The Beauty of Flavour Physics

Malami, Eleftheria

2024

DOI (link to publisher)
10.5463/thesis.893

document version
Publisher's PDF, also known as Version of record

The Beauty of Flavour Physics
B Meson Decays: Do They Reveal New Physics?

Eleftheria Malami

ISBN: 978-90-834632-6-1
DOI: http://doi.org/10.5463/thesis.893

The Beauty of Flavour Physics
B Meson Decays: Do They Reveal New Physics?
Thesis, Vrije Universiteit, Amsterdam
Cover design: Esther van Hoevelaken-Wilbrink, concept and photo by Eleftheria Malami
Printed by: proefschriftenprinten.nl

This work is financed by the Netherlands Organization for Scientific Research (NWO) and carried out at the National Institute for Subatomic Physics (Nikhef) in Amsterdam, The Netherlands, and Vrije Universiteit (VU) Amsterdam, The Netherlands.

VRIJE UNIVERSITEIT

THE BEAUTY OF FLAVOUR PHYSICS

B Meson Decays: Do They Reveal New Physics?

ACADEMISCH PROEFSCHRIFT

ter verkrijging van de graad Doctor aan
de Vrije Universiteit Amsterdam,
op gezag van de rector magnificus
prof.dr. J.J.G. Geurts,
in het openbaar te verdedigen
ten overstaan van de promotiecommissie
van de Faculteit der Bètawetenschappen
op woensdag 6 november 2024 om 13.45 uur
in een bijeenkomst van de universiteit,
De Boelelaan 1105

door

Eleftheria Malami

geboren te Athene, Griekenland

promotor:	prof.dr. R. Fleischer
copromotor:	prof.dr. M.H.M. Merk
promotiecommissie:	prof.dr. J. Rojo prof.dr. E.L.M.P. Laenen prof.dr. A.P. Colijn dr. D. van Dyk dr. A. Perrevoort dr. J. de Vries

Contents

List of Figures

List of Tables

This manuscript is based on the following publications:

- R. Fleischer and E. Malami, "Revealing new physics in $B_s^0 \to D_s^{\mp} K^{\pm}$ decays," Eur. Phys. J. C **83**, no.5, 420
- K. De Bruyn, R. Fleischer, E. Malami and P. van Vliet, "New physics in B_q^0–$\bar{B}_q^0$ mixing: present challenges, prospects, and implications for $B_q^0 \to \mu^+\mu^-$" J. Phys. G **50**, no.4, 045003
- R. Fleischer and E. Malami, "Using $B_s^0 \to D_s^{\mp} K^{\pm}$ Decays as a Portal to New Physics," Phys. Rev. D **106**, no.5, 056004
- M. Z. Barel, K. De Bruyn, R. Fleischer and E. Malami, "In pursuit of new physics with $B_d^0 \to J/\psi K^0$ and $B_s^0 \to J/\psi\phi$ decays at the high-precision Frontier," J. Phys. G **48**, no.6, 065002
- R. Fleischer, R. Jaarsma, E. Malami and K. K. Vos, "Exploring $B \to \pi\pi, \pi K$ decays at the high-precision frontier," Eur. Phys. J. C **78**, no.11, 943

and the following proceedings contributions:

- E. Malami, "Theoretical Highlights of CP Violation in B Decays," PoS **HQL2023** (2024), 058
- E. Malami, "Manifestations of CP Violation in B Mesons: Theoretical Perspective," Contribution to: **Beauty 2023**
- K. De Bruyn, R. Fleischer, E. Malami and P. van Vliet, "Studies of New Physics in $B_q^0 - \bar{B}_q^0$ Mixing and Implications for Leptonic Decays," PoS **DISCRETE2022** 082
- E. Malami, "CP Violation and mixing in beauty sector: A theoretical overview," PoS **LHCP2022**, 056
- V. Chobanova, *et al.* "Summary of Working Group 4: Mixing and mixing-related CP violation in the $\boldsymbol{B}$ system: Δm, $\Delta\Gamma$, ϕ_s, ϕ_1/β, ϕ_2/α, ϕ_3/γ," PoS **CKM2021**, 017
- E. Malami and R. Fleischer, "Puzzles in the $B_s^0 \to D_s^{\pm} K^{\mp}$ System," PoS **CKM2021**, 077
- E. Malami and R. Fleischer, "Searching for New Physics with $B_s^0 \to D_s^{\pm} K^{\mp}$ Decays," PoS **PANIC2021**, 159
- E. Malami, "Exploring New Physics in $B \to \pi K$ Decays," PoS **CORFU2019**, 025
- E. Malami, "$B_s^0 \to D_s^{\pm} K^{\mp}$ decays: Can they reveal New Physics?," PoS **CORFU2019**, 026

1 Introduction

What are the fundamental constituents of matter? What are their fundamental interactions? Such questions play a central role in understanding nature. A fascinating description of the subatomic world is given by the Standard Model (SM) of particle physics [1–3]; the framework that describes the electromagnetic, weak and strong interactions. Gravity, the fourth fundamental interaction, is not part of the SM. In this thesis, gravity does not play any role – it consitutes a separate problem. In general, the SM is a very successful theory, having passed impressive experimental tests. Key player in experimental particle physics is currently the Large Hadron Collider (LHC) at CERN, which led to the breakthrough discovery of the Higgs particle in 2012 [4, 5].

Despite the success of the SM, there are phenomena that it cannot explain and we have indications that it is not complete. We do not know the origin of the SM, which shows very intriguing patterns and features. In order to understand these patterns, physics beyond the SM might be required [6, 7]. Examples of phenomena that are not incorporated in the SM, other than gravity, are the matter–antimatter asymmetry in Universe and the dark matter. The first refers to the observed imbalance between matter and antimatter in the Universe after the Big Bang, leading to a matter–dominated Universe [8]. The second is a hypothetical form of matter, which does not interact with electromagnetic forces and for which the SM does not provide a candidate to explain its properties [9, 10].

How can we search for physics beyond the SM? In general, there are two approaches. We can perform:

- either *direct searches,*
  where we can try to produce and detect new real particles directly at colliders
- or *indirect searches,*
  where we try to find traces of virtual particles, which are manifestations of quantum effects, by performing high precision measurements.

Let us now discuss in more detail these two avenues. On the one hand, we can try to produce particles directly at particle colliders at the "high-energy frontier". Then, we can study the decays of these new particles into SM particles with the use of general purpose detectors. The mass-reach is limited by the energy of the collider. Nowadays, the most powerful collider is the LHC at CERN, colliding protons at energies up to 13.7 TeV. Unfortunately, no particles from beyond the SM have been found so far, suggesting that the particles are too heavy to be produced directly.

On the other hand, we can also search for New Physics (NP) indirectly through precision measurements of known decay processes. An essential point in these studies is that we can probe very high energy scales of NP, much higher than the directly accessible regimes in particle colliders, thereby moving to the "high precision frontier". In this case, we utilise quantum fluctuations, very suppressed processes, and can obtain indirect evidence of new particles via such quantum effects. The idea is to find and identify processes and observables which theorists can calculate with high precision and also experimentalists can measure very precisely. If there are new particles entering, we would find discrepancies between the measured quantities and the ones calculated in the SM.

Indirect access to NP effects is the main approach we follow in this thesis. The powerful tool of quantum field theory (QFT) is used in the quest of possible indirect indications of NP. Working at the "high precision frontier", the SM offers a particularly interesting sector, which runs under the terminology of the "flavour sector". Flavour physics describes the different interactions between different flavours (i.e. types) of quarks and leptons, which are the building blocks of matter in the SM. We can obtain very intriguing transitions between different quark and lepton flavours. In this thesis, we focus on the quark flavour sector.

A particularly promising tool providing reliable tests of the SM flavour dynamics and searching for signals of NP is given by decays of B mesons. B mesons are bound states of a bottom anti-quark, which is also known as a "beauty" quark, and a light quark (which can be either up, down, or strange) or charm quark. In our studies, we present benchmark B decay processes, which are sensitive to physics from beyond the SM.

We have now reached an interesting era of particle physics, where there is a plethora of experimental data. A number of puzzling patterns arise in these data sets. This may indicate that we have finally reached a level of precision where it is possible to reveal such discrepancies between experimental measurements and theoretical predictions. Unfortunately, the individual precision is not yet high enough to draw definite conclusions. It is very exciting though that we start to see these puzzles. Moving towards higher precision in the future, we might eventually be able to establish NP. In this thesis, we will revisit intriguing cases and also point out new puzzles that had not been observed before.

In general, there are puzzling cases which arise from decays where the observables are robust with respect to theoretical uncertainties. In this sense, these decays have "simple dynamics" with respect to strong interactions. The corresponding puzzles are called flavour anomalies and are associated to a class of decays called semileptonic, which we will introduce in Chapter 3.[1] Additionally, observables related to $B_s^0 \to \mu^+\mu^-$ modes [14, 15], which are

[1]Examples are the ratios $R(D)$, $R(D^*)$ [11], and the angular observable P_5' [12,13]. The first observable refers to ratios between the branching fractions of the decays $B \to D^{(*)}\ell\bar{\nu}$ involving taus with respect to those involving muons or electrons, as we will discuss in Sec. 3.4.3, while P_5' arises from an analysis of the

"rare" decays, are in the spotlight, too. We will further explore these observables in the $B^0_{(s)} \to \mu^+\mu^-$ system in the present thesis in Chapter 8.[2]

On the other hand, there are further puzzles which also have important implications, playing a central role in understanding flavour physics, but are related to modes with much more complicated dynamics due to strong interactions. Calculations in this case are very difficult and a lot of sophistication is required in the analysis of these decays. These are called non-leptonic decays, and we will extensively discuss them in this thesis. Prime examples here are the $B^0_d \to J/\psi K^0$ and $B^0_s \to J/\psi\phi$ modes as well as the $B \to \pi K$ and $B^0_s \to D^\mp_s K^\pm$ channels. Key role in the anomalies observed in this case plays CP violation. An overview of all these puzzling cases is given in Fig. 1.

In this thesis, studies of CP violation are a primary focus. The term C stands for the charge conjugation operator and changes a particle into its antiparticle, while the term P stands for the parity operator, which leads to space inversion. The violation of the CP symmetry refers to the non-invariance of the weak interactions with respect to a combined C and P transformation. It was firstly discovered in 1964 through the observation of the $K_L \to \pi^+\pi^-$ decay [8]. Today, this phenomenon is also established in B decays and the charm sector.

CP violation is a topic crucial for our existence. Prime point is the observed baryon asymmetry in the Universe. Sakharov proposed a set of conditions [16], which must be satisfied in order to have matter and antimatter production at different rates. These conditions are: baryon number violation, CP violation, as well as conditions where thermodynamic equilibrium does not hold. Studies of the baryon asymmetry within the SM indicate that the corresponding CP violation is too small by many orders of magnitude [17], thereby suggesting new sources of CP violation.

CP violation manifests itself in various ways in B-meson decays. We can categorise the decays we study as follows:

- the $B^0_d \to J/\psi K^0_S$ and $B^0_s \to J/\psi\phi$ decays,
- the $B^0_s \to D^\mp_s K^\pm$ system,
- the $B \to \pi K$ system and
- the rare $B^0_{(s)} \to \mu^+\mu^-$ decays.

The first three categories include no leptons in the final state and are challenging due to strong interactions. In these channels, we perform state-of-the-art studies of CP violation

$B^0 \to K^{*0}\mu^+\mu^-$ channel.

[2] These observables are the branching fractions $\mathcal{B}$ and the mass eigenstate rate asymmetries $\mathcal{A}_{\Delta\Gamma_s}$, as we will discuss in detail in Chapter 8.

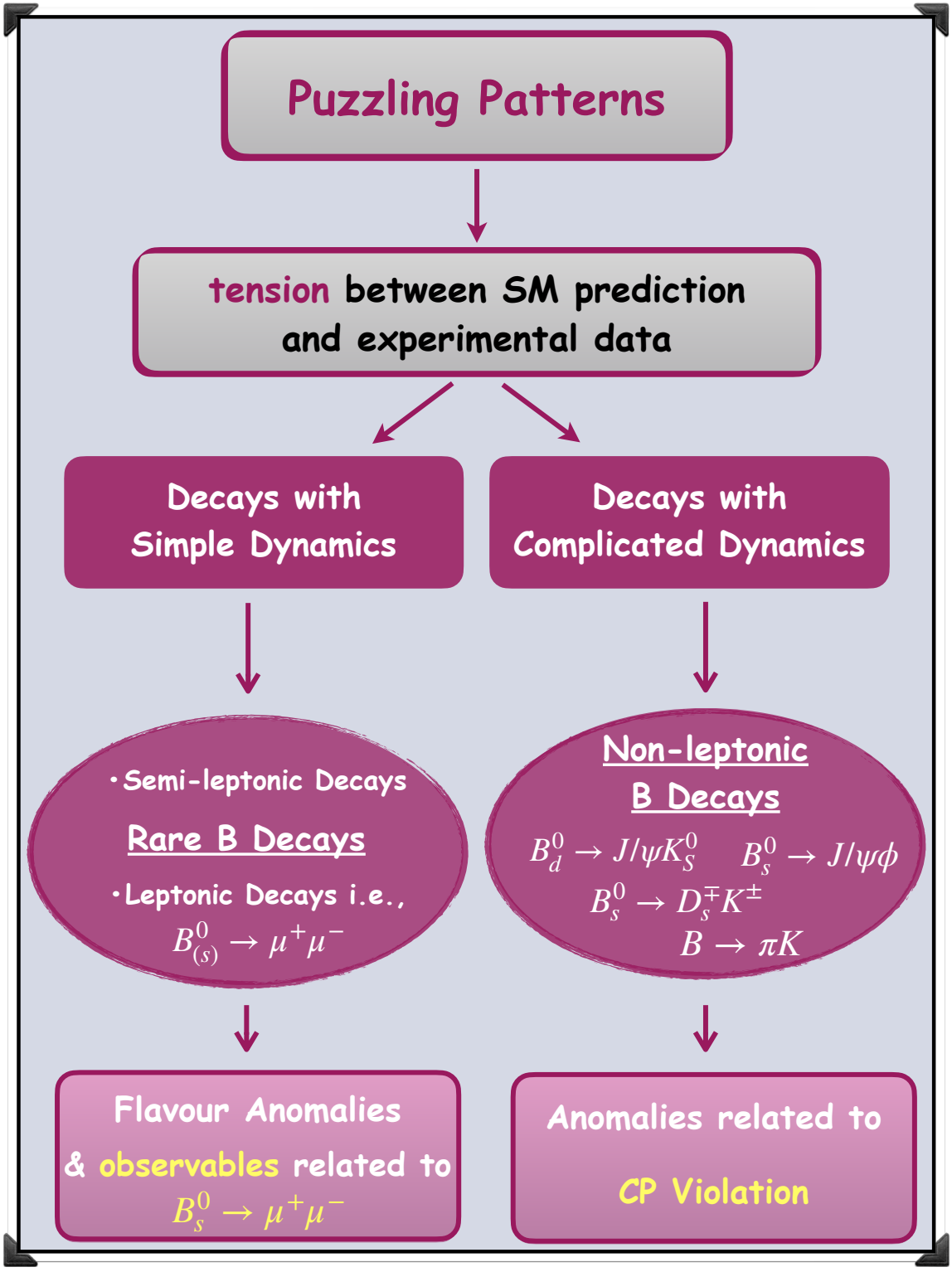

Figure 1: Overview of puzzling cases as described in the text.

and explore how much space is left for NP. The last category is a simpler case. Although CP violation in this channel is also interesting, it is not part of our analysis in this thesis. Instead, we focus on aspects of NP.

B decays offer fascinating strategies to deal with both CP violation and searches for hints of NP. As a result, the B-meson system receives a lot of attention from both theorists and experimentalists, having dedicated experiments to explore these decays. LHCb and Belle II are currently the main players, building on a long history of the exploration of the flavour sector, but also ATLAS and CMS can make interesting contributions. Concerning searches of NP in this thesis, we focus on model-independent studies and not constructing a specific model. Our aim is to find indications of NP, investigating correlations between observables in various benchmark B decays.

The outline of this thesis is as follows. Firstly, in Chapter 2, we describe the theoretical framework of the SM. The focus is on the quark flavour sector, both heuristically and in a more formal way. We introduce the concept of CP violation and discuss the Cabibbo–Kobayashi–Maskawa mechanism, as well as the unitarity triangle (UT).

Chapter 3 introduces the B-meson system, discussing both charged and neutral B mesons. We pay special attention to the neutral ones, showing the phenomenon of B_q^0–$\bar{B}_q^0$ mixing (where $q = d, s$), which plays an important role in testing the SM. We provide the theoretical tools we use in the analyses of B decays and discuss the classification of these decays according to their final states. We set up the formalism for each of these classes, analysing their dynamics, and discuss interesting aspects, mostly within the SM framework. An essential topic in our analysis is related to the determination of the apex of the UT, as we describe in Chapter 3.4.2.

In Chapter 4, we specifically discuss CP violation in B decays, focusing on how CP asymmetries arise. We classify the various types of CP violation and present interesting observables. Having the formalism at hand, we utilise benchmark B decays to further explore the topic both within and beyond the SM.

Moving to Chapter 5, we study applications of the B_q^0–$\bar{B}_q^0$ mixing phenomenon. Central role in our studies is played by specific parameters which are associated with the mixing effects, i.e. decay widths, mass differences and CP-violating mixing phases. Key modes for exploring these parameters are $B_d^0 \to J/\psi K_S^0$ and $B_s^0 \to J/\psi\phi$, which are considered to be "golden modes" for analysing CP violation. At the level of precision that we have now reached, we have to include uncertainties coming from certain decay contributions, which cannot be calculated reliably from first principles in strong interactions. However, we have identified ways to take them into account through related control channels. This will result in a state-of-the-art determination of the mixing parameters. These parameters are then

further used as key inputs to explore how much room is left for NP in B_q^0–$\bar{B}_q^0$.

Chapter 6 covers the analysis of the $B_s^0 \to D_s^{\mp} K^{\pm}$ system. These decays allow a theoretically clean determination of one of the parameters of the UT, the angle γ. Considering experimental data, we observe intriguing patterns related to CP violation, suggesting NP at the decay amplitude level. The same trend also arises in other modes with similar dynamics. We shed more light on this puzzling situation, utilising the experimental data and performing a theoretical analysis. We propose strategies to explore possible NP effects and generalise the description of these decays to allow for NP at the decay amplitude level.

In Chapter 7, we discuss $B \to \pi K$ decays. The puzzles arising there are a long-standing issue. We focus on the $B_d^0 \to \pi^0 K_S$ channel, which is the most interesting channel with respect to CP violation. Exploiting the current data, we explore the correlations between the CP asymmetries in this mode, which are theoretically very robust regarding theoretical uncertainties. In doing so, we encounter discrete ambiguities. Although difficult to remove these ambiguities, one solution is finally left, which shows interesting tension with respect to the corresponding measurement. We propose a strategy which allows an optimal determination of the parameters that describe the puzzling effects. This strategy can be applied in the high precision B physics era, eventually answering the question of whether these decays imply NP.

Last but not least, in Chapter 8, we present the $B_s^0 \to \mu^+\mu^-$ decay, which is a very rare process in the SM. We expect only 3 out of one billion B_s mesons produced at the LHC to decay into the final state $\mu^+\mu^-$. After searching for this decay for decades, the LHCb and CMS collaborations have finally managed to observe the $B_s^0 \to \mu^+\mu^-$ channel in 2012 [18], representing a key result of the previous LHC running. In this thesis, we utilise this very interesting decay as a probe of NP. In particular, we focus on minimising the impact of theoretical uncertainties arising within the SM, and employ new observables of $B_s^0 \to \mu^+\mu^-$ to explore possible NP contributions. Applying the results of the NP analysis in B_q^0–$\bar{B}_q^0$ mixing obtained in Chapter 5, we constrain the NP parameter space.

Finally, we note that this thesis covers a broad variety of different processes in flavour physics. We collect all the main strategies and findings of our analyses in Chapter 9 and conclude with a brief outlook.

2 Exploring the Flavour Sector

In this chapter, we set up the stage for exploring the quark flavour sector. We introduce the SM framework, firstly heuristically and then in a more formal way, and derive the corresponding Lagrangian. We study the concept of CP violation within the SM and discuss the Cabibbo-Kobayashi-Maskawa (CKM) mechanism, which is the origin of CP violation.

2.1 The Standard Model in a Nutshell

The SM framework describes the interactions of the elementary particles that we know today, which are the leptons and the quarks [1–3].[3] As we have already mentioned in Chapter 1, three of the four fundamental forces that act in the universe; the weak, the electromagnetic and the strong interactions, are incorporated in this framework. The fourth one, gravity, is not included in the SM. As we will discuss in Sec. 2.1.1, a highlight regarding the interactions in the SM is that the electromagnetic and weak interactions are "unified" in an electroweak sector. Thus, the SM compromises two parts, one describing electroweak interactions and the other referring to strong interactions.

Let us now begin our discussion of the SM first by presenting its main features. An illustration of the SM is given in Fig. 1. As we know, the fermions, which are the leptons and quarks, are the building blocks of matter. They arise in three "generations", which differ in their mass spectra, with the particles of the first generation being less heavy than those of the second generation, which are less heavy than those of the third. The forces are mediated by four vector bosons, thus particles with spin equal to 1, which are: the photon γ for the electromagnetic force, the charged $W^{\pm}$ and the neutral Z boson for the electroweak force, and the gluon for the strong force. These are all gauge bosons, arising in the framework of gauge theory, as we will discuss below. In addition, on July 4th, 2012, the discovery of a scalar boson was announced through the independent measurements of ATLAS and CMS, which was related to the Brout–Englert–Higgs (BEH) mehcanisms [32, 33], completing the current picture of the SM. This particle was the Higgs boson, with spin equal to 0.

The SM utilises gauge theories to implement local symmetries, with special field transformations at each space-time point to ensure that the theory is gauge invariant, thus unchanged under transformations. A major problem was to assign masses to particles in this framework. Explicit mass terms would break the gauge symmetries. In order to avoid that in a consistent way, spontaneous symmetry breaking was introduced. The concept of

[3] For a detailed discussion of the SM, we provide here a number of interesting textbooks [19–31].

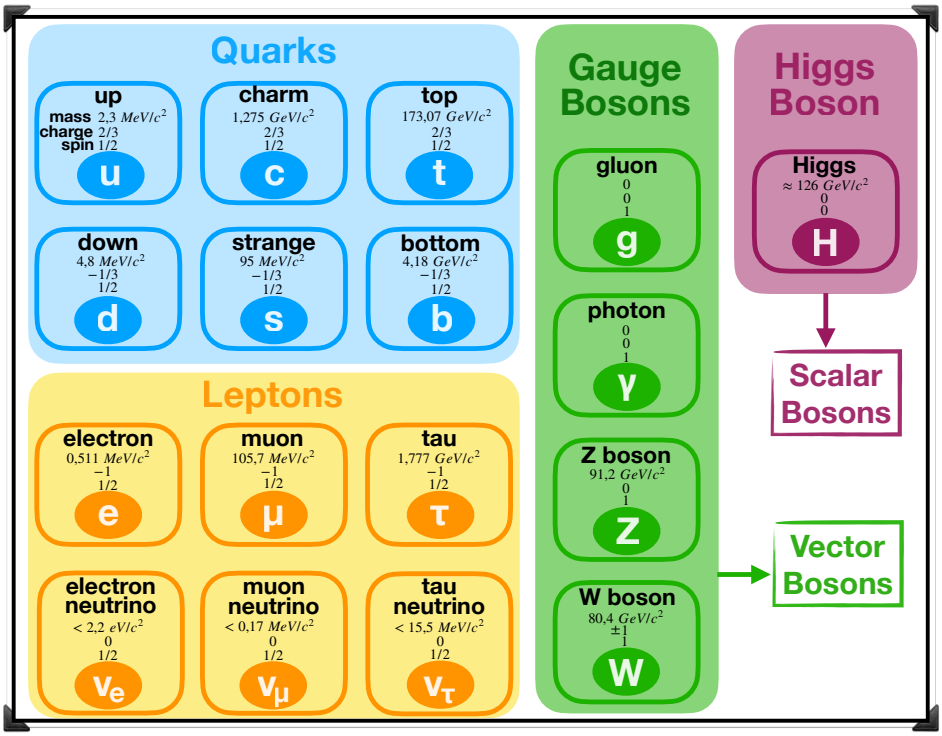

Figure 2: The Standard Model of elementary particles.

spontaneous symmetry breaking originates from condensed matter physics. In the SM, it is implemented in the most minimal and simplistic way, utilising the BEH field. The mechanism responsible for mass generation, involving this spontaneous symmetry breaking, is the BEH mechanism, or simply Higgs mechanism. An important note to add is that these theories are renormalizable[4], thus consistent quantum field theories [34].

Let us say a few more words about the masses of the elementary particles. We emphasize again that to break the symmetry in the most minimal way, an elementary scalar field has to be added, which is the BEH field (or simply the Higgs field). The Higgs boson is an excitation of this field. Through the process of electroweak symmetry breaking, the Higgs field develops a non-vanishing vacuum expectation value. Due to this non-zero expectation value, the gauge bosons W and Z become massive and as we will discuss later in the thesis, leptons and quarks also acquire masses via Yukawa interactions with the same Higgs field.

[4]Renormalizability is an intrinsic feature of quantum field theory. When calculating quantum corrections, infinities (like loops which diverge) might arise. Applying a renormalizable theory, allows these infinities to be absorbed by properly redefining the couplings, fields and masses of the theory. Renormalizability ensures that divergencies and infinities can be absorbed into a finite number of parameters, thus obtain a finite result. These technicalities will not be directly addressed in this thesis, however it is an essential feature of the SM.

On the other hand, the photons are massless, since the corresponding symmetry, the $U(1)$ symmetry of quantum electrodynamics, remains unbroken. Gluons, mediating the strong interactions, also remain massless. Last but not least, the Higgs boson also interacts with the Higgs field, hence it gains mass itself.

2.1.1 Electroweak Interactions

Let us firstly discuss the electroweak (EW) part of the SM, which provides the unified description of electromagnetic and weak interactions. Historically, the EW sector preceded the understanding of strong interactions in the SM. The triumph of the SM, and what makes it such a beautiful theory, is that for the first time we have a unification of two interactions that were previously viewed as very different and separate. This unification was suggested independently by Glashow [35], Salam [36] and Weinberg [1] in the late 1960s, and was a breakthrough discovery, playing a key role in our understanding of the EW interactions. For their contributions, all three of them were awarded the Nobel Prize in physics in the year 1979.

In this unified EW sector, the theory of quantum electrodynamics (QED) describes the electromagnetic part, which generalises the classical electrodynamics with the Maxwell equations to the quantum level. At the heart of the unified electroweak theory lies the notion of gauge symmetry, which we will formally discuss in Sec. 2.2.1. Key role to this framework is the concept of spontaneous symmetry breaking, manifesting through the Higgs mechanism.

The electromagnetic and weak interactions, though distinct in their manifestations at low energies, become indistinguishable at high energies, on the order of 246 GeV, which is the vacuum expectation value of the Higgs field. This unified theory has been extensively tested, in particular at LEP and SLC colliders (for an overview, see Ref. [37] and references therein), and confirmed through experiments conducted at particle accelerators such as the Large Hadron Collider (LHC), which is currently the "main player".

The electroweak sector of the SM stands as a testament to the power of theoretical insight and experimental verification. It showcases the remarkable unity underlying the fundamental forces of nature. In early 1970s, 't Hooft and Veltman showed that the EW theory is renormalizable [38], for which they were awarded the Nobel prize in 1999.

2.1.2 Strong Interactions

The second important theoretical framework in the SM is quantum chromodynamics (QCD). Describing strong interactions between quarks, mediated by the massless gluons,

QCD operates within the framework of a non-abelian gauge symmetry $SU_c(3)$, which is not spontaneously broken. We note that only quarks can participate in these interactions.

QCD exhibits two regimes: the perturbative regime, related to high energies or short distances, where perturbation theory can be applied in order to calculate QCD corrections, and the non-perturbative one, corresponding to low energies, where perturbation theory cannot be used. Key feature of QCD is asymptotic freedom [39], which implies that the quarks and gluons have reduced coupling strength at high energies. Asymptotic freedom results from the self couplings of the gluons in non-abelian gauge theories.

Due to the fact that the coupling α_s, describing the strength of the QCD interactions, is small at high energies (perturbative part), these elementary particles behave like quasi-independent particles. Thus, the feature of asymptotic freedom makes perturbative calculations of strong interaction effects at small distances possible[5]. It is important to recognize the groundbreaking work of D. Gross, F. Wilczek, and D. Politzer, who were awarded the 2004 Nobel Prize for demonstrating that QCD has the feature of asymptotic freedom [41–44]. Our knowledge of the complex dynamics regulating strong interactions within the SM is largely based on their remarkable work.

However, at lower energies/greater distances, where perturbative techniques cannot be applied, QCD interactions become stronger, with α_s value becoming very large, thereby leading to hadronic bound states. Therefore, quarks and gluons are confined within composite particles known as hadrons. This phenomenon is known as confinement. Confinement binds quarks and gluons inside hadrons to bind, preventing the particles from being free. This effect is essential in our studies of meson decays, in particular decays of B meson, since these processes are non-perturbative and difficult to calculate. Given the complex nature of confinement and hadronic effects, we explore methodologies and approaches which allow us to deal with these challenging calculations.

As an epilogue, it is worth mentioning that already in the 1980s researchers started considering larger gauge groups that would incorporate both QCD and EW sector, aiming towards a Grand Unified Theory (GUT) [45, 46], albeit not experimentally confirmed. Intrinsic feature of this effort is that when attempting to establish a unified framework of EW and strong interactions, leptoquark particles emerge, which are capable to experience both interactions. However, so far, there is no convincing theory to describe QCD and EW SM in a unified manner.

[5]Here renormalization group techniques [40] can also be used.

2.2 Theoretical Ingredients of the Standard Model

Having provided a general description of the SM framework, let us now move on to a more formal description, looking at the theoretical foundation and derive the Lagrangian.

2.2.1 Gauge Group

The SM is based on the gauge group [25, 47]:

$$SU_c(3) \times SU_L(2) \times U_Y(1), \tag{2.1}$$

where $SU_c(3)$ represents the symmetry of strong interactions described by QCD, while $SU_L(2) \times U_Y(1)$ describes the electroweak interaction.

$SU_c(3)$ is a 3rd order unitary group, representing 3×3 matrices acting on three-dimensional vectors. The quantum number of $SU_c(3)$ is "colour", indicated by the subscript "c". We note that only the quarks are subject to the effects of QCD since leptons do not interact via the strong force. Quarks are triplets under $SU_c(3)$ (denoted as **3**) with the quantum numbers "red", "green" and "blue". Leptons are singlets under $SU_c(3)$ and as a result they are colour neutral. The group $SU_L(2)$ includes all two-dimensional complex unitary matrices with unit determinant[6]. The quantum number of the $SU_L(2)$ group is the weak isospin and there are two states ($\pm1/2$). The left-handed fields are doublets under $SU_L(2)$ and the right-handed fields are singlets under $SU_L(2)$. In the charged weak interactions which are mediated by the $W^{\pm}$ bosons, it is only the doublets that participate. Finally, the $U_Y(1)$ group includes all one-dimensional complex unitary matrices[7]. The quantum number of $U_Y(1)$ is the hypercharge Y and in principle can be any real number. The hypercharge can be normalised following the Gell-Mann−Nishijima relation [48, 49]:

$$Q = T_3 + Y, \tag{2.2}$$

where Q is the electric charge and T_3 is the third component of the weak isospin of $SU_L(2)$.

As already discussed, the symmetry has to be broken in order to give masses to the particles. In particular, heavy EW gauge bosons W and Z are required to make the interactions "weak"[8]. As a result of EW symmetry breaking, the $U(1)$ symmetry of QED remains exact. The strong interactions, described by the $SU_c(3)$ symmetry, also remain unbroken. Consequently, the photons and the gluons are massless particles in this framework, whereas the W and Z gain masses of 80 GeV and 90 GeV, respectively. Now, the

[6] It is related to the rotation group $SO(3)$, indicating sphere symmetry in 3 dimensions.

[7] It corresponds to the symmetry of the circle remaining unchanged under rotations in a plane.

[8] We emphasize that these interactions are not weak because of a small coupling constant but due to the very heavy gauge bosons.

$SU_L(2) \times U_Y(1)$ symmetry of electroweak interactions is spontaneously broken by the Higgs mechanism as follows [1, 50, 51]:

$$SU_L(2) \times U_Y(1) \xrightarrow{\text{SSB}} U(1)_{\text{QED}}, \tag{2.3}$$

where SSB stands for the spontaneous symmetry breaking and $U(1)_{\text{QED}}$ denotes the symmetry group of QED. We point out again that this symmetry breaking, which is needed to give masses to particles, is done in the most minimal way, adding a single scalar particle. Looking at the current experimental information on the Higgs, it is very remarkable that nature really follows this simplistic way.

2.2.2 Standard Model Lagrangian

We can now encode all the above information in the Lagrangian. Following the conventions of [52, 53], we first of all consider the spinor fields ψ, which account for the fermion generations and for which

$$\bar{\psi} = \psi^\dagger \gamma^0, \tag{2.4}$$

where γ^0 is one of the Dirac matrices. We write:

$$\gamma^0 = \begin{pmatrix} \mathbb{1} & 0 \\ 0 & -\mathbb{1} \end{pmatrix}, \quad \gamma^i = \begin{pmatrix} 0 & \vec{\sigma} \\ -\vec{\sigma} & 0 \end{pmatrix}, \tag{2.5}$$

where $\mathbb{1}$ is the 2×2 unit matrix and $\vec{\sigma}$ are the 2×2 Pauli matrices, which are given in the Appendix A. The full SM Lagrangian consists of the kinetic term $\mathcal{L}_{\text{kin}}$, the Higgs part $\mathcal{L}_\phi$ and the Yukawa part $\mathcal{L}_{\text{Yukawa}}$, and can be written as follows:

$$\mathcal{L}_{\text{total}} = \mathcal{L}_{\text{kin}} + \mathcal{L}_\phi + \mathcal{L}_{\text{Yukawa}}. \tag{2.6}$$

Let us examine each term separately [54]. We start with the kinetic part and as a first step, we consider the case of free fields, i.e. without interactions. This is the kinematic term of the Dirac spinor, with the Dirac equation for a free Dirac field describing fermions. The Lagrangian governing the dynamics of the spinor fields is given by:

$$\mathcal{L}_{\text{kin}} = i\bar{\psi}(\partial^\mu \gamma_\mu)\psi, \qquad \mu = 0, 1, 2, 3\ , \tag{2.7}$$

where we introduce the partial derivative acting on ψ.

How do we next include the interaction terms? The interactions for gauge theories are introduced through the gauge principle, making the symmetry of the SM a local symmetry. This ensures that the Lagrangian remains invariant under local transformations. To achieve

this, the partial derivative has to be replaced by the covariant derivative D^μ. In this procedure, for each generator of our gauge group we have to introduce a gauge field:

$$D^\mu = \partial^\mu + ig_w W^\mu \sigma + ig' B^\mu Y + ig_s G^\mu T^\alpha. \tag{2.8}$$

Here, we have the three bosons of the electroweak interaction W^μ with the Pauli matrices σ and the g_w which is the coupling for $SU_L(2)$, the single hypercharge boson B with the g' coupling for the $U_Y(1)$ as well as the eight gluon fields G^μ with the Gell-Mann matrices T^α (which are given in Appendix A), and the g_s coupling for $SU_c(3)$. We note at this point, that these gauge bosons are massless. The kinetic part of the Lagrangian is written as:

$$\mathcal{L}_{\text{kin}} = i\bar{\psi}(D^\mu \gamma_\mu)\psi. \tag{2.9}$$

We can now write the kinetic part of the Lagrangian for quarks and leptons. Here, for simplicity, we focus only on the Q_i quarks interaction part. The quarks experience both the strong and the EW interactions:

$$\mathcal{L}_{\text{kin}} = i\bar{Q}_i \gamma_\mu (\partial^\mu + \frac{i}{2} g_w W^\mu \sigma + \frac{i}{6} g' B^\mu Y + \frac{i}{2} g_s G^\mu T^\alpha) Q_i, \tag{2.10}$$

where only the last term corresponds to the QCD part, with G^μ describing the involvement of the gluons, while the other terms refer to the EW sector.

For the charged weak interaction, where only Q_i doublets participate, thus for the interaction between the left-handed quarks, which carry weak isospin $-1/2$, we obtain:

$$\begin{aligned} \mathcal{L}_{\text{weak}} &= i\bar{Q}_{i,\text{left}} \gamma_\mu (\partial^\mu + \frac{i}{2} g_w W^\mu \sigma) Q_{i,\text{left}} \\ &= i\overline{(u \;\; d)}_{i,\text{left}} \gamma_\mu (\partial^\mu + \frac{i}{2} g_w W^\mu \sigma) \begin{pmatrix} u \\ d \end{pmatrix}_{i,\text{left}} . \end{aligned} \tag{2.11}$$

Considering that $W^\pm = \frac{1}{\sqrt{2}}(W_1 \mp iW_2)$, and denoting left as L, we can rewrite the above equation in the form:

$$\mathcal{L}_{\text{weak}} = i\bar{u}_{i,L} \gamma_\mu \partial^\mu u_{i,L} + i\bar{d}_{i,L} \gamma_\mu \partial^\mu d_{i,L} - \frac{g}{\sqrt{2}} \bar{u}_{i,L} \gamma_\mu W^{-\mu} d_{i,L} - \frac{g}{\sqrt{2}} \bar{d}_{i,L} \gamma_\mu W^{+\mu} u_{i,L} + ... \tag{2.12}$$

So far, we have only massless gauge bosons and the gauge symmetry does not allow explicit mass terms. The symmetry has to be broken in order to introduce mass terms. Focusing on the weak interactions, we need heavy gauge bosons. A solution to this challenge of making the bosons heavy can be given through spontaneous symmetry breaking. So, how

does the EW symmetry breaking work now? In the SM, in the most minimal version, an elementary scalar field is introduced, the Higgs field ϕ, which is an isospin doublet:

$$\phi = \begin{pmatrix} \phi^+ \\ \phi^0 \end{pmatrix}. \tag{2.13}$$

This field is responsible for the spontaneous symmetry breaking through developing a non-vanishing vacuum expectation value, minimizing the Higgs potential $V(\phi)$ of the SM which is written as follows:

$$V(\phi) = \mu^2(\phi^\dagger\phi) + \lambda(\phi^\dagger\phi)^2, \tag{2.14}$$

where μ^2 is the mass term and λ is the Higgs self coupling. So, we break the EW symmetry $SU_L(2) \times U_Y(1)$ in such a way that $U(1)_{\text{QED}}$ remains unbroken, as presented in Eq. (2.3). Therefore, we write the Higgs part of the Lagrangian as

$$\mathcal{L}_\phi = (D_\mu\phi)^\dagger(D^\mu\phi) - \mu^2(\phi^\dagger\phi) - \lambda(\phi^\dagger\phi)^2, \tag{2.15}$$

which includes the kinetic term for the Higgs with the couplings to the Higgs potential and the gauge bosons.

We move now to the third part of the Lagrangian. The Yukawa sector includes interactions between the Higgs and the fermions involving the Yukawa couplings. These couplings are allowed and can be added by hand. Since the Higgs couples to $SU_L(2)$ doublet and singlet in a gauge invariant way (hence the Lagrangian does not change under transformations), the $\mathcal{L}_{\text{Yukawa}}$ part of the Lagrangian is written as follows:

$$-\mathcal{L}_{\text{Yukawa}} = Y^d_{ij}\bar{Q}_{i,L}\ \phi\ d_{j,R} + Y^u_{ij}\bar{Q}_{i,L}\ \tilde{\phi}\ u_{j,R} + Y^l_{ij}\bar{L}_{i,L}\ \phi\ l_{j,R} + \text{h.c.}\ , \tag{2.16}$$

where h.c. stands for hermitian conjugate, the $\bar{Q}$ and $\bar{L}$ denote the quarks and leptons, while the subscripts L and R stand for left and right, respectively. The fermion fields are three-component vectors, so all three generations are included. The Y^d_{ij}, Y^u_{ij} and Y^l_{ij} are 3×3 Yukawa-matrices, which operate in flavour space producing the quark mixing (thus the couplings between different families), while $\tilde{\phi}$ is:

$$\tilde{\phi} = i\sigma_2\phi^* = \begin{pmatrix} \phi^0 \\ -\phi^- \end{pmatrix}. \tag{2.17}$$

2.2.3 Quark Mixing in the Standard Model

Let us now have a closer look into the Yukawa interactions, needed to have fermion masses, which give rise to interesting phenomena like flavour-changing transitions. These transitions play a very important role for this thesis. We explore how these phenomena occur,

discussing the links between the Yukawa couplings and the quark mixing. Quark mixing refers to the interaction between different quark generations in the SM. As we will show, an essential point is the difference between the mass eigenstates and flavour eigenstates.

We are interested in showing how the quarks obtain their masses from the Yukawa Lagrangian. Starting from Eq. (2.16), we write the Yukawa Lagrangian for the quarks. We choose ϕ^0 to be $\frac{1}{\sqrt{2}}(\upsilon + h(x))$, where υ is the vacuum expectation value of the Higgs potential and h is the physical Higgs field, thus we obtain [54, 55]:

$$\phi(x) = \begin{pmatrix} \phi^+ \\ \phi^0 \end{pmatrix} \quad \xrightarrow{\text{SSB}} \quad \frac{1}{\sqrt{2}} \quad \begin{pmatrix} 0 \\ \upsilon + h(x) \end{pmatrix}. \tag{2.18}$$

Therefore, the mass terms which are derived from this equation after the symmetry breaking are the following:

$$-\mathcal{L}_{\text{mass}} = Y^d_{ij}\bar{d}_{i,L}\frac{\upsilon}{\sqrt{2}}d_{j,R} + Y^u_{ij}\bar{u}_{i,L}\frac{\upsilon}{\sqrt{2}}u_{j,R} + \text{h.c.} + \text{interaction terms} \tag{2.19}$$

$$= \bar{d}_{i,L}M^d_{ij}d_{j,R} + \bar{u}_{i,L}M^u_{ij}u_{j,R} + \text{h.c.} + \text{interaction terms}\ , \tag{2.20}$$

where the different indices describe different quark flavours $i, j = 1, 2, 3$ and one has to sum over these. The matrices M^f (where $f = u, d$) can be diagonalised by unitary matrices V^f_R, V^f_L in order to obtain proper mass terms:

$$M^f_{\text{diag}} = V^f_L M^f V^{f\dagger}_R. \tag{2.21}$$

So far, the fermion fields have been expressed in the interaction basis, therefore d, u are interaction eigenstates. Due to the fact that the V matrices are unitary, satisfying $V^f V^{f\dagger} = \mathbb{1}$, and utilising Eq. (2.21), Eq. (2.20) becomes:

$$-\mathcal{L}_{\text{mass}} = \bar{d}_{i,L}V^{d\dagger}_L V^d_L M^d_{ij} V^{d\dagger}_R V^d_R d_{j,R} + \bar{u}_{i,L}V^{u\dagger}_L V^u_L M^u_{ij} V^{u\dagger}_R V^u_R u_{j,R} \tag{2.22}$$

$$= \bar{d}_{i,L}V^{d\dagger}_L (M^d_{ij})_{\text{diag}} V^d_R d_{j,R} + \bar{u}_{i,L}V^{u\dagger}_L (M^u_{ij})_{\text{diag}} V^u_R u_{j,R}. \tag{2.23}$$

We now rewrite the quark fields as $\bar{d}'_{i,L} = \bar{d}_{i,L}V^{d\dagger}_L$ and $d'_{j,R} = V^d_R d_{j,R}$ (and correspondingly for the up-type quarks), and obtain

$$-\mathcal{L}_{\text{mass}} = \bar{d}'_{i,L}(M^d_{ij})_{\text{diag}} d'_{j,R} + \bar{u}'_{i,L}(M^u_{ij})_{\text{diag}} u'_{j,R}, \tag{2.24}$$

where the quark fields are written in their mass eigenstates, thus the primes denote the quark mass eigenstates.

The Lagrangian for the charged-current interaction in terms of the weak interaction eigenstates is written as

$$\mathcal{L}_{\text{cc}} = \frac{g}{\sqrt{2}}\bar{u}_{iL}\gamma_\mu W^{-\mu} d_{iL} + \frac{g}{\sqrt{2}}\bar{d}_{iL}\gamma_\mu W^{+\mu} u_{iL}. \tag{2.25}$$

If we now rewrite the Lagrangian in terms of the quark mass eigenstates, the quark mixing arises between generations in the charged-current interaction, since every interaction field is replaced with a combination of the mass eigenstates:

$$\mathcal{L}_{\rm cc} = \frac{g}{\sqrt{2}}\bar{u}'_{iL}(V_L^u V_L^{d\dagger})_{ij}\gamma_\mu W^{-\mu} d_{iL} + \frac{g}{\sqrt{2}}\bar{d}'_{iL}(V_L^d V_L^{u\dagger})_{ij}\gamma_\mu W^{+\mu} u_{iL}, \tag{2.26}$$

where $(V_L^u V_L^{d\dagger})_{ij}$ and $(V_L^d V_L^{u\dagger})_{ij}$ refer to the Cabibbo-Kobayashi-Maskawa (CKM) matrix $V_{\rm CKM}$ [56, 57], which will be discussed in Sec. 2.4. We note that as a convention we choose the weak and mass eigenstates to be equal for the up-type quarks $u_i = u'_j$. On the other hand, the down-type quarks are rotated when going from one basis to the other, thus $d_i = V_{\rm CKM} d'_j$. We see that within the SM, the analysis for flavour physics actually begins from a charged-current Lagrangian.

2.3 CP Violation in the SM

In this section, we explore how discrete symmetries, parity and charge conjugation, are implemented in the SM and focus on the violation of the symmetry called CP through EW interactions. The operator P stands for parity and is related to space inversion. This operator flips the sign of the space coordinates, thus for a wavefunction $\psi(t, x, y, z)$ we obtain:

$$\mathrm{P}\psi(t, x, y, z) = \psi(t, -x, -y, -z). \tag{2.27}$$

Parity conservation suggests that the physical processes act in an identical way once they are viewed as in a mirror, simply speaking. Experimental data indicate that parity is conserved in strong and electromagnetic interactions but is violated in weak interactions. This parity violation in weak interactions was proposed theoretically in 1957 and was shortly after established by the Wu experiment [58].

The operator C denotes the charge conjugation which changes a particle into its anti-particle (or vice versa), therefore changing the sign of the charges of the elementary particles:

$$\mathrm{C}\,|\psi\rangle = |\bar{\psi}\rangle\,. \tag{2.28}$$

We note that the space-time coordinates are not changed in this operation. Similarly to parity, the charge conjugation is conserved in strong and electromagnetic interactions but is maximally violated in weak interactions.

Therefore, weak interactions maximally violate parity and charge conjugation. Initially, it was believed that applying both symmetries would lead to invariance of weak interactions with respect to the combined C and P, thus the CP transformation. However, it came as a surprise in 1964 through precision measurements by observing the kaon decay $K_L \to \pi^+\pi^-$

[8] that CP is not a good symmetry of weak interaction. CP violation is a very profound aspect of particle physics, which also plays a key role in our studies. In the SM, we can actually accommodate CP violation, and below we will see how we can accomplish this.

Last but not least, we note that a third discrete symmetry is that of time reversal, which is related to the operator T:

$$\mathrm{T} : t \to -t. \tag{2.29}$$

Combining the C, P and T operators, the CPT symmetry is a conjecture and appears to be a very fundamental symmetry in quantum field theory. Any Lorentz invariant local field theory must obey the combined CPT symmetry. Simply speaking, giving up on CPT symmetry for local quantum field theories, one would run into serious problems, as the whole formulation of theoretical physics would break down. Tests are performed on how well it holds and so far, no CPT violation has been found. The key point is that if CPT is conserved, then in case there is CP violation, there should also be T violation, so in this sense they are really closely linked.

2.3.1 CP Violation in Quark Flavour Physics

We continue with the discussion of the origin of CP violation in the quark sector (for detailed studies see, e.g., [59–62]). Within the SM, CP violation arises in the complex Yukawa couplings. Since both the kinetic term of the Lagrangian in the interaction basis and the Higgs part conserve CP symmetry, our starting point is again the Yukawa sector and the corresponding Lagrangian reads:

$$-\mathcal{L}_{\text{Yukawa}} = Y_{ij}\bar{\psi}_{i,L}\ \phi\ \psi_{j,R} + Y^*_{ij}\bar{\psi}_{j,R}\ \phi^\dagger\ \psi_{i,L}\ . \tag{2.30}$$

Under CP transformation, we obtain:

$$\mathrm{CP}(\bar{\psi}_{i,L}\ \phi\ \psi_{j,R}) = \bar{\psi}_{j,R}\ \phi^\dagger\ \psi_{i,L}. \tag{2.31}$$

As a result, the CP-transformed Yukawa Lagrangian takes the form

$$-\mathcal{L}^{\text{CP}}_{\text{Yukawa}} = Y_{ij}\ \bar{\psi}_{j,R}\ \phi^\dagger\ \psi_{i,L} + Y^*_{ij}\ \bar{\psi}_{i,L}\ \phi\ \psi_{j,R}. \tag{2.32}$$

We observe that if $Y_{ij} = Y^*_{ij}$, the Yukawa Lagrangian remains invariant. Therefore, CP violation appears in the Yukawa complex couplings.

Diagonalising the Yukawa matrices, we arrive again at the Lagrangian in terms of quark mass eigenstates, as presented in Eq. (2.26). Simplifying the notation regarding the CKM matrix, we write:

$$\mathcal{L}_{cc} = \frac{g}{\sqrt{2}}\ \bar{u}'_{i,L}V_{ij}\gamma_\mu W^{-\mu}d_{i,L} + \frac{g}{\sqrt{2}}\bar{d}'_{i,L}V^*_{ij}\gamma_\mu W^{+\mu}u_{i,L}. \tag{2.33}$$

Applying a CP operation in Eq. (2.33) provides us with the following expression:

$$\mathcal{L}_{cc}^{\mathrm{CP}} = \frac{g}{\sqrt{2}}\, \bar{d}'_{i,L} V_{ij} \gamma_\mu W^{+\mu} u_{i,L} + \frac{g}{\sqrt{2}} \bar{u}'_{i,L} V_{ij}^{*} \gamma_\mu W^{-\mu} d_{i,L}. \tag{2.34}$$

We observe again that if $V_{ij} = V_{ij}^{*}$, the Yukawa Lagrangian remains invariant. So, if V_{ij} is real, there is no CP violation. It is the complex nature of the CKM matrix that gives rise to CP violation within the SM.

To summarise, the Yukawa couplings, describing the interactions between the Higgs field and the fermions, give rise to off-diagonal elements in the matrix between the different generations. After the diagonalization of the Yukawa matrix, these off-diagonal elements arise in the charged current couplings described by the CKM matrix, thereby suggesting that this CKM matrix is the source of CP violation in the quark flavour sector.

So, we already see that we can accommodate CP violation, if the CKM matrix is complex. But can we have physical phases in the CKM matrix? Let us answer this question in the following Section.[9]

2.4 CKM Matrix

We have already introduced the CKM matrix in a more formal way, discussing how it connects the flavour states with the mass eigensates and highlighting the important role that it plays as a source of CP violation. For instance, in Eqs. (2.34) and (2.26), we see how it enters the Lagrangian via formal arguments. Let us now move on to a more phenomenological interpretation of this matrix and explore what this implies.

The CKM matrix $V_{\mathrm{CKM}} = (V_{\mathrm{ij}})$ [56, 57] is a 3×3 unitary matrix for 3 generations:

$$V_{\mathrm{CKM}} = \begin{pmatrix} V_{ud} & V_{us} & V_{ub} \\ V_{cd} & V_{cs} & V_{cb} \\ V_{td} & V_{ts} & V_{tb} \end{pmatrix}, \tag{2.35}$$

which describes the quark mixing effects. It connects the weak interaction eigenstates with their mass eigenstates. Conventionally, for the up-type quarks, the interaction and the mass

[9] Another open issue in theoretical physics is the "strong CP problem" (see for instance Refs. [63, 64]). Simply speaking, the problem is that in principle, there could be CP violation in strong interactions but it turns out that the phenomenon is very small. So, the question is: Why is CP violation so small in strong interactions? Proposed solutions include the introduction of pseudoparticles called axions. Readers are referred to Ref. [65] for further details. However, this issue is not relevant to our studies. Consequently, in this thesis, we assume that the strong interactions conserve CP symmetry, taking the strong CP problem aside, without exploring it further.

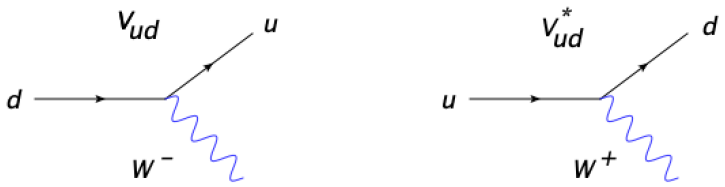

Figure 3: Illustration of charged current processes in the SM.

eigenstates are equal while the down-type quarks are being rotated through the following transformation:

$$\begin{pmatrix} d \\ s \\ b \end{pmatrix}_{\text{weak}} = \begin{pmatrix} V_{ud} & V_{us} & V_{ub} \\ V_{cd} & V_{cs} & V_{cb} \\ V_{td} & V_{ts} & V_{tb} \end{pmatrix} \begin{pmatrix} d' \\ s' \\ b' \end{pmatrix}_{\text{mass}} . \tag{2.36}$$

By construction the CKM matrix is unitary, thus we may write:

$$V_{\text{CKM}} V_{\text{CKM}}^\dagger = \begin{pmatrix} V_{ud} & V_{us} & V_{ub} \\ V_{cd} & V_{cs} & V_{cb} \\ V_{td} & V_{ts} & V_{tb} \end{pmatrix} \begin{pmatrix} V_{ud}^* & V_{cd}^* & V_{td}^* \\ V_{us}^* & V_{cs}^* & V_{ts}^* \\ V_{ub}^* & V_{cb}^* & V_{tb}^* \end{pmatrix} = \begin{pmatrix} 1 & 0 & 0 \\ 0 & 1 & 0 \\ 0 & 0 & 1 \end{pmatrix} = V_{\text{CKM}}^\dagger V_{\text{CKM}}. \tag{2.37}$$

The unitarity ensures that there is no flavour-changing neutral current (FCNC) at the tree level in the SM [3]. Looking at the structure of the Lagrangian given in Eqs. (2.33) and (2.34), the transition from a down- to an up-type quark is described by the V_{ud} element, which characterises the corresponding coupling strength. Similarly, the V_{ud}^* element enters the transition from an up to a down type quark. An illustration of these charged-current processes and the corresponding CKM matrix elements governing them is given in Fig. 3.

In addition to these transitions, there are also CP-conjugate processes. In the first case, for the CP-conjugate process an anti-down would transition to anti-up quark, still with the same CKM element as depicted in the left plot of Fig. 3. In the second case, an anti-up would transition to anti-down quark, again with the same CKM element as shown in the right plot of Fig. 3.

We have seen that the complex phases are related to the possibility of CP violation. Can we actually have complex phases in the CKM matrix? In order to explore whether we might actually have a complex phase in this matrix and to determine how many physical parameters we have, we perform a counting of the free parameters.

2.4.1 Counting the Number of Parameters

In the SM, there are 3 generations, so the CKM matrix is a 3×3 unitary matrix. It is useful though to extend the discussion and assume N fermion generations. The $N \times N$ matrix is characterised by N^2 complex elements and hence $2N^2$ real parameters. The unity of the diagonal elements, as given in Eq. (2.37), leads to N normalization constraints and due to the fact that the off-diagonal elements vanish, there are $N^2 - N$ orthogonality relations. Consequently, the number of constraints in this case is

$$N + N^2 - N = N^2. \tag{2.38}$$

We note that we have the freedom to redefine the up- and down-type quark field phases as follows:

$$u^{'}_{i,L} = e^{i\xi^{u'}_i} u^{'}_{i,L}, \tag{2.39}$$

$$d^{'}_{j,L} = e^{i\xi^{d'}_i} d^{'}_{j,L}, \tag{2.40}$$

where ξ is an arbitrary convention-dependent phase, which cannot be measured. We emphasize that if we had physical observables, these phases would have to cancel.

For the up-type quarks, there are N such quantities and for their down-type counterparts also N quantities, therefore $2N$ in total. Concerning the right-handed quark fields, they are rotated simultaneously in order to maintain the mass terms invariant. In order to ensure the invariance of the charged-current Lagrangian, we have the following phase transformation of the CKM matrix elements:

$$V \to \begin{pmatrix} e^{-\xi(u')} & 0 & 0 \\ 0 & e^{-\xi(c')} & 0 \\ 0 & 0 & e^{-\xi(t')} \end{pmatrix} \begin{pmatrix} V_{ud} & V_{us} & V_{ub} \\ V_{cd} & V_{cs} & V_{cb} \\ V_{td} & V_{ts} & V_{tb} \end{pmatrix} \begin{pmatrix} e^{\xi(d')} & 0 & 0 \\ 0 & e^{\xi(s')} & 0 \\ 0 & 0 & e^{\xi(b')} \end{pmatrix} = \exp[i(\xi^{u'}_i - \xi^{d'}_i)]V_{ij}.$$

Having though the freedom to make redefinitions of phases as above, we can apply this to the CKM matrix to eliminate phases and eventually see how many physical parameters we actually need.

There are $2N$ phases leading to $2N-1$ phase differences. The number of free parameters can be determined by subtracting the number of the constraints coming from the unitarity as well as the number of the phase differences from the total number of the real parameters:

$$\begin{aligned} n_{\text{free parameters}} &= 2N^2 - N^2 - 2N + 1 \\ &= (N-1)^2. \end{aligned} \tag{2.41}$$

These parameters can consist of rotation angles and complex phases.

Since the CKM matrix is a unitary matrix, there are $(N^2 - N)/2$ constraints, which involve the angles that describe the rotations among the N dimensions, which are the Euler angles that we already mentioned earlier. We find the number of angles by subtracting from the N^2 real parameters the N normalization constraints and the $(N^2 - N)/2$ orthogonality constraints:

$$\begin{aligned} n_{\text{angles}} &= N^2 - N - \frac{1}{2}(N^2 - N) \\ &= \frac{1}{2}N(N-1). \end{aligned} \tag{2.42}$$

The remaining parameters represent the number of complex phases:

$$\begin{aligned} n_{\text{phases}} &= n_{\text{free parameters}} - n_{\text{angles}} \\ &= (N-1)^2 - \frac{1}{2}N(N-1) \\ &= \frac{1}{2}(N-1)(N-2). \end{aligned} \tag{2.43}$$

Therefore, for an $N \times N$ unitary matrix, there are $N(N-1)/2$ Euler angles, which describe rotations between the N generations, and $(N-1)(N-2)/2$ complex phases.

Specifically, for the case of $N = 2$ generations, we obtain no complex phase and there is only one parameter, which is the Cabibbo angle [56]. Here, we could not accommodate CP violation through the quark-mixing matrix. On the other hand, moving to $N = 3$ generations, the 3×3 CKM matrix involves three Euler angles (real parameters) and a single complex phase. This single complex phase allows us to accommodate CP violation. The question is whether this phase is different from 0 (or π) or not but in principle, we may have a CP-violating phase.

Kobayashi and Maskawa were the first who pointed this out in 1973, making a link to the number of generations and the phenomenon of CP violation [57]. The main conclusion is that a third generation would be needed in the SM. This is a crucial point for our existence, as it is one of the requirements for the generation of the baryon asymmetry of the universe, as proposed by the Sakharov conditions [16], already presented in Sec. 1. So, the counting of the parameters may look simple but it has profound implications. In 2008, Kobayashi and Maskawa were rewarded with a Nobel prize for their pioneering work.

Having presented the parameter counting, we discuss how we can parametrize the CKM matrix. There is freedom of choosing different parametrizations. The one which is typically used for applications in phenomenological studies is the one advocated by the Particle Data

Group (PDG) [66]:

$$V_{\rm CKM} = \begin{pmatrix} c_{12}c_{13} & s_{12}c_{13} & s_{13}e^{-i\delta_{13}} \\ -s_{12}c_{23} - c_{12}s_{23}s_{13}e^{i\delta_{13}} & c_{12}c_{23} - s_{12}s_{23}e^{i\delta_{13}} & s_{23}c_{13} \\ s_{12}s_{23} - c_{12}c_{23}s_{13}e^{i\delta_{13}} & -c_{12}s_{23} - s_{12}c_{23}e^{i\delta_{13}} & c_{23}c_{13} \end{pmatrix}. \tag{2.44}$$

This is the "standard parametrization", where $c_{ij} \equiv \cos\theta_{ij}$ and $s_{ij} \equiv \sin\theta_{ij}$ and θ_{ij} denote the Euler rotation angles with i, j being the generation labels. The CKM matrix is expressed in terms of three Euler angles θ_{12}, θ_{13} and θ_{23} and a complex phase δ_{13}, which allows us to accommodate the CP-violating phenomena in flavour-changing processes in the SM.[10]

2.4.2 Hierarchy of the CKM Matrix Elements

Looking at the CKM matrix, an interesting question comes up: what is the magnitude of the CKM matrix elements? Does this matrix show any underlying patterns? In order to answer this question, we can measure processes, which are governed by certain CKM matrix elements, and can use them to determine these CKM factors. This procedure can be quite involved, as hadronic physics enters as well as nuclear physics in some cases. For an overview of these measurements, the reader is referred to the PDG Review in Ref. [66], which provides the state-of-the-art status of these measurements. The data reveal a very intriguing hierarchy, as illustrated in Fig. 4.

Wolfenstein introduced a parametrization to make this hierarchy explicit [69]. The steps on how to obtain it and the framework of particularly including higher order corrections are presented in Ref. [70]. We introduce a set of four new parameters, λ, A, ρ and η, and we need to get back to the PDG parametrization. For this purpose, we use the following relations:

$$s_{12} \equiv |V_{us}| = \lambda \approx 0.22, \quad s_{23} \equiv A\lambda^2, \quad s_{13}e^{-i\delta_{13}} \equiv A\lambda^3(\rho - i\eta). \tag{2.45}$$

[10] We note that in the lepton sector, with the neutrino masses, we have a similar matrix, which is the Pontecorvo-Maki-Nakagawa-Sakata (PMNS) matrix [67, 68]. For three generations, it is written as:

$$\begin{pmatrix} \nu_e \\ \nu_\mu \\ \nu_\tau \end{pmatrix} = \begin{pmatrix} U_{e1} & U_{e2} & U_{e3} \\ U_{\mu 1} & U_{\mu 2} & U_{\mu 3} \\ U_{\tau 1} & U_{\tau 2} & U_{\tau 3} \end{pmatrix} \begin{pmatrix} \nu_1 \\ \nu_2 \\ \nu_3 \end{pmatrix},$$

connecting the mass eigenstates (ν_1, ν_2, ν_3) to their flavour eigenstates $(\nu_e, \nu_\mu, \nu_\tau)$. The components $U_{\alpha i}$ are the PMNS matrix elements. However, the hierarchy is very different than the CKM matrix. It does not have the hierarchy structures of the quarks. Another tricky part is related to the parameter counting. For instance, in the case of Majorana neutrinos, there may be two more phases in the PMNS matrix. This is due to the fact that the states are real and hence have less phase freedom. Here, focusing on the quark sector, we do not further elaborate on the leptonic mixing matrix.

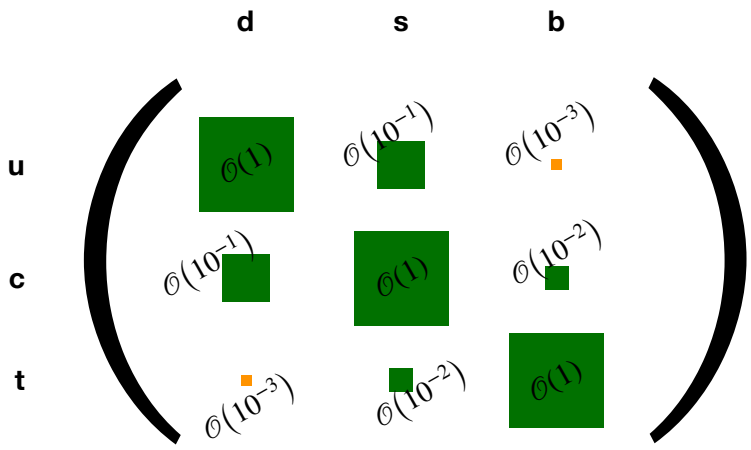

Figure 4: Illustration of the hierarchy of the CKM matrix elements.

Here λ is an expansion parameter related to kaon decays, and more specifically from the class of decays called semi-leptonic (a term that we will discuss in detail in Sec. 3.4). Now, we only give the order of λ in Eq. (2.45). As λ is an important parameter, we will elaborate more on it later in the thesis. The parameter η gives rise to an imaginary part, i.e. complex CKM matrix elements.

We can now perform a Taylor expansion on every element of the CKM matrix in powers of λ. Neglecting terms of $\mathcal{O}(\lambda^4)$, yields

$$V_{\text{CKM}} = \begin{pmatrix} 1 - \frac{1}{2}\lambda^2 & \lambda & A\lambda^3(\rho - i\eta) \\ -\lambda & 1 - \frac{1}{2}\lambda^2 & A\lambda^2 \\ A\lambda^3(1 - \rho - i\eta) & -A\lambda^2 & 1 \end{pmatrix} + \mathcal{O}(\lambda^4), \tag{2.46}$$

which reflects the hierarchical structure of the CKM matrix elements in terms of order of λ that we already presented in Fig. 4. As we can see, the transitions between the same generation are governed by CKM matrix elements of $\mathcal{O}(1)$, hence transitions within a family are strongly favoured. The transitions between the first and second generations are suppressed by CKM factors of $\mathcal{O}(10^{-1})$, thus by one power of λ. The transitions between the second and third generation are suppressed by $\mathcal{O}(10^{-2})$, thus by two powers of λ. Finally, transitions between the first and third generations are even more suppressed, by $\mathcal{O}(10^{-3})$, so by at least three powers of λ. Consequently, it becomes clear that this Taylor expansion is very useful in phenomenological applications. In terms of the experimental precision we have nowadays, higher-order terms have to be included in the expansion [70].

2.4.3 Additional requirements for CP violation

As we have already seen, within the SM, CP violation may arise in the Yukawa sector, as we could have a complex phase in the CKM matrix. In order to have a non-vanishing phase, at least three fermion generations are required. However, for observable effects violating the CP symmetry, further requirements are needed.

Closer studies by Jarlskog [71] have shown that another criterion has to be satisfied, which is related to the following parameter:

$$J_{\rm CP} = |\Im(V_{i\alpha}V_{j\beta}V_{i\beta}^*V_{j\alpha}^*)|, \qquad (i \neq j, \alpha \neq \beta). \tag{2.47}$$

This "Jarlskog parameter" characterizes the strength of CP violation in the SM and is invariant under phase transformations of the CKM matrix.

In particular, CP violation requires that the Jarlskog parameter is different from 0, thus $J_{\rm CP} \neq 0$. Applying the PDG parametrization, we obtain

$$J_{\rm CP} = s_{12}s_{13}s_{23}c_{12}c_{23}c_{13}^2 \sin\delta_{13}, \tag{2.48}$$

and observe that this parameter is proportional to $\sin\delta_{13}$. Indeed, for $\delta_{13} = 0$ or π, $J_{\rm CP}$ would vanish and we would not have CP violation. In the Wolfenstein parametrization, neglecting higher-order terms in λ, $J_{\rm CP}$ takes the following form:

$$J_{CP} = A^2\lambda^6\eta. \tag{2.49}$$

So, $J_{\rm CP}$ is proportional to η, which plays the role of the CP-violating weak phase in this case. The experimental information implies that $J_{\rm CP}$ is $\mathcal{O}(10^{-5})$, suggesting that CP violation is a small effect.

In addition to the non-vanishing Jarlskog parameter, another condition that needs to be satisfied in order to have CP violating effects is related to the quark masses and is the following [71, 72]:

$$(m_t^2 - m_c^2)(m_t^2 - m_u^2)(m_c^2 - m_u^2)(m_b^2 - m_s^2)(m_b^2 - m_d^2)(m_s^2 - m_d^2) \times J_{\rm CP} \neq 0. \tag{2.50}$$

These mass factors reflect the feature that if any two quarks of the same charge had the same mass, the CP-violating phase of the CKM matrix vanishes. This would be like the case with two generations where the phase can be eliminated. We observe that CP violation is closely linked to the hierarchy of masses and the number of fermion generations. A better fundamental understanding of the origin of CP violation in the SM suggests a connection to the hierarchy in the CKM matrix but it is challenging.

We observe that within the SM, CP violation is a small effect and hence, difficult to measure. It indeed took until 1964 and came as a surprise to reveal CP violation in the

neutral kaon system, described by an observable ε_K [73]. This phenomenon was discovered through the observation of $K_L \to \pi^+\pi^-$ decays. It is a manifestation of indirect CP violation, a term that we will discuss in Sec. 4. In 1999, a non-vanishing value of a quantity called $\mathrm{Re}(\varepsilon'_K/\varepsilon_K)$ was established [74, 75], characterising CP violation arising directly at the decay amplitude level of the neutral kaons. CP violation was also observed in the B meson system in 2001 by the BaBar and Belle experiments [76,77]. It was established in the $B^0_d \to J/\psi K_S$ decay. Here we have a large CP asymmetry of about 70%, thus suggesting a large effect. However, the decay rates are still small at the order of $\mathcal{O}(10^{-4})$, showing again that observing CP-violating phenomena is indeed difficult. In 2019, CP violation was also finally established in the neutral charm system, through the measurement of the difference between the CP asymmetries of $D^0 \to K^+K^-$ and $D^0 \to \pi^+\pi^-$ channels by the LHCb Collaboration [78].

2.5 Unitarity Triangles

The unitarity of the CKM matrix, characterised by Eq. (2.37), requires that the rows and the columns must be orthogonal and normalised. This gives rise to nine relations [79]. Three of them are the normalisation relations, referring to the diagonal elements:

$$V_{ud}V^*_{ud} + V_{us}V^*_{us} + V_{ub}V^*_{ub} = 1, \tag{2.51}$$

$$V_{cd}V^*_{cd} + V_{cs}V^*_{cs} + V_{cb}V^*_{cb} = 1, \tag{2.52}$$

$$V_{td}V^*_{td} + V_{ts}V^*_{ts} + V_{tb}V^*_{tb} = 1. \tag{2.53}$$

The other six are the orthogonal relations, corresponding to the non-diagonal elements:

$$V_{ud}V^*_{us} + V_{cd}V^*_{cs} + V_{td}V^*_{ts} = 0, \tag{2.54}$$

$$V_{us}V^*_{ub} + V_{cs}V^*_{cb} + V_{ts}V^*_{tb} = 0, \tag{2.55}$$

$$V_{ud}V^*_{ub} + V_{cd}V^*_{cb} + V_{td}V^*_{tb} = 0, \tag{2.56}$$

$$V_{cd}V^*_{ud} + V_{cs}V^*_{us} + V_{cb}V^*_{ub} = 0, \tag{2.57}$$

$$V_{cd}V^*_{td} + V_{cs}V^*_{ts} + V_{cb}V^*_{tb} = 0, \tag{2.58}$$

$$V_{td}V^*_{ud} + V_{ts}V^*_{us} + V_{tb}V^*_{ub} = 0. \tag{2.59}$$

These orthogonality relations have the structure of the sum of three complex numbers adding up to zero, which can be represented in the complex plane as triangles.

We can now apply the Wolfenstein parametrization and explore the magnitude of the CKM matrix elements in powers of λ, thus check how these triangles would look like [80].

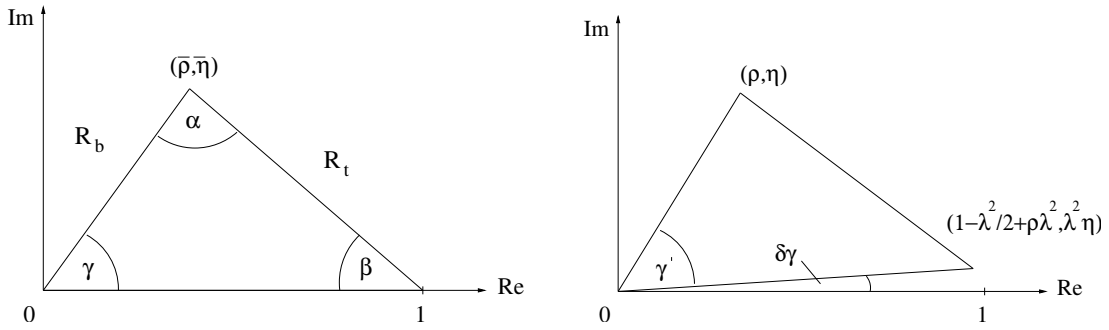

Figure 5: The two non-squashed triangles of the CKM matrix [80]. The left one represents the "unitarity triangle" with the apex given by $(\bar{\rho}, \bar{\eta})$, as defined in the text, while the right one is shifted by $\delta\gamma$ and the apex is given by (ρ, η).

Eqs. (2.56) and (2.59) are the only two cases that refer to triangles with all three sides of the same order of magnitude, thus the only non-squashed triangles. In the remaining four equations, the three terms in the sum are characterised by different powers of λ, thus there is always one side which is suppressed with respect to the others.

Let us elaborate a bit more on the non-squashed triangle relations:

$$V_{ud}V_{ub}^* + V_{cd}V_{cb}^* + V_{td}V_{tb}^* = 0, \tag{2.60}$$

$$V_{td}V_{ud}^* + V_{ts}V_{us}^* + V_{tb}V_{ub}^* = 0. \tag{2.61}$$

At leading non-vanishing order, the two non-squashed cases agree with each other, thereby describing the same triangle, which would be the "unitarity triangle". However, including higher order terms in the Wolfenstein expansion, a small difference of $\mathcal{O}(\lambda^2)$ rises between them. One of these relations is then the "unitarity triangle" in the complex plane:

$$V_{ud}V_{ub}^* + V_{cd}V_{cb}^* + V_{td}V_{tb}^* = 0. \tag{2.62}$$

This is the one that the basis agrees with the real axis. So, one is constructed in a way that the basis is still aligned with the real axis while the other one is shifted by a tiny $\delta\gamma = -\lambda^2\eta$ angle with respect to the real axis. An illustration is given in Fig. 5, which is presented in Ref. [80].

Let us introduce the sides and the angles of the "unitarity triangle", which is again shown in Fig. 6. One side of the triangle points along the real axis, having unit length by definition. The other two sides are [81]:

$$R_b \equiv |V_{ud}V_{ub}^*/V_{cd}V_{cb}^*| = \left(1 - \frac{\lambda^2}{2}\right)\frac{1}{\lambda}\left|\frac{V_{ub}}{V_{cb}}\right| = \sqrt{\bar{\rho}^{\,2} + \bar{\eta}^{\,2}}\,, \tag{2.63}$$

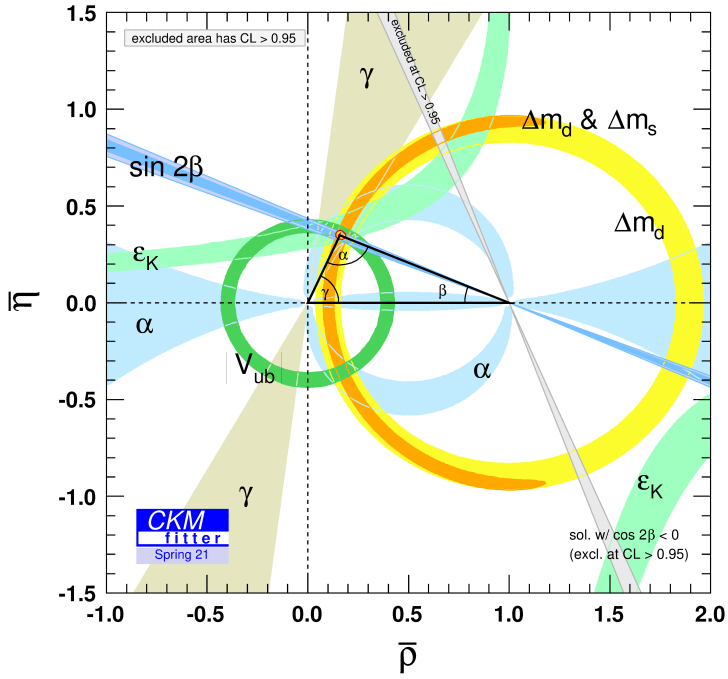

Figure 6: Illustration of a global analysis of the UT in the $\bar{\rho} - \bar{\eta}$ plane by the CKM Collaboration [82].

$$R_t \equiv |V_{td}V_{tb}^*/V_{cd}V_{cb}^*| = \frac{1}{\lambda}\left|\frac{V_{td}}{V_{ts}}\right|\left[1 - \frac{\lambda^2}{2}(1-2\bar{\rho})\right] + \mathcal{O}\left(\lambda^4\right) = \sqrt{(1-\bar{\rho})^2 + \bar{\eta}^{\,2}}, \tag{2.64}$$

which we will discuss in detail in Sec. 3.4.2. The apex is given by $(\bar{\rho}, \bar{\eta})$, with

$$\bar{\rho} = \rho\left(1 - \frac{1}{2}\lambda^2\right), \qquad \bar{\eta} = \eta\left(1 - \frac{1}{2}\lambda^2\right), \tag{2.65}$$

where ρ, η and λ are the Wolfenstein parameters. The three angles of the triangle are defined as

$$\alpha \equiv \arg\left[-\frac{V_{td}V_{tb}^*}{V_{ud}V_{ub}^*}\right], \quad \beta \equiv \arg\left[-\frac{V_{cd}V_{cb}^*}{V_{td}V_{tb}^*}\right], \quad \gamma \equiv \arg\left[-\frac{V_{ud}V_{ub}^*}{V_{cd}V_{cb}^*}\right] \tag{2.66}$$

and are convention-independent observables.

We can determine the UT using experimental data for appropriate observables and convert them, with application of theory and assuming the SM, into contours in the $\bar{\rho} - \bar{\eta}$ plane. If we had only the SM, all these contours should intersect in one point, the apex of the UT. If we had NP, we should expect discrepancies. An illustration of these contours and the corresponding UT are illustrated in Fig. 6, where we see a CKM global fit [82].

For completeness, we briefly mention here where these contours come from. The indirect CP violation in the neutral kaon system with the ε_K parameter can be converted into a hyperbola in the $\bar{\rho} - \bar{\eta}$ plane (Sec. 3.4.2). The $|V_{ub}|$ (and $|V_{cb}|$) matrix element, determined by B decays (Sec. 3.4.1), as well as the parameters Δm_d and Δm_s, which are mass differences related to the phenomenon called neutral B meson mixing (Sec. 3.1), lead to contours that allow the determination of the sides R_b and R_t. CP-violating observables from the $B_d^0 \to J/\psi K_S$ decay allow the extraction of the $\sin 2\beta$ and hence the β angle. Similarly, measurements of CP-violating effects in B meson decays are converted into direct information on the angles α and γ (Sec. 6), allowing their determination.

A key goal is to overconstrain the UT, adding more and more constraints. When adding these constraints, validity of the SM is assumed. Should there be NP entering, then we would expect discrepancies. Looking at the current data, the apex is already impressively constrained and the picture looks consistent within the uncertainties. However, there is still a lot of room for improvement. Subtleties already arise which have to be included, and this will also be important while moving towards higher precision in the future. Currently we have for certain CKM parameters discrepancies between different determinations, which play key role in this thesis. Therefore, a careful analysis of the UT is needed and we will explicitly study the topic in Sec. 3.4.2.

2.6 Summary

In this chapter, we have set the stage for investigating the quark flavour sector. Beginning with an overview of the SM framework and discussing the corresponding Lagrangian, we introduced the concept of CP symmetry violation and discussed the CKM mechanism, which gives rise to CP violation in the SM. An essential point is the intriguing hierarchical structure characterising the CKM matrix, as determined by experimental measurements. Associated to the CKM matrix are the corresponding unitarity triangles, which play an important role in our studies. We have thoroughly introduced the properties of the UT in this chapter. Discrepancies arise between different determinations for certain CKM parameters. Therefore, a careful analysis of the UT is needed in order to unravel the implications of these deviations, which will be presented in Sec. 3.4.2.

With the framework now established, we proceed to investigate the dynamics of the B meson system in Chapter 3. B decays govern the sector of quark flavour physics, therefore the main focus of this thesis is the exploration of the topic of CP violation and searches of NP through benchmark B transitions.

3 B Meson System

In our studies, we focus on decays of B mesons, which are hadronic bound states of an anti-b quark and a light quark. The B-meson system includes both charged and neutral B mesons. The quark content of the different B mesons is given in Table 1. We note that from the charged mesons, we only use those with the u quark in the present work, while we do not study the mesons with the c quark, which are less frequently produced at the LHC.

Regarding neutral B mesons, as we will discuss in detail in Sec. 5, an important feature is B_q^0–$\bar{B}_q^0$ mixing, where q represent the d and s quarks. Thanks to this phenomenon, B_q^0 and $\bar{B}_q^0$ may transition into each other (so-called flavour-oscillation) before decaying into a final state f or its CP-conjugate state $\bar{f}$, thereby leading to interesting quantum mechanical phenomena. Decay-time dependent oscillations can give rise to very intriguing interference effects, also including CP violation. An illustration of neutral B meson mixing and interference effects is given in Fig. 7.

Key aspect of this thesis is to test the SM through its flavour sector, accommodating CP violation and searching for physics beyond the SM. In this respect, B mesons are the main players. B mesons are hadronic states, so there are no free b quark decays. The quarks are confined inside the hadrons, bound by the exchange of soft gluons. As we are interested in a clean extraction of electroweak (EW) information on CKM matrix elements and CP asymmetries, hadronic interactions cause complications. For studies of CP violation, resolving the hadronic uncertainties are a key part of the analysis.

Decades of research have suggested beautiful strategies, which allow us to control these uncertainties. Benchmark processes permit us to determine the underlying EW physics even in a theoretically clean way. The B-meson system is very favourable in this sense. More specifically, there are two ways to handle these hadronic terms. Firstly, in one strategy, there are decays where hadronic matrix elements cancel out in the CP asymmetries. Secondly, in another strategy, there are cases where we can use experimental data in order to determine the hadronic parameters. In addition, from the point of view of strong interactions, the B meson is considered to be "heavy". This leads to certain simplifications, and flavour symmetries of strong interactions can also be utilised in this case.

Due to all these very interesting features of the B-meson system, big experimental efforts have been made, also to unveil and explore CP violation. Major "players" in the beginning were ARGUS at DESY [83–85], as well as CLEO at Cornell [86–88] later, while the 2000-2010 decade was governed by the e^+e^- B factories built at SLAC with the BaBar experiment [76,89], and at KEK with the Belle detector [77,90]. The phenomenon of B_s^0–$\bar{B}_s^0$

Mesons	Quark content	Mesons	Quark content
B^+	$u\bar{b}$	B_d^0	$d\bar{b}$
B^-	$\bar{u}b$	$\bar{B}_d^0$	$\bar{d}b$
B_c^+	$c\bar{b}$	B_s^0	$s\bar{b}$
B_c^-	$\bar{c}b$	$\bar{B}_s^0$	$\bar{s}b$

Table 1: Quark content of B mesons.

Figure 7: Oscillations between B_q^0 and $\bar{B}_q^0$ before decaying into the final state f (left plot) and the CP-conjugate final state $\bar{f}$ (right plot). The mixing phenomenon generates interference effects between different decay processes.

mixing was discovered in 2006 by Tevatron with CDF [91, 92] and D0 experiments [93, 94]. LHC has also a very rich B-physics programme, in particular the LHCb experiment [95], but also ATLAS [96] and CMS [97] can look at specific B-meson decays. The new feature offered by the LHC are studies of the B_s system, complementing the physics of BaBar and Belle. Nowadays, it is mostly in the "hands" of LHCb and Belle II and future upgrades, to further explore the B system and to offer a window towards the SM. Further exciting options may arise at the FCC-ee collider (for an overview the reader is referred to Ref. [98]).

3.1 The Phenomenon of B_q^0–$\bar{B}_q^0$ Mixing

Let us have a closer look at B_q^0–$\bar{B}_q^0$ mixing. This phenomenon describes the fact that neutral B meson oscillates between its matter and antimatter counterpart before it decays. Within the SM, the mixing is described by loop diagrams, called box topologies, illustrated in Fig. 8. Here, we discuss the formalism of the neutral B-meson mixing. For a detailed review, the reader is referred to Ref. [66] and references therein. We mostly follow Ref. [99] and the lectures notes presented in Ref. [100].

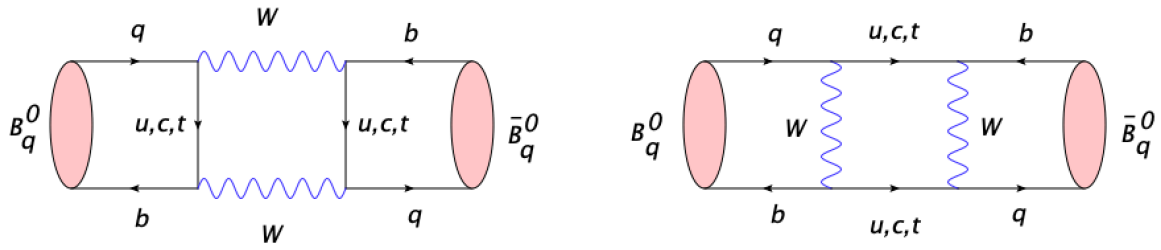

Figure 8: Box diagrams contributing to B_q^0–$\bar{B}_q^0$ in the SM.

3.1.1 Formalism of B_q^0–$\bar{B}_q^0$ Mixing

Let us assume that we have a B_q^0-meson state at time $t = 0$. Here, for simplicity, we refer to the B_q^0 state simply as B^0. Any differences between B_s and B_d, will be explicitly denoted by the corresponding quark label. Due to the time evolution, the initial B^0 state evolves into the following linear combination:

$$|B(t)\rangle = a(t)\left|B^0\right\rangle + b(t)\left|\bar{B}^0\right\rangle, \tag{3.1}$$

where the states $|B^0\rangle$ and $\left|\bar{B}^0\right\rangle$ have the same mass and $a(t)$, $b(t)$ are time-dependent coefficients. Introducing $B(t)$ as a state vector:

$$B(t) = \begin{pmatrix} a(t) \\ b(t) \end{pmatrix}, \tag{3.2}$$

in the subspace of B^0 and $\bar{B}^0$ and following Schrödinger equation, we obtain:

$$i\frac{dB}{dt} = HB \implies i\frac{d}{dt}\begin{pmatrix} a(t) \\ b(t) \end{pmatrix} = H\begin{pmatrix} a(t) \\ b(t) \end{pmatrix}. \tag{3.3}$$

The Hamiltonian H is a 2×2 matrix, which can explicitly be written in terms of the mass matrix M and the decay matrix Γ as follows:

$$H = M - \frac{i}{2}\Gamma = \begin{pmatrix} M_{11} - \frac{i}{2}\Gamma_{11} & M_{12} - \frac{i}{2}\Gamma_{12} \\ M_{21} - \frac{i}{2}\Gamma_{21} & M_{22} - \frac{i}{2}\Gamma_{22} \end{pmatrix}. \tag{3.4}$$

The next step is to solve the Schrödinger equation by calculating the eigenvalues and the eigenstates. We consider the equation for the determinant:

$$\begin{vmatrix} M - \frac{i}{2}\Gamma - \kappa & M_{12} - \frac{i}{2}\Gamma_{12} \\ M_{21}^* - \frac{i}{2}\Gamma_{21}^* & M - \frac{i}{2}\Gamma - \kappa \end{vmatrix} = 0, \tag{3.5}$$

leading to the eigenvalues $\kappa_\pm$:

$$\kappa_\pm = M - \frac{i}{2}\Gamma \pm \sqrt{(M_{12} - \frac{i}{2}\Gamma_{12})(M_{21}^* - \frac{i}{2}\Gamma_{21}^*)}. \tag{3.6}$$

The eigenstates $|B_H\rangle$ and $|B_L\rangle$, where H stands for "heavy" and L for "light", are written as follows:

$$|B_H\rangle = p\left|B^0\right\rangle + q\left|\bar{B}^0\right\rangle, \tag{3.7}$$

$$|B_L\rangle = p\left|B^0\right\rangle - q\left|\bar{B}^0\right\rangle, \tag{3.8}$$

where the p and the q are determined by solving:

$$\begin{pmatrix} M - \frac{i}{2}\Gamma & M_{12} - \frac{i}{2}\Gamma_{12} \\ M_{21}^* - \frac{i}{2}\Gamma_{21}^* & M - \frac{i}{2}\Gamma \end{pmatrix} \begin{pmatrix} p \\ q \end{pmatrix} = \kappa_\pm \begin{pmatrix} p \\ q \end{pmatrix}. \tag{3.9}$$

Consequently, we obtain the ratio:

$$\frac{q}{p} = \pm\sqrt{\frac{M_{21}^* - \frac{i}{2}\Gamma_{21}^*}{M_{12} - \frac{i}{2}\Gamma_{12}}}, \tag{3.10}$$

where we consider $|q/p| = 1$, so choosing a convention where $CP\left|B^0\right\rangle = \left|\bar{B}^0\right\rangle$

3.1.2 Expressions for the Time Evolution

The time-dependent mass eigenstates can be writtten as

$$|B_H(t)\rangle = e^{-im_H t - \frac{1}{2}\Gamma_H t}|B_H(0)\rangle = e^{-im_H t - \frac{1}{2}\Gamma_H t}(p\left|B^0\right\rangle + q\left|\bar{B}^0\right\rangle), \tag{3.11}$$

$$|B_L(t)\rangle = e^{-im_L t - \frac{1}{2}\Gamma_L t}|B_L(0)\rangle = e^{-im_L t - \frac{1}{2}\Gamma_L t}(p\left|B^0\right\rangle - q\left|\bar{B}^0\right\rangle), \tag{3.12}$$

where the decomposition of the states $\left|B^0\right\rangle$ and $\left|\bar{B}^0\right\rangle$ is:

$$\left|B^0\right\rangle = \frac{1}{2p}\left(|B_H\rangle + |B_L\rangle\right), \tag{3.13}$$

$$\left|\bar{B}^0\right\rangle = \frac{1}{2q}\left(|B_H\rangle - |B_L\rangle\right). \tag{3.14}$$

Combining the above expressions, we obtain:

$$\begin{aligned}\left|B^0(t)\right\rangle &= \frac{1}{2p}\left[e^{-im_H t - \frac{1}{2}\Gamma_H t}(p\left|B^0\right\rangle + q\left|\bar{B}^0\right\rangle) + e^{-im_L t - \frac{1}{2}\Gamma_L t}(p\left|B^0\right\rangle - q\left|\bar{B}^0\right\rangle)\right] \\ &= \frac{1}{2}\left(e^{-im_H t - \frac{1}{2}\Gamma_H t} + e^{-im_L t - \frac{1}{2}\Gamma_L t}\right)\left|B^0\right\rangle + \frac{q}{2p}\left(e^{-im_H t - \frac{1}{2}\Gamma_H t} - e^{-im_L t - \frac{1}{2}\Gamma_L t}\right)\left|\bar{B}^0\right\rangle.\end{aligned} \tag{3.15}$$

Introducing the functions

$$g_+ = \frac{1}{2}\left(e^{-im_H t-\frac{1}{2}\Gamma_H t} + e^{-im_L t-\frac{1}{2}\Gamma_L t}\right), \tag{3.16}$$

$$g_- = \frac{1}{2}\left(e^{-im_H t-\frac{1}{2}\Gamma_H t} - e^{-im_L t-\frac{1}{2}\Gamma_L t}\right), \tag{3.17}$$

we can rewrite $|B^0(t)\rangle$, and in a similar way $\left|\bar{B}^0(t)\right\rangle$, in a more compact way:

$$\left|B^0(t)\right\rangle = g_+(t)\left|B^0\right\rangle + \ g_-(t)\ \frac{q}{p}\left|\bar{B}^0\right\rangle, \tag{3.18}$$

$$\left|\bar{B}^0(t)\right\rangle = g_-(t)\ \frac{p}{q}\ \left|B^0\right\rangle + g_+(t)\left|\bar{B}^0\right\rangle. \tag{3.19}$$

Denoting the following combination of heavy and light masses as M and the combination of heavy and light decay rates as Γ:

$$M = (m_H + m_L)/2, \tag{3.20}$$

$$\Gamma = (\Gamma_H + \Gamma_L)/2, \tag{3.21}$$

while the difference between heavy and light masses as Δm and the difference between light and heavy decay rates as $\Delta\Gamma$:

$$\Delta m = m_H - m_L, \tag{3.22}$$

$$\Delta\Gamma = \Gamma_L - \Gamma_H, \tag{3.23}$$

the functions g_+ and g_- are rewritten as follows:

$$g_+ = \frac{1}{2}e^{iMt}e^{-\Gamma t/2}\left(e^{i\frac{1}{2}\Delta mt}\ e^{-\frac{1}{4}\Delta\Gamma t} + e^{-i\frac{1}{2}\Delta mt}\ e^{\frac{1}{4}\Delta\Gamma t}\right) = e^{-\Gamma t/2}\left(\frac{e^{i\Delta mt/2} + e^{-i\Delta mt/2}}{2}\right), \tag{3.24}$$

$$g_- = \frac{1}{2}e^{iMt}e^{-\Gamma t/2}\left(e^{i\frac{1}{2}\Delta mt}\ e^{-\frac{1}{4}\Delta\Gamma t} - e^{-i\frac{1}{2}\Delta mt}\ e^{\frac{1}{4}\Delta\Gamma t}\right) = e^{-\Gamma t/2}\left(\frac{e^{i\Delta mt/2} - e^{-i\Delta mt/2}}{2}\right). \tag{3.25}$$

In the last equation, for simplicity, we assumed the B_d^0 system, where the decay rate difference is tiny, thus $\Delta\Gamma_d \approx 0$. Due to this, we could choose a phase convention that allowed us to remove the factor e^{iMt}. For the B_s system though, the $\Delta\Gamma_s$ is sizeable.

Consequently, for the simplified case of B_d^0 meson, we write:

$$g_+ = e^{-\Gamma t/2}\cos\frac{\Delta mt}{2}, \tag{3.26}$$

$$g_- = e^{-\Gamma t/2}\ i\sin\frac{\Delta mt}{2}, \tag{3.27}$$

we finally obtain the expressions for the time evolution of the B^0 and $\bar{B}^0$: [11]

$$\left|B^0(t)\right\rangle = e^{-\Gamma t/2}\left(\cos\frac{\Delta m t}{2}\left|B^0\right\rangle + \; i\sin\frac{\Delta m t}{2}\;\frac{q}{p}\left|\bar{B}^0\right\rangle\right), \tag{3.28}$$

$$\left|\bar{B}^0(t)\right\rangle = e^{\Gamma t/2}\left(-i\sin\frac{\Delta m t}{2}\;\frac{p}{q}\left|B^0\right\rangle + \cos\frac{\Delta m t}{2}\left|\bar{B}^0\right\rangle\right). \tag{3.29}$$

We will utilise these time-dependent vector states later in this thesis to calculate the time-dependent decay rates and observables.

Having set up the formalism, let us now discuss the parameters which are related to the mixing phenomenon and which also play important role in our studies.

3.1.3 Mixing Parameters

Associated to the mixing effects are the phases ϕ_d and ϕ_s for the B_d and the B_s meson system, respectively, as well as the mass difference Δm_q ($q \in \{u, s\}$) and the decay width difference $\Delta\Gamma_q$, which were introduced in Eqs. (3.22) and (3.23).

The SM expressions for the mixing phases, originating from box topologies (shown in Fig. 8), are:

$$\phi_d^{\rm SM} = 2\beta = 2\arg\left(-\frac{V_{cd}V_{cb}^*}{V_{td}V_{tb}^*}\right) = 2\tan^{-1}\left(\frac{\bar{\eta}}{1-\bar{\rho}}\right), \tag{3.30}$$

$$\phi_s^{\rm SM} = -2\delta\gamma = -2\arg\left(V_{ts}V_{tb}^*\right) \approx -2\lambda^2\bar{\eta} + \mathcal{O}(\lambda^4), \tag{3.31}$$

We highlight that the $\phi_d^{\rm SM}$ phase is related to the 2β UT angle, defined in Sec. 2.5. We also note that for the $\phi_s^{\rm SM}$ phase, the dependence on the apex of the UT is doubly Cabibbo-suppressed due to the λ^2 term. These phases are measured through CP violating processes, which we will discuss in more detail in the next Chapters.

Regarding the mass difference, we have the relation:

$$\Delta m_q = 2\left|M_{12}^q\right|, \tag{3.32}$$

where in the SM the mass element M_{12}^q is given as [101]:

$$\left|M_{12}^q\right|^{\rm SM} = \frac{G_{\rm F}^2 m_W^2}{12\pi^2} m_{B_q}\left|V_{tq}V_{tb}\right|^2 \; S_0(x_t)\,\eta_{2B}\hat{B}_{B_q}f_{B_q}^2\,. \tag{3.33}$$

Here, $G_{\rm F}$ is the Fermi constant, m_W is the W mass, m_{B_q} is the B_q mass, $S_0(x_t)$ is the Inami–Lim function [102] describing the top quark mass dependence, η_{2B} is a short-distance QCD

[11] In an analogous way, we would work for the case of the B_s^0 system. The only difference is that in the expressions of $g_\pm$, we would not be able to set $\Delta\Gamma$ to zero.

correction factor [103, 104], $\hat{B}_{B_q}$ is the renormalisation group invariant bag parameter, and f_{B_q} is the B_q decay constant. Since

$$|M_{12}^q|^{\rm SM} \propto |V_{tq}V_{tb}|^2, \tag{3.34}$$

we can rewrite the CKM matrix elements in terms of the UT apex and the experimental inputs. Using the Wolfenstein parametrisation [69, 70], we have for $q = d$:

$$|V_{td}V_{tb}| = \lambda|V_{cb}|\sqrt{(1-\bar{\rho})^2+\bar{\eta}^{\,2}} + \mathcal{O}\left(\lambda^7\right) , \tag{3.35}$$

$$= \lambda|V_{cb}|\sqrt{1-2\bar{\rho}+R_b^2} \tag{3.36}$$

$$= \lambda|V_{cb}|\sqrt{1-2R_b\cos\gamma+R_b^2} + \mathcal{O}\left(\lambda^7\right) , \tag{3.37}$$

where we have used $R_b^2 = \bar{\rho}^2+\bar{\eta}^2$ and $\bar{\rho} = R_b\cos\gamma$, following the definitions in Sec. 2.5. We note that $|V_{td}V_{tb}|$, hence $\Delta m_d^{\rm SM}$, depends at leading order on $\bar{\rho}$ and $\bar{\eta}$. On the other hand, for $q = s$ we have:

$$|V_{ts}V_{tb}| = |V_{cb}|\left[1-\frac{\lambda^2}{2}(1-2\bar{\rho})\right] + \mathcal{O}\left(\lambda^6\right) , \tag{3.38}$$

$$= |V_{cb}|\left[1-\frac{\lambda^2}{2}(1-2R_b\cos\gamma)\right] + \mathcal{O}\left(\lambda^6\right) , \tag{3.39}$$

where $|V_{ts}V_{tb}|$, hence $\Delta m_s^{\rm SM}$ depends on UT at next-to-leading order in λ.

All these relations will be very useful in our numerical analysis, allowing us to get clean SM predictions for the mixing parameters (Sec. 5.4). This is closely linked to the determination of the UT apex as we will discuss in Sec. 3.4.2. In addition, clean SM results will help us to explore how much space is still left for NP, as we will present in Chapter 5.

3.2 Weak Decays

Let us now move on to the discussion of the B-meson transitions. As we know, hadrons decay via the weak interactions. Before discussing specific decays, we firstly introduce the theoretical tools that we utilise in our analysis and discuss the different categories of the B-meson decays.

Interactions are represented by Feynman diagrams. These diagrams are powerful tools, which allow us to have an intuitive description of decay processes by converting them into mathematical expressions for quantum field theory calculations. Two different topologies contribute to these decays, allowing us to categorize them into different classes of Feynman diagrams: "tree" and "penguin" (loop) topologies, as shown in Fig. 9.

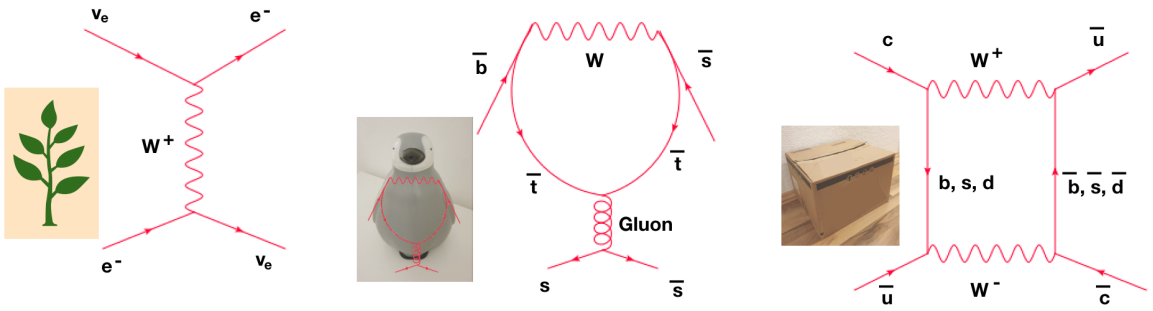

Figure 9: Examples of decay topologies: tree (left), penguin (middle) and box (right).

We mention that there are decays that arise at the tree level at the leading order. On the other hand, there are transitions, especially those coming from flavour-changing neutral currents, which in the SM do not arise at the tree level because of the GIM mechanism [3], but may emerge at the loop level. In addition, there are cases where both trees and penguins can contribute but the tree contribution is suppressed via a tiny CKM factor, therefore playing a less important role than the penguins at lowest order. Other examples are "annihilation" and "exchange" topologies, which are actually types of tree topologies, as well as "box" topologies. The latter fall under the category of the loop diagrams and can, for instance, arise along with EW penguins. Fig. 9 provides an illustration of the main categories we listed here, to give an impression of how these topologies look like.

Classifying according to the final state of the decays, there are three different categories: the leptonic, the semileptonic and the non-leptonic decays. In the following Sections, we will explicitly discuss the different dynamics of these decays and illustrate the corresponding Feynman diagrams. Let us firstly present the way to simplify the weak decays calculations and then specifically discuss the formalism of the three different decay classes.

3.2.1 Theoretical tools

Starting point of any analysis is to calculate the amplitude of the weak decays of B mesons. We have to deal with EW interactions, governed by exchanges of W and Z bosons, occuring at the EW scale, thus corresponding to $\mathcal{O}(100\text{ GeV})$, as well as with processes which are governed by energies of the decaying b quark, which has a mass of about 5 GeV. The various energy scales characterising the B meson decays suggest that different aspects of QCD are probed. Therefore, in order to be able to calculate the decay amplitudes at all energy regimes, it is essential to construct effective field theories.

One can apply an effective field theory picture by integrating out the heavy degrees of freedom. Low energy-effective Hamiltonians describe the given decays. These effective

Hamiltonians involve operators and their corresponding coefficients. As we will see in the following sections, the effective theory is a very powerful tool both in the SM (particularly for QCD corrections in the category of the non-leptonic decays) and for NP studies. Concerning the latter, effective Hamiltonians provide an efficient way for accounting NP effects by simply adding new operators into the equation, and allowing short-distance coefficients of SM operators to take values deviating from the SM.

Consequently, the effective theory approach has two aspects. The first one is to integrate out the heavy degrees of freedom and to have a description of low-energy processes, allowing us to look at different quark-level transitions and write the corresponding operators for that. The second one is to generalise the theory in order to include possible NP contributions. In the case of extensions of the SM, we examine whether new operators emerge (or not). This allows us to deal with NP in a model-independent way, thus without specifying a model. However, if we assume specific NP scenario, one could express the Wilson coefficients in terms of the parameters of the new theory. Keeping these in mind, we now move on and discuss in practice how we apply these effective theories, introducing each one of the three different decay classes separately.

3.3 Leptonic Decays

From the point of view of strong interactions, the simplest class is given by the leptonic decays. In these channels, only leptons appear in the final state, such as $B^- \to \ell\bar{\nu}$, where $\ell = e, \mu$ or τ. The Feynman diagram that describes this process is illustrated[12] in Fig. 10. In the SM, the quarks of the decaying hadron annihilate into a W boson. These decays have the simplest hadronic structure, since there are no hadrons in the final state. Here, we first discuss these charged leptonic channels. We also note that there are neutral leptonic decays of the kind $B_q^0 \to \ell^+\ell^-$. However, these channels have different dynamics (loop processes) and we explore them separately. We will explicitly study $B_q^0 \to \mu^+\mu^-$ in Chapter 8.

3.3.1 The Decay Amplitudes and Decay Rates

Applying the Feynman rules, the Feynman diagram contributing in the SM, shown in Fig. 10, can be converted into a mathematical expression for the transition amplitude. Thus, we write the amplitude for this decay as follows [99]:

$$A(B^- \to \ell\bar{\nu}) = -\frac{g_2^2}{8} V_{ub}[\bar{u}_\ell \gamma^\alpha (1-\gamma_5) v_\nu] \left[\frac{g_{\alpha\beta}}{k^2 - M_W^2}\right] \langle 0|\bar{u}\gamma^\beta(1-\gamma_5)b|B^-\rangle, \tag{3.40}$$

[12] We also show the interior gluons in the Feynman diagram.

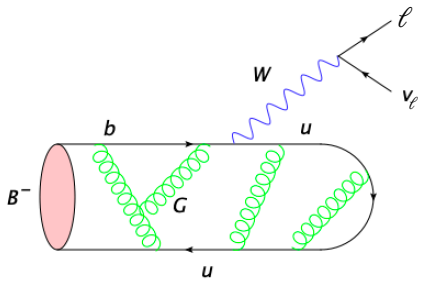

Figure 10: Topology for the B-meson leptonic decay in the SM.

where we have two parts: the Dirac spinors for the outgoing leptons, representing the spinor fields of the fermions as described by the Dirac equation, and the hadronic matrix element, encoding the physics of strong interactions. Therefore,

$$\text{Dirac spinors:} \qquad \bar{u}_\ell \gamma^\alpha (1-\gamma_5) v_\nu,$$

$$\text{hadronic matrix element:} \qquad \langle 0|\bar{u}\gamma^\beta(1-\gamma_5)b|B^-\rangle.$$

Furthermore, g_2 is the gauge coupling of the $SU_L(2)$[13], V_{ub} is the corresponding CKM matrix element, k is the four-momentum carried by W, M_W is the W mass and α and β are Lorentz indices. Due to the fact that $k^2 = M_B^2 \ll M_W^2$, we can write

$$\frac{1}{k^2 - M_W^2} \quad \longrightarrow \quad -\frac{1}{M_W^2} \equiv -\left(\frac{8G_\text{F}}{\sqrt{2}g_2^2}\right). \tag{3.41}$$

"Integrating out" the heavy W boson, Eq. (3.40) is rewritten as:

$$A(B^- \to \ell\bar{\nu}) = \frac{G_\text{F}}{\sqrt{2}} V_{ub} \left[\bar{u}_\ell \gamma^\alpha (1-\gamma_5) v_\nu\right] \langle 0|\bar{u}\gamma_\alpha(1-\gamma_5)b|B^-\rangle, \tag{3.42}$$

where we used $g_{\alpha\beta}\gamma^\beta = \gamma_\alpha$. The hadronic matrix element includes all the hadronic physics. There are no other QCD effects from strong interactions in the final state. The matrix element can be parametrised as

$$\langle 0|\bar{u}\gamma_\alpha(1-\gamma_5)b|B^-\rangle = \langle 0|\bar{u}\gamma_\alpha\gamma_5 b|B^-\rangle = i f_B q_\alpha, \tag{3.43}$$

where f_B is the B-meson decay constant, an important input for phenomenological studies that we will explore further later in our analysis, and q_α the four momentum of the decaying meson. We note that

$$\langle 0|\bar{u}\gamma_\alpha b|B^-\rangle = 0 \tag{3.44}$$

[13]The gauge coupling of the $SU_L(2)$ is already introduced in Sec. 2.2.2. Here, to be consistent with the notation in Ref. [99], we denote it as g_2.

since the B^- meson is a pseudoscalar particle.

Having the transition amplitude available, we can calculate the decay rate Γ. The decay rates describe decay probabilities, and are proportional to the squared decay amplitudes. In order to derive the decay rates, we have to perform the corresponding phase-space integration over all components of p_ℓ and p_ν [14], denoting the momenta of the lepton and neutrino, respectively:

$$\Gamma = \int \frac{d^3p_\ell}{(2\pi)^3 2E_\ell} \frac{d^3p_\nu}{(2\pi)^3 2E_\nu} \frac{(2\pi)^4}{2E_B} \delta^4(p_B - p_\ell - p_\nu) \left| A(B^- \to \ell\bar{\nu}) \right|^2 . \tag{3.45}$$

The $E_{\ell,\nu,B}$ terms denote the energy of the particles and the four dimensional delta function ensures the energy-momentum conservation.

Now, we can also write the expression for the branching ratio, which is defined as:

$$\mathcal{B}(B^- \to \ell^- \bar{\nu}_\ell) = \Gamma(B^- \to \ell^- \bar{\nu}_\ell)\ \tau_{B^-}, \tag{3.46}$$

where τ_{B^-} is the lifetime of the B^- meson. In the SM, this quantity, which measures the probability that a B^- meson decays into the final state $\ell^-\bar{\nu}_\ell$, takes the following form [105]:

$$\mathcal{B}(B^- \to \ell^- \bar{\nu}_\ell)|_{\rm SM} = \frac{G_{\rm F}^2}{8\pi} |V_{ub}|^2 M_{B^-} m_\ell^2 \left(1 - \frac{m_\ell^2}{M_{B^-}^2}\right)^2 f_{B^-}^2 \tau_{B^-}. \tag{3.47}$$

We note that the mass of the neutrino has been neglected. We highlight the fact that the branching ratio is proportional to the squared lepton mass, indicating helicity suppression.

What values do we obtain for the branching ratios of the leptonic B decays? Before answering this question, let us note/summarise here some key points for these transitions. The leptonic decays of charged B mesons are CKM-suppressed in the SM due to the tiny value of $|V_{ub}|$ which is proportional to the term λ^3. In addition, they are helicity suppressed since the SM contribution to the decay amplitude is proportional to the square of the mass of the lepton. The hierarchy of the masses of the electrons, muons and taus is also to be considered. Due to these reasons, for transitions with muonic and electronic modes, we obtain very small SM branching ratios, $\mathcal{O}(10^{-7})$ and $\mathcal{O}(10^{-10})$, respectively.

More specifically, the decays with muons in the final state have been observed, and for the $B^- \to \mu^-\bar{\nu}_\mu$ channel the measured branching fraction is [106]:

$$\mathcal{B}(B^- \to \mu^-\bar{\nu}_\mu) = (6.46 \pm 2.22(\text{stat}) \pm 1.60(\text{syst})) \times 10^{-7} = (6.46 \pm 2.74(\text{tot})) \times 10^{-7}, \tag{3.48}$$

while for electrons only an upper bound is available [107]:

$$\mathcal{B}(B^+ \to e^+\nu_e) < 9.8 \times 10^{-7}. \tag{3.49}$$

[14] We note that in order to derive the decay rates, we apply Dirac algebra relations, summing over the spins of the leptons in the final state and neglecting the neutrino masses.

The large mass of the tau makes the helicity suppression ineffective in the $B^- \to \tau\bar{\nu}$ decays. However, the challenging τ reconstruction makes this mode difficult to handle from an experimental point of view. Nevertheless, data for this channel have already been reported and the corresponding branching fraction is [108]:

$$\mathcal{B}(B^- \to \tau\bar{\nu}) = (1.79^{+0.56}_{-0.49}(\text{stat})^{+0.46}_{-0.51}(\text{syst})) \times 10^{-4}. \tag{3.50}$$

Considering effects from beyond the SM, NP may lift the helicity suppression, as we will discuss for neutral leptonic B decays in Sec. 8. Detailed discussions of specific constraints on NP and SM predictions as well as interpretations in the searches of NP and comparisons with the SM can be found on Ref. [105].

3.3.2 The Effective Hamiltonian within the SM and beyond

Let us now focus on how the low-energy effective Hamiltonian arises and analyze the profound feature of integrating out the very heavy W boson. We will show in practice how we make the transition from the full to the effective theory.

Working again with the $B^- \to \ell\bar{\nu}$ decay, we guide the way towards the theoretical tools that we apply and which we briefly introduced in the previous Section. The starting point is the Feynman diagram that describes this process in the "full theory", which is illustrated on the left-hand side of Fig. 11. In the "effective theory", we integrate out the W boson and the propagator is contracted to a point, illustrated by a blob here. In a more formal way, we can describe the process by a 4-Fermi operator. As a historical point, we mention that Fermi did not know where suc operators came from, studying the nuclear β decay in 1933 [109] . However, nowadays, we know that the origin of the charged-current operator is in the exchange of a W boson, within the SM. Hence we can resolve what it is happening in this blob, which is illustrated in the diagram on the right-hand side of Fig. 11.

Therefore, at low energy scale we simplify the theory, as certain degrees of freedom can be integrated out. We highlight again that this is the effective description of a B meson decay, mediated by the very heavy W boson and this works because the energy release of the decaying b quark is much smaller than the W mass.

This effective theory description leads to the following effective Hamiltonian in the SM, which is constructed in such a way that the transition amplitude we presented above can be calculated through a matrix element of the following Hamiltonian [105]:

$$\mathcal{H}_{\text{eff}} = \frac{4G_{\text{F}}}{\sqrt{2}} V_{qb} \left[C_{V_L} \mathcal{O}^{\ell}_{V_L} \right] + \text{h.c.} \ , \tag{3.51}$$

where the four-fermion operator is given by

$$\mathcal{O}^{\ell}_{V_L} = (\bar{q}\gamma^{\mu} P_L b)(\bar{\ell}\gamma_{\mu} P_L \nu_{\ell}), \tag{3.52}$$

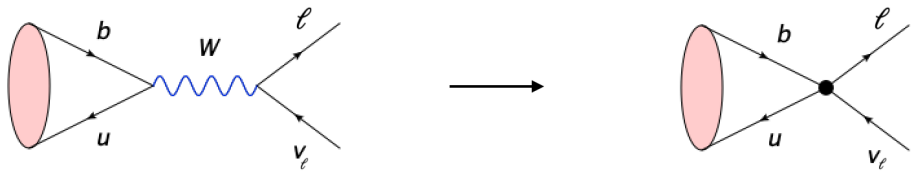

Figure 11: Illustration of going from the "full theory" to an "effective theory", integrating out the W boson.

where $q = u$ and we define $P_L \equiv (1 - \gamma_5)/2$. Thus, there is only one operator contributing in the SM.

This concept is very powerful, and even though it might look unnecessarily complicated for the case of the SM Hamiltonian where only one operator contributes, it becomes very important in the case where we allow for NP effects. Therefore, if we go beyond the SM and assume that we have NP entering far above the EW scale, we can integrate out these heavy NP particles in an analogous way as we integrated out the heavy W boson.

Then we can write the Hamiltonian including NP effects. Here, as an example, we examine the case of NP contributions on (Pseudo-)Scalar operators. The reason to focus on new (Pseudo-)Scalar contributions is due to the interesting point that they could in principle lift the helicity suppression, thereby enhancing the branching ratio. In general though, the Hamiltonian could have more operators.[15]. Therefore, for our specific example here, following from Eq. (3.51), we obtain

$$\mathcal{H}_{\text{eff}} = \frac{4G_{\text{F}}}{\sqrt{2}} V_{qb} \left[C_{V_L} \mathcal{O}^{\ell}_{V_L} + C^{\ell}_{S} \mathcal{O}^{\ell}_{S} + C^{\ell}_{P} \mathcal{O}^{\ell}_{P} \right] + \text{h.c.} \,, \tag{3.53}$$

where again $q = u$ and the following four-fermion operators arise:

$$\mathcal{O}^{\ell}_{S} = (\bar{q} b)(\bar{\ell} P_L \nu_\ell), \tag{3.54}$$

$$\mathcal{O}^{\ell}_{P} = (\bar{q} \gamma_5 b)(\bar{\ell} P_L \nu_\ell), \tag{3.55}$$

which we do not have in the SM. Therefore, the corresponding Wilson coefficients in the SM take the values $C_{V_L} = 1$, $C^{\ell}_{S} = 0$, $C^{\ell}_{P} = 0$. The coefficients C^{ℓ}_{S}, C^{ℓ}_{P} allow model-

[15]Here, for the charged leptonic Hamiltonian in Eq. (3.53), we only show the left-handed current-current operators and the new (Pseudo-)Scalar ones. However, there could be more, such as the right-handed operators. Similarly, we can write the Hamiltonian for the neutral neutral leptonic decays, which we will explicitly show and discuss in Chapter 8, (where the right-handed operators will be denoted as primed). More details can be found in Ref. [110].

independent studies of such decays. Moreover, in case of having a specific model, one could calculate these coefficients and express them in terms of parameters of this model. So, we have presented a theoretical framework which is very powerful, especially for NP studies, and which we will use throughout this thesis.

3.3.3 Note: What About Neutral Leptonic $B_q^0 \to \ell^+\ell^-$ Decays?

So far, we have discussed the case of charged leptonic decays, which are caused by flavour-changing charged-current interactions. However, the neutral leptonic decays, rising from flavour-changing neutral currents, are also very interesting and powerful. The neutral ones have different dynamics, not arising at the tree level in the SM but only from loop processes, and are very rare processes. However, they do have similar features. In our studies the rare leptonic transitions are key players and we discuss them in detail in Chapter 8, highlighting the points of the helicity suppression and the structure with the $B_{(s)}$ decay constant, where all hadronic physics is encoded since, as we have already mentioned, gluons do not couple to the leptonic final states.

3.4 Semileptonic Decays

In this decay class, both leptons and hadrons appear in the final state. The general structure is more complicated. Here, both the initial and the final states involve the binding of hadrons. There are also strong interactions between the initial and final state particles.

Let us consider now semileptonic decays like $\bar{B}_d^0 \to D^+\ell\nu_\ell$, illustrated in Fig. 12, where we also show gluons, which are responsible for hadronic binding and hadronic effects. Starting from the Feynman diagrams of the $b \to c$ case, we write the decay amplitude in a similar way as in the leptonic case [99]:

$$A(\bar{B}_d^0 \to D^+\ell\nu_\ell) = -\frac{g_2^2}{8} V_{cb}[\bar{u}_\ell \gamma^\alpha (1-\gamma_5) v_\nu] \left[\frac{g_{\alpha\beta}}{k^2 - M_W^2}\right] \langle D^+|\bar{c}\gamma^\beta(1-\gamma_5)b|\bar{B}_d^0\rangle \tag{3.56}$$

$$= \frac{G_{\rm F}}{\sqrt{2}} V_{cb}\,[\bar{u}_\ell \gamma^\alpha (1-\gamma_5) v_\nu]\,\langle D^+|\bar{c}\gamma_\alpha(1-\gamma_5)b|\bar{B}_d^0\rangle, \tag{3.57}$$

utilising again that $k^2 \sim M_B^2 \ll M_W^2$. Taken that $\langle D^+|\bar{c}\gamma_\alpha\gamma_5 b|\bar{B}_d^0\rangle = 0$, since both D^+ and B_d^0 are pseudoscalar particles, the transition matrix element can be written as follows [99]:

$$\langle D^+(k)|\bar{c}\gamma_\alpha b|\bar{B}_d^0(p)\rangle = F_1(q^2)\left[(p+k)_\alpha - \left(\frac{M_B^2 - M_D^2}{q^2}\right) q_\alpha\right] + F_0(q^2)\left(\frac{M_B^2 - M_D^2}{q^2}\right) q_\alpha, \tag{3.58}$$

where $q \equiv p - k$. The quantities $F_1(q^2)$ and $F_0(q^2)$ are form factors of the $\bar{B} \to D$ transitions. The form factors are non-perturbative objects and, as a result, we cannot calculate them

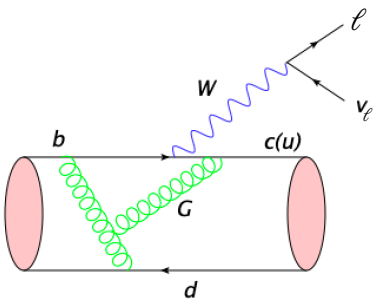

Figure 12: Topology for semileptonic B-meson decays in the SM.

in perturbation theory. We notice that in the semileptonic decays, the hadronic matrix element involves two form factors while in the leptonic case the matrix element depends only on one decay constant. Therefore, due to these hadronic form factors in the transition amplitude calculation, the structure of the semileptonic decays is more complicated than the leptonic case. We note that the following normalisation condition [111] holds, which can be generalised for all $B \to P$ transitions, where P denotes a pseudoscalar meson:

$$F_1^{B\to P}(0) = F_0^{B\to P}(0). \tag{3.59}$$

This is an important point that we will use for our calculations in the next Chapters.

Having calculated the decay amplitude, we can obtain the expressions for the differential decay rate, which leads to the full branching ratio once we integrate over q^2. So, for the $B \to D\ell\bar{\nu}_\ell$ transition, assuming again the SM, the differential decay rate can be written in the following form [111–114]:

$$\begin{aligned}\frac{\mathrm{d}\Gamma(B\to D\ell\bar{\nu}_\ell)}{\mathrm{d}q^2} = \frac{G_{\rm F}^2\,|V_{cb}|^2}{192\,\pi^3 m_B^3}\,\frac{q^2-m_\ell^2}{(q^2)^2}\left[\frac{(q^2-m_\ell^2)^2}{q^2}\right]^{1/2}\left[\frac{(m_B^2-m_D^2-q^2)^2}{4q^2}-m_D^2\right]^{1/2}\\ \Big[(m_\ell^2+2q^2)(q^2-(m_B-m_D)^2)(q^2-(m_B+m_D)^2)\left[F_1^{B\to D}(q^2)\right]^2\\ +\,3m_\ell^2(m_B^2-m_D^2)^2\left[F_0^{B\to D}(q^2)\right]^2\Big],\end{aligned} \tag{3.60}$$

where $|V_{cb}|$ is the CKM matrix element and $F_1^{B\to D}(q^2)$, $F_0^{B\to D}(q^2)$ the form factors for the $B \to D$ transitions parametrising the corresponding quark-current matrix element, as in Eq. (3.58). We note that a similar expression holds for the $B \to \pi\ell\bar{\nu}_\ell$ modes, where instead of $|V_{cb}|$, the $|V_{ub}|$ matrix element enters.

We mention that the expression in Eq. (3.60) is the general one which applies also for the taus. But since in our studies we are interested in decays only with electrons and muons,

which are light leptons, we can neglect the lepton masses. Then, we can rewrite the above equation for the $B \to P$ transitions in a more compact way, for $m_\ell = 0$ [115]:

$$\frac{\mathrm{d}\Gamma(\bar{B} \to P\ell\bar{\nu}_\ell)}{\mathrm{d}q^2} = \frac{G_{\mathrm{F}}^2 \left|V_{rb}\right|^2}{192\,\pi^3} \left[m_B\, \Phi\left(\frac{m_P}{m_B}, \frac{\sqrt{q^2}}{m_B}\right)\right]^3 \left[F_1^{B\to P}(q^2)\right]^2, \tag{3.61}$$

where $\Phi(x, y)$ is the phase-space function, which is defined as:

$$\Phi(x, y) \equiv \sqrt{[1 - (x + y)^2][1 - (x - y)^2]}. \tag{3.62}$$

This decay rate expression is the one we will utilise in Sec. 5.3 and Sec. 6.6. We note that only the $F_1^{B\to P}(q^2)$ form factor survives when we have vanishing lepton masses.

3.4.1 Determining $|V_{ub}|$ and $|V_{cb}|$ elements

In our studies, an important point is the determination of the CKM matrix elements, in particular $|V_{ub}|$ and $|V_{cb}|$, which are necessary for the extraction of the UT apex, as we will see in the following Section. Having determined the decay rate of the semileptonic decays, we discuss how this rate allows us to obtain the CKM elements.

Recalling the differential decay rate expression in Eq. (3.60), it becomes clear that, if we know the hadronic form factors, we can determine the $|V_{cb}|$ element from the measured rate. This is actually the method that researchers follow, making use of lattice results[16]. Such determinations of the $|V_{cb}|$ element, where for the decay rate measurement, the final state hadron of the corresponding decay is considered to be a specific meson are called "exclusive". This approach can be applied not only to the $\bar{B}_d \to D^+$ transitions which we examine here as an example, but also to other decay modes coming from the same quark level transition, for instance $B \to D^*\ell\nu$ or further excited D-meson states.

Consequently, knowing the form factors, one can determine $|V_{cb}|$. However, determining the form factors is the difficult part. In the 1990s, for the $b \to c$ decays, the concept of heavy quark effective theory (HQET) was developed [116, 117], allowing simplifications, which are applied in the determinations of $|V_{cb}|$. The concept of HQET goes beyond the scope of this thesis and we will not elaborate this framework further. All the form factors are related to one function, the Isgur–Wise function in the heavy quark limit. This method works only for $b \to c$ case, which is a so-called "heavy to heavy" transition, since charm is considered to be a heavy quark as well. The form factors are calculated non-perturbatively and encode all the low-energy hadronic physics information. For their calculations, either the method of lattice-QCD or the approach of light-cone sum rules (LCSR) is applied. We

[16] There has been excellent progress in lattice results over the recent years and later in the thesis we will discuss the form factors in more detail.

note that lattice-QCD calculations work better at high momentum regions, thus high q^2, while LCSR works better at low q^2 regions, so near $q^2 = 0$ [118].

In an analogous way, we can write the differential decay rate for the $b \to u\ell\bar{\nu}_\ell$ transitions, for instance the $B \to \pi\ell\bar{\nu}$ decays. Knowing the corresponding form factors, we can determine the CKM matrix element $|V_{ub}|$ from the measured rates. This is again an exclusive determination since we focus on specific final state meson.[17]

In addition to these exclusive determinations, other methods have been developed for obtaining the CKM elements. Another approach for obtaining $|V_{ub}|$ and $|V_{cb}|$ is the "inclusive determination", where the measurement of the decay rate refers to the sum over all possible final states. We only mention here that concepts like the heavy quark expansions can be performed and are implemented in the corresponding state-of-the-art calculations [118]. Again, this topic is beyond the scope of the thesis.

The main message of this discussion is that there are different approaches of determining the CKM matrix elements $|V_{ub}|$ and $|V_{cb}|$, utilising semileptonic decays: the exclusive and inclusive determinations. The current experimental values for $|V_{ub}|$ and $|V_{cb}|$ using the two different approaches are the following:

$$|V_{ub}|_{\text{incl}} = (4.19 \pm 0.17) \times 10^{-3} \ \ [119] \ , \qquad |V_{ub}|_{\text{excl}} = (3.51 \pm 0.12) \times 10^{-3} \ [120], \quad (3.63)$$

$$|V_{cb}|_{\text{incl}} = (42.16 \pm 0.50) \times 10^{-3} \ \ [121], \qquad |V_{cb}|_{\text{excl}} = (39.10 \pm 0.50) \times 10^{-3} \ [120]. \quad (3.64)$$

Even though these two approaches should yield results that agree with each other, we observe that tensions arise between the inclusive and exclusive values. More specifically, the $|V_{ub}|$ results differ by 3.9 standard deviations and the $|V_{cb}|$ values differ by 4.3 standard deviations. This is a long-standing issue, and as we will discuss in the following Section, these deviations have profound impacts on the UT apex extraction as well as in the NP searches (Chapter 5). They lead to different pictures for the allowed parameter space for NP in B_q^0–$\bar{B}_q^0$ mixing, making it important to further investigate their origin and eventually resolve them. So, special care is needed when using the $|V_{ub}|$ and$|V_{cb}|$ matrix elements.

As a final remark, we emphasize again that the semileptonic decays are prime players for extracting the CKM elements. Another way of determining the CKM elements though is via the leptonic decays, which we already described in Sec. 3.3. For instance, the decay of a B^- meson to muon and neutrino, could also be used for such determinations using

[17] We note though that contrary to the $b \to c$ case, here we have a heavy to light transition. HQET does not apply in the $b \to u$ modes, since it does not seem to work sufficiently when both heavy and light quarks are involved. In this case, other theoretical tools like lattice QCD have to be used for the theoretical calculations. We note again that these methodologies are not part of our studies.

the decays constants as inputs. However, the level of precision in the leptonic modes is not competitive to the semileptonic ones.

3.4.2 Key Application: UT Apex Determination Through R_b and γ

The Unitarity Triangle (UT) plays a central role in our studies. Determinations of the UT parameters mainly result from global UT analyses [122, 123]. However, these analyses include inputs which could be affected by NP contributions in B_q^0–$\bar{B}_q^0$ mixing. Therefore, we cannot rely on them in order to obtain the SM predictions. Instead, we have a careful look at the analyses of the determination of the apex of the UT following our studies in Refs. [81, 124]. The extraction of the UT apex is a key application of the semileptonic decays. Here, we present the impact of the tensions that arise between inclusive and exclusive determinations of the CKM matrix elements $|V_{ub}|$ and $|V_{cb}|$. The knowledge of the UT apex is needed for SM predictions of the B_q^0–$\bar{B}_q^0$ mixing parameters, namely the CP-violating phases ϕ_q and the mass difference ΔM_q. As we will see later in our studies, the SM predictions are crucial in order to explore how much space for NP is available.

Following our analysis in Refs. [81,124], we choose to extract the apex of the UT relying only on two observables, the UT side R_b and the angle γ, trying to keep possible contamination of input parameters from NP effects to a minimum level[18]. Let us discuss in more detail how we determine the UT apex in this case.

First of all, the R_b, defined in Eq. (2.63), depends on the CKM elements $|V_{ub}|$ and $|V_{cb}|$. Therefore, knowing $|V_{ub}|$ and $|V_{cb}|$ from semileptonic decays allows us to fix the R_b side of the UT. More specifically, we can fix a circle in the $\bar{\rho} - \bar{\eta}$ plane with radius R_b around the origin. Using in addition information on γ, we can determine the apex of the UT, since:

$$\bar{\rho} + i\bar{\eta} = R_b \; e^{i\gamma}. \tag{3.65}$$

As R_b depends on $|V_{ub}|$ and $|V_{cb}|$, it is affected by the tensions that arise between the various theoretical and experimental approaches. We will present the values separately for the inclusive and the exclusive case below. Trying to better understand the situation [125–128], a third possibility is used, where we combine the exclusive $|V_{ub}|$ with the inclusive $|V_{cb}|$ value, referring to this scenario as hybrid. As a result, in our analysis, we use and explicitly show our results for the inclusive, exclusive and hybrid cases.

Making use of Eq. (2.63), we have all input parameters available and we calculate the

[18] Here, we only use tree charged-current processes.

Determination	$\bar{\rho}$	$\bar{\eta}$
Inclusive	0.160 ± 0.025	0.404 ± 0.022
Exclusive	0.144 ± 0.022	0.365 ± 0.018
Hybrid	0.134 ± 0.021	0.338 ± 0.017

Table 2: Values of the UT apex $\bar{\rho}$ and $\bar{\eta}$ for the inclusive, exclusive and hybrid case.

R_b side for the three cases, finding:

$$R_{b,\text{incl}} = 0.434 \pm 0.018\,, \tag{3.66}$$

$$R_{b,\text{excl}} = 0.392 \pm 0.014\,, \tag{3.67}$$

$$R_{b,\text{hybrid}} = 0.364 \pm 0.013\,. \tag{3.68}$$

The inclusive differs from the exclusive result by 2.4 standard deviations. The hybrid value differs from the inclusive by 3.7 and from the exclusive by 1.5 standard deviations.

Regarding the angle γ, we use the numerical value:

$$\gamma_{\text{avg}} = (68.4 \pm 3.3)^\circ, \tag{3.69}$$

which is an average value coming from determinations on the one hand, from $B \to DK$ decays and on the other hand, from an isospin analysis of $B \to \pi\pi, \rho\pi, \rho\rho$ modes. Here, we only present this value since it is necessary for pinning down the UT apex. However, as this angle plays an important role in our studies, we will discuss in detail in the following Chapters how we determined it through the different decay processes and what its implications are in studies of CP violation and NP effects.

Having the numerical values for the angle γ and the R_b side for the inclusive, exclusive and hybrid case, we can perform a fit and we finally obtain the coordinates $(\bar{\rho}, \bar{\eta})$ of the UT apex [81]. We note that the analysis in Ref. [81] was performed in collaboration with K. De Bruyn, who brought to our attention and utilised the GammaCombo framework [129], in order to produce the corresponding plots. Following these lines, we obtain results for $\bar{\rho}$ and $\bar{\eta}$, which are presented in Table 2 for all three cases.

To visualise the results, we provide an illustration of these solutions in Fig. 13 using the "Mathematica" tool [130]. The green contour represents the γ value, the orange band shows the R_b side and the yellow region indicates the area where γ and R_b contours overlap. The contours are shown for 39% confidence level (CL) and 87% CL. The top plot corresponds to the inclusive case, the middle to the exclusive and the bottom plot to the hybrid

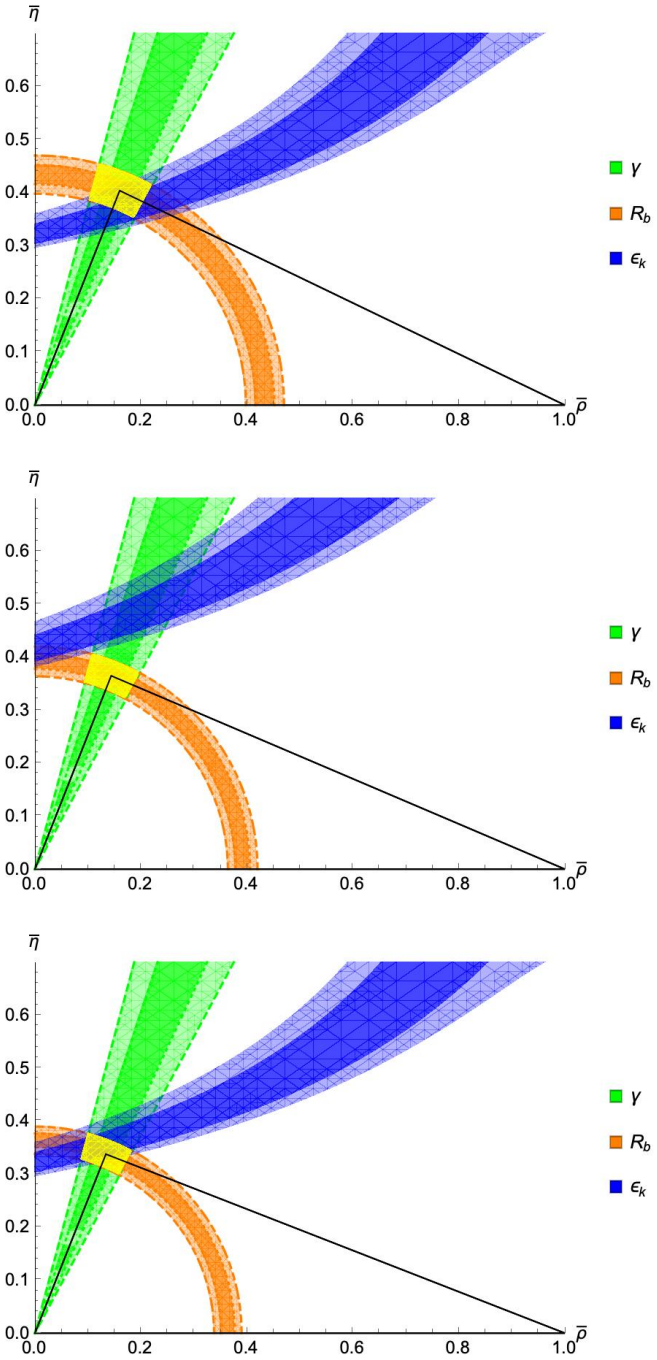

Figure 13: UT apex determination using the angle γ and the side R_b for the inclusive, exclusive and hybrid case. The plots show the angle γ (green), the side R_b (orange) and the overlap region between these two observables (yellow). The hyperbola $|\varepsilon_K|$ (blue contour) is also illustrated for comparison [81].

case. The same plot also presents the $|\varepsilon_K|$ hyperbola (blue contour), which we discuss below.

The parameter $|\varepsilon_K|$

Most of the observables that constrain the UT apex originate from B decays. However, the $|\varepsilon_K|$ observable describes "indirect" CP violation in the neutral kaon system. This is the observable where CP violation was discovered in 1964. This indirect CP violation comes from the fact that the mass eigenstates $K_{\rm L,S}$ of the K^0 system, characterised by the K^0–$\bar{K}^0$ mixing phenomenon, are not CP eigenstates. More specifically, the state $K_{\rm L}$ is dominated by the CP-odd eigenstate, but it also has a tiny admixture of the CP-even eigenstate. The latter may decay into the final $\pi^+\pi^-$ state via CP-conserving interactions. Review on the topic can be found for instance on Refs. [131–133].

In this thesis we focus on decays of B mesons but not on the kaon system. However, the $|\varepsilon_K|$ parameter provides interesting insights in our analysis. Therefore, we provide the formalism, which is needed for the numerical analysis.

Formalism

The SM expression for ε_K is given by [134]:

$$|\varepsilon_K| = \frac{G_{\rm F}^2 m_W^2 m_K f_K^2}{6\sqrt{2}\pi^2 \Delta m_K} \kappa_\epsilon \hat{B}_K |V_{cb}|^2 \lambda^2 \bar{\eta} \left[|V_{cb}|^2 (1-\bar{\rho}) \eta_{tt}^{\rm EW} \eta_{tt}\, \mathcal{S}(x_t) - \eta_{ut}\, \mathcal{S}(x_c, x_t) \right] , \tag{3.70}$$

where we note the strong dependence on the $|V_{cb}|$ value, since it is proportional to the square and fourth power of the $|V_{cb}|$ element. Here, we have $G_{\rm F} = 1.1663787 \times 10^{-11}$ MeV^{-2} [66], which is the Fermi constant, m_W and m_K are the W and kaon masses, respectively:

$$m_W = (80\ 377 \pm 12)\ \text{MeV}\ [66], \qquad m_K = (497.611 \pm 0.013)\ \text{MeV}\ [66], \tag{3.71}$$

the kaon decay constant $f_K = (155.7 \pm 0.3)$ MeV [135], the mass difference between the $K_{\rm S}^0$ and $K_{\rm L}^0$ mass eigenstates $\Delta m_K = (0.005289 \pm 0.000010)\ \text{ps}^{-1}$ [66], and the kaon bag parameter $\hat{B}_K = 0.7625 \pm 0.0097$ [135]. The parameter $\kappa_\epsilon = 0.94 \pm 0.02$ [136] is a multiplicative correction factor coming from long-distance contributions that are not included in the kaon bag parameter. The functions

$$\mathcal{S}(x_t) = S_0(x_t) + S_0(x_c) - 2S_0(x_c, x_t)\ , \qquad \mathcal{S}(x_c, x_t) = S_0(x_c) - S_0(x_c, x_t) \tag{3.72}$$

are combinations of the Inami–Lim functions (coming from box topologies) given by [102]:

$$S_0(x_i) = x_i \left[\frac{1}{4} + \frac{9}{4(1-x_i)} - \frac{3}{2(1-x_i)^2} - \frac{3x_i^2 \ln x_i}{2(1-x_i)^3} \right] , \tag{3.73}$$

$$S_0(x_i,x_j) = \frac{x_i x_j}{x_i - x_j}\left[\frac{1}{4} + \frac{3}{2(1-x_i)} - \frac{3}{4(1-x_i)^2}\right]\ln x_i + \frac{x_j x_i}{x_j - x_i}\left[\frac{1}{4} + \frac{3}{2(1-x_j)} - \frac{3}{4(1-x_j)^2}\right]\ln x_j - \frac{3x_i x_j}{4(1-x_i)(1-x_j)}\,, \tag{3.74}$$

where $x_i \equiv [\bar{m}_i(\bar{m}_i)/m_W]^2$ with $i = c, t$ and $\bar{m}_i(\bar{m}_i)$ is the running mass of quark i in the $\overline{\text{MS}}$ scheme (a renormalization scheme) evaluated at the scale $(\bar{m}_i)$. For the charm quark we have $\bar{m}_c(\bar{m}_c) = (1.278 \pm 0.013)$ GeV [135]. For the top quark, for which we have $m_t = (172.69 \pm 0.30)$ GeV [66], the pole mass (value observed experimentally) is converted into $\bar{m}_t(\bar{m}_t) = (162.19 \pm 0.30)$ GeV, using the RunDec tool [137, 138]. We note that for the latter case, we ignore light-quark mass effects and use experimental data for the mass of Z boson $m_Z = (91.1876 \pm 0.0021)$ GeV [66] and the QCD coupling $\alpha_s(m_Z) = 0.1179 \pm 0.0009$ [66]. Last but not least, η_{tt}^{EW}, η_{tt} and η_{ut} are correction factors to $\mathcal{S}(x_t)$ and $\mathcal{S}(x_c, x_t)$ [134, 139]. The factor $\eta_{tt}^{\text{EW}} = 0.990 \pm 0.004$ [139] shows the impact of next-to-leading order (NLO) electroweak corrections based on the first calculations of two-loop electroweak effects on ε_K. The factor $\eta_{tt} = 0.550 \pm 0.023$ [134] parametrises the QCD corrections and is known to next-to-leading-logarithmic (NLL) precision. The $\eta_{ut} = 0.402 \pm 0.005$ [134] is also due to QCD corrections and is known to next-next-to-leading-logarithmic (NNLL) precision.

Numerical Values

Following from Eq. (3.70), the measured value of the CP-violating observable $|\varepsilon_K|$ in the SM describes a hyperbola in the $\bar{\rho} - \bar{\eta}$ plane:

$$\bar{\eta} = \frac{|\varepsilon_K|}{A - B\bar{\rho}}. \tag{3.75}$$

We obtain the SM predictions, utilising the inclusive, exclusive and hybrid values of $\bar{\rho}$ and $\bar{\eta}$ given in Table 2. Since $|\varepsilon_K|_{\text{SM}}$ depends only on $|V_{cb}|$, the inclusive scenario also covers the hybrid one. Therefore, the SM values are:

$$|\varepsilon_K|_{\text{SM}} = (2.54 \pm 0.22) \times 10^{-3} \quad \text{Inclusive/Hybrid,} \tag{3.76}$$

$$|\varepsilon_K|_{\text{SM}} = (1.74 \pm 0.15) \times 10^{-3} \quad \text{Exclusive.} \tag{3.77}$$

Regarding A and B, the values for the inclusive (thus also hybrid) and exclusive cases are given as follows:

$$A = (6.94 \pm 0.40) \times 10^{-3}, \quad B = (5.11 \pm 0.35) \times 10^{-3} \qquad \text{Inclusive/Hybrid,} \tag{3.78}$$

$$A = (5.36 \pm 0.32) \times 10^{-3}, \quad B = (3.78 \pm 0.27) \times 10^{-3} \qquad \text{Exclusive.} \tag{3.79}$$

Let us now compare these SM predictions with the experimental value [66]

$$|\varepsilon_K| = (2.228 \pm 0.011) \times 10^{-3}. \tag{3.80}$$

We observe that this result differs from the inclusive/hybrid case by 1.4 standard deviations while it differs from the exclusive case by 3.2 standard deviations. Even though there seems to be a preference for the inclusive/hybrid case, the uncertainty on the SM value is not sufficient to draw conclusions.

Fig. 13 shows that the blue contour, indicating the $|\varepsilon_K|$ observable, lies below the yellow region (overlap area between γ and R_b) in the inclusive scenario, while it is completely above the yellow region in the exclusive case. On the other hand, in the hybrid determination, the contour lies between those of the inclusive and exclusive cases while overlaps completely with the yellow solution, giving the most consistent picture of the UT apex within the SM. This illustrates again the strong dependence on $|V_{cb}|$. In the future, it will be interesting to see how the interplay between $|\varepsilon_K|$ and the UT will evolve and this could help to understand the tensions between the inclusive and exclusive determinations of $|V_{ub}|$ and $|V_{cb}|$.

3.4.3 Impact of New Physics in Semileptonic Decays

Discussing the impact of NP in semileptonic decays, we generalise the low-energy effective Hamiltonian to allow for NP effects[19] as in Eq. (3.53):

$$\mathcal{H}_{\text{eff}} = \frac{4G_{\text{F}}}{\sqrt{2}} V_{qb} \left[C_{V_L} \mathcal{O}^{\ell}_{V_L} + C^{\ell}_{S} \mathcal{O}^{\ell}_{S} + C^{\ell}_{P} \mathcal{O}^{\ell}_{P} \right] + \text{h.c.} \, . \tag{3.81}$$

Similarly to the leptonic case, there is only one operator contributing in the SM, the $\mathcal{O}^{\ell}_{V_L}$, indicating that the construction of the effective theories is convenient in the NP searches.

We would like to mention here that an interesting point related to the tau semileptonic modes is given by the ratios of the branching fractions of the decays with taus with respect to decays with muons or electrons. We have the ratios $R(D)$ and $R(D^*)$ defined as follows:

$$R(D) = \frac{\mathcal{B}(B \to D\tau\nu_\tau)}{\mathcal{B}(B \to D\ell\nu_\ell)}, \tag{3.82}$$

$$R(D^*) = \frac{\mathcal{B}(B \to D^*\tau\nu_\tau)}{\mathcal{B}(B \to D^*\ell\nu_\ell)}, \tag{3.83}$$

where $\ell = e, \mu$. These ratios are excellent tools to test lepton flavour universality (LFU) in charged-current processes. The SM predictions are very precise, since there is a minimal

[19] In the most general case, there could be more operators, thus right-handed as well as tensor operators can also be included. Here, we focus again on the (Pseudo-)Scalar contributions similarly to Eq. (3.53).

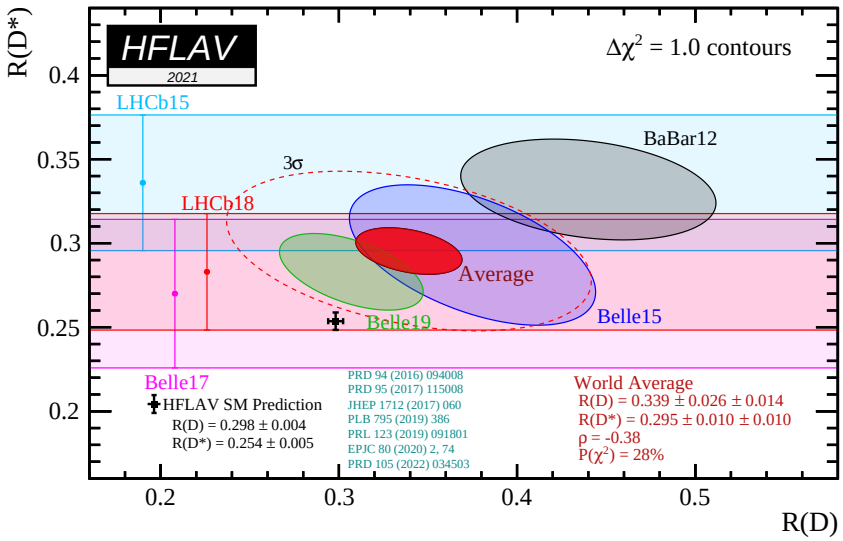

Figure 14: Overview of measurements of the $R(D)$ and $R(D^*)$ ratios [11].

dependence on the form factor[20] of the $B \to D^{(*)}$ transitions and they do not depend at all on the $|V_{cb}|$ matrix elements. The corresponding HFLAV predictions are [11]:

$$R(D)_{\rm SM} = 0.298 \pm 0.004 \tag{3.84}$$

$$R(D^*)_{\rm SM} = 0.254 \pm 0.005. \tag{3.85}$$

These ratios have been measured by BaBar, Belle and LHCb collaborations and the current world average is given as follows [11]:

$$R(D) = 0.339 \pm 0.026 \pm 0.014 \tag{3.86}$$

$$R(D^*) = 0.295 \pm 0.010 \pm 0.010. \tag{3.87}$$

We note that a new measurement of these ratios has recently been reported by LHCb [140]: $R(D) = 0.441 \pm 0.060 \pm 0.066$ and $R(D^*) = 0.281 \pm 0.018 \pm 0.024$. This has not yet been included in the current HFLAV overview in Ref. [11].

Comparing the theoretical predictions with the experimental world averages, there are tensions up to the level of 3.3 σ. An overview[21] of all the measurements of these ratios as well

[20] Neglecting the lepton masses for the semileptonic decays later on, there is only one form factor contributing, while for the taus, due to their heavy mass which cannot be neglected, there are two form factors entering. Thus, comparing the tau mode (with two form factors) with the muon or electron modes (having one form factor), in the $R(D(^*))$ ratios the form factors do not fully cancel but they are still considered to be very robust theoretically.

[21] An alternative illustration is provided in Appendix C.

as the SM predictions are given in Fig. 14. In this thesis, we are not exploring further these ratios. However, it is a very intriguing topic, and as in NP studies it is usually assumed that NP enters via the tau leptons, these ratios serve as an excellent probe for physics beyond the SM. This is due to the fact that semileptonic decays with taus in the final state, can be sensitive to NP effects due to their large mass. Thus, in the future it will be important to further study these modes. Last but not least, we mention that $B \to K^{(*)}\ell^+\ell^-$ modes offer also interesting probes for tests of LFU in FCNC processes [141–146].

3.5 Non-leptonic decays

In this category, the final state consists only of hadrons. Therefore, the hadronic sector here is much more complicated in comparison with the leptonic and the semileptonic decays. The hadronic effects are very difficult to handle, making these transitions the most challenging B decays. The process describing the non-leptonic decays is given as follows:

$$b \to q_1 \bar{q}_2 d(s) \quad \text{where } q_1, q_2 \ \in \ \{u, d, c, s\}. \tag{3.88}$$

Regarding the Feynman diagrams of the non-leptonic B decays, there are three different cases depending on the flavour content of the final state. We observe that in the case the quarks q_1 and q_2 are not the same and they are either u or c, only tree topologies appear. In the case where the quarks q_1 and q_2 are equal and are either u or c, then we have both tree and penguin diagrams contributing. In the last case, if again the quarks q_1 and q_2 are equal but they are either d or s, only penguin diagrams contribute. Fig. 15(a) depicts the tree topologies, Fig. 15(b) shows the QCD (gluonic) penguin, while Fig. 15(c) and (d) illustrate the electroweak (EW) penguins.

The examples in Fig. 15 can also help us to understand better the terminology which is used regarding the Feynman diagrams. Thus, the tree diagrams include no loops[22] whereas the penguins are the loop topologies, where the W boson reconnects back to the quark line from which it was emitted. There are two kinds of penguin diagrams, the QCD penguins, where the gluon is the emitted particle from the loop, and the electroweak penguins, where the emitted particle from the loop is either a photon or a Z boson.

3.5.1 Operator Product Expansion

Our starting point for the challenging case of non-leptonic B decays is to use again the low energy effective Hamiltonian $\mathcal{H}_{\text{eff}}$ framework. The tool we use in order to calculate this Hamiltonian and deal with effects of strong interactions of QCD is the "Operator Product Expansion" (OPE) [147–149]. Applying the OPE,

[22] In tree diagrams, the W boson leads to a different quark line than the line that starts out as b quark.

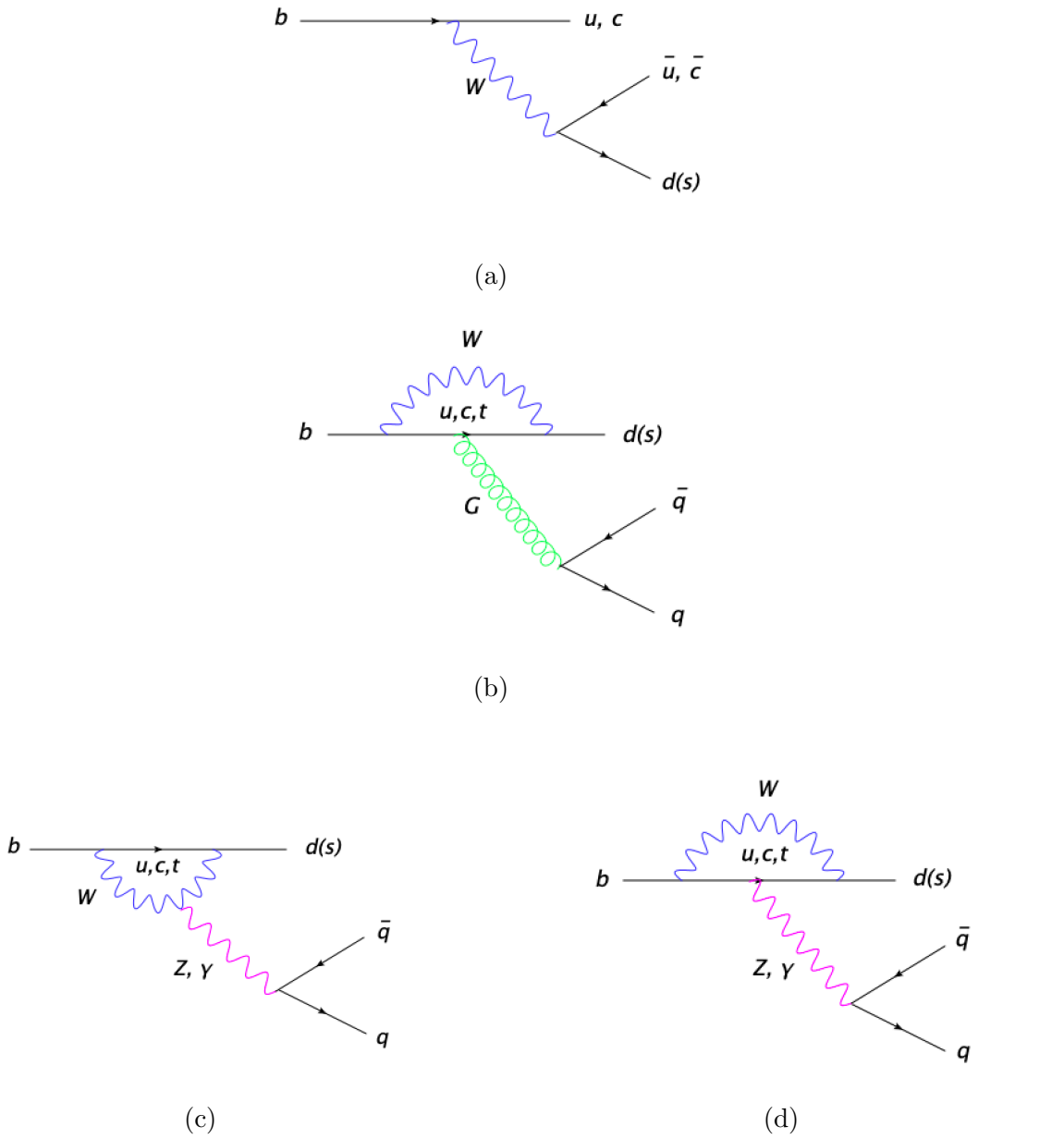

Figure 15: Topologies for non-leptonic B decays: (a) tree diagrams, (b) QCD penguins, (c) and (d) EW penguins.

- the exchange of the very heavy W boson can be approximated to a point-like four-quark interaction and
- the local four-quark operator is interpreted as a four-quark interaction vertex with the Wilson coefficient being the respective coupling constant.

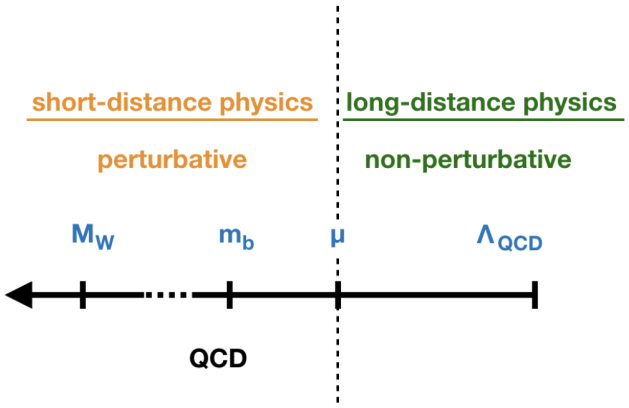

Figure 16: Illustration of different energy regimes for weak B decays.

As a result, the low-energy effective Hamiltonian takes the schematic form:

$$\mathcal{H}_{\text{eff}} \propto G_F \sum_i C_i(\mu) \times O_i + \text{terms suppressed by } (1/M_W^2), \tag{3.89}$$

where μ indicates the renormalization scale, which separates the regimes of low energy from the high energy regimes [116]. The $C_i(\mu)$ coefficients refer to the short-distance effects and include all the QCD interactions above the scale μ. On the other hand, we have the O_i operators and when calculating the amplitude of a specific decay process, we have to deal with the hadronic matrix elements. They refer to the long distance effects and include the low energy contributions below the scale μ. The short-distance part is the one that can be calculated in perturbation theory. However, the long-distance part, referring to the matrix elements, requires non-perturbative techniques. The situation though is already simplified compared to the original case, allowing for a systematic framework to calculate and include higher-order QCD corrections. An illustration of the different energy scales for the B-meson decays is given in Fig. 16.

In a nutshell, the OPE technique allows us to separate the short-distance part or the high energy scale part, where we can make perturbative calculations in QCD, from the non-perturbative part of QCD, which leads to the hadronic binding and which in perturbation theory we cannot calculate, therefore non-perturbative methods are required.

Writing the low-energy effective Hamiltonian for the non-leptonic decays in a formal way, we obtain:

$$\mathcal{H}_{\text{eff}} = \frac{G_F}{\sqrt{2}} \lambda_{\text{CKM}} \sum_k C_k(\mu) Q_k, \tag{3.90}$$

where the transition matrix element is:

$$\langle f\,|\mathcal{H}_{\rm eff}|\,i\rangle = \frac{G_F}{\sqrt{2}}\lambda_{\rm CKM}\sum_k C_k(\mu)\langle f\,|Q_k(\mu)|\,i\rangle. \tag{3.91}$$

Here, f and i denote the final and initial state, respectively, $\lambda_{\rm CKM}$ is a CKM factor, $C_k(\mu)$ are the Wilson coefficients, which are the perturbative quantities, and the $\langle f\,|Q_k(\mu)|\,i\rangle$ denote the hadronic matrix elements, which are the non-perturbative objects. We highlight that the quantity Q_k is a local operator arising from both QCD and EW interactions while the coefficients $C_k(\mu)$ are couplings related to the vertices described by the corresponding Q_k.

Taken that non-leptonic B decays may have both tree and penguin topologies, we have many more operators compared to the leptonic and the semi-leptonic decays:

- Q_1^{jr} and Q_2^{jr}: current-current operators
- Q_3^r, Q_4^r, Q_5^r and Q_6^r: QCD penguin operators
- Q_7^r, Q_8^r, Q_9^r and Q_{10}^r: EW penguin operators,

where $r \in \{d, s\}$ and $j \in \{u, c\}$. The structure of the operators is given in Appendix B. The effective Hamiltonian takes the following form:

$$\mathcal{H}_{\rm eff} = \frac{G_F}{\sqrt{2}}\left[\sum_{j=u,c} V_{jr}^* V_{jb}\left\{\sum_{k=1}^{2} C_k(\mu)Q_k^{jr} + \sum_{k=3}^{10} C_k(\mu)Q_k^r\right\}\right], \tag{3.92}$$

and applies to any non-leptonic B decay in the SM.

How did we derive the $\mathcal{H}_{\rm eff}$ for the non-leptonic decays?

Let us use as an example the pure tree decay $\bar{B}_d^0 \to K^- D^+$. Note that in terms of colour flow, the tree topologies are divided into two categories: colour-allowed and colour-suppressed ones. In the colour-allowed tree diagrams, the quark and antiquark pair, which is generated by the W boson, end up in the same meson, while in the colour-suppressed trees, the quark and antiquark coming from the W end up in different final mesons. An illustration of these Feynman diagrams is given in Fig. 17, where the left plot corresponds to the colour-allowed tree topologies, using the $B_d^0 \to K^- D^+$ decay as an example, while the right plot refers to the colour-suppressed tree topologies as seen in the $\bar{B}_d^0 \to D^0\pi^0$ decay. It becomes clear that at the leading-order Feynman diagram in the colour-allowed case, the colour indices of the K^- meson and the $\bar{B}_d^0$–D^+ system run independently from each other. So, there are two independent colour degrees of freedom in the colour-allowed case (denoted as α and β), while there is only one in the colour-suppressed (α index).

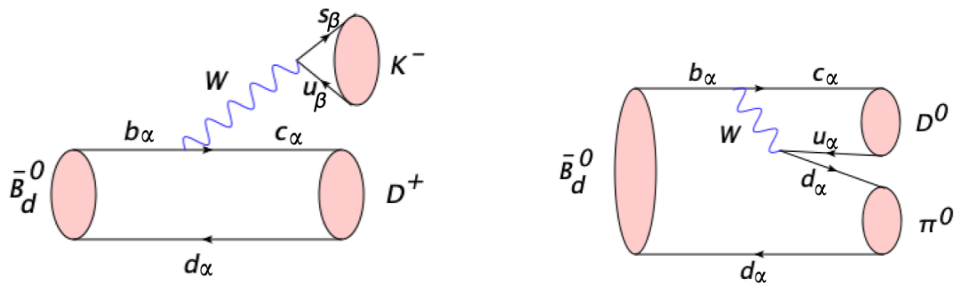

Figure 17: Colour-allowed tree (left) and colour-suppressed tree (right) topology.

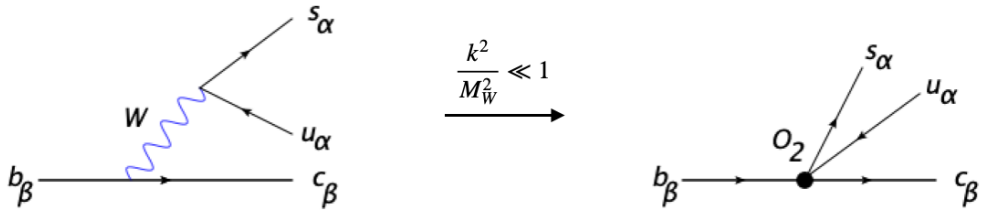

Figure 18: Effective theory picture: Integrating out the W boson leads to the effective theory with the four quark operator O_2. We note that the indices α and β are colour indices of the $SU(3)_{\rm C}$ group.

Let us continue with exploring the $B_d^0 \to K^- D^+$ transition. As previously, applying the Feynman rules, we evaluate the transition amplitude in the SM (using the notation of [99]):

$$A(\bar{B}_d^0 \to K^- D^+) = -\frac{g_2^2}{8} V_{us}^* V_{cb} \left[\bar{s}\gamma^\nu(1-\gamma_5)u\right] \left[\frac{g_{\nu\mu}}{k^2 - M_W^2}\right] \left[\bar{c}\gamma^\mu(1-\gamma_5)b\right]. \tag{3.93}$$

Due to the fact that $k^2/M_W^2 \ll 1$, as we have already seen before, we integrate out the heavy W boson:

$$\frac{g_{\nu\mu}}{k^2 - M_W^2} \to -\left(\frac{8G_F}{\sqrt{2}g_2^2}\right) g_{\nu\mu}, \tag{3.94}$$

thus we move from the full theory to the effective one, obtaining the four quark operator O_2. A depiction of this process, which is now described by the current-current operator

$$O_2 \equiv \left[\bar{s}_\alpha \gamma_\mu(1-\gamma_5)u_\alpha\right] \left[\bar{c}_\beta \gamma^\mu(1-\gamma_5)b_\beta\right], \tag{3.95}$$

where the α and β indices denote the colour of the $SU(3)_{\rm C}$ gauge group, is given in Fig. 18.

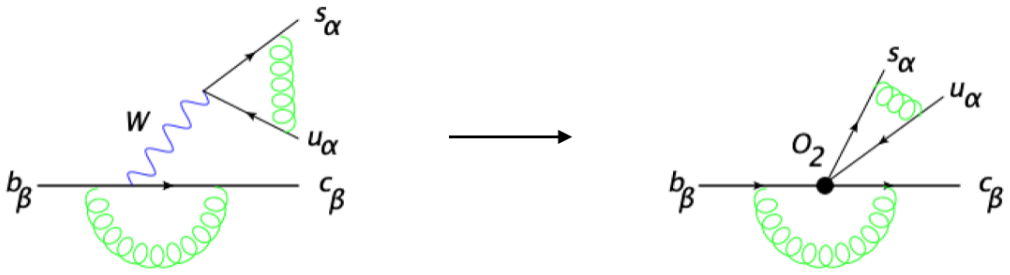

Figure 19: Impact of factorizable QCD effects, going from the full (left plot) to an effective theory (right plot).

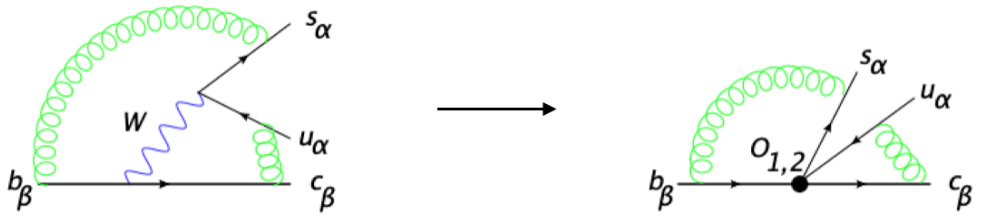

Figure 20: Impact of non-factorizable QCD effects, going from the full (left plot) to an effective theory (right plot).

Therefore, we obtain the following effective Hamiltonian:

$$\mathcal{H}_{\text{eff}} = \frac{G_{\text{F}}}{\sqrt{2}} V_{us}^* V_{cb} \left[\bar{s}_\alpha \gamma_\mu (1-\gamma_5) u_\alpha\right] \left[\bar{c}_\beta \gamma^\mu (1-\gamma_5) b_\beta\right] \equiv \frac{G_{\text{F}}}{\sqrt{2}} V_{us}^* V_{cb} C_2 O_2 . \tag{3.96}$$

Let us now explore the impact of QCD, due to the exchange of gluons, since so far we have not included QCD corrections. There are two cases:

- factorizable QCD corrections, depicted in Fig. 19. These effects result in the Wilson coefficient C_2 acquiring a dependence on the renormalization scale μ, therefore $C_2(\mu) \neq 1$, and
- non-factorizable QCD corrections, depicted in Fig. 20, which lead to the generation of a second current–current operator O_1 and the renormalization of the operator O_2. The O_1 operator is defined as

$$O_1 \equiv \left[\bar{s}_\alpha \gamma_\mu (1-\gamma_5) u_\beta\right] \left[\bar{c}_\beta \gamma^\mu (1-\gamma_5) b_\alpha\right] . \tag{3.97}$$

Finally, we may write the low-energy effective Hamiltonian in the following form:

$$\mathcal{H}_{\text{eff}} = \frac{G_{\text{F}}}{\sqrt{2}} V_{us}^* V_{cb} \left[C_1(\mu) O_1 + C_2(\mu) O_2 \right], \tag{3.98}$$

or in a more compact and general way:

$$H_{\text{eff}} = \frac{G_F}{\sqrt{2}} \left[\sum_{j=u,c} V_{jr}^* V_{jb} \left\{ \sum_{k=1}^{2} C_k(\mu) Q_k^{jr} \right\} \right]. \tag{3.99}$$

This expression is in the form of Eq. (3.92), taking only tree topologies into account (purple part). The Wilson coefficients $C_1(\mu)$ and $C_2(\mu)$ [150–152] can be calculated through "matching" between the full and the effective theory. More specifically, the first step is to calculate the QCD corrections both in the full theory, explicitly considering the W exchange, and in the effective theory, where the W boson is integrated out. Then we express the transition amplitude, as presented in Eq. (3.91), in terms of the Wilson coefficients and the matrix elements which are now QCD-corrected.

We highlight that the results for the Wilson coefficients $C_k(\mu)$ contain $\log(\mu/M_W)$ terms which become large for renormalization scales μ in the GeV regime, thus for $\mu = \mathcal{O}(m_b)$, which is the scale that governs the hadronic matrix elements of the operators O_k. So, what should we do? Utilise the renormalization-group improved perturbation theory. The transition matrix element $\langle f | \mathcal{H}_{\text{eff}} | i \rangle$ cannot depend on the chosen renormalization scale μ. This implies a renormalization group equation:

$$\mu \frac{d}{d\mu} \langle f | \mathcal{H}_{\text{eff}} | i \rangle = 0. \tag{3.100}$$

Its solution can be written in the following form:

$$\vec{C}(\mu) = \hat{U}(\mu, M_W) \cdot \vec{C}(M_W), \tag{3.101}$$

where the initial conditions of $\vec{C}(M_W)$ describe the short-distance physics at high-energy scales. Through Eq. (3.101), the following terms of the Wilson coefficients can be systematically summed up:

$$\alpha_s^n \left[\log\left(\frac{\mu}{M_W} \right) \right]^n \text{ (LO)}, \quad \alpha_s^n \left[\log\left(\frac{\mu}{M_W} \right) \right]^{n-1} \text{ (NLO)}, \quad \ldots \quad . \tag{3.102}$$

As this goes beyond the scope of our analysis, the reader is referred to Ref. [104] for a detailed discussion.

Continuing with the expression of the effective Hamiltonian, our final step is to move forward and allow for penguin topologies to enter. Therefore, having both tree and penguin

contributions, the operator basis is further enhanced. Recalling the unitarity of the CKM matrix, we apply the relation:

$$V_{ur}^* V_{ub} + V_{cr}^* V_{cb} + V_{tr}^* V_{tb} = 0 \quad (r \in \{d, s\}). \tag{3.103}$$

The top quark, just like in the case of the W boson, is a heavy degree of freedom. Therefore, both the W boson and the top quark, which enters through penguins, are integrated out, as well as the Z bosons. Consequently, we obtain the expression we have already shown in Eq. (3.92), which we repeat here:

$$\mathcal{H}_{\text{eff}} = \frac{G_F}{\sqrt{2}} \left[\sum_{j=u,c} V_{jr}^* V_{jb} \left\{ \sum_{k=1}^{2} C_k(\mu) Q_k^{jr} + \sum_{k=3}^{10} C_k(\mu) Q_k^r \right\} \right], \tag{3.104}$$

where the blue part refers to the penguin contributions. We highlight once again that the effective Hamiltonian is the prime theoretical tool for the analysis of the weak decays and the neutral meson mixing phenomenon, not only for the B mesons that we are interested in for this thesis but also for the kaons and the D mesons.

Formalism of Decay Amplitudes

Since we have presented the low-energy effective Hamiltonian, we can also provide the formalism for the decay amplitudes for both the $\bar{B} \to \bar{f}$ process, where f denotes the final state, and the CP-conjugate process $B \to f$. Applying Eq. (3.104), we obtain:

$$\begin{aligned} A(\bar{B} \to \bar{f}) &= \langle \bar{f} | \mathcal{H}_{\text{eff}} | \bar{B} \rangle \\ &= \frac{G_{\text{F}}}{\sqrt{2}} \left[\sum_{j=u,c} V_{jr}^* V_{jb} \left\{ \sum_{k=1}^{2} C_k(\mu) \langle \bar{f} | Q_k^{jr}(\mu) | \bar{B} \rangle + \sum_{k=3}^{10} C_k(\mu) \langle \bar{f} | Q_k^r(\mu) | \bar{B} \rangle \right\} \right], \end{aligned} \tag{3.105}$$

$$\begin{aligned} A(B \to f) &= \langle f | \mathcal{H}_{\text{eff}}^\dagger | B \rangle \\ &= \frac{G_{\text{F}}}{\sqrt{2}} \left[\sum_{j=u,c} V_{jr} V_{jb}^* \left\{ \sum_{k=1}^{2} C_k(\mu) \langle f | Q_k^{jr\dagger}(\mu) | B \rangle + \sum_{k=3}^{10} C_k(\mu) \langle f | Q_k^{r\dagger}(\mu) | B \rangle \right\} \right]. \end{aligned} \tag{3.106}$$

These are the most general expressions in the SM. We will explicitly make use of these important relations in our studies of CP violation, as we will discuss in detail in Chapter 4.

3.5.2 The Concept of Factorisation

As we mentioned, the non-leptonic decays are very challenging due to the hadronic effects. When we want to calculate a transition amplitude specifically for a given decay, we face the

problem that now we have to calculate matrix elements of four-quark operators[23]. These are very complicated objects. So, how can we handle them?

A very important concept that helps us to deal with such decays with involved dynamics and derive the non-leptonic B decays amplitudes, is the framework of "factorisation". More specifically, the hadronic matrix elements of four-quark operators are factorised/separated into the product of hadronic matrix elements of quark currents [153]. There are decays like $B \to D\pi$ transitions, that factorisation is really intuitive and is the most obvious strategy. The main advantage is that the theoretical description of the decay amplitude calculation gets simplified. In the factorised expressions the decay constant for the decay products (mesons in the final state) are involved as well as the form factors, which we obtain from semi-leptonic decays.

We note that factorisation is not a universal feature but is process dependent. The concept of factorisation plays central role in our analysis. We will explicitly make use of this tool in Chapters 5 and 6, and further elaborate on the formalism. We already highlight here that there are decays where factorisation is expected to work very well, as in the case of "colour-allowed" $b \to c$ transitions. Key example in this category is the $B_s^0 \to D_s^+ K^-$ decay, which is one of the main transitions we study in this thesis. We will discuss this channel in Sec. 6.5. On the other hand, in colour-suppressed decays, it is expected not to work so well. An interesting example in this case, is the $B \to J/\psi K_S$ decay which we will discuss in Sec 5.2 and Sec. 5.3.

Factorisation and colour-allowed decays

Let us now see in practice how we may factorise the hadronic matrix elements. For this purpose, we once again make use of the $\bar{B}_d^0 \to D^+ K^-$ decay, utilising the Feynman diagram in Fig. 21. We firstly have to calculate the transition amplitude. We encounter the hadronic matrix elements of the operators $O_{1,2}$. We need to consider the $SU(N_{\rm C})$ colour-algebra relation [99]:

$$T^a_{\alpha\beta} T^a_{\gamma\delta} = \frac{1}{2}\left(\delta_{\alpha\delta}\delta_{\beta\gamma} - \frac{1}{N_{\rm C}}\delta_{\alpha\beta}\delta_{\gamma\delta}\right) \tag{3.107}$$

$$= \frac{1}{2}\delta_{\alpha\delta}\delta_{\beta\gamma} - \frac{1}{2}\frac{\delta_{\alpha\beta}\delta_{\gamma\delta}}{N_{\rm C}}, \tag{3.108}$$

which allows us to write the operator O_1 as:

$$O_1 = \frac{1}{N_{\rm C}} O_2 + 2\left(\bar{s}_\alpha T^a_{\alpha\beta} u_\beta\right)_{\rm V-A}\left(\bar{c}_\gamma T^a_{\gamma\delta} b_\delta\right)_{\rm V-A}. \tag{3.109}$$

[23] In the case of semileptonic decays, the matrix elements literally factorise automatically as the gluons do not "talk" with the lepton antineutrino pair. However, this is not happening in the non-leptonic case due to the gluon exchanges between the quarks in the final states.

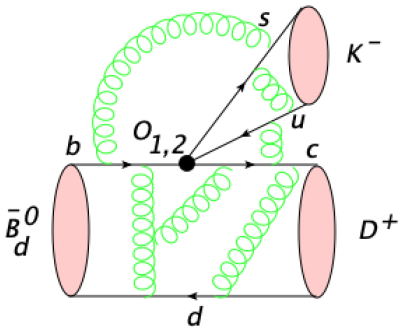

Figure 21: Feynman diagram for the $\bar{B}_d^0 \to D^+ K^-$ decay within the effective theory.

Here, for completeness, we note that one can straightforwardly show that this is the expression of O_1 by simply plugging Eq. (3.108) into Eq. (3.109):

$$\begin{aligned} O_1 &= \frac{1}{N_\mathrm{C}} O_2 + \frac{1}{2} 2 \left(\underbrace{\bar{s}_\alpha \delta_{\alpha\delta}}\, u_\beta \right)_{\mathrm{V-A}} \left(\underbrace{\bar{c}_\gamma \delta_{\beta\gamma}}\, b_\delta \right)_{\mathrm{V-A}} - \frac{1}{2} 2 \frac{1}{N_\mathrm{C}} \left(\bar{s}_\alpha \underbrace{\delta_{\alpha\beta} u_\beta} \right)_{\mathrm{V-A}} \left(\bar{c}_\gamma \underbrace{\delta_{\gamma\delta} b_\delta} \right)_{\mathrm{V-A}} \\ &= \frac{1}{N_\mathrm{C}} O_2 \; + \quad \underbrace{(\bar{s}_\delta \;\; u_\beta)_{\mathrm{V-A}} \quad (\bar{c}_\beta \;\; b_\delta)_{\mathrm{V-A}}} - \quad \frac{1}{N_\mathrm{C}} \quad \underbrace{(\bar{s}_\alpha \;\; u_\alpha)_{\mathrm{V-A}} \quad (\bar{c}_\gamma \;\; b_\gamma)_{\mathrm{V-A}}} \\ &= \frac{1}{N_\mathrm{C}} O_2 \; + \qquad\qquad O_1 \qquad\qquad - \quad \frac{1}{N_\mathrm{C}} \qquad\qquad O_2. \end{aligned} \tag{3.110}$$

Therefore, rearranging the operator and utilising the colour algebra relation for $SU(N_\mathrm{C})$, we can rewrite the operator O_1 as in Eq. (3.109). This allows us to obtain the amplitude:

$$\begin{aligned} \langle K^- D^+ | \mathcal{H}_\mathrm{eff} | \bar{B}_d^0 \rangle = \frac{G_\mathrm{F}}{\sqrt{2}} V_{us}^* V_{cb} \Big[\left(\frac{C_1}{N_\mathrm{C}} + C_2 \right) \langle K^- D^+ | (\bar{s}_\alpha u_\alpha)_{\mathrm{V-A}} (\bar{c}_\beta b_\beta)_{\mathrm{V-A}} | \bar{B}_d^0 \rangle \\ + 2\, C_1 \langle K^- D^+ | (\bar{s}_\alpha\, T^a_{\alpha\beta}\, u_\beta)_{\mathrm{V-A}} (\bar{c}_\gamma\, T^a_{\gamma\delta}\, b_\delta)_{\mathrm{V-A}} | \bar{B}_d^0 \rangle \Big]. \end{aligned} \tag{3.111}$$

We introduce the important quantity a_1:

$$a_1 = \frac{C_1}{N_\mathrm{C}} + C_2 \sim 1, \tag{3.112}$$

which is the phenomenological "colour factor" governing the "colour-allowed" decays.

We can now factorise the hadronic matrix elements as follows:

$$\begin{aligned} \langle K^- D^+ | (\bar{s}_\alpha u_\alpha)_{\mathrm{V-A}} (\bar{c}_\beta b_\beta)_{\mathrm{V-A}} | \bar{B}_d^0 \rangle |_\mathrm{fact} &= \langle K^- | \left[\bar{s}_\alpha \gamma_\mu (1-\gamma_5) u_\alpha \right] | 0 \rangle \langle D^+ | \left[\bar{c}_\beta \gamma^\mu (1-\gamma_5) b_\beta \right] | \bar{B}_d^0 \rangle \\ &= i f_K \times F_0^{(B\to D)}(M_K^2) \times (M_B^2 - M_D^2), \end{aligned} \tag{3.113}$$

where f_K is the kaon decay constant, $F_0^{(B\to D)}(M_K^2)$ is a hadronic form factor and $(M_B^2 - M_D^2)$ refers to the kinematical factor. Regarding the second term in Eq. (3.111), we notice that

it vanishes in factorisation:

$$\begin{aligned}&\langle K^- D^+|(\bar{s}_\alpha\, T^a_{\alpha\beta}\, u_\beta)_{\text{V–A}}(\bar{c}_\gamma\, T^a_{\gamma\delta}\, b_\delta)_{\text{V–A}}|\bar{B}^0_d\rangle\big|_{\text{fact}}\\ &= \langle K^-|(\bar{s}_\alpha\, T^a_{\alpha\beta}\, u_\beta)_{\text{V–A}}|0\rangle\langle D^+|(\bar{c}_\gamma\, T^a_{\gamma\delta}\, b_\delta)_{\text{V–A}}|\bar{B}^0_d\rangle = 0,\end{aligned} \tag{3.114}$$

as the mesons are colour-singlets, thereby implying that $\alpha = \beta$ and $\gamma = \delta$. The $T^a_{\alpha\beta}$, $T^a_{\gamma\delta}$ are traceless and as a result the above term vanishes.

Factorisation and colour-suppressed decays

So far, our working example is the "colour-allowed" tree decay $\bar{B}^0_d \to D^+K^-$. Moving to the case of "colour-suppressed" trees, such as the $\bar{B}^0_d \to D^0\pi^0$ mode shown in Fig. 17 (right plot), we can repeat the same steps in the decay amplitude calculation, keeping in mind that now in Eq. (3.111), instead of the quantity a_1, the following combination is introduced:

$$a_2 = C_1 + \frac{C_2}{N_{\text{C}}} \sim 0.25. \tag{3.115}$$

The a_2 parameter is the "colour-supprression" factor. In this case, there is only one colour index, running the whole Feynman diagram. A more formal description of the a_2 factor will be presented in Sec. 5.3.1.

3.5.3 Remarks Concerning the Colour Factors: The μ dependence

The Wilson coefficients depend on the renormalization scale μ[24]. When calculating the whole matrix element, the transition amplitude does not depend on μ. The factorised hadronic matrix element in Eq. (3.113) is a μ independent quantity. This shows that factorisation can not be exact. It also indicates that the μ dependence should come from non-factorisable effects. So, the interesting question, studied by Buras in Ref. [154], is to explore how the phenomenological coefficients depend on μ. The a_1 combination is very robust with respect to the μ dependence while the a_2 is very strongly dependent on the renormalization scale. From this observation, one can already see that factorisation for colour-allowed decays are on much better ground than in the colour suppressed decays. A detailed analysis can be found in Ref. [155].

[24]Regarding the Wilson coefficients, we note that renormalization scheme dependence arises at the next-to-leading order. Calculating the overall amplitude, it is the scheme dependence of the matrix element which ensures that finally this dependence cancels out.

3.5.4 Developments Beyond Naive Factorisation

We note here that the concept of factorisation has a long history [153, 156–160]. Originally, it simply started as the separation of the hadronic matrix elements of four-quark operators into the product of hadronic matrix elements of quark currents. This "naive factorisation" can be justified in weak decays in the large-N_C limit [156, 161–163]. Phenomenologically, it was a very important concept to deal theoretically with non-leptonic decays. Developments around 2000 led to the concept of "QCD factorisation" (QCDF) [164, 165]. This framework puts factorisation on a more solid ground for certain decay classes, providing the formalism to obtain the decay amplitudes in the heavy quark limit.

QCDF applies to B meson decays of the following kind:

$$\bar{B} \to M_1^{\{\text{Heavy or Light}\}}\, M_2^{\{\text{Light}\}} \tag{3.116}$$

where the meson $M_1^{\{\text{Heavy or Light}\}}$ picks up the spectator quark. The corresponding decay amplitude in QCDF takes the following form:

$$A(\bar{B} \to M_1 M_2)|_{\text{QCDF}} = \underbrace{\langle M_2|\zeta_2|0\rangle\langle M_1|\zeta_1|\bar{B}\rangle}_{\text{[naive factorisation]}} \times \underbrace{[1 + \text{non-factorisable corr.} + \mathcal{O}(\Lambda_{\text{QCD}}/m_b)]}_{\text{[hard scattering picture]}}, \tag{3.117}$$

where $\zeta_{1,2}$ are bilinear quark currents. In this approach, in addition to naive factorisation, one can also calculate non-factorisable corrections within a hard scattering picture utilising the heavy quark limit[25]. These non-factorisable effects are determined through perturbation theory. On top of these, there also other non-factorisable effects of non-parturbative nature which may arise at Λ_{QCD}/m_b, where Λ_{QCD} denotes the scale parameter of QCD. These terms appear as power corrections in Λ_{QCD}/m_b, giving rise to the main limitations of the theoretical accuracy.

Closely related to QCDF is the framework of the soft collinear effective theory (SCET) [166, 167]. SCET is simply speaking an alternative formulation of QCDF, which is very important in studies in collider physics. For completeness, we mention that further interesting approaches have been developed such as the perturbative hard-scattering technique (PQCD) for non-leptonic decays [168, 169]. These frameworks go beyond the scope of this thesis, thus we will not further elaborate on them.

3.5.5 Prime Strategy: Ratios with Partner Semileptonic Decays

In addition to determinations of the CKM elements, the semileptonic channels are also useful in other applications. They are particularly of key importance in the analysis of

[25] Simply speaking, the hard scattering picture refers to the exchange of high energetic gluons, called "hard gluons", in non-factorisable Feynman diagrams, where perturbation theory would still apply.

non-leptonic decays. One of our goals is to determine the colour factors $|a_1|$, $|a_2|$ from the data and to have a reference to check how well factorisation works. The calculation of the non-leptonic decay rates depends on CKM matrix elements and on hadronic form factors, arising in the factorisation approach. Thus, it becomes important to minimise their impact. For this purpose, the semileptonic modes can be used in order to create ratios with the branching fractions of non-leptonic decays [170]. These ratios indeed allow us to minimise the dependence on both:

- $|V_{ub}|$ and $|V_{cb}|$ matrix elements and
- hadronic form factors,

while determining the colour factors and testing the factorisation hypothesis.

Consequently, we create ratios between the non-leptonic B decays and their partner B semileptonic transitions. For the non-leptonic channels, we utilise the decay rate Γ, and knowing that $\Gamma \propto |A_{\text{fact}}|^2$, we consider the expression of the factorised decay amplitude. Similarly, for the semileptonic modes, we recall the expression of the decay rate in Eq. (3.61). We point out again that for these determinations we only refer to semileptonic decays that involve electrons or muons, which are well measured, but not to taonic modes. We will explicitly use this methodology with the ratios of semileptonic decays and provide the corresponding formalism in Sec. 5.3 and Sec. 6.6.

3.6 Reserved Threads: Insights on New Physics in the B System

The final topic we introduce to complete our presentation of the B-meson system is the impact of NP. Searches of possible hints from beyond the SM will be explored and explicitly discussed in the next Chapters. Here, we briefly present the status of NP searches and discuss in a heuristic manner how NP effects may enter in the B-meson decays.

One can search for NP particles directly at the high-energy frontier, as done by ATLAS and CMS at the LHC. So far, no new particles have been found. As an illustration, a plot by the ATLAS Collaboration [171] is given in Fig. 22, showing limits on masses of NP particles, arising in a plethora of different NP models. These are mapped out by assuming specific models – resulting in exclusion limits. Similar plots with bounds for direct NP searches are also provided by CMS.

In this thesis though, we follow a different approach. As already mentioned in Chapter 1, we use precision physics and search for indirect signals of NP. We can probe much higher energy scales than directly at colliders. NP particles, too heavy to be directly produced, could still leave their footprints on these decays and rare processes. In this case, we would

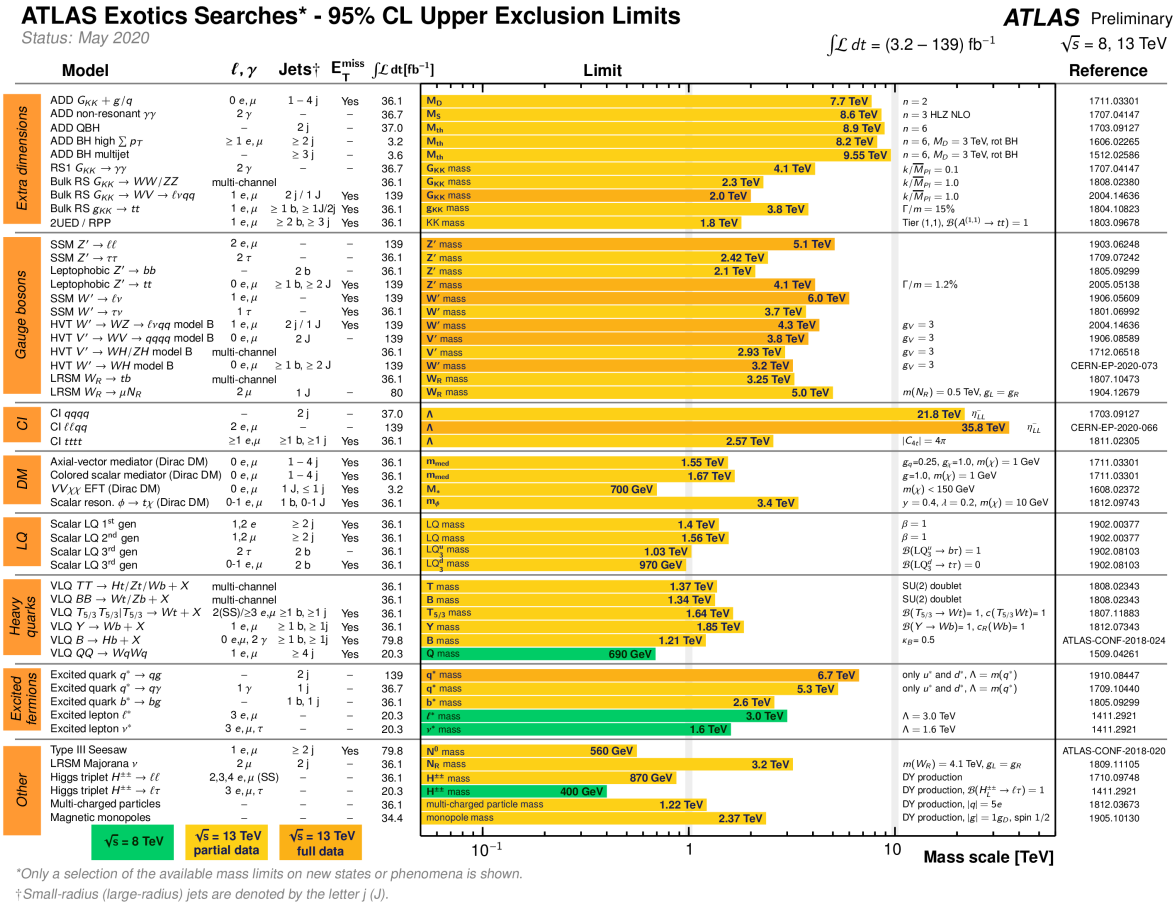

Figure 22: Exclusion limits (95% CL) for direct searches of NP with ATLAS [171].

get deviations between the theoretical predictions and the experimental measurements, thereby indicating the presence of NP.

So, more specifically, we assume that we have very heavy NP entering, far beyond the EW scale[26]. In an effective field theory picture[27] the heavy degrees of freedom of NP would be integrated out. In the low-energy effective Hamiltonian, these NP effects would then only be manifested through:

i) the Wilson coefficients of SM operators, taking values different from the SM or

ii) new operators, which might arise and which we do not have in the SM. However, no new particle fields would be present in these operators.

[26] We assume that NP is very heavy, otherwise we would have seen it

[27] As we discussed for the SM how the W, Z bosons and top quarks are integrated out, the same can be done for NP particles.

We emphasize that this powerful effective field theory approach is a model-independent method.

Why do we prefer model-independent searches?

Alternatively, one could utilise models. Such models can also be applied on given flavour processes and one can calculate everything in terms of parameters of these models. Thus, one can use processes to specifically constrain parameters of the specific models. However, this specific model might not be realised in Nature. Therefore, we prefer having a model-independent analysis and for this we apply effective field theory. We have already seen earlier in the Chapter that this method is very useful for the description of the B decays but so far, we had only studied it within the SM. Now, we can go beyond the SM. We highlight again that as we have not seen any new particles up to the TeV regime[28] we assume very NP.

Consequently, let us summarize how we explore the impact of NP effects in a schematic way. For NP searches:

- either we assume a specific model, as it is assumed in the exclusions plots in Fig. 22, and we study what happens for flavour processes in such models
- or one uses the model-independent effective field theory, noting that it assumes very heavy NP. Integrating out the heavy degrees of freedom, the NP only manifests through changes of Wilson coefficient function or/and new operators.[29] Having the effective Hamiltonian as a starting point, there are two options for NP to enter [172]:
  - In the first case, NP can modify the Wilson coefficients in such a way that they have two parts; the SM and the NP part, in which also new CP-violating phases may arise through complex phases:

$$C_k \to C_k^{\rm SM} + C_k^{\rm NP}.$$

  - In the second case, new operators could appear. This new operator basis, where new sources of flavour and CP violation are taken into account (noting that there can also be operators with more complicated structures or Dirac matrices), takes the form:

[28] unless particles are very elusive and have escaped detection, thus having invisible particles of low energy

[29] In this case, we are left with operators and Wilson coefficients, so we can in a model-independent way explore NP effects. We mention that in principle, one could also take specific models and work in a similar way as people do for these direct searches. But this is not the strategy we follow in this thesis.

$$\text{New operator} \to \{Q_k^{\rm SM}, Q_l^{\rm NP}\}.$$

Therefore, the operator basis can be enhanced from the NP. Due to this enhancement, operators which are either not present or strongly suppressed within SM may eventually play an important role.

In the following Chapters, we will elaborate more on the NP searches studying specific, benchmark B-meson decays and will propose strategies that will allow us to explore how much room for NP there is in the different B modes.

3.7 Synopsis

In this chapter we have discussed the B-meson system, which is a prime player in quark flavour physics. Firstly, focusing on the neutral B mesons, we introduced the important feature of the B_q^0–$\bar{B}_q^0$ mixing. Since this phenomenon offers great opportunities to test the SM, we set up the formalism and explicitly discussed the associated mixing parameters. As we will see later, the mixing parameters are very useful in our analysis. Obtaining their SM predictions, we can also utilise them to constrain the parameter space for NP.

Providing an introduction to the weak interactions of quarks and the theoretical tools we use in the analysis of the decays, we classify the B decays according to their final state. There are three categories – leptonic, semileptonic and non-leptonic decays – and we investigate each one of them separately. The starting point is the derivation of the decay amplitude and the corresponding low-energy effective Hamiltonian, applying effective theories. Having the transitions amplitudes, we also determined the decay rates, and as a result the branching ratios, which are important observables in our studies.

The case of the leptonic decays is the simplest one as there are no strong interaction effects of the final-state particles. We described their dynamics using as an example a charged leptonic B decay. We pointed out the differences that may arise due to different leptons in the final state. We highlighted features, like the helicity suppression, that play an essential role in obtaining SM predictions and constraints on NP through the branching ratio. Similar strategies can be applied for the neutral leptonic B decays, which we will present in Chapter 8.

The second category, the semileptonic B transitions, is another interesting class of decays. We have seen that one of the most important aspects is the determination of the CKM matrix elements $|V_{ub}|$ and $|V_{cb}|$. We specifically discussed how these quantities can be extracted with the help of semileptonic decays. Different approaches can be used to obtain $|V_{ub}|$ and $|V_{cb}|$, the exclusive and inclusive determinations. The remarkable point is that tensions arise between these two determinations, which is a long-standing puzzle.

This requires specific care when making predictions as well as on how to deal with the corresponding CKM matrix elements. In particular, we emphasized the importance of not making averages, but carefully examining every case separately. In addition, a third possibility, which is a hybrid combination of exclusive $|V_{ub}|$ and inclusive $|V_{cb}|$ values, is explored. Hopefully, in the future, with better analysis, this puzzle will be resolved. These CKM matrix elements enter in a plethora of SM calculations. Here, we focused on utilising them for determining the apex of the UT.

A key application of the semileptonic B decays is the extraction of the coordinates of the UT apex, which is a central topic of our analysis. For the SM determination of the UT in this Chapter, we chose to use only two observables, the angle γ and the side R_b, since they are less prone to be affected by NP effects. The R_b side is determined through the $|V_{ub}|$ and $|V_{cb}|$ matrix elements, thereby the unresolved discrepancies between inclusive and exclusive determinations play a crucial role. We performed fits using γ and R_b as inputs and taking into account all three cases (inclusive, exclusive and hybrid), we extracted the $\bar{\rho}$ and $\bar{\eta}$ values. Sizeable differences were found between these cases, advocating that it is important in the future to resolve these deviations. The solutions were also compared with a constraint coming from the $|\varepsilon_K|$, which could help to eventually solve this puzzle. In Chapter 5, we will use this analysis for further exploring NP effects in B_q^0–$\bar{B}_q^0$ mixing.

The last class of decays, the non-leptonic ones, is the most complicated case due to the presence of the hadronic effects, which are very difficult to handle. We discussed the low-energy effective Hamiltonians which set the theoretical stage for analysing these decays. We utilised the OPE which allows the separation of the short-distance from the long-distance contributions. The short-distance contributions are encoded in perturbatively calculable Wilson coefficients while the long-distance physics is described by hadronic matrix elements of four-quark operators. A very important concept for dealing with the hadronic matrix elements is factorisation. Here, we provided its framework and more technical details will follow later on, while discussing specific B decays. In addition, we briefly introduced the method of combining information between non-leptonic and semileptonic decays in order to simplify the analysis and extract useful information on testing the factorisation hypothesis. We will present the corresponding formalism in Chapters 5 and 6. The rich phenomenology of the non-leptonic decays makes them prime candidates for studying CP violation and we will discuss this in detail in the subsequent Chapter 4.

So far, we have mostly focused on the description of the SM framework, while giving some information about NP. For completeness, we provided a heuristic description of how NP contributions can enter in the B decays. Once again, we highlighted that in our analysis we aim at indirect searches at the high precision frontier. In the next Chapters, we will explicitly explore NP contributions and obtain constraints for various benchmark processes.

4 CP Violation in B Meson Decays

CP violation is a central topic in our studies and B-meson decays are the main actors in exploring this topic. As we have already stated, CP violation in the SM arises from complex phases in the CKM matrix. In this chapter, we will focus on how CP asymmetries arise and explore the interesting observables which are offered through benchmark B decays. A detailed analysis of the topic can be found i.e. in Refs. [99, 173–176].

4.1 Direct CP Violation in SM

Let us firstly discuss the type of CP violation that originates directly at the level of the decay amplitudes. The CP asymmetry is defined as follows:

$$\mathcal{A}_{\rm CP} \equiv \frac{\Gamma(B \to f) - \Gamma(\bar{B} \to \bar{f})}{\Gamma(B \to f) + \Gamma(\bar{B} \to \bar{f})} = \frac{|A(B \to f)|^2 - |A(\bar{B} \to \bar{f})|^2}{|A(B \to f)|^2 + |A(\bar{B} \to \bar{f})|^2}. \tag{4.1}$$

As introduced in Chapter 3, the leptonic and semileptonic classes of decays involve only a single weak amplitude in the SM. As a result, dealing with the squared absolute value of the amplitudes $|A(B \to f)|^2$ and $|A(\bar{B} \to \bar{f})|^2$ in Eq. (4.1), these quantities are the same for the decay and its CP-conjugate. Therefore, the $\mathcal{A}_{\rm CP} = 0$, meaning that these decay classes do not manifest direct CP violation. On the other hand, the non-leptonic decays (characterised by strong interactions), having different topologies and with different CKM factors at play, involve more than one weak amplitude, thus they can generate this type of CP violation. So, we consider the non-leptonic transitions and discuss the concept of "direct" CP violation, presenting the formalism in the SM.

Regarding the decay amplitudes, we recall the formalism given in Eqs. (3.105) and (3.106). In order to introduce the same hadronic matrix elements in the decay amplitudes $A(B \to f) = \langle f|\mathcal{H}_{\rm eff}^{\dagger}|B\rangle$ and $A(\bar{B} \to \bar{f}) = \langle \bar{f}|\mathcal{H}_{\rm eff}|\bar{B}\rangle$, we have to perform CP operations. Since the strong interactions are invariant under CP transformations and taken that

$$(\mathcal{CP})^{\dagger}(\mathcal{CP}) = \hat{1}, \tag{4.2}$$

we rewrite the decay amplitudes as follows:

$$\begin{aligned} A(B \to f) = \frac{G_{\rm F}}{\sqrt{2}} \Bigg[\sum_{j=u,c} V_{jr} V_{jb}^{*} \Bigg\{ \sum_{k=1}^{2} C_k(\mu) \langle f|(\mathcal{CP})^{\dagger}(\mathcal{CP}) Q_k^{jr\dagger}(\mu)(\mathcal{CP})^{\dagger}(\mathcal{CP})|B\rangle \\ + \sum_{k=3}^{10} C_k(\mu) \langle f|(\mathcal{CP})^{\dagger}(\mathcal{CP}) Q_k^{r\dagger}(\mu)(\mathcal{CP})^{\dagger}(\mathcal{CP})|B\rangle \Bigg\} \Bigg]. \end{aligned} \tag{4.3}$$

Due to the relations

$$(\mathcal{CP})|B\rangle = e^{i\phi_{\rm CP}(B)}|\bar{B}\rangle, \tag{4.4}$$

$$(\mathcal{CP})|f\rangle = e^{i\phi_{\rm CP}(f)}|\bar{f}\rangle, \tag{4.5}$$

where $\phi_{\rm CP}(B)$ and $\phi_{\rm CP}(f)$ are convention-dependent phases, and

$$(\mathcal{CP})Q_k^{jr\dagger}(\mathcal{CP})^\dagger = Q_k^{jr}, \tag{4.6}$$

$$(\mathcal{CP})Q_k^{r\dagger}(\mathcal{CP})^\dagger = Q_k^{r}, \tag{4.7}$$

we rewrite the decay amplitude as follows:

$$A(B\to f) = e^{i[\phi_{\rm CP}(B)-\phi_{\rm CP}(f)]} \times\frac{G_{\rm F}}{\sqrt{2}}\left[\sum_{j=u,c} V_{jr}V_{jb}^*\left\{\sum_{k=1}^{2} C_k(\mu)\langle\bar{f}|Q_k^{jr}(\mu)|\bar{B}\rangle + \sum_{k=3}^{10} C_k(\mu)\langle\bar{f}|Q_k^{r}(\mu)|\bar{B}\rangle\right\}\right]. \tag{4.8}$$

As a result, the hadronic matrix elements here are the same as those entering Eq. (3.105). However, regarding the CKM elements, still one amplitude has the CKM factors while the other has the complex conjugate of these factors.

Finally, we can write the amplitudes for the decay and the CP-conjucate case:

$$A(B\to f) = \langle f|\mathcal{H}_{\rm eff}^\dagger|B\rangle = e^{i[\phi_{\rm CP}(B)-\phi_{\rm CP}(f)]}\left[e^{-i\varphi_1}|A_1|e^{i\delta_1} + e^{-i\varphi_2}|A_2|e^{i\delta_2}\right], \tag{4.9}$$

$$A(\bar{B}\to \bar{f}) = \langle \bar{f}|\mathcal{H}_{\rm eff}|\bar{B}\rangle = e^{+i\varphi_1}|A_1|e^{i\delta_1} + e^{+i\varphi_2}|A_2|e^{i\delta_2}, \tag{4.10}$$

where $|A_{1,2}|e^{i\delta_{1,2}}$ are CP-conserving "strong" amplitudes involving the hadronic matrix elements of the four-quark operators and $\delta_{1,2}$ are CP-conserving phases arising from the hadronic matrix elements, which indicates the important role that hadronic physics plays here. Thus, we have:

$$|A_j|e^{i\delta_j} = \sum_k C_k(\mu)\times\langle f|Q_k^j(\mu)|B\rangle, \tag{4.11}$$

where we repeat that $C_k(\mu)$ refers to the perturbative QCD part while the $\langle f|Q_k^j(\mu)|B\rangle$ term encodes the hadronic dynamics of the decay. The phases $\varphi_{1,2}$ are CP-violating weak phases coming from the CKM elements $V_{jr}V_{jb}^*$. The term $e^{i[\phi_{\rm CP}(B)-\phi_{\rm CP}(f)]}$ contains the convention-dependent phase factors. These quantities cancel in all physical observables, in particular in the CP asymmetries. We point out that in the SM, Eqs. (4.9) and (4.10) present the most general structure of the amplitudes of the weak $B\to f$ and $\bar{B}\to\bar{f}$ decays.

Using the above equations for the decay amplitudes, we obtain:

$$\mathcal{A}_{\rm CP} = \frac{2|A_1||A_2|\sin(\delta_1-\delta_2)\sin(\varphi_1-\varphi_2)}{|A_1|^2+2|A_1||A_2|\cos(\delta_1-\delta_2)\cos(\varphi_1-\varphi_2)+|A_2|^2}, \tag{4.12}$$

which is the "direct" CP asymmetry.

Requirements and Applications

Based on Eq. (4.12), we note that one needs at least two decay amplitudes for having direct CP violation, since a non-vanishing value of $\mathcal{A}_{\rm CP}$ is generated through the interference between the two weak amplitudes.

Consequently, the criteria for having direct CP violation $\mathcal{A}_{\rm CP} \neq 0$ are:

1) $|A_1| \neq 0$ and $|A_2| \neq 0$,

2) $\varphi_1 - \varphi_2 \neq 0, \pi$,

3) $\delta_1 - \delta_2 \neq 0, \pi$.

If one looks at specific decays, the difference $\varphi_1 - \varphi_2$ is usually related to the CKM angle γ, which is the δ_{13} phase in the PDG parametrization. When measuring the direct CP asymmetry, the angle γ can be determined. However, the strong amplitudes $|A_{1,2}|e^{i\delta_{1,2}}$ entering Eq. (4.12) suffer from hadronic uncertainties. Therefore, in order to extract γ, these hadronic uncertainties have to be taken into account. Strategies have been developed over the years to determine this angle, while handling the hadronic matrix elements. For this purpose, pure tree $B \to DK$ decays play a key role. One can utilise amplitude relations between these modes to eliminate hadronic matrix elements. Measuring the direct asymmetries, the angle γ can eventually be extracted. Therefore, this is a very useful application of direct CP violation. We provide more information in Sec. 4.3.

4.2 CP Violation Induced Through B_q^0–$\bar{B}_q^0$ Mixing

Non-vanishing CP violating asymmetries require certain conditions to be met and these conditions arise from interference between two weak decay amplitudes. However, we can also obtain interference effects through B_q^0–$\bar{B}_q^0$ mixing in the time-dependent decay rates.

4.2.1 CP Violation in Mixing

CP violation in mixing can be probed by considering flavour specific B-meson decays where the final states are specific to the B^0 or $\bar{B}^0$ meson. A prime example is given by semileptonic decays, where the charge of the lepton determines whether we have initially present B^0 or a $\bar{B}^0$ meson. Particularly interesting are decay processes, where we have final states which can only be reached if the initially present B^0 meson oscillates into a $\bar{B}^0$ or vice versa. Then the asymmetry, assuming $\bar{B}^0(0) = \bar{B}^0$ and $B^0(0) = B^0$, takes the following form:

$$\frac{\Gamma(\bar{B}^0(t) \to X\ell^+) - \Gamma(B^0(t) \to X\ell^-)}{\Gamma(\bar{B}^0(t) \to X\ell^+) + \Gamma(B^0(t) \to X\ell^-)} = \frac{1 - |q/p|^4}{1 + |q/p|^4}. \tag{4.13}$$

We observe that this observable can take a non-vanishing value only if[30]:

$$|q/p| \neq 1. \tag{4.14}$$

We note that CP violation in B_q^0–$\bar{B}_q^0$ mixing is very small in the SM, at the order of $\mathcal{O}(10^{-4})$, and strongly experimentally constrained. Experimental measurements of such "wrong charge" lepton asymmetries have been made (i.e. in Ref. [177]) and upper bounds have been studied in Ref. [178]. In the following, we will neglect those tiny effects.

We emphasize that for the time-dependence formulae below, we use the assumption:

$$|q/p| = 1. \tag{4.15}$$

4.2.2 Time-Dependent CP Asymmetries

Interference effects arise when both B_q^0 and $\bar{B}_q^0$ decay into the same final state. An illustration of these effects was given in Fig. 7. Interference through mixing and the decay signals another type of CP violation. Let us firstly examine the case where the neutral B mesons decay into a final state which is a CP-eigenstate, thus Eq. (4.5) reads as follows:

$$(\mathcal{CP})|f\rangle = \pm|f\rangle. \tag{4.16}$$

Before defining the time-dependent CP asymmetry, let us introduce some of the key quantities in our studies, assuming $|q/p| = 1$:

$$\xi_f^{(q)} = e^{-i\Theta_{M_{12}}^{(q)}} \frac{A(\bar{B}_q^0 \to f)}{A(B_q^0 \to f)}, \quad \xi_{\bar{f}}^{(q)} = e^{-i\Theta_{M_{12}}^{(q)}} \frac{A(\bar{B}_q^0 \to \bar{f})}{A(B_q^0 \to \bar{f})}. \tag{4.17}$$

These observables describe mathematically the interference effects and are convention-independent with

$$\Theta_{M_{12}}^{(q)} = \pi + 2\text{arg}(V_{tq}^* V_{tb}) - \phi_{\text{CP}}(B_q), \tag{4.18}$$

where $\phi_{\text{CP}}(B_q)$ cancels in the amplitude ratio. In addition, starting again from Eqs. (3.16) and (3.17) while utilising Eqs. (3.20)-(3.23)[31], we obtain:

$$\begin{aligned} |g_\pm^{(q)}(t)|^2 &= \frac{1}{4}\left[e^{-\Gamma_{\text{L}}^{(q)}t} + e^{-\Gamma_{\text{H}}^{(q)}t} \pm 2\, e^{-\Gamma_q t}\cos(\Delta m_q t)\right] \\ &= \frac{e^{-\Gamma_q t}}{2}\left[\cosh\frac{1}{2}\Delta\Gamma_q t \pm \cos(\Delta m_q t)\right] \end{aligned} \tag{4.19}$$

[30] We note that neutral kaons and D mesons also show mixing effects between particles and anti-particles and we can also have $|q/p|$ deviating from 1 in these cases.

[31] We note that here we present the formulas for the general case of B_q. Thus, we do not simplify things by assuming only the case of the B_d system, where $\Delta\Gamma_d$ is negligible, as in Eqs. (3.26) and (3.27).

$$g_-^{(q)}(t)\, g_+^{(q)}(t)^* = \frac{1}{4}\left[e^{-\Gamma_{\rm L}^{(q)}t} - e^{-\Gamma_{\rm H}^{(q)}t} + 2\,i\,e^{-\Gamma_q t}\sin(\Delta m_q t)\right]$$
$$= \frac{e^{-\Gamma_q t}}{2}\left[\sinh\frac{1}{2}\Delta\Gamma_q t + i\sin(\Delta m_q t)\right], \tag{4.20}$$

$$g_-^{(q)}(t)^* g_+^{(q)}(t) = \frac{1}{4}\left[e^{-\Gamma_{\rm L}^{(q)}t} - e^{-\Gamma_{\rm H}^{(q)}t} - 2\,i\,e^{-\Gamma_q t}\sin(\Delta m_q t)\right]$$
$$= \frac{e^{-\Gamma_q t}}{2}\left[\sinh\frac{1}{2}\Delta\Gamma_q t - i\sin(\Delta m_q t)\right], \tag{4.21}$$

Combining the above formulas, the decay rate can be written as follows:

$$\Gamma(\overset{(-)}{B}{}_q^0\,(t) \to f) = \left[|g_\mp^{(q)}(t)|^2 + |\xi_f^{(q)}|^2|g_\pm^{(q)}(t)|^2 - 2\,{\rm Re}\left\{\xi_f^{(q)} g_\pm^{(q)}(t) g_\mp^{(q)}(t)^*\right\}\right]\tilde{\Gamma}_f, \tag{4.22}$$

where $\tilde{\Gamma}_f$ denotes the "unevolved" decay rate[32], calculated from $|A|^2$ with the usual phase-space integration.

Now, we keep in mind that the "untagged" decay rates correspond to the average of the decay rate of the B_q^0 going into the final state f and the $\bar{B}_q^0$ decaying into the same final state f. Utilising Eq. (4.22), we obtain:

$$\langle\Gamma(B_q(t) \to f)\rangle \equiv \Gamma(B_q^0(t) \to f) + \Gamma(\bar{B}_q^0(t) \to f)$$
$$\propto \left[\cosh(\Delta\Gamma_q t/2) - \mathcal{A}_{\Delta\Gamma}(B_q \to f)\sinh(\Delta\Gamma_q t/2)\right] e^{-\Gamma_q t}, \tag{4.23}$$

where we mention again that $\Delta\Gamma_s$ is sizeable while $\Delta\Gamma_d \approx 0$. We can now write the time-dependent CP asymmetry as follows:

$$\mathcal{A}_{\rm CP}(t) \equiv \frac{\Gamma(B_q^0(t) \to f) - \Gamma(\bar{B}_q^0(t) \to f)}{\Gamma(B_q^0(t) \to f) + \Gamma(\bar{B}_q^0(t) \to f)}$$
$$= \left[\frac{\mathcal{A}_{\rm CP}^{\rm dir}(B_q \to f)\,\cos(\Delta m_q t) + \mathcal{A}_{\rm CP}^{\rm mix}(B_q \to f)\,\sin(\Delta m_q t)}{\cosh(\Delta\Gamma_q t/2) - \mathcal{A}_{\Delta\Gamma}(B_q \to f)\,\sinh(\Delta\Gamma_q t/2)}\right], \tag{4.24}$$

where we have separated the two types of CP violation. The first one, $\mathcal{A}_{\rm CP}^{\rm dir}$, stands for the direct CP-violating contributions (already introduced in Sec. 4.1). The second part, $\mathcal{A}_{\rm CP}^{\rm mix}$, refers to the interference between the different decay amplitudes coming from the mixing and is called mixing-induced CP violation. The sizeable $\Delta\Gamma_s$ gives access to another observable, the $\mathcal{A}_{\Delta\Gamma}$. Consequently, only in the decay of the B_s^0 meson we get access to the latter observable. So, for the decays of the B_d^0 meson, the time-dependent asymmetry takes the form:

$$\mathcal{A}_{\rm CP}(t) = \mathcal{A}_{\rm CP}^{\rm dir}(B_d \to f)\,\cos(\Delta m_q t) + \mathcal{A}_{\rm CP}^{\rm mix}(B_d \to f)\,\sin(\Delta m_q t), \tag{4.25}$$

[32] Analogous expressions can be written for the CP-conjugate states.

since $\Delta\Gamma_d$ is equal to 0, thereby the denominator in Eq. (4.24) gets equal to 1.

In terms of the $\xi^{(q)}$ observable, these CP asymmetries are written as follows:

$$\mathcal{A}_{\rm CP}^{\rm dir}(B_q \to f) \equiv \frac{|A(B_q^0 \to f)|^2 - |A(\bar{B}_q^0 \to \bar{f})|^2}{|A(B_q^0 \to f)|^2 + |A(\bar{B}_q^0 \to \bar{f})|^2} = \frac{1 - \left|\xi_f^{(q)}\right|^2}{1 + \left|\xi_f^{(q)}\right|^2} \tag{4.26}$$

$$\mathcal{A}_{\rm CP}^{\rm mix}(B_q \to f) \equiv \frac{2\,{\rm Im}\,\xi_f^{(q)}}{1 + \left|\xi_f^{(q)}\right|^2}, \qquad \mathcal{A}_{\Delta\Gamma}(B_s \to f) \equiv \frac{2\,{\rm Re}\,\xi_f^{(s)}}{1 + \left|\xi_f^{(s)}\right|^2}. \tag{4.27}$$

The three observables satisfy the relation:

$$\left[\mathcal{A}_{\rm CP}^{\rm dir}(B_q \to f)\right]^2 + \left[\mathcal{A}_{\rm CP}^{\rm mix}(B_q \to f)\right]^2 + \left[\mathcal{A}_{\Delta\Gamma}(B_q \to f)\right]^2 = 1, \tag{4.28}$$

consequently, they are not independent from each other.

It becomes clear that the quantity $\xi_f^{(q)}$ includes all the necessary information to calculate the asymmetries. Following the definition in Eq. (4.17) and utilising the expressions of the decay amplitudes in Eqs. (4.9) and (4.10), we calculate $\xi_f^{(q)}$ as follows:

$$\xi_f^{(q)} = \mp\, e^{-i\phi_q} \left[\frac{e^{+i\varphi_1}|A_1|e^{i\delta_1} + e^{+i\varphi_2}|A_2|e^{i\delta_2}}{e^{-i\varphi_1}|A_1|e^{i\delta_1} + e^{-i\varphi_2}|A_2|e^{i\delta_2}}\right], \tag{4.29}$$

where the "$\mp$" sign comes from the CP eigenvalue. Let us remind the reader that φ_1, φ_2 are weak phases, δ_1, δ_2 strong phases and $\phi_q = 2\arg(V_{tq}^* V_{tb})$ the B_q^0–$\bar{B}_q^0$ mixing phase. As we have already seen in Eqs. (3.30) and (3.31), we have:

$$\phi_d = +2\beta, \qquad \phi_s = -2\delta\gamma, \tag{4.30}$$

where β and $\delta\gamma$ are related to the UT angles. We note that:

$$e^{-i\phi_{\rm CP}(f)} = \pm 1 \;\; \text{due to Eq. (4.16).} \tag{4.31}$$

We mention that an analogous methodology can be applied for decays where the final state is not a CP-eigenstate but again both the B_q^0 and $\bar{B}_q^0$ mesons decay into the same final state f. Prime example in this case is the $B_s \to D_s^{\pm} K^{\mp}$ system, which we will study in detail in Chapter 6.

What do we learn from Eq. (4.29)?

In order to determine the CP asymmetries, we have to calculate the observable in Eq. (4.29). Still discussing the formalism in the SM framework, in this equation, CP-violating phases φ_1 and φ_2 enter, which come from complex phases in the CKM matrix elements. The $|A_1|e^{i\delta_1}$ and $|A_2|e^{i\delta_2}$ quantities encode the hadronic matrix elements, suffering from hadronic

uncertainties. So, examining Eq. (4.29), we observe that if there is only one amplitude, for instance $|A_1|$, while the other amplitude (i.e., the $|A_2|$) vanishes, we obtain:

$$\xi_f^{(q)} = \mp\, e^{-i\phi_q} \left[\frac{e^{+i\phi_f/2}|M_f|e^{i\delta_f}}{e^{-i\phi_f/2}|M_f|e^{i\delta_f}}\right] = \mp\, e^{-i(\phi_q-\phi_f)}. \tag{4.32}$$

Thus, the hadronic matrix element $|M_f|e^{i\delta_f}$ fully cancels in this equation and we are only left with the difference of the decay phases and the ϕ_q. No hadronic uncertainties remain. In this case, the criteria for direct CP violation given in Sec. 4.1 are no longer satisfied, and as a result $\mathcal{A}_{\rm CP}^{\rm dir}$ vanishes:

$$\mathcal{A}_{\rm CP}^{\rm dir}(B_q \to f) = 0. \tag{4.33}$$

The mixing-induced CP asymmetry is the only one that survives:

$$\mathcal{A}_{\rm CP}^{\rm mix}(B_q \to f) = \pm \sin(\phi_q - \phi_f) = \pm \sin\phi, \tag{4.34}$$

where ϕ is the CP-violating weak phase difference that governs the asymmetry. We emphasize that $\mathcal{A}_{\rm CP}^{\rm mix}$ is free from hadronic uncertainties. Consequently, the time-dependent CP asymmetry given in Eq. (4.24) takes the following form for $\Delta\Gamma_q = 0$:

$$\mathcal{A}_{\rm CP}(t) = \pm \sin\phi\, \sin(\Delta M_q t). \tag{4.35}$$

The best setting for studying this special case is provided by the $B^0 \to J/\psi K_S$ decay, which we will explicitly discuss in Chapter 5. Another instructive example is the $B_d^0 \to \pi^+\pi^-$, which we will discuss below.

Concluding, the main message is that if the decay is dominated by only one CKM amplitude, all the hadronic contributions would cancel out and the direct CP violation would vanish. Then, only the mixing induced CP asymmetry is left, which would be a clean observable.

4.2.3 Application: Extraction of the UT Angle α

Let us discuss an interesting application of the analysis of the CP asymmetries through the $B_d^0 \to \pi^+\pi^-$ decay. This channel is characterised by colour-allowed trees, which give the leading contributions, but also include penguin corrections. An illustration of the corresponding topologies is given in Fig. 23. The final state of this channel is a CP-even eigenstate, thus its CP-eigenvalue is equal to +1.

The decay amplitude is written as [179, 180]:

$$A(B_d^0 \to \pi^+\pi^-) = \lambda_u^{(d)} \left(A_{\rm cc}^u + A_{\rm pen}^u\right) + \lambda_c^{(d)} A_{\rm pen}^c + \lambda_t^{(d)} A_{\rm pen}^t\,, \tag{4.36}$$

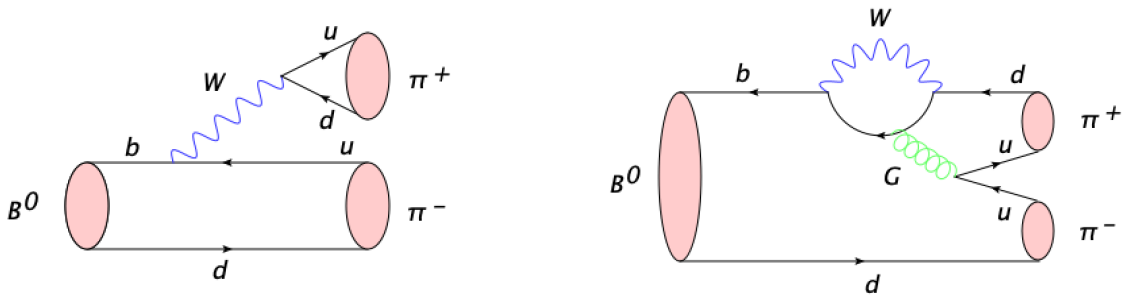

(a) (b)

Figure 23: Colour-allowed tree (left) and penguin (right) topologies for the $B_d^0 \to \pi^+\pi^-$ decay.

where $\lambda_j^{(d)} \equiv V_{jd}V_{jb}^*$ are the CKM factors with $j \in \{u, c, t\}$, the $A_{\rm cc}^u$ denotes the amplitude from the "current–current" contributions while the $A_{\rm pen}^j$ indicate the "penguin" amplitudes. All three CKM factors are of the same order in λ (specifically $\mathcal{O}(\lambda^3)$). In contrast to the colour-allowed trees, the QCD penguins amplitudes, as loop processes, are suppressed with respect to the tree, so we expect them to be smaller[33]. Using the unitarity relation between the CKM factors:

$$V_{td}V_{tb}^* = -V_{ud}V_{ub}^* - V_{cd}V_{cb}^*, \tag{4.37}$$

we can eliminate one factor:

$$\lambda_t^{(d)} = -\lambda_u^{(d)} - \lambda_c^{(d)}, \tag{4.38}$$

thereby simplifying the amplitude equation:

$$A(B_d^0 \to \pi^+\pi^-) = \lambda_u^{(d)}\left(A_{\rm cc}^u + A_{\rm pen}^u - A_{\rm pen}^t\right) + \lambda_c^{(d)}\left(A_{\rm pen}^c - A_{\rm pen}^t\right) . \tag{4.39}$$

Then the term referred as "tree" is:

$$T = \lambda_u^{(d)}\left(A_{\rm cc}^u + A_{\rm pen}^u - A_{\rm pen}^t\right) , \ ^{34} \tag{4.40}$$

while the "penguin" term is:

$$P = \lambda_c^{(d)}\left(A_{\rm pen}^c - A_{\rm pen}^t\right) , \tag{4.41}$$

[33] How small they are is a challenge related to QCD and we will not elaborate more on this topic. We only mention that using factorisation, it can be estimated that penguins are at the level of 20% of the tree.

[34] For completeness, we mention that the current-current operators $A_{\rm cc}^u$ include both tree and exchange contributions.

As a result, we can rewrite the decay amplitude as [181, 182]:

$$A(B^0 \to \pi^+\pi^-) = T + P \tag{4.42}$$

$$= |T|e^{i\delta^T}e^{i\gamma} + |P|e^{i\delta^P} \tag{4.43}$$

$$= |T|e^{i\delta^T}\left(e^{i\gamma} + re^{i\delta}\right) \ , \tag{4.44}$$

where we factored out the weak phase $\gamma = \arg\left(-V_{ud}V_{ub}^*/V_{cd}V_{cb}^*\right)$, introduced $r = |P|/|T|$ and used $\delta \equiv \delta^P - \delta^T$ for the strong phases.

The time-dependent CP asymmetry is given by [180, 183]:

$$\begin{aligned}\mathcal{A}_{\rm CP}(t)(B_d \to \pi^+\pi^-) &\equiv \frac{\Gamma(B_d^0(t) \to \pi^+\pi^-) - \Gamma(\bar{B}_d^0(t) \to \pi^+\pi^-)}{\Gamma(B_d^0(t) \to \pi^+\pi^-) + \Gamma(\bar{B}_d^0(t) \to \pi^+\pi^-)} \\ &= \mathcal{A}_{\rm CP}^{\rm dir}\cos(\Delta m_d t) + \mathcal{A}_{\rm CP}^{\rm mix}\sin(\Delta m_d t) \ . \end{aligned} \tag{4.45}$$

Let us firstly recall the quantity ξ, which encodes all the necessary information. Following Refs. [179, 184] and with the amplitude given in Eqs. (4.44) we have:

$$\xi^{(d)}_{\pi^+\pi^-} = -e^{-i\phi_d}\frac{A(\bar{B}^0 \to \pi^+\pi^-)}{A(B^0 \to \pi^+\pi^-)} \tag{4.46}$$

$$= -e^{-i\phi_d}\left[\frac{e^{-i\gamma} + re^{i\delta}}{e^{i\gamma} + re^{i\delta}}\right], \tag{4.47}$$

where γ has flipped its sign in $A(\bar{B}^0 \to \pi^+\pi^-)$. Due to the interference between trees and penguins we could get a direct CP asymmetry. These parameters also enter the mixing-induced CP asymmetry.

We observe though that if we neglect the penguin contributions, which are loop suppressed[35] and assume that the decay is fully dominated by the colour-allowed tree topology, the situation becomes simpler. Then the $\xi^{(d)}_{\pi^+\pi^-}$ gets the form:

$$\xi^{(d)}_{\pi^+\pi^-} = e^{-i\phi_d}e^{-2i\gamma} = -e^{-i(\phi_d+2\gamma)} \tag{4.48}$$

where the hadronic amplitudes cancel. We note that in the SM $\phi_d = 2\beta$. Key relation[36] here is:

$$\phi_d + 2\gamma = -2\alpha \ , \tag{4.49}$$

[35] As mentioned earlier, a generic estimate suggests that the penguin contributions are up to 20% of the tree contributions.

[36] For completeness, we mention that in the most general case, we allow also for NP effects and we have:

$$\phi_d + 2\gamma = \phi_d^{\rm NP} - 2\alpha$$

Here, we discuss things in the SM, thus we assume that $\phi_d^{\rm NP} = 0$.

which is commonly reported as a measurement of the CKM angle α. Regarding the CP asymmetries then we obtain:

$$\mathcal{A}_{\rm CP}^{\rm dir} = \frac{1 - \left|\xi^{(d)}_{\pi^+\pi^-}\right|^2}{1 + \left|\xi^{(d)}_{\pi^+\pi^-}\right|^2} \approx 0, \qquad \mathcal{A}_{\rm CP}^{\rm mix} = \frac{2\,{\rm Im}\,\xi^{(d)}_{\pi^+\pi^-}}{1 + \left|\xi^{(d)}_{\pi^+\pi^-}\right|^2} \approx -\sin(2\alpha). \tag{4.50}$$

As a result, we write the time-dependent CP asymmetry in the following form

$$\mathcal{A}_{\rm CP}(t)(B_d \to \pi^+\pi^-) = -\sin(2\alpha)\sin(\Delta m_d\, t), \tag{4.51}$$

which allows the α determination since $\sin(2\alpha)$ can be measured.

However, penguins do contribute. So, it is important to take them into account and the question is how big these penguin contributions are. Interestingly, using isospin relations, the penguin corrections can be included. Thus, we write the isospin relations[37] [185, 186]:

$$\sqrt{2}A(B^+ \to \pi^+\pi^-) = A(B_d^0 \to \pi^+\pi^-) + \sqrt{2}A(B_d^0 \to \pi^0\pi^0). \tag{4.52}$$

This allows the determination of α. A similar relation holds also for the CP-conjugate modes. We note that this strategy has experimentally been applied to $B \to \pi\pi$ and in a similar way can be applied to $B \to \rho\pi$ and $B \to \rho\rho$ and even a combination can be utilised for obtaining α. The latest experimental determination is given as follows [187]

$$\alpha = (85.2^{+4.8}_{-4.3})^\circ\,. \tag{4.53}$$

We emphasize that it is important that we have determined the angle α for one more reason; this value can also be used in order to obtain γ. To do this, we convert this result, thus the $\phi_d + 2\gamma$ into a γ value. Let us discuss this in the coming Section.

4.3 Summary Thread: Different Ways of Determining γ

The CKM angle γ plays a major role in our analysis. In order to prepare the setting, we provide here an overview of different γ determinations. We have already presented in Eq. (3.69) the value which we utilise for the UT apex extraction and which will be used in our analyses, especially when information relevant to the UT apex is required. Let us now give more information on how we obtain this result.

[37] We will explicitly discuss the isospin relations of the $B \to \pi\pi$ system and the corresponding amplitude parametrization in Chapter 7.

Pure Tree $B_s^0 \to D_s^\mp K^\pm$ Decays

Traditionally, for the determinations of γ, pure level tree decays of the kind $B \to DK$ have been in the focus. Particularly interesting transitions, falling into this category, is the $B_s^0 \to D_s^\mp K^\pm$ system. A detailed analysis of these decays is provided in Chapter 6, as they play central role in our studies for this thesis. However, for completeness, we also briefly address the topic here. Due to the B_s^0–$\bar{B}_s^0$ mixing phenomenon, interference effects arise between these decay channels, leading to a time-dependent rate asymmetry. The corresponding observables of this asymmetry allow a theoretically clean determination of $\phi_s + \gamma$, where ϕ_s is a $B_s^0 - \bar{B}_s^0$ mixing phase. As this phase can be determined through the decay $B_s^0 \to J/\psi\phi$, even in the presence of NP contributions in $B_s^0 - \bar{B}_s^0$ mixing, we can actually extract γ. These decays historically are considered to be very robust with respect to NP but we have now reached the level of precision where we start seeing puzzling patterns.

LHCb reported a surprisingly large value of the angle γ of the UT[38], making a convoluted analysis in the $B_s^0 \to D_s^\mp K^\pm$ system [189]. In order to gain a better understanding of this result, a transparent analysis of the corresponding CP asymmetries has been performed [115,190]. Paying also special attention to discrete ambiguities, the LHCb picture has been confirmed. Updating the value of $\phi_s = \left(-5^{+1.6}_{-1.5}\right)^\circ$, including penguin corrections in the $B_s^0 \to J/\psi\phi$ modes [191], the LHCb result shifts to the value [115,190]:

$$\gamma_{B_s \to D_s K} = \left(131^{+17}_{-22}\right)^\circ , \tag{4.54}$$

which is in tension with the regime of 70°. This value would require NP contributions at the decay amplitude level. Even though, so far, we have focused on SM studies, for completeness here, we give a few details regarding NP searches. In the presence of NP, the UT angle γ enters as an effective angle, so Eq. (4.54) can be written as

$$\gamma_{\text{eff}} \equiv \gamma + \delta\gamma_{\text{NP}}, \tag{4.55}$$

where γ is the CKM value while $\delta\gamma_{\text{NP}}$ refers to the NP part. Investigating branching ratios of individual modes, as discussed in [115,190], puzzling patterns arise also at the branching ratio level, which one would expect if there is NP entering at the decay amplitude level. Complementing the analysis with decays with similar dynamics, consistent patterns are found, making the intriguing situation even more exciting. In Ref. [115,190] a model independent strategy has been presented, describing that data can be accommodated with NP

[38] A new measurement was recently reported by LHCb [188]. This new result only uses Run II data and has not been included in the world average yet, so we will not use it in our analysis. However, it is very interesting to explore further. We point out, as we will also see in detail in Chapter 6, that the main points arising from our $B_s \to D_s K$ studies and the strategies we propose, especially regarding NP studies, still hold and provide very useful insights.

contributions at the level of 30% of the SM amplitudes. We note that model-dependent studies have also been discussed in Refs. [192–194].

Pure Tree $B \to DK$ Decays

Even though these $B_s^0 \to D_s^\mp K^\pm$ studies are recent developments, the $B \to DK$ tree transitions through various time-independent studies are key modes for γ determinations [195, 196]. In the latter case, direct CP violation is utilised while the interference effects are different from the $B_s^0 \to D_s^\mp K^\pm$ system, where mixing-induced CP-violation plays the central role. The latest average from the LHCb collaboration of γ coming from time-independent analyses of $B^+ \to D^{(*)}h^+$ and $B^0 \to Dh$ decays only, where h is pion, kaon or K^*, is [197] [39]

$$\gamma_{B\to DK} = (64.9^{+3.9}_{-4.5})^\circ \, . \tag{4.56}$$

In principle, this value could also have a NP component. NP would enter differently as there are topologies, like color-suppressed modes, that do not contribute to the $B_s^0 \to D_s^\mp K^\pm$ system and the sensitivity on γ now arises from different interference effects. In such a simultaneous fit to a variety of B decays, NP effects may be averaged out, thus resulting in an effective angle that can not be quantified. In order to better understand what happens in these modes, it would be important to have individual measurements of the different modes aiming to perform them with highest precision, instead of making averages.

Decays Involving Penguins: $B \to \pi\pi,\ \rho\pi,\ \rho\rho$

The other interesting system which can be used is provided by $B \to \pi\pi,\ \rho\pi,\ \rho\rho$ modes [185, 199]. The sensitivity to γ, specifically referring to the $B^0 \to \pi^+\pi^-$ decay, which we will later use in our analysis of the $B \to \pi K$ system, comes from mixing-induced CP violation [200]. In this case, we determine α from an isospin analysis, as discussed above, and we convert its value into γ through Eq. (4.48). The ϕ_d value, which is measured in the $B_d^0 \to J/\psi K^0$ channel and corrected for contributions from penguin topologies, is given as follows [191, 201]:

$$\phi_d = \left(44.4^{+1.6}_{-1.5}\right)^\circ \, . \tag{4.57}$$

Combining the result for $\phi_d + 2\gamma$ in Eq. (4.53) with the measurement of ϕ_d in Eq. (4.57), we find the value:

$$\gamma_{\rm iso} = (72.6^{+4.3}_{-4.9})^\circ \, , \tag{4.58}$$

[39] LHCb Collaboration performs such γ measurements using self-tagging charged or neutral decays. For more details, the reader is referred to Refs. [197, 198].

which could be affected by possible NP at the amplitudes through penguin topologies[40].

Other Useful Modes Including Penguins: $B_s \to K^+K^-$, $B_d \to \pi^+\pi^-$

In addition, we mention that there is another interesting way of extracting the angle γ, proposed in Ref. [202, 203]. This strategy utilises the U-spin symmetry and combines the direct and the mixing-induced CP asymmetries of the $B_d \to \pi^+\pi^-$ modes with the penguin-dominated $B_s \to K^+K^-$ decay[41] without relying on information from the branching ratios. The result:

$$\gamma = (65^{+11}_{-7})^\circ, \tag{4.59}$$

agrees excellently with the γ values from the $B \to DK$ decays. In our numerical analysis, and due to the dynamics of the $B_s \to K^+K^-$ decay, we will not explore further this value.

Final Average Value of γ Utilised in our Numerical Analysis

We note that the two γ determinations in Eqs. (4.56) and (4.58), which have different origin, are consistent within 1.1 standard deviations. We also see that both approaches have similar precision. This allows us to average the two results yielding the value that we already presented in Eq. (3.69). For completeness, we repeat it here:

$$\gamma_{\rm avg} = (68.4 \pm 3.3)^\circ. \tag{4.60}$$

However, we highlight that in the future, with improved precision, differences between the two approaches might become more significant. Then using an averaged value will no longer be justified, as these deviations might hint NP.

[40] We mention that the penguins are the preferred avenue for NP. However, in principle, NP could also enter through the tree topologies.

[41] LHCb recently reported the first observation of CP violation in the $B_s \to K^+K^-$ decay, suggesting significant differences in the direct asymmetries between the $B^0_d \to \pi^+\pi^-$ and $B^0_s \to K^-\pi^+$ as well as the $B^0_s \to K^-K^+$ and $B^0_d \to \pi^-K^+$ modes.

4.4 Closing Remarks

CP violation plays a very important role in the B system studies. So far, we have provided the formalism within the SM framework. The various types of CP violation can be classified as follows [204]:

- **CP violation in decay**
  This type of CP violation refers to the case where the rate of a B meson decaying into a final state f is different from the rate of the $\bar{B}$ (anti-B) decaying into the CP conjugate final state $\bar{f}$. As we had already mentioned, the neutral B mesons are characterised by the mixing phenomenon while in charged mesons there is no mixing. Therefore, this case is the only type of CP violation that can occur in both charged and neutral mesons.

- **CP violation in mixing**
  This type refers only to the neutral B mesons. In the SM, it is very small and experimentally strongly constrained, so in the following these effects will not be considered.

- **CP violation coming through the interference provided by B_q^0–$\bar{B}_q^0$ mixing**
  This case again refers only to neutral mesons. It corresponds to cases where both B^0 and $\bar{B}^0$ decay into the same final state.

Non-leptonic decays play the key role for studying CP violation in the SM because of interference effects that arise. We have decays that despite the challenge to calculate the hadronic matrix elements, allow us to test the SM descripion of CP violation in a very clean way. There are transitions where these hadronic matrix elements either exactly cancel out or to a very good approximation. There are two options [205]:

- ◇ either we use amplitude relations to eliminate the hadronic matrix elements. In this case, exact relations utilising pure tree decays (i.e. $B^\pm \to K^\pm D$ modes) are distinguished from relations arising from flavour symmetries of strong interactions, such as $B_q \to \pi\pi, \pi K, KK$ decays

- ◇ or in the case of neutral B_q mesons, mixing-induced CP violation may arise from interference effects between mixing and decay. If there is only a single CKM amplitude dominating the decay, the hadronic matrix elements cancel in the CP asymmetries. Benchmark decay here is the $B_d^0 \to J/\psi K_S$ channel, which we will study in detail in the subsequent Chapter.

In the next Chapters, we will utilise benchmark decays that will help us to further explore the topic not only within the SM but also in searches of NP.

Intermezzo: CP Violation Roadmap

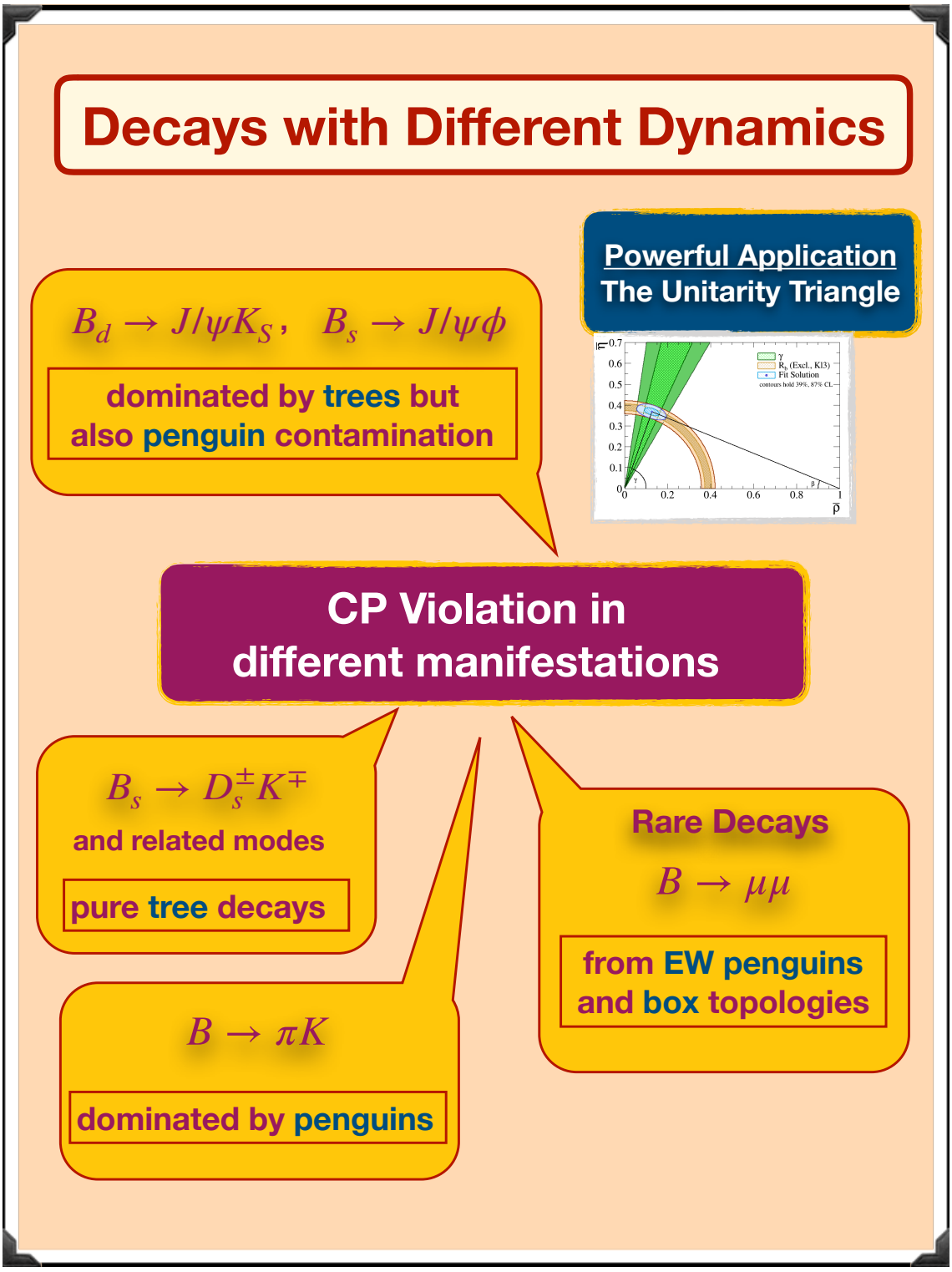

5 $B_d^0 \to J/\psi K_S^0$, $B_s^0 \to J/\psi\phi$: Penguins & New Physics in B_q^0–$\bar{B}_q^0$

Having discussed the concept of CP violation in B mesons and introduced $B_{(s)}^0$–$\bar{B}_{(s)}^0$ mixing within the SM, we can now study applications of this phenomena and explore effects of NP. Key decays for this endeavour are the $B_d^0 \to J/\psi K_S^0$ and $B_s^0 \to J/\psi\phi$ modes. Historically, these channels have received a lot of attention and are considered to be the "golden modes" for CP violation in B decays.

A problem that we encounter with these two decays is that the corresponding expressions include doubly Cabibbo suppressed terms, which are difficult to calculate. Prime quantities associated with mixing phenemona characterising these channels are the mixing phases ϕ_d and ϕ_s. Therefore, we have to pay special attention in their determination. In order to deal with the penguin effects in the determination of the mixing phases, we propose a formalism that employs the $SU(3)$ flavour symmetry and utilises CP violation measurements. This formalism will be applied to the data leading to the current results for the mixing phases and the penguin parameters. These results will be combined with information from branching ratios, allowing us to determine the hadronic parameters. A new strategy is suggested, which relies on information from semileptonic decays and provides factorisation tests in the corresponding colour-suppressed decays.

Our next goal is to explore how much space for NP is left through the current available data. Since the knowledge of the UT apex is needed in our analysis, we will utilise the results of the UT studies in Sec. 3.4.2, highlighting again the importance of studying separately the inclusive and exclusive determinations. Considering NP scenarios and performing future projections, we will discuss the impact of improved precision on key input quantities. This chapter is based on our work presented on Refs. [81, 124, 191, 201, 206, 207].

5.1 Setting the Stage

The decays $B_d^0 \to J/\psi K_S^0$ and $B_s^0 \to J/\psi\phi$, caused by $\bar{b} \to \bar{c}c\bar{s}$ quark level transitions, are dominated by colour-suppressed tree diagrams but they also receive contributions from penguin topologies, which are doubly Cabibbo suppressed. The topologies that characterise these two systems are illustrated in Fig. 24. We note, here, that the $B_s^0 \to J/\psi\phi$ mode receives also contributions from exchange and penguin-annihilation topologies but as they are expected to be small, we neglect them in our analysis.

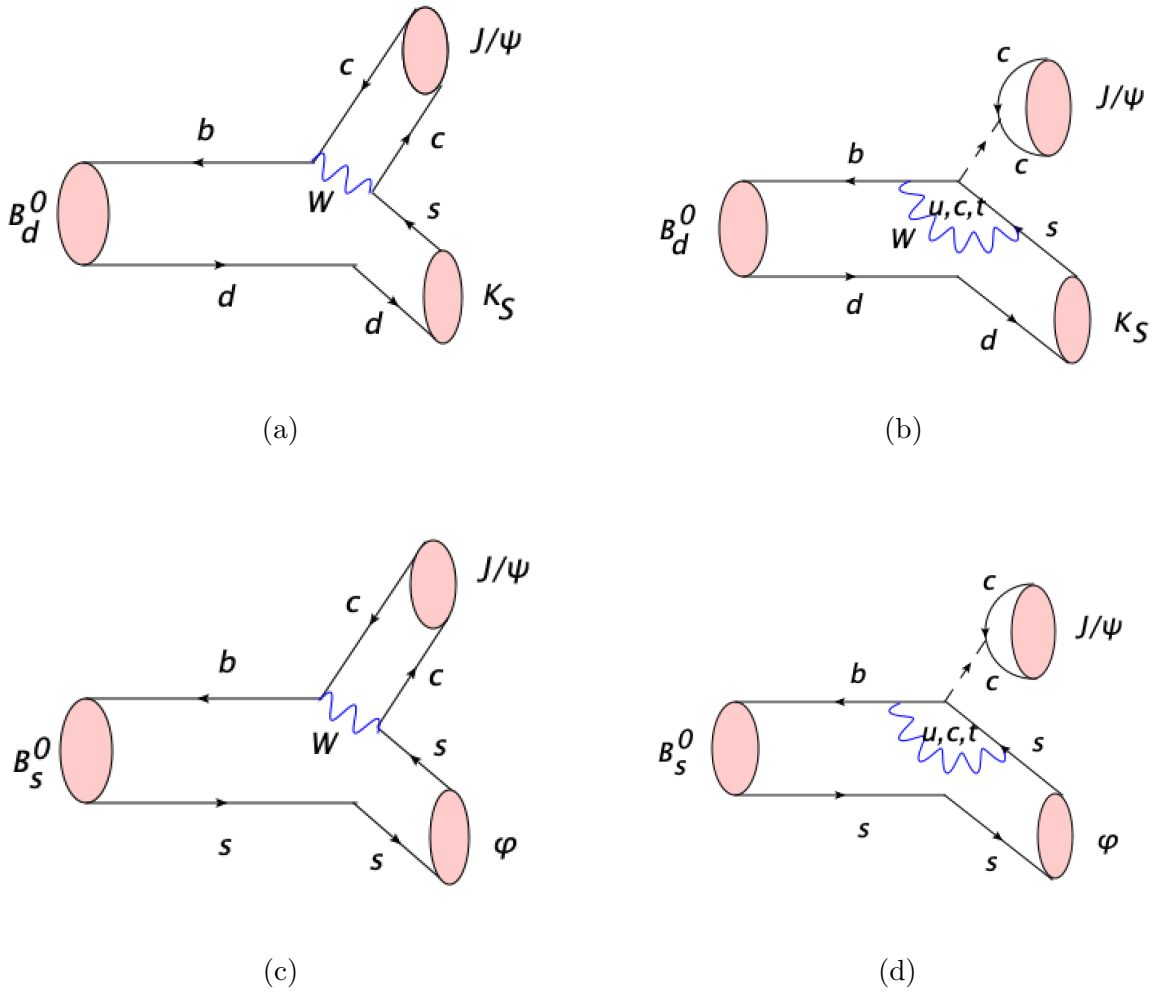

Figure 24: Topologies characterising the golden modes: (a) Colour-suppressed tree topology for $B_d^0 \to J/\psi K_S^0$ decay, (b) penguin topology for $B_d^0 \to J/\psi K_S^0$ decay: doubly Cabibbo suppressed, (c) colour-suppressed tree topology for $B_d^0 \to J/\psi\phi$ decay and (d) penguin topology for $B_d^0 \to J/\psi\phi$ decay: doubly Cabibbo suppressed.

5.1.1 Decay Amplitudes

Having introduced the Feynman diagrams for the channels we are interested in, we can write the decay amplitudes for these modes. Firstly, we work with the $B_d \to J/\psi K_S^0$, which is a decay into a CP eigenstate with eigenvalue -1. Within the SM, we write [208]:

$$A(B_d^0 \to J/\psi\, K_S^0) = \lambda_c \left(A_{\rm tree}^{c'} + A_{\rm pen}^{c'} \right) + \lambda_u A_{\rm pen}^{u'} + \lambda_t A_{\rm pen}^{t'}\,, \tag{5.1}$$

where $A_{\rm tree}$ refers to the tree contributions while $A_{\rm pen}$ describes the penguin topologies with internal quarks c, u, t respectively. We note here, that keeping the notation of Ref. [208], the primes are used to denote the $\bar{b} \to \bar{c}c\bar{s}$ transitions. The terms λ_q, with q standing again for c, u, t quarks are the usual CKM factors $\lambda_q \equiv V_{qs}V_{qb}^*$: We can eliminate λ_t,[42] using the unitarity of the CKM matrix and applying the Wolfenstein parametrization [69], we obtain the following expression for the decay amplitude[43] [191, 208]:

$$A\left(B_d^0 \to J/\psi\, K_{\rm S}\right) = \left(1 - \frac{\lambda^2}{2}\right)\mathcal{A}'\left[1 + \epsilon a' e^{i\theta'}e^{i\gamma}\right]\,. \tag{5.2}$$

This is a general parametrization of the decay amplitude in the SM. Here, $\mathcal{A}'$ is the hadronic amplitude while $a'e^{i\theta'}$ denotes the penguin parameter and they can be written with the help of the tree and the penguin topologies as [191, 208]:

$$\mathcal{A}' \equiv \lambda^2 A\left(A_{\rm tree}^{c'} + A_{\rm pen}^{c'} - A_{\rm pen}^{t'}\right), \tag{5.3}$$

$$a'e^{i\theta'} \equiv R_b\left(\frac{A_{\rm pen}^{u'} - A_{\rm pen}^{t'}}{A_{\rm tree}^{c'} + A_{\rm pen}^{c'} - A_{\rm pen}^{t'}}\right), \tag{5.4}$$

where $A \equiv |V_{cb}|/\lambda^2$, and R_b the UT side.The factor ϵ suppresses the contributions from the penguin topologies and is written in terms of the Wolfenstein parameter λ as [191]:

$$\epsilon \equiv \frac{\lambda^2}{1-\lambda^2} = 0.05238 \pm 0.00035\,, \tag{5.5}$$

where the numerical value is based on the measurement of the Flavour Lattice Averaging Group (FLAG) of the CKM element $|V_{us}| = 0.2231 \pm 0.0007$ [209]. Therefore, we see that the quantity $a'e^{i\theta'}$ enters in a doubly Cabibbo-suppressed way.

Ignoring the time evolution, the "unevolved" transition amplitudes of the neutral B meson decays into a CP final eigenstate f can be expressed in a compact way as follows [208, 210]:

$$A(B_q^0 \to f) \equiv \quad \mathcal{N}_f\left[1 - b_f e^{i\rho_f}e^{+i\gamma}\right]\,, \tag{5.6}$$

$$A(\bar{B}_q^0 \to f) \equiv \eta_f\mathcal{N}_f\left[1 - b_f e^{i\rho_f}e^{-i\gamma}\right]\,, \tag{5.7}$$

[42] We utilise the relation [99]

$$V_{ur}^*V_{ub} + V_{cr}^*V_{cb} + V_{tr}^*V_{tb} = 0 \quad (r \in \{d, s\}),$$

as we already introduced earlier in Chapter 2.

[43] Here, the amplitude has been written for the K_S final state, neglecting CP violation in the neutral kaon system.

where η_f is the CP-eigenvalue of the f final state, $\mathcal{N}_f$ is a normalisation factor for which we have the following substitution:

$$\mathcal{N}_f \to \left(1 - \frac{\lambda^2}{2}\right) \mathcal{A}' \,, \tag{5.8}$$

while b_f shows the relative contribution of penguins with respect to tree contributions, ρ_f is the CP-conserving strong phase while γ is the weak phase and we have:

$$b_f e^{i\rho_f} \to -\epsilon a' e^{i\theta'}. \tag{5.9}$$

The same holds for the B_s^0-meson counterpart of the $B_d^0 \to J/\psi K_S$ decay, which is the $B_s^0 \to J/\psi\phi$ channel, arising from replacing the down spectator quark by a strange quark. The difference is that now we have two vector mesons in the final state, therefore there is an admixture of different CP eigenstates. The system can be described with three polarization states: the CP-even 0 and $\|$ eigenstates and the CP-odd $\perp$ eigenstates. Therefore, the system has more complicated dynamics as the hadromic parameters depend on the final state configuration. The decay amplitude though is completely analogous to Eq. (5.2), so it is written as [210–212]:

$$A\left(B_s^0 \to (J/\psi\phi)_f\right) = \left(1 - \frac{\lambda^2}{2}\right) \mathcal{A}'_f \left[1 + \epsilon a'_f e^{i\theta'_f} e^{i\gamma}\right] \,, \tag{5.10}$$

where f refers to the different configurations $\{0, \|, \perp\}$ of the final state of the vector meson. We note that, in principle, the $\mathcal{A}'_f$ amplitude and the a'_f, θ'_f penguin parameters should be considered for each polarisation state f individually. Applying naive factorisation for the hadronic matrix elements, the penguin parameters do not depend on the final-state configuration f [210]. In the remainder of the text, we label the penguin parameters of this vector–vector decay channel as a'_V and θ'_V. Here, we focus on polarisation-independent measurements in the analysis of the current data, following the experimental analyses of CP violation in these channels. It would be important in the future measurements to have also a polarisation-dependent analysis.

5.1.2 The CP Asymmetries in $B_{(s)}^0 \to J/\psi X$ System

The three asymmetries, defined in Sec. 4.2, depend on the penguin parameters b_f and ρ_f, as well as the B_q^0–$\bar{B}_q^0$ mixing phase ϕ_q as follows [210]:

$$\mathcal{A}_{\rm CP}^{\rm dir}(B_q \to f) = \frac{2b_f \sin\rho_f \sin\gamma}{1 - 2b_f \cos\rho_f \cos\gamma + b_f^2}\,, \tag{5.11}$$

$$\eta_f \mathcal{A}_{\rm CP}^{\rm mix}(B_q \to f) = \left[\frac{\sin\phi_q - 2b_f \cos\rho_f \sin(\phi_q+\gamma) + b_f^2 \sin(\phi_q+2\gamma)}{1 - 2b_f \cos\rho_f \cos\gamma + b_f^2}\right] \tag{5.12}$$

$$\eta_f \mathcal{A}_{\Delta\Gamma}(B_q \to f) = -\left[\frac{\cos\phi_q - 2b_f \cos\rho_f \cos(\phi_q+\gamma) + b_f^2 \cos(\phi_q+2\gamma)}{1 - 2b_f \cos\rho_f \cos\gamma + b_f^2}\right]\,, \tag{5.13}$$

where η_f is the CP eigenvalue of the final state f.

5.1.3 Dictionary for CP Violating Phases

The CP-violating phase ϕ_q is experimentally accessible through the CP asymmetry arising from the interference of the B_q^0–$\bar{B}_q^0$ mixing and the decay processes of B_q to the final CP eigenstate f. It can be written as:

$$\phi_q \equiv \phi_q^{\rm SM} + \phi_q^{\rm NP}, \tag{5.14}$$

where $\phi_q^{\rm SM}$ denotes the SM part which is determined with the UT and $\phi_q^{\rm NP}$ describes contributions from potential new sources of CP violation lying beyond the SM. However, due to the presence of the doubly Cabibbo suppressed penguin topologies, the mixing-induced CP asymmetry allows us to measure an effective phase $\phi_{q,f}^{\rm eff}$ which is connected to ϕ_q through:

$$\phi_{q,f}^{\rm eff} = \phi_q + \Delta\phi_q^f, \tag{5.15}$$

where $\Delta\phi_q^f$ is a hadronic phase shift. This phase shift is a function of the penguin parameters a and θ and it measures the ratio of the penguin over tree contributions. It is decay-channel specific and it arises from non-perturbative, strong interaction effects. Therefore, it shows the impact of penguins on the effective mixing phases. If there were only contributions from tree topologies, we would get $\Delta\phi_q^f = 0$. Since there are contributions from the doubly Cabibbo suppressed penguins, the hadronic phase shift $\Delta\phi_q^f$ is of the order of 0.5° [208, 211, 213–219].

Starting from the quantity [211, 212]:

$$\sin\left(\phi_{q,f}^{\rm eff}\right) \equiv \frac{\eta_f \mathcal{A}_{\rm CP}^{\rm mix}(B_q \to f)}{\sqrt{1 - \left(\mathcal{A}_{\rm CP}^{\rm dir}(B_q \to f)\right)^2}} = \sin\left(\phi_q + \Delta\phi_q^f\right), \tag{5.16}$$

which allows the determination of the effective mixing phase experimentally, and utilising Eqs. (5.11) and (5.12), we obtain:

$$\sin\Delta\phi_q^f = \frac{-2b_f\cos\rho_f\sin\gamma + b_f^2\sin 2\gamma}{\left(1-2b_f\cos\rho_f\cos\gamma+b_f^2\right)\sqrt{1-\left(\mathcal{A}_{\rm CP}^{\rm dir}(B\to f)\right)^2}}\,, \tag{5.17}$$

$$\cos\Delta\phi_q^f = \frac{1-2b_f\cos\rho_f\cos\gamma + b_f^2\cos 2\gamma}{\left(1-2b_f\cos\rho_f\cos\gamma+b_f^2\right)\sqrt{1-\left(\mathcal{A}_{\rm CP}^{\rm dir}(B\to f)\right)^2}}\,. \tag{5.18}$$

Here, we have allowed for the penguin effects, i.e. $b_f \neq 0$. These relations yield

$$\tan\Delta\phi_q^f = -\left[\frac{2b_f\cos\rho_f\sin\gamma - b^2\sin 2\gamma}{1-2b_f\cos\rho_f\cos\gamma+b_f^2\cos 2\gamma}\right]\,. \tag{5.19}$$

We highlight that in the case there is no doubly Cabibbo-suppressed penguin contributions, i.e. $b_f = 0$, the expressions of the CP asymmetries would take the simplified form

$$\mathcal{A}_{\rm CP}^{\rm dir} = 0\,, \qquad \eta_f\mathcal{A}_{\rm CP}^{\rm mix} = \sin\phi_q\,, \tag{5.20}$$

therefore, the ϕ_q would be determined directly from the mixing-induced CP asymmetry. However, when allowing for the penguin effects, additional information is needed in order to correctly interpret the experimental measurements and determine the mixing phase ϕ_q, distinguishing these phases from the effective ones.

5.1.4 Branching Ratio

An interesting observable to work with, after having determined the decay amplitudes, is the branching ratio. Working with the $B_s \to J/\psi K_{\rm S}^0$ channel, the experimental time-integrated untagged rate is written as [220]:

$$\begin{aligned}\mathcal{B}(B_s\to J/\psi K_{\rm S}^0) &\equiv \frac{1}{2}\int_0^\infty \langle\Gamma(B_s(t)\to J/\psi K_{\rm S}^0)\rangle dt \\ &= \frac{1}{2}\int_0^\infty \left[\Gamma(B_s^0(t)\to J/\psi K_{\rm S}^0) + \Gamma(\bar{B}_s^0(t)\to J/\psi K_{\rm S}^0)\right] dt.\end{aligned} \tag{5.21}$$

The "theoretical" branching ratio is defined by the untagged decay rate at a decay time $t = 0$ [208]. The conversion relation between the experimental and the theoretical branching ratio for this channel is written as [221]:

$$\mathcal{B}\left(B_s\to J/\psi K_{\rm S}^0\right)_{\rm theo} = \left[\frac{1-y_s^2}{1+\mathcal{A}_{\Delta\Gamma}(B_s\to J/\psi K_{\rm S}^0)\,y_s}\right]\mathcal{B}\left(B_s\to J/\psi K_{\rm S}^0\right)\,. \tag{5.22}$$

We the determine the observable $\mathcal{A}_{\Delta\Gamma}(B_s \to J/\psi K_{\rm S}^0)$, thus we fix the conversion factor utilising the effective lifetime [221]:

$$\tau^{\rm eff}_{J/\psi K_{\rm S}^0} \equiv \frac{\int_0^\infty t\,\langle\Gamma(B_s(t) \to J/\psi K_{\rm S}^0)\rangle\,dt}{\int_0^\infty \langle\Gamma(B_s(t) \to J/\psi K_{\rm S}^0)\rangle\,dt} \tag{5.23}$$

$$= \frac{\tau_{B_s}}{1-y_s^2}\left[\frac{1+2\mathcal{A}_{\Delta\Gamma}(B_s \to J/\psi K_{\rm S}^0)\,y_s + y_s^2}{1+\mathcal{A}_{\Delta\Gamma}(B_s \to J/\psi K_{\rm S}^0)\,y_s}\right]. \tag{5.24}$$

Similar relations can be written for the other $B_q^0 \to J/\psi X$ channels.

5.2 Obtaining the Phases ϕ_q through $B_{(s)}^0 \to J/\psi X$ Decays

To determine the CP-violating phases ϕ_q and to get the picture from the current data, we perform a simultaneous analysis, using not only the two decays that we introduced in the previous Sections but also a number of partner decays that enter in a Cabibbo–favoured way. Applying $SU(3)$ flavour symmetry of strong interactions, we make use of the following channels: the $B_s^0 \to J/\psi K_S^0$ [211, 222] and $B_d^0 \to J/\psi\pi^0$ modes [210, 215], which are the key control channels for the $B_d^0 \to J/\psi K_S^0$ decay, as well as $B_d^0 \to J/\psi\rho^0$ [210–212], which is the main control mode for the $B_s^0 \to J/\psi\phi$ decay. Let us describe our strategy in more detail below.

5.2.1 The Status from the Current Data

First of all, we work with the $B_s^0 \to J/\psi K_S^0$ channel, which is the U-spin[44] partner of the $B_d^0 \to J/\psi K_S^0$, thus we interchange all strange and down quarks. The SM decay amplitude can be written as follows [208]:

$$A\left(B_s^0 \to J/\psi K_S^0\right) = -\lambda\mathcal{A}\left[1 - ae^{i\theta}e^{i\gamma}\right], \tag{5.25}$$

where the hadronic parameters are defined in analogy to Eqs. (5.3) and (5.4):

$$\mathcal{A} \equiv \lambda^2 A\left(A^c_{\rm tree} + A^c_{\rm pen} - A^t_{\rm pen}\right), \tag{5.26}$$

$$ae^{i\theta} \equiv R_b\left(\frac{A^u_{\rm pen} - A^t_{\rm pen}}{A^c_{\rm tree} + A^c_{\rm pen} - A^t_{\rm pen}}\right). \tag{5.27}$$

Since these are $\bar{b} \to dc\bar{c}$ quark level transitions, we use unprimed parameters. Again, the amplitude is a general parametrization within the SM, relying only on the unitarity of the

[44] The U-spin symmetry is a subgroup of the $SU(3)$ flavour symmetry of strong interactions that relates down and strange quarks to each other.

CKM matrix. In Eq. (5.25), $ae^{i\theta}$ enters the decay amplitude in a Cabibbo-allowed way. Due to the absence of the Cabibbo suppression factor ϵ, the penguin effects are amplified in these $\bar{b} \to dc\bar{c}$ modes with respect to their $\bar{b} \to \bar{s}c\bar{c}$ counterparts.

The other partner decay of $B_d^0 \to J/\psi K_S^0$ is the $B_d^0 \to J/\psi\pi^0$, where we replace the strange spectator quark with a down quark. Neglecting exchange and penguin-annihilation topologies, the SM decay amplitude takes the form [215]:

$$\sqrt{2}A(B^0 \to J/\psi\pi^0) = \lambda\mathcal{A}\left[1 - ae^{i\theta}e^{i\gamma}\right], \tag{5.28}$$

where $\mathcal{A}$ and $ae^{i\theta}$ are defined in a similar way as in Eqs. (5.3) and (5.4). The factor of $\sqrt{2}$ is related to the normalization of the π^0 wavefunction. We note again the absence of the factor ϵ.

So far, we have introduced the amplitudes of the partner decays of the $B_d^0 \to J/\psi K_S^0$ channel, where we have the pseudoscalar mesons K_S^0 and π^0 in the final state. Now, we move to $B_s^0 \to J/\psi\phi$ with its partner decay $B_d^0 \to J/\psi\rho^0$, originating from $\bar{b} \to dc\bar{c}$ quark-level transitions, where we have two vector mesons in the final state. In analogy to the structure of the decay amplitude in Eq. (5.10), we have:

$$A(B_d^0 \to [J/\psi\,\rho^0]_f) = -\lambda\,\mathcal{A}_f\left[1 - a_f\,e^{i\theta_f}e^{i\gamma}\right] \tag{5.29}$$

for a given final state configuration $f \in \{0, \|, \perp\}$ with

$$\mathcal{A}_f \equiv \lambda^2 A\left(A^{c'}_{\text{tree,f}} + A^{c'}_{\text{pen,f}} - A^{t'}_{\text{pen,f}}\right), \tag{5.30}$$

$$a_f\,e^{i\theta_f} \equiv R_b\left(\frac{A^{u}_{\text{pen,f}} - A^{t}_{\text{pen,f}}}{A^{c}_{\text{tree,f}} + A^{c}_{\text{pen,f}} - A^{t}_{\text{pen,f}}}\right). \tag{5.31}$$

Similar to the $B_s^0 \to J/\psi\phi$ decay, an angular analysis of the decay products of the vector mesons is needed [210].

Taking these five decays into account and using the CP asymmetries, we can perform a simultaneous analysis and finally determine the mixing phases ϕ_d and ϕ_s, as it is presented in Ref. [191]. The interplay between these channels follows the scheme illustrated in Fig. 25. Starting with the $B_s^0 \to J/\psi K_S^0$ decay, the mixing phase ϕ_s (not the effective one) is required in order to determine the $\Delta\phi_d$ penguin shift from $B_s^0 \to J/\psi K_S^0$. The $\Delta\phi_d$ is needed in order to extract ϕ_d from $B_d^0 \to J/\psi K_S^0$. The mixing phase ϕ_d (again, not the effective one) is needed as an input to determine the $\Delta\phi_s$ penguin shift from $B_d^0 \to J/\psi\rho^0$, which is then required in order to get the phase ϕ_s using the CP asymmetries of the $B_s^0 \to J/\psi\phi$ decay.

Due to the $SU(3)$ symmetry, the following relations hold:

$$a' = a, \qquad \theta' = \theta, \tag{5.32}$$

$$\mathcal{A}' = \mathcal{A}\,. \tag{5.33}$$

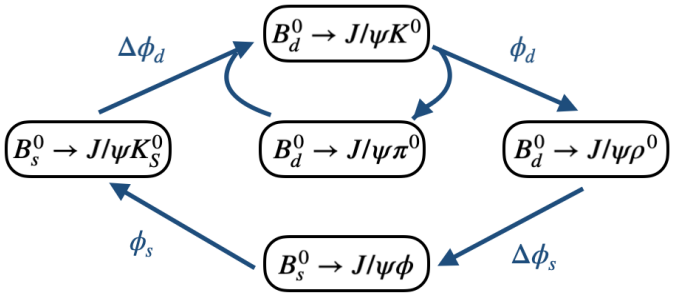

Figure 25: Interplay between the $B \to J\psi X$ modes in the determination of the ϕ_q phases and the dependence on the hadronic penguin shifts

However, we should note that the $SU(3)$ flavour symmetry globally works up to corrections at the 20% level. Therefore, the Eqs. (5.32) and (5.33) get $SU(3)$-breaking corrections. In Eq. (5.32), these corrections can enter only through non-factorisable effects while in Eq. (5.33) through both factorisable and non-factorisable corrections. This happens because in the factorisation approximation, in the ratio presented in Eq. (5.26), the hadronic form factors and the decay constants cancel, while this not the case for the hadronic amplitude presented in Eq. (5.27).

We emphasize here that Eq. (5.32) does not imply that a and θ for the vector modes are the same as for the pseudoscalar modes. Moreover, in factorisation these penguin parameters would not dependent on the polarization state. From now on, we will denote the penguin parameters for the vector case as a_V and θ_V while for the pseudoscalar, simply as a and θ.

Using external input on the angle γ [45] and combining it with the values of the direct and mixing-induced CP asymmetries which are shown in Table 3, we perform the combined analysis of the five $B^0 \to J/\psi X$ decays. The $SU(3)$ symmetry relations in Eq. (5.32) indicate that the penguin parameters of the $B_d^0 \to J/\psi K^0$, $B_s^0 \to J/\psi K_S^0$ and $B_d^0 \to J/\psi\pi^0$ decays are equal to one another. Similarly, the penguin parameters of the $B_s^0 \to J/\psi\phi$ and $B_d^0 \to J/\psi\rho^0$ are equal. Our assumptions are that, due to lack of sensitivity on the current data, we ignore $SU(3)$-breaking effects, polarisation-dependent effects as well as exchange and penguin-annihilation topologies contributions.

[45] We mention here that in our analysis in Ref. [191] we had used the value of γ coming only from $B \to DK$ decays. For the updated results presented at the CKM 2021 conference [201], we used $\gamma = (64.9 \pm 4.5)^\circ$ which was the most recent value from $B \to DK$ modes reported by the LHCb collaboration [197].

Decay Channels	$\mathcal{A}_{\rm CP}^{\rm dir}$	$\eta\mathcal{A}_{\rm CP}^{\rm mix}$	References
$B_s^0 \to J/\psi K_S^0$	-0.28 ± 0.42	0.08 ± 0.41	[223]
$B_d^0 \to J/\psi K^0$	-0.007 ± 0.018	0.690 ± 0.018	[187]
$B_d^0 \to J/\psi \pi^0$	0.04 ± 0.12	0.86 ± 0.14	[187]
$B_s^0 \to J/\psi\phi$	0.006 ± 0.013	-0.085 ± 0.025	[224]
$B_d^0 \to J/\psi\rho^0$	-0.064 ± 0.059	0.66 ± 0.15	[225]

Table 3: Values of the direct $\mathcal{A}_{\rm CP}^{\rm dir}$ and mixing-induced $\mathcal{A}_{\rm CP}^{\rm mix}$ CP Asymmetries of the five $B^0 \to J/\psi X$ used for the simultaneous fit.

Fit Results for the Penguin Parameters and the Mixing Phases

The solutions of the fit for the vector–pseudoscalar final state are [191]:

$$a = 0.13^{+0.16}_{-0.10}\,, \qquad \theta = \left(173^{+34}_{-43}\right)^\circ\,, \qquad \phi_d = \left(44.4^{+1.6}_{-1.5}\right)^\circ\,. \tag{5.34}$$

These correspond to a hadronic phase shift $\Delta\phi_d = \left(-0.73^{+0.60}_{-0.91} \pm 1.4\right)^\circ$.

The solutions of the fit for the vector–vector final state are [191]:

$$a_V = 0.043^{+0.082}_{-0.037}\,, \qquad \theta_V = \left(306^{+\ 48}_{-112}\right)^\circ\,, \qquad \phi_s = \left(-5.0^{+1.6}_{-1.5}\right)^\circ\,, \tag{5.35}$$

and correspond to a hadronic phase shift $\Delta\phi_s = (0.1 \pm 0.5)^\circ$.

These ϕ_d and ϕ_s mixing phases include corrections from penguin contributions. In order to see the impact of the penguin topologies we compare the values of ϕ_d and ϕ_s coming from the fit with the corresponding experimental input, thus the effective phases $\phi^{\rm eff}_{d,J/\psi K^0}$ and $\phi^{\rm eff}_{s,J/\psi\phi}$, respectively:

$$\phi^{\rm eff}_{d,J/\psi K^0} = (43.6 \pm 1.4)^\circ\,, \tag{5.36}$$

$$\phi^{\rm eff}_{s,J/\psi\phi} = (-4.1 \pm 1.3)^\circ. \tag{5.37}$$

Consequently, the comparison between Eqs. (5.34) and (5.36) as well as Eqs. (5.35) and (5.37) indicates the non-negligible impact of the penguin contributions. Fig. 26 illustrates the two-dimensional confidence regions of this simultaneous fit of the five $B^0 \to J/\psi X$ decay channels for the penguin parameters and the mixing phases ϕ_d and ϕ_s arising from the CP asymmetries. The fit is performed using the GammaCombo framework [129], which as we already mentioned in Sec. 3.4.2 was originally developed by the LHCb collaboration.

Comparing the fit solutions (a, θ) and (a_V, θ_V), i,e. the blue areas on the top left and right panel of Fig. 26, we note that even though the results are compatible, the shape of the

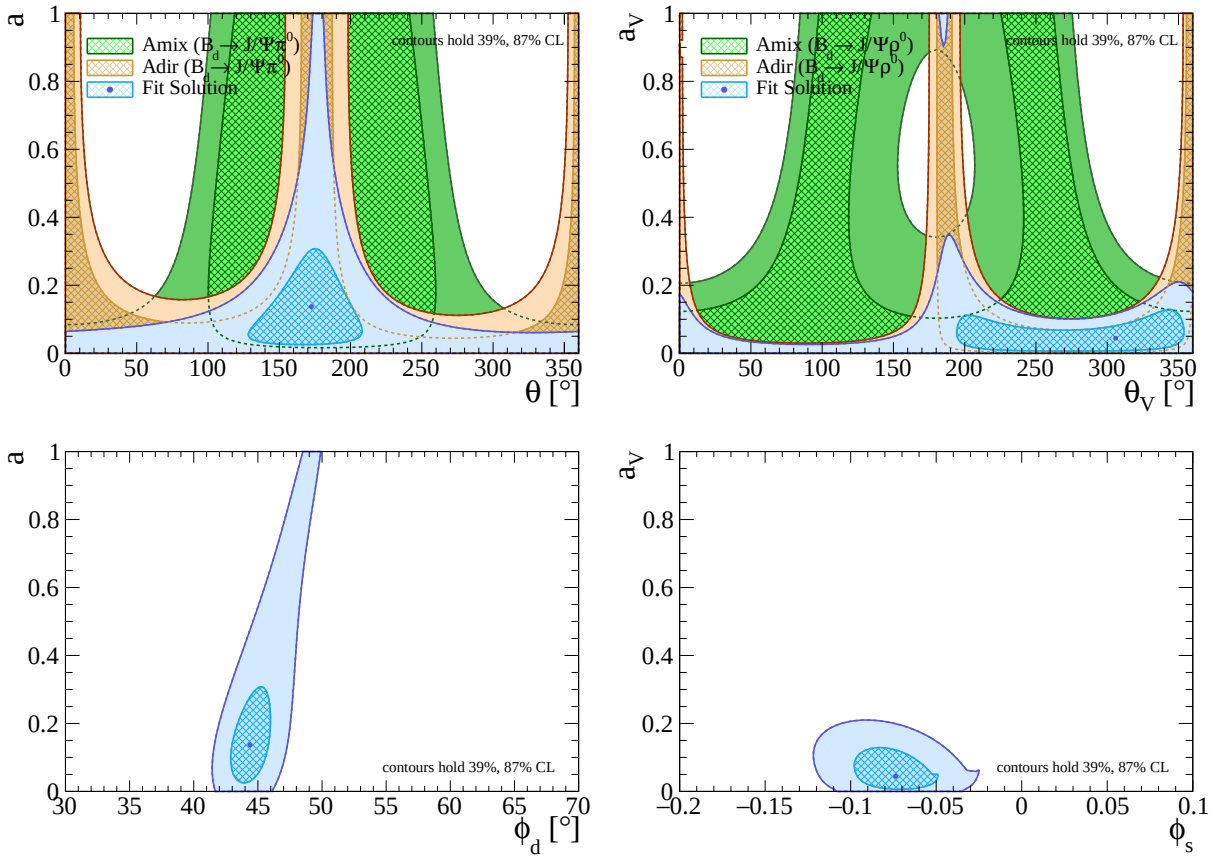

Figure 26: Simultaneous fit for the penguin parameters a, θ, a_V, θ_V and mixing phases ϕ_d and ϕ_s from the CP asymmetries utilising the five $B^0 \to J/\psi X$ decay channels [191]. The plots are produced with GammaCombo.

contours (confidence regions) show the different dynamics between the vector–pseudoscalar and the vector–vector final states. The contours for the CP asymmetries, $\mathcal{A}^{\rm mix}_{\rm CP}$ and $\mathcal{A}^{\rm dir}_{\rm CP}$ are added only for illustration.

We also observe, in the lower panel of Fig. 26, that there is a strong correlation between a and ϕ_d for the vector–pseudoscalar final states while the correlation between a_V and ϕ_s is a lot smaller for the vector–vector final states. As we already mentioned, within the current precision, there is agreement between the three polarisation states in the $B^0_s \to J/\psi\phi$ decay. However, in the future upgrade programmes of LHCb and Belle II, reaching higher precision and providing improved input measurements, may allow to observe and resolve differences.

Determining the Available NP Space

Recalling Eq. (5.14), we can now compare the current values of the mixing phases with the SM predictions and find the possible available space for the NP contributions. Here, in order to be consistent with the numerical analysis within this section, we present the values given in Ref. [191] for the inclusive and exclusive case.[46]

Firstly, for the B_s system, following the definition of the SM predictions for the mixing phase ϕ_s, given in (3.31), and utilising the UT apex coordinates, we obtain the SM values. Then, combining this SM prediction with the fit value of the mixing phase in Eq. (5.35), we determine the NP phases as follows:

$$\phi_s^{\rm SM} = (-2.49 \pm 0.14)^\circ, \quad \phi_s^{\rm NP} = (-2.5 \pm 1.6)^\circ, \qquad \text{Inclusive,} \tag{5.38}$$

$$\phi_s^{\rm SM} = (-2.15 \pm 0.11)^\circ, \quad \phi_s^{\rm NP} = (-2.9 \pm 1.6)^\circ, \qquad \text{Exclusive.} \tag{5.39}$$

We note that the precision on the $\phi_s^{\rm NP}$ result is limited by the experimental fit in Eq. (5.35). Thus, ϕ_s is a powerful probe for NP and it will be interesting to see how the picture evolves in the future. In addition, improvements in the measurements of the CP asymmetries of all five $B_q^0 \to J/\psi X$ channels are also important in order to be able to discover possible NP in the B_s mixing.

Similarly, for the B_d system, starting from the SM prediction of ϕ_d in Eq. (3.30) and combining it with the fit solution in Eq. (5.34), we obtain:

$$\phi_d^{\rm SM} = (52.7 \pm 2.4)^\circ, \quad \phi_d^{\rm NP} = (-8.3 \pm 2.8)^\circ, \ \text{Inclusive,} \tag{5.40}$$

$$\phi_d^{\rm SM} = (45.7 \pm 2.0)^\circ, \quad \phi_d^{\rm NP} = (-1.3 \pm 2.6)^\circ, \ \text{Exclusive.} \tag{5.41}$$

The situation for ϕ_d is different from the case for ϕ_s. The precision on $\phi_d^{\rm NP}$ is limited by the SM prediction uncertainty. It becomes clear that there is significant difference between the inclusive and exclusive case, which already indicates the necessity of resolving the discrepancies between the $|V_{ub}|$ and $|V_{cb}|$ determinations for NP studies utilising the B_d^0–$\bar{B}_d^0$ mixing phase.

5.2.2 Improving the data

Our strategy can be exploited in the future high precision era, where significant improvements in uncertainties of the penguin parameters and their impact on the mixing phases are expected. Studies and analyses regarding the increased luminosity expected from the

[46] Here, this is sufficient since we are interested in showing the main strategy. In the following Sections, where we will perform a careful analysis of the NP effects, we will provide the most recent predictions and explore all three cases, the inclusive, exclusive and hybrid in order to draw our conclusions.

HL-LHC and Belle II can be found in Refs. [226–228]. Here, in order to show the potential that our strategy has and how effective it can be, we compare the current precision with future benchmark scenarios in a simplified way, without taking into account the experimental challenges of the different decay channels or the time scales that these improvements would require.

More specifically, we choose two benchmark scenarios [191] and keep the central values of the current data. First, we divide all the experimental uncertainties by a factor of 2 and then by a factor of 5. Fig. 27 shows the central values of the penguin parameters and the mixing phases (denoted by dots) with the associated uncertainties for both the current precision (blue colour) and the two future scenarios; the red lines show the improved uncertainties by a factor of 2 while the greens denote the improvement by a factor of 5.

Interestingly, we note that already an improvement of the experimental precision by a factor of 2 would have a large impact on the determination of the penguin parameters, allowing to establish non-zero penguin contributions. This demonstrates that the measurements of the CP asymmetries of all five $B^0 \to J/\psi X$ decays are equally important.

Controlling the penguin contributions has a large impact on the knowledge of the phases ϕ_q. What we get from the numerics is that in the future, we can pin down NP with significance of more than five standard deviations[47]. More specifically, regarding the phase ϕ_s, it becomes clear that it is possible to control penguins with precision that allows to establish non-zero NP phases $\phi_s^{\rm NP}$ with significance of more than 5σ. Regarding ϕ_d though, NP contributions are limited by the large uncertainties of the SM predictions. Hopefully, in the future the discrepancies between inclusive and exclusive $|V_{ub}|$ and $|V_{cb}|$ will be resolved.

5.3 Information from the Branching Ratio

Having utilised the information from the CP asymmetries for extracting the penguin parameters and mixing phases, we can make use of the measurements of the branching fractions to study the dynamics of the five $B^0 \to J/\psi X$ decays. The theoretical framework to calculate decay amplitudes and therefore branching ratios is given by factorisation, which we already introduced in Chapter 3.

The SM structure for the tree amplitude of a B_q^0 meson, where $q \in \{s, d\}$, decaying into J/ψ (vector) and a pseudoscalar P meson can be written in factorisation as follows

[47] We note that for the illustration of $\phi_s^{\rm NP}$ and $\phi_d^{\rm NP}$ phases, we chose to work with the value coming from the exclusive case.

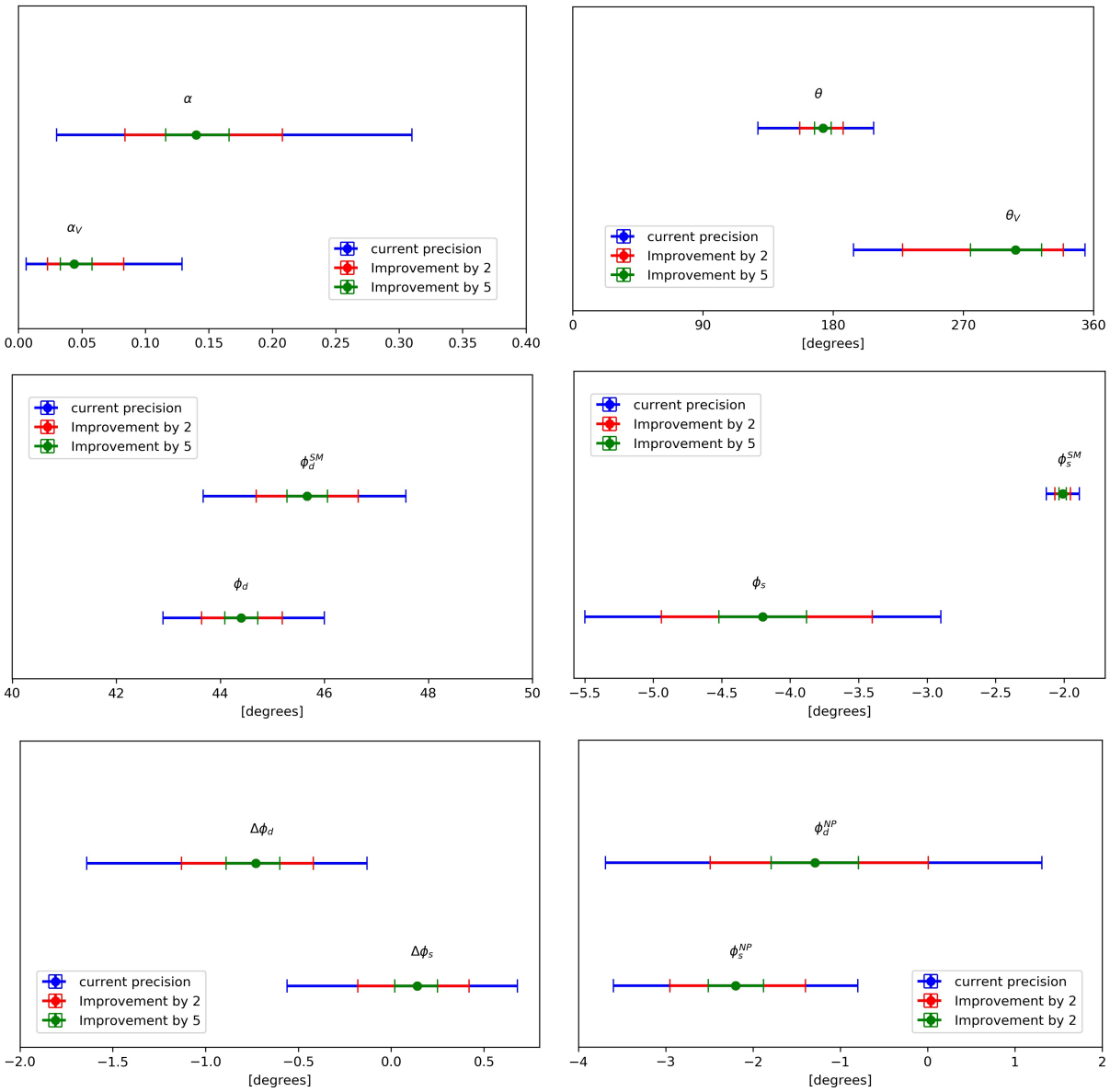

Figure 27: Penguin parameters and mixing phases for current precision (blue), an improved precision by a factor of 2 (red) and an improved precision by a factor of 5 (green).

[104, 163, 229]:

$$
\begin{aligned}
A(B_q^0 \to J/\psi P)|_{\text{fact}}^{\text{tree}} &= \frac{G_{\text{F}}}{\sqrt{2}} V_{cq'} V_{cb}^* \, a_2 \;\; \langle J/\psi P | (\bar{c}\gamma^\mu c)(\bar{b}\gamma_\mu q) | B_q^0 \rangle |_{\text{fact}}, \\
&= \frac{G_{\text{F}}}{\sqrt{2}} V_{cq'} V_{cb}^* \, a_2 \;\; \underbrace{\langle J/\psi | (\bar{c}\gamma^\mu c) | 0 \rangle} \; \underbrace{\langle P | (\bar{b}\gamma_\mu q) | B_q^0 \rangle}, \\
&= \frac{G_{\text{F}}}{\sqrt{2}} V_{cq'} V_{cb}^* \, a_2 \;\; m_{J/\psi} f_{J/\psi} \varepsilon_{J/\psi}^\mu \left[p_{B\mu} + p_{P\mu} - \left(\frac{m_B^2 - m_P^2}{q^2} \right) q_\mu \right] f_{B\to P}^+(q^2).
\end{aligned}
\tag{5.42}
$$

Here $G_{\rm F}$ is the Fermi constant, $V_{cq'}$ and V_{cb} denote CKM matrix elements, a_2 is a phenomenological "colour suppression" factor, $m_{J/\psi}$ is the mass and $f_{J/\psi}$ the decay constant of the J/ψ meson, $\varepsilon_{J/\psi}$ is its polarisation vector, $f^+_{B\to P}$ is the hadronic $B \to P$ form factor, p_B and p_P are the four momentum vectors of the B and pseudoscalar mesons, respectively, and $q_\mu = p_{B\mu} - p_{P\mu}$ their momentum transfer.

We can generalise the decay amplitude in order to allow for penguin effects as well. Specifically, for the $B_d^0 \to J/\psi\pi^0$ decay, the generalised amplitude can be written as [191]:

$$\begin{aligned}\sqrt{2}\, A(B_d^0 \to J/\psi\pi^0) =& \frac{G_{\rm F}}{\sqrt{2}} V_{cd}V_{cb}^*\, m_{J/\psi}\, f_{J/\psi} f^+_{B_d\to\pi}(m^2_{J/\psi})\, (p_{B\mu} + p_{K\mu}) \cdot \varepsilon^\mu_{J/\psi} \\ & \times \left(1 - a e^{i\theta} e^{i\gamma}\right) \times a_2(B_d^0 \to J/\psi\pi^0)\,, \end{aligned} \tag{5.43}$$

where $a_2(B_d^0 \to J/\psi\pi^0)$ is a generalisation of the naive colour-suppression factor.

We calculate the CP averaged branching ratio:

$$\begin{aligned} 2\,\mathcal{B}(B_d^0 \to J/\psi\pi^0) = \tau_{B_d}\, \frac{G_{\rm F}^2}{32\pi} |V_{cd}V_{cb}|^2\, m_{B_d}^3 \left[f_{J/\psi} f^+_{B_d\to\pi}(m^2_{J/\psi})\right]^2 \left[\Phi\left(\frac{m_{J/\psi}}{m_{B_d}}, \frac{m_{\pi^0}}{m_{B_d}}\right)\right]^3 \\ \times (1 - 2a\cos\theta\cos\gamma + a^2) \times \left[a_2(B_d^0 \to J/\psi\pi^0)\right]^2, \end{aligned} \tag{5.44}$$

where τ_{B_d} is the lifetime of the B_d^0 meson, Φ is the phase-space function defined in Eq. (3.62) and the factor 2 on the left-hand side is again related to the π^0 wave function. The value of the decay constant, using the most recent lattice QCD result [230] is:

$$f_{J/\psi} = (410.4 \pm 1.7)\ \text{MeV}\,. \tag{5.45}$$

Regarding the form factors, there are different approaches that can be used in order to determine their values. Here, we work with the results from the lattice QCD approach. The values that we obtain using FLAG [209] are the following:

$$f^+_{B_d\to\pi}(m^2_{J/\psi}) = 0.371 \pm 0.069\,, \tag{5.46}$$

$$f^+_{B_d\to K}(m^2_{J/\psi}) = 0.645 \pm 0.022\,, \tag{5.47}$$

$$f^+_{B_s\to K}(m^2_{J/\psi}) = 0.470 \pm 0.024\,. \tag{5.48}$$

Here we had to extrapolate the results from high q^2 to the low kinematic point of $q^2 = m^2_{J/\psi}$. For this purpose, we followed the Bourrely–Caprini–Lellouch (BCL) parametrisation [231]. Our goal is to determine the parameter a_2 for the $B \to J/\psi$ modes. Let us discuss this parameter and its determination in more detail below.

5.3.1 The parameter a_2

The quantity a_2 is the phenomenological "colour suppression" factor, as already introduced in Eq. (3.115). In factorisation, it is written as follows:

$$a_2 = C_1 + \frac{C_2}{3}, \tag{5.49}$$

where C_1 and C_2 are the short-distance Wilson coefficients of the current–current operators $\mathcal{O}_1$ and $\mathcal{O}_2$, respectively:

$$\mathcal{O}_1 = \left(\bar{c}_\alpha \gamma_\mu (1-\gamma_5) q'_\beta\right)\left(\bar{b}_\beta \gamma^\mu (1-\gamma_5) c_\alpha\right) \equiv (\bar{c}_\alpha q'_\beta)_{\mathrm{V-A}} (\bar{b}_\beta c_\alpha)_{\mathrm{V-A}} \,, \tag{5.50}$$

$$\mathcal{O}_2 = \left(\bar{c}_\beta \gamma_\mu (1-\gamma_5) q'_\beta\right)\left(\bar{b}_\alpha \gamma^\mu (1-\gamma_5) c_\alpha\right) \equiv (\bar{c}_\beta q'_\beta)_{\mathrm{V-A}} (\bar{b}_\alpha c_\alpha)_{\mathrm{V-A}} \,. \tag{5.51}$$

Naive factorisation predicts [155]:

$$a_2 = 0.21 \pm 0.05 \,. \tag{5.52}$$

The factor a_2 depends strongly on the renormalisation scale μ (contrary to a_1 for colour-allowed mesons) reflecting that factorisation is not expected to work well for such colour-suppressed decays.

Using the values of form factors in Eqs. (5.46)–(5.48) we can determine the parameter a_2, utilising Eq. (5.42) and the penguin parameters a and θ. Thus, for $B_d^0 \to J/\psi\pi^0$, we have:

$$|a_2(B_d^0 \to J/\psi\pi^0)|^2 \times (1 - 2a\cos\theta\cos\gamma + a^2) = 0.145 \pm 0.055 \,, \tag{5.53}$$

$$\xRightarrow[\text{to}]{\text{leading}} a_2(B_d^0 \to J/\psi\pi^0) = 0.363^{+0.066}_{-0.079} \,. \tag{5.54}$$

In analogy, we obtain for the $B_d^0 \to J/\psi K^0$ and $B_s^0 \to J/\psi K_S^0$ decays:

$$|a'_2(B_d^0 \to J/\psi K^0)|^2 \times (1 + 2\epsilon a\cos\theta\cos\gamma + \epsilon^2 a^2) = 0.0714 \pm 0.0059 \,, \tag{5.55}$$

$$\xRightarrow[\text{to}]{\text{leading}} a'_2(B_d^0 \to J/\psi K^0) = 0.268^{+0.011}_{-0.012} \,, \tag{5.56}$$

$$|a_2(B_s^0 \to J/\psi K_S^0)|^2 \times (1 - 2a\cos\theta\cos\gamma + a^2) = 0.097 \pm 0.013 \,, \tag{5.57}$$

$$\xRightarrow[\text{to}]{\text{leading}} a_2(B_s^0 \to J/\psi K_S^0) = 0.296^{+0.024}_{-0.027} \,. \tag{5.58}$$

The numerical results in Eqs. (5.56) and (5.58) agree surprisingly well with the factorisation range in Eq. (5.52). The a_2 result for the decay $B_d^0 \to J/\psi\pi^0$ has larger uncertainties, which arises from the uncertainty of the corresponding form factor in Eq. (5.46), showing

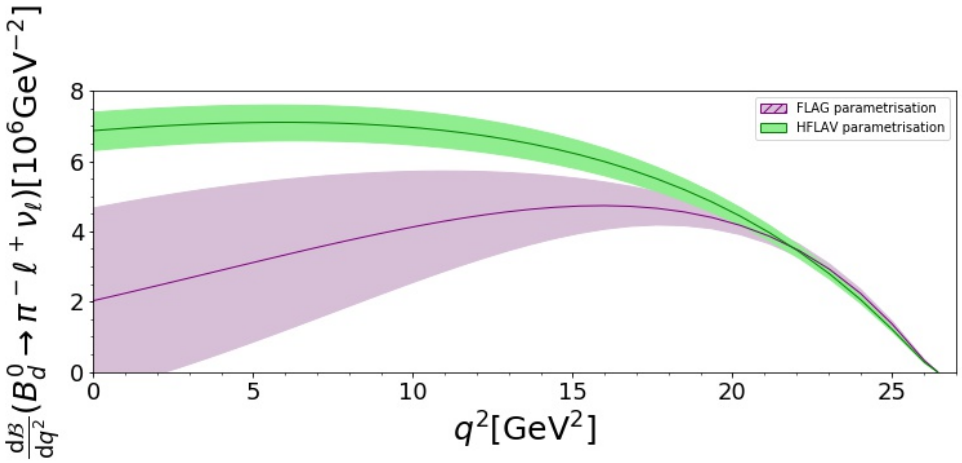

Figure 28: The differential branching ratio of $B_d^0 \to \pi^- \ell^+ \nu_\ell$ using the FLAG (purple contour) and HFLAV (green contour) parametrisations.

the limitations of the lattice calculations. When it comes to lower q^2, the limited precision of the lattice calculations gets amplified. We can illustrate this feature by plotting the differential branching ratio of the $B_d^0 \to \pi^- \ell^+ \nu_\ell$ semileptonic partner decay for different q^2 bins, as given in Fig. 28. As we can see, the band is wider in the lower q^2 regions.

Using FLAG parametrisation [209], which was also used in order to calculate the form factor $f^+_{B_d \to \pi}$ in Eq. (5.46), the differential branching ratio of the $B_d^0 \to \pi^- \ell^+ \nu_\ell$ decay in the limit $m_\ell \to 0$ is written as:

$$\frac{d\mathcal{B}}{dq^2}(B_d^0 \to \pi^- \ell^+ \nu_\ell) = \tau_{B_s} \left[\frac{d\Gamma}{dq^2}(B_d^0 \to \pi^- \ell^+ \nu_\ell) \right] , \tag{5.59}$$

$$= \tau_{B_s} \left[\frac{G_F^2}{24\pi^3} |V_{ub}|^2 \eta_{\text{EW}}^2 p_\pi^3 \left[f^+_{B_d \to \pi}(q^2) \right]^2 \right] , \tag{5.60}$$

$$= \tau_{B_s} \left[\frac{G_F^2}{24\pi^3} |V_{ub}|^2 \eta_{\text{EW}}^2 \left[\frac{m_{B_d}}{2} \Phi \left(\frac{m_\pi}{m_{B_d}}, \frac{q}{m_{B_d}} \right) \right]^3 \left[f^+_{B_d \to \pi}(q^2) \right]^2 \right] , \tag{5.61}$$

where $\eta_{\text{EW}} = 1.0066 \pm 0.0050$ [232] denotes the one-loop electroweak correction factor. Fig. 28 illustrates the corresponding contour with purple colour. The differential rate was measured by the BaBar and Belle collaborations. The uncertainties are due to the form factor parametrisation. This curve is compared to another contour, denoted by green colour in Fig. 28, which uses the HFLAV parametrisation that combines lattice QCD and light–cone sum–rule calculations. This leads to the following value of the form factor:

$$f^+_{B_d \to \pi}(m^2_{J/\psi}) = 0.487 \pm 0.018 , \tag{5.62}$$

which agrees much better with the value of the form factor in Eq. (5.48). As we can see, there is a large discrepancy between the two contours, showing the issues that arise when using the form factors and illustrating the necessity to minimise the dependence on them when determining the parameters a_2 from the data.

5.3.2 Utilising Semileptonic Decays

It is essential to determine the parameters a_2 in a clean way from the data and to obtain insights into how well factorisation works. In order to do so, it is important to handle the form factors, which are difficult to calculate, as there are challenges with extrapolating lattice results and handling the theoretical uncertainties. Therefore, following the strategy introduced in Sec. 3.5.4, we use semileptonic decays and more specifically, we construct ratios between the branching fractions of the $B^0 \to J/\psi X$ and corresponding partner decays, which allow us to avoid the form factor dependence.

Let us firstly work with the decay $B_d^0 \to J/\psi\pi^0$. Its partner semileptonic decay is $B_d^0 \to \pi^-\ell^+\nu_\ell$ which has the same form factor dependence. Therefore, constructing the following ratio

$$R_d^\pi \equiv \frac{\Gamma(B_d^0 \to J/\psi\pi^0)}{d\Gamma/dq^2|_{q^2=m_{J/\psi}^2}(B_d^0 \to \pi^-\ell^+\nu_\ell)} = \frac{\mathcal{B}(B_d^0 \to J/\psi\pi^0)}{d\mathcal{B}/dq^2|_{q^2=m_{J/\psi}^2}(B_d^0 \to \pi^-\ell^+\nu_\ell)}\,, \tag{5.63}$$

$$= 3\pi^2 \left(\frac{1-\lambda^2}{R_b^2}\right)\left(\frac{f_{J/\psi}}{\eta_{\rm EW}}\right)^2 \times (1 - 2a\cos\theta\cos\gamma + a^2) \times \left[a_2(B_d^0 \to J/\psi\pi^0)\right]^2\,, \tag{5.64}$$

the $|V_{ub}|$ matrix element and the form factors fully cancel, thereby allowing a clean extraction of $|a_2(B_d^0 \to J/\psi\pi^0)|$. However, it still requires knowledge of the penguin parameters. In the above equation, we have used the relation

$$\left|\frac{V_{cd}V_{cb}}{V_{ub}}\right|^2 = \frac{1-\lambda^2}{R_b^2} + \mathcal{O}(\lambda^4), \tag{5.65}$$

neglecting the $\mathcal{O}(\lambda^4)$ corrections.

Regarding the numerical analysis, we use the $B_d^0 \to J/\psi\pi^0$ branching ratio, given in PDG [233]. For the differential branching ratio of $B \to \pi\ell\nu$ we use the following experimental average for the $q^2 = m_{J/\psi}^2$ bin [187]:

$$\frac{d\mathcal{B}}{dq^2|_{q^2=[8,10]\,\text{GeV}^2}}(B \to \pi\ell\nu) = (6.44 \pm 0.43) \times 10^{-6}\,\text{GeV}^{-2}. \tag{5.66}$$

This value is an average of the BaBar and Belle measurements, assuming isospin symmetry in order to combine the experimental data from both $B_d^0 \to \pi^-\ell^+\nu_\ell$ and $B^+ \to \pi^0\ell^+\nu$

channels. Finally, we obtain the following value of the ratio R_d^π [191]:

$$R_d^\pi = (2.58 \pm 0.23) \times 10^{-6}\,\text{MeV}^2\,. \tag{5.67}$$

Utilising this result with Eq. (5.64), as well as the penguin parameters in Eq. (5.34), we finally determine the value a_2 as follows:

$$\left|a_2(B_d^0 \to J/\psi\pi^0)\right|^2 \times (1 - 2a\cos\theta\cos\gamma + a^2) = (0.0832 \pm 0.0079)\,, \tag{5.68}$$

$$|a_2(B_d^0 \to J/\psi\pi^0)| = 0.275^{+0.018}_{-0.023}\,. \tag{5.69}$$

This result agrees better with naive factorisation, in Eq. (5.52) [155], than the form-factor based result in Eq. (5.54), showing the advantages of using our strategy with the semileptonic decays. The central value in Eq. (5.54) is larger, a fact that is related to the discrepancies between FLAG and HFLAV parametrisations (as shown in Fig. 28), while the uncertainties are also larger, due to the fact that the form factor in Eq. (5.46) has large uncertainties.

A similar ratio can be constructed for the $B_s^0 \to J/\psi K_S^0$ decay. Its semileptonic partner is the $B_s^0 \to K^-\ell^+\nu_\ell$ channel. Thus, we write

$$R_s^K \equiv \frac{\Gamma(B_s^0 \to J/\psi K_S^0)}{d\Gamma/dq^2|_{q^2=m^2_{J/\psi}}(B_s^0 \to K^-\ell^+\nu_\ell)} = \frac{\mathcal{B}(B_s^0 \to J/\psi K_S^0)}{d\mathcal{B}/dq^2|_{q^2=m^2_{J/\psi}}(B_s^0 \to K^-\ell^+\nu_\ell)}\,. \tag{5.70}$$

However, we cannot determine the rate R_s^K yet. Even though the LHCb collaboration has given a first measurement of the branching fraction of the $B_s^0 \to K^-\ell^+\nu_\ell$ channel [234], a measurement of the differential branching fraction is not available yet. Therefore, the form factors information is needed and we still use the value of Eq. (5.58).

Last but not least, for the $B_d^0 \to J/\psi K^0$ decay, there is no semileptonic partner. As a result, for this case, the form factor information in the analysis will be required. For the value of a_2 we use Eq. (5.56).

We illustrate the correlation of the effective colour-suppression factors of the various decays with the size a of the penguin parameters in Fig. 29. So, we show the values of a_2 as functions of a, and the corresponding uncertainty contours, for the $B_s^0 \to J/\psi K_S^0$ (green), $B_d^0 \to J/\psi\pi^0$ (brown) and $B_d^0 \to J/\psi K^0$ (blue) decay channels. We point out that comparing with naive factorisation [155] deviations arise at the (30–40)% level. This may appear to be large. However, we should keep in mind that this is a class of decays where factorisation is not expected to work well.

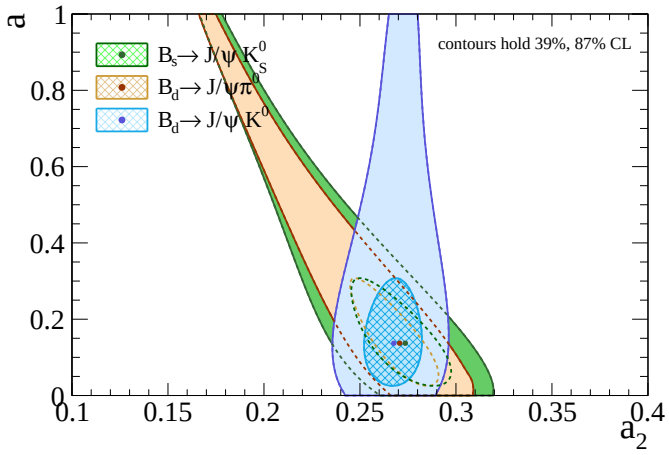

Figure 29: The effective colour-suppression factors in terms of the size a of the penguin parameters [201].

5.4 Towards NP in B_q^0–$\bar{B}_q^0$ Mixing

Let us now move towards NP and perform careful studies to explore the allowed parameter space for NP in B_q-meson mixing. For this purpose, as we already saw earlier, we have to compare the SM predictions of the B_q^0–$\bar{B}_q^0$ mixing parameters with the corresponding experimental values. This will allow us to constrain possible NP contributions in the neutral B_q-meson mixing.

Our first step is to properly determine the mixing parameters in the SM. We highlight that these parameters strongly depend on the CKM matrix elements and the determinations of the UT apex. Recalling the UT analysis in Sec. 3.4.2, we will discuss the impact that the different experimental inputs (related to CKM factors) have on the NP parameter space. Here, we will study each one of the inclusive, exclusive and hybrid case separately.

Following the definitions of the SM predictions for the mixing phases ϕ_d and ϕ_s given in Eqs. (3.30) and (3.31), respectively, and utilising the UT apex coordinates for the inclusive, exclusive and hybrid case, we obtain the SM values [81] presented in Table 4.

We also obtain the numerical predictions for the mass difference Δm_q between the heavy and light mass eigenstates of the neutral B_q-meson system, defined in Eq. (3.32). We use the values of the masses of the B_s and B_d system [66]:

$$m_{B_d} = 5279.66 \pm 0.12 \text{ MeV}, \quad m_{B_s} = 5366.92 \pm 0.10 \text{ MeV}, \tag{5.71}$$

where the mass element M_{12}^q in the SM is given in Eq. (3.33). Finally, the results for the mass difference in the SM are shown in Table 5.

Case	$\phi_d^{\rm SM}$	$\phi_s^{\rm SM}$
Inclusive	$(51.4 \pm 2.8)^\circ$	$(-2.30 \pm 0.13)^\circ$
Exclusive	$(46.2 \pm 2.3)^\circ$	$(-2.08 \pm 0.10)^\circ$
Hybrid	$(42.6 \pm 2.2)^\circ$	$(-1.93 \pm 0.10)^\circ$

Table 4: SM predictions for the mixing phases $\phi_d^{\rm SM}$ and $\phi_s^{\rm SM}$ for the inclusive, exclusive and hybrid case.

Case	$\Delta m_d^{\rm SM}$	$\Delta m_s^{\rm SM}$
Inclusive	(0.513 ± 0.040) ps^{-1}	(17.23 ± 0.87) ps^{-1}
Exclusive	(0.439 ± 0.033) ps^{-1}	(14.80 ± 0.76) ps^{-1}
Hybrid	(0.510 ± 0.037) ps^{-1}	(17.19 ± 0.87) ps^{-1}

Table 5: SM predictions for the mass differences $\Delta m_d^{\rm SM}$ and $\Delta m_s^{\rm SM}$ for the inclusive, exclusive and hybrid case.

The experimental values for Δm_d and Δm_s are [120, 235]:

$$\Delta m_d = (0.5065 \pm 0.0019)\ \text{ps}^{-1}\,, \tag{5.72}$$

$$\Delta m_s = (17.7656 \pm 0.0057)\ \text{ps}^{-1}\,. \tag{5.73}$$

Comparing the SM predictions with the experimental values, we find that the latter are more precise (one to two orders of magnitude). A combined analysis of lattice and light-cone sum rules (LQSR) [236] gives similar results. We note that in the exclusive scenario, the Δm_d SM prediction differs from the corresponding measured value by 2 standard deviations while the Δm_s SM value differs from the experimental one by 3 standard deviations. We also observe that the central values in the exclusive scenario are smaller than those of the inclusive and exclusive cases, following the pattern of the value of the $|V_{cb}|$ CKM matrix element.

5.4.1 Introducing the NP parameters

Our next goal is to quantify the impact of NP in the neutral B_q-meson mixing. In general, we may write:

$$M_{12}^{(q)} = M_{12}^{q,\rm SM}\left(1 + \kappa_q e^{i\sigma_q}\right), \tag{5.74}$$

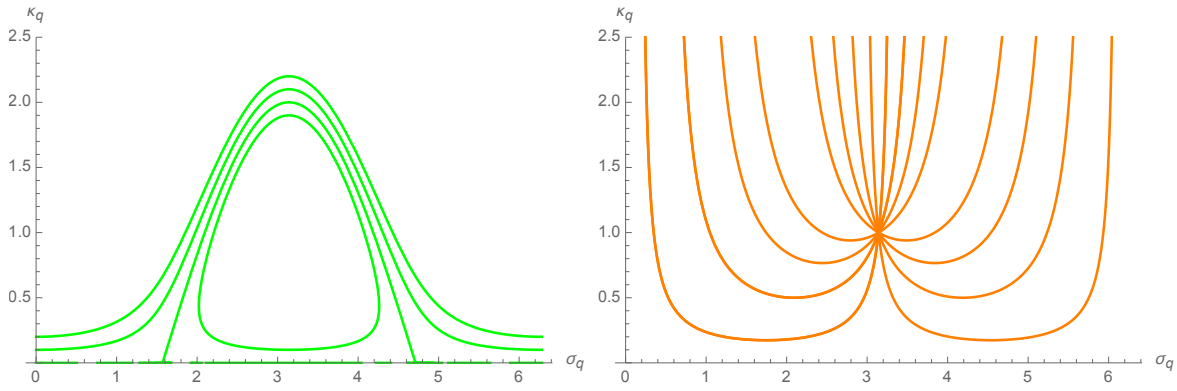

Figure 30: Contours on the σ_q-κ_q plane. The left panel shows the dependence on the ρ parameter while the right one indicates the dependence on the $\phi_q^{\rm NP}$ phase.

where we introduce the NP parameters κ_q and σ_q while the SM mass $M_{12}^{q,\rm SM}$ is given in Eq. (3.33). We can now generalise the expression of the mixing parameters in such a way that we have two parts, the SM and the NP one, following [237]:

$$\Delta m_q = \Delta m_q^{\rm SM} + \Delta m_q^{\rm NP} = \Delta m_q^{\rm SM} \left|1 + \kappa_q e^{i\sigma_q}\right| , \tag{5.75}$$

$$\phi_q = \phi_q^{\rm SM} + \phi_q^{\rm NP} = \phi_q^{\rm SM} + \arg\left(1 + \kappa_q e^{i\sigma_q}\right) . \tag{5.76}$$

The parameter κ_q describes the size of the NP effects while the σ_q is a complex phase accounting for additional CP-violating effects. This is a model independent parametrisation in the sense that we make no assumptions concerning the NP origin.

Following Eq. (5.75) we obtain the first constraint from the Δm_q parameter and the κ_q in terms of σ_q can be written as follows [237]:

$$\rho_d \equiv \left|\Delta m_q / \Delta m_q^{\rm SM}\right| = \sqrt{1 + 2\kappa_q \cos\sigma_q + \kappa_q^2} , \tag{5.77}$$

$$\kappa_q = -\cos\sigma_q \pm \sqrt{\rho_q^2 - \sin^2\sigma_q} . \tag{5.78}$$

An illustration of the contours in the σ_q-κ_q plane for different values of ρ is given in the left panel of Fig. 30. As an example, we vary the value of ρ between 1.2 and 0.8. We choose a step of 0.1 and the upper contour corresponds to $\rho = 1.2$ while the lower to $\rho = 0.8$.

The second constrain on the NP parameters comes from the ϕ_q. The parameter κ_q as a function of σ_q is [237]:

$$\kappa_q = \frac{\tan\phi_q^{\rm NP}}{\sin\sigma_q - \cos\sigma_q \tan\phi_q^{\rm NP}} , \tag{5.79}$$

for a given value of $\phi_q^{\rm NP}$. We provide the corresponding plot in the right panel of Fig. 30. in the σ_q-κ_q plane for different $\phi_q^{\rm NP}$ values. As an example, we pick a few values of the

Case	κ_d	σ_d	κ_s	σ_s
Inclusive	$0.121^{+0.056}_{-0.055}$	$\left(261^{+37}_{-35}\right)^\circ$	$0.045^{+0.048}_{-0.033}$	$\left(312^{+37}_{-77}\right)^\circ$
Exclusive	$0.156^{+0.093}_{-0.084}$	$\left(347^{+21}_{-25}\right)^\circ$	$0.205^{+0.064}_{-0.059}$	$\left(347.6^{+8.5}_{-9.8}\right)^\circ$
Hybrid	$0.031^{+0.057}_{-0.031}$	$\left(104^{+256}_{-104}\right)^\circ$	$0.053^{+0.046}_{-0.034}$	$\left(309^{+34}_{-65}\right)^\circ$

Table 6: Values of the NP parameters κ_q, σ_q for the B_s and B_d systems in Scenario I for inclusive, ecxlusive and hybrid case.

NP phase between $0^\circ < \sigma_q < 180^\circ$ and $180^\circ < \sigma_q < 360^\circ$, corresponding to positive and negative $\phi_q^{\rm NP}$, respectively.

With the help of Eqs. (5.75) and (5.76), we explore two different NP scenarios. The first one, namely Scenario I is the most general case, having the least assumptions. The second case that we consider, Scenario II, assumes Flavour Universal NP (FUNP). The purpose of the latter is to explore the impact of additional assumptions on the allowed parameter space for NP in B_q^0–$\bar{B}_q^0$ mixing.

5.4.2 Exploring NP Scenarios

Scenario I

The first scenario, which as we mentioned is the most general, uses the UT side R_b and the angle γ as inputs for the SM predictions. The only assumption in this case is that there is no NP in R_b and γ.

Therefore, we utilise the UT apex determination, which does not rely on information from mixing in order to determine the SM predictions of Δm_q and ϕ_q. These predictions are compared with their measured values and allow us to constrain the NP parameters. Here, the NP parameter space is determined separately for the B_d and the B_s system, thus (κ_d, σ_d) and (κ_s, σ_s) are obtained independently from each other. The results, obtained from GammaCombo, are presented in Table 6.

In order to guide the eye, a simplified version of the κ_d and σ_d fit is shown in Fig. 31. Including the constraints from Δm_d and ϕ_d we show the plots for the B_d system for the inclusive, exclusive and hybrid case. We draw the individual constraints from ϕ_d and Δm_d and show the central value[48] of the κ_d and σ_d for all three cases (indicated by black dot). Similarly, Fig. 32 illustrates the κ_s and σ_s correlation. A more sophisticated fit for both B_d and B_s systems, produced using the GammaCombo tool, is given in Ref. [81]. It shows

[48]Here, since the allowed regions can be read off from the overlap of the countours from ϕ_q and Δm_q, we do not add the error bands for the κ_q and σ_q points in the plot.

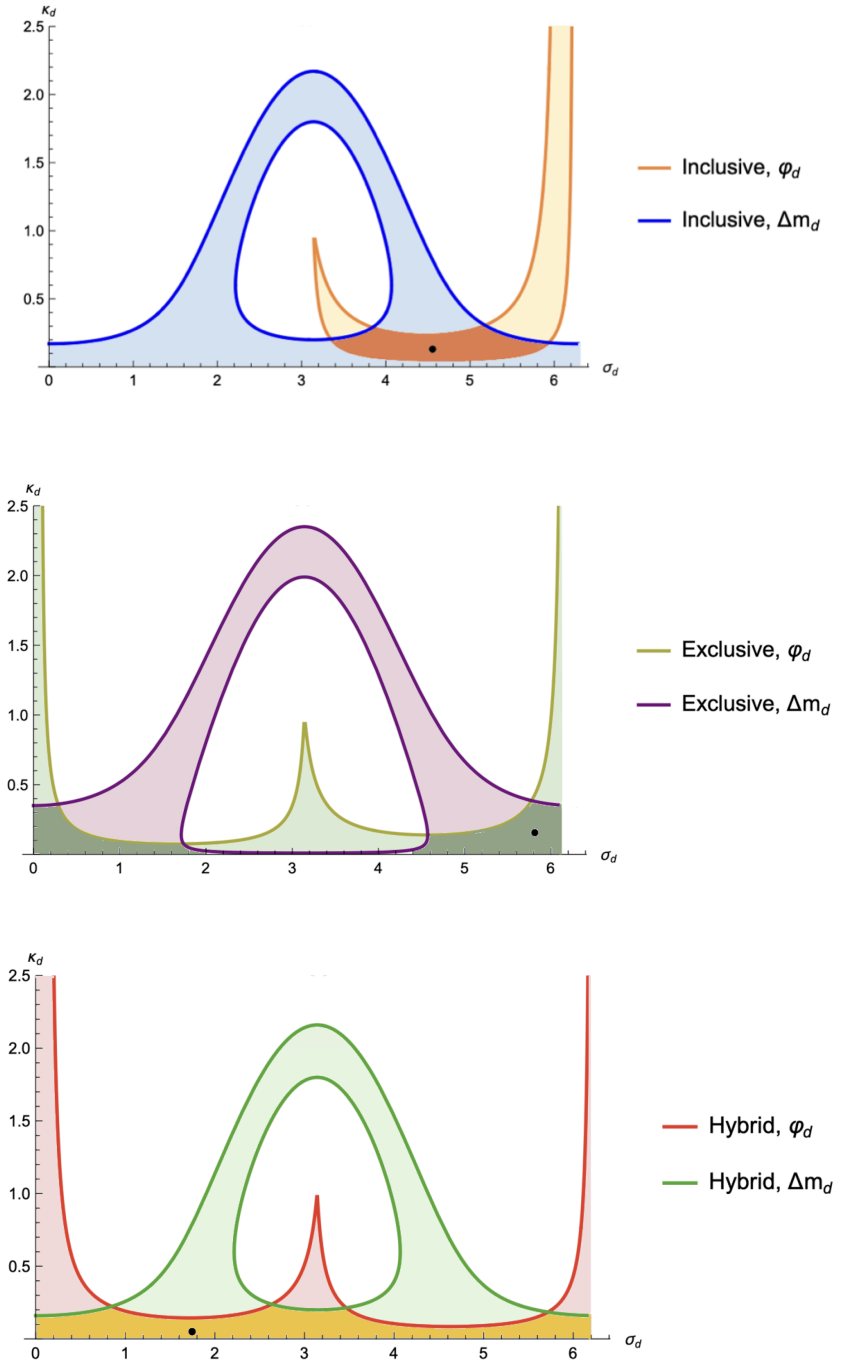

Figure 31: Simplified version of the fit for the NP parameters in the B_d system for Scenario I. We show the central values of κ_d and σ_d (denoted as black dot) for the inclusive (top), exclusive (middle) and hybrid (bottom) case including the constraints from ϕ_d and Δm_d.

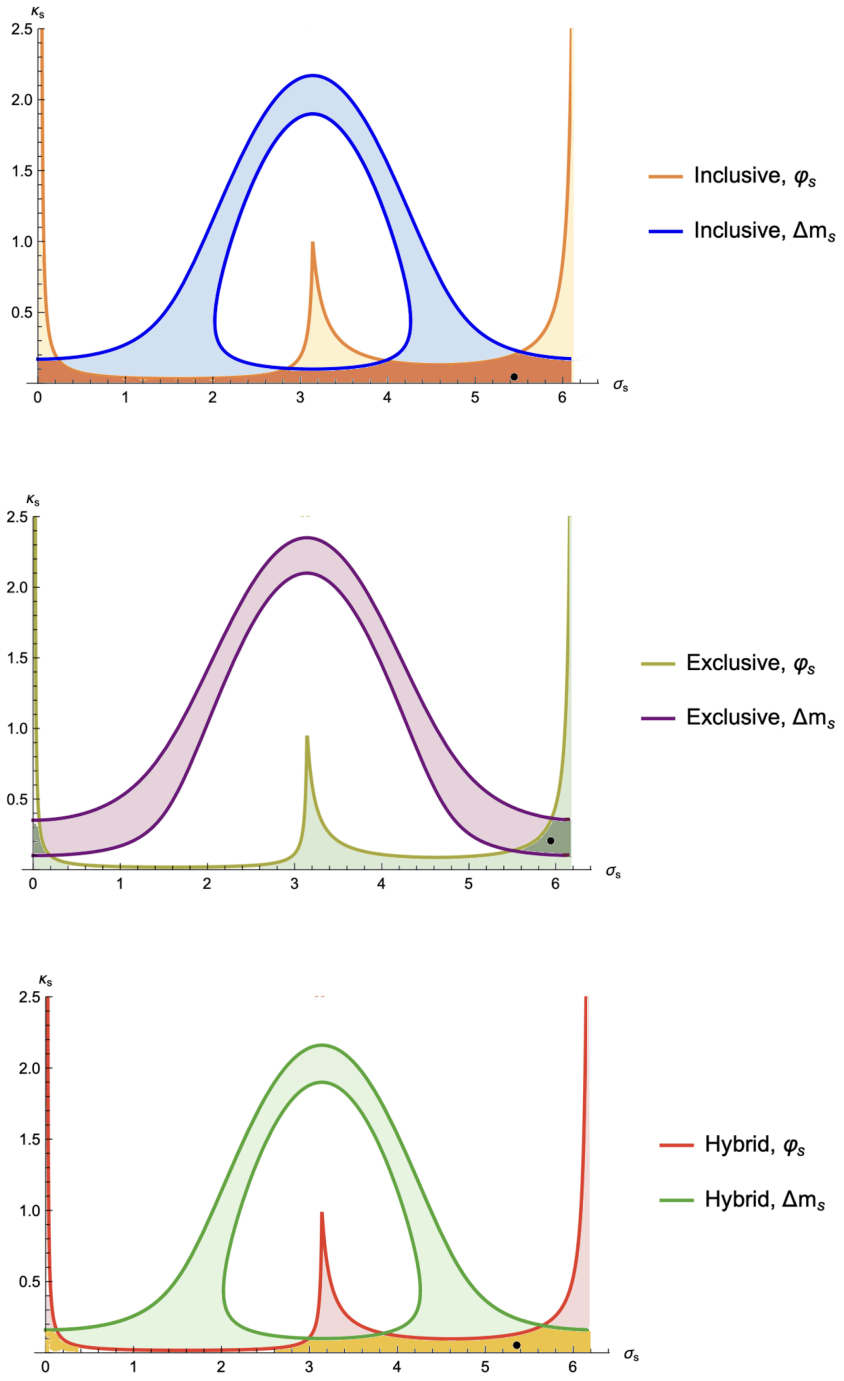

Figure 32: Simplified version of the fit for the NP parameters in the B_s system for Scenario I. We show the central values of κ_s and σ_s (denoted as black dot) for the inclusive (top), exclusive (middle) and hybrid (bottom) case including the constraints from ϕ_s and Δm_s.

that the conclusions regarding the presence of NP are different for the three cases. In the inclusive case, the κ_s is compatible with 0 while κ_d is different from 0 at the 2.2 σ level. In the exclusive determination, the κ_d deviates from 0 at the 1.9 σ level, whereas κ_s differs from zero at the 3.5 σ level, suggesting a strong hint of NP. Last but not least, in the hybrid case, the κ_d is compatible with 0 while κ_s deviates at the 1.6 σ level.

Scenario II

For the second NP scenario, we have the FUNP case, where we assume that [81]:

$$(\kappa_d, \sigma_d) = (\kappa_s, \sigma_s), \tag{5.80}$$

thus the NP contributions are equal in the B_d and B_s system. This is not a Minimal Flavour Violation scenario, in which there would be no CP-violating NP phase, but it can be realised in NP models with $U(2)$ symmetry [238, 239].

Here, we do not determine the UT apex based on the side R_b and the angle γ but instead the fit relies on the R_b and R_t sides. This is a very useful method, in particular when discrepancies between the various γ determinations arise. Therefore, possible NP in γ will not affect the findings. Let us make a small parenthesis here to describe this alternative way of the UT determination.

Unitarity Triangle Apex through R_b and R_t side

Recalling the definition in Eq. (2.64), the side R_t can be written as [81]:

$$R_t = \frac{1}{\lambda}\left|\frac{V_{td}}{V_{ts}}\right|\left[1 - \frac{\lambda^2}{2}(1-2\bar{\rho})\right] + \mathcal{O}\left(\lambda^4\right) . \tag{5.81}$$

The ratio of the CKM matrix elements $|V_{td}|$ and $|V_{ts}|$ is expressed in terms of the B_q^0–$\bar{B}_q^0$ mixing parameters as follows [81]:

$$\left|\frac{V_{td}}{V_{ts}}\right| = \xi\sqrt{\frac{m_{B_s}\Delta m_d^{\rm SM}}{m_{B_d}\Delta m_s^{\rm SM}}}. \tag{5.82}$$

Here the SU(3)-breaking parameter ξ is the ratio of bag parameters and decay constants of the B_d and the B_s systems that can be calculated on the lattice. We obtain [135, 240]:

$$\xi \equiv \frac{f_{B_s}\sqrt{\hat{B}_{B_s}}}{f_{B_d}\sqrt{\hat{B}_{B_d}}} = 1.212 \pm 0.016 . \tag{5.83}$$

Determination	$\bar{\rho}$	$\bar{\eta}$
Inclusive	0.180 ± 0.014	0.395 ± 0.020
Exclusive	0.163 ± 0.013	0.357 ± 0.017
Hybrid	0.153 ± 0.013	0.330 ± 0.016

Table 7: Values of the UT apex $\bar{\rho}$ and $\bar{\eta}$, determined from the R_b and R_t sides, for the inclusive, exclusive and hybrid case.

The individual results for the decay constant and bag parameters are [135, 240]:

$$f_{B_d}\sqrt{\hat{B}_{B_d}} = (210.6 \pm 5.5)\,\text{MeV}\,, \tag{5.84}$$

$$f_{B_s}\sqrt{\hat{B}_{B_s}} = (256.1 \pm 5.7)\,\text{MeV}\,. \tag{5.85}$$

The advantage of this ratio compared to the individual results is that uncertainties cancel, making it cleaner. Using the values of the masses of the B_s and B_d system given in Eq. (5.71) and the experimental values for Δm_d and Δm_s given in Eqs. (5.72) and (5.73), we obtain the ratio of the CKM matrix elements:

$$\left|\frac{V_{td}}{V_{ts}}\right| = 0.2063 \pm 0.0004 \pm 0.0027\,. \tag{5.86}$$

Here, the first uncertainty corresponds to experimental measurements while the second one is due to the lattice input.

Therefore, the R_t side can be determined.[49] However, in this case we have to make the assumption that we use SM expressions for the mixing parameters Δm_d and Δm_s.

UT Apex Results through R_b and R_t

Having determined R_t, we can now make a fit to the R_b and R_t sides and we obtain the results [81] in Table 7. Comparing these results with the ones that relies on information from γ shown in Table 2, we notice that there is a similar precision for $\bar{\eta}$ while $\bar{\rho}$ is a factor 2 more precise.

Consequently, the extraction of the UT apex coordinates utilising R_b and R_t is more precise than the determination through R_b and γ, presented in Sec. 3.4.2. On the other hand, R_t requires the SM expressions of Δm_d and Δm_s and as a result, possible NP contributions in B_q^0-$\bar{B}_q^0$ mixing are ignored.

[49] We mention here that since we will revisit the discussion about the side R_t in Chapter 8, we will gather the corresponding values in Table 17, for completeness.

Case	$\kappa_d = \kappa_s = \kappa$	$\sigma_d = \sigma_s = \sigma$
Inclusive	$0.057^{+0.040}_{-0.026}$	$(294^{+34}_{-53})^\circ$
Exclusive	$0.203^{+0.062}_{-0.057}$	$(347.7^{+7.4}_{-8.3})^\circ$
Hybrid	$0.043^{+0.049}_{-0.036}$	$(326^{+32}_{-90})^\circ$

Table 8: Values of $\kappa_d = \kappa_s = \kappa$ and $\sigma_d = \sigma_s = \sigma$ in the NP Scenario II for the inclusive, exclusive and hybrid case.

Obtaining the NP Parameters in Scenario II

Let us finally define the NP space using the FUNP assumption. An important consequence of this assumption is that in the ratio $\Delta m_d/\Delta m_s$, any NP contributions cancel. Therefore, the R_t (defined in Eq. (5.81)) will not receive any contributions from NP at order λ^2. Employing the UT apex, coming from R_b and R_t, we obtain the SM values of Δm_q and ϕ_q without relying on γ. These SM predictions are compared with the experimental counterparts and lead to constraints on κ and σ. The GammaCombo fit results [81] are presented in Table 8.

Comparing Scenario I and Scenario II

Comparing the values from Scenario II with the results from Scenario I, where the UT apex was relying on R_b and γ, we observe that they are similar to the κ_s and σ_s parameters for the inclusive, exclusive and hybrid case, indicating that the B_s system dominates the fits.

A comparison between the two scenarios allows us to test the FUNP assumption and explore its impact on the constraints on the parameter space of NP in B_q^0-$\bar{B}_q^0$ mixing. Within uncertainties, the FUNP case interpolates between B_d and B_s system, with B_s still playing the dominant role. So, the FUNP scenario seems to be compatible with Scenario I for both B_d and B_s, which means that we can not rule out FUNP assumption[50]. Fig. 33 illustrates the correlation between κ_d and κ_s. The three contours represent the three R_b solutions (for the inclusive, exclusive and hybrid case) while the black diagonal line denotes that $\kappa_d = \kappa_s$, which is used in the FUNP scenario. We observe again that all three solutions are compatible with the FUNP assumption.

[50] A comparison between the fit solutions for the B_d and B_s systems coming from GammaCombo is presented in Ref. [81] and for completeness we add it in Appendix D.

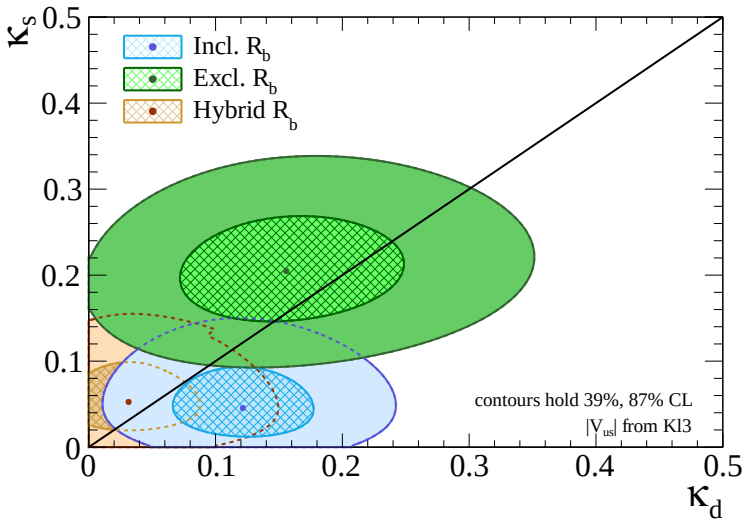

Figure 33: Comparing the inclusive, exclusive and hybrid scenarios through a combined fit for κ_d and κ_s. The black diagonal line denotes the FUNP scenario, where $\kappa_d = \kappa_s$. The analysis has been made using GammaCombo fit.

5.4.3 Future Improvements

In the future, it will be important to achieve increased precision on the key input measurements. Let us firstly discuss the case of improvements on the NP parameters κ_q and σ_q. Regarding the phases ϕ_q, it is only the $\phi_s^{\rm SM}$ which is more precisely known than the corresponding experimental value. On the other hand, the $\phi_d^{\rm SM}$ phase is limited by the UT apex knowledge and particularly the R_b side. The $\Delta m_d^{\rm SM}$ and $\Delta m_s^{\rm SM}$ parameters have large uncertainties due to non-perturbative terms. As it is difficult to improve these calculations and it is not easy to predict the associated time-scale, we avoid future estimates. As a result, we focus on the $|V_{cb}|$ matrix element, the lattice calculations and the UT apex.

We get a feeling of the future prospects, by making the hypothetical assumption that each one of the above mentioned input parameters is reduced by 50%. The corresponding values are presented in Table 9, where we compare the current results (Scenario I) of κ_q and σ_q for the inclusive, exclusive and hybrid case for both the B_d and B_s systems with the 50% improved precision on each one of the parameters: $|V_{cb}|$, lattice and UT apex [81]. We obtain interesting findings, which of course depend on these assumptions.

Regarding the B_s-meson system, we note that the precision on κ_q and σ_q is limited by the lattice uncertainty. The impact from improvements on the UT apex seems to be negligible, especially for the phase ϕ_s. From the scenarios that we consider, it is the exclusive case which assumes improvement from lattice that appears to be the most exciting. Such a case,

	κ_d			σ_d		
Scenario	Inclusive	Exclusive	Hybrid	Inclusive	Exclusive	Hybrid
Current	$0.121^{+0.056}_{-0.055}$	$0.156^{+0.093}_{-0.084}$	$0.031^{+0.057}_{-0.031}$	$\left(261^{+37}_{-35}\right)^\circ$	$\left(347^{+21}_{-25}\right)^\circ$	$\left(104^{+256}_{-104}\right)^\circ$
$\lvert V_{cb}\rvert_{50\%\text{ improv.}}$	$0.121^{+0.056}_{-0.055}$	$0.156^{+0.089}_{-0.081}$	$0.031^{+0.056}_{-0.031}$	$\left(261^{+37}_{-35}\right)^\circ$	$\left(347^{+21}_{-24}\right)^\circ$	$\left(104^{+256}_{-104}\right)^\circ$
$\text{lattice}_{50\%\text{ improv.}}$	$0.121^{+0.056}_{-0.055}$	$0.156^{+0.074}_{-0.069}$	$0.031^{+0.050}_{-0.031}$	$\left(261^{+31}_{-31}\right)^\circ$	$\left(347^{+21}_{-22}\right)^\circ$	$\left(104^{+256}_{-104}\right)^\circ$
$\text{UT Apex}_{50\%\text{ improv.}}$	$0.121^{+0.037}_{-0.036}$	$0.156^{+0.078}_{-0.071}$	$0.031^{+0.046}_{-0.031}$	$\left(261^{+31}_{-28}\right)^\circ$	$\left(347^{+10}_{-15}\right)^\circ$	$\left(104^{+256}_{-104}\right)^\circ$
	κ_s			σ_s		
Current	$0.045^{+0.048}_{-0.033}$	$0.205^{+0.064}_{-0.059}$	$0.053^{+0.046}_{-0.034}$	$\left(312^{+37}_{-77}\right)^\circ$	$\left(347.6^{+8.5}_{-9.8}\right)^\circ$	$\left(309^{+34}_{-65}\right)^\circ$
$\lvert V_{cb}\rvert_{50\%\text{ improv.}}$	$0.045^{+0.046}_{-0.032}$	$0.205^{+0.058}_{-0.053}$	$0.053^{+0.044}_{-0.033}$	$\left(312^{+37}_{-73}\right)^\circ$	$\left(347.6^{+8.5}_{-9.4}\right)^\circ$	$\left(309^{+33}_{-61}\right)^\circ$
$\text{lattice}_{50\%\text{ improv.}}$	$0.045^{+0.032}_{-0.028}$	$0.205^{+0.042}_{-0.040}$	$0.053^{+0.030}_{-0.029}$	$\left(312^{+36}_{-47}\right)^\circ$	$\left(347.6^{+8.5}_{-8.8}\right)^\circ$	$\left(309^{+31}_{-39}\right)^\circ$
$\text{UT Apex}_{50\%\text{ improv.}}$	$0.045^{+0.048}_{-0.033}$	$0.205^{+0.064}_{-0.059}$	$0.053^{+0.046}_{-0.034}$	$\left(312^{+37}_{-77}\right)^\circ$	$\left(347.6^{+8.5}_{-9.7}\right)^\circ$	$\left(309^{+34}_{-64}\right)^\circ$

Table 9: Results for NP parameters κ_q and σ_q, assuming a hypothetical scenario of reducing the uncertainty on the $|V_{cb}|$ matrix element, the lattice calculations and the UT apex by 50%. Both B_d and B_s systems are studied for the inclusive, exclusive and hybrid case [81].

would suggest NP in B_s^0–$\bar{B}_s^0$ with a significance of more than 5 standard deviations.

As far as the B_d-meson system is concerned, the situation is different. We demonstrate in our studies that, the UT apex plays a limiting factor. We note that it is the inclusive scenario which assumes improvement on the UT apex the one that stands out. In order to fully explore the potentials of this system, progress on the UT apex has to be made. Things are very different from the B_s-system where the SM prediction of ϕ_s is more robust. Consequently, searches of NP in B_s^0-$\bar{B}_s^0$ mixing are more promising than in the B_d-system. Of course, it is of key importance to manage to constrain NP in both the B_d and B_s systems as much as possible.

Another essential point regarding future prospects is related to NP in the angle γ. As we have already mentioned, there are two ways of determining γ and with the current data, they are in good agreement with each other. However, these measurements have different origin. If in the future, there is improved precision on the input quantities of these measurements, the different γ determinations might show significant discrepancies due to NP effects. In this case, it would no longer be justified to perform an average of the different results, as we performed here. Therefore, the UT analysis should be revisited. Then, independent information from additional observables would be necessary to resolve such a situation, which could also provide exciting new opportunities in NP searches, not only in γ but also in B_q^0-$\bar{B}_q^0$ mixing, which is strongly correlated with the UT apex coordinates.

As we also discussed the case of determining the UT without using γ information but the R_t side instead, we highlight the issue in this case, which is the SM determination of the R_t. Utilising additional assumptions like the FUNP, we make sure that in ratios like $\Delta m_d/\Delta m_s$, any NP contributions drop out, thus remain SM-like.

5.5 To sum up

In this Chapter we have presented a detailed analysis of the $B_d^0 \to J/\psi K^0$ and $B_s^0 \to J/\psi\phi$ channels, discussing the state-of-the-art picture of the penguin effects. Special care has to be taken in the extraction of the mixing phases ϕ_q. The determination of ϕ_d from the $B_d^0 \to J/\psi K^0$ channel and ϕ_s from the $B_s^0 \to J/\psi\phi$ is limited due to penguin effects.

We are entering a phase where hadronic uncertainties have to be included. Therefore, we have developed a strategy of including these corrections with the help of data. Having employed $SU(3)$ flavour symmetry, we have made use of the corresponding control channels, which are the $B_d^0 \to J/\psi\pi^0$, $B_s^0 \to J/\psi K_S^0$ and $B_d^0 \to J/\psi\rho^0$ modes. All these five channels have been used in a simultaneous fit. Since their mixing-induced asymmetries depend on ϕ_q, this analysis allows the extraction of the mixing phases and the hadronic parameters, taking directly the penguin effects into account.

Considering future scenarios, we have highlighted again how essential it is to improve the precision on R_b side and eventually resolve the $|V_{ub}|$ and $|V_{cb}|$ inclusive-exclusive tensions as these are limiting factors concerning ϕ_d determination. Regarding ϕ_s, it will be important for polarization-dependent measurements from $B_s^0 \to J/\psi\phi$ to become available. As we have shown in these scenarios that it will be possible to obtain non-zero contributions to ϕ_s with more than 5 σ, it becomes clear that the penguin uncertainties have to be controlled and that the five channels we have used can be benchmark channels for CP violation studies.

Moreover, we have utilised information from branching ratios in order to determine the effective colour suppression factors a_2. These parameters can be used as reference for future QCD calculations, thus to help gain insight into the dynamics of the $B^0 \to J/\psi P$ decays. In order to extract the a_2 factors in a theoretically clean way and to minimise the dependence on hadronic formn factors, we have introduced ratios of the $B^0 \to J/\psi P$ modes that we are interested in, with their semi-leptonic partner decays. The results are in the ballpark of theoretical predictions, suffering though from large uncertainties. They also show the impact of non-factorisable $SU(3)$ breaking effects, where no deviation from the $SU(3)$ limit has been indicated within the current precision. Therefore, the $SU(3)$-based strategy suggested in our analysis works well and it can offer exciting potential for establishing new sources of CP violation in the future.

Having the SM predictions of the mixing parameters as inputs, we have moved towards

our main goal, which is to explore the allowed parameter space for NP. We have introduced the NP parameters κ_q and σ_q and have explored two different NP scenarios. In the first scenario, we have constrained the NP parameters separately for the B_s and the B_d system in a model-independent way. We have shown that out of the three cases, it is the exclusive one for the B_s system that gives a strong NP evidence.

In the second scenario, we have assumed Flavour Universal NP, thus NP contributions are the same in the B_s and B_d system and as a result, NP effects are dropped out in the $\Delta m_d/\Delta m_s$ ratio. As we have noted, the B_s system is the dominant one. Comparing the three cases for the CKM matrix elements, we have found that in the exclusive one the fit contours overlap well with those coming from the general NP case for the B_s system while in the inclusive and hybrid case the shapes are different. Thus, the FUNP assumption might not be realised in the nature, although we can not exclude such kind of NP given the current uncertainties.

Moving to the high precision era, we have performed future projections for the main input parameters, thus the CKM matrix elements, the UT apex as well as the lattice calculations. Interestingly, we have demonstrated that in the B_d system the UT apex plays a limiting factor and progress on the UT apex is required in order to fully explore this system's potential. Contrary to B_d, in the B_s system we do not have this issue as the SM prediction of the phase ϕ_s is more robust. Therefore, NP searches in the neutral mixing of B_s system are more promising than in the B_d. However, constraining NP in both systems as much as possible is of key importance. Last but not least, essential future prospect is also related to the UT angle γ, because improved precision on the input quantities might lead to discrepancies between the different γ determinations due to NP, which will not allow anymore an averaged result as it is used here.

Our Decays Roadmap - Highlights

Decays with Different Dynamics

UT
Important to study
inclusive & exclusive cases
separately for $|V_{ub}|$ & $|V_{cb}|$

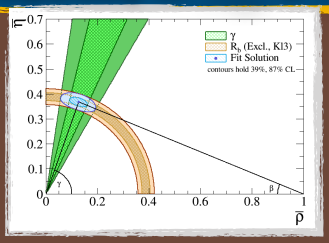

$B_d \to J/\psi K_S$, $B_s \to J/\psi\phi$

Performing combined fit with their control channels
↓
allows the determination of the mixing phases $\phi_{d,s}$
including the impact of penguins on CP asymmetries

CP Violation in different manifestations

$B_s \to D_s^{\pm} K^{\mp}$
and related modes
pure tree decays

Rare Decays
$B \to \mu\mu$
from EW penguins
and box topologies

$B \to \pi K$
dominated by penguins

6 The $B_s^0 \to D_s^\mp K^\pm$ System

In this Chapter we explore the $B_s^0 \to D_s^\mp K^\pm$ system, which is a very interesting example of non-leptonic decays, offering a powerful probe for testing the SM description of CP violation [241–243]. In the SM, the channels $\bar{B}_s^0 \to D_s^+ K^-$ and $B_s^0 \to D_s^+ K^-$ with their counterparts decaying into the CP-conjugate final state $D_s^- K^+$ originate from pure tree topologies caused by $b \to c\bar{u}s$ and $\bar{b} \to \bar{u}c\bar{s}$ quark-level processes, respectively, as shown in Fig. 34(a,b). Dealing with neutral B_s^0 mesons, the phenomenon of B_s^0–$\bar{B}_s^0$ mixing occurs. Due to B_s^0–$\bar{B}_s^0$ mixing, interference effects arise between the $\bar{B}_s^0 \to D_s^+ K^-$ and $B_s^0 \to D_s^+ K^-$ decay processes. Therefore, the $B_s^0 \to D_s^\mp K^\pm$ system allows a theoretically clean determination of the phase $\phi_s + \gamma$. As the mixing phase ϕ_s is determined through $B_s^0 \to J/\psi\phi$ and similar modes [191, 211, 212, 220, 244], it finally leads to the extraction of γ.

Historically, these decays were considered very robust with respect to NP contributions. However, we have now reached the level of precision that allows us to see puzzling patterns. One of these puzzles, which was also our motivation to further explore the $B_s^0 \to D_s^+ K^-$ system, was a surprisingly large γ value which was reported by LHCb Collaboration [189]

$$\gamma = \left(128^{+17}_{-22}\right)^\circ . \tag{6.1}$$

This result is in tension with the regime of 70°, which is given by global analyses of the UT [122, 187, 233, 245] as illustrated in Fig. 35. Could this value indicate physics beyond the SM?

In order to answer this question, we complement our analysis with information from branching ratios. Extracting the individual branching ratios of the $B_s^0 \to D_s^+ K^-$ decays and combining with information from semi-leptonic $B_{(s)}$ decays, we arrive at yet another tension with SM predictions, which we also obtain in other decays with similar dynamics.

In view of all these puzzles, we need to shed more light on the situation. Therefore, we develop a model-independent strategy and generalise our analysis of the $B_s^0 \to D_s^\mp K^\pm$ system in order to include NP effects.

The outline of this Chapter is the following: first, we provide the theoretical framework, having a closer look at CP violation and discussing the $\phi_s + \gamma$ determination, while paying special attention to discrete ambiguities. We determine the individual branching ratios of the $B_s^0 \to D_s^+ K^-$ and $B_s^0 \to D_s^- K^+$ decay channels from the experimental data. We convert them into effective colour factors $|a_1|$, which characterise the colour-allowed tree decays, and obtain the corresponding SM predictions. We extract the $|a_1|$ parameters in the cleanest possible way with respect to uncertainties from CKM parameters and form factors, utilising

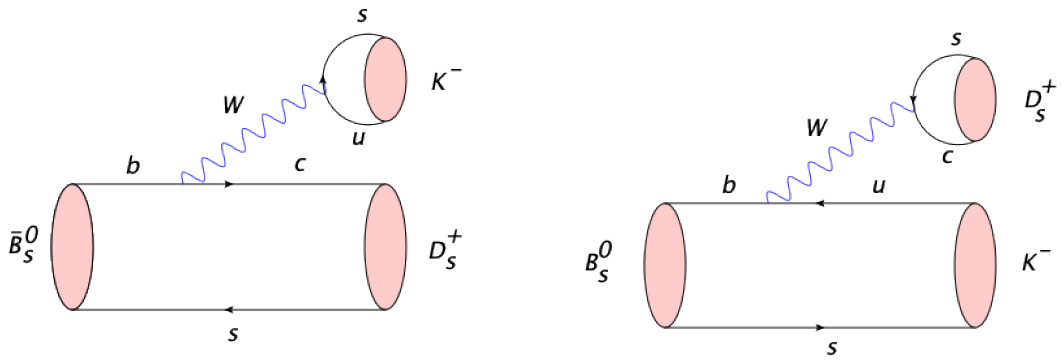

Figure 34: Colour-allowed tree topologies for the $B_s^0 \to D_s^\mp K^\pm$ system in the SM.

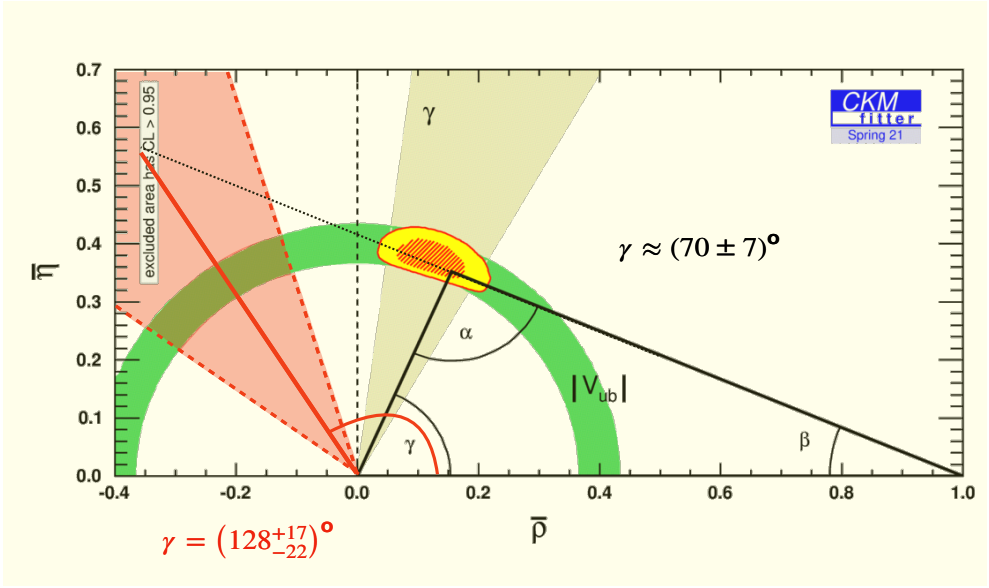

Figure 35: Tension between the angle γ form the global UT analyses (shaded brown area) and the result from the LHCb Collabration (shaded red area) in Ref. [189].

$B_{(s)}$ semileptonic decays. In view of the puzzles that arise, we propose a model-independent framework to reveal possible NP effects. We apply our strategy to the data and explore the space left for NP. We finally summarise our conclusions. The chapter is based on our studies in Refs. [115, 190] and the proceedings contributions [206, 207, 246–248].

For completeness, we emphasize that we only focus on the value of γ (and related observables) reported in Ref. [189], which was the available data when our papers discussed

in this thesis were published. Very recently, the LHCb Collaboration came up with a new analysis of the $B_s^0 \to D_s^{\mp} K^{\pm}$ system, reporting a standalone RUN II measurement corresponding to $\gamma = (74 \pm 11)^\circ$ [188]. By the time the present manuscript was submitted, this result had not been included in the average of the γ values yet. Hence, for the numerical analysis of this thesis, we will not take it into account. However, this is a very interesting result, where the large uncertainties still leave a lot of room, and needs to be further explored. Despite of what the future data will bring, the key points of our proposed strategies and the main results arising from our studies still hold and provide useful insights, setting the basis for future explorations of these decays.

6.1 Standard Model Amplitudes

Our starting point is to express the SM amplitude as:

$$A(B_s^0 \to D_s^+ K^-) = \langle K^- D_s^+ | \mathcal{H}_{\rm eff}(B_s^0 \to D_s^+ K^-) | B_s^0 \rangle \ , \tag{6.2}$$

where $\mathcal{H}_{\rm eff}$ is the low-energy effective Hamiltonian of the system. A similar relation can also be written for the CP-conjugate case. Following here the notation of Ref. [242], we denote the CKM factors[51] as υ_s, $\bar{\upsilon}_s$, υ_s^*, $\bar{\upsilon}_s^*$ and the hadronic matrix elements as M_s, $\bar{M}_s$. The decay amplitude is rewritten as follows:

$$A(\bar{B}_s^0 \to D_s^+ K^-) = \frac{G_F}{\sqrt{2}} \bar{\upsilon}_s \bar{M}_s, \tag{6.3}$$

$$A(B_s^0 \to D_s^+ K^-) = (-1)^L e^{i\phi_{\rm CP}} \frac{G_F}{\sqrt{2}} \upsilon_s^* M_s, \tag{6.4}$$

where L is the angular momentum of the final state system, which in this case is equal to 0, and $\phi_{\rm CP}$ is a convention dependent CP-phase. This phase arises from performing CP operations, as was already presented in Eqs. (4.4) and (4.5). Similarly, for the CP-conjugate final state:

$$A(\bar{B}_s^0 \to D_s^- K^+) = \frac{G_F}{\sqrt{2}} \upsilon_s M_s, \tag{6.5}$$

$$A(B_s^0 \to D_s^- K^+) = (-1)^L e^{i\phi_{\rm CP}} \frac{G_F}{\sqrt{2}} \bar{\upsilon}_s^* \bar{M}_s. \tag{6.6}$$

Let us recall Sec. 4.2.2, where we introduced the quantities ξ and $\bar{\xi}$ which measure the strength of the interference effects. Employing the CP transformations in Eqs. (4.4)

[51] These CKM factors are products of CKM matrix elements.

and (4.5), we can now write these physical observables for the $B_s^0 \to D_s^{\mp} K^{\pm}$ system as follows [242]:

$$\xi_s = -e^{-i\phi_s} \left[e^{i\phi_{\rm CP}} \frac{A(\bar{B}_s^0 \to D_s^+ K^-)}{A(B_s^0 \to D_s^+ K^-)} \right], \tag{6.7}$$

$$\bar{\xi}_s = -e^{-i\phi_s} \left[e^{i\phi_{\rm CP}} \frac{A(\bar{B}_s^0 \to D_s^- K^+)}{A(B_s^0 \to D_s^- K^+)} \right]. \tag{6.8}$$

The next step is to implement the formulas of the decay amplitudes in the above expressions. Therefore, the $\phi_{\rm CP}$ phase gets cancelled by the amplitude ratios and we obtain the simpler form:

$$\xi_s = -(-1)^L e^{-i(\phi_s+\gamma)} \left[\frac{1}{x_s e^{i\delta_s}} \right], \tag{6.9}$$

$$\bar{\xi}_s = -(-1)^L e^{-i(\phi_s+\gamma)} \left[x_s e^{i\delta_s} \right]. \tag{6.10}$$

Here, the hadronic parameter x_s and the strong phase δ_s are introduced. The parameter x_s is defined as in Ref. [242]

$$x_s = R_b a_s, \tag{6.11}$$

where R_b is the UT side, while for a_s:

$$a_s e^{i\delta_s} = e^{-i[\phi_{\rm CP}(D) - \phi_{\rm CP}(K)]} \frac{M_s}{\overline{M}_s}. \tag{6.12}$$

The phases $\phi_{\rm CP}$ are cancelled in the ratio of the hadronic matrix elements.

Due to the structure of Eqs. (6.9) and (6.10), we utilise the product of the two parameters and arrive at a theoretically clean relation:

$$\xi_s \times \bar{\xi}_s = e^{-i2(\phi_s+\gamma)}, \tag{6.13}$$

where the non-perturbative hadronic parameter $x_s e^{i\delta_s}$ cancels. This relation allows the extraction of $\phi_s + \gamma$, once ξ_s and $\bar{\xi}_s$ are determined. So, let us see in the following Section how we determine them.

6.2 CP Asymmetries

Due to the B_s^0–$\bar{B}_s^0$ oscillations, and having both neutral mesons decaying into the same final state f, interference effects arise between B_s^0–$\bar{B}_s^0$ mixing and the decay processes. These effects lead to the time-dependent rate asymmetry, which takes the following form for the $B_s^0 \to D_s^{\mp} K^{\pm}$ system [242, 243]:

$$\mathcal{A}_{CP}(t) = \frac{\Gamma(B_s^0(t) \to f) - \Gamma(\bar{B}_s^0(t) \to f)}{\Gamma(B_s^0(t) \to f) + \Gamma(\bar{B}_s^0(t) \to f)} = \frac{C\, \cos(\Delta m_s\, t) + S\, \sin(\Delta m_s\, t)}{\cosh(y_s\, t/\tau_{B_s}) + \mathcal{A}_{\Delta\Gamma}\, \sinh(y_s\, t/\tau_{B_s})}. \tag{6.14}$$

This asymmetry allows us to probe the corresponding CP-violating effects. Here, f is the $D_s^+ K^-$ final state, the $\Delta m_s \equiv m_{\rm H}^{(s)} - m_{\rm L}^{(s)}$ describes the mass difference of the B_s mass eigenstates, as we already introduced in Eq. (3.22), and y_s is defined as

$$y_s \equiv \frac{\Delta\Gamma_s}{2\,\Gamma_s} = 0.062 \pm 0.004, \tag{6.15}$$

where $\Delta\Gamma_s \equiv \Gamma_{\rm L}^{(s)} - \Gamma_{\rm H}^{(s)}$ is the decay width difference, as in Eq. (3.23), and $\Gamma_s \equiv \tau_{B_s}^{-1}$ is the inverse of the average lifetime of the B_s system. The numerical value of y_s corresponds to the current experimental average [233]. The coefficients of the oscillatory terms $\cos(\Delta m_s t)$ and $\sin(\Delta m_s t)$ are the observables C and S, respectively, which are now expressed as follows[52]:

$$C = \frac{|A(B_s^0 \to D_s^+ K^-)|^2 - |A(\bar{B}_s^0 \to D_s^+ K^-)|^2}{|A(B_s^0 \to D_s^+ K^-)|^2 + |A(\bar{B}_s^0 \to D_s^+ K^-)|^2} = \frac{1 - |\xi_s|^2}{1 + |\xi_s|^2}, \tag{6.16}$$

$$S = \left(\frac{2}{1 + |\xi_s|^2}\right)\ {\rm Im}\,\xi_s, \tag{6.17}$$

with S indicating the mixing induced CP violation. Due to the sizeable differential decay width $\Delta\Gamma_s$, we get access to a third observable, the $\mathcal{A}_{\Delta\Gamma}$:

$$\mathcal{A}_{\Delta\Gamma} = \left(\frac{2}{1 + |\xi_s|^2}\right)\ {\rm Re}\,\xi_s. \tag{6.18}$$

We remind the reader that the $\mathcal{A}_{\Delta\Gamma}$ depends on the other two asymmetries, satisfying the sum rule:

$$\Delta_{\rm SR} \equiv 1 - C^2 - S^2 - \mathcal{A}_{\Delta\Gamma}^2 = 0. \tag{6.19}$$

As we can see from the above relations, the absolute value of ξ_s can be determined from the measured value of C while information from S and $\mathcal{A}_{\Delta\Gamma}$ allows the extraction of the imaginary and real part of ξ_s, respectively, through the relations

$$|\xi_s| = \sqrt{\frac{1 - C}{1 + C}}, \qquad {\rm Re}\,\xi_s = \frac{\mathcal{A}_{\Delta\Gamma}}{1 + C}, \qquad {\rm Im}\,\xi_s = \frac{S}{1 + C}, \tag{6.20}$$

fixing ξ_s in the complex plane from the data. Therefore, we can determine ξ_s unambiguously from the measured observables.

We note that analogous relations hold for $\bar{f}$, thus the CP-conjugate $D_s^- K^+$ final state, where C, S and $\mathcal{A}_{\Delta\Gamma}$ are replaced by $\overline{C}$, $\overline{S}$ and $\overline{\mathcal{A}}_{\Delta\Gamma}$, respectively. Similarly, we obtain the following sum rule:

$$\overline{\Delta}_{\rm SR} \equiv 1 - \overline{C}^2 - \overline{S}^2 - \overline{\mathcal{A}}_{\Delta\Gamma}^2 = 0. \tag{6.21}$$

[52] The notation now is in line with Refs. [115, 190].

Observables	
$C = -0.73 \pm 0.15$	$\overline{C} = +0.73 \pm 0.15$
$S = +0.49 \pm 0.21$	$\overline{S} = +0.52 \pm 0.21$
$\mathcal{A}_{\Delta\Gamma} = +0.31 \pm 0.32$	$\overline{\mathcal{A}}_{\Delta\Gamma} = +0.39 \pm 0.32$

Table 10: CP-violating $B_s^0 \to D_s^\mp K^\pm$ observables corresponding to the LHCb analysis [189].

Again, we extract $\bar{\xi}_s$ from the measured values of the three observables. The observables corresponding to the LHCb analysis [189] are collected in Table 10, taking the proper sign conventions into account and having added the statistical and systematic uncertainties in quadrature. For completeness, we mention that these measured values are consistent with the sum rules in Eqs. (6.19) and (6.21):

$$\Delta_{\rm SR} = 0.13 \pm 0.36, \quad \overline{\Delta}_{\rm SR} = 0.04 \pm 0.40. \tag{6.22}$$

6.3 Determining γ and Resolving Ambiguities

We already introduced Eq. (6.13), which is one of the relations that play the central role in our analysis and we described in the previous Section how both ξ_s and $\bar{\xi}_s$ can be determined through the asymmetries C, S, $\mathcal{A}_{\Delta\Gamma}$ and $\overline{C}$, $\overline{S}$, $\overline{\mathcal{A}}_{\Delta\Gamma}$, respectively. Therefore, Eq. (6.13) allows the extraction of $\phi_s + \gamma$ using only the observables. Since ϕ_s is already determined through $B_s^0 \to J/\psi\phi$ and similar modes [191, 211, 212, 220, 244], we extract the UT angle γ. We note that due to the multiplicative factor of two, which is associated with this phase, we obtain a twofold ambiguity, modulo 180°.

The observables $\mathcal{A}_{\Delta\Gamma}$ and $\overline{\mathcal{A}}_{\Delta\Gamma}$ play an important role in the reduction of the number of the ambiguities. More specifically, if only measurements of C and S were available, we would obtain a twofold ambiguity for ξ_s, and similarly for $\bar{\xi}_s$. Consequently, when applying Eq. (6.13), we would have a fourfold ambiguity for $2(\phi_s + \gamma)$, resulting in an eightfold ambiguity for $\phi_s + \gamma$, thus for γ itself. However, combining the information obtained from S_s, $\bar{S}_s$, $\mathcal{A}_{\Delta\Gamma_s}$ and $\bar{\mathcal{A}}_{\Delta\Gamma_s}$, the number of discrete ambiguities can be reduced, as it is pointed out in Refs. [242, 243]. We are then left with a twofold ambiguity, which can further be resolved. Thus, $\mathcal{A}_{\Delta\Gamma_s}$ and $\bar{\mathcal{A}}_{\Delta\Gamma_s}$ are crucial to resolve ambiguities.

In the SM framework, due to the fact that Eqs. (6.9) and (6.10) rely on the structure of the corresponding decay amplitudes, the following relations hold

$$|\bar{\xi}_s| = \frac{1}{|\xi_s|} = \sqrt{\frac{(1+C)}{(1-C)}}, \qquad C + \overline{C} = 0, \tag{6.23}$$

which were assumed by the LHCb Collaboration in their analysis [189]. LHCb performed a sophisticated fit to their data, taking relevant correlations into account, and obtained the following picture:

$$|\bar{\xi}_s| = 0.37^{+0.10}_{-0.09}, \quad \phi_s + \gamma = \left(126^{+17}_{-22}\right)^\circ, \quad \delta_s = (-2^{+13}_{-14})^\circ, \quad \text{[modulo } 180^\circ\text{]}, \tag{6.24}$$

where we have omitted the solutions modulo 180° and used $\phi_s = (-1.7 \pm 1.9)^\circ$ in order to convert the value of γ in Eq. (6.1) into $\phi_s + \gamma$. Using an updated value of $\phi_s = \left(-5^{+1.6}_{-1.5}\right)^\circ$, as we already introduced in Eq. (5.35), which is the average of the corresponding measurements and includes corrections from doubly Cabibbo-suppressed penguin topologies, [191] we obtain

$$\gamma = \left(131^{+17}_{-22}\right)^\circ. \tag{6.25}$$

This result is in tension with the SM, which suggests a value of γ at the regime of 70°. In view of this puzzling value and as LHCb performed an intricate analysis to obtain their results, working under the assumption $C + \overline{C} = 0$, it is crucial to transparently understand the situation. Let us see how we can achieve this.

Applying Eq. (6.23) using the measured value of C, which is given in Table 10, we obtain:

$$|\xi_s| = 2.53^{+1.43}_{-0.59}, \qquad |\bar{\xi}_s| = 0.40 \pm 0.13. \tag{6.26}$$

Using the following combinations of the observables:

$$\langle S \rangle_+ \equiv \frac{\overline{S} + S}{2} = 0.50 \pm 0.15, \qquad \langle S \rangle_- \equiv \frac{\overline{S} - S}{2} = 0.02 \pm 0.15 \tag{6.27}$$

$$\langle \mathcal{A}_{\Delta\Gamma} \rangle_+ \equiv \frac{\overline{\mathcal{A}}_{\Delta\Gamma} + \mathcal{A}_{\Delta\Gamma}}{2} = 0.35 \pm 0.23, \qquad \langle \mathcal{A}_{\Delta\Gamma} \rangle_- \equiv \frac{\overline{\mathcal{A}}_{\Delta\Gamma} - \mathcal{A}_{\Delta\Gamma}}{2} = 0.04 \pm 0.23, \tag{6.28}$$

we are able to determine $\phi_s + \gamma$ as well as δ_s with the help of experimental data, utilising the following relations [115, 190, 242, 243]:

$$\tan(\phi_s + \gamma) = -\frac{\langle S \rangle_+}{\langle \mathcal{A}_{\Delta\Gamma} \rangle_+} = -1.45^{+0.73}_{-2.76}, \tag{6.29}$$

$$\tan \delta_s = \frac{\langle S \rangle_-}{\langle \mathcal{A}_{\Delta\Gamma} \rangle_+} = 0.04^{+0.70}_{-0.40}. \tag{6.30}$$

The situation is illustrated in Fig. 36. As we can see on the left-hand side plot, the points where the contours coming from the tangent function and the line corresponding to the value of $(\tan \phi_s + \gamma)$ intersect, are the $\phi_s + \gamma$ solutions. There is a twofold solution for $\phi_s + \gamma$ arising from the measured observables:

$$\phi_s + \gamma = (-55^{+18}_{-22})^\circ \quad \vee \quad (125^{+22}_{-18})^\circ. \tag{6.31}$$

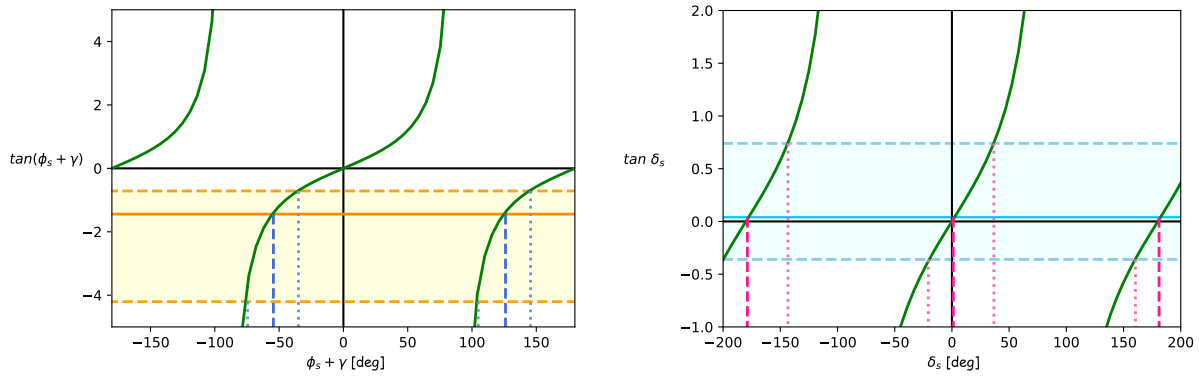

Figure 36: Illustration of the determination of $\phi_s+\gamma$ (left) and δ_s (right) [115], as described in the text.

Similarly, on the right-hand side plot in Fig. 36, for the CP-conserving strong phase δ_s, the numerical values corresponding to the LHCb measurements give

$$\delta_s = (182^{+34}_{-22})^\circ \quad \vee \quad (2^{+34}_{-22})^\circ. \tag{6.32}$$

Taking the signs of $\langle S\rangle_+$ and $\langle \mathcal{A}_{\Delta\Gamma}\rangle_+$ into account and using the relations

$$\frac{\langle S\rangle_+}{\sqrt{1-C^2}} = +\cos\delta_s \sin(\phi_s+\gamma), \quad \frac{\langle \mathcal{A}_{\Delta\Gamma}\rangle_+}{\sqrt{1-C^2}} = -\cos\delta_s \cos(\phi_s+\gamma), \tag{6.33}$$

we observe that $(\phi_s+\gamma) \sim -55^\circ$ and 125° are associated with $\delta_s \sim 180^\circ$ and 0°, respectively. Regarding $\langle S\rangle_-$ and $\langle \mathcal{A}_{\Delta\Gamma}\rangle_-$, they are both proportional to $\sin\delta_s$, and this is also reflected by their small experimental values. The case of $\delta_s \sim 180^\circ$ would be in huge conflict with factorization, which predicts $\delta_s \sim 0^\circ$, as we will discuss in more detail in Subsection 6.5. Consequently, we can single out the final solution $\phi_s+\gamma = (125^{+22}_{-18})^\circ$ with $\delta_s = (2^{+34}_{-22})^\circ$, thereby excluding the solutions modulo 180°.

Therefore, we find excellent agreement between this transparent picture and the LHCb analysis. The result in Eq. (6.25), despite its significant uncertainty, is much larger than the regime of 70°, indicating a discrepancy at the 3σ level. Could this tension indicate NP entering the $B_s^0 \to D_s^\mp K^\pm$ system?

This puzzle would require new sources of CP violation. It could not arise from any long distance effects since the determination of the angle γ is theoretically clean. CP-violating NP effects could, in principle, enter through B_s^0–$\bar{B}_s^0$ mixing. However, the experimental value of ϕ_s which we use in the analysis already includes these effects. Therefore, such new contributions would only enter directly at the level of the decay amplitude of the $B_s^0 \to D_s^\mp K^\pm$ system. As a result, they would manifest themselves also in the corresponding

branching ratios. So, in order to answer the above question and shed more light on this puzzling situation, a closer look at the branching ratios is required. Let us explore all these quantities in detail in the subsequent Section.

6.4 Theoretical Branching Ratios

Information from branching ratios will complement the CP-violating observables and as we will describe in the following Sections, they will give rise to a second puzzling situation. We first determine the individual branching ratios for the different decay channels.

We consider $\bar{B}_s^0$ and B_s^0 decays into the final state $D_s^+ K^-$. Due to B_s^0–$\bar{B}_s^0$ mixing effects, we have to distinguish between the time-integrated "experimental" branching ratios [220]

$$\mathcal{B}_{\rm exp} = \frac{1}{2}\int_0^\infty \left[\Gamma(\bar{B}_s^0(t) \to D_s^+ K^-) + \Gamma(B_s^0(t) \to D_s^+ K^-)\right] {\rm d}t, \tag{6.34}$$

and the "theoretical" branching ratios where these effects are switched off, thus for decay time $t = 0$,

$$\mathcal{B}_{\rm th} \equiv \frac{1}{2}\left[\mathcal{B}(\bar{B}_s^0 \to D_s^+ K^-)_{\rm th} + \mathcal{B}(B_s^0 \to D_s^+ K^-)_{\rm th}\right], \tag{6.35}$$

where the factor of $1/2$ arises from the average of the $\bar{B}_s^0$ and B_s^0 decays. We have to disentangle the interference effects between the two decay paths arising from B_s^0–$\bar{B}_s^0$ mixing:

$$\mathcal{B}(\bar{B}_s^0 \to D_s^+ K^-)_{\rm th} = |A(\bar{B}_s^0 \to D_s^+ K^-)|^2\, \Phi_{\rm Ph}\, \tau_{B_s} \tag{6.36}$$

$$\mathcal{B}(B_s^0 \to D_s^+ K^-)_{\rm th} = |A(B_s^0 \to D_s^+ K^-)|^2\, \Phi_{\rm Ph}\, \tau_{B_s}. \tag{6.37}$$

Here $\Phi_{\rm Ph}$ is the phase-space factor defined as

$$\Phi_{\rm Ph} \equiv \frac{1}{16\,\pi\, m_{B_s}}\, \Phi\left(\frac{m_{D_s}}{m_{B_s}}, \frac{m_K}{m_{B_s}}\right), \tag{6.38}$$

where the meson masses m_{B_s}, m_{D_s} and m_K enter the phase-space function, which we have already presented in Eq. (3.62).

The "theoretical" and the "experimental" branching ratios are related to each other as follows [221]:

$$\mathcal{B}_{\rm th} = \left[\frac{1 - y_s^2}{1 + \mathcal{A}_{\Delta\Gamma_s} y_s}\right] \mathcal{B}_{\rm exp}. \tag{6.39}$$

Using the definition of ξ_s in Eq. (6.7), we may write

$$\mathcal{B}_{\rm th} = \frac{1}{2}\left(1 + |\xi_s|^2\right) \mathcal{B}_{\rm th}(B_s^0 \to D_s^+ K^-) \tag{6.40}$$

$$= \frac{1}{2}\left(1 + |\xi_s|^{-2}\right) \mathcal{B}_{\rm th}(\bar{B}_s^0 \to D_s^+ K^-), \tag{6.41}$$

allowing us to determine the individual theoretical branching ratios [115, 190]:

$$\mathcal{B}(B_s^0 \to D_s^+ K^-)_{\rm th} = 2\left(\frac{1}{1+|\xi|^2}\right)\mathcal{B}_{\rm th}, \tag{6.42}$$

$$\mathcal{B}(\bar{B}_s^0 \to D_s^+ K^-)_{\rm th} = 2\left(\frac{|\xi|^2}{1+|\xi|^2}\right)\mathcal{B}_{\rm th} = |\xi|^2 \mathcal{B}(B_s^0 \to D_s^+ K^-)_{\rm th}. \tag{6.43}$$

The $\mathcal{B}_{\rm th}$ can be determined from the experimental branching ratio through Eq. (6.39). Analogous expressions hold for the B_s^0 and $\bar{B}_s^0$ decays into the final state $D_s^- K^+$, replacing $\mathcal{B}_{\rm exp}$, $\mathcal{B}_{\rm th}$, $\mathcal{A}_{\Delta\Gamma_s}$ and ξ_s through their counterparts $\bar{\mathcal{B}}_{\rm exp}$, $\bar{\mathcal{B}}_{\rm th}$, $\bar{\mathcal{A}}_{\Delta\Gamma_s}$ and $\bar{\xi}$, respectively. Unfortunately, separate measurements of the experimental branching ratios for these final states have not yet been reported. However, the following average is available

$$\langle \mathcal{B}_{\rm exp} \rangle \equiv \frac{1}{2}\left(\mathcal{B}_{\rm exp} + \bar{\mathcal{B}}_{\rm exp}\right) = \frac{1}{2}\,\mathcal{B}_{\Sigma}^{\rm exp}, \tag{6.44}$$

$$\mathcal{B}_{\Sigma}^{\rm exp} \equiv \mathcal{B}_{\rm exp} + \bar{\mathcal{B}}_{\rm exp} = (2.27 \pm 0.19) \times 10^{-4}, \tag{6.45}$$

where the numerical value in Eq. (6.45) is given in Ref. [233]. In the SM framework, the following relations hold:

$$\mathcal{B}(\bar{B}_s^0 \to D_s^+ K^-)_{\rm th} \overset{\rm SM}{=} \mathcal{B}(B_s^0 \to D_s^- K^+)_{\rm th} \tag{6.46}$$

$$\mathcal{B}(B_s^0 \to D_s^+ K^-)_{\rm th} \overset{\rm SM}{=} \mathcal{B}(\bar{B}_s^0 \to D_s^- K^+)_{\rm th}, \tag{6.47}$$

$$\mathcal{B}_{\rm th} \overset{\rm SM}{=} \bar{\mathcal{B}}_{\rm th}. \tag{6.48}$$

Consequently, assuming SM relations for the amplitudes, as was also done by the LHCb collaboration [189], we obtain [243]:

$$\mathcal{B}_{\rm th} = \bar{\mathcal{B}}_{\rm th} = \left[\frac{1-y_s^2}{1+y_s\langle \mathcal{A}_{\Delta\Gamma}\rangle_+}\right]\langle \mathcal{B}_{\rm exp}\rangle. \tag{6.49}$$

Using the numerical values in Eqs. (6.15), (6.28) and (6.44), we determine the value of $\mathcal{B}_{\rm th}$ [115, 190]:

$$\mathcal{B}_{\rm th} = (1.10 \pm 0.09) \times 10^{-4} \tag{6.50}$$

and finally obtain the values of the individual theoretical branching ratios characterising the $B_s^0 \to D_s^{\mp} K^{\pm}$ system:

$$\mathcal{B}(\bar{B}_s^0 \to D_s^+ K^-)_{\rm th} = (1.94 \pm 0.21) \times 10^{-4}, \tag{6.51}$$

$$\mathcal{B}(B_s^0 \to D_s^+ K^-)_{\rm th} = (0.26 \pm 0.12) \times 10^{-4}. \tag{6.52}$$

These results follow from the current data, through Eqs. (6.42), and (6.43) and the $|\xi_s|$, which is extracted from the experimental study of CP violation [115, 190]. Here, we assume

Parameters	CP conjugate	Values
$\mathcal{B}_{\rm th}$	$\bar{\mathcal{B}}_{\rm th}$	$(1.10 \pm 0.09) \times 10^{-4}$
$\mathcal{B}(\bar{B}_s^0 \to D_s^+ K^-)_{\rm th}$	$\mathcal{B}(B_s^0 \to D_s^- K^+)_{\rm th}$	$(1.94 \pm 0.21) \times 10^{-4}$
$\mathcal{B}(B_s^0 \to D_s^+ K^-)_{\rm th}$	$\mathcal{B}(\bar{B}_s^0 \to D_s^- K^+)_{\rm th}$	$(0.26 \pm 0.12) \times 10^{-4}$

Table 11: Theoretical branching ratios characterising the $B_s^0 \to D_s^\mp K^\pm$ system, assuming the SM framework, as discussed in the text [115].

vanishing NP contributions to the corresponding amplitudes. We note that due to our assumption of the SM, the theoretical branching ratios of these decays are equal to their CP conjugates. We collect the values for the individual decay channels in Table 11.

We have determined the individual branching ratios of the two decay channels from the data. For the theoretical SM interpretation, these branching ratios are converted into quantities $|a_1|$, which are phenomenological colour factors that characterise colour-allowed tree decays, as we have already introduced in Sec. 3.5.2. Let us discuss below how we obtain these $|a_1|$ factors.

6.5 Factorisation

Due to the impact of strong interactions, it is challenging to calculate the non-leptonic B-meson decays. The factorisation approach is a particularly useful tool for the calculation of the decay amplitudes and the branching ratios. As already discussed in Sec. 3.5.2, the hadronic matrix elements of the corresponding four-quark operators are factorised into the product of the matrix elements of their quark currents. Factorisation is not a universal feature of non-leptonic B decays. It is expected to work well in decay transitions that originate only from colour-allowed tree topologies [153, 159, 170]. A lot of effort has been put also in QCDF for these decays [164–166]. Prime examples where factorisation is on solid ground are the $b \to c$ transitions like the $\bar{B}_s^0 \to D_s^+ K^-$ channel, which plays a key role in our analysis, as well as the decays $\bar{B}_s^0 \to D_s^+ \pi^-$ and $\bar{B}_d^0 \to D_d^+ K^-$. Let us now see factorisation at work.

6.5.1 Introduction to Partner Decays and Branching Ratio Comparison

Let us firstly discuss the $\bar{B}_d^0 \to D_d^+ K^-$ and $B_d^0 \to D_s^+ \pi^-$ modes, which are the partner decays of the $\bar{B}_s^0 \to D_s^+ K^-$ and $B_s^0 \to D_s^+ K^-$ modes, respectively. They originate from the same quark-level processes while differing only through the spectator quarks. We note that the B_s modes receive additional contributions from exchange topologies, while their

Masses	Values	Masses	Values
m_{B_s}	(5366.88 ± 0.14) MeV	m_{D_d}	(1869.66 ± 0.05) MeV
m_{B_d}	(5279.64 ± 0.12) MeV	m_K	(493.677 ± 0.016) MeV
m_{D_s}	(1968.34 ± 0.07) MeV	m_π	(139.5704 ± 0.0002) MeV

Table 12: Meson masses relevant for our numerical analysis [233]

B_d counterparts do not have such contributions. We can determine the branching ratios of the partner decays and compare them with the results collected in Table 11.

Working with the $\bar{B}_d^0 \to D_d^+ K^-$ and $\bar{B}_s^0 \to D_s^+ K^-$ channels, we may determine the following ratio [115]

$$\left|\frac{T_{D_sK}}{T_{D_dK}}\right|^2 \left|1 + \frac{E_{D_sK}}{T_{D_sK}}\right|^2 = \frac{\tau_{B_d}}{\tau_{B_s}} \frac{m_{B_s}}{m_{B_d}} \left[\frac{\Phi(m_{D_d}/m_{B_d}, m_K/m_{B_d})}{\Phi(m_{D_s}/m_{B_s}, m_K/m_{B_s})}\right] \left[\frac{\mathcal{B}(\bar{B}_s^0 \to D_s^+ K^-)_{\rm th}}{\mathcal{B}(\bar{B}_d^0 \to D_d^+ K^-)}\right], \quad (6.53)$$

where the T_{D_sK} and T_{D_dK} amplitudes describe colour-allowed tree topologies, while E_{D_sK} denotes the exchange topologies. The $SU(3)$ flavour symmetry of strong interactions implies

$$T_{D_sK} \approx T_{D_dK}. \quad (6.54)$$

The $SU(3)$-breaking corrections only arise from spectator quarks. The current experimental branching ratio, which is CP-averaged, reads as follows [233]:

$$\mathcal{B}(\bar{B}_d^0 \to D_d^+ K^-) = (1.86 \pm 0.20) \times 10^{-4}. \quad (6.55)$$

Using the value of $\mathcal{B}(\bar{B}_d^0 \to D_d^+ K^-)$ in Table 11, the meson masses in Table 12 and the average lifetime of the B_s^0 meson [233]

$$\tau_{B_s} = (1.527 \pm 0.011)\,\text{ps}, \quad (6.56)$$

we obtain

$$\left|\frac{T_{D_sK}}{T_{D_dK}}\right| \left|1 + \frac{E_{D_sK}}{T_{D_sK}}\right| = 1.03 \pm 0.08. \quad (6.57)$$

Similarly, we use the $B_d^0 \to D_s^+ \pi^-$ and $B_s^0 \to D_s^+ K^-$ decays and determine [115]

$$\left|\frac{T_{KD_s}}{T_{\pi D_s}}\right|^2 \left|1 + \frac{E_{KD_s}}{T_{KD_s}}\right|^2 = \frac{\tau_{B_d}}{\tau_{B_s}} \frac{m_{B_s}}{m_{B_d}} \left[\frac{\Phi(m_{D_s}/m_{B_d}, m_\pi/m_{B_d})}{\Phi(m_{D_s}/m_{B_s}, m_K/m_{B_s})}\right] \left[\frac{\mathcal{B}(B_s^0 \to D_s^+ K^-)_{\rm th}}{\mathcal{B}(B_d^0 \to D_s^+ \pi^-)}\right], \quad (6.58)$$

where the T_{KD_s}, $T_{\pi D_s}$ and E_{KD_s} describe the corresponding colour-allowed tree and exchange topologies, respectively. Due to the $SU(3)$ flavour symmetry, we have

$$T_{KD_s} \approx T_{\pi D_s}. \tag{6.59}$$

The current experimental CP-averaged branching ratio is [233]:

$$\mathcal{B}(B_d^0 \to D_s^+ \pi^-) = (2.16 \pm 0.26) \times 10^{-5}. \tag{6.60}$$

Using again the values in Tables 11 and 12 as well as the average lifetime of the B_d^0 meson [233]:

$$\tau_{B_d} = (1.519 \pm 0.004)\,\text{ps}, \tag{6.61}$$

we determine the ratio:

$$\left|\frac{T_{KD_s}}{T_{\pi D_s}}\right| \left|1 + \frac{E_{KD_s}}{T_{KD_s}}\right| = 1.11 \pm 0.26. \tag{6.62}$$

The findings in Eqs. (6.57) and (6.62) are consistent with a small impact of the exchange topologies, which was also found in Refs. [243, 249]. We will examine the situation in more detail in a following Section.

As a next step, we compare the $\bar{B}_d^0 \to D_d^+ \pi^-$ and $\bar{B}_s^0 \to D_s^+ \pi^-$ decays , arising from $b \to c\bar{u}d$ quark-level processes, with the $\bar{B}_s^0 \to D_s^+ K^-$ and $\bar{B}_d^0 \to D_d^+ K^-$ channels, which are related through the U-spin symmetry of strong interactions [242, 243]. We determine the ratio

$$\left|\frac{T_{D_d\pi}}{T_{D_s\pi}}\right|^2 \left|1 + \frac{E_{D_d\pi}}{T_{D_d\pi}}\right|^2 = \frac{\tau_{B_s}}{\tau_{B_d}} \frac{m_{B_d}}{m_{B_s}} \left[\frac{\Phi(m_{D_s}/m_{B_s}, m_\pi/m_{B_s})}{\Phi(m_{D_d}/m_{B_d}, m_\pi/m_{B_d})}\right] \left[\frac{\mathcal{B}(\bar{B}_d^0 \to D_d^+ \pi^-)}{\mathcal{B}(\bar{B}_s^0 \to D_s^+ \pi^-)_{\text{th}}}\right] \tag{6.63}$$

with the colour-allowed tree amplitudes $T_{D_d\pi}$, $T_{D_s\pi}$ and the exchange topologies $E_{D_d\pi}$. The values for the experimental branching ratios are the following [233]:

$$\mathcal{B}(\bar{B}_d^0 \to D_d^+ \pi^-) = (2.52 \pm 0.13) \times 10^{-3}, \tag{6.64}$$

$$\mathcal{B}(\bar{B}_s^0 \to D_s^+ \pi^-)_{\text{exp}} = (3.00 \pm 0.23) \times 10^{-3}. \tag{6.65}$$

We can convert the experimental $\bar{B}_s^0 \to D_s^+ \pi^-$ branching ratio into the theoretical one, utilising the relation [221]

$$\mathcal{B}(\bar{B}_s^0 \to D_s^+ \pi^-)_{\text{th}} = (1 - y_s^2)\, \mathcal{B}(\bar{B}_s^0 \to D_s^+ \pi^-)_{\text{exp}}. \tag{6.66}$$

Using the values in Tables 11 and 12 with the average B_s and B_d lifetimes, we obtain [115]

$$\left|\frac{T_{D_d\pi}}{T_{D_s\pi}}\right| \left|1 + \frac{E_{D_d\pi}}{T_{D_d\pi}}\right| = 0.91 \pm 0.04. \tag{6.67}$$

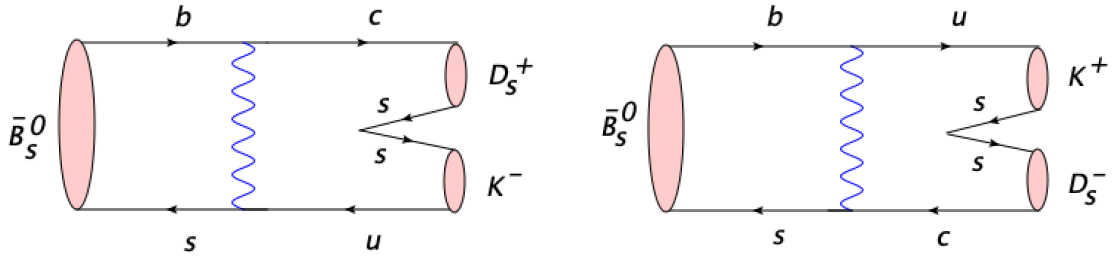

(a) (b)

Figure 37: Exchange topologies for (a) the $\bar{B}_s^0 \to D_s^+ K^-$ and (b) the $\bar{B}_s^0 \to K^+ D_s^-$ decays.

Comparing with Eq. (6.57), the results agree within the uncertainties.

So far, we have found consistent branching ratios with the partner decays and have already presented the first information on exchange topologies. We can now gain insights for more decay channels. In the following Secs. 6.5.2 and 6.5.3, we will discuss how we can determine separately the ratios of the colour-allowed tree amplitudes as well as the terms r_E, defined as

$$r_E = |1 + E/T| \,, \tag{6.68}$$

which include the ratios of exchange over tree topologies.

6.5.2 Theoretical Prediction of $a_1^{D_s K}$

Let us now focus on the $\bar{B}_s^0 \to D_s^+ K^-$ decay, which is caused by $b \to c\bar{u}s$ quark-level transition. This decay receives an additional contribution from an exchange topology which involves the spectator quark and is not factorisable. An illustration of this topology is given in Fig. 37a. However, experimental data indicate that these exchange topologies play a minor role as they contribute to the decay amplitudes at the few-percent level [249]. Within the SM, we may write the amplitude of the $\bar{B}_s^0 \to D_s^+ K^-$ mode as follows:

$$A^{\rm SM}_{\bar{B}_s^0 \to D_s^+ K^-} = \frac{G_{\rm F}}{\sqrt{2}} \, V_{us}^* V_{cb} \, f_K \, F_0^{B_s \to D_s}(m_K^2) \, (m_{B_s}^2 - m_{D_s}^2) \, a_{1\,\rm eff}^{D_s K} , \tag{6.69}$$

where $G_{\rm F}$ is the Fermi constant, $V_{us}^* V_{cb}$ is a factor of CKM matrix elements, f_K the kaon decay constant, and $F_0^{B_s \to D_s}(m_K^2)$ a form factor parametrising the hadronic $b \to c$ quark-current matrix element, as presented in Eq. (3.58). As we have already mentioned, there is a variety of approaches for calculating the form factors, most notably lattice QCD [209, 250, 251]. The parameter

$$a_{1\,\rm eff}^{D_s K} = a_1^{D_s K} \left(1 + \frac{E_{D_s K}}{T_{D_s K}} \right) \tag{6.70}$$

describes the deviation from naive factorisation. The parameter $a_1^{D_s K}$ characterises the non-factorisable effects entering the colour-allowed tree amplitude $T_{D_s K}$, while $E_{D_s K}$ describes the non-factorisable exchange topologies, which were introduced in Eq. (6.53).

Within the QCD factorisation approach, the a_1 parameters for colour-allowed $\bar{B} \to D\pi$ and $\bar{B} \to DK$ decays, which arise from $b \to c\bar{u}d$, $b \to c\bar{u}d$ quark-level transitions, are found as $|a_1| \approx 1.07$, with uncertainties at the percent level, showing a quasi-universal behaviour [164]. As we have noted, factorisation is expected to work very well in this decay class. This is also indicated by the fact that the parameter a_1 has a stable behaviour under the QCD renormalization group evolution [154, 155], as discussed in Sec. 3.5.3. This is in contrast to the a_2 coefficient characterising colour-suppressed decays, where factorisation is not expected to work well[53].

The current state-of-the-art results within QCD factorisation for the $\bar{B}_d^0 \to D_d^+ K^-$, $\bar{B}_d^0 \to D_d^+ \pi^-$ and $\bar{B}_s^0 \to D_s^+ \pi^-$ decays, which are related to one another through the $SU(3)$ flavour symmetry of strong interactions, are given as [252, 253]:

$$|a_1^{D_d K}| = 1.0702^{+0.0101}_{-0.0128} \tag{6.71}$$

$$|a_1^{D_d \pi}| = 1.073^{+0.012}_{-0.014}\ , \tag{6.72}$$

$$|a_1^{D_s \pi}| = 1.0727^{+0.0125}_{-0.0140}\ . \tag{6.73}$$

Here, we observe an essentially negligible difference of the values of their $|a_1|$ parameter. Recently, in Ref. [254], even QED effects have been studied. These effects are small and fully included within the uncertainties.

We may now obtain the $|a_1|$ parameter of $\bar{B}_s^0 \to D_s^+ K^-$, utilising the $\bar{B}_d^0 \to D^+ K^-$ channel, which differs only through the spectator quarks and use:

$$|a_1^{D_s K}| = 1.07 \pm 0.02, \tag{6.74}$$

where in view of $SU(3)$-breaking effects in the spectator quarks, we have doubled the tiny uncertainty, considering the spread of the $SU(3)$-related values in Eq. (6.71). Moving on to the impact of the exchange topologies, we note that in the $\bar{B}_s^0 \to D_s^+ K^-$ decay this topology is non-factorizable and we cannot calculate it reliably from first principles. As we will see next, we use experimental data in order to constrain this contribution.

[53] Interestingly though, as we have already seen in Chapter 5, for decays of the kind $\bar{B}_d^0 \to J/\psi\pi^0$, experimental data give values for $a_2(\bar{B}_d^0 \to J/\psi\pi^0)$ that are surprisingly consistent with the picture of naive factorisation [191].

Constraints on Exchange Topologies

With the help of the $|a_1^{D_d K}|$ and $|a_1^{D_s K}|$ values and the form-factor ratio [127]

$$\left| \frac{F_0^{B_s \to D_s}(m_K^2)}{F_0^{B_d \to D_d}(m_K^2)} \right| = 1.01 \pm 0.02, \tag{6.75}$$

we may calculate the ratio of the colour-allowed tree amplitudes [115, 190], which enters the expression in Eq. (6.57):

$$\left| \frac{T_{D_s K}}{T_{D_d K}} \right| = \left[\frac{F_0^{B_s \to D_s}(m_K^2)}{F_0^{B_d \to D_d}(m_K^2)} \right] \left[\frac{m_{B_s}^2 - m_{D_s}^2}{m_{B_d}^2 - m_{D_d}^2} \right] \left| \frac{a_1^{D_s K}}{a_1^{D_d K}} \right| = 1.03 \pm 0.03. \tag{6.76}$$

This ratio finally allows us to obtain the result for the parameter [115, 190]

$$r_E^{D_s K} \equiv \left| 1 + \frac{E_{D_s K}}{T_{D_s K}} \right| = 1.00 \pm 0.08, \tag{6.77}$$

which follows from experimental data. We note that no anomalous behaviour of the exchange topology, that could come from large rescattering or other non-factorizable effects, is indicated. There is consistency with Refs. [243, 249].

Similarly, using the values of the $|a_1^{D_d \pi}|$ and $|a_1^{D_s \pi}|$ parameters, the ratio of the form factors [127]

$$\left| \frac{F_0^{B_s \to D_s}(m_\pi^2)}{F_0^{B_d \to D_d}(m_\pi^2)} \right| = 1.01 \pm 0.02, \tag{6.78}$$

and the masses in Table 12, we obtain the colour-allowed tree amplitude ratio entering in Eq. (6.67):

$$\left| \frac{T_{D_d \pi}}{T_{D_s \pi}} \right| = \left[\frac{F_0^{B_d \to D_d}(m_\pi^2)}{F_0^{B_s \to D_s}(m_\pi^2)} \right] \left[\frac{m_{B_d}^2 - m_{D_d}^2}{m_{B_s}^2 - m_{D_s}^2} \right] \left| \frac{a_1^{D\pi}}{a_1^{D_s \pi}} \right| = 0.99 \pm 0.03. \tag{6.79}$$

This finally leads to the result

$$r_E^{D_d \pi} \equiv \left| 1 + \frac{E_{D_d \pi}}{T_{D_d \pi}} \right| = 0.92 \pm 0.05. \tag{6.80}$$

Again, there is no anomalous behaviour of the exchange topologies with respect to the theoretical estimates. The current state-of-the-art results in Eqs. (6.77) and (6.80) are consistent with those obtained in Refs. [243, 249].

Another interesting decay which gives us information about the exchange topologies is the $\bar{B}_s^0 \to D^+ \pi^-$ channel. It arises only from exchange diagrams and it is related to the exchange contribution in $\bar{B}_s^0 \to D_s^+ K^-$ decay through the $SU(3)$ symmetry, replacing the

pair of $d\bar{d}$ quarks by $s\bar{s}$. Regarding the experimental status, constraints on its branching ratio have not yet been reported. There is only the following upper bound available [187]:

$$\mathcal{B}(B_s^0 \to D^{*\mp}\pi^\pm)_{\rm exp} < 6.1 \times 10^{-6} \;\; (90\%\ \text{C.L.}) \; . \tag{6.81}$$

Last but not least, we discuss the $\bar{B}_d^0 \to D_s^+ K^-$ decay, which also originates only from exchange topologies. It differs from the $\bar{B}_s^0 \to D_s^+ K^-$ channel only through the down quark of the $\bar{B}_d^0$ meson in the initial state. Therefore, through $SU(3)$ symmetry, the following relations for the amplitudes are obtained:

$$A(\bar{B}_d^0 \to D_s^+ K^-) \equiv V_{cb} V_{ud}^* \, E'_{D_s K}, \tag{6.82}$$

$$A(\bar{B}_s^0 \to D_s^+ K^-) \equiv V_{cb} V_{us}^* \, (T_{D_s K} + E_{D_s K}). \tag{6.83}$$

Employing these relations, we may write the following expression:

$$\left| \frac{E'_{D_s K}}{T_{D_s K} + E_{D_s K}} \right|^2 = \frac{\tau_{B_s}}{\tau_{B_d}} \frac{m_{B_d}}{m_{B_s}} \left[\frac{\Phi(m_{D_s}/m_{B_s}, m_K/m_{B_s})}{\Phi(m_{D_s}/m_{B_d}, m_K/m_{B_d})} \right] \left| \frac{V_{us}}{V_{ud}} \right|^2 \left[\frac{\mathcal{B}(\bar{B}_d^0 \to D_s^+ K^-)}{\mathcal{B}(\bar{B}_s^0 \to D_s^+ K^-)_{\rm th}} \right] . \tag{6.84}$$

Experimentally the following branching ratio is measured [187]:

$$\mathcal{B}(\bar{B}_d^0 \to D_s^+ K^-) = (2.7 \pm 0.5) \times 10^{-5}. \tag{6.85}$$

Using the values for the CKM elements [233] and the results in Table 11, we finally obtain:

$$\left| \frac{E'_{D_s K}}{T_{D_s K} + E_{D_s K}} \right| = 0.08 \pm 0.01. \tag{6.86}$$

This result provides direct access to the size of the exchange contribution and agrees excellently with the picture in Eq. (6.77). Due to the non-factorisable contributions to the exchange amplitude, as pointed out in [243, 249], a large strong phase difference between the colour-allowed tree amplitudes and the exchange topologies is indicated. This feature is also supported by data for other modes. The current uncertainties do not allow us to draw further conclusions. Consequently, the ranges we consider in Eq. (6.77) are conservative assessments of the impact of the exchange topologies.

6.5.3 Theoretical Prediction of $a_1^{KD_s}$

The amplitude of the decay $\bar{B}_s^0 \to K^+ D_s^-$, which is caused by $b \to u\bar{c}s$ processes, can be expressed in a similar manner as the amplitude of the $\bar{B}_s^0 \to D_s^+ K^-$ decay ($b \to c$ process). In the SM, we write

$$A^{\rm SM}_{\bar{B}_s^0 \to K^+ D_s^-} = \frac{G_{\rm F}}{\sqrt{2}} \, V_{cs}^* V_{ub} \, f_{D_s} \, F_0^{B_s \to K}(m_{D_s}^2) \, (m_{B_s}^2 - m_K^2) \, a_{1\,\rm eff}^{KD_s}, \tag{6.87}$$

with the corresponding CKM factors are replaced correspondingly, the D_s decay constant f_{D_s}, and the form factor $F_0^{B_s\to K}(m_{D_s}^2)$ which parametrises the hadronic matrix element of the $b \to u$ transition and the parameter

$$a_{1\,\text{eff}}^{KD_s} = a_1^{KD_s}\left(1 + \frac{E_{KD_s}}{T_{KD_s}}\right). \tag{6.88}$$

As in Eq. (6.70), the coefficient $a_1^{KD_s}$ describes non-factorisable contributions entering the colour-allowed T_{KD_s} tree amplitude, while the E_{KD_s} amplitude arises from non-factorisable exchange topologies. The exchange topology is illustrated in Fig. 37b.

In this case, even though it is also a colour-allowed channel, there may be significant non-factorisable effects, as the heavy-quark arguments for QCD factorisation in $b \to c$ tree-level transitions do not apply in this case [164]. Using Eq. (6.74) as guidance, we assume the following value as a reference point:

$$|a_1^{KD_s}| = 1.1 \pm 0.1. \tag{6.89}$$

Interestingly, the strong phase difference δ_s in Eq. (6.24), with a central value close to 0°, agrees excellently with factorisation, thereby supporting factorisation also in the $b \to u\bar{c}s$ channel[54].

Constraints on Exchange Topologies

We continue now with the ratios entering in Eq. (6.62), and consider the $\bar{B}_d^0 \to \pi^+ D_s^-$ decay. Its amplitude takes the same form as Eq. (6.87). Due to the fact that this channel does not receive any contributions from exchange topologies, we obtain

$$a_{1\,\text{eff}}^{\pi D_s} = a_1^{\pi D_s}. \tag{6.90}$$

Applying the $SU(3)$ flavour symmetry to the spectator quarks, we assume

$$|a_1^{\pi D_s}| = |a_1^{KD_s}| = 1.1 \pm 0.1, \tag{6.91}$$

with the numerical value in Eq. (6.89). We can now write the ratio of the colour-allowed tree topologies as follows:

$$\left|\frac{T_{KD_s}}{T_{\pi D_s}}\right| = \left[\frac{F_0^{B_s\to K}(m_{D_s}^2)}{F_0^{B_d\to\pi}(m_{D_s}^2)}\right]\left[\frac{m_{B_s}^2 - m_K^2}{m_{B_d}^2 - m_\pi^2}\right]\left|\frac{a_1^{KD_s}}{a_1^{\pi D_s}}\right| = 1.15 \pm 0.19, \tag{6.92}$$

[54]We emphasize here again that if factorisation didn't work, we would expect a much bigger phase difference δ_s. This small value of δ_s though shows that factorisation is supported even in the $b \to u\bar{c}s$ channel, where in general, it appears to be on less solid ground.

where we utilise the meson masses in Table 12 and Eq. (6.91). The $B_s \to K$ and $B_d \to \pi$ form factors, describing $SU(3)$-breaking effects, are calculated with QCD light cone sum rules in Ref. [255]. Therefore, the ratio of form factors is:

$$\left[\frac{F_0^{B_s\to K}(m_{D_s}^2)}{F_0^{B\to\pi}(m_{D_s}^2)}\right] = 1.12 \pm 0.11. \tag{6.93}$$

Finally, the ratio in Eq. (6.92) and the numerical result in Eq. (6.62) allow the determination of the quantity

$$r_E^{KD_s} \equiv \left|1 + \frac{E_{KD_s}}{T_{KD_s}}\right| = 0.97 \pm 0.17, \tag{6.94}$$

which folllows from the experimental data. We observe a pattern similar to the constraints in Eqs. (6.77) and (6.80), although with larger uncertainty.

The decay $\bar{B}_s^0 \to D^-\pi^+$ is related to the exchange contribution to $\bar{B}_s^0 \to D_s^- K^+$ channel. The branching ratio has not been measured but only an upper bound is available.

In addition, the $\bar{B}_d^0 \to D_s^- K^+$ is related to the exchange topology of the $\bar{B}_s^0 \to K^+ D_s^-$ channel, which differs only through the down quark of the initial $\bar{B}_d^0$ meson. A measurement of the corresponding branching ratio is not yet available [187]. Using the experimental results in Table 11 and Eq. (6.85), we write

$$\left|\frac{E'_{D_sK}}{T_{KD_s}+E_{KD_s}}\right|^2 = \frac{\tau_{B_s}}{\tau_{B_d}}\frac{m_{B_d}}{m_{B_s}}\left[\frac{\Phi(m_{D_s}/m_{B_s}, m_K/m_{B_s})}{\Phi(m_{D_s}/m_{B_d}, m_K/m_{B_d})}\right]\left|\frac{V_{ub}V_{cs}}{V_{cb}V_{ud}}\right|^2\left[\frac{\mathcal{B}(\bar{B}_d^0 \to D_s^- K^+)}{\mathcal{B}(\bar{B}_s^0 \to K^+ D_s^-)_{\rm th}}\right], \tag{6.95}$$

where

$$\left|\frac{V_{ub}V_{cs}}{V_{cb}V_{ud}}\right| = \left[\frac{\lambda R_b}{1-\lambda^2/2}\right]\left[1+\mathcal{O}(\lambda^2)\right] = 0.089 \pm 0.005, \tag{6.96}$$

having used the Wolfenstein parameterization with R_b denoting the UT side from the origin to the apex [122]. Therefore, we obtain:

$$\left|\frac{E'_{D_sK}}{T_{KD_s}+E_{KD_s}}\right| = 0.09 \pm 0.02, \tag{6.97}$$

which is in excellent agreement with Eq. (6.86). The hadronic matrix elements of the exchange amplitudes scale with the product of the decay constants. Thus, $f_{B_{ds}} f_{D_s} f_K$ for our modes, we obtain that $E'_{D_sK} \approx E_{KD_s}$. We finally consider the numerical range

$$r_E^{KD_s} = 1.00 \pm 0.08, \tag{6.98}$$

which is fully consistent with (6.94), although giving a sharper picture. Comparing with our analysis regarding the $\bar{B}_s^0 \to K^+ D_s^-$ decay, this range is similar as the one for $r_E^{D_sK}$ in Eq. (6.77).

6.6 Information from Semileptonic Decays

Our next step is to extract the $|a_1|$ parameters of the $\bar{B}_s^0 \to D_s^+ K^-$ and $\bar{B}_s^0 \to K^+ D_s^-$ channels from the data in the cleanest possible way. For this purpose, it is important to minimise the dependence on uncertainties from CKM parameters and hadronic form factors. In order to achieve this, semileptonic decays provide again a very useful tool [153, 164, 249]. The experimental results of $|a_1|$ can then be compared with the corresponding theoretical expectations. It is interesting to see whether we will encounter another puzzling situation.

6.6.1 Extracting the Experimental Value of $|a_1^{D_s K}|$

We can now determine $|a_1|$ in a clean way, utilising information from $B_{(s)}$ semileptonic decays. We firstly discuss the $\bar{B}_s^0 \to D_s^+ K^-$ mode. As we already mentioned, it originates from a $b \to c$ transition and its partner semileptonic decay is the $\bar{B}_s^0 \to D_s^+ \ell \bar{\nu}_\ell$. We introduce the following ratio [153, 164, 249]:

$$R_{D_s^+ K^-} \equiv \frac{\mathcal{B}(\bar{B}_s^0 \to D_s^+ K^-)_{\rm th}}{\mathrm{d}\mathcal{B}\left(\bar{B}_s^0 \to D_s^+ \ell^- \bar{\nu}_\ell\right)/\mathrm{d}q^2|_{q^2=m_K^2}}. \tag{6.99}$$

We remind the reader that the differential branching ratio is related to the differential rate through the average lifetime τ_{B_s} of the B_s meson:

$$\frac{\mathrm{d}\mathcal{B}\left(\bar{B}_s^0 \to D_s^+ \ell^- \bar{\nu}_\ell\right)}{\mathrm{d}q^2} = \tau_{B_s} \left[\frac{\mathrm{d}\Gamma\left(\bar{B}_s^0 \to D_s^+ \ell^- \bar{\nu}_\ell\right)}{\mathrm{d}q^2}\right]. \tag{6.100}$$

The $\bar{B}_s^0 \to D_s^+ \ell^- \bar{\nu}_\ell$ differential rate has recently been measured by the LHCb collaboration [256]. We apply the Caprini–Lellouch–Neubert (CLN) parametrisation [257] of the relevant form factor with the following parameters:

$$|V_{cb}| = (41.4 \pm 1.3) \times 10^{-3}, \tag{6.101}$$

$$G(0) = 1.102 \pm 0.034, \tag{6.102}$$

$$\rho^2 = 1.27 \pm 0.05, \tag{6.103}$$

resulting from the LHCb analysis [256]. Using Eq. (6.100) with the value of τ_{B_s} in Eq. (6.56) to convert the differential rate into the differential branching ratio, we finally obtain [55]

$$\left.\frac{\mathrm{d}\mathcal{B}\left(\bar{B}_s^0 \to D_s^+ \ell^- \bar{\nu}_\ell\right)}{\mathrm{d}q^2}\right|_{q^2=m_K^2} = (3.97 \pm 0.47) \times 10^{-3}\ \mathrm{GeV}^{-2}. \tag{6.104}$$

[55] For completeness and to be consistent with our analysis in [115,190], we mention that we have calculated the uncertainty neglecting correlations between the parameters. Taking them into account would reduce the error but for our numerical analysis, we prefer to use the larger uncorrelated error, also in view of the different form factors parametrizations that can be used.

We note that in the future, it would be useful if the experimental Collaborations provided measurements of the differential rates at the relevant q^2 bins. As a result, there would be no need to use different form factor parametrisations. The numerical values in Table 11 and in Eq. (6.104) yield

$$R_{D_s^+K^-} = 0.05 \pm 0.01. \tag{6.105}$$

Utilising Eqs. (6.36) and (3.62) with (6.100) and (3.61), the ratio $R_{D_s^+K^-}$ in Eq. (6.99) can be written as

$$R_{D_s^+K^-} = 6\pi^2 f_K^2 |V_{us}|^2 |a_{1\,\mathrm{eff}}^{D_sK}|^2 X_{D_sK}, \tag{6.106}$$

where the CKM matrix element $|V_{cb}|$ cancels. We note that for the momentum transfer $q^2 = m_K^2$ the same phase space-functions enter the semileptonic and non-leptonic $\bar{B}_s^0$ decays. The term X_{D_sK} includes the following masses and the corresponding form factor ratio:

$$X_{D_sK} = \frac{(m_{B_s}^2 - m_{D_s}^2)^2}{[m_{B_s}^2 - (m_{D_s} + m_K)^2][m_{B_s}^2 - (m_{D_s} - m_K)^2]} \left[\frac{F_0^{B_s\to D_s}(m_K^2)}{F_1^{B_s\to D_s}(m_K^2)}\right]^2, \tag{6.107}$$

where the relevant meson masses are collected in Table 12. The ratio of hadronic form factors for $q^2 = m_K^2$ is close to the normalisation given in Eq. (3.59) and the form-factor information from lattice QCD studies [209, 250, 251] yields:

$$\left[\frac{F_0^{B_s\to D_s}(m_K^2)}{F_1^{B_s\to D_s}(m_K^2)}\right] = 1.00 \pm 0.03. \tag{6.108}$$

The product of the kaon decay constant f_K and the CKM factor $|V_{us}|$ can be extracted from data for leptonic K decays, yielding $f_K|V_{us}| = (35.09 \pm 0.04 \pm 0.04)\,\mathrm{MeV}$ [258]. Consequently, with the numerical value in Eq. (6.105), we determine

$$|a_{1\,\mathrm{eff}}^{D_sK}| = 0.82 \pm 0.09. \tag{6.109}$$

Using the expression in (6.70) with the numerical value of $r_E^{D_sK}$ given in Eq. (6.77) to take the exchange topology contributions into account, we obtain the result

$$|a_1^{D_sK}| = 0.82 \pm 0.11, \tag{6.110}$$

which follows from the data and is very robust with respect to the hadronic form factors in Eq. (6.108). We observe that the result has a surprisingly small central value. Comparing it with the corresponding theoretical expectation in Eq. (6.74), it differs at the $2.2\,\sigma$ level.

6.6.2 Extracting the Experimental Value of $|a_1^{KD_s}|$

We discuss now the $\bar{B}_s^0 \to K^+ D_s^-$ channel, which originates from a $b \to u$ transition. We use the rate of the theoretical branching ratio of this transition with the differential branching ratio of its partner semileptonic decay $\bar{B}_s^0 \to K_s^+ \ell \bar{\nu}_\ell$:

$$R_{K^+D_s^-} \equiv \frac{\mathcal{B}(\bar{B}_s^0 \to D_s^- K^+)_{\rm th}}{\mathrm{d}\mathcal{B}\left(\bar{B}_s^0 \to K^+ \ell^- \bar{\nu}_\ell\right)/\mathrm{d}q^2|_{q^2=m_{D_s}^2}} = 6\pi^2 f_{D_s}^2 |V_{cs}|^2 |a_{1\,\rm eff}^{KD_s}|^2 X_{KD_s}, \tag{6.111}$$

in analogy to Eqs. (6.99) and (6.106). The product of the D_s decay constant f_{D_s} and the CKM factor $|V_{cs}|$ can be determined from leptonic D_s decays measurements, yielding $f_{D_s}|V_{cs}| = (250.9 \pm 4.0)\,\mathrm{MeV}$ [258]. The term X_{KD_s} is written as

$$X_{KD_s} = \frac{(m_{B_s}^2 - m_K^2)^2}{[m_{B_s}^2 - (m_K + m_{D_s})^2][m_{B_s}^2 - (m_K - m_{D_s})^2]} \left[\frac{F_0^{B_s\to K}(m_{D_s}^2)}{F_1^{B_s\to K}(m_{D_s}^2)}\right]^2. \tag{6.112}$$

Even though the semileptonic $\bar{B}_s^0 \to K^+ \ell \bar{\nu}_\ell$ channel has recently been observed by the LHCb collaboration and a first measurement of its branching ratio is available [234], the corresponding differential decay rate for various q^2 bins has not yet been reported.

As a result, in order to be able to determine the ratio $R_{K^+D_s^-}$ from the data, we apply the $SU(3)$ flavour symmetry: instead of using the semileptonic $\bar{B}_s^0 \to K^+ \ell \bar{\nu}_\ell$, we make use of its partner decay $B_d^0 \to \pi^+ \ell^- \bar{\nu}_\ell$. For this channel, we do have measurements of the differential rate by the BaBar and Belle collaborations [187, 233].

We introduce now the following ratio:

$$R_{K^+D_s^-}^{SU(3)} \equiv \frac{\mathcal{B}(\bar{B}_s^0 \to D_s^- K^+)_{\rm th}}{\mathrm{d}\mathcal{B}\left(\bar{B}^0 \to \pi^+ \ell^- \bar{\nu}_\ell\right)/\mathrm{d}q^2|_{q^2=m_{D_s}^2}} = 6\pi^2 f_{D_s}^2 |V_{cs}|^2 |a_{1\,\rm eff}^{KD_s}|^2 X_{SU(3)}, \tag{6.113}$$

where in the expression of $X_{SU(3)}$ different phase-space factors enter, in contrast to the decay ratios considered above e.g., in Eq. (6.112), and we have:

$$X_{SU(3)} = \left[1 - \frac{m_K^2}{m_{B_s}^2}\right]^2 \frac{\left[\Phi\left(\frac{m_K}{m_{B_s}}, \frac{m_{D_s}}{m_{B_s}}\right)\right]}{\left[\Phi\left(\frac{m_\pi}{m_B}, \frac{m_{D_s}}{m_{B_s}}\right)\right]^3} \left[\frac{F_0^{B_s\to K}(m_{D_s}^2)}{F_1^{B\to\pi}(m_{D_s}^2)}\right]^2. \tag{6.114}$$

The non-perturbative form factors have been determined with lattice QCD [259, 260] and QCD light-cone sum rule analyses [255, 261]. The ratio of form factors can be written as

$$\left[\frac{F_0^{B_s\to K}(m_{D_s}^2)}{F_1^{B\to\pi}(m_{D_s}^2)}\right]^2 = \left[\frac{F_0^{B_s\to K}(m_{D_s}^2)}{F_1^{B_s\to K}(m_{D_s}^2)}\right]^2 \left[\frac{F_1^{B_s\to K}(m_{D_s}^2)}{F_1^{B\to\pi}(m_{D_s}^2)}\right]^2. \tag{6.115}$$

We assume that the first ratio satisfies the relation in Eq. (3.59) for $q^2 = m_{D_s}^2$, in view of the currently large experimental $\mathcal{B}(\bar{B}_s^0 \to D_s^- K^+)_{\rm th}$ uncertainty, and as a result it is close

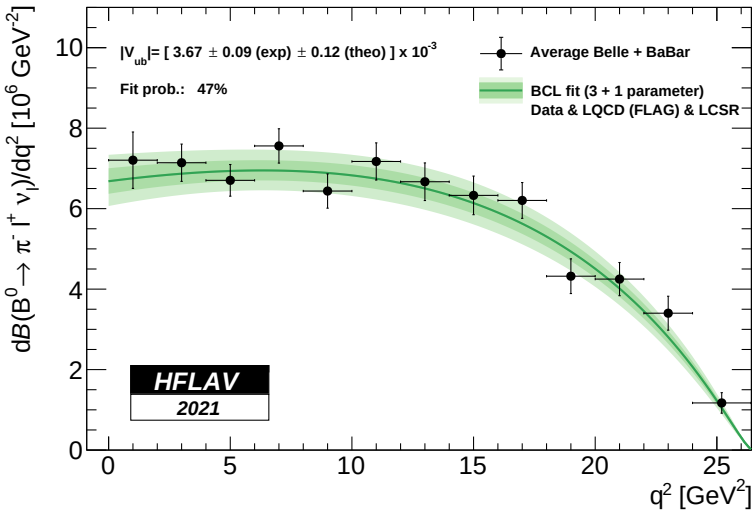

Figure 38: Result of the fit for the BCL parametrization to the averaged q^2, as given in [11].

to 1. This agrees with the analysis in Ref. [262]. It would be important to have a dedicated lattice QCD study of this form-factor ratio in the future. The second ratio of form factors represents the $SU(3)$-breaking corrections. Using the results for $q^2 = 0$ given in Ref. [255] and neglecting again the $q^2 = m_{D_s}^2$ evolution, we have

$$\left[\frac{F_1^{B_s\to K}(m_{D_s}^2)}{F_1^{B\to\pi}(m_{D_s}^2)}\right] = 1.12 \pm 0.12. \tag{6.116}$$

If we apply the formalism of Ref. [255] to perform a study of the q^2 evolution and determine the form factors at $q^2 = m_{D_s}^2$, we obtain:

$$F_1^{B_s\to K}(m_{D_s}^2) = 0.366 \pm 0.028, \tag{6.117}$$

$$F_1^{B\to\pi}(m_{D_s}^2) = 0.323 \pm 0.028, \tag{6.118}$$

yielding

$$\left[\frac{F_1^{B_s\to K}(m_{D_s}^2)}{F_1^{B\to\pi}(m_{D_s}^2)}\right] = 1.13 \pm 0.13, \tag{6.119}$$

As this result is in excellent agreement with Eq. (6.116), the effect of the evolution of q^2 is negligible within the given errors.

Last but not least, we determine the value of $R_{K^+D_s^-}$ in Eq. (6.113) using the following experimental value of the differential semileptonic branching ratio [187]:

$$\mathrm{d}\mathcal{B}\left(\bar{B}^0 \to \pi^+\ell^-\bar{\nu}_\ell\right)/\mathrm{d}q^2|_{q^2=m_{D_s}^2} = (7.14 \pm 0.46) \times 10^{-6}\ \mathrm{GeV}^{-2}, \tag{6.120}$$

and the theoretical branching ratio for the $\bar{B}_s^0 \to D_s^- K^+$ decay in Table 11. We note that the most recent fit for the differential $\bar{B}^0 \to \pi^+ \ell^- \bar{\nu}_\ell$ branching ratio presented by HFLAV[56] is shown in Fig. 38. We obtain

$$R_{K^+ D_s^-} = 3.64 \pm 1.70. \tag{6.121}$$

This yields the effective value

$$|a_{1\,\text{eff}}^{KD_s}| = 0.77 \pm 0.20 \tag{6.122}$$

utilising Eq. (6.113). Finally, the range for $r_E^{KD_s}$ in Eq. (6.98) yields

$$|a_1^{KD_s}| = 0.77 \pm 0.21. \tag{6.123}$$

We find again a pattern that favours a central value smaller than the theoretical reference value given in Eq. (6.89). Even though factorisation may here not work as well as in the $\bar{B}_s^0 \to D_s^+ K^-$ decay, this result is another intriguing observation. Comparing with Eq. (6.110), the uncertainty is now significantly larger. Due to the large current uncertainties, we can again not draw further conclusions.

We stress that it would be very interesting and important to reduce both the theoretical and the experimental uncertainties. It is also desirable to have in the future a measurement of the differential decay rate of the $\bar{B}_s^0 \to K_s^+ \ell \bar{\nu}_\ell$ channel, therefore to be able to implement this rate directly into Eq. (6.111). This semileptonic mode would also be very useful for an analysis of the $\bar{B}_s^0 \to K^+ K^-$ decay [263].

6.7 Puzzles in the $|a_1|$ parameters

When we compare the theoretical predictions with the values arising from the data, both $|a_1^{D_s K}|$ and $|a_1^{KD_s}|$ show a similar pattern with the experimental central values being much smaller than the theoretical ones. Let us now see whether we observe similar trends in $B_{(s)}$ decays with similar dynamics.

We firstly discuss the decay $\bar{B}_d^0 \to D_d^+ K^-$, arising from $b \to c\bar{u}s$ processes in analogy to the $\bar{B}_s^0 \to D_s^+ K^-$ channel. There are no exchange topologies in this mode. Utilising again the information from semileptonic decays, following the same strategy that we presented above, we introduce the ratio

$$R_{D_d^+ K^-} \equiv \frac{\mathcal{B}(\bar{B}_d^0 \to D_d^+ K^-)}{\mathrm{d}\mathcal{B}\left(\bar{B}_d^0 \to D_d^+ \ell^- \bar{\nu}_\ell\right)/\mathrm{d}q^2|_{q^2=m_K^2}} = 6\pi^2 f_K^2 |V_{us}|^2 |a_1^{D_d K}|^2 X_{D_d K}, \tag{6.124}$$

[56] We mention that in Fig. 28 we had already produced the contour that corresponds to the values of the differential branching ratio of the $\bar{B}^0 \to \pi^+ \ell^- \bar{\nu}_\ell$ channel in the HFLAV parametrisation. In that plot we had made the comparison between the HFLAV and the FLAG parametrisation. Here, we show the plot as it is presented in Ref. [11].

which allows us to extract the $|a_1^{D_dK}|$ from the data. We define the differential branching ratio of the $\bar{B}_d^0 \to D_d^+ \ell^- \bar{\nu}_\ell$ decay at the relevant value of $q^2 = m_K^2$, applying the CLN parametrisation [257] with the parameters [187]:

$$\eta_{\rm EW} G(1)|V_{cb}| = (42.00 \pm 1.00) \times 10^{-3}, \tag{6.125}$$

$$\rho^2 = 1.131 \pm 0.033, \tag{6.126}$$

and the lifetime τ_{B_d} in Eq. (6.61). We obtain the value: [57]

$$\mathrm{d}\mathcal{B}\left(\bar{B}_d^0 \to D_d^+ \ell^- \bar{\nu}_\ell\right)/\mathrm{d}q^2|_{q^2=m_K^2} = (3.65 \pm 0.23) \times 10^{-3}\ \mathrm{GeV}^{-2}. \tag{6.127}$$

The term X_{D_dK} is written as:

$$X_{D_dK} = \frac{(m_{B_d}^2 - m_{D_d}^2)^2}{[m_{B_d}^2 - (m_{D_d} + m_K)^2][m_{B_d}^2 - (m_{D_d} - m_K)^2]} \left[\frac{F_0^{B_d \to D_d}(m_K^2)}{F_1^{B_d \to D_d}(m_K^2)}\right]^2, \tag{6.128}$$

The form-factor ratio, in accordance with the normalisation condition (3.59), is:

$$\left[\frac{F_0^{B_d \to D_d}(m_K^2)}{F_1^{B_d \to D_d}(m_K^2)}\right] = 1, \tag{6.129}$$

and with the meson masses in Table 12, we obtain

$$|a_1^{D_dK}| = 0.83 \pm 0.05. \tag{6.130}$$

We may now compare this result with the theoretical value in Eq. (6.71). The central value is again significantly smaller, showing a discrepancy at the at the $4.8\,\sigma$ level.

The next decay that we study is $\bar{B}_d^0 \to D_d^+ \pi^-$, which is the U-spin partner of the $\bar{B}_s^0 \to D_s^+ K^-$ channel [242]. We introduce

$$R_{D^+\pi^-} \equiv \frac{\mathcal{B}(\bar{B}_d^0 \to D_d^+ \pi^-)}{\mathrm{d}\mathcal{B}\left(\bar{B}_d^0 \to D_d^+ \ell^- \bar{\nu}_\ell\right)/\mathrm{d}q^2|_{q^2=m_\pi^2}} = 6\pi^2 f_\pi^2 |V_{ud}|^2 |a_{1\,\mathrm{eff}}^{D_d\pi}|^2 X_{D_d\pi}. \tag{6.131}$$

The experimental differential semileptonic branching ratio for $q^2 = m_\pi^2$ is [187],

$$\mathrm{d}\mathcal{B}\left(\bar{B}_d^0 \to D_d^+ \ell^- \bar{\nu}_\ell\right)/\mathrm{d}q^2|_{q^2=m_\pi^2} = (3.80 \pm 0.24) \times 10^{-3}\ \mathrm{GeV}^{-2}, \tag{6.132}$$

while $f_\pi |V_{ud}| = (127.13 \pm 0.02)$ MeV [258] and

$$X_{D_d\pi} = \frac{(m_{B_d}^2 - m_{D_d}^2)^2}{[m_{B_d}^2 - (m_{D_d} + m_\pi)^2][m_{B_d}^2 - (m_{D_d} - m_\pi)^2]} \left[\frac{F_0^{B_d \to D_d}(m_\pi^2)}{F_1^{B_d \to D_d}(m_\pi^2)}\right]^2. \tag{6.133}$$

[57] We do not take correlations between the parameters into account, as in Eq. (6.104). Including them, leads to a smaller uncertainty but we prefer to keep the more conservative uncorrelated uncertainty, following Refs. [115, 190].

The term $a_{1\,\text{eff}}^{D_d\pi}$ takes the exchange topology into account and we have:

$$a_{1\,\text{eff}}^{D_d\pi} = a_1^{D_d\pi}\left(1 + \frac{E_{D_d\pi}}{T_{D_d\pi}}\right). \tag{6.134}$$

With these numerical values, we obtain:

$$|a_{1\,\text{eff}}^{D_d\pi}| = 0.83 \pm 0.03. \tag{6.135}$$

Assuming $r_E^{D_d\pi} = r_E^{D_sK}$ with the numerical value in Eq. (6.77), we find

$$|a_1^{D_d\pi}| = 0.83 \pm 0.07\,. \tag{6.136}$$

Comparing this result with the theoretical prediction in Eq. (6.71), we observe again that the experimental value is much smaller, differing at the $3.3\,\sigma$ level.

We continue with the decay $\bar{B}_s^0 \to D_s^+\pi^-$ which differs from the $\bar{B}_d^0 \to D_d^+\pi^-$ channel only through the spectator quarks. As there is no contribution from exchange topologies in this mode, we have a cleaner setting. We introduce

$$R_{D_s^+\pi^-} \equiv \frac{\mathcal{B}(\bar{B}_s^0 \to D_s^+\pi^-)_\text{th}}{\mathrm{d}\mathcal{B}\left(\bar{B}_s^0 \to D_s^+\ell^-\bar{\nu}_\ell\right)/\mathrm{d}q^2|_{q^2=m_\pi^2}} = 6\pi^2 f_\pi^2 |V_{ud}|^2 |a_1^{D_s\pi}|^2 X_{D_s\pi} \tag{6.137}$$

and in analogy to the discussion above the term $X_{D_s\pi}$ is

$$X_{D_s\pi} = \frac{(m_{B_s}^2 - m_{D_s}^2)^2}{[m_{B_s}^2 - (m_{D_s}+m_\pi)^2][m_{B_s}^2 - (m_{D_s}-m_\pi)^2]}\left[\frac{F_0^{B_s\to D_s}(m_\pi^2)}{F_1^{B_s\to D_s}(m_\pi^2)}\right]^2. \tag{6.138}$$

In order to determine the theoretical branching ratio of $\bar{B}_s^0 \to D_s^+\pi^-$, we use Eqs. (6.66) and (6.64), and get:

$$\mathcal{B}(\bar{B}_s^0 \to D_s^+\pi^-)_\text{th} = (2.99 \pm 0.23) \times 10^{-3}. \tag{6.139}$$

For the differential rate of the semileptonic $\bar{B}_s^0 \to D_s^+\ell^-\bar{\nu}_\ell$ decay, we apply the CLN parametrisation with the parameters given by the LHCb collaboration in Ref. [256]. We obtain:

$$\mathrm{d}\mathcal{B}\left(\bar{B}_s^0 \to D_s^+\ell^-\bar{\nu}_\ell\right)/\mathrm{d}q^2|_{q^2=m_\pi^2} = (4.12 \pm 0.46) \times 10^{-3}\ \text{GeV}^{-2}, \tag{6.140}$$

where we used the $\bar{B}_s^0$ lifetime in Eq. (6.56). We finally arrive at the result:

$$|a_1^{D_s\pi}| = 0.87 \pm 0.06\,, \tag{6.141}$$

which we compare with the theoretical value in Eq. (6.71). The central value is again too small, with a discrepancy at the $3.2\,\sigma$ level.

Last but not least, we consider the counterpart decay of $\bar{B}_s^0 \to K^+ D_s^-$, which is the $\bar{B}_d^0 \to \pi^+ D_s^-$ channel. It only differs through the spectator quarks and does not receive any contributions from exchange topologies. We introduce

$$R_{\pi^+ D_s^-} \equiv \frac{\mathcal{B}(\bar{B}_d^0 \to \pi^+ D_s^-)}{\mathrm{d}\mathcal{B}\left(\bar{B}^0 \to \pi^+ \ell^- \bar{\nu}_\ell\right)/\mathrm{d}q^2|_{q^2=m_{D_s}^2}} = 6\pi^2 f_{D_s}^2 |V_{cs}|^2 |a_1^{\pi D_s}|^2 X_{\pi D_s} \tag{6.142}$$

with

$$X_{\pi D_s} = \frac{(m_{B_d}^2 - m_\pi^2)^2}{[m_{B_d}^2 - (m_\pi + m_{D_s})^2][m_{B_d}^2 - (m_\pi - m_{D_s})^2]} \left[\frac{F_0^{B_d\to\pi}(m_{D_s}^2)}{F_1^{B_d\to\pi}(m_{D_s}^2)}\right]^2, \tag{6.143}$$

where we have again assumed that the form-factor ratio still satisfies the relation in Eq. (3.59) for $q^2 = m_{D_s}^2$, i.e., is close to 1. A dedicated lattice QCD study of this form-factor ratio would be really useful for future analysis. Using the experimental differential branching ratio [187]:

$$\mathrm{d}\mathcal{B}\left(\bar{B}^0 \to \pi^+ \ell^- \bar{\nu}_\ell\right)/\mathrm{d}q^2|_{q^2=m_{D_s}^2} = (7.14 \pm 0.46) \times 10^{-6}\ \mathrm{GeV}^{-2}, \tag{6.144}$$

we finally determine

$$|a_1^{\pi D_s}| = 0.78 \pm 0.05\,. \tag{6.145}$$

This result is consistent with the value in Eq. (6.123), although with significantly smaller uncertainty. The experimental value differs from the theoretical reference value in Eq. (6.91) at the $2.9\,\sigma$ level.

Summarising, we had a detailed look at $B_{(s)}$ decays with similar dynamics. We observed again a similar pattern, with the parameters following from the data being smaller than the corresponding theoretical values:

$$\begin{aligned}
\bar{B}_d^0 \to D_d^+ K^- \text{decay:} &\quad |a_1^{D_d K}| = 0.83 \pm 0.05, \quad \text{differs at } 4.8\,\sigma \text{ level},\\
\bar{B}_d^0 \to D_d^+ \pi^- \text{decay:} &\quad |a_1^{D_d \pi}| = 0.83 \pm 0.07, \quad \text{differs at } 3.3\,\sigma \text{ level},\\
\bar{B}_s^0 \to D_s^+ \pi^- \text{decay:} &\quad |a_1^{D_s \pi}| = 0.87 \pm 0.06, \quad \text{differs at } 3.2\,\sigma \text{ level},\\
\bar{B}_d^0 \to \pi^+ D_s^- \text{decay:} &\quad |a_1^{\pi D_s}| = 0.78 \pm 0.05, \quad \text{differs at } 2.9\,\sigma \text{ level}.
\end{aligned}$$

We illustrate and compare the experimental and theoretical SM values of the $|a_1|$ parameters for various decay processes in Fig. 39. The left panel shows decays which are caused by $b \to c\bar{u}s$ and $b \to c\bar{u}d$ processes. The right panel illustrates decays originating from $b \to u\bar{c}s$ transitions. We also show in one plot these results for the various $|a_1|$ parameters coming from the experimental data and compare them with the theoretical SM expectations in Appendix E.1. We note that in Ref. [249], the same pattern was found for $\bar{B}_d^0 \to D_d^+ \pi^-$ and

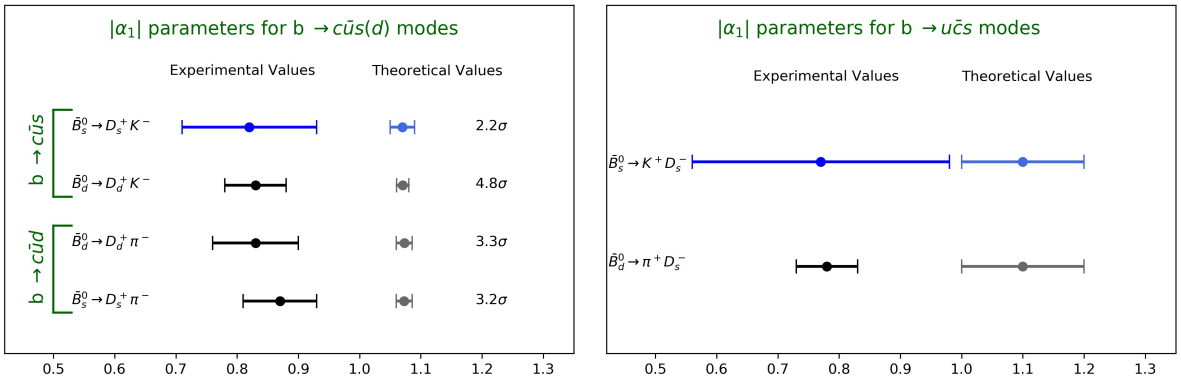

Figure 39: Experimental and theoretical SM values of the $|a_1|$ parameters for various decay processes. The left panel illustrates decays which are caused by $b \to c\bar{u}s$ and $b \to c\bar{u}d$ processes while the right panel shows decays originating from $b \to u\bar{c}s$ transitions.

$\bar{B}_d^0 \to D_d^+ K^-$ decays with $|a_1|$ values smaller than one. It has also recently been discussed within QCD factorisation also for $\bar{B}_s^0 \to D_s^+ \pi^-$ in Ref. [253].

So far, we have only considered the SM framework. We have identified an intriguing result for the angle γ arising from measurements of CP violation in the $B_s^0 \to D_s^\mp K^\pm$ system. This picture is complemented by information from the branching ratios, which is encoded in the parameters a_1. We note that the latter puzzle is not related to CP violation. Before moving on to generalise this description to allow also for contributions coming from NP in Sec. 6.8, let us still point out some further remarks in the next Section.

6.7.1 Further Remarks

Possible NP Effects in Semileptonic Modes

Recalling Eq. (3.61) for the semileptonic $B \to P\ell\bar{\nu}_\ell$ decays, we note that we have assumed the SM for the semileptonic decay amplitude. The corresponding modes may be affected by physics from beyond the SM [264–267]. It is possible to include NP effects in such decays, as discussed in Refs. [105, 110, 268, 269]. A popular scenario in the literature suggests that NP should enter exclusively through couplings to heavy leptons. In the case of τ leptons, we remind here the reader about the discussion regarding the ratios $R(D)$ and $R(D^*)$ in Sec. 3.4.3. However, in our analysis we utilise experimental data for semileptonic $B_{(s)}$ decays having only electrons and muons in the final states. As a result, should NP enter via taus, our studies would not be affected. In analogy, for determinations of $|V_{ub}|$ and $|V_{cb}|$ in Chapter 3, only $B_{(s)}$ decays to $\ell = e, \mu$ were used.

Power Corrections

As we already presented in Fig. 39, the experimental values of $|a_1|$ are much smaller than the theoretical ones for various $b \to c\bar{u}s(d)$ and $b \to u\bar{c}s$ modes. Following from this feature, recent analyses within scenarios for physics beyond the SM have been studied [192–194]. Within the SM, a suppression of the $|a_1|$ parameters could arise from universal power-suppressed corrections of order $\Lambda_{\rm QCD}/m_b$ [252]. However, such effects would not explain the intriguing γ value coming from the CP-violating observables of the $B_s^0 \to D^\mp K^\pm$ decays, as it would require new sources of CP violation. We note that in Refs. [270, 271] NP effects in non-leptonic B meson tree-level decays are also discussed.

Regarding QCD factorisation, we highlight again that we have puzzles in the $|a_1|$, not only in the $b \to c$ transitions, where factorisation is expected to work excellently, but also in channels like $\bar{B}_s^0 \to K^+ D_s^-$ and $\bar{B}_d^0 \to \pi^+ D_s^-$, where this framework is on less solid ground. Interestingly, in our analysis in the previous Sections, there was no indication of anomalous enhancement due to the exchange topologies, which could arise from large non-factorisable effects. The small strong phase δ_s in Eq. (6.24) also supports the factorisation picture. Anomalously enhanced power corrections are also disfavoured by these observations.

6.8 Pursuing New Physics

In view of these puzzles that we have extensively discussed in the previous Sections, we generalise our discussion and extend our analysis to include NP effects in $\bar{B}_s^0 \to D_s^\mp K^\pm$.

6.8.1 Generalising the Amplitudes

The decay amplitudes consist of the SM and the NP part:

$$\text{Amplitude} = P_{\rm SM} + P_{\rm NP} = P_{\rm SM}\left(1 + \frac{P_{\rm NP}}{P_{\rm SM}}\right). \tag{6.146}$$

We generalise the transition amplitudes of the four decays as follows:

$$A(\bar{B}_s^0 \to D_s^+ K^-) = A(\bar{B}_s^0 \to D_s^+ K^-)_{\rm SM}\left[1 + \bar{\rho}\, e^{i\bar{\delta}} e^{+i\bar{\varphi}}\right], \tag{6.147}$$

$$A(B_s^0 \to D_s^+ K^-) = A(B_s^0 \to D_s^+ K^-)_{\rm SM}\left[1 + \rho\, e^{i\delta} e^{-i\varphi}\right], \tag{6.148}$$

$$A(B_s^0 \to D_s^- K^+) = A(B_s^0 \to D_s^- K^+)_{\rm SM}\left[1 + \bar{\rho}\, e^{i\bar{\delta}} e^{-i\bar{\varphi}}\right], \tag{6.149}$$

$$A(\bar{B}_s^0 \to D_s^- K^+) = A(\bar{B}_s^0 \to D_s^- K^+)_{\rm SM}\left[1 + \rho\, e^{i\delta} e^{+i\varphi}\right]. \tag{6.150}$$

Here $\bar{\rho}$ and ρ describe the strength of the NP contributions to $b \to c\bar{u}s$ and $\bar{b} \to \bar{u}c\bar{s}$ quark-level transitions with respect to the corresponding SM amplitudes, respectively, with $\bar{\delta}$, δ

denoting CP-conserving strong phases while $\bar{\varphi}$, φ are CP-violating NP phases[58]:

$$\bar{\rho}\, e^{i\bar{\delta}} e^{i\bar{\varphi}} \equiv \frac{A(\bar{B}_s^0 \to D_s^+ K^-)_{\rm NP}}{A(\bar{B}_s^0 \to D_s^+ K^-)_{\rm SM}}, \qquad \rho\, e^{i\delta} e^{-i\varphi} \equiv \frac{A(B_s^0 \to D_s^+ K^-)_{\rm NP}}{A(B_s^0 \to D_s^+ K^-)_{\rm SM}}, \tag{6.151}$$

$$\bar{\rho}\, e^{i\bar{\delta}} e^{-i\bar{\varphi}} \equiv \frac{A(B_s^0 \to D_s^- K^+)_{\rm NP}}{A(B_s^0 \to D_s^- K^+)_{\rm SM}}, \qquad \rho\, e^{i\delta} e^{+i\varphi} \equiv \frac{A(\bar{B}_s^0 \to D_s^- K^+)_{\rm NP}}{A(\bar{B}_s^0 \to D_s^- K^+)_{\rm SM}}. \tag{6.152}$$

Using these parametrisations of NP effects, we may generalise the expressions of the branching ratios and the CP asymmetries, which are related to decay amplitudes.

6.8.2 Direct CP Asymmetries

The definitions of the direct CP asymmetries for the $B_s^0 \to D_s^\mp K^\pm$ system are:

$$\bar{\mathcal{A}}_{\rm CP}^{\rm dir} \equiv \frac{|A(B_s^0 \to D_s^- K^+)|^2 - |A(\bar{B}_s^0 \to D_s^+ K^-)|^2}{|A(B_s^0 \to D_s^- K^+)|^2 + |A(\bar{B}_s^0 \to D_s^+ K^-)|^2}, \tag{6.153}$$

$$\mathcal{A}_{\rm CP}^{\rm dir} \equiv \frac{|A(B_s^0 \to D_s^+ K^-)|^2 - |A(\bar{B}_s^0 \to D_s^- K^+)|^2}{|A(B_s^0 \to D_s^+ K^-)|^2 + |A(\bar{B}_s^0 \to D_s^- K^+)|^2}. \tag{6.154}$$

In the SM framework, these direct asymmetries vanish, as reflected by the following decay amplitude relations:

$$|A(\bar{B}_s^0 \to D_s^+ K^-)_{\rm SM}| = |A(B_s^0 \to D_s^- K^+)_{\rm SM}|, \tag{6.155}$$

$$|A(B_s^0 \to D_s^+ K^-)_{\rm SM}| = |A(\bar{B}_s^0 \to D_s^- K^+)_{\rm SM}|. \tag{6.156}$$

In contrast to the SM, NP contributions may generate non-vanishing direct CP asymmetries. Applying the generalised amplitude Eqs. (6.147) and (6.150), in Eqs. (6.153)-(6.154), we obtain

$$\bar{\mathcal{A}}_{\rm CP}^{\rm dir} = \frac{2\,\bar{\rho}\sin\bar{\delta}\sin\bar{\varphi}}{1 + 2\,\bar{\rho}\cos\bar{\delta}\cos\bar{\varphi} + \bar{\rho}^2}, \tag{6.157}$$

$$\mathcal{A}_{\rm CP}^{\rm dir} = \frac{2\,\rho\sin\delta\sin\varphi}{1 + 2\,\rho\cos\delta\cos\varphi + \rho^2}. \tag{6.158}$$

Therefore, provided we have non-vanishing CP-conserving and CP-violating phases, the direct CP asymmetries do not vanish, in line with the general requirements for direct CP violation.

[58] For a detailed analysis of how one defines these NP parameters, the reader is referred to Ref. [115].

6.8.3 Branching Ratio Observables

We have already introduced the ratios R of theoretical branching ratios with the differential branching ratios of their corresponding semileptonic decay channels. In the presence of NP, we use CP-averaged ratios $\langle R \rangle$ as follows:

$$\langle R_{D_sK} \rangle \equiv \frac{\mathcal{B}(\bar{B}_s^0 \to D_s^+ K^-)_{\rm th} + \mathcal{B}(B_s^0 \to D_s^- K^+)_{\rm th}}{\left[{\rm d}\mathcal{B}\left(\bar{B}_s^0 \to D_s^+ \ell^- \bar{\nu}_\ell\right)/{\rm d}q^2 + {\rm d}\mathcal{B}\left(B_s^0 \to D_s^- \ell^+ \nu_\ell\right)/{\rm d}q^2 \right]|_{q^2=m_K^2}}, \tag{6.159}$$

$$\langle R_{KD_s} \rangle \equiv \frac{\mathcal{B}(\bar{B}_s^0 \to K^+ D_s^-)_{\rm th} + \mathcal{B}(B_s^0 \to K^- D_s^+)_{\rm th}}{\left[{\rm d}\mathcal{B}\left(\bar{B}_s^0 \to K^+ \ell^- \bar{\nu}_\ell\right)/{\rm d}q^2 + {\rm d}\mathcal{B}\left(B_s^0 \to K^- \ell^+ \nu_\ell\right)/{\rm d}q^2 \right]|_{q^2=m_{D_s}^2}}, \tag{6.160}$$

which take the form:

$$\langle R_{D_sK} \rangle = 6\pi^2 f_K^2 |V_{us}|^2 |a_{1\,\rm eff}^{D_sK}|^2 X_{D_sK} \ \left[1 + 2\,\bar{\rho}\cos\bar{\delta}\cos\bar{\varphi} + \bar{\rho}^2\right], \tag{6.161}$$

$$\langle R_{KD_s} \rangle = 6\pi^2 f_{D_s}^2 |V_{cs}|^2 |a_{1\,\rm eff}^{KD_s}|^2 X_{KD_s} \ \left[1 + 2\,\rho\cos\delta\cos\varphi + \rho^2\right]. \tag{6.162}$$

We note here that for vanishing direct CP asymmetries, we have $\langle R_{D_sK} \rangle = R_{D_s^+K^-}$ and $\langle R_{KD_s} \rangle = R_{K^+D_s^-}$. We can introduce the following quantities:

$$\bar{b} = \frac{\langle R_{D_sK} \rangle}{6\pi^2 f_K^2 |V_{us}|^2 |a_{1\,\rm eff}^{D_sK}|^2 X_{D_sK}}, \tag{6.163}$$

$$b = \frac{\langle R_{KD_s} \rangle}{6\pi^2 f_{D_s}^2 |V_{cs}|^2 |a_{1\,\rm eff}^{KD_s}|^2 X_{KD_s}}, \tag{6.164}$$

where for the effective values of $|a_{1\,\rm eff}|$ we use the product of the theoretical expectations in Eqs. (6.74) and (6.89), which are obtained within QCD factorisation, and the numerical values of $r_E^{D_sK}$ and $r_E^{KD_s}$ in Eqs. (6.77) and (6.98), respectively, yielding:

$$|a_{1\,\rm eff}^{D_sK}| = 1.07 \pm 0.09, \qquad |a_{1\,\rm eff}^{KD_s}| = 1.1 \pm 0.13. \tag{6.165}$$

Regarding the ratios R, we use the experimental values in Eqs. (6.105) and (6.121). Finally, the parameters $\bar{b}$ and b take the following form:

$$\bar{b} \equiv \frac{\langle \mathcal{B}(\bar{B}_s^0 \to D_s^+ K^-)_{\rm th} \rangle}{\mathcal{B}(\bar{B}_s^0 \to D_s^+ K^-)_{\rm th}^{\rm SM}} = 1 + 2\,\bar{\rho}\cos\bar{\delta}\cos\bar{\varphi} + \bar{\rho}^2, \tag{6.166}$$

$$b \equiv \frac{\langle \mathcal{B}(\bar{B}_s^0 \to K^+ D_s^-)_{\rm th} \rangle}{\mathcal{B}(\bar{B}_s^0 \to K^+ D_s^-)_{\rm th}^{\rm SM}} = 1 + 2\,\rho\cos\delta\cos\varphi + \rho^2, \tag{6.167}$$

Within the SM, these observables would be equal to 1. However, using the values in Eqs. (6.165), (6.105) and (6.121), these parameters take the values

$$\bar{b} = 0.58 \pm 0.16, \qquad b = 0.50 \pm 0.26. \tag{6.168}$$

The deviations of the branching ratio observables $\bar{b}$ and b from the value of 1 reflect the puzzling picture coming from the $|a_1|$ parameters presented in Fig. 39.

6.8.4 Generalised Expressions for ξ_s and $\bar{\xi}_s$

As we noted above, for the CP-violating phenomena in the $B_s^0 \to D_s^{\mp} K^{\pm}$ system, interference effects between B_s^0–$\bar{B}_s^0$ mixing and decay processes play a key role and are described by the physical observables ξ_s and $\bar{\xi}_s$. We generalise their expressions to allow for NP contributions with new sources of CP violation as follows:

$$\xi_s = \xi_s^{\rm SM} \left[\frac{1 + \bar{\rho}\, e^{i\bar{\delta}} e^{+i\bar{\varphi}}}{1 + \rho\, e^{i\delta} e^{-i\varphi}} \right], \qquad \bar{\xi} = \bar{\xi}_s^{\rm SM} \left[\frac{1 + \rho\, e^{i\delta} e^{+i\varphi}}{1 + \bar{\rho}\, e^{i\bar{\delta}} e^{-i\bar{\varphi}}} \right]. \tag{6.169}$$

Using the SM expressions in Eqs. (6.9) and (6.10), interchanging the NP parameters ρ, δ, φ and $\bar{\rho}$, $\bar{\delta}$, $\bar{\varphi}$, we write:

$$\xi_s = -e^{-i(\phi_s+\gamma)} \left[\frac{1}{x_s e^{i\delta_s}} \right] \left[\frac{1 + \bar{\rho}\, e^{i\bar{\delta}} e^{+i\bar{\varphi}}}{1 + \rho\, e^{i\delta} e^{-i\varphi}} \right], \tag{6.170}$$

$$\bar{\xi}_s = -e^{-i(\phi_s+\gamma)} \left[x_s e^{i\delta_s} \right] \left[\frac{1 + \rho\, e^{i\delta} e^{+i\varphi}}{1 + \bar{\rho}\, e^{i\bar{\delta}} e^{-i\bar{\varphi}}} \right]. \tag{6.171}$$

Introducing a phase $\Delta\varphi$, the above relations are rewritten as:

$$\xi_s = -|\xi_s| e^{-i\delta_s} e^{-i(\phi_s+\gamma)} e^{i\Delta\varphi}, \tag{6.172}$$

$$\bar{\xi}_s = -|\bar{\xi}_s| e^{+i\delta_s} e^{-i(\phi_s+\gamma)} e^{i\Delta\bar{\varphi}}, \tag{6.173}$$

where

$$\tan\Delta\varphi = \frac{\rho\sin(\varphi-\delta) + \bar{\rho}\sin(\bar{\varphi}+\bar{\delta}) + \bar{\rho}\rho\sin(\bar{\delta}-\delta+\bar{\varphi}+\varphi)}{1 + \rho\cos(\varphi-\delta) + \bar{\rho}\cos(\bar{\varphi}+\bar{\delta}) + \bar{\rho}\rho\cos(\bar{\delta}-\delta+\bar{\varphi}+\varphi)}, \tag{6.174}$$

$$\tan\Delta\bar{\varphi} = \frac{\bar{\rho}\sin(\bar{\varphi}-\bar{\delta}) + \rho\sin(\varphi+\delta) + \rho\bar{\rho}\sin(\delta-\bar{\delta}+\varphi+\bar{\varphi})}{1 + \bar{\rho}\cos(\bar{\varphi}-\bar{\delta}) + \rho\cos(\varphi+\delta) + \rho\bar{\rho}\cos(\delta-\bar{\delta}+\varphi+\bar{\varphi})}. \tag{6.175}$$

In the SM case, the product $\xi_s \times \bar{\xi}_s$ is central for studying CP violation. We rewrite the generalised product as follows:

$$\xi_s \times \bar{\xi}_s = \left(\xi_s^{\rm SM} \times \bar{\xi}_s^{\rm SM}\right) \left[\frac{1 + \rho\, e^{i\delta} e^{+i\varphi}}{1 + \rho\, e^{i\delta} e^{-i\varphi}} \right] \left[\frac{1 + \bar{\rho}\, e^{i\bar{\delta}} e^{+i\bar{\varphi}}}{1 + \bar{\rho}\, e^{i\bar{\delta}} e^{-i\bar{\varphi}}} \right], \tag{6.176}$$

$$= \; e^{-i2(\phi_s+\gamma)} \quad \left[\frac{1 + \rho\, e^{i\delta} e^{+i\varphi}}{1 + \rho\, e^{i\delta} e^{-i\varphi}} \right] \left[\frac{1 + \bar{\rho}\, e^{i\bar{\delta}} e^{+i\bar{\varphi}}}{1 + \bar{\rho}\, e^{i\bar{\delta}} e^{-i\bar{\varphi}}} \right], \tag{6.177}$$

where again the hadronic parameter x_s with its strong phase δ_s cancels.

We may then write the first ratio in Eq. (6.177), expressing the NP parameters in terms of the direct CP asymmetries, using:

$$\frac{1+\rho\, e^{i\delta}e^{+i\varphi}}{1+\rho\, e^{i\delta}e^{-i\varphi}} = e^{-i\Delta\Phi}\sqrt{\frac{1-\mathcal{A}_{\rm CP}^{\rm dir}}{1+\mathcal{A}_{\rm CP}^{\rm dir}}} \tag{6.178}$$

where we introduce a phase $\Delta\Phi$, which is given through:

$$\cos\Delta\Phi = \sqrt{\frac{1-\mathcal{A}_{\rm CP}^{\rm dir}}{1+\mathcal{A}_{\rm CP}^{\rm dir}}}\left[\frac{1+2\rho\cos\delta\cos\varphi+\rho^2\cos 2\varphi}{1+2\rho\cos(\delta-\varphi)+\rho^2}\right], \tag{6.179}$$

$$\sin\Delta\Phi = \sqrt{\frac{1-\mathcal{A}_{\rm CP}^{\rm dir}}{1+\mathcal{A}_{\rm CP}^{\rm dir}}}\left[\frac{-2\rho\cos\delta\sin\phi+\rho^2\sin(-2\phi)}{1+2\rho\cos(\delta-\phi)+\rho^2}\right], \tag{6.180}$$

and

$$\tan\Delta\Phi = -\left[\frac{2\rho\cos\delta\sin\varphi+\rho^2\sin 2\varphi}{1+2\rho\cos\delta\cos\varphi+\rho^2\cos 2\varphi}\right]. \tag{6.181}$$

In an analogous way, we express the second ratio in Eq. (6.177) in terms of the direct asymmetries $\bar{\mathcal{A}}_{\rm CP}^{\rm dir}$ and the corresponding counterparts for the phase $\Delta\bar{\Phi}$ that are related to $\bar{\rho}$, $\bar{\varphi}$ and $\bar{\delta}$.

We may now rewrite the product $\xi_s \times \bar{\xi}_s$ with the help of the direct CP asymmetries as

$$\xi_s \times \bar{\xi}_s = e^{-i2(\phi_s+\gamma)}\sqrt{\left[\frac{1-\mathcal{A}_{\rm CP}^{\rm dir}}{1+\mathcal{A}_{\rm CP}^{\rm dir}}\right]\left[\frac{1-\bar{\mathcal{A}}_{\rm CP}^{\rm dir}}{1+\bar{\mathcal{A}}_{\rm CP}^{\rm dir}}\right]}\, e^{-i(\Delta\Phi+\Delta\bar{\Phi})}. \tag{6.182}$$

Moreover, applying Eqs. (6.172) and (6.173), the product of $\xi_s \times \bar{\xi}_s$ takes the form

$$\xi_s \times \bar{\xi}_s = |\xi_s|\;|\bar{\xi}_s|\; e^{-i2(\phi_s+\gamma)}\; e^{i(\Delta\varphi+\Delta\bar{\varphi})} \tag{6.183}$$

where

$$\begin{aligned}
|\xi_s|\;|\bar{\xi}_s| &= \left|\frac{A(\bar{B}_s^0\to D_s^+K^-)}{A(B_s^0\to D_s^+K^-)}\right|\left|\frac{A(\bar{B}_s^0\to D_s^-K^+)}{A(B_s^0\to D_s^-K^+)}\right| \\
&= \left|\frac{A(\bar{B}_s^0\to D_s^-K^+)}{A(B_s^0\to D_s^+K^-)}\right|\left|\frac{A(\bar{B}_s^0\to D_s^+K^-)}{A(B_s^0\to D_s^-K^+)}\right| \\
&= \sqrt{\left[\frac{1-\mathcal{A}_{\rm CP}^{\rm dir}}{1+\mathcal{A}_{\rm CP}^{\rm dir}}\right]\left[\frac{1-\bar{\mathcal{A}}_{\rm CP}^{\rm dir}}{1+\bar{\mathcal{A}}_{\rm CP}^{\rm dir}}\right]}.
\end{aligned} \tag{6.184}$$

Comparing Eqs. (6.182) and (6.183)-(6.184), we note that the CP-violating NP phase shifts satisfy the following sum rule:

$$\Delta\Phi + \Delta\bar{\Phi} = -\left(\Delta\varphi + \Delta\bar{\varphi}\right). \tag{6.185}$$

We can further simplify the expression of the product of the two physical observables ξ_s and $\bar{\xi}_s$:

$$\left|\xi \times \bar{\xi}\right|^2 = \left[\frac{1-\mathcal{A}_{\rm CP}^{\rm dir}}{1+\mathcal{A}_{\rm CP}^{\rm dir}}\right]\left[\frac{1-\bar{\mathcal{A}}_{\rm CP}^{\rm dir}}{1+\bar{\mathcal{A}}_{\rm CP}^{\rm dir}}\right]. \tag{6.186}$$

We note that for vanishing direct CP asymmetries, the squared product in Eq. (6.186) is equal to 1. However, for non-vanishing direct asymmtries, we obtain

$$\left|\xi \times \bar{\xi}\right|^2 = 1+\epsilon, \tag{6.187}$$

yielding

$$\xi_s \times \bar{\xi}_s = \sqrt{1+\varepsilon}\; e^{-i[2(\phi_s+\gamma)+\Delta\Phi+\Delta\bar{\Phi}}. \tag{6.188}$$

Using the observable C in Eq. (6.16) and its CP-conjugate $\bar{C}$, we obtain

$$C+\bar{C} = -\frac{\varepsilon}{1+|\xi_s|^2}\left(1+\bar{C}\right). \tag{6.189}$$

Regarding the term $1+|\xi_s|^2$, we recal the relation of $|\xi_s|$ in terms of the observable C:

$$|\xi|^2 = \frac{(1-C)}{(1+C)} \tag{6.190}$$

$$1+|\xi|^2 = \frac{2}{(1+C)}. \tag{6.191}$$

Therefore, we obtain the following expression which generalises the relation in Eq. (6.23) that was assumed by the LHCb collaboration in Ref. [189]:

$$-\frac{1}{2}\,\epsilon = \frac{C+\bar{C}}{(1+C)\left(1+\bar{C}\right)} = \mathcal{A}_{\rm CP}^{\rm dir} + \bar{\mathcal{A}}_{\rm CP}^{\rm dir} + \mathcal{O}((\mathcal{A}_{\rm CP}^{\rm dir})^2). \tag{6.192}$$

Finally, we arrive at the following result [115,190], which is the generalisation of Eq. (6.13) for the presence of NP:

$$\xi \times \bar{\xi} = \sqrt{1-2\left[\frac{C+\bar{C}}{(1+C)\left(1+\bar{C}\right)}\right]}\, e^{-i\left[2(\phi_s+\gamma)+\Delta\Phi+\Delta\bar{\Phi}\right]}. \tag{6.193}$$

We emphasize that this product is theoretically clean, as in the SM. Making use of the observables of the time-dependent rate asymmetries of the $B_s^0 \to D_s^\mp K^\pm$ system, the corresponding product of ξ and $\bar{\xi}$ can still be determined. We notice that now the UT angle γ, due to the CP-violating NP phases, enters with a shift. Consequently, it results in an

"effective" angle [115, 190]

$$\gamma_{\text{eff}} \equiv \gamma + \delta\gamma_{\text{NP}}, \tag{6.194}$$

$$\equiv \gamma + \frac{\left(\Delta\Phi + \Delta\bar{\Phi}\right)}{2} \tag{6.195}$$

$$= \gamma - \frac{(\Delta\varphi + \Delta\bar{\varphi})}{2}. \tag{6.196}$$

We highlight here the following regarding the extraction of the γ value. When performing combined fits to the data using various B decays, as discussed for instance in Ref. [197], NP effects might be averaged out to some extend. Thus, it might yield an effective angle with NP contributions which cannot transparently be quantified, in contrast to Eq. (6.194).

Instead of these fits, it will be important to look for patterns being in tension with SM utilising individual γ determinations. The main goal then is to perform these analyses with the highest possible precision. In this respect, the strategy that we follow here, exploring CP violation in the $B_s^0 \to D_s^\mp K^\pm$ system and studying the branching ratios which are associated to these channels as well as their partner decays, is a prime example.

6.8.5 Correlations of New Physics Parameters

Our next step is to apply our new model-independent formalism to the currently available measurements [115,190]. Employing the direct CP asymmetry $\mathcal{A}_{\text{CP}}^{\text{dir}}$ and the branching ratio observable b, we can obtain correlations between the NP parameters. Therefore, we may determine ρ as function of the CP-violating phase φ with the help of

$$\rho = \sqrt{[b - 1 + 2\cos^2\varphi] \pm \sqrt{[b - 1 + 2\cos^2\varphi]^2 - \left[(b-1)^2 + \left(\frac{b\,\mathcal{A}_{\text{CP}}^{\text{dir}}}{\tan\varphi}\right)\right]}}. \tag{6.197}$$

Similar expression hold for the CP-conjugate quantities, allowing the extraction of the NP parameter $\bar{\rho}$ as function of $\bar{\varphi}$.

Since we are interested in applying our method to the current experimental data, we set the strong phases equal to 0°, thus

$$\delta = \bar{\delta} = 0^\circ, \tag{6.198}$$

in order to be consistent with the LHCb assumption $C = -\bar{C}$. This implies vanishing direct CP asymmetries $\bar{\mathcal{A}}_{\text{CP}}^{\text{dir}}$ and $\mathcal{A}_{\text{CP}}^{\text{dir}}$ as we can see in Eqs. (6.157) and (6.158), in agreement with the $B \to DK$ data within the current uncertainties [233]. Factorisation also favours the small δ_s phases, especially for the $b \to c$ mode $\bar{B}_s^0 \to D_s^+ K^-$. Therefore, the strong

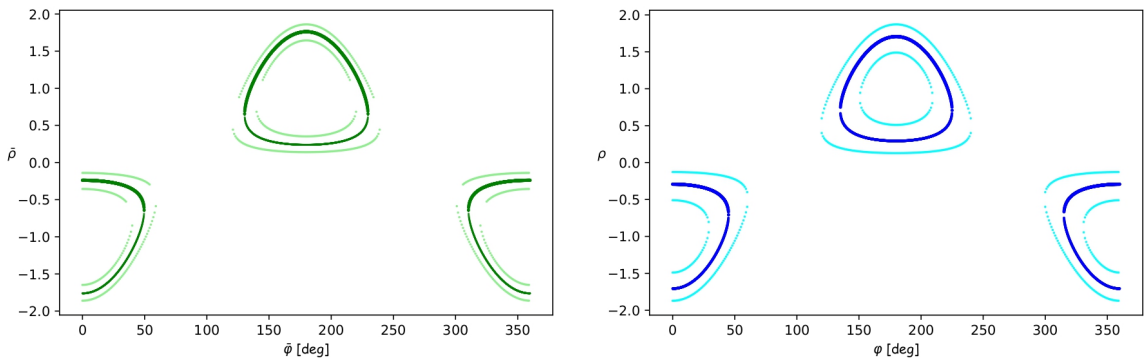

Figure 40: Illustration of the NP parameter $\bar{\rho}$ as function of the CP-violating phase $\bar{\varphi}$, utilising the branching ratio observable $\bar{b}$ (left panel) and the corresponding analysis for ρ and φ, using the observable b (right panel) [115].

phase difference δ_s result, which is presented in Eq. (6.24), within the uncertainties would be fully consistent with this picture.

Let us now assume vanishing strong phases, as in Eq. (6.198) and use the branching ratio information encoded in the observables b and $\bar{b}$. Then the expressions of the NP parameters $\bar{\rho}$ and ρ in terms of the CP-violating NP phases, presented in Eq. (6.197), take the simplified form:

$$\bar{\rho} = -\cos\bar{\varphi} \pm \sqrt{\bar{b} - \sin^2\bar{\varphi}}, \tag{6.199}$$

$$\rho = -\cos\varphi \pm \sqrt{b - \sin^2\varphi}. \tag{6.200}$$

Using the values of b and $\bar{b}$ in Eq. (6.168), we illustrate the constraints on NP parameters in Fig. 40. The green contour shows the NP parameter $\bar{\rho}$ as a function of the phase $\bar{\varphi}$ for the central value of the observable $\bar{b}$. The blue one represents the corresponding analysis of ρ in terms of ϕ for the b central value. In order to include uncertainties, we vary the values of the observable $\bar{b}$ and b within the $1\,\sigma$ range, leading to the contours in lighter colours.

We may also calculate correlations between the NP parameters in the $\bar{\varphi}$–φ plane as well as at the $\bar{\rho}$–ρ plane, utilising the time-dependent rates of the $B^0 \to D_s^{\mp} K^{\pm}$. Looking at Eqs. (6.174) and (6.175) and using the assumption in Eq. (6.198), we obtain

$$\tan\Delta\varphi = \frac{\rho\sin\varphi + \bar{\rho}\sin\bar{\varphi} + \bar{\rho}\rho\sin(\bar{\varphi}+\varphi)}{1 + \rho\cos\varphi + \bar{\rho}\cos\bar{\varphi} + \bar{\rho}\rho\cos(\bar{\varphi}+\varphi)}. \tag{6.201}$$

Now, Eq. (6.196) under the assumption of setting the strong phases equal to 0 in Eq. (6.198) implies:

$$\Delta\varphi = \Delta\bar{\varphi} = \gamma - \gamma_{\text{eff}} = -(61 \pm 20)^\circ, \tag{6.202}$$

where, summarising the picture from analyses of CP violation in tree-level decays of the kind $B \to DK$ [187], $\gamma = (70 \pm 7)^\circ$ is the UT value [187, 233] and $\gamma_{\rm eff}$ corresponds to the result in Eq. (6.25).

Let us stress here a few points regarding the angle γ and the $\Delta\varphi$ phase. As we have stated before, γ is determined with the help of pure tree decays, where large CP violation has not been observed. As we already work in the case where the strong phases are equal to 0°, the direct CP asymmetries vanish. Therefore, we ensure we do not encounter any issues with direct CP violation in modes with similar dynamics. In addition, this condition allows us to be consistent with the LHCb assumption for C and $\bar{C}$. Generalising this analysis and measuring every decay channel separately is very important. What we would also like to emphasize regarding the NP phase shift is that it is extracted in a theoretically clean way from the data. In particular, it does not rely on SM predictions of the ξ and $\bar{\xi}$ observables, a significant finding which is non-trivial.

Obtaining the NP Constraints

In order to convert the measured observables in constraints on the NP parameter space, Eq. (6.201) plays a central role. Firstly, utilising again the values of b and $\bar{b}$ in Eq. (6.168), we implement the expressions of Eqs. (6.199) and (6.200) into Eq. (6.201). As the experimental value of $\Delta\varphi$ is given in Eq. (6.202), we can determine φ as a function of $\bar{\varphi}$, thereby fixing contours in the $\bar{\varphi}$–φ plane. This is illustrated in the left panel of Fig. 41. Interestingly, at least one of the CP-violating phases has to take a non-trivial value, highlighting the need for new sources of CP violation.

Finally, having the values of $\bar{\varphi}$ and φ, we may use again $\bar{\rho}(\bar{\varphi})$ and $\rho(\varphi)$ in Eqs. (6.199) and (6.200), allowing us to obtain the correlations in the $\bar{\rho}$–ρ plane. Each point is linked with a specific value of the CP-violating NP phases $\bar{\varphi}$ and φ, illustrated in the right panel of Fig. 41. In order to show this better, we pick, as an example, four random points in the $\bar{\varphi}$–φ plane, illustrated as square, circle, diamond and star in Fig. 41, and we show the corresponding values in the $\bar{\rho}$–ρ plane. The sets of values that we have used are the following:

$$(\rho, \varphi) = (-0.43, 37.0^\circ), \quad (\bar{\rho}, \bar{\varphi}) = (-0.64, 49.6^\circ) \tag{6.203}$$

$$(\rho, \varphi) = (-0.48, 40.3^\circ), \quad (\bar{\rho}, \bar{\varphi}) = (0.58, 229.0^\circ) \tag{6.204}$$

$$(\rho, \varphi) = (0.40, 146.0^\circ), \quad (\bar{\rho}, \bar{\varphi}) = (1.14, 221.0^\circ) \tag{6.205}$$

$$(\rho, \varphi) = (0.36, 209.0^\circ), \quad (\bar{\rho}, \bar{\varphi}) = (-0.74, 49.2^\circ). \tag{6.206}$$

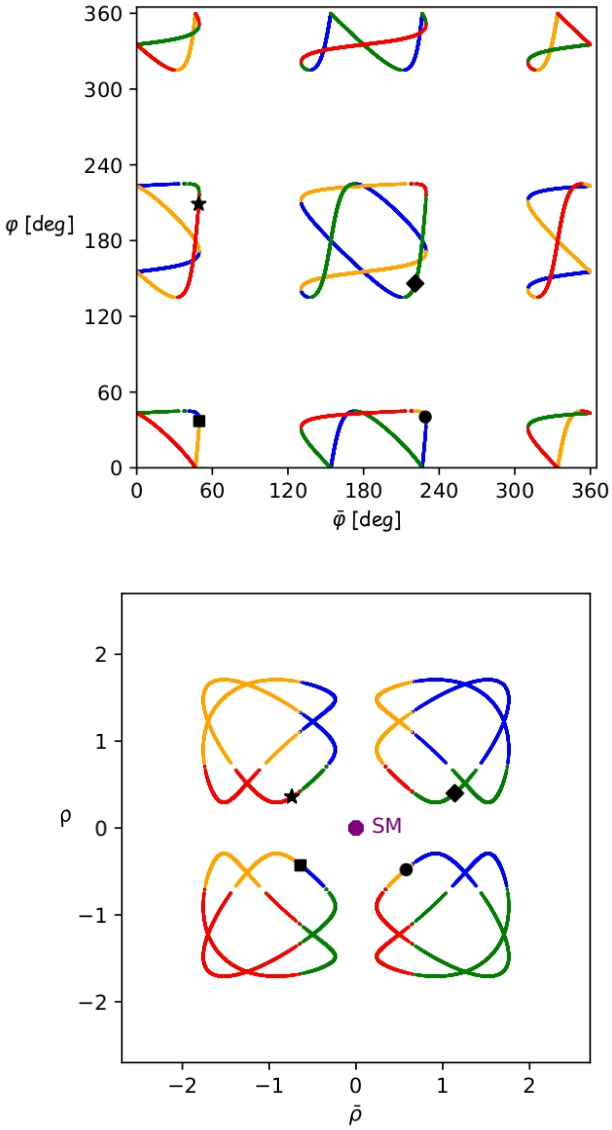

Figure 41: NP parameter correlations for the central values of the current experimental data in the $\bar{\varphi}$–φ plane (left) and the $\bar{\rho}$–ρ plane (right), as discussed in the text. We have indicated four points (square, circle, diamond and star) to illustrate the connection in the two correlations, and have highlighted the SM point [115].

We note that the SM point, which corresponds to the origin $(0, 0)$ in the $\bar{\rho}$–ρ plane, is excluded. The points of ρ and $\bar{\rho}$ are bounded to values below two. Last but not least, the gaps between the contours arise from the algebraic structure of the corresponding expressions and are in particular related to the fact that the values of b and $\bar{b}$ are smaller than 1. We explore how the plots in Fig. 41 change for different values of b and $\bar{b}$ in Appendix E.2.

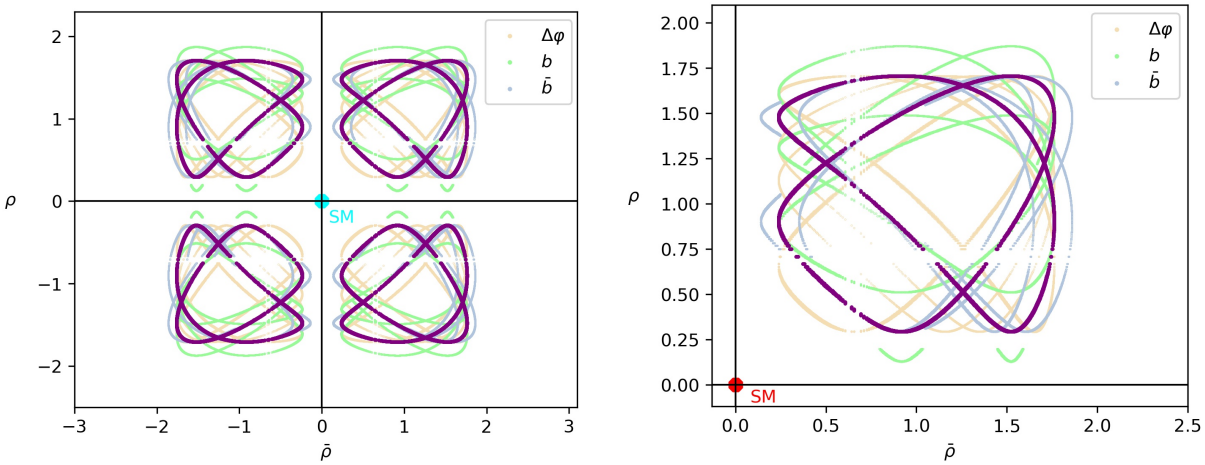

Figure 42: Impact of uncertainties of the input quantities $\bar{b}$, b and $\Delta\varphi$ in the full $\bar{\rho}$–ρ plane (left) and focusing only on the positive values of $\bar{\rho}$ and ρ (right) [115, 190].

We emphasize that Fig. 41 shows the NP parameters correlations for the central values of the current experimental data. The four different colours represent the four different combinations that we obtain for the product $\rho\bar{\rho}$ in Eq. (6.201). This is due to the different signs before the square root in the Eqs. (6.199) and (6.200), giving rise to two solutions for every ρ and $\bar{\rho}$.

The interesting point following from the $\bar{\rho}$–ρ plot is that it would be possible for values as small as in the regime around 0.5 to accommodate the central values of the current data. Therefore, this would resolve the puzzling patterns in both the measurements of CP violation as well as in the branching ratios. We would then have NP contributions at he level of 50% of the SM amplitudes, a feature that we also observe in the NP parameter sets in Eqs. (6.203)–(6.206).

Let us now move on and explore the NP parameters correlations including uncertainties. Varying each of the input quantities $\bar{b}$, b and $\Delta\varphi$ separately, we illustrate their impact on the contours in the $\bar{\rho}$–ρ plane. As it is shown in the left panel of Fig. 42, each one of the three contours with the pale colours corresponds to one of the input parameters. In the right panel of Fig. 42, we zoom in to the positive values of ρ and $\bar{\rho}$. We nicely see now that we could accommodate the current data with NP contributions at the level of 30% of the SM amplitudes.

Concluding, we have presented a NP analysis which, in the future, will serve as benchmark as the data improve, allowing us to narrow down specific models and scenarios. In view of this, we mention again that specific NP scenarios which could affect the decays $B_{(s)} \to D_{(s)}\pi$ and $B \to DK$ were studied with respect to the branching ratios and the puzzles that are associated with them for these channels in Refs. [192–194]. Another inter-

esting example of such kind of physics beyond the SM entering the $B_s^0 \to D_s^\mp K^\pm$ system is the one that involves left-handed W' bosons [192]. As we have demonstrated in our analysis, this offers an exciting probe for CP-violating NP phases. These first proposed models have potential challenges with collider data for direct NP searches and could be interesting illustrations of possible scenarios.

6.9 Conclusion

The pure tree $B_s^0 \to D_s^\mp K^\pm$ decays and their CP conjugates play a key role in testing the SM. Due to interference effects, CP-violating asymmetries arise, allowing theoretical clean determinations of the UT angle γ within the SM. Performing an analysis of these CP asymmetries measured by the LHCb Collaboration, and paying special attention to resolving ambiguities, we find an intriguing γ value, consistent with the LHCb measurement.[59] This result is in tension with the values suggested by the global UT analyses at the 3σ level. We note that these tensions cannot be explained through non-factorisable effects

This intriguing case is complemented by a second puzzle which arises from the analysis of the branching ratios of the $B_s^0 \to D_s^\mp K^\pm$ decays as well as modes with similar dynamics. More specifically, starting from experimental branching ratios, we determine the individual theoretical ones. The $B_{(s)}^0$–$\bar{B}_{(s)}^0$ mixing effects are properly taken into account. Associated to the branching ratios are the parameters $|a_1|$, where we clearly observe tensions between theoretical predictions and experimental results. This is not only for the $\bar{B}_s^0 \to D_s^+ K^-$ decay but also for the $\bar{B}_s^0 \to K^+ D_s^-$ channel.

In particular, within QCD factorisation, the SM predictions for the $|a_1|$ parameters suggest a value of 1.07 with uncertainties at the percent level. Concerning the experimental values, our goal is to minimise the impact of the CKM matrix elements $|V_{cb}|$ and $|V_{ub}|$ as well as the uncertainties of hadronic form factors. In order to achieve that, we have introduced ratios of the $\bar{B}_s^0 \to D_s^+ K^-$ and $\bar{B}_s^0 \to K^+ D_s^-$ branching ratios with the differential rates of semileptonic $\bar{B}_s^0 \to D_s^+ \ell^- \bar{\nu}_\ell$ and $\bar{B}_s^0 \to K_s^+ \ell^- \bar{\nu}_\ell$ decays, respectively. As a result, we determine $|a_1^{D_s K}|$ and $|a_1^{K D_s}|$ from the data in a clean way.

For the $b \to c$ modes, factorisation is expected to work very well [164]. Examples are the $\bar{B}_d^0 \to D_d^+ K^-$, $\bar{B}_d^0 \to D_d^+ \pi^-$ and $\bar{B}_s^0 \to D_s^+ \pi^-$ channels, which are tree decays and have dynamics similar to the $\bar{B}_s^0 \to D_s^+ K^-$. In these channels, we observe again the same pattern for the $|a_1|$ parameters with the experimental values being small with respect to

[59] The new LHCb Run II measurement, which was recently reported in Ref. [188], is interesting and needs to be further explored. This value has not yet been included in the average of the γ measurements, hence we did not use it in the present numerical analysis. Despite this measurement, the key points of our strategies still hold.

QCD factorisation [249, 253]. The tensions between theory and experiment in this case are even up to 4.8σ. In the case of the $b \to u$ transition, like the $\bar{B}_d^0 \to \pi^+ D_s^-$ channel, which has similar dynamics to $\bar{B}_s^0 \to K^+ D_s^-$, factorisation is on less solid ground. However, we find a similar pattern with theoretical predictions being larger than the experimental results. Due to large uncertainties though, we cannot yet draw any further conclusions in this case.

In view of these intriguing results, we have generalised our analysis and allow for NP contributions with new sources of CP violation. We have suggested a model-independent strategy utilising the CP-violating observables. This results in an effective angle $\gamma_{\rm eff}$, which enters the generalised expressions with a CP-violating NP phase shift.

As we know, NP effects with new sources of CP violation can generate direct CP asymmetries. We highlight that the general formalism we have proposed holds also for non-vanishing direct CP violation. However, LHCb uses the assumption of $C + \bar{C} = 0$, as in the SM. As a result, our strategy allows us to go beyond this condition. In order to obtain the full picture, it would be important that the LHCb generalises its analysis correspondingly.

In our numerical analysis, where we explore what the measurements imply for NP, we also make an assumption to have vanishing CP-conserving phases. This would then be consistent with LHCb and would correspond to the strict limit in factorisation. Employing our formalism to the current data, we obtain correlations between the NP parameters of the $b \to c\bar{u}s$ and $b \to u\bar{c}s$ modes. We find strongly correlated NP effects, which could have large CP-violating phases. Interestingly, we find that we can accommodate the data with NP contributions as small as 30% of the SM amplitudes.

A summary of our strategy is presented in Fig. 43. Our analysis has three main pillars:

- Focusing on CP Violation: we utilise the CP asymmetries C, S, $\mathcal{A}_{\Delta\Gamma}$ and their CP conjugates, which allow the unambiguous determination of ξ and $\bar{\xi}$ from the data. The gemeralised $\xi \times \bar{\xi}$ product, accounting for NP effects, leads to the theoretically clean extraction of $\gamma_{\rm eff} \equiv \gamma + \gamma_{\rm NP}$. The angle $\gamma_{\rm NP}$, depending on NP parameters, is determined using information on γ from other processes.

- Utilising Branching Ratios: we combine the branching fractions of the non-leptonic decays with the differential branching fractions of their semi-leptonic partners, which allow a theoretically clean extraction of the $|a_1|$ parameters. Constraining exchange contributions using control channels, we complement the data with theoretical $|a_1|$ predictions. This allows the determination of the b and $\bar{b}$ quantities.

- Mapping out the NP Parameter Space: we utilise the three observables $\gamma_{\rm eff}$, b and $\bar{b}$ and obtain correlations between the NP parameters $\rho(\varphi)$ and $\bar{\rho}(\bar{\varphi})$, allowing us to explore the available space for NP.

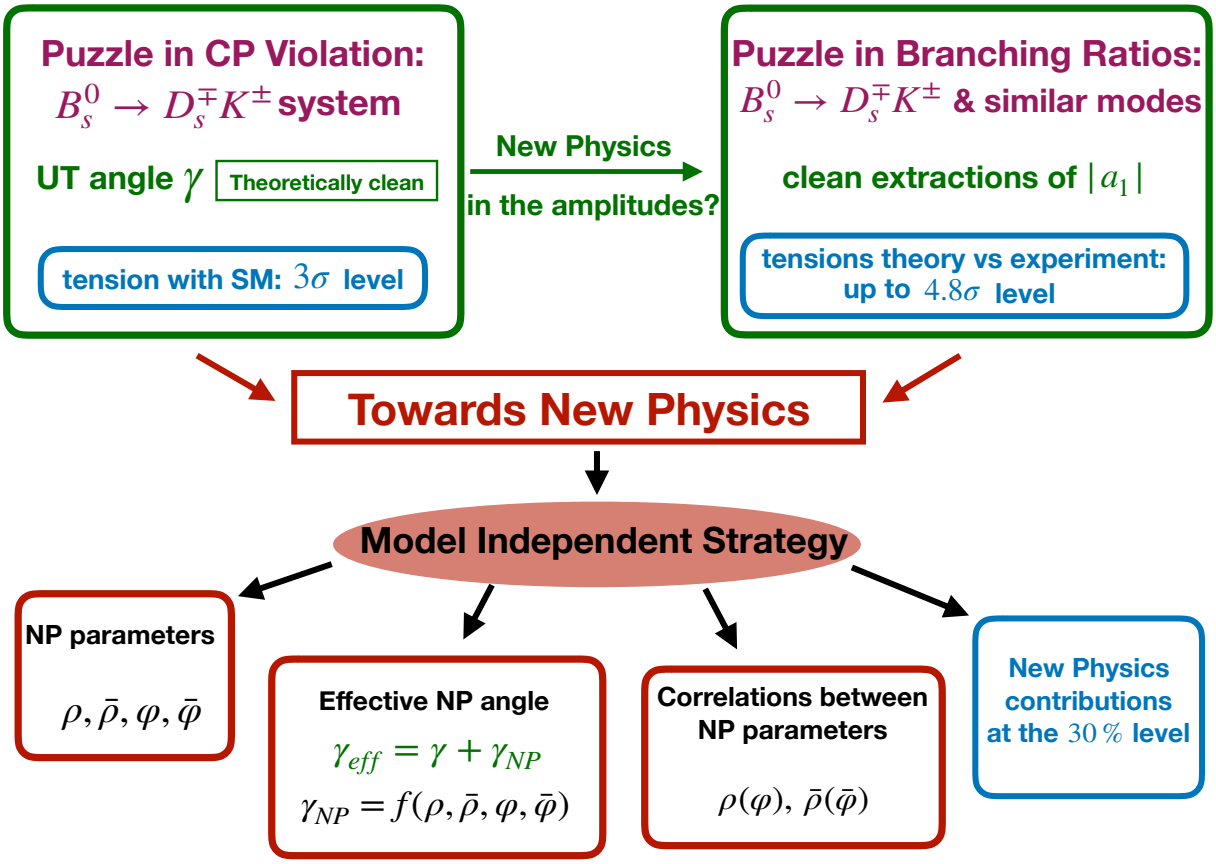

Figure 43: Illustration of the strategy to search for NP in the $B_s^0 \to D_s^\mp K^\pm$ system [190].

Our formalism can be utilised in future measurements of the $B_s^0 \to D_s^\mp K^\pm$ system, taking also the semileptonic decays $\bar{B}_s^0 \to D_s^+ \ell^- \bar{\nu}_\ell$ and $\bar{B}_s^0 \to K_s^+ \ell^- \bar{\nu}_\ell$ into account. It will be exciting to see how the data will evolve in the future high-precision physics era. Will we finally be able to establish new sources of CP violation in the $B_s^0 \to D_s^\mp K^\pm$ system?

Our Decays Roadmap - Highlights

Decays with Different Dynamics

UT
Important to study inclusive & exclusive cases separately for $|V_{ub}|$ & $|V_{cb}|$

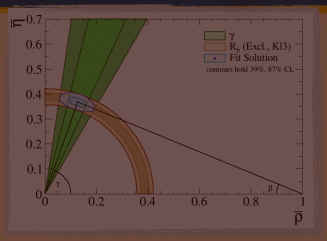

$B_d \to J/\psi K_S$, $B_s \to J/\psi\phi$

Performing combined fit with their control channels

↓

allows the determination of the mixing phases $\phi_{d,s}$ including the impact of penguins on CP asymmetries

CP Violation in different manifestations

$B_s \to D_s^{\pm} K^{\mp}$ & related modes

- Intriguing puzzles in CP violation and in branching ratio
- Utilising our model independent strategy in high precision era of B physics → may establish new sources of CP Violation

Rare Decays

$B \to \mu\mu$

from EW penguins and box topologies

$B \to \pi K$

dominated by penguins

7 The $B \to \pi K$ System

In this Chapter, we explore another case of non-leptonic decays, the $B \to \pi K$ transitions. As already discussed, theory calculations in this category suffer from uncertainties due to the presence of hadronic matrix elements. In order to handle the associated hadronic uncertainties, we apply flavour symmetries of strong interactions. These symmetries allow us to relate the amplitudes of the $B \to \pi K$ decays to those of two other systems: the $B \to \pi\pi$ and the $B \to KK$ channels. As a result, the matrix elements can either be eliminated or determined by experimental data.

The $B \to \pi K$ system of decays consists of four channels: $B^+ \to \pi^+ K^0$, $B^+ \to \pi^0 K^+$, $B_d^0 \to \pi^- K^+$ and $B_d^0 \to \pi^0 K^0$. Inconsistencies arise among the branching ratios and the CP asymmetries of these four channels, resulting in a puzzling situation. This $B \to \pi K$ puzzle is a long standing problem (see for instance Refs. [179, 186, 200, 272–277]). Here, we will revisit this puzzle and try to shed more light on the situation and possible resolutions.

Discussing the topologies of these modes, one would naively assume that the contributions that play the leading role are the tree topologies. However, this is not the case. These contributions are strongly suppressed because of the tiny CKM matrix element $|V_{ub}|$. Consequently, these decays are dominated by QCD penguin topologies. In addition, EW penguins also play an important role.

As an example, we illustrate the Feynman diagrams contributing to the $B_d^0 \to \pi^0 K^0$ channel in Fig 44. As we can see, for this $b \to q\bar{q}s$ transition, we have the colour-suppressed tree, the gluonic penguin as well as the colour-suppressed and the colour-allowed EW penguins. In our analysis, we will pay special attention to the $B_d^0 \to \pi^0 K^0$ decay. This is an important mode since it is the only one that exhibits mixing-induced CP violation, thereby making it a great candidate for testing the SM.

In view of searches for physics beyond the SM, we highlight that EW penguins offer a promising path for NP effects to enter [186, 278–280], making the $B \to \pi K$ channels very promising for NP searches. Considering that NP contributions are related to new sources of CP violation arising from CP-violating observables, it becomes more clear why $B_d^0 \to \pi^0 K^0$, with its mixing-induced CP asymmetry, is so important.

In this Chapter, starting from the deviations between the experimental measurements of the B-factories and the SM predictions, we will present a state-of-the-art analysis. We will explore the correlations between the CP asymmetries and obtain an updated picture. We will suggest a new strategy which permits the determination of the parameters that describe the EW penguin contributions. This new method can be applied to the data

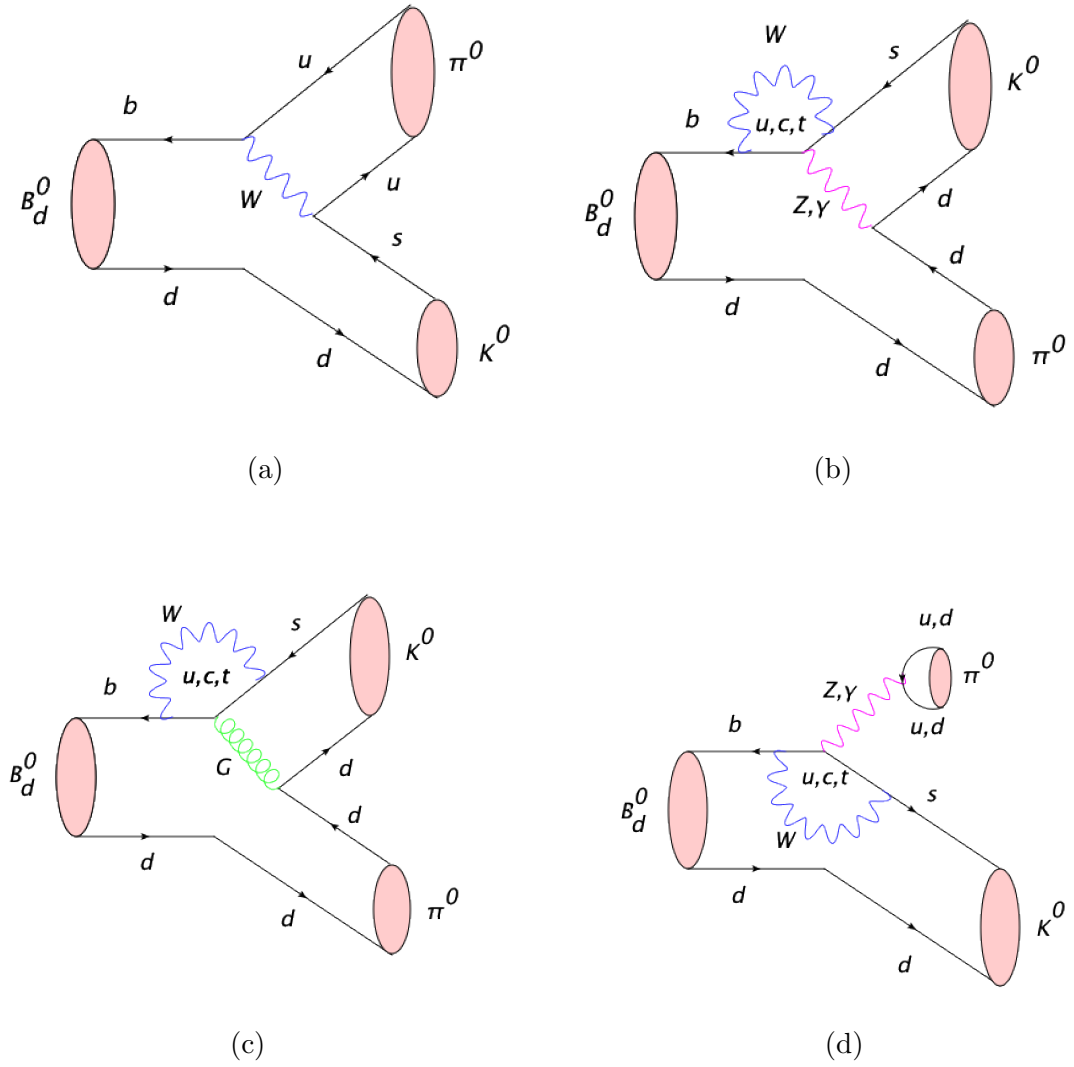

Figure 44: Feynman diagrams for the $B_d^0 \to \pi^0 K_s$ decay: (a) colour-suppressed tree, (b) colour-suppressed EW penguin, (c) QCD (gluonic) penguin, (d) colour-allowed EW penguin.

allowing us to constrain the parameter space for NP. For this purpose, we will utilise both charged and neutral $B \to \pi K$ modes. In the future, this strategy can be fully exploited, offering insights into the EW penguin sector. This Chapter follows our analysis presented in Refs. [281–284].

7.1 Amplitude Parametrization for the $B \to \pi K$ Modes

Let us first express the amplitudes of the four $B \to \pi K$ modes with the help of the flavour topologies which are relevant to these decays. In the SM we obtain correspondingly [272, 273, 285, 286]:

$$A\left(B_d^0 \to \pi^- K^+\right) = -[(\hat{P} - \frac{1}{3}\hat{P}_{EW}^C) + (\hat{T} + \hat{P}_{EW}^C)], \tag{7.1}$$

$$\sqrt{2}A\left(B_d^0 \to \pi^0 K^0\right) = (\hat{P} - \frac{1}{3}\hat{P}_{EW}^C) - (\hat{C} + \hat{P}_{EW}), \tag{7.2}$$

$$A\left(B^+ \to \pi^+ K^0\right) = (\hat{P} - \frac{1}{3}\hat{P}_{EW}^C) + \hat{A}, \tag{7.3}$$

$$\sqrt{2}A\left(B^+ \to \pi^0 K^+\right) = -[(\hat{P} - \frac{1}{3}\hat{P}_{EW}^C) + (\hat{T} + \hat{P}_{EW}^C) + (\hat{C} + \hat{P}_{EW}) + \hat{A}], \tag{7.4}$$

where $\hat{T}$ describes the colour-allowed trees while $\hat{C}$ the colour-suppressed trees, $\hat{P}$ denotes the QCD penguins, $\hat{P}_{EW}$ denotes the color-allowed EW penguin whereas $\hat{P}_{EW}^C$ the color-suppressed EW penguin contributions and $\hat{A}$ stands for annihilation. We notice that the amplitudes of $B_d^0 \to \pi^- K^+$ and $B^+ \to \pi^+ K^0$ have contributions only from colour-suppressed EW penguins while the $B_d^0 \to \pi^0 K^0$ and $B^+ \to \pi^0 K^+$ amplitudes have additional contributions from colour-allowed EW penguins.

Employing the isospin symmetry of strong interactions, the above amplitudes can be rewritten as follows, using the parametrization of Ref. [186]:

$$A(B_d^0 \to \pi^- K^+) = P' \left[1 + \frac{2}{3} a_C e^{i\Delta_C} q e^{i\omega} e^{i\phi}\, r_c e^{i\delta_c} - r e^{i\delta} e^{i\gamma}\right], \tag{7.5}$$

$$\sqrt{2}A(B_d^0 \to \pi^0 K^0) = -P' \left[1 - r e^{i\delta} e^{i\gamma} + \left\{e^{i\gamma} - \left(1 - \frac{2}{3} a_C e^{i\Delta_C}\right) q e^{i\phi} e^{i\omega}\right\} r_c e^{i\delta_c}\right], \tag{7.6}$$

$$A(B^+ \to \pi^+ K^0) = -P' \left[1 + \rho_c e^{i\theta_c} e^{i\gamma} - \frac{1}{3} \hat{a}_C e^{i\Delta_{\hat{C}}} q e^{i\omega} e^{i\phi}\, r_c e^{i\delta_c}\right], \tag{7.7}$$

$$\sqrt{2}A(B^+ \to \pi^0 K^+) = P' \left[1 + \rho_c e^{i\theta_c} e^{i\gamma} - \left\{e^{i\gamma} - \left(1 - \frac{1}{3} \hat{a}_C e^{i\Delta_{\hat{C}}}\right) q e^{i\phi} e^{i\omega}\right\} r_c e^{i\delta_c}\right] . \tag{7.8}$$

Let us introduce all the parameters in these expressions. The normalization factor P' is defined as:

$$P' \equiv \frac{\lambda^3 A}{\sqrt{\epsilon}} (\mathcal{P}'_t - \mathcal{P}'_c) \ , \tag{7.9}$$

where $\mathcal{P}'_t$ and $\mathcal{P}'_c$ are the strong QCD penguin amplitudes with internal t and c quarks exchanges, respectively, and the primes indicate that we deal with $\bar{b} \to \bar{s}$ transitions.

Moreover, $\epsilon \equiv \lambda^2/(1-\lambda^2)$ is given in Eq. (5.5), where $\lambda \equiv |V_{us}| = 0.2231 \pm 0.0007$ following [209], and $A \equiv |V_{cb}|/\lambda^2 = 0.8227^{+0.0066}_{-0.0136}$ given in Ref. [69, 70].

In Eqs. (7.5)-(7.8), the parameter $qe^{i\phi}e^{i\omega}$ describes the EW penguin contributions and is given by the following expression:

$$qe^{i\phi}e^{i\omega} \equiv -\left(\frac{\hat{P}'_{EW} + \hat{P}'^{\rm C}_{EW}}{\hat{T}' + \hat{C}'}\right). \tag{7.10}$$

The ϕ and ω are CP-violating and CP-conserving phases, repsectively. In these equations, we have also the parameters a_C and $\hat{a}_C$, which are related to colour-suppressed EW penguins, and the CP-conserving phases Δ_C and $\Delta_{\hat{C}}$ for the B^0_d and B^+ decays, respectively, for which:

$$a_C e^{i\Delta_C} \equiv \frac{\hat{P}'^{\rm C}_{EW}}{\hat{P}'_{EW} + \hat{P}'^{\rm C}_{EW}} \ . \tag{7.11}$$

Due to isospin symmetry, the following relation holds:

$$a_C = \hat{a}_C, \quad \Delta_C = \Delta_{\hat{C}} \ . \tag{7.12}$$

We observe that these quantities enter with the parameters q and ϕ, which are EW penguin parameters, playing an important role in our analysis.

Finally, the hadronic parameters entering Eqs. (7.5)-(7.8) are defined as follows:

$$re^{i\delta} = \left(\frac{\lambda^2 R_b}{1-\lambda^2}\right)\left[\frac{\mathcal{T}' - (\mathcal{P}'_t - \mathcal{P}'_u)}{\mathcal{P}'_t - \mathcal{P}'_c}\right], \tag{7.13}$$

$$r_{\rm c}e^{i\delta_{\rm c}} = \left(\frac{\lambda^2 R_b}{1-\lambda^2}\right)\left[\frac{\mathcal{T}' + \mathcal{C}'}{\mathcal{P}'_t - \mathcal{P}'_c}\right], \tag{7.14}$$

$$\rho_c e^{i\theta_c} = \left(\frac{\lambda^2 R_b}{1-\lambda^2}\right)\left[\frac{\mathcal{P}'_t - \tilde{\mathcal{P}}'_u - \mathcal{A}'}{\mathcal{P}'_t - \mathcal{P}'_c}\right] \approx 0, \tag{7.15}$$

$$\rho_n e^{i\theta_n} = \left(\frac{\lambda^2 R_b}{1-\lambda^2}\right)\left[\frac{\mathcal{C}' + (\mathcal{P}'_t - \mathcal{P}'_u)}{\mathcal{P}'_t - \mathcal{P}'_c}\right] = r_c e^{i\delta_c} - re^{i\delta}, \tag{7.16}$$

where $\tilde{\mathcal{P}}'_u$ is a QCD penguin amplitude, $\mathcal{A}'$ an annihilation amplitude and $\mathcal{T}'$, $\mathcal{C}'$ are the colour-allowed and the colour-suppressed tree contributions, respectively. Introducing the normalized amplitudes

$$\hat{T}' = |V_{ub}V^*_{us}|\mathcal{T}' \quad \text{and} \quad \hat{C}' = |V_{ub}V^*_{us}|\mathcal{C}', \tag{7.17}$$

we rewrite the hadronic parameters for the QCD penguin and the tree topologies as

$$re^{i\delta} \equiv \frac{\hat{T}' - \hat{P}'_{tu}}{P'} \quad \text{and} \quad r_{\rm c}e^{i\delta_{\rm c}} \equiv \frac{\hat{T}' + \hat{C}'}{P'}, \tag{7.18}$$

with $\hat{P}'_{tu}$ indicating the difference between QCD penguin amplitudes with t and u quarks.

7.2 Determining the Hadronic Parameters

Let us determine the hadronic parameters we introduced above. The parameters $re^{i\delta}$ and $r_c e^{i\delta_c}$ are non-perturbative terms, thus difficult to calculate. In order to determine them we use the $B \to \pi\pi$ system, which has been extensively studied in [186]. More specifically, we utilise the $SU(3)$ symmetry of strong interactions, which relates the $B \to \pi K$ with the $B \to \pi\pi$ system. This allows us to convert the $B \to \pi\pi$ parameters into the corresponding $B \to \pi K$ ones.

7.2.1 Information from the $B \to \pi\pi$ System

Let us now give the structure of the amplitudes of the $B \to \pi\pi$ decays. There are three modes: the $B^+ \to \pi^+\pi^0$, $B_d^0 \to \pi^+\pi^-$ and $B_d^0 \to \pi^0\pi^0$ channel. Their amplitudes receive contributions from colour-allowed trees ($\mathcal{T}$), colour-suppressed trees ($\mathcal{C}$), penguins ($\mathcal{P}$), exchange topologies ($\mathcal{E}$), and penguin-annihilation topologies ($\mathcal{PA}$). Using the parametrization given in Refs. [186, 275], we have:

$$\sqrt{2}A(B^+ \to \pi^+\pi^0) = -\tilde{T}e^{i\gamma}(1 + xe^{i\Delta})(1 + \tilde{q}e^{-i\beta}e^{-i\gamma}) \tag{7.19}$$

$$A(B_d^0 \to \pi^-\pi^+) = -\tilde{T}(e^{i\gamma} - de^{i\theta}) \tag{7.20}$$

$$\sqrt{2}A(B_d^0 \to \pi^0\pi^0) = P\left[1 + \frac{x}{d}e^{i\gamma}e^{i(\Delta-\theta)} + \tilde{q}\left(\frac{1 + xe^{i\Delta}}{d}e^{-i\theta}e^{-i\beta}\right)\right] , \tag{7.21}$$

where d, x are the hadronic parameters describing the $B \to \pi\pi$ decays and θ, Δ are their strong phases. The factors $\tilde{T}$ and P are expressed as

$$\tilde{T} = \lambda^3 AR_b(\mathcal{T} - \mathcal{P}_{tu} + \mathcal{E} - \mathcal{PA}_{tu}) , \tag{7.22}$$

$$P = \lambda^3 A(\mathcal{P}_t - \mathcal{P}_c) , \tag{7.23}$$

with $\mathcal{P}_{tq}$ denoting the difference between penguin topologies with internal t and q quarks and PA_{tu} the corresponding difference between penguin-annihilation topologies. The parameter $\tilde{q}$ describes the EW penguin topologies [200, 287]

$$\tilde{q} \equiv \left|\frac{P_{EW} + P_{EW}^{C}}{T + C}\right| \sim 1.3 \times 10^{-2}\left|\frac{V_{td}}{V_{ub}}\right| \sim 3 \times 10^{-2}, \tag{7.24}$$

where $T = \lambda^3 AR_b\mathcal{T}$ and $C = \lambda^3 AR_b\mathcal{C}$. However, the EW penguins play a minor role and their effect on d, θ, x and Δ is negligible due to the current uncertainties [186]. This picture could change in the future with more sophisticated analyses. Considering the $de^{i\theta}$ and $xe^{i\Delta}$,

we introduce:

$$de^{i\theta} \equiv -\frac{1}{R_b}\frac{\mathcal{P}_{tc}+\mathcal{P}\mathcal{A}_{tc}}{\mathcal{T}-\mathcal{P}_{tu}+\mathcal{E}-\mathcal{P}\mathcal{A}_{tu}}\ , \tag{7.25}$$

$$xe^{i\Delta} \equiv \frac{\mathcal{C}+\mathcal{P}_{tu}-\mathcal{E}+\mathcal{P}\mathcal{A}_{tu}}{\mathcal{T}-\mathcal{P}_{tu}+\mathcal{E}-\mathcal{P}\mathcal{A}_{tu}}\ . \tag{7.26}$$

Our next step is to consider the CP asymmetries, as presented in Chapter 4. Reminding the reader about Eq. (4.25), we specifically write the time-dependent CP asymmetry for the decay of a B_d^0 meson into a final state which is an eigenstate of the CP operator:

$$\mathcal{A}_{\rm CP}(t) \equiv \frac{\Gamma(\bar{B}_d^0(t)\to f)-\Gamma(B_d^0(t)\to f)}{\Gamma(\bar{B}_d^0(t)\to f)+\Gamma(B_d^0(t)\to f)} = A_{\rm CP}^f\cos(\Delta m_d t)+S_{\rm CP}^f\sin(\Delta m_d t)\ . \tag{7.27}$$

With the expressions of the decay amplitudes, we obtain the direct and mixing induced CP asymmetries of the $B_d^0\to\pi^+\pi^-$ channel. These asymmetries are expressed in terms of the parameters in Eq. (7.25), the mixing phase ϕ_d in Eq. (4.57) [191, 201], which includes penguin corrections, and the angle γ in Eq. (4.60), as

$$A_{\rm CP}^{\pi^-\pi^+} = \frac{2d\sin\theta\sin\gamma}{1-2d\cos\theta\cos\gamma+d^2}\ , \tag{7.28}$$

$$S_{\rm CP}^{\pi^-\pi^+} = -\left[\frac{d^2\sin\phi_d-2d\cos\theta\sin(\phi_d+\gamma)+\sin(\phi_d+2\gamma)}{1-2d\cos\theta\cos\gamma+d^2}\right]. \tag{7.29}$$

The experimental values of these asymmetries, available in PDG [66] are

$$A_{\rm CP}^{\pi^-\pi^+} = 0.31\pm0.03, \qquad S_{\rm CP}^{\pi^-\pi^+} = -0.67\pm0.03. \tag{7.30}$$

This allows us to determine the d and θ parameters purely from data. We obtain their values:

$$d = 0.58\pm0.08,\ \ \theta = (150.6\pm4.1)^\circ. \tag{7.31}$$

Similarly, we write the CP asymmetries of the $B_d^0\to\pi^0\pi^0$ decay in terms of the parameters in Eq. (7.26):

$$A_{\rm CP}^{\pi^0\pi^0} = \frac{-2dx\sin(\theta-\Delta)\sin\gamma}{d^2+2dx\cos(\theta-\Delta)\cos\gamma+x^2}\ , \tag{7.32}$$

$$S_{\rm CP}^{\pi^0\pi^0} = -\left[\frac{d^2\sin\phi_d+2dx\cos(\theta-\Delta)\sin(\phi_d+\gamma)+x^2\sin(\phi_d+2\gamma)}{d^2+2dx\cos(\theta-\Delta)\cos\gamma+x^2}\right]\ . \tag{7.33}$$

The mixing-induced CP asymmetry of this channel is not yet measured. As a result, in order to extract the values of x and Δ from the data, we utilise ratios of branching ratios. The first ratio we use is the following:

$$R_{+-}^{\pi\pi} \equiv 2\frac{M_{B^+}}{M_{B_d}}\frac{\Phi(m_\pi/M_{B_d}, m_\pi/M_{B_d})}{\Phi(m_{\pi^0}/M_{B^+}, m_\pi/M_{B^+})}\left[\frac{\mathcal{B}(B^+\to\pi^+\pi^0)}{\mathcal{B}(B_d^0\to\pi^+\pi^-)}\right]\frac{\tau_{B_d^0}}{\tau_B^+}, \tag{7.34}$$

Mode	$\mathcal{B}[\times 10^{-6}]$	Mode	$\mathcal{B}[\times 10^{-6}]$
$B^0 \to \pi^0\pi^0$	1.59 ± 0.26	$\bar{B}^0 \to \pi^0\bar{K}^0$	9.9 ± 0.5
$B^0 \to \pi^+\pi^-$	5.12 ± 0.19	$\bar{B}^0 \to \pi^+K^-$	19.6 ± 0.5
$B^+ \to \pi^+\pi^0$	5.5 ± 0.4	$B^+ \to \pi^+K^0_S$	23.7 ± 0.8
		$B^+ \to \pi^0K^+$	12.9 ± 0.5

Table 13: Branching ratios of the $B \to \pi\pi$ and the $B \to \pi K$ decays [233]

where Φ is the usual phase-space function $\Phi(X,Y) = \sqrt{[1-(X+Y)^2][1-(X-Y)^2]}$ with the values of the masses following Ref. [66]. The experimental values for the lifetimes are $\tau_{B^+}/\tau_{B^0_d} = 1.076 \pm 0.004$ [66, 288] and for the branching ratios [66]:

$$\mathcal{B}(B^+ \to \pi^+\pi^0) = (5.5 \pm 0.4) \times 10^{-6}, \tag{7.35}$$

$$\mathcal{B}(B^0_d \to \pi^+\pi^-) = (5.12 \pm 0.19) \times 10^{-6}. \tag{7.36}$$

We collect all the values of the branching ratios of these decays in Table 13. Consequently, the experimental value for the ratio $R^{\pi\pi}_{+-}$ is:

$$R^{\pi\pi}_{+-} = 2.00 \pm 0.16. \tag{7.37}$$

In terms of the hadronic parameters this ratio is written as

$$R^{\pi\pi}_{+-} = \frac{1 + 2x\cos\Delta + x^2}{1 - 2d\cos\theta\cos\gamma + d^2}, \tag{7.38}$$

which leads to the following relation between x and Δ:

$$x = -\cos\Delta \pm \sqrt{r_\pi R^{\pi\pi}_{+-} - \sin^2\Delta}, \tag{7.39}$$

where

$$r_\pi \equiv 1 - 2d\cos\theta\cos\gamma + d^2. \tag{7.40}$$

The second ratio we introduce is the following:

$$R^{\pi\pi}_{00} \equiv 2\frac{\Phi(m_\pi/M_{B_d}, m_\pi/M_{B_d})}{\Phi(m_{\pi^0}/M_{B_d}, m_{\pi^0}/M_{B_d})}\left[\frac{\mathcal{B}(B^0_d \to \pi^0\pi^0)}{\mathcal{B}(B^0_d \to \pi^+\pi^-)}\right], \tag{7.41}$$

where $\mathcal{B}(B^0_d \to \pi^+\pi^-) = (5.12 \pm 0.19) \times 10^{-6}$ [66], which is also listed in Table 13. Thus, the experimental value is

$$R^{\pi\pi}_{00} = 0.621 \pm 0.104\ . \tag{7.42}$$

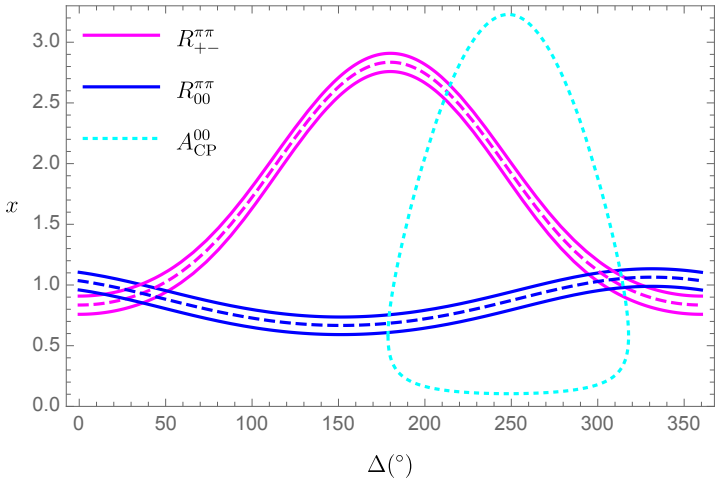

Figure 45: Determination of the parameters x and Δ with the help of the ratios $R_{00}^{\pi\pi}$ and $R_{+-}^{\pi\pi}$. The direct CP asymmetry $A_{\rm CP}^{\pi^0\pi^0}$ resolves the two-fold ambiguity.

We then obtain

$$R_{00}^{\pi\pi} = \frac{d^2 + 2dx\cos(\Delta-\theta)\cos\gamma + x^2}{1 - 2d\cos\theta\cos\gamma + d^2} \ , \tag{7.43}$$

which leads to

$$x = -d\cos\gamma\cos(\Delta-\theta) \pm \sqrt{r_\pi R_{00}^{\pi\pi} - (1-\cos^2(\Delta-\theta))d^2} \ . \tag{7.44}$$

The system of Eqs. (7.39) and (7.44) allows us to fix contours in the Δ–x plane, as illustrated in Fig. 45. The blue contour corresponds to the ratio $R_{00}^{\pi\pi}$ while the mangenta curve to the $R_{+-}^{\pi\pi}$ ratio. The points where the contours intersect provide the values of x and Δ. We observe that there are two points of intersection, resulting in two solutions. This ambiguity can be resolved by using the measured value of the direct CP asymmetry of the $B_d^0 \to \pi^0\pi^0$ channel [66]:

$$A_{\rm CP}^{\pi^0\pi^0} = 0.33 \pm 0.22, \tag{7.45}$$

which generates the dotted contour in cyan in Fig. 45 [281]. Finally, we obtain:

$$x = 1.06 \pm 0.09 \ , \quad \Delta = -(54.0 \pm 12.3)^\circ. \tag{7.46}$$

This determination of the hadronic parameters coming from the $B \to \pi\pi$ system is theoretically clean. It only depends on the experimental values of the CP asymmetries, the angle γ and the phase ϕ_d. There are no assumptions beyond the SM parametrizations. Now, that we have determined the parameters x, Δ, d, θ, we continue with the determination of the $B \to \pi K$ parameters r, δ and $r_{\rm c}$, $\delta_{\rm c}$.

7.2.2 Numerical Results for the Hadronic Parameters of the $B \to \pi K$ System

Regarding the parameters r and δ, we use the relation

$$re^{i\delta} = -\frac{e^{-i\Delta_{SU(3)}}}{\xi_{SU(3)}}\left[\frac{\epsilon}{d}e^{-i\theta}\right], \tag{7.47}$$

where $\Delta_{SU(3)}$ and $\xi_{SU(3)}$ describe non-factorizable U-spin-breaking corrections. We assume these non-factorizable effects at the level of 20%:

$$\xi_{SU(3)} = 1.0 \pm 0.2, \quad \Delta_{SU(3)} = (0 \pm 20)^\circ. \tag{7.48}$$

We will discuss the parameters d and θ in Sec 7.2.1. In addition, we define

$$r_{\rm c}^{\pi\pi}e^{i\delta_{\rm c}^{\pi\pi}} \equiv \epsilon R_b\left[\frac{\mathcal{T}+\mathcal{C}}{\mathcal{P}_{tc}+\mathcal{P}\mathcal{A}_{tc}}\right] = -\frac{\epsilon}{de^{i\theta}}(1+xe^{i\Delta}) \ , \tag{7.49}$$

leading to the following expression with the help of the $SU(3)$ flavour symmetry:

$$r_{\rm c}e^{i\delta_{\rm c}} = r_{\rm c}^{\pi\pi}e^{i\delta_{\rm c}^{\pi\pi}} = \xi_{SU(3)}^{r_{\rm c}} r_{\rm c}^{\pi\pi}e^{i(\Delta_{SU(3)}^{r_{\rm c}}+\delta_{\rm c}^{\pi\pi})} \ , \tag{7.50}$$

where $\xi_{SU(3)}^{r_{\rm c}}$ and $\Delta_{SU(3)}^{r_{\rm c}}$ parametrize the $SU(3)$-breaking effects, allowing again for such effects of up to 20%:

$$\xi_{SU(3)}^{r_{\rm c}} = 1.0 \pm 0.2, \quad \Delta_{SU(3)}^{r_{\rm c}} = (0 \pm 20)^\circ. \tag{7.51}$$

With the value of $\epsilon = 0.0535 \pm 0.0002$ [122] and the hadronic parameters from the $B \to \pi\pi$ system determined in Sec 7.2.1, the results following from Eqs. (7.47) and (7.50) are

$$re^{i\delta} = (0.09 \pm 0.03)\, e^{i(29.4\pm20.4)^\circ}, \tag{7.52}$$

$$r_c e^{i\delta_c} = (0.18 \pm 0.04)\, e^{i(1.7\pm21.3)^\circ}. \tag{7.53}$$

We note that in the analysis of the $B \to \pi K$ as well as the $B \to \pi\pi$ and $B \to KK$ modes, no indication of anomalous large non-factorizable $SU(3)$-breaking corrections or exchange and penguin-annihilation topologies contribution has been found [263, 281, 289].

Information from the $B \to KK$ System

Regarding the hadronic parameter $\rho_{\rm c}$, which is doubly Cabibbo-suppressed, we make use of the $B \to KK$ system [186, 290]. More specifically, employing the U-spin symmetry of strong interactions, we may utilise data from $B^+ \to K^+\bar{K}^0$. Following the analysis presented in [289], we the obtain:

$$\rho_{\rm c} = 0.03 \pm 0.01 \ , \ \ \theta_{\rm c} = (2.6 \pm 4.6)^\circ \ . \tag{7.54}$$

7.3 Electroweak Penguin Parameters q and ϕ in the SM

Let us now focus on the parametrization of the EW penguin parameters q and the CP-violating phase ϕ. Our starting point is Eq. (7.10), which we repeat here for convenience:

$$qe^{i\phi}e^{i\omega} \equiv -\left(\frac{\hat{P}'_{EW} + \hat{P}'^{\rm C}_{EW}}{\hat{T}' + \hat{C}'}\right). \tag{7.55}$$

We remind the reader that ω is the CP-conserving phase. In the SM, in order to calculate this parameter, we utilise the general expressions of the four-quark operators and recal the structure of the Q_k given in Appendix B. Applying then the $SU(3)$ symmetry to the hadronic matrix elements, and with the help of the Wilson coefficients and the UT triangle side R_b, we obtain [200, 291, 292]:

$$qe^{i\phi}e^{i\omega} \equiv \underbrace{\frac{-3}{2\lambda^2 R_b}\left[\frac{C_9(\mu) + C_{10}(\mu)}{C_1(\mu) + C_2(\mu)}\right]} R_q \tag{7.56}$$

$$= \qquad (0.68 \pm 0.05) \qquad R_q \ . \tag{7.57}$$

The parameter R_q describes the $SU(3)$-breaking corrections and can be written as the ratio of the following operator matrix elements [200, 292]:

$$R_q = \frac{\langle \pi K|\bar{Q}_1 - \bar{Q}_2|B^+\rangle}{\langle \pi K|\bar{Q}_1 + \bar{Q}_2|B^+\rangle}, \qquad \text{where } \bar{Q}_i = \frac{1}{2}\left(\bar{Q}_i^u - \bar{Q}_i^d\right). \tag{7.58}$$

Regarding its numerical value, we allow for $SU(3)$-breaking corrections of 30%, following the analysis in Ref. [293]:

$$R_q = 1.00 \pm 0.3. \tag{7.59}$$

Based on expected future progress on lattice calculations [293], a theory benchmark scenario can be assumed of $R_q = 1.00 \pm 0.05$.

Concerning the Wilson coefficients in Eq. (7.56), we note the following: for the Q_7 and Q_8 EW penguin operators, the coefficients C_7 and C_8, respectively, are tiny, thus they can be neglected. On the other hand, the coefficients C_9 and C_{10} are sizeable. Hence, we have connected the corresponding Q_9 and Q_{10} penguin operators with the current-current operators Q_1 and Q_2, which are related to the tree amplitudes [294], applying Fierz transformations:

$$Q_9^{u,d}|_{\rm Fierz} = Q_1^{u,d}, \qquad Q_{10}^{u,d}|_{\rm Fierz} = Q_2^{u,d}. \tag{7.60}$$

In the $SU(3)$ limit, the strong phase ω vanishes. Performing numerical studies, values of up to 10° would not have any impact on our analysis. The feature of small values for

the ω phase is model-independent [292]. In our studies, we set $\omega = 0^\circ$. Within the SM, the CP-violating phase ϕ vanishes. Consequently, if ϕ gets a sizeable value, this would be a signal of NP. Therefore, it is important to test whether there are any deviations from the SM values and if these deviations indicate NP.

7.4 CP Violation in $B \to \pi K$ Decays

Our next step is to study CP violation. A reliable SM prediction of the mixing-induced and the direct CP asymmetries is essential in order to search for signs of NP. Therefore, we will focus on the $B^0_d \to \pi^0 K_s$ channel, which is the only $B \to \pi K$ mode that exhibits mixing-induced CP violation. Before examining this channel in more detail and dive into the analysis of the CP-violating asymmetries, let us briefly present here important aspects of the other key observables, which are given by the branching ratios of the $B \to \pi K$ decays.

Branching Ratios

Regarding the branching fractions, we can determine ratios between the different $B \to \pi K$ channels, following Refs. [200, 292, 295]:

$$R \equiv \left[\frac{\mathcal{B}(B^0_d \to \pi^- K^+)}{\mathcal{B}(B^+ \to \pi^+ K^0)}\right] \frac{\tau_{B^+}}{\tau_{B^0_d}}, \tag{7.61}$$

$$R_{\rm c} \equiv 2\left[\frac{\mathcal{B}(B^+ \to \pi^0 K^+)}{\mathcal{B}(B^+ \to \pi^+ K^0)}\right], \tag{7.62}$$

$$R_{\rm n} \equiv \frac{1}{2}\left[\frac{\mathcal{B}(B^0_d \to \pi^- K^+}{\mathcal{B}(B^0_d \to \pi^0 K^0)}\right] \ . \tag{7.63}$$

With the values of the corresponding branching ratios in Table 13, we can determine the experimental values of these ratio [281]:

$$R = 0.89 \pm 0.04, \qquad R_{\rm c} = 1.09 \pm 0.06, \qquad R_{\rm n} = 0.99 \pm 0.06 \ . \tag{7.64}$$

With the help of the hadronic parameters, we can rewrite the above ratios [281]. The ratio R involves only colour-suppressed EW penguins, described by

$$\tilde{a}_C \equiv a_C \cos(\delta_{\rm c} + \Delta_C). \tag{7.65}$$

Expanding in terms of the small r and $r_{\rm c}$ and the tiny $\rho_{\rm c}$ parameters, we obtain

$$R = 1 - 2\, r \cos\delta \cos\gamma + 2\, r_{\rm c}\, \tilde{a}_{\rm C}\, q \cos\phi - 2\rho_{\rm c} \cos\theta_{\rm c} \cos\gamma + \mathcal{O}(r^2_{\rm (c)}, \rho^2_c) \ . \tag{7.66}$$

On the other hand, the ratios $R_{\rm c}$ and $R_{\rm n}$ depend on the EW penguin parameters q and ϕ. Expanding again in terms of the small r and $r_{\rm c}$ of the order of $\mathcal{O}(0.1)$, we obtain

$$R_{\rm c} = 1 - 2\, r_{\rm c} \cos\delta_{\rm c}(\cos\gamma - q\cos\phi) + \mathcal{O}(r_{\rm c}^2) \ , \tag{7.67}$$

$$R_{\rm n} = 1 - 2 r_{\rm c} \cos\delta_{\rm c}(\cos\gamma - q\cos\phi) + \mathcal{O}(r_{\rm (c)}^2) \ . \tag{7.68}$$

With the help of the numerics in Eq. (7.64), we get the following interesting relation [281]:

$$R_{\rm c} - R_{\rm n} = 0 + \mathcal{O}(r_{\rm (c)}^2) = 0.10 \pm 0.08, \tag{7.69}$$

which is satisfied by the experimental data at the 1σ level.

Let us now discuss the special case with $\phi = 0^\circ$, including SM, but also allowing for NP contributions through values of q that are not SM-like. Neglecting contributions from colour-suppressed EW penguins, the above ratios are rewritten as follows [186]:

$$R = \frac{1 - 2r\cos\delta\cos\gamma + r^2}{1 + \rho_c^2 + 2\rho_c\cos\gamma\cos\theta_c} \ , \tag{7.70}$$

$$R_{\rm n} = \frac{1}{b}(1 - 2r\cos\delta\cos\gamma + r^2) \ , \tag{7.71}$$

$$R_{\rm c} = 1 + \frac{r_c^2 r_q - 2\rho_c r_c\cos(\delta_c - \theta_c)(1 - q\cos\gamma) - 2(-q + \cos\gamma) r_c\cos\delta_c}{1 + \rho_c^2 + 2\rho_c\cos\gamma\cos\theta_c} \ , \tag{7.72}$$

where we have introduced:

$$\begin{aligned} b \equiv\ & 1 - 2r\cos\delta\cos\gamma + r^2 + 2r_c\cos\delta_c(-q + \cos\gamma) + 2r\cos(\delta - \delta_c) r_c(-1 + q\cos\gamma) \\ & + r_c^2(1 + q^2 - 2q\cos\gamma) \ , \end{aligned} \tag{7.73}$$

$$r_q = 1 - 2q\cos\gamma + q^2. \tag{7.74}$$

The tiny parameter ρ_c is also included, as presented in Ref. [281].

7.4.1 CP Violation in the $B_d^0 \to \pi^0 K_{\rm S}$ Decay

Let us now focus on the $B_d^0 \to \pi^0 K_{\rm S}$ channel, which is a CP-odd eigenstate, and specifically discuss the CP asymmetries, starting again from the expression of the time-dependent CP asymmetry. Recalling Eq. (7.27), we have

$$\begin{aligned} A_{\rm CP}(t) &= \frac{\Gamma(\bar{B}^0(t) \to \pi^0 K_{\rm S}) - \Gamma(B^0(t) \to \pi^0 K_{\rm S})}{\Gamma(\bar{B}^0(t) \to \pi^0 K_{\rm S}) + \Gamma(B^0(t) \to \pi^0 K_{\rm S})} \\ &= A_{\rm CP}^{\pi^0 K_{\rm S}} \cos(\Delta m t) + S_{\rm CP}^{\pi^0 K_{\rm S}} \sin(\Delta m t). \end{aligned} \tag{7.75}$$

The direct CP asymmetry takes the form

$$A_{\rm CP}^{\pi^0 K_{\rm S}} = \frac{|\bar{A}_{00}|^2 - |A_{00}|^2}{|\bar{A}_{00}|^2 + |A_{00}|^2}, \tag{7.76}$$

where we have used the notation

$$A_{00} = A\left(B^0 \to \pi^0 K_{\rm S}\right), \tag{7.77}$$

$$\bar{A}_{00} = A\left(\bar{B}^0 \to \pi^0 \bar{K}_{\rm S}\right). \tag{7.78}$$

The mixing-induced CP asymmetry, arising from interference between B_d^0–$\bar{B}_d^0$ mixing and decay processes of B_d^0 and $\bar{B}_d^0$ mesons into the final state $\pi^0 K_{\rm S}$, is written as:

$$\begin{aligned} S_{\rm CP}^{\pi^0 K_{\rm S}} &= \frac{2|A_{00}\bar{A}_{00}|}{|\bar{A}_{00}|^2 + |A_{00}|^2} \sin(2\beta - 2\phi_{\pi^0 K_{\rm S}}) \\ &= \frac{2|A_{00}\bar{A}_{00}|}{|\bar{A}_{00}|^2 + |A_{00}|^2} \sin(\phi_d - \arg(\bar{\rm A}_{00}{\rm A}_{00}^*)), \end{aligned} \tag{7.79}$$

where 2β denotes the CP-violating B_d^0–$\bar{B}_d^0$ mixing phase ϕ_d. We also introduce the angle between the decay amplitude A_{00} and its CP conjugate $\bar{A}_{00}$:

$$2\phi_{\pi^0 K_{\rm S}} = \arg(\bar{\rm A}_{00}{\rm A}_{00}^*) \equiv \phi_{00}. \tag{7.80}$$

Regarding the angle ϕ_{00}, utilising the parametrizations of the amplitudes, we obtain the following expression for the SM case corresponding to $\phi = 0^\circ$ [281]:

$$\tan\phi_{00}|_{\phi=0^\circ} = 2\left(\frac{Q}{W}\right)\sin\gamma\ , \tag{7.81}$$

where

$$\begin{aligned} Q &= r\cos\delta - r_c\cos\delta_c + qr_c^2 - qrr_c\cos(\delta-\delta_c) \\ &\quad - (r_c^2 - 2rr_c\cos(\delta-\delta_c) + r^2)\cos\gamma\ , \\ W &= 1 - 2(qr_c^2 - r_c\cos\delta_c + r\cos\delta - qrr_c\cos(\delta-\delta_c))\cos\gamma - 2qr_c\cos(\delta_c) \\ &\quad + (r_c^2 - 2rr_c\cos(\delta-\delta_c) + r^2)\cos(2\gamma) + q^2r_c^2\ . \end{aligned} \tag{7.82}$$

Since ϕ_{00} plays a central role in our analysis, our next step is to discuss how we can determine this angle.

7.4.2 Isospin Analysis

As we already introduced in the previous Section, we can measure the angle ϕ_{00} through Eq. (7.79). The calculation of ϕ_{00} requires the determination of the decay amplitudes. For this purpose, we will make use of isospin relations.

Having as a starting point the isospin analysis [285], the $B \to \pi K$ decays involve a weak Hamiltonian which has two terms, the $\Delta I = 0$ and $\Delta I = 1$ components:

$$\mathcal{H}_{\rm eff} = \mathcal{H}_{\Delta I=0} + \mathcal{H}_{\Delta I=1}, \tag{7.83}$$

where the $\Delta I = 0$ piece leads to a final state with $I = 1/2$ whereas the $\Delta I = 1$ term leads to both $I = 1/2$ and $I = 3/2$ final states. More specifically, for $B \to \pi K$ decays, the initial B meson states have $I = 1/2$ while the πK final states are decomposed into both $I = 1/2$ and $I = 3/2$ final states.

A key parameter in these studies is the amplitude $A_{3/2}$, which corresponds to isospin $I = 3/2$, and its CP conjugate $\bar{A}_{3/2}$. Applying the isospin relations [272, 293], we may write

$$3A_{3/2} \equiv \sqrt{2}A(B_d^0 \to \pi^0 K^0) + A(B^0 \to \pi^- K^+), \tag{7.84}$$

$$3\bar{A}_{3/2} \equiv \sqrt{2}A(\bar{B}_d^0 \to \pi^0 \bar{K}^0) + A(\bar{B}^0 \to \pi^+ K^-), \tag{7.85}$$

where

$$3A_{3/2} \equiv 3|A_{3/2}|e^{i\phi_{3/2}} \tag{7.86}$$

$$= -(\hat{T}' + \hat{C}')e^{i\gamma} + \left(\hat{P}'_{EW} + \hat{P}'^{\rm C}_{EW}\right) \tag{7.87}$$

$$= -\left[\hat{T}' + \hat{C}'\right](e^{i\gamma} - qe^{+i\phi}). \tag{7.88}$$

Here, we have made use of Eq. (7.55) and note that the term $|\hat{T}'+\hat{C}'|$ normalizes Eq. (7.135). This quantity can be expressed with the help of the $B^+ \to \pi^+\pi^0$ channel utilising the $SU(3)$ symmetry. Assuming vanishing strong phase (as a convention), we obtain

$$\hat{T}' + \hat{C}' = |\hat{T}' + \hat{C}'|e^{i\gamma}. \tag{7.89}$$

The amplitude $|\hat{T}' + \hat{C}'|$ can be determined with the help of the $SU(3)$ flavour symmetry as follows [296]:

$$|\hat{T}' + \hat{C}'| = R_{T+C}\left|\frac{V_{us}}{V_{ud}}\right|\sqrt{2}|A(B^+ \to \pi^+\pi^0)| \ . \tag{7.90}$$

where $R_{T+C} = |\mathcal{T}' + \mathcal{C}'|/|\mathcal{T} + \mathcal{C}|$ parametrizes $SU(3)$-breaking effects. The calligraphic $|\mathcal{T} + \mathcal{C}|$ amplitude is determined via the $B^+ \to \pi^+\pi^0$ decay while the $|\mathcal{T}' + \mathcal{C}'|$ aplitude

corresponds to its $B \to \pi K$ counterpart. The numerical value of R_{T+C} (which was used in the analysis in Ref. [281]) is

$$R_{T+C} = 1.2 \pm 0.2 \ . \tag{7.91}$$

Therefore, the amplitude of $3A_{3/2}$ can be determined for a given $qe^{i\phi}$.

Similarly, the amplitude $3\bar{A}_{3/2}$ can be written as

$$3\bar{A}_{3/2} \equiv 3|\bar{A}_{3/2}|e^{i\bar{\phi}_{3/2}} \tag{7.92}$$

$$= -\left[\hat{T}' + \hat{C}'\right](e^{-i\gamma} - qe^{-i\phi}) \ , \tag{7.93}$$

where we observe the relation $\bar{\phi}_{3/2} = -\phi_{3/2}$. We note again that $\omega = 0^\circ$ while the EW penguin parameters take the SM values[60] $q = 0.66$ and $\phi = 0^\circ$. Thus, the value of $3\bar{A}_{3/2}$ can also be determined. Finally, we obtain the following numerical values:

$$3A_{3/2} \equiv A_{3/2} = (0.3 - 0.8i) \cdot 10^{-3}, \tag{7.94}$$

$$3\bar{A}_{3/2} \equiv \bar{A}_{3/2} = (0.3 + 0.8i) \cdot 10^{-3}, \tag{7.95}$$

which, as we have already discussed, represent sides of the isospin triangles in the complex plane. At this point, we are only interested in the central values, as we will use them for illustrating the corresponding triangles. In the coming Sections, we will discuss in detail how we construct the isospin triangles in the complex plane. For this purpose, we will utilise these values and apply the isospin relations in Eqs. (7.84)-(7.85).

7.4.3 Isospin Triangles in the Complex Plane - Neutral B Decays

Before we continue our analysis, we adopt a notation for the amplitudes that is analogous to the one in Eqs. (7.77)-(7.78) in order to simplify the expressions and write

$$A_{-+} = A\left(B^0 \to \pi^- K^+\right), \qquad \bar{A}_{-+} = A\left(\bar{B}^0 \to \pi^+ K^-\right), \tag{7.96}$$

$$A_{+0} = A\left(B^+ \to \pi^+ K^0,\right) \qquad \bar{A}_{+0} = A\left(B^- \to \pi^- \bar{K}^0\right), \tag{7.97}$$

$$A_{0+} = A\left(B^+ \to \pi^0 K^+\right), \qquad \bar{A}_{0+} = A\left(B^- \to \pi^0 K^-\right). \tag{7.98}$$

An analogous notation can be applied for the branching ratios of the corresponding decay channels.

[60] We note that in order to be consistent with our published analysis, for the rest of the Chapter, we will use the numerics as given in Ref. [281].

Decay Channel	$A_{\rm CP}$	$S_{\rm CP}$
$\bar{B}^0_d \to \pi^+ K^-$	-0.082 ± 0.006	–
$\bar{B}^0_d \to \pi^0 \bar{K}^0$	0.00 ± 0.13	0.58 ± 0.17
$B^+ \to \pi^+ K_S$	-0.017 ± 0.016	–
$B^+ \to \pi^0 K^+$	0.037 ± 0.021	–

Table 14: Direct and mixing induced CP asymmetries for the $B \to \pi K$ system as presented in Ref. [281].

We firstly study the case of the decays of the neutral B mesons. We have to determine the quantities $|A_{00}|$, $|\bar{A}_{00}|$ as well as $|A_{-+}|$ and $|\bar{A}_{-+}|$. For this purpose, we make use of the direct CP asymmetries (as already given in Eq. (7.76))

$$A_{\rm CP}^{\pi^0 K_{\rm S}} = \frac{|\bar{A}_{00}|^2 - |A_{00}|^2}{|\bar{A}_{00}|^2 + |A_{00}|^2}, \qquad A_{\rm CP}^{\pi^- K^+} = \frac{|\bar{A}_{-+}|^2 - |A_{-+}|^2}{|\bar{A}_{-+}|^2 + |A_{-+}|^2}, \tag{7.99}$$

and the branching ratios, which can be expressed as linear combinations of the amplitudes as follows:

$$\mathcal{B}_{00} = \frac{1}{2}\left[|\bar{A}_{00}|^2 + |A_{00}|^2\right], \qquad \mathcal{B}_{-+} = \frac{1}{2}\left[|\bar{A}_{-+}|^2 + |A_{-+}|^2\right]. \tag{7.100}$$

Solving the above system, we are able to determine the lengths of the decay amplitudes and their CP-conjugates. We obtain:

$$|A_{00}| = \sqrt{\mathcal{B}_{00}(1 - A_{\rm CP}^{\pi^0 K_{\rm S}})}, \tag{7.101}$$

$$|A_{-+}| = \sqrt{\mathcal{B}_{-+}(1 - A_{\rm CP}^{\pi^- K^+})}, \tag{7.102}$$

$$|\bar{A}_{00}| = \sqrt{\mathcal{B}_{00}(1 + A_{\rm CP}^{\pi^0 K_{\rm S}})}, \tag{7.103}$$

$$|\bar{A}_{-+}| = \sqrt{\mathcal{B}_{-+}(1 + A_{\rm CP}^{\pi^- K^+})}. \tag{7.104}$$

The current values of the branching ratios in the $B \to \pi K$ channels are presented in Table 13 while the measurements of the CP asymmetries are given in Table 14.

Having all the necessary formulae and numerical values, we are now ready to draw isospin triangles in the complex plane. Visualising things via triangles will help us to determine the angles ϕ_{00} and eventually, resolve any ambiguities and obtain the final "correct" ϕ_{00} value. Let us explain the methodology below.

We keep $A_{\rm CP}^{\pi^0 K_{\rm S}}$ as a free parameter and substitute the values of the other asymmetries and branching ratios. This allows us to calculate $|A_{00}|$ and $|\bar{A}_{00}|$ by utilising the $3A_{3/2}$ and $3\bar{A}_{3/2}$ values determined in Sec 7.4.1. We can then construct the following systems in the complex x–y plane:

$$x^2 + y^2 = 2|A_{00}|^2, \qquad (x - \Re[A_{3/2}])^2 + (y + \Im[A_{3/2}])^2 = |A_{-+}|^2, \tag{7.105}$$

$$x^2 + y^2 = 2|\bar{A}_{00}|^2, \qquad (x - \Re[\bar{A}_{3/2}])^2 + (y - \Im[\bar{A}_{3/2}])^2 = |\bar{A}_{-+}|^2. \tag{7.106}$$

We get 4 possible combinations between A_{00} and $\bar{A}_{00}$, hence 4 angles between the two different solutions.

We can now illustrate the decay amplitudes and angles in the complex plane. The above systems represent circles, as shown in Appendix F.1. We fistly discuss the system in Eq. (7.105). Starting with $3A_{3/2}$, we draw a line that starts at $(0, 0)$ and ends at $(0.3, -0.8)$, as calculated in Sec 7.4.2. With the middlepoint $(0, 0)$, we draw a circle with radius $\sqrt{2}|A_{00}|$. A second circle is drawn, where the middlepoint is $(0.3, -0.8)$ and the radius is $|\bar{A}_{-+}|$. The two circles intersect in two points, which fix the A_{00}. This system of the two intersecting circles and the corresponding triangles is illustrated in the left panel of Fig 46. The blue lines denote the A_{00} (pointing towards the intersecting points), the orange one is the amplitude $A_{3/2}$ and the yellow lines, completing the triangles, denote the A_{-+} side. Similarly, we obtain the picture for the CP-conjugate case, which is described in Eq. (7.106). The corresponding circles and triangles are shown in the right panel of Fig. 46, where the red lines denote the $\bar{A}_{00}$ while the green ones show the $\bar{A}_{-+}$ sides. We show all isospin triangles which relate the A_{00} and A_{-+} to the $A_{3/2}$ amplitude as well as those that relate the $\bar{A}_{00}$ and $\bar{A}_{-+}$ to the $\bar{A}_{3/2}$ in Fig. 47, using the same colours as in Fig. 46.

In this way, we eventually determine ϕ_{00}, which is the angle between A_{00} and $\bar{A}_{00}$. Having shown all the amplitude triangles, we provide specifically an illustration of the angle ϕ_{00} in Fig. 48. The two A_{00} and $\bar{A}_{00}$ sides and the corresponding angle are denoted in red. The dashed lines represent the CP-conjugate case. As we have already mentioned, there are four (combinations) orientations of the A_{00} and $\bar{A}_{00}$ amplitudes, therefore four angles ϕ_{00}. We discuss how we utilise this angle in more detail in the following Section.

7.4.4 Correlations Between Mixing Induced and Direct CP Asymmetries

Let us now see how we obtain the mixing-induced CP asymmetry as a function of the direct CP asymmetry $A_{\rm CP}^{\pi^0 K_{\rm S}}$. The generalised expression for the mixing-induced CP violation, which we have already introduced in Eq. (7.79), is written as [212, 293]:

$$S_{\rm CP}^{\pi^0 K_{\rm S}} = \sqrt{1 - (A_{\rm CP}^{\pi^0 K_{\rm S}})^2}\, \sin(\phi_d - \phi_{00}). \tag{7.107}$$

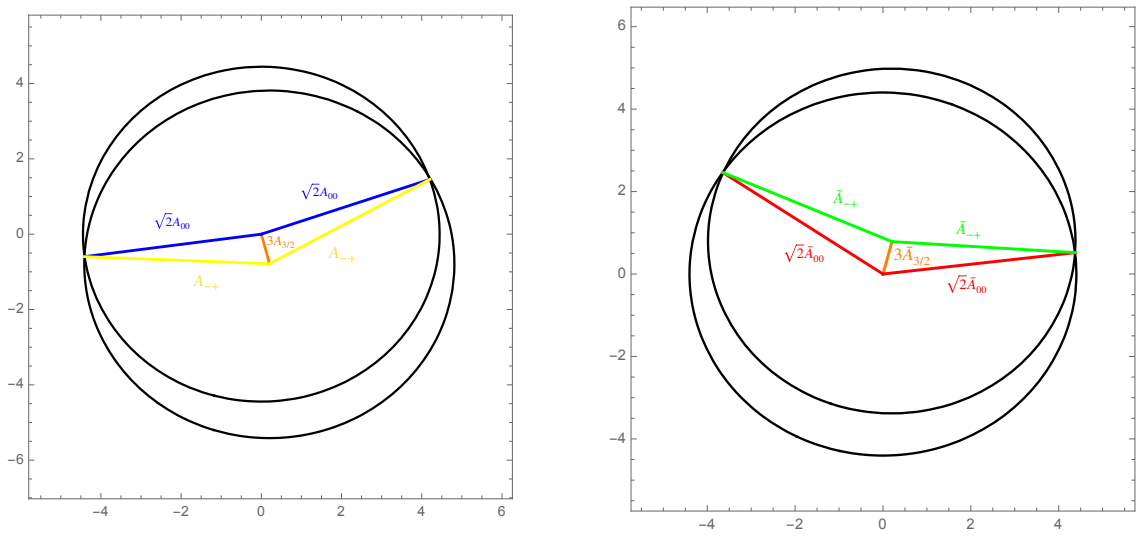

Figure 46: System of the two intersecting circles and the corresponding triangles. The two solutions for A_{00} are given in the left panel while the two $\bar{A}_{00}$ solutions for the CP-conjugate case are shown in the right panel.

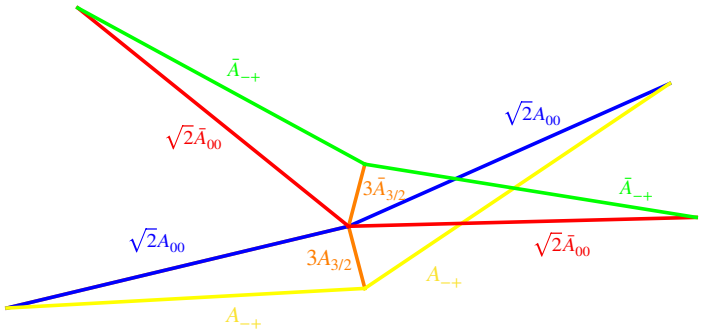

Figure 47: Triangles that relate the A_{00} and A_{-+} to the fixed $A_{3/2}$ amplitude as well as the triangles for the CP conjugate case.

This relation, which correlates the two CP asymmetries, plays a central role in our analysis. The direct CP asymmetry can be measured. The value of the angle ϕ_{00} has already been determined as we discussed in the previous Section. As a result, we are able to make a prediction of the mixing-induced CP asymmetry through Eq. (7.107).

Employing ϕ_{00}, we obtain a four-fold ambiguity for this angle since the triangles can be flipped around the $A_{3/2}$ and $\bar{A}_{3/2}$ axes. The four orientations of the triangles, that we collectively show in Fig. 47, can be illustrated separately in Fig. 49. The solid triangles refer to the $B_d^0 \to \pi^0 K_S^0$ case whereas the dashed one corresponds to its CP conjugate case.

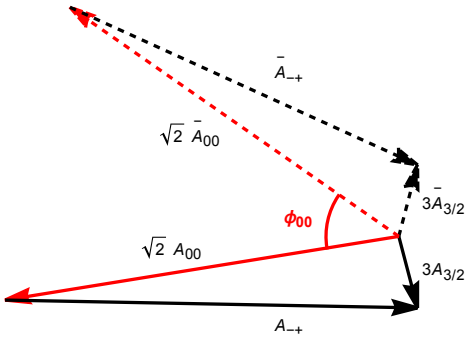

Figure 48: Illustration of the angle ϕ_{00}.

The four angles, hence orientations, are denoted by different colours: (a) green, (b) blue, (c) grey and (d) orange. Starting from Fig. 49(a), we firstly flip the dashed triangle around $\bar{A}_{3/2}$ and we arrive at the second orientation in Fig. 49(b). Then, flipping the solid triangle around the $A_{3/2}$ axis, we obtain Fig. 49(c). Finally, we flip the dashed triangle around $\bar{A}_{3/2}$ and get the last orientation in Fig. 49(d).

Varying the values of $A_{\rm CP}^{\pi^0 K_{\rm S}}$ in Eq. (7.107), using the mixing phase ϕ_d as input and with ϕ_{00} at hand, we calculate the correlation between the direct and the mixing induced CP asymmetry of the $B_d^0 \to \pi^0 K_{\rm S}^0$ decay [186, 293]. The four possibilities for the angle ϕ_{00} lead to four branches for $S_{\rm CP}^{\pi^0 K_{\rm S}}$ in the $S_{\rm CP}^{\pi^0 K_{\rm S}} - A_{\rm CP}^{\pi^0 K_{\rm S}}$ plane. The corresponding plots for the central values are presented in Fig. 50, where the colours of the branches are labelled with the same colour as the four ϕ_{00} angles in Fig. 49. For completeness, these four contours for the central values are also shown in Appendix F.2.

We finally illustrate the correlations between $S_{\rm CP}^{\pi^0 K_{\rm S}}$ and $A_{\rm CP}^{\pi^0 K_{\rm S}}$, taking the experimental errors and uncertainties of the parameters R_{T+C} and R_q into account. Fig. 51 provides the full picture. The colours of the branches still correspond to the colours of the ϕ_{00} angles and matches the description in Fig. 50. We also present the current experimental measurements for the direct and the mixing-induced CP asymmetries with the associated uncertainties (black), which are given in Table 14. Moreover, the red vertical band shows the prediction coming from the sum rule [281], which we will discuss in the next pages.

We note that additional narrow bands are illustrated in Fig. 51 that correspond to future scenarios. More specifically, we consider the following benchmark case [293]:

$$R_{T+C} = 1.22 \pm 0.02, \tag{7.108}$$

$$R_q = 1.00 \pm 0.05. \tag{7.109}$$

In this case, only the expected theory uncertainties are taken into account, based on ex-

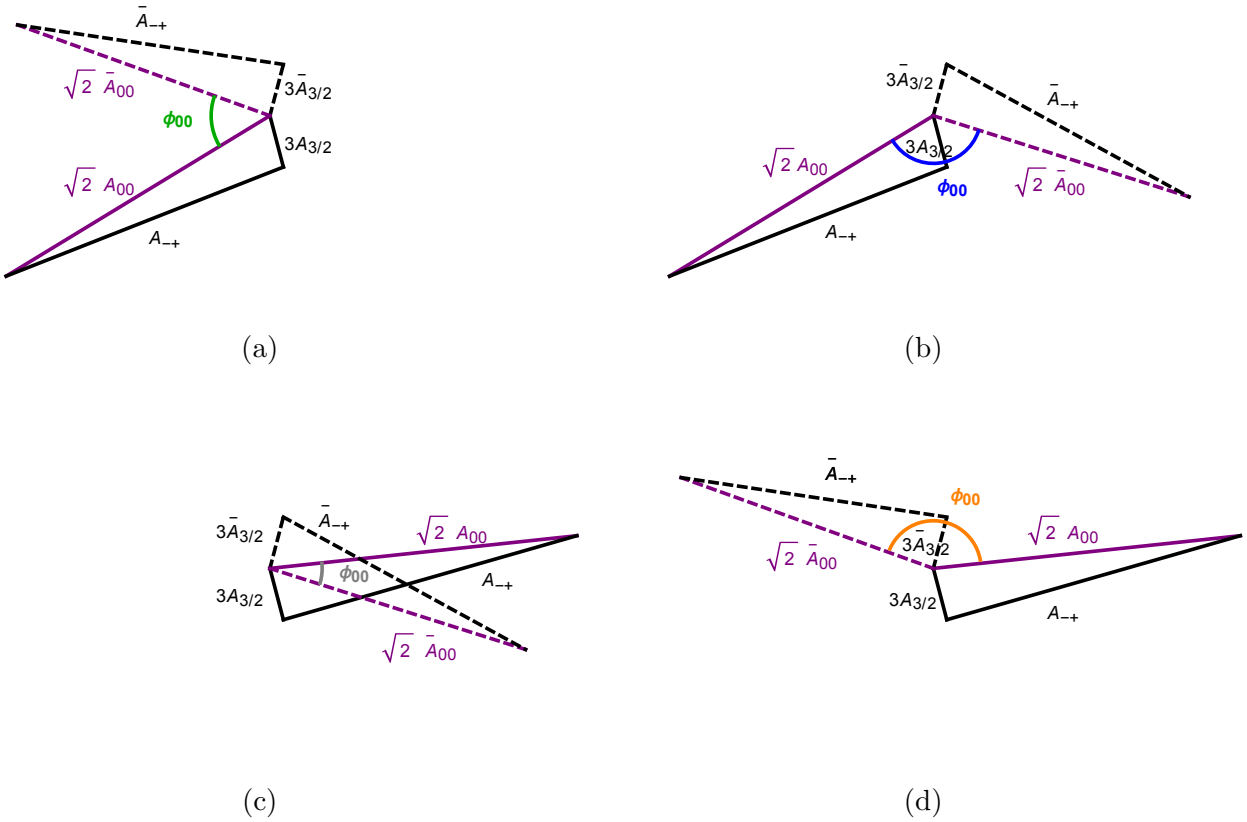

Figure 49: The four ϕ_{00} solutions, as discussed in the text. The A_{00} and $\bar{A}_{00}$ are denoted by purple, the dashed lines represent the CP conjugate cases and the four angles are denoted by (a) green, (b) blue, (c) grey and (d) orange.

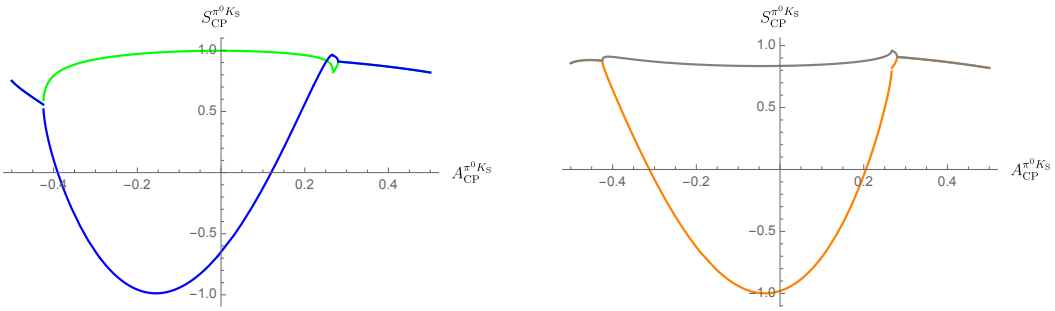

Figure 50: Plots of the mixing-induced CP asymmetry in terms of the direct CP asymmetry (central values). The four branches correspond to the four angles ϕ_{00} shown in Fig. 49.

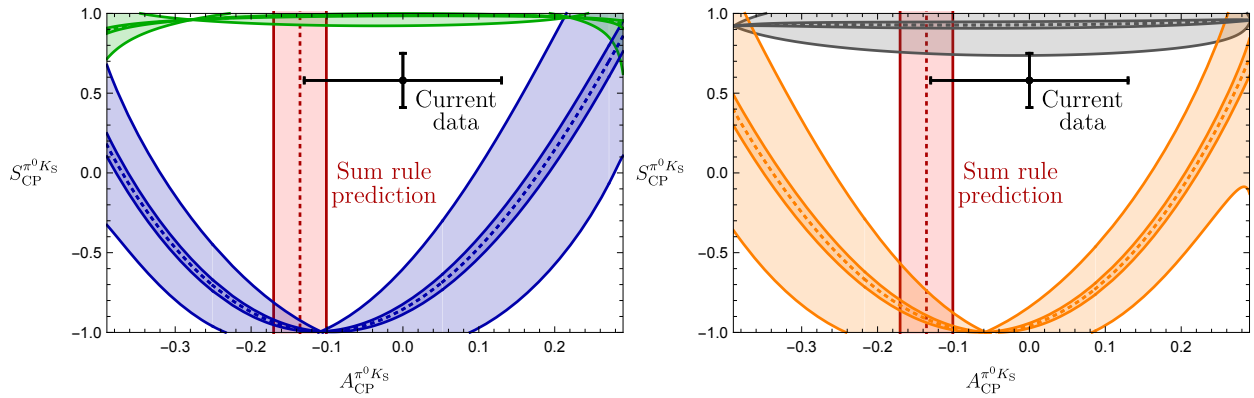

(a) (b)

Figure 51: Correlations between $S_{\rm CP}^{\pi^0 K_S}$ and $A_{\rm CP}^{\pi^0 K_S}$ taking the uncertainties into account. The current data for the CP asymmetries (black cross) and the sum rule prediction (red band) are also shown. The narrow bands correspond to a future scenario.

pected future progress in lattice calculations.

Sum Rules

An interesting test of the SM is given by the sum rule, which is defined with the help of the branching ratios as follows [297, 298]:

$$\Delta_{\rm SR}^{(\rm I)} = A_{\rm CP}^{\pi^\pm K^\mp} + A_{\rm CP}^{\pi^\pm K^0} \frac{\mathcal{B}(B^+ \to \pi^+ K^0)}{\mathcal{B}(B_d^0 \to \pi^- K^+)} \frac{\tau_{B^0}}{\tau_{B^+}} - A_{\rm CP}^{\pi^0 K^\pm} \frac{2\mathcal{B}(B^+ \to \pi^0 K^+)}{\mathcal{B}(B_d^0 \to \pi^- K^+)} \frac{\tau_{B^0}}{\tau_{B^+}}$$
$$- A_{\rm CP}^{\pi^0 K^0} \frac{2\mathcal{B}(B_d^0 \to \pi^0 K^0)}{\mathcal{B}(B_d^0 \to \pi^- K^+)} = 0 + \mathcal{O}(r_{(\rm c)}^2, \rho_{\rm c}^2) \ . \tag{7.110}$$

Utilising the current measurements of branching ratios and CP asymmetries, as presented in Tables 13 and 14, we obtain the experimental value [281]:

$$\Delta_{\rm SR}^{(\rm I)}|_{\rm exp} = -0.15 \pm 0.14. \tag{7.111}$$

We are also interested in calculating the SM prediction for the sum rule. For this purpose, we discuss further the direct asymmetries, rewriting them also in terms of the hadronic parameters. We obtain the following expression [281]:

$$A_{\rm CP}^{\pi^- K^+} \equiv \mathcal{A}_{\rm CP}^{\rm dir}(B_d^0 \to \pi^- K^+) = \frac{4}{3} r_c \, \tilde{a}_S q \sin\phi - 2r \sin\delta \sin\gamma + \mathcal{O}(r_{(\rm c)}^2), \tag{7.112}$$

where the colour-suppressed EW penguin contribution $\tilde{a}_S$ is defined as:

$$\tilde{a}_S \equiv a_C \sin(\delta_c + \Delta_C) \ . \tag{7.113}$$

We note that for small phases δ_c and Δ_C, the parameter $\tilde{a}_S$ is strongly suppressed. Combining Eqs. (7.112) and (8.33), and using the values of the hadronic parameters, we can determine $\tilde{a}_S$ and $\tilde{a}_C$ through:

$$\tilde{a}_S \; q \sin\phi = \frac{3(A_{\rm CP}^{\pi^- K^+} + 2r \sin\delta \sin\gamma)}{4r_c} \; , \tag{7.114}$$

$$\tilde{a}_C \; q \cos\phi = \frac{R - 1 + 2r\cos\delta\cos\gamma + 2\rho_c \cos\theta_c \cos\gamma}{2r_c} \; . \tag{7.115}$$

Similarly, we express the other direct CP asymmetries [281], yielding:

$$\begin{aligned} A_{\rm CP}^{\pi^+ K^0} &\equiv A_{\rm CP}^{\rm dir}(B^+ \to \pi^+ K^0) = 2\rho_{\rm c} \sin\theta_{\rm c} \sin\gamma - \frac{2}{3}\tilde{a}_S q r_{\rm c} \sin\phi + \mathcal{O}(r_{\rm c}^2, \rho_{\rm c}^2) \; , \\ A_{\rm CP}^{\pi^0 K^+} &\equiv A_{\rm CP}^{\rm dir}(B^+ \to \pi^0 K^+) = 2\rho_{\rm c} \sin\theta_{\rm c} \sin\gamma - 2r_{\rm c} \sin\delta_{\rm c}[\sin\gamma - q\sin\phi] \\ &\qquad - \frac{2}{3}\tilde{a}_S q r_{\rm c} \sin\phi + \mathcal{O}(r_{\rm c}^2, \rho_{\rm c}^2) \; , \end{aligned}$$

$$\begin{aligned} A_{\rm CP}^{\pi^0 K^0} \equiv A_{\rm CP}^{\rm dir}(B_d^0 \to \pi^0 K^0) &= 2r_{\rm c} \sin\delta_{\rm c}[\sin\gamma - q\sin\phi] + \frac{4}{3}\tilde{a}_S q r_{\rm c} \sin\phi \\ &\quad - 2r\sin\delta\sin\gamma + \mathcal{O}(r_{\rm (c)}^2) \; , \end{aligned} \tag{7.116}$$

where we have expanded again in terms of the the small $r_{\rm c}$ and the tiny $\rho_{\rm c}$.

We return now to the calculation of the SM prediction of the sum rule. The sub-leading terms lead to the following expression [281]:

$$\Delta_{\rm SR}^{\rm (I)} = 2qr_{\rm c} \left[\frac{r\sin(\delta_{\rm c} - \delta) + \rho_{\rm c}\sin(\delta_{\rm c} - \theta_{\rm c})}{1 - 2r\cos\delta\cos\gamma + r^2} \right] \sin(\gamma - \phi). \tag{7.117}$$

Using the values of the hadronic parameters in Sec. 7.2.2 and the SM values of the EW penguin parameters q and ϕ in Sec. 7.4.2, we find the SM value:

$$\Delta_{\rm SR}^{\rm (I)}|_{\rm SM} = -0.009 \pm 0.013. \tag{7.118}$$

Comparing the experimental value in Eq. (7.111) and the SM prediction in Eq. (7.118), we see that the experimental result for the sum rule is consistent with zero as well as the SM value within uncertainties.

Last but not least, since we have presented the direct CP asymmetries in terms of the hadronic parameters, we also discuss the case of vanishing CP violation in the EW penguins,

thus for $\phi = 0°$. In this case, the direct asymmetries can be rewritten as [186, 281]:

$$A_{\rm CP}^{\pi^- K^+} = \frac{-2r \sin\delta \sin\gamma}{1 - 2r\cos\delta\cos\gamma + r^2} \ , \tag{7.119}$$

$$A_{\rm CP}^{\pi^+ K^0} = \frac{2\rho_c \sin\theta_c \sin\gamma}{1 + 2\rho_c\cos\theta_c\cos\gamma + \rho_c^2} \ , \tag{7.120}$$

$$A_{\rm CP}^{\pi^0 K^+} = -\frac{2r_c \sin\delta_c \sin\gamma - 2\rho_c \sin\theta_c \sin\gamma + 2q\rho_c r_c \sin(\delta_c - \theta_c)}{R_c(1 + \rho_c^2 + 2\rho_c\cos\gamma\cos\theta_c)} \ , \tag{7.121}$$

$$A_{\rm CP}^{\pi^0 K^0} = A_{\rm CP}^{\pi^0 K_{\rm S}} = \frac{2\sin\gamma}{b}\Big[- r\sin\delta + r_c(qr\sin(\delta - \delta_c) + \sin\delta_c)\Big], \tag{7.122}$$

where we have included the tiny ρ_c parameter as in [281].

7.4.5 Obtaining the Final Single Solution

The different orientations of the isospin triangles have left us with a four-fold ambiguity. Our goal now is to resolve these ambiguities and determine the correct contour in the $A_{\rm CP}^{\pi^0 K_{\rm S}}$–$S_{\rm CP}^{\pi^0 K_{\rm S}}$ plane.

The first parameter we consider is the strong phase δ_c [293]. Let us describe how we work with this parameter. We have already provided the expression of the direct CP asymmetry of the $B^0 \to \pi^- K^+$ channel in Eq. (7.119), rewriting it here as

$$A_{-+} = \frac{-2r\sin\delta\sin\gamma}{r_r}, \tag{7.123}$$

where we simplified it by expressing the denominator in the following form

$$r_r = 1 - 2r\cos\delta\cos\gamma + r^2. \tag{7.124}$$

The value of A_{-+} is known. As a result, we can extract the parameter r in terms of δ. We recall the expression:

$$r_c = \frac{|\hat{T} + \hat{C}|}{\sqrt{\mathcal{B}_{-+}}}\sqrt{r_r}, \tag{7.125}$$

where we employ again the $SU(3)$ flavour symmetry and obtain:

$$r_c = \sqrt{2}\left|\frac{V_{us}}{V_{ud}}\right| R_{T+C}\sqrt{\frac{\mathcal{B}(B^+ \to \pi^0\pi^+)}{\mathcal{B}(B_d^0 \to \pi^- K^+)}\frac{\tau_{B_d^0}}{\tau_{B^+}}}\sqrt{r_r}. \tag{7.126}$$

Therefore, utilising the expressions for r_c, A_{-+}, and b in Eq. (7.73), we determine the quantity $R_n = r_r/b = \text{const}$ in such a way that it depends only on δ and δ_c. The values that correspond to $|\delta_{\rm c}| < 90°$ can be found on the contours in Fig. 51a while those that refer

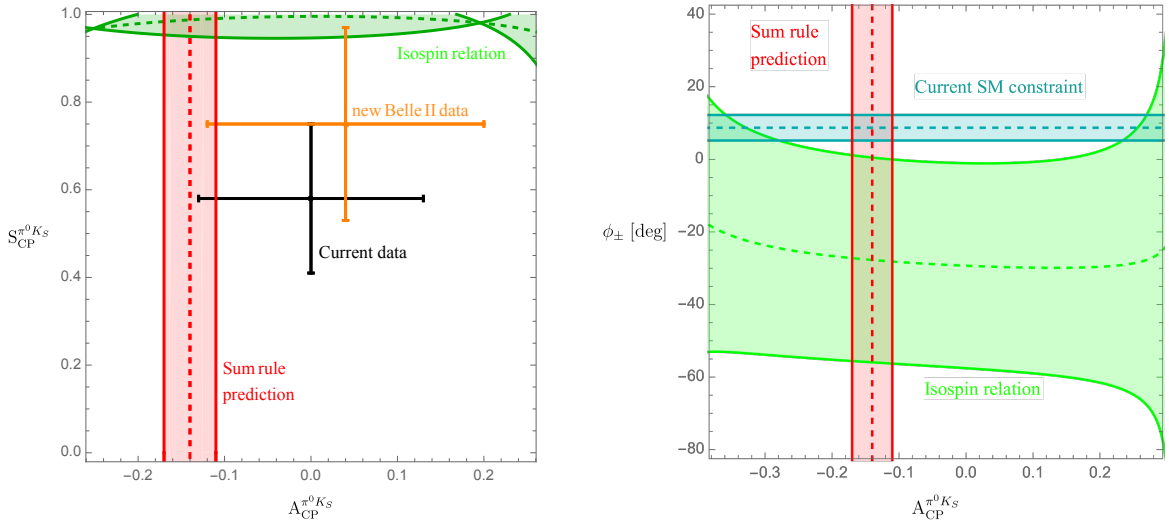

(a) (b)

Figure 52: (a) Resolving the discrete ambiguity and pinning down the correct contour in the $A_{\rm CP}^{\pi^0 K_S}$–$S_{\rm CP}^{\pi^0 K_S}$ plane, coming from the isospin relations [300, 301]. (b) Illustration of $\phi_\pm$ in terms of $A_{\rm CP}^{\pi^0 K_S}$ for the correct triangle configuration. The current SM constraint in Eq. (7.130) is given by the petrol horizontal band.

to $|\delta_c| > 90°$ can be found on the contours in Fig. 51b. The range of δ_c has been calculated in Eq. (7.53). This leads to the conclusion that only the upper (green) contour in Fig. 51a is allowed. This also agrees with the picture associated to the value of r_c, since the lower contour of Fig. 51a leads to large values of r_c, thus allowing again only the upper contour.

The final correct contour is illustrated in Fig. 52a. In addition to the (world-averaged) current data (black cross), we also show a new Belle II measurement for the CP asymmetries [299] denoted as the orange cross. This measurement agrees better with the isospin results within uncertainties. This is an interesting development to explore further, especially once it is included in the current world average.

Another tool that can be used for resolving the ambiguities is the angle $\phi_\pm$ between the amplitudes $A_{-+} \equiv A(B_d^0 \to \pi^- K^+)$ and $\bar{A}_{-+} \equiv A(\bar{B}_d^0 \to \pi^+ K^-)$, defined as [302]:

$$\phi_\pm = \text{Arg}\left[\bar{A}_{-+} A_{-+}^*\right] . \tag{7.127}$$

Every triangle configuration is associated with an angle $\phi_\pm$, allowing us to illustrate contours of $\phi_\pm$ in terms of the direct CP asymmetry (as shown in Appendix F.3). For $\phi = 0°$, we can write [281]:

$$\tan\phi_\pm|_{\phi=0°} = \frac{-r^2 \sin 2\gamma + r\sin(\gamma-\delta) + r\sin(\gamma+\delta) + C_\pm}{1 + r^2\cos 2\gamma - r\cos(\gamma-\delta) - r\cos(\gamma+\delta) + B_\pm} , \tag{7.128}$$

where

$$B_\pm = \frac{4}{3} q r_{\rm c} [\tilde{a}_C - r \cos\gamma (\tilde{a}_C \cos\delta + \tilde{a}_S \sin\delta) + \frac{1}{3} q r_{\rm c} (\tilde{a}_C^2 + \tilde{a}_S^2)],$$
$$C_\pm = \frac{4}{3} q r r_{\rm c} \sin\gamma (\tilde{a}_C \cos\delta + \tilde{a}_S \sin\delta) \ . \tag{7.129}$$

Utilising the hadronic parameters, we can determine the numerical values of $B_\pm$ and $C_\pm$, and as a result the $\tan\phi_\pm|_{\phi=0^\circ}$, thus the value of $\phi_\pm$ in the SM. We find [281]:

$$\phi_\pm = 2r \cos\delta \sin\gamma + \mathcal{O}(r_{(c)}^2) = (8.7 \pm 3.5)^\circ \ . \tag{7.130}$$

This additional constraint is illustrated as the petrol horizontal band in Fig. 52b. As shown in Appendix F.3, following our analysis in [281], the blue and the orange contours from the triangle analysis are excluded by this constraint. Moreover, there is tension with the grey contour, which is already eliminated due to the range of δ_c. Therefore, Fig. 52b shows the angle $\phi_\pm$ in terms of $A_{\rm CP}^{\pi^0 K_{\rm S}}$ for the final triangle configuration (green contour). We observe for this configuration a tension with the SM prediction for $\phi_\pm$ at the 1 σ level.

How to Resolve the $B \to \pi K$ Puzzle?

Let us focus on the current world average of the CP asymmetries (black cross in Fig. 52a). We will not explore the new Belle II measurement further, since it is not included in the world average yet.[61] Since there is a discrepancy between the experimental data and the constraint following from the triangle construction, as shown in Fig. 52a, we are interested in examining how this puzzle can be resolved.

One way is through a change in the data. Prime candidate is the branching ratio (due to the large experimental uncertainty on $B^0 \to \pi^0 K^0$). In Ref. [281], an interesting example has been illustrated where lowering the branching ratio's central value (by 2.5 σ) and at the same time moving the central value of the mixing-induced CP asymmetry up (by 2.5 σ) gives a picture consistent with the SM. Hence, it seems challenging to fulfil all constraints simultaneously in order to achieve agreement with the SM in this case.

On the other hand, this tension might imply effects of NP. As we have already discussed, a very promising avenue for NP to enter is through the EW penguin sector, which is characterised by the q and ϕ parameters. The sensitivity to new sources of CP violation is a key point here.[62]

[61] We note that the new Belle II measurement agrees better with the theoretical solution arising from the triangles. It will be interesting to monitor how the situation will evolve in the future.

[62] We also mention here for completeness that there could be NP scenarios with extra Z' bosons, where we may have links with anomalies in rare B decays.

7.5 New Strategy to Determine q and ϕ

In the first part of this Chapter, after providing the technical details, we focused on the determination of correlations between the mixing-induced and the direct CP asymmetry of the $B^0 \to \pi^0 K_S$ channel. Comparing the corresponding SM predictions for the CP asymmetries coming from Eq. (7.107) and the triangle analysis with the experimental data, tensions arise. More specifically, in the $A_{\rm CP}^{\pi^0 K_{\rm S}}$–$S_{\rm CP}^{\pi^0 K_{\rm S}}$ plane in Fig. 52, we see the deviation between the green contour, reflecting the theory prediction for the CP asymmetries, and the black cross denoting the data. As a result, revisiting this $B \to \pi K$ puzzle and considering the picture we obtained from the current data, there could be NP entering in the EW penguin sector, which is characterised by q and ϕ. The importance of these EW penguin parameters q and ϕ in studying possible NP effects require a careful analysis of their determination.

This brings us to the second part of our analysis. In the following Sections, we present a new method of determining these EW penguin parameters. So far, we have only worked with the neutral $B \to \pi K$ decays. Here, our first step is to utilise the charged $B \to \pi K$ modes, which exhibit only direct CP violation.

7.5.1 Utilising Charged $B \to \pi K$ Decays

Similar to the case of neutral $B \to \pi K$ modes, our starting point are the isospin relations:

$$3A_{3/2} \equiv \sqrt{2}A(B^+ \to \pi^0 K^+) + A(B^+ \to \pi^+ K^0), \tag{7.131}$$

$$3\bar{A}_{3/2} \equiv \sqrt{2}A(B^- \to \pi^0 K^-) + A(B^- \to \pi^- \bar{K}^0), \tag{7.132}$$

which we may write using a simplified notation for the decay amplitudes as follows:

$$3A_{3/2} = \sqrt{2}A_{0+} + A_{+0}, \tag{7.133}$$

$$3\bar{A}_{3/2} = \sqrt{2}\bar{A}_{0+} + \bar{A}_{+0}. \tag{7.134}$$

As we have already discussed, with the help of the direct CP asymmetries and the CP-averaged branching ratios, the isospin relations represent triangles in the complex plane, assuming a given value of $|A_{3/2}| = |\bar{A}_{3/2}|$. In analogy to the case of the neutral $B \to \pi K$ modes, we have:

$$3A_{3/2} \equiv 3|A_{3/2}|e^{i\phi_{3/2}} = -\left[\hat{T}' + \hat{C}'\right](e^{i\gamma} - qe^{+i\phi}), \tag{7.135}$$

$$3\bar{A}_{3/2} \equiv 3|\bar{A}_{3/2}|e^{i\bar{\phi}_{3/2}} = -\left[\hat{T}' + \hat{C}'\right](e^{-i\gamma} - qe^{-i\phi}). \tag{7.136}$$

The term $(e^{i\gamma} - qe^{i\phi})$ can be expressed as follows:

$$\begin{aligned}(e^{i\gamma} - qe^{i\phi}) &= \cos\gamma + i\sin\gamma - q\cos\phi - iq\sin\phi \\ &= (\cos\gamma - q\cos\phi)\left[1 + i\left(\frac{\sin\gamma - q\sin\phi}{\cos\gamma - q\cos\phi}\right)\right]. \end{aligned} \tag{7.137}$$

In a similar way, we can rewrite the term $(e^{-i\gamma} - qe^{-i\phi})$.

To construct the amplitude triangles for the charged $B \to \pi K$ decays, it is useful to draw them in such a way that the amplitudes $|A_{+0}|$ and $|\bar{A}_{+0}|$ coincide. We consider two circles: one with $(0,0)$ as centre and $3|A_{3/2}|$ as a radius and the other one with $(|A_{+0}|, 0)$ as middlepoint and $\sqrt{2}A_{0+}$ as a radius. In the example we study here, we consider the SM values of q and ϕ. For a given value $|A_{3/2}| = |\bar{A}_{3/2}|$, we have the following system of equations:

$$x^2 + y^2 = 3|A_{3/2}|, \qquad (x - |A_{+0}|)^2 + y^2 = 2|A_{0+}|^2, \tag{7.138}$$

$$x^2 + y^2 = 3|A_{3/2}|, \qquad (x - |A_{+0}|)^2 + y^2 = 2|\bar{A}_{0+}|^2, \tag{7.139}$$

where the second system stands for the CP-conjugate case. Eq. (7.138) represents two circles which intersect in two points. These circles are indicated by green colour in Fig. 53a. The points of intersection guide the construction of the triangles, which is indicated by the blue solid lines. The full picture is given in Appendix F.4. Similarly, Eq. (7.139) represents two circles, which are denoted by black. The small black circle is the same as the small green one. There are again two intersection points and the pink dashed lines show the corresponding triangles. In Fig. 53b, we zoom in and show one orientation of the isospin triangles of the charged $B \to \pi K$ decays (where the pink dashed one stands for the CP-conjugate case), where we see which decay amplitude corresponds to every side of the triangle.

Since the triangles can be flipped around the $A_{3/2}$ and $\bar{A}_{3/2}$ axes, we have again a four-fold ambiguity for $\Delta\phi_{3/2}$, which is determined as follows [281]:

$$\Delta\phi_{3/2} \equiv \phi_{3/2} - \bar{\phi}_{3/2}. \tag{7.140}$$

This difference between the phases $\phi_{3/2}$ of the decay amplitude $A_{3/2}$ and $\bar{\phi}_{3/2}$ of the amplitude $\bar{A}_{3/2}$ is given by $\Delta\phi_{3/2} = 2\phi_{3/2}$, due to the relation $\bar{\phi}_{3/2} = -\phi_{3/2}$. We also note that the relative orientation of the triangles, which is the angle between the amplitudes $A_{+0} \equiv A(B^+ \to \pi^+ K^0)$ and $\bar{A}_{+0} \equiv A(B^- \to \pi^- \bar{K}^0)$, is given by

$$\phi_{\rm c} \equiv \mathrm{Arg}\left[\bar{A}_{+0} A^*_{+0}\right] = \mathcal{O}(1^\circ). \tag{7.141}$$

Employing the amplitude parametrization given in Eq. (7.7) and neglecting the colour-suppressed EW penguin contributions, we obtain

$$\tan\phi_{\rm c} = \frac{-\rho_{\rm c}^2 \sin 2\gamma - \rho_{\rm c}\sin(\gamma - \theta_{\rm c}) - \rho_{\rm c}\sin(\gamma + \theta_{\rm c})}{1 + \rho_{\rm c}^2\cos 2\gamma + \rho_{\rm c}\cos(\gamma - \theta_{\rm c}) + \rho_{\rm c}\cos(\gamma + \theta_{\rm c})}\,. \tag{7.142}$$

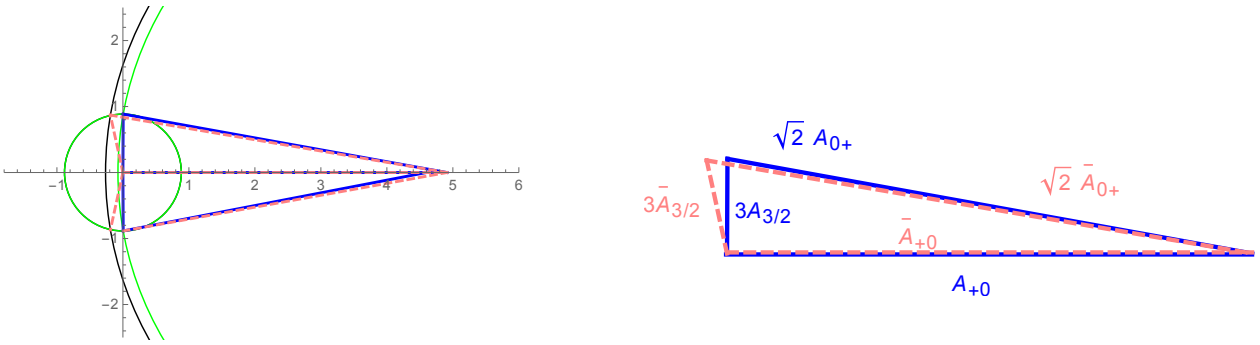

(a) (b)

Figure 53: (a) Constructing the isospin triangles for the charged $B \to \pi K$ decays, applying Eqs. (7.138)-(7.139). (b) Illustration of the isospin triangles for the charged $B^+ \to \pi^0 K^+$ and $B^+ \to \pi^+ K^0$ modes (solid blue), and for the CP-conjugate case (dashed pink).

7.5.2 Extracting the Parameters q and ϕ

Let us now discuss the new strategy we have developed for extracting the EW penguin parameters, as presented in Ref. [281]. Utilising the phase difference $\Delta\phi_{3/2}$ introduced in Eq. (7.140), we firstly work with the amplitudes $A_{3/2}$.

We recall that for the strong phase $\omega = 0°$, we have the condition $|A_{3/2}| = |\bar{A}_{3/2}|$. Using the definitions in Eqs. (7.135)-(7.136), we obtain

$$\frac{\bar{A}_{3/2}}{A_{3/2}} = e^{\bar{\phi}_{3/2}-\phi_{3/2}} = \frac{e^{-i\gamma} - qe^{-i\phi}}{e^{i\gamma} - qe^{i\phi}}. \tag{7.143}$$

Multiplying both the numerator and the denominator with the factor $(e^{-i\gamma} - qe^{-i\phi})$, we get

$$e^{\bar{\phi}_{3/2}-\phi_{3/2}} = \frac{e^{-2i\gamma} - qe^{-i(\phi+\gamma)} - qe^{-i(\phi+\gamma)} + q^2 e^{-2i\phi}}{1 - qe^{i(\phi-\gamma)} - qe^{-i(\phi-\gamma)} + q^2}. \tag{7.144}$$

Let us now introduce

$$\sqrt{N} = 3\left|\frac{A_{3/2}}{\hat{T} + \hat{C}}\right|, \tag{7.145}$$

which again comes from Eq. (7.135). Our next step is to provide the relation between N and q. For this purpose, we make use of the following identities:

$$e^{ix} = \cos(x) + i\sin(x) \tag{7.146}$$

$$\sin(x \pm y) = \sin x \cos y \pm \cos x \sin y \tag{7.147}$$

$$\cos(x \pm y) = \cos x \cos y \mp \sin x \sin y, \tag{7.148}$$

and Eq. (7.135) implies

$$\left[\frac{3\left|A_{3/2}\right|}{\left|\hat{T}+\hat{C}\right|}\right]^2 - \sin^2(\phi-\gamma) = \left[q - \cos(\phi-\gamma)\right]^2. \tag{7.149}$$

Hence, taking the square root of this expression, we solve the equation for q and obtain

$$q = \cos(\phi-\gamma) \pm \sqrt{\left[\frac{3\left|A_{3/2}\right|}{\left|\hat{T}+\hat{C}\right|}\right]^2 - \sin^2(\phi-\gamma)} \tag{7.150}$$

$$= \cos(\phi-\gamma) \pm \sqrt{\frac{3\left|A_{3/2}\right|}{\left(\hat{T}+\hat{C}\right)} + \cos^2(\phi-\gamma) - 1}, \tag{7.151}$$

where the trigonometric identity $\sin^2(x) + \cos^2(x) = 1$ has been used.

Combining the two expressions

$$\sqrt{N}e^{i\frac{(\bar{\phi}_{3/2}-\phi_{3/2})}{2}} = \sqrt{N}\left[\cos\left(\frac{\bar{\phi}_{3/2}-\phi_{3/2}}{2}\right) + i\sin\left(\frac{\bar{\phi}_{3/2}-\phi_{3/2}}{2}\right)\right] \tag{7.152}$$

and

$$e^{-i\gamma} - qe^{-i\phi} = \cos\gamma - q\cos\phi - i\left(\sin\gamma - q\sin\phi\right), \tag{7.153}$$

we are able to determine both $\cos\left((\bar{\phi}_{3/2}-\phi_{3/2})/2\right)$ and $\sin\left((\bar{\phi}_{3/2}-\phi_{3/2})/2\right)$, yielding

$$\tan\left(\frac{\bar{\phi}_{3/2}-\phi_{3/2}}{2}\right) = \frac{\sin\gamma - q\sin\phi}{\cos\gamma - q\cos\phi}. \tag{7.154}$$

Then we introduce the useful notation [281]:

$$c = \pm\sqrt{N}\cos\left(\frac{\phi_{3/2}-\bar{\phi}_{3/2}}{2}\right) = \cos\gamma - q\cos\phi, \tag{7.155}$$

$$s = \pm\sqrt{N}\sin\left(\frac{\phi_{3/2}-\bar{\phi}_{3/2}}{2}\right) = \sin\gamma - q\sin\phi. \tag{7.156}$$

These expressions get the form:

$$c = \pm\sqrt{N}\cos\left(\frac{\Delta\phi_{3/2}}{2}\right), \tag{7.157}$$

$$s = \pm\sqrt{N}\sin\left(\frac{\Delta\phi_{3/2}}{2}\right). \tag{7.158}$$

Finally, for obtaining the relation between N and q, we write

$$N = 1 - 2q\cos(\gamma - \phi) + q^2 \tag{7.159}$$

$$= 1 - 2q\cos\phi\cos\gamma - 2q\sin\phi\sin\gamma + q^2 \tag{7.160}$$

$$= 1 - 2\cos(\gamma - c)\cos\gamma - 2(\sin\gamma - s)\sin\gamma + q^2, \tag{7.161}$$

where we implemented the expressions of c and s in the latter expression. Consequently,

$$q^2 = N + 1 - 2c\cos\gamma - 2s\sin\gamma, \tag{7.162}$$

$$q = \pm\sqrt{N + 1 - 2c\cos\gamma - 2s\sin\gamma}. \tag{7.163}$$

So far, we have determined the parameter q. The final step is to also provide a relation between the phase ϕ and N. As a result, recalling Eqs. (7.155) and (7.156), we obtain

$$q\cos\phi = \cos\gamma - c, \tag{7.164}$$

$$q\sin\phi = \sin\gamma - s, \tag{7.165}$$

yielding

$$\tan\phi = \frac{\sin\phi}{\cos\phi} = \frac{\sin\gamma - s}{\cos\gamma - c}. \tag{7.166}$$

Consequently, both the EW penguin parameters q and ϕ can be determined. We collect the important relations of our strategy in Fig. 54.

$$\Delta\phi_{3/2} = \phi_{3/2} - \bar{\phi}_{3/2}, \qquad \sqrt{N} = 3\left|\frac{A_{3/2}}{\hat{T} + \hat{C}}\right|$$

$$c = \pm\sqrt{N}\cos\left(\frac{\Delta\phi_{3/2}}{2}\right), \qquad s = \pm\sqrt{N}\sin\left(\frac{\Delta\phi_{3/2}}{2}\right)$$

$$q = \pm\sqrt{N + 1 - 2c\cos\gamma - 2s\sin\gamma}$$

$$\tan\phi = \frac{\sin\gamma - s}{\cos\gamma - c}$$

Figure 54: Important relations for determining the EW penguin parameters q and ϕ.

7.5.3 Constraints on ϕ–q Plane Utilising Charged $B \to \pi K$ Decays

As we have already mentioned, concerning the charged $B \to \pi K$ system, there is a four-fold ambiguity for the $\Delta\phi_{3/2}$. For every value of $\Delta\phi_{3/2}$, we solve a quadratic equation which leads to two contours in the $q - \phi$ plane, thus eight contours in total.

Similarly to the neutral case, we can eliminate contours by considering

$$\phi_{0+} = \text{Arg}\left[\bar{A}_{0+} A^*_{0+}\right] \ , \tag{7.167}$$

which is the angle between the $A_{0+} \equiv A(B^+ \to \pi^0 K^+)$ and $\bar{A}_{0+} \equiv A(B^- \to \pi^0 K^-)$ decay amplitudes. This angle can be obtained from the triangle construction and depends on ϕ. In addition, we consider the theoretical prediction, as presented in Ref. [281]:

$$\tan\phi_{0+} = 2r_{\rm c}\left[\cos\delta_{\rm c}\sin\gamma - \left(\cos\delta_{\rm c} - \frac{1}{3}\tilde{a}_C\right) q\sin\phi\right] + \mathcal{O}(r^2_{\rm (c)}, \rho_c) \ , \tag{7.168}$$

with the colour-suppressed EW penguin parameter $\tilde{a}_C$ which has already been introduced in Sec 7.4. The theoretical value depends on both q and ϕ.

Fig. 55 illustrates the contours coming from the triangle analysis in the $q - \phi$ plane. The contours are denoted by purple, green, grey and orange. In addition to the angle ϕ_{0+}, we impose another constraint, which is related to the parameter R_c and leads to the cyan dotted line. We observe that the contours coming from the triangle analysis show discontinuities around the values of $q \sim 1$ and $\phi \sim 70°$. This is due to the fact that $|A_{3/2}|$ cannot become arbitrarily small and as a result, the corresponding decay amplitudes cannot form triangles anymore.

Let us now discuss in more detail the constraint coming from the R_c, thus the ratio of the CP-averaged branching fractions of the charged $B \to \pi K$ decays defined in Eq. (7.67). Utilising the strong phase $\delta_{\rm c}$ and the parameters $r_{\rm c}$ and $\rho_{\rm c}$ and setting [281]:

$$A_{R_{\rm c}} \equiv r^2_{\rm c} \ , \tag{7.169}$$

$$B_{R_{\rm c}} \equiv 2r_{\rm c}\left[\cos\delta_{\rm c}\cos\phi - (r_{\rm c} - \rho_{\rm c}\cos(\theta_{\rm c} - \delta_{\rm c}))\cos(\gamma - \phi)\right] \ , \tag{7.170}$$

$$\begin{aligned} C_{R_{\rm c}} \equiv & \left[1 + 2\rho_{\rm c}\cos\theta_{\rm c}\cos\gamma + \rho^2_{\rm c}\right][1 - R_{\rm c}] - 2\rho_{\rm c} r_{\rm c}\cos(\theta_{\rm c} - \delta_{\rm c}) \\ & - 2r_{\rm c}\cos\delta_{\rm c}\cos\gamma + r^2_{\rm c}, \end{aligned} \tag{7.171}$$

we obtain a relation between q and R_c in the following compact way [281]:

$$q = \frac{-B_{R_{\rm c}} \pm \sqrt{B^2_{R_{\rm c}} - 4A_{R_{\rm c}}C_{R_{\rm c}}}}{2A_{R_{\rm c}}} \ . \tag{7.172}$$

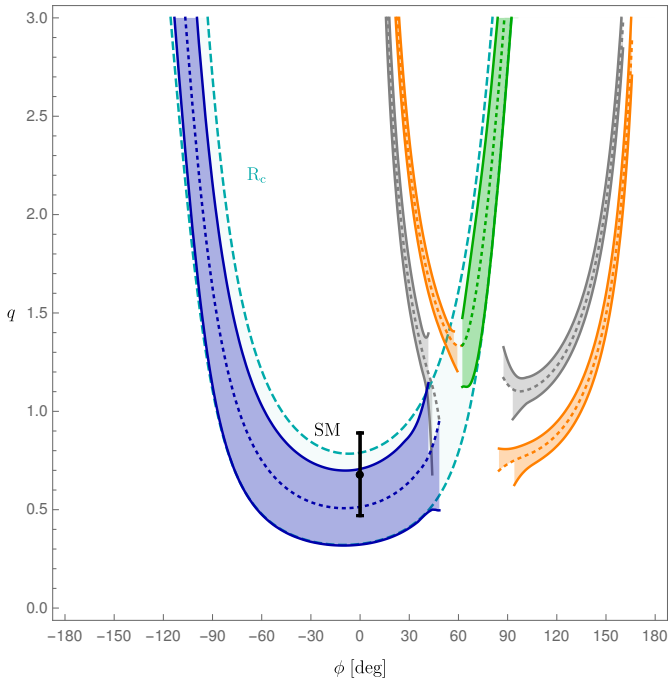

Figure 55: Contours in the $q - \phi$ plane, arising from the triangle analysis of the charged $B \to \pi K$ decays, where constraints have been imposed as discussed in the text. The contour R_c gives rise to the cyan dotted line [281].

This allows us to convert the measured value of R_c, using also the numerical values of δ_c, r_c and ρ_c, into the cyan dotted contour in the $q - \phi$ plane in Fig. 55, complementing the analysis. This contour is in excellent agreement with two of the contours coming from the triangle construction as well as with the SM values for q and ϕ.

7.5.4 Utilizing Mixing-Induced CP Violation in $B^0 \to \pi^0 K_S$ Decay

Let us discuss how we can get further information for the q and ϕ determination and obtain a sharper picture. For this purpose, we work again with the $B^0 \to \pi^0 K_S$ channel and utilise the mixing-induced CP asymmetry $S_{CP}^{\pi^0 K_S}$. This allows us to extract the phase ϕ_{00}.

With the help of the values of the hadronic parameters and the mixing-induced CP asymmetry, the following expression can be obtained, which provides another contour in the q–ϕ plane [281]:

$$q = \frac{-B_c + \sqrt{B_c^2 - 4A_c D_c}}{2A_c} \,, \tag{7.173}$$

where

$$A_c \equiv r_c^2(-\tan\phi_{00}\cos 2\phi - \sin 2\phi)\ , \tag{7.174}$$

$$\begin{aligned} B_c \equiv\ & 2r_c\cos\delta_c(\tan\phi_{00}\cos\phi + \sin\phi) - \frac{4}{3}\hat{c}_+ A_c \\ & -(2r_c^2 - 2r_c r\cos(\delta_c-\delta))(-\tan\phi_{00}\cos(\gamma+\phi) - \sin(\gamma+\phi)) \end{aligned} \tag{7.175}$$

$$\begin{aligned} D_c \equiv\ & -\tan\phi_{00} - (2r_c\cos\delta_c - 2r\cos\delta)(\tan\phi_{00}\cos\gamma + \sin\gamma) \\ & + (r_c^2 + r^2 - 2r_c r\cos(\delta_c-\delta))(-\tan\phi_{00}\cos 2\gamma - \sin 2\gamma) \\ & + \frac{4}{3}\tilde{a}_C\ q r_c(-\tan\phi_{00}\cos\phi - \sin\phi) + \frac{4}{9}q^2(\tilde{a}_S^2 + \tilde{a}_C^2)A_c \\ & + \frac{4}{3}(-\tan\phi_{00}\cos(\gamma+\phi) - \sin(\gamma+\phi))(r_c^2\hat{c}_+ - r_c r(\tilde{a}_C\cos\delta + \tilde{a}_S\sin\delta)) \end{aligned} \tag{7.176}$$

with

$$\hat{c}_+ \equiv \tilde{a}_C\ q\cos\delta_c + \tilde{a}_S\ q\sin\delta_c\ . \tag{7.177}$$

We can now calculate the value of ϕ_{00} using the current measurement of $S_{\rm CP}^{\pi^0 K_{\rm S}}$, which we have presented in Table 14, and implement it in Eqs. (7.173)-(7.176) in order to convert the mixing-induced CP asymmetry into another contour in the q–ϕ plane. We obtain [281]:

$$\phi_{00} = (7.7 \pm 12.1)^\circ. \tag{7.178}$$

This results in the purple contour illustrated in Fig. 56a, where contributions from colour-suppressed EW penguin topologies are included. In the same plot, we also show the contours coming from the isospin analysis that are in agreement with the $R_{\rm c}$ constraint.

7.5.5 Illustrating a Future Scenario

The strategy we presented in Sec. 7.5.4 can be used to illustrate a future application. We assume a scenario, as given in [281]:

$$S_{\rm CP}^{\pi^0 K_{\rm S}} = 0.67 \pm 0.042, \quad A_{\rm CP}^{\pi^0 K_{\rm S}} = -0.07 \pm 0.042, \quad \phi_{00} = (0.9 \pm 3.3)^\circ. \tag{7.179}$$

Including colour-suppressed EW penguin effects, we assume that the uncertainty of $S_{\rm CP}^{\pi^0 K_{\rm S}}$ is the same as $A_{\rm CP}^{\pi^0 K_{\rm S}}$. The resulting picture is illustrated in Fig. 56b. The purple contour shows the constraint coming from $S_{\rm CP}^{\pi^0 K_{\rm S}}$. The experimental uncertainties are those given in Eq. (7.179) and are illustrated by the solid purple line. We also take into account the theoretical uncertainties, which are the $SU(3)$ uncertainties related to the hadronic

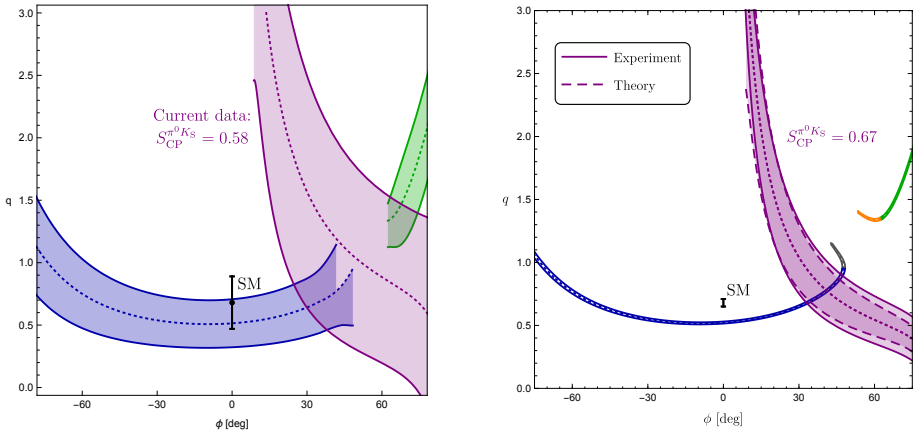

(a) (b)

Figure 56: (a) Constraints in the q–ϕ plane utilising information from the mixing-induced CP asymmetry $S_{CP}^{\pi^0 K_S}$. (b) Illustrating a future application of our strategy considering a scenario for measurement of mixing induced CP asymmetry [281].

parameters which we use in order to determine q in Eq. (7.173). The theoretical uncertainties are denoted by the dashed purple line. We observe that the experimental and the theoretical precision can be matched, which is very promising for future analyses.

Fig. 56b also shows the four contours (blue, green, orange, gray) coming from the triangle analysis. We note that the contours which remain after taking into account constraints from the phase ϕ_{0+} and the ratio R_c [281].

7.6 Concluding

In this Chapter, we have discussed the $B \to \pi K$ system, which is another interesting case of non-leptonic decays. As we have emphasized numerous times through this thesis, in this class of decays, we have to deal with the challenging hadronic matrix elements entering through the low-energy effective Hamiltonian. This system is dominated by loop topologies. In addition to the QCD penguin diagrams, EW penguins also play an important role. Therefore, we had to pay special attention to the EW penguin sector in our studies.

Our first goal was to present a state-of-the-art analysis. Utilising expressions of the decay amplitudes of the $B \to \pi K$ channels, we applied a specific parametrization [186], which introduces hadronic parameters. In order to determine these parameters, we made use of the powerful tool of the $SU(3)$ flavour symmetry of the strong interactions. This allowed us to obtain relations between the $B \to \pi K$ decay amplitudes and those of the $B \to \pi\pi$ and $B \to KK$ systems. Experimental information for the hadronic parameters of the latter systems are available. Consequently, employing the $SU(3)$ flavour symmetry, we

converted the hadronic parameters of these systems into their $B \to \pi K$ counterparts and finally extracted their values.

Our next step was to study CP violation in the $B \to \pi K$ system. The key mode for these studies is the $B_d^0 \to \pi^0 K^0$ channel, which is the only one that exhibits mixing-induced CP violation. Therefore, we aimed at obtaining correlations between the corresponding direct and the mixing-induced CP asymmetries. For this purpose, a central role was played by an isospin analysis, while keeping the theoretical assumptions as minimal as possible. Isospin relations between the amplitudes of the neutral $B \to \pi K$ decays allowed us to represent these amplitudes as triangles in the complex plane. The different orientations of these triangles result in different contours in the $A_{\rm CP}^{\pi^0 K_{\rm S}}$–$S_{\rm CP}^{\pi^0 K_{\rm S}}$ plane, describing correlations between the CP asymmetries. These contours can be obtained in a very clean way within the SM, and we can unambiguously pick the final contour. Comparing it with the experimental values of the CP asymmetries, we revealed tensions between this final contour, which reflects the theory SM predictions, and the data.

These tensions could be resolved either via a change in the values of the measured observables or assuming NP in the EW penguin sector. A recent highlight was a new Belle II measurement [299], which shifted towards the direction of the band characterising the SM correlation. However, the uncertainties of these measurements are unfortunately still too large to draw any definite conclusions. In addition, the new results for these CP asymmetries have not yet been included in the corresponding world average. Therefore, we did not explore the situation in further detail, although it will be very interesting to follow the future experimental developments.

In the last part of our analysis, we focused on the EW sector since EW penguins could offer an avenue for effects of new particles to enter the $B \to \pi K$ channels. The puzzling patterns in the data with respect to the SM could be an indication of NP of this kind. Consequently, the EW penguin parameters q and ϕ played a key role. We proposed a new strategy to extract these parameters from the data. Our method exploited both neutral and charged $B \to \pi K$ channels, employing again isospin relations between their decay amplitudes. Applying our strategy to the current data, we obtained contours in the ϕ–q plane. In order to get a more complete picture and actually determine q and ϕ, we utilised additional information from the mixing-induced CP asymmetry of the $B_d^0 \to \pi^0 K_S$ decay.

This methodology was also applied to a future benchmark scenario assuming experimental and theoretical progress. We found that the experimental precision can match the theoretical uncertainties, thereby demonstrating the power of the method. Therefore, implementing our strategy to future data from Belle II as well as the LHCb upgrade(s) will offer exciting new opportunities - either by confirming again the SM or eventually revealing NP with new sources of CP violation.

Our Decays Roadmap - Highlights

Decays with Different Dynamics

UT
Important to study inclusive & exclusive cases separately for $|V_{ub}|$ & $|V_{cb}|$

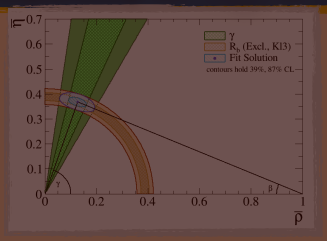

$B_d \to J/\psi K_S$, $B_s \to J/\psi\phi$

Performing combined fit with their control channels
↓
allows the determination of the mixing phases $\phi_{d,s}$
including the impact of penguins on CP asymmetries

CP Violation in different manifestations

$B_s \to D_s^{\pm} K^{\mp}$ & related modes

- Intriguing puzzles in CP violation and in branching ratio
- Utilising our model independent strategy in high precision era of B physics → may establish new sources of CP Violation

Rare Decays

$B \to \mu\mu$

from EW penguins and box topologies

$B \to \pi K$

These modes also indicate interesting puzzles

- Highlights
- Key mode $B_d^0 \to \pi^0 K_S$: the only one exhibiting mixing-induced CP asymmetry $\xrightarrow[\text{correlations}]{\text{obtain}} A_{CP}^{\pi^0 K_S} - S_{CP}^{\pi^0 K_S}$
- New Belle II measurement of $A_{CP}^{\pi^0 K_S}$, $S_{CP}^{\pi^0 K_S}$ — Might resolve $B \to \pi K$ puzzle
- New Strategy for extracting ϕ, q — EW penguin parameters

8 Rare $B_q^0 \to \mu^+\mu^-$ Decays

Other interesting cases that provide reliable tests of the SM flavour dynamics and work as powerful probes of NP are the decays mediated by $b \to s\ell^+\ell^-$ quark-level transitions. In this Chapter we mostly focus on one of the decays originating from these processes, which is the $B_s^0 \to \mu^+\mu^-$. This is a purely leptonic mode.

Having already introduced the leptonic decays in Sec. 3.3, we now present the formalism specifically for the neutral B_s^0 meson decaying into the final state $\mu^+\mu^-$. In an analogous way, we can approach the $B_d^0 \to \mu^+\mu^-$ mode, which we will also explore in the following Sections. It is worth noting that the decays of the neutral $B_{(s)}^0$ meson into the final states e^+e^- and $\tau^+\tau^-$ are also interesting. However, so far, they have received less attention, both theoretically and experimentally. We will not elaborate more on these modes but for the interested reader, more information can be found in Ref. [303].

The $B_s^0 \to \mu^+\mu^-$ decay is a flavour-changing neutral current (FCNC) process, thus a transition involving different quark flavours but of the same electric charge. Within the SM, these decays are forbidden at the tree level. The leading contributions arise from one-loop diagrams; the box and penguin topologies, as illustrated in Fig. 57. They are theoretically very clean as they involve only the B_s decay constant. In addition, in the SM these decays are helicity suppressed by a factor $(m_\mu^2/M_{B_s}^2)$, where m_μ denotes the mass of the muon and M_{B_s} the mass of the B_s meson [304]. Therefore, these decays are strongly suppressed and thus very rare. Experiments had been searching the $B_s^0 \to \mu^+\mu^-$ decay for decades [305]. The first observation of this decay was announced by the LHCb and CMS collaborations in 2012, with the result that about three out of one billion B_s^0 mesons decay into $\mu^+\mu^-$ [18]. The corresponding plot for the LHC Run I analysis in given in the Appendix G.

Useful and interesting observables are connected to the $B_s^0 \to \mu^+\mu^-$ channel and one of them is the branching ratio. As we have already discussed in previous Chapters, the phenomenon of the B_s^0–$\bar{B}_s^0$ mixing leads to time-dependent decay rates. The sizeable decay width difference $\Delta\Gamma_s$ gives access to another interesting observable, the mass-eigenstate rate asymmetry $\mathcal{A}_{\Delta\Gamma_s}^{\mu\mu}$, which is connected to the effective lifetime $\tau_{\mu\mu}$ [306, 307]. Fig. 58 shows the $B_s^0 \to \mu^+\mu^-$ and $B^0 \to \mu^+\mu^-$ branching ratio measurements for the combined results by ATLAS, CMS and LHCb (left plot), and the most recent LHCb data (right plot), comparing the experimental results with the SM predictions.

This decay offers an excellent path to search for physics beyond the SM, as NP could have an impact on the FCNC sector. There could be new particles entering the loop diagrams or might even arise at the tree level. Examples of NP scenarios are Z' models,

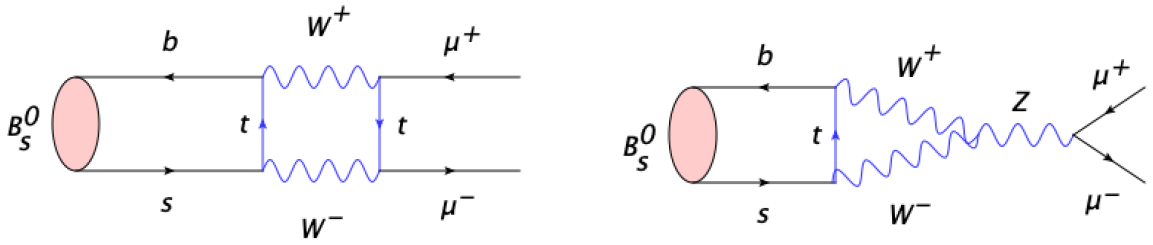

Figure 57: Feynman diagrams describing the $B_s^0 \to \mu^+\mu^-$ decay in the SM: box (left) and penguin (right) topologies.

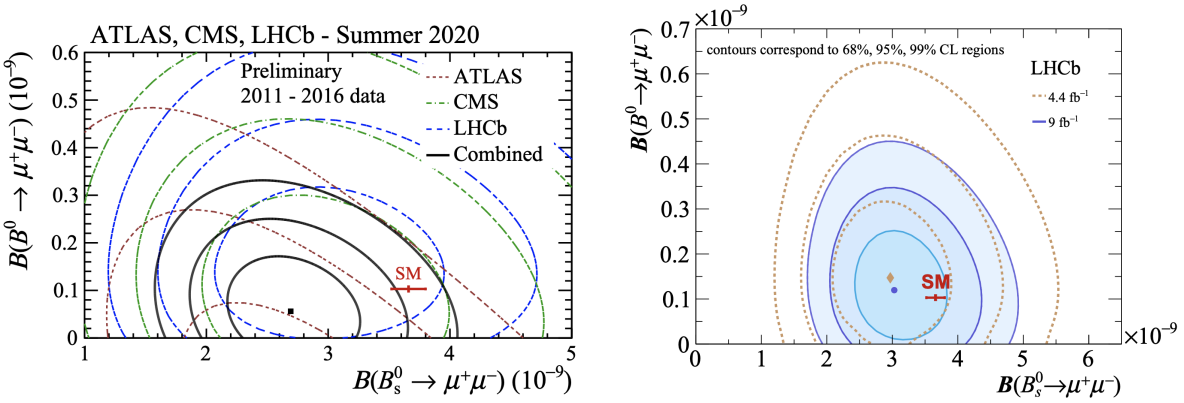

Figure 58: Branching fraction measurements for $B_s^0 \to \mu^+\mu^-$ and $B^0 \to \mu^+\mu^-$, combining the ATLAS, CMS and LHCb 2011-2016 data [14] (left) and the 2021 results by the LHCb Collaboration [15] (right). The SM point in both plots is denoted by the red cross. The ellipses are likelihood contours for different confidence levels for every experiment.

leptoquarks and models with extended Higgs sectors (see for instance Refs. [308–312]). A significant characteristic of the $B_s^0 \to \mu^+\mu^-$ decay is that it is sensitive to NP leading to scalar and pseudoscalar contributions, which are described by complex coefficients S and P, respectively. In terms of these quantities, the branching ratio is expressed as

$$\mathcal{B} \propto f_{B_s}\, m_\mu^2\, (|P|^2 + |S|^2), \tag{8.1}$$

where f_{B_s} is the decay constant of the B_s meson. As we mentioned before, this channel is characterised by helicity suppression in the SM, which is reflected by m_μ^2. We note that the scalar and pseudoscalar operators can lift this helicity suppression and as a result, NP may enhance or reduce the branching ratio. Thus, as we will discuss in the following Sections,

- this decay is a probe of NP with new scalar and pseudoscalar contributions and
- NP can be studied by measuring the $\mathcal{A}_{\Delta\Gamma_s}^{\mu\mu}$ observable and compared with the SM predictions. When allowing for NP effects, this observable is fully unconstrained.

A detailed analysis of NP searches in the leptonic modes in a model-independent way is given in Refs. [303, 313].

In the following Sections, we will mainly explore puzzling patterns that are related to the branching fractions $\mathcal{B}$ of the $B_q^0 \to \mu^+\mu^-$ channel and the $\mathcal{A}_{\Delta\Gamma_s}^{\mu\mu}$ observable [14, 15]. For completeness, we mention that on top of these, there are more puzzling cases, which are called flavour anomalies. An example of such a flavour anomaly is the angular observable P_5'. Recently, CMS [13] reported results, coming from the angular analysis of the decay $B^0 \to K^{*0}\mu^+\mu^-$, which are in good agreement with the corresponding LHCb measurements [12], hence confirming the tension in P_5'. In addition, there is the $R_{K^{(*)}}$ observable, which is the ratio of the branching fractions of the decay $B \to K^{(*)}\mu^+\mu^-$ to the decay $B \to K^{(*)}e^+e^-$. In the previous years, this ratio was also suggesting tensions with the SM. However, a new LHCb measurement in December 2022 [144,314] reported values which are compatible with the SM. The $R_{K^{(*)}}$ ratio offer tests of lepton flavour universality (LFU) (see Sec. 8.2.5). Both P_5' and $R_{K^{(*)}}$ involve decays mediated by $b \to s\ell^+\ell^-$ transitions. The analysis of these rare semileptonic decays can also offer links to the purely leptonic modes (see for instance Refs. [145, 146, 315]). Therefore, flavour anomalies are very interesting but they go beyond the scope of this thesis, hence we will not study them here.

We also note, even though this is not the topic of this Chapter, that CP violation has interesting manifestations in these rare decays. For the rare semileptonic decays, $R_{K^{(*)}}$ is such an example. For the leptonic $B_q^0 \to \mu^+\mu^-$ modes, it was very recently found in Ref. [315] that there are very constrained regions in the observable space for searches of new CP-violating (pseudo)-scalar contributions.

Returning to the central point of our analysis, we remind the reader of the discussions in Sec. 3.4.2 as well as in Chapter 5 about the discrepancies that arise between the measurements of the CKM matrix elements. These unresolved tensions have an impact on the UT apex determination and the NP searches in B_q^0–$\bar{B}_q^0$ mixing. In addition, they may also affect other NP searches, such as the $B_s^0 \to \mu^+\mu^-$ branching ratio measurements. The application of these results on the rare leptonic modes is the main topic of this Chapter.

The outline of this Chapter is the following: We firstly set the stage for the $B_s^0 \to \mu^+\mu^-$ decay, presenting the quantities and observables that play the key role in our studies. We aim at exploring whether there is room for NP in this case and focus on the branching ratio which is a probe of NP with new (pseudo)-scalar contributions. Additionally, for constraining NP, the dependence on the $|V_{cb}|$ and $|V_{ub}|$ CKM matrix elements has to be

minimised. This can be achieved by introducing the ratio between the branching fraction of the $B_s^0 \to \mu^+\mu^-$ channel and the mixing parameter Δm_s, as pointed out in Refs. [316–318]. Here, we properly take into account NP contributions to B_q^0–$\bar{B}_q^0$ mixing. Hence, we allow for possible NP not only in the branching fraction but also in the Δm_s in this ratio. For this purpose, we apply our results from the general, model-independent NP analysis presented in Chapter 5. This allows us to provide an interesting alternative constraint on NP entering through the (pseudo)-scalar sector. Last but not least, similar strategies can be applied to the $B_d^0 \to \mu^+\mu^-$ decay. However, we have to be careful, because here a different CKM factor enters. Instead of the $|V_{ts}|$ we have the $|V_{td}|$ matrix element, which is a factor of λ smaller in the Wolfenstein parametrization. This means that there is a suppression of λ^2 in the branching ratio, making this mode even more rear. As a result, this channel has not been observed yet and only upper bounds of the branching ratio are available. The main points of this Chapter follow our analysis presented in Refs. [81, 124].

8.1 Setting the Theoretical Framework

Our starting point is the effective Hamiltonian which describes the $b \to s\ell^+\ell^-$ transitions. Having already introduced the leptonic decays in Sec. 3.3, we now consider the $B_q^0 \to \ell^+\ell^-$ process and obtain in the SM [104]:

$$\mathcal{H}_{\text{eff}} = -\frac{G_{\text{F}}}{\sqrt{2}}\left[\frac{\alpha}{2\pi \sin^2\theta_{\text{W}}}\right] V_{tb}^* V_{tq} \eta_Y Y_0(x_t) (\bar{b}q)_{\text{V}-\text{A}} (\bar{\ell}\ell)_{\text{V}-\text{A}} + \text{h.c.}\,, \tag{8.2}$$

where G_F is the Fermi constant, $\alpha = e^2/4\pi$ the QED fine structure constant, θ_{W} the weak mixing angle, $V_{tb}^* V_{tq}$ denotes the product of the CKM matrix elements, $\eta_Y = 1.0113$ [319] a perturbative QCD correction and $Y_0(x_t)$ the Inami–Lim function describing the top-quark mass dependence [102].[63]

Having the low-energy effective Hamiltonian allows us to calculate the transition matrix element. Within the SM, it is only the matrix element of the axial-vector operator which contributes to the Hamiltonian, which has the structure $O_{10} = (\bar{b}\gamma_\mu P_L s) \otimes (\bar{\mu}\gamma^\mu\gamma_5\mu)$. At this point, we make a small parenthesis and discuss the structure of the matrix elements, including also the case of physics beyond the SM. In general, the matrix element for the B_s^0 decays caused by $b \to s\ell^+\ell^-$ processes consists of two parts:

$$\langle \ell^+\ell^- | O_i | B_s^0 \rangle = \langle \ell^+\ell^- | O_i^{\ell\ell} | 0 \rangle \otimes \langle 0 | O_i^{qq} | B_s^0 \rangle, \tag{8.3}$$

where $\langle \ell^+\ell^- | O_i^{\ell\ell} | 0 \rangle$ denotes the leptonic matrix element while $\langle 0 | O_i^{qq} | B_s^0 \rangle$ is the hadronic matrix element including the non-perturbative strong interaction effects. We emphasize

[63] The term $\eta_Y Y_0(x_t)$ describes the short-distance physics.

Leptonic Part $O^{\ell\ell}$	Hadronic Part O^{qq}
Scalar	Scalar
Scalar	Pseudoscalar
Pseudoscalar	Scalar
Pseudoscalar	Pseudoscalar
Vector	Vector
Vector	Axial-Vector
Axial-Vector	Vector
Axial-Vector	Axial-Vector
Tensor	Tensor

Scalar (S)	Pseudoscalar (P)	Vector (V)	Axial-Vector (A)	Tensor (T)
1	γ_5	γ_μ	$\gamma_\mu\gamma_5$	$\gamma_\mu\gamma_\nu - \gamma_\mu\gamma_\nu$

Table 15: Possible combinations between the leptonic and the hadronic part.

that gluons do not couple to the leptons, and as a result, we have perfect factorisation.[64] Therefore, we obtain the scheme

$$O = O^{\ell\ell} \otimes O^{qq}, \tag{8.4}$$

where $O^{\ell\ell}$ is the leptonic and O^{qq} is the hadronic part. Depending on the possible combinations between the leptonic and the hadronic part, the matrix element can be scalar (S), pseudoscalar (P), vector (V), axial-vector (A) or tensor (T). Due to Lorentz invariance, these possible combinations are presented in Table 15.

Let us now write the decay amplitude of the $B_s^0 \to \mu^+\mu^-$ channel:

$$\begin{aligned} A(B_s^0 \to \mu^+\mu^-) &= \langle \mu^+\mu^- | \mathcal{H}_{\text{eff}} | B_s^0 \rangle \\ &= \frac{G_F}{\sqrt{2}} \sum_i \; C_i(\mu) \; \times \langle \mu^+\mu^- | O_i | B_s^0 \rangle. \end{aligned} \tag{8.5}$$

[64] In comparison to the non-leptonic decays that we extensively studied in the previous Chapters, here things are much simpler. This is due to the fact that factorisation arises automatically, since gluons do not couple to $\ell^+\ell^-$, as we have already mentioned in Chapter 3.

We remind here the reader that C_i are the Wilson coefficients, which are obtained within perturbation theory. They are well defined in the SM and can be affected by NP. The term $\langle \mu^+\mu^-|O_i|B_s^0\rangle$ is the non-perturbative part.

Recalling Eq. (8.3), we observe that concerning the hadronic matrix element part, only the $\langle 0|(\bar{b}q)_{\mathrm{V-A}}|B_q^0\rangle$ term is required. Taking into account that B_s^0 is a pseudoscalar meson, the vector current piece vanishes. Then, in analogy to Eq. (3.43), the matrix element is simply given by the f_{B_q} decay constant. Regarding the leptonic part in Eq. (8.3), it can be expressed in terms of Dirac spinors and apply Dirac algrebra [320]. Consequently, out of all the general possible combinations presented in Table 15, those that finally contribute to the $B_s^0 \to \mu^+\mu^-$ decay, are the following:

- scalar⊗pseudoscalar,
- pseudoscalar⊗pseudoscalar,
- axial-vector⊗axial-vector,

where we mention again that we consider also structures that are not present in the SM.

We can now present the operators that contribute to the non-perturbative B_s^0 matrix element for the $B_s^0 \to \mu^+\mu^-$ channel:

- $O_S = m_b(\bar{b}P_R s)\otimes(\bar{\mu}\mu)$ $\qquad$ $O'_S = m_b(\bar{b}P_L s)\otimes(\bar{\mu}\mu)$
- $O_P = m_b(\bar{b}P_R s)\otimes(\bar{\mu}\gamma_5\mu)$ $\qquad$ $O'_P = m_b(\bar{b}P_L s)\otimes(\bar{\mu}\gamma_5\mu)$
- $O_{10} = (\bar{b}\gamma_\mu P_L s)\otimes(\bar{\mu}\gamma^\mu\gamma_5\mu)$ $\qquad$ $O'_{10} = (\bar{b}\gamma_\mu P_R s)\otimes(\bar{\mu}\gamma^\mu\gamma_5\mu)$,

where m_b is the mass of the b quark and

$$P_L = \frac{(1-\gamma_5)}{2}, \qquad P_R = \frac{(1+\gamma_5)}{2}. \tag{8.6}$$

Finally, the effective Hamiltonian with the help of these operators can be written as follows [304, 306, 311, 312]:

$$\mathcal{H}_{\mathrm{eff}} = -\frac{G_F}{\sqrt{2\pi}} V_{ts}^* V_{tb}\alpha \left[C_{10}O_{10} + C'_{10}O'_{10} + C_S O_S + C'_S O_S + C_P O_P + C'_P O'_P\right]. \tag{8.7}$$

The only contribution in SM comes from the operator O_{10} with a real coefficient. Hence, in the SM we have $C_{10} = C_{10}^{\mathrm{SM}}$ for which:

$$C_{10}^{\mathrm{SM}} = -\eta_Y Y_0(x_t)\sin^{-2}\theta_W. \tag{8.8}$$

The numerical value for this coefficient is [311]:

$$C_{10}^{\rm SM} = -4.134\ . \tag{8.9}$$

The coefficients C'_{10}, $C_S^{(\prime)}$ and $C_P^{(\prime)}$ in Eq. (8.7) do not contribute in the SM. However, they can play an important role if there is physics entering from beyond the SM. We note for completeness that the coefficients C_{10} and C'_{10} are dimensionless while the $C_S^{(\prime)}$ and $C_P^{(\prime)}$ have dimension $[\text{GeV}]^{-1}$.

8.1.1 Observables and Important Quantities

Concerning the decay observables, we start with the branching ratio for the $B_s^0 \to \mu^+\mu^-$ decay. The time-integrated branching ratio measured experimentally is [220]:

$$\overline{\mathcal{B}}(B_s \to \mu^+\mu^-) \equiv \frac{1}{2}\int_0^\infty \langle \Gamma(B_s(t) \to \mu^+\mu^-)\rangle\, dt. \tag{8.10}$$

The theoretical branching fraction of the decay $B_s^0 \to \mu^+\mu^-$ at lowest order in the SM takes the form [311]:

$$\mathcal{B}(B_s \to \mu^+\mu^-)_{\rm th} = \frac{\tau_{B_s} G_{\rm F}^4 m_W^4 \sin^4\theta_W}{8\pi^5} \left|C_{10}^{\rm SM}\right|^2 |V_{ts}V_{tb}^*|^2 f_{B_s}^2 m_{B_s} m_\mu^2 \sqrt{1-\frac{4m_\mu^2}{m_{B_s}^2}}\ . \tag{8.11}$$

Here, we highlight again the importance of the decay constant, which encodes all the hadronic physics. It is a non-perturbative parameter and is calculated with lattice QCD. The values of f_{B_s}, reviewed in [135], are presented in Fig. 59. Moreover, the branching ratio exhibits helicity suppression, which is reflected by the m_μ^2 factor.

The conversion relation between the thoeretical and the experimental branching ratio, which we have already discussed in previous Sections and especially in Sec. 6.4, is:

$$\mathcal{B}(B_s \to \mu^+\mu^-)_{\rm th} = \frac{1-y_s^2}{1+y_s\mathcal{A}_{\Delta\Gamma_s}^{\mu\mu}} \bar{\mathcal{B}}(B_s \to \mu^+\mu^-). \tag{8.12}$$

Here, the second interesting observable arises, which is the $\mathcal{A}_{\Delta\Gamma_s}^{\mu\mu}$. We remind the reader that we get access to this observable due to the sizeable $\Delta\Gamma_s$. As discussed in [306,311,312], $\mathcal{A}_{\Delta\Gamma_s}^{\mu\mu}$ takes the values:

$$\mathcal{A}_{\Delta\Gamma_s}^{\mu\mu} \in [-1,1] \tag{8.13}$$

$$\mathcal{A}_{\Delta\Gamma_s}^{\mu\mu} = +1 \text{ in SM.} \tag{8.14}$$

This observable can be determined from measurements of the $B_s \to \mu^+\mu^-$ effective lifetime, defined as [306, 313]:

$$\tau_{\mu\mu}^s \equiv \frac{\int_0^\infty t\langle\Gamma(B_s(t) \to \mu^+\mu^-)\rangle dt}{\int\int_0^\infty \langle\Gamma(B_s(t) \to \mu^+\mu^-)\rangle dt}\ . \tag{8.15}$$

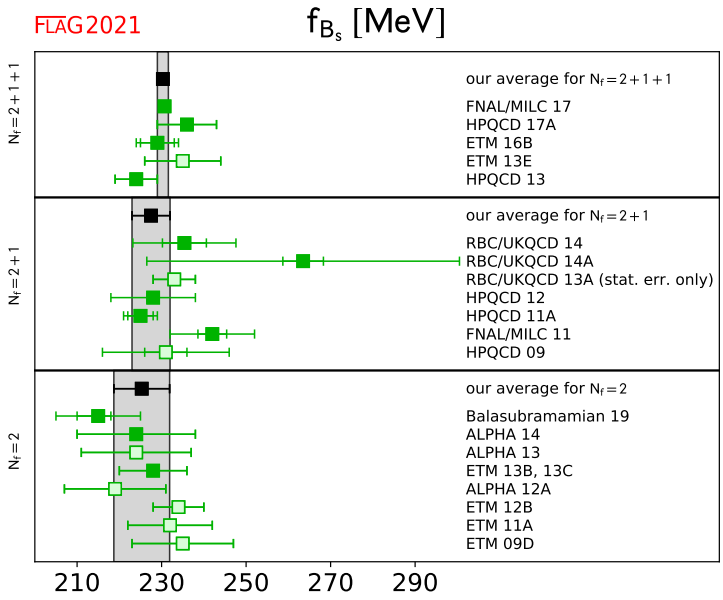

Figure 59: Lattice QCD results for the decay constant for the B_s meson [135].

The expression of $\mathcal{A}^{\mu\mu}_{\Delta\Gamma_s}$ in terms of the effective lifetime is the following:

$$\mathcal{A}^{\mu\mu}_{\Delta\Gamma_s} = \frac{1}{y_s}\left[\frac{(1-y_s^2)\tau^s_{\mu\mu} - (1+y_s^2)\tau_{B_s}}{2\tau_{B_s} - (1-y_s^2)\tau^s_{\mu\mu}}\right]. \tag{8.16}$$

We note that there are recent measurements of $\tau^s_{\mu\mu}$ by ATLAS [321], CMS [322] and the LHCb Collaboration [15], allowing us to derive bounds of $\mathcal{A}^{\mu\mu}_{\Delta\Gamma_s}$. However, the uncertainties are very large to constrain the observable [315].

For completeness, we also rewrite the conversion relation in terms of $\tau^s_{\mu\mu}$ and obtain:

$$\mathcal{B}(B_s \to \mu^+\mu^-)_{\rm th} = \left[2 - (1-y_s^2)\frac{\tau^s_{\mu\mu}}{\tau_{B_s}}\right]\bar{\mathcal{B}}(B_s \to \mu^+\mu^-). \tag{8.17}$$

Considering the experimental results, the branching fraction of the $B_s^0 \to \mu^+\mu^-$ decay has been measured by the CMS [323], with the most recent update given in Ref. [324], LHCb [325] and ATLAS [326] collaborations.[65]

At this point, let us introduce the following quantities which describe the pseudoscalar and scalar operators, $O_P^{(\prime)}$ and $O_S^{(\prime)}$, respectively [313]:

$$P = \frac{C_{10} - C'_{10}}{C_{10}^{\rm SM}} + \frac{M_{B_s}^2}{2m_\mu}\left(\frac{m_b}{m_b + m_s}\right)\left(\frac{C_P - C'_P}{C_{10}^{\rm SM}}\right) \tag{8.18}$$

[65] As a comment regarding $b \to s\ell\ell$ anomalies, we note that averages for these results have been performed by multiple groups [327–329].

$$S = \sqrt{1-4\frac{m_\mu^2}{M_{B_s}^2}}\,\frac{M_{B_s}^2}{2m_\mu}\left(\frac{m_b}{m_b+m_s}\right)\left(\frac{C_S-C_S'}{C_{10}^{\rm SM}}\right) \tag{8.19}$$

where we have to pay special attention to the dependence on the mass of the muon m_μ. We recall Eq. (8.11), where m_μ^2 reflects the helicity suppression. The expressions of P and S suggest that the helicity suppression can be lifted by the $C_P^{(\prime)}$ and $C_S^{(\prime)}$ coefficients, entering with a factor $1/m_\mu$. These quantities can be defined as:

$$P \equiv |P| e^{i\phi_P}, \tag{8.20}$$

$$S \equiv |S| e^{i\phi_S}, \tag{8.21}$$

where ϕ_P and ϕ_S are CP-violating phases. Within the SM, these quantities by definition take the values

$$P|_{\rm SM} = 1, \tag{8.22}$$

$$S|_{\rm SM} = 0, \tag{8.23}$$

and they will be very useful later on, especially when using the generalised expression of the branching ratios, allowing for NP contributions.

Last but not least, we present the CP-violating rate asymmetry for the $B_s^0 \to \mu^+\mu^-$ decay. We emphasize that, so far, the expressions for the rates were helicity summed. Here, for the discussion of CP violation, it is important to look at decays with specific lepton helicities. A flavour-tagged analysis would give access to the following CP-violating decay rate [311]

$$\frac{\Gamma(B_s^0(t)\to\mu_\lambda^+\mu_\lambda^-)-\Gamma(\bar B_s^0(t)\to\mu_\lambda^+\mu_\lambda^-)}{\Gamma(B_s^0(t)\to\mu_\lambda^+\mu_\lambda^-)+\Gamma(\bar B_s^0(t)\to\mu_\lambda^+\mu_\lambda^-)} = \frac{\mathcal{C}_{\mu\mu}^\lambda\cos(\Delta m_s t)+\mathcal{S}_{\mu\mu}\sin(\Delta m_s t)}{\cosh\left(\frac{y_s t}{\tau_{B_s}}\right)+\mathcal{A}_{\Delta\Gamma}^{\mu\mu}\sinh\left(\frac{y_s t}{\tau_{B_s}}\right)}, \tag{8.24}$$

with $\lambda = L, R$ denoting the helicity of the $\ell^+\ell^-$ pair. The following observables arise:

$$\mathcal{C}_{\mu\mu}^\lambda = -\eta_\lambda\left[\frac{2|P_{\mu\mu}^s S_{\mu\mu}^s|\cos(\varphi_P-\varphi_S)}{|P_{\mu\mu}^s|^2+|S_{\mu\mu}^s|^2}\right], \tag{8.25}$$

$$\mathcal{S}_{\mu\mu} = \frac{|P_{\mu\mu}^s|^2\sin(2\varphi_P-\phi_s^{\rm NP})-|S_{\mu\mu}^s|^2\sin(2\varphi_S-\phi_s^{\rm NP})}{|P_{\mu\mu}^s|^2+|S_{\mu\mu}^s|^2}, \tag{8.26}$$

where we have generalised the expressions and allowed for NP. We repeat that φ_P and φ_S are CP-violating phases. The phase $\phi_s^{\rm NP}$ arises from possible CP-violating NP effects originating from the B_s^0–$\bar B_s^0$ mixing. We note that in the SM, both these CP asymmetries are zero.[66] We stress that the observable $\mathcal{C}_{\mu\mu}^\lambda$ depends on the muon pair helicity: $\mathcal{C}_{\mu\mu}^\lambda = -\eta_\lambda\mathcal{C}_{\mu\mu}$.

[66] We mention that $\eta_L = +1$ and $\eta_R = -1$.

Hence, it is difficult to measure. On the other hand, the observable $\mathcal{S}_{\mu\mu}$, as well as the $\mathcal{A}_{\Delta\Gamma}^{\mu\mu}$, do not depend on the helicity of the muons.

As it is difficult to measure the decays with muon helicities, we now sum over the helicities. We obtain:

$$\frac{\Gamma(B_s^0(t) \to \mu^+\mu^-) - \Gamma(\bar{B}_s^0(t) \to \mu^+\mu^-)}{\Gamma(B_s^0(t) \to \mu^+\mu^-) + \Gamma(\bar{B}_s^0(t) \to \mu^+\mu^-)} = \frac{\mathcal{S}_{\mu\mu}\sin(\Delta m_s t)}{\cosh(y_s t/\tau_{B_s}) + \mathcal{A}_{\Delta\Gamma}^{\mu\mu}\sinh(y_s t/\tau_{B_s})} \,. \tag{8.27}$$

For completeness, we also write the observable $\mathcal{A}_{\Delta\Gamma}^{\mu\mu}$ in terms of the pseudoscalar and scalar contributions and finally have [306, 311]:

$$\mathcal{A}_{\Delta\Gamma}^{\mu\mu} = \frac{|P_{\mu\mu}^s|^2\cos(2\varphi_P - \phi_s^{\rm NP}) - |S_{\mu\mu}^s|^2\cos(2\varphi_S - \phi_s^{\rm NP})}{|P_{\mu\mu}^s|^2 + |S_{\mu\mu}^s|^2} \,. \tag{8.28}$$

We emphasize that this observable is fully unconstrained within its physical range $[-1, 1]$ when allowing for NP. We also stress that in all three observables; $\mathcal{C}_{\mu\mu}^{\lambda}$, $\mathcal{S}_{\mu\mu}^{\lambda}$ and $\mathcal{A}_{\Delta\Gamma}^{\mu\mu}$, the decay constant f_{B_s} cancels, making them theoretically clean. These three observables are not independent of one another, since they satisfy the relation:

$$\mathcal{C}_{\mu\mu}^2 + \mathcal{S}_{\mu\mu}^2 + \mathcal{A}_{\Delta\Gamma}^{\mu\mu\,2} = 1 \,, \tag{8.29}$$

which we have already applied before, i.e. in Eq. (6.19).

8.2 Searching for New Physics

Let us now move towards searches of NP in the leptonic modes. The $B_s^0 \to \mu^+\mu^-$ channel is sensitive to scalar and pseudoscalar lepton densities, which enter the $O_S^{(\prime)}$ and $O_P^{(\prime)}$ operators. The corresponding Wilson coefficients C_P and C_S are largely unconstrained. Recalling Eqs. (8.18) and (8.19), the scalar and pseudoscalar operators can lift the helicity suppression. Since NP may enhance or reduce the branching ratio, this decay channel is a sensitive probe of NP with new scalar and pseudoscalar contributions. In principle, NP could modify the branching ratio of the leptonic modes also through B_q^0–$\bar{B}_q^0$ mixing.[67] However, NP in B_q^0–$\bar{B}_q^0$ mixing is already taken into account through the experimental values of the mixing parameters.

Following these lines, the branching ratio is a key observable for exploring NP in the (pseudo)-scalar sector. So, our starting point is the expression of the measured branching

[67] In other words, B_q^0–$\bar{B}_q^0$ mixing could enter and lead to subtleties regarding the measurement of the experimental branching ratio and the comparison with the SM predictions.

Parameter	Value	Parameter	Value
f_{B_s}	230.3 ± 1.3 MeV [135]	$\hat{B}_s$	1.232 ± 0.053 [135, 240]
$\tau_{B_s,H}$	1.624 ± 0.009 ps [120]	$\hat{B}_s/\hat{B}_d$	1.008 ± 0.025 [135, 240]
$\tau^s_{\mu\mu}$	2.07 ± 0.29 ps [325]	$2y_s \equiv \Delta\Gamma_s/\Gamma_s$	0.128 ± 0.007 [120]
τ_{B_s}	1.520 ± 0.005 ps [120]	$2y_d \equiv \Delta\Gamma_d/\Gamma_d$	0.001 ± 0.010 [120]

Table 16: Values for the decay constants, effective lifetimes, bag parameters and width difference parameters, which are used in the determination of the SM branching ratios of the $B_q^0 \to \mu^+\mu^-$ system.

ratio, where we allow for NP contributions. We obtain [81, 304]:

$$\bar{\mathcal{B}}(B_s \to \mu^+\mu^-) = \frac{\tau_{B_s} G_F^4 M_W^4 \sin^4\theta_W}{8\pi^5} \frac{\left|C_{10}^{\rm SM} V_{ts} V_{tb}^*\right|^2}{(1-y_s)} f_{B_s}^2 M_{B_s} m_\mu^2 \sqrt{1-4\frac{m_\mu^2}{M_{B_s}^2}}$$
$$\times \frac{1+\mathcal{A}^{\mu\mu}_{\Delta\Gamma_s} y_s}{1+y_s} \left(|P^s_{\mu\mu}|^2 + |S^s_{\mu\mu}|^2\right) \tag{8.30}$$
$$= \bar{\mathcal{B}}(B_s \to \mu^+\mu^-)^{\rm SM} \times \frac{1+\mathcal{A}^{\mu\mu}_{\Delta\Gamma_s} y_s}{1+y_s} \left(|P^s_{\mu\mu}|^2 + |S^s_{\mu\mu}|^2\right) . \tag{8.31}$$

We have already given the expression of the observable $\mathcal{A}^{\mu\mu}_{\Delta\Gamma_s}$ in Eq. (8.28). We collect input values that are used in the determination of the SM branching ratio of the $B_q^0 \to \mu^+\mu^-$ decay in Table 16.[68]

8.2.1 Constraining New Physics

A key quantity in order to constrain the NP parameter space is given by the ratio between the measured and the SM branching ratios [306]:

$$\overline{R} \equiv \frac{\overline{\mathcal{B}}(B_s \to \mu^+\mu^-)}{\overline{\mathcal{B}}(B_s \to \mu^+\mu^-)_{\rm SM}}. \tag{8.32}$$

Applying Eq. (8.30), this ratio can be rewritten as

$$\overline{R} = \left[\frac{1+\mathcal{A}^{\mu\mu}_{\Delta\Gamma_s} y_s}{1+y_s}\right] \left(|P^s_{\mu\mu}|^2 + |S^s_{\mu\mu}|^2\right) . \tag{8.33}$$

[68] We note that the lifetime of the heavy B_s mass eigenstate $\tau_{B_s,H}$ can be expressed in terms of the τ_{B_s} and y_s as $\tau_{B_s}/(1-y_s)$.

By definition, this quantity is equal to 1 in the SM. Let us firstly simplify the discussion and show the contour we can derive in the $|P|$–$|S|$ plane.[69] If y_s is not taken into account in the comparison between theory and experiment, then the expression takes the simple form:

$$\overline{R} = |P^s_{\mu\mu}|^2 + |S^s_{\mu\mu}|^2, \tag{8.34}$$

which fixes a circle in the $|P|$–$|S|$ plane. Combining the SM prediction[70] given in Ref. [330]

$$\bar{\mathcal{B}}(B_s \to \mu^+\mu^-)|_{\rm SM} = (3.66 \pm 0.14) \times 10^{-9}, \tag{8.35}$$

and the measured value coming given in the analysis in Ref. [329]:

$$\bar{\mathcal{B}}(B_s \to \mu^+\mu^-) = (2.85^{+0.34}_{-0.31}) \times 10^{-9}\,, \tag{8.36}$$

we determine:

$$\overline{R} = 0.779^{+0.098}_{-0.090}. \tag{8.37}$$

This value gives rise to the orange circular band in Fig. 60.

However, this quantity does not allow us to separate the scalar and pseudoscalar contributions. As a result, there could still be a large amount of NP present. How do we resolve this situation? We use the measurement of the effective lifetime $\tau^s_{\mu\mu}$ which allows us to convert $\tau^s_{\mu\mu}$ into bounds on $\mathcal{A}^{\mu\mu}_{\Delta\Gamma_s}$. The second constraint is given by $\mathcal{A}^{\mu\mu}_{\Delta\Gamma_s}$, assuming $P^s_{\mu\mu}$ and $S^s_{\mu\mu}$ are real:

$$\mathcal{A}^{\mu\mu}_{\Delta\Gamma_s} = \cos\phi^{\rm NP}_s \left[\frac{(P^s_{\mu\mu})^2 - (S^s_{\mu\mu})^2}{(P^s_{\mu\mu})^2 + (S^s_{\mu\mu})^2}\right]. \tag{8.38}$$

This fixes straight lines in the $|P|$–$|S|$ plane, denoted by the green lines in Fig. 60. Consequently, knowing $\overline{R}$ and $\mathcal{A}^{\mu\mu}_{\Delta\Gamma_s}$, we can not only separate the (pseudo)-scalar contributions but also fully determine $|P^s_{\mu\mu}|$ and $|S^s_{\mu\mu}|$. The recent measurements of the effective lifetime provided by ATLAS [321], CMS [322] and LHCb [15] are the following:

$$\tau^s_{\mu\mu}|_{\rm ATLAS\ 2023} = (0.99 \pm 0.45)\ {\rm ps}\ . \tag{8.39}$$

$$\tau^s_{\mu\mu}|_{\rm CMS\ 2022} = (1.83 \pm 0.23)\ {\rm ps}\ , \tag{8.40}$$

$$\tau^s_{\mu\mu}|_{\rm LHCb\ 2021} = (2.07 \pm 0.29)\ {\rm ps}\ , \tag{8.41}$$

and give rise to values of $\mathcal{A}^{\mu\mu}_{\Delta\Gamma_s}$. Unfortunately though, these first experimental constraints have very large uncertainties. The yielded values of $\mathcal{A}^{\mu\mu}_{\Delta\Gamma_s}$ are not even within the range of $-1 \leq \mathcal{A}^{\mu\mu}_{\Delta\Gamma_s} \leq 1$. Hence, it is important to measure it further in the future.

[69] In terms of notation, we simplify the labels in the axes.

[70] At this point, for simplicity, we do not consider the implications arising from the inclusive and exclusive determinations of the CKM parameters.

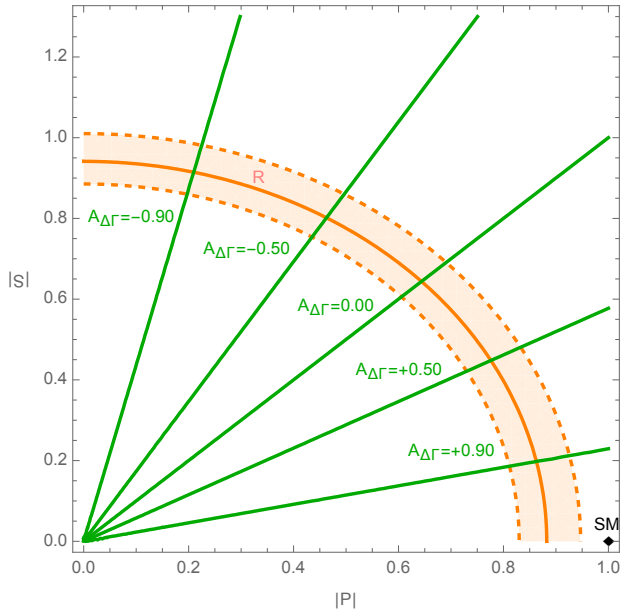

Figure 60: Constraints on $|P|$ and $|S|$ plane.

Summarising, Fig. 60 shows the current constraints in the $|P|$–$|S|$ plane, reflected by the orange circular band, as well as future constraints related to the $\mathcal{A}_{\Delta\Gamma_s}^{\mu\mu}$ observable, denoted by the green straight lines. Consequently, the branching ratio and the $\mathcal{A}_{\Delta\Gamma_s}^{\mu\mu}$ complement each other in identifying and discriminating NP.

Here, we have given a first impression of how we derive the ratio $\overline{R}$ and the corresponding plot. In order to achieve this, we have simplified the discussion. Hence, we have not discussed yet how the uncertainties of the relevant CKM matrix elements affect these studies. Below, we will properly present the impact that the different determinations of these quantities –inclusive, exclusive and hybrid– have on the NP searches in the leptonic modes.

8.2.2 Minimising the impact of CKM elements in New Physics Searches

Our starting point is again the measured branching ratio, which is given in Eq. (8.30). As we see, the SM prediction depends on the CKM element $|V_{ts}|$. Following the Wolfenstein parametrisation [69, 70]:

$$|V_{ts}V_{tb}| = \lambda|V_{cb}|\left[1 - \frac{\lambda^2}{2}\left(1 - 2\bar{\rho}\right)\right] + \mathcal{O}\left(\lambda^6\right) \ , \tag{8.42}$$

we observe that $|V_{ts}|$ is determined through the UT apex solution and the CKM element $|V_{cb}|$. As a result, the branching ratio is proportional to the square of $|V_{cb}|$, thus again depending on the exclusive and inclusive determinations. It becomes clear that it is impor-

tant to study every case (inclusive, exclusive and hybrid) separately. Unfortunately, this is usually not done "properly" in the literature.

Consequently, we can obtain the SM predictions of the branching ratio for the inclusive, exclusive and hybrid case:

$$\bar{\mathcal{B}}(B_s \to \mu^+\mu^-) = (3.81 \pm 0.11) \times 10^{-9}\,, \quad \text{Inclusive,} \tag{8.43}$$

$$\bar{\mathcal{B}}(B_s \to \mu^+\mu^-) = (3.27 \pm 0.10) \times 10^{-9}\,, \quad \text{Exclusive,} \tag{8.44}$$

$$\bar{\mathcal{B}}(B_s \to \mu^+\mu^-) = (3.80 \pm 0.10) \times 10^{-9} \quad \text{Hybrid.} \tag{8.45}$$

We observe again the variation depending on the CKM parametrization. We note that the spread between inclusive, hybrid and exclusive case is wider than the uncertainties.

Comparing now our SM predictions with the experimental value of the branching ratio given in Eq. (8.36), we are able to constrain the parameters $|P^s_{\mu\mu}|$ and $|S^s_{\mu\mu}|$, in the way we described in Sec. 8.2.1. The numerical values for the ratio $\overline{R}$ for the inclusive, exclusive and hybrid case are the following:

$$\overline{R} = 0.748^{+0.092}_{-0.084}, \quad \text{Inclusive,} \tag{8.46}$$

$$\overline{R} = 0.871^{+0.107}_{-0.098}, \quad \text{Exclusive,} \tag{8.47}$$

$$\overline{R} = 0.750^{+0.100}_{-0.094}, \quad \text{Hybrid.} \tag{8.48}$$

Here, we would like to note that for the numerical analysis and the plots in this Chapter, we utilise the value of the experimental branching ratio in Eq. (8.36) in order to be consistent with our published analysis in Ref. [81]. The most recent measured value though includes also the 2022 CMS measurement reported in Ref. [322]. For completeness, we mention that the new world average then is $\overline{\mathcal{B}}(B_s \to \mu^+\mu^-) = (3.45 \pm 0.29) \times 10^{-9}$ [120]. Interestingly, this value is larger than the exclusive SM prediction in Eq. (8.44) which would give rise to a value of $\overline{R}$ larger than 1.

We point out that Eq. (8.33) can also be written as [311]

$$\overline{R} = \left[\frac{1 + y_s \cos(2\varphi_P - \phi_s^{\rm NP})}{1 + y_s}\right] |P^s_{\mu\mu}|^2 + \left[\frac{1 - y_s \cos(2\varphi_S - \phi_s^{\rm NP})}{1 + y_s}\right] |S^s_{\mu\mu}|^2\,. \tag{8.49}$$

Having the numerical values of the ratios $\overline{R}$ for inclusive, exclusive and hybrid case, and utilising the above expression, we derive the $|P|$–$|S|$ plot. The corresponding band is given in Fig. 61 (purple) and presented for inclusive, exclusive and hybrid case. We note that for our studies we assume the scenario where NP phases for the pseudo-scalar and scalar contributions are zero (or π), so we have $\varphi_P = 0$ (or π) and $\varphi_S = 0$ (or π). The phase $\phi_s^{\rm NP}$ is the usual phase determined through the $B_s^0 \to J/\psi\phi$ channel, as discussed in Chapter 5.

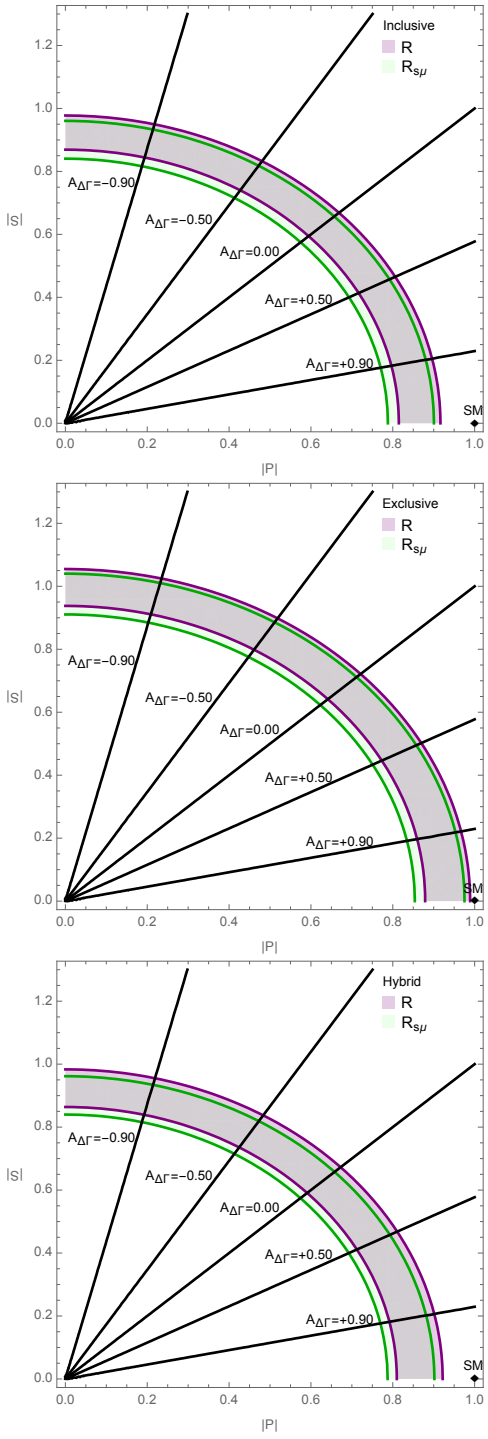

Figure 61: Constraints in the $|P|$–$|S|$ plane coming from the ratio $\overline{R}$ (purple) and the $R_{s\mu}$ (green), for the inclusive (top), exclusive (middle) and hybrid (bottom) case of the CKM parameters, as discussed in the text. We assume that $\varphi_P = 0$ (or π) and $\varphi_S = 0$ (or π).

We obtain the contours, thus the constraints, that correspond to the branching ratio of the $B_s^0 \to \mu^+\mu^-$ decay for all three cases.

Our next goal is to eliminate the dependence on $|V_{cb}|$ when allowing for NP. How can we achieve this? Key quantity, which can be used in order to minimise the impact of $|V_{cb}|$ and UT apex, as suggested in Refs. [316–318], is the ratio with the B_s mass difference Δm_s:

$$\mathcal{R}_{s\mu} \equiv \frac{\bar{\mathcal{B}}(B_s \to \mu^+\mu^-)}{\Delta m_s} \,. \tag{8.50}$$

Looking at $\mathcal{R}_{s\mu}$ in the SM the CKM factor in Eq. (8.42) cancels in this ratio, as we will discuss below. However, we have to correct for the possible NP effects entering the B_q^0-$\bar{B}_q^0$ mixing. This is now possible following the analysis presented in [81, 124].

Let us study the situation in more detail. We refer again to Fig. 61, which illustrates constraints from the branching ratio of $B_s^0 \to \mu^+\mu^-$. Comparing the light purple contours in these plots, we observe how the NP searches with the branching ratio depend on $|V_{cb}|$ and the UT apex. In order to minimise this dependence, we utilise the Eq. (8.50), repeating here that in the SM, the state-of-the-art picture for Δm_s (as it is already introduced in Sec. 3.1.3) is [81]

$$\Delta m_s|_{\rm SM} \equiv 2|M_{12}^s|_{\rm SM} = \frac{G_F^2 m_W^2}{12\pi^2} m_{B_s} |V_{ts}V_{tb}|^2 S_0(x_t)\eta_{2B}\hat{B}_{B_s} f_{B_s}^2 \,. \tag{8.51}$$

Combining it with the SM expression for the branching ratio we obtain:

$$\mathcal{R}_{s\mu}^{\rm SM} = \frac{\tau_{B_s}}{1-y_s}\frac{3G_{\rm F}^2 m_W^2 \sin^4\theta_W}{4\pi^3}\frac{|C_{10}^{\rm SM}|^2}{S_0(x_t)\eta_{2B}\hat{B}_{B_s}} m_\mu^2 \sqrt{1-4\frac{m_\mu^2}{m_{B_s}^2}} \,. \tag{8.52}$$

Interestingly, the CKM elements fully drop out in the SM. Moreover, the decay constant also cancels out. Here, only the bag parameter survives and takes the value [135, 240]:

$$\hat{B}_{B_s} = (1.232 \pm 0.053) \,. \tag{8.53}$$

However, the Δm_s could also be affected by NP contributions. Including NP contributions, the term Δm_s can be written, as presented in Sec. 5.4.1, in the following form [81]:

$$\Delta m_s = \Delta m_s|_{\rm SM} \, \left|1 + \kappa_q e^{i\sigma_q}\right| , \tag{8.54}$$

where κ_s and σ_s denote NP parameters. Consequently, we now allow for NP effects in both branching ratio $\bar{\mathcal{B}}(B_s \to \mu^+\mu^-)$ and mass difference Δm_s. We obtain the generalised expression for $\mathcal{R}_{s\mu}$ as follows [81]:

$$\mathcal{R}_{s\mu} = \mathcal{R}_{s\mu}^{\rm SM} \times \frac{1 + \mathcal{A}_{\Delta\Gamma_s}^{\mu\mu} y_s}{1+y_s} \frac{|P_{\mu\mu}^s|^2 + |S_{\mu\mu}^s|^2}{\sqrt{1 + 2\kappa_s \cos\sigma_s + \kappa_s^2}} \,. \tag{8.55}$$

Here, due to the NP parameters κ_s and σ_s in $\mathcal{R}_{s\mu}$, a dependence on the CKM matrix elements is introduced. However, this dependence is much weaker than the one that we originally had. We highlight again the main advantage of our strategy, which is the fact that the leading dependence on the CKM factors in $\mathcal{R}_{s\mu}^{\rm SM}$, cancels out due to the ratio with respect to Δm_s.

Having introduced all the formulas, we can now finalise our analysis and determine the values of $\mathcal{R}_{s\mu}^{\rm SM}$ and $\mathcal{R}_{s\mu}$. Firstly, Eq. (8.52), leads to the numerical result [81]:

$$\mathcal{R}_{s\mu}^{\rm SM} = (2.22 \pm 0.10) \times 10^{-10}\,{\rm ps}\,, \tag{8.56}$$

which is similar to the result coming from the analysis presented in Ref. [317]

$$\mathcal{R}_{s\mu}^{\rm SM} = (2.042^{+0.083}_{-0.058}) \times 10^{-10}\,{\rm ps}\,. \tag{8.57}$$

Then, Eq. (8.50) combining the experimental measurements of branching ratio in Eq. (8.36) and the mass difference Δm_s in Eq. (5.73), we obtain:

$$\mathcal{R}_{s\mu} = (1.60 \pm 0.19) \times 10^{-10}\,. \tag{8.58}$$

Comparing the values of $\mathcal{R}_{s\mu}^{\rm SM}$ and $\mathcal{R}_{s\mu}$, utilising Eq. (8.55) and the results coming from the general, model-independent NP fit in Sec. 5.4.2, we obtain extra contours, thus constraints in the $|P|$–$|S|$ plane. These contours are denoted in Fig. 61 with green colour, and are presented for the inclusive, exclusive and hybrid case. Illustrating this alternative constraint in the $|P|$–$|S|$ plane, it becomes again clear that the choice of the CKM factor and the apex of the UT enters now only through NP in B_s^0–$\bar{B}_s^0$ mixing.

8.2.3 Utilising the $B_d^0 \to \mu^+\mu^-$ decay

So far, the considerations regarding NP studies have been presented for the $B_s^0 \to \mu^+\mu^-$ decay. In principle, they can also be applied to the $B_d^0 \to \mu^+\mu^-$ channel. However, as we already mentioned in the introduction of this Chapter, the matrix element which enters now is $|V_{td}|$ (instead of $|V_{ts}|$). $|V_{td}|$ is a factor of λ smaller than $|V_{ts}|$ in the Wolfenstein parametrization, leading to a suppression of λ^2 in the branching ratio. As a result, this channel is very rare and has not been observed yet. Only upper limits are provided by the LHCb [325], ATLAS [326] and CMS [323]. The most stringent result is the following upper bound [329]:

$$\bar{\mathcal{B}}(B_d \to \mu^+\mu^-) < 0.26 \times 10^{-9}\,. \tag{8.59}$$

In addition, a combined analysis with $B_s^0 \to \mu^+\mu^-$, as presented in [328], leads to the following average value of branching ratio:

$$\bar{\mathcal{B}}(B_d \to \mu^+\mu^-) = (0.56 \pm 0.70) \times 10^{-10}\,. \tag{8.60}$$

The uncertainty is still too big to draw any conclusions. It will be really interesting though to measure this decay and compare with the SM.

An interesting point is that we can combine the branching ratio information from both the $B_s^0 \to \mu^+\mu^-$ and the $B_d^0 \to \mu^+\mu^-$ channel. Creating the ratio of these branching fractions provides a determination of the UT side R_t. As we already discussed in Sec. 5.4.2, utilising the R_t and R_b sides, we are able to determine the UT apex without relying on information from the angle γ. This is important, in particular, when searching for possible NP effects entering the γ measurements.

However, using the sides R_b and R_t in the extraction of the apex of the UT, has a main limitation related to the determination of the R_t. Following Eq. (5.81), the R_t side depends on the ratio of CKM matrix elements $|V_{td}/V_{ts}|$. The processes which are used to determine R_t can also be affected by NP contributions. Exploring this situation in Sec. 5.4.2, we determined the matrix elements ratio using the B_q^0–$\bar{B}_q^0$ mixing parameters. Here, we study the determination of R_t with the help of the rare decays $B_q^0 \to \mu^+\mu^-$.

Our starting point is to use the SM expressions of the $B_s^0 \to \mu^+\mu^-$ branching fractions given in Eqs. (8.11) and (8.12). Analogous relations can be written for the $B_d^0 \to \mu^+\mu^-$ mode which allows us to calculate the ratio of these branching fractions. In order to avoid the $|V_{td}/V_{ts}|$ dependence, we recall the definition of the R_t side in Eq. (5.81) and consequently, rewrite $|V_{td}/V_{ts}|$ in terms of the R_t. As a result, we obtain the following ratio [81]:

$$\left.\frac{\bar{\mathcal{B}}(B_d \to \mu^+\mu^-)}{\bar{\mathcal{B}}(B_s \to \mu^+\mu^-)}\right|_{\rm SM} = \lambda^2 R_t^2 \left[1 + \frac{\lambda^2}{2}\,(1-2\bar{\rho})\right]^2 \frac{\sqrt{m_{B_d}^2 - 4m_\mu^2}}{\sqrt{m_{B_s}^2 - 4m_\mu^2}} \frac{f_{B_d}^2}{f_{B_s}^2} \frac{1-y_s}{1-y_d}\,. \tag{8.61}$$

Regarding the values of R_t, we use those that we determined from our previous UT analysis in Sec. 5.4.2. These values correspond to the $\bar{\eta}$ and $\bar{\rho}$ solutions presented in Table 7, thus arising from the fit to the R_b and R_t sides of the UT. These R_t values are collected now in Table 17. Concerning the ratio of the decay constants, we use $f_{B_s}/f_{B_d} = 1.209 \pm 0.005$ [135]. Therefore, using the numerical values of the parameters entering Eq. (8.61), we obtain the SM ratio of the branching ratios of the leptonic decays for all three cases; inclusive, exclusive and hybrid. We collect the corresponding results in Table 17. We observe that within the current precision, the differences between these three cases are negligible.

Comparing now the SM values with the experimental result [328]

$$\frac{\bar{\mathcal{B}}(B_d \to \mu^+\mu^-)}{\bar{\mathcal{B}}(B_s \to \mu^+\mu^-)} = 0.019 \pm 0.024\,, \tag{8.62}$$

where the average branching ratio of the $B_d \to \mu^+\mu^-$ in Eq. (8.60) has been used, we find

Case	R_t	$\left.\frac{\bar{\mathcal{B}}(B_d \to \mu^+\mu^-)}{\bar{\mathcal{B}}(B_s \to \mu^+\mu^-)}\right\|_{\rm SM}$
Inclusive	0.910 ± 0.012	0.0282 ± 0.0019
Exclusive	0.909 ± 0.012	0.0281 ± 0.0018
Hybrid	0.909 ± 0.012	0.0281 ± 0.0017

Table 17: Results for the ratios $\left.\frac{\bar{\mathcal{B}}(B_d \to \mu^+\mu^-)}{\bar{\mathcal{B}}(B_s \to \mu^+\mu^-)}\right\|_{\rm SM}$ for the inclusive, exclusive and hybrid case. These ratios are calculated using the R_t values for all three cases, which we obtained from our previous analysis in Sec. 5.4.2, as discussed in the text.

an uncertainty of 125%. This result would then lead to the following value of R_t:

$$R_t = 0.77 \pm 0.48\,, \tag{8.63}$$

which has an uncertainty of the factor 40 larger than the values of R_t given in Table 17. The precision on the ratio of branching fractions scales with the precision on R_t^2. This indicates that more precise measurements of the branching ratios of the rare leptonic decays in the future will allow us to further explore the NP studies in B_q^0–$\bar{B}_q^0$ mixing.

8.2.4 Future Prospects

It becomes clear from the discussion above that the ratio of the branching fractions of the $B_s^0 \to \mu^+\mu^-$ and the $B_d^0 \to \mu^+\mu^-$ decays provides an alternative way to determine the UT side R_t. However, as we have already presented in Sec. 5.4.2, where we obtained R_t utilising Δm_d and Δm_s measurements, additional assumptions about flavour universal NP (FUNP) are required, so that the ratios of B_d and B_s observables still remain SM-like. Thus, it is not sufficient to allow for a general model-independent strategy for searching for NP.

The current experimental uncertainties though are still very large to allow us to fully explore this alternative determination of the R_t side. In the future, LHCb expects to reduce the branching fractions uncertainties on the ratios of the leptonic decays. More specifically, they expect a reduction on the uncertainty on the ratio of branching fractions to 34% by 2025 and to 10% by the end of the HL-LHC era [228]. We can illustrate the potential of the upgrade programme of the LHCb collaboration. For this purpose, we will now not consider

the SM values of R_t in Table 17. Instead, we will assume the following

$$R_t = 0.932 \pm 0.024 \quad \text{Inclusive}, \tag{8.64}$$

$$R_t = 0.930 \pm 0.021 \quad \text{Exclusive}, \tag{8.65}$$

$$R_t = 0.930 \pm 0.021 \quad \text{Hybrid}. \tag{8.66}$$

These are the SM values of R_t calculated from $\bar{\rho}$ and $\bar{\eta}$ given in Table 2, hence the solutions of the UT apex determined through the side R_b and the angle γ, as discussed in Sec. 3.4.2. Therefore, the future prospects for the side R_t are [81]:

$$R_t = 0.93 \pm 0.16\,(2025)\,, \tag{8.67}$$

$$R_t = 0.931 \pm 0.047\,(\text{Upgrade II})\,. \tag{8.68}$$

The main uncertainties still come from the measurements of the branching fractions while all the other uncertainties combined contribute only at the level of 1% level, thus they can be neglected.

Another useful application of the ratios of the branching fractions of the leptonic B_d and B_s modes is the following quantity [303]:

$$U_{\mu\mu}^{ds} \equiv \sqrt{\frac{|P_{\mu\mu}^d|^2 + |S_{\mu\mu}^d|^2}{|P_{\mu\mu}^s|^2 + |S_{\mu\mu}^s|^2}}\,, \tag{8.69}$$

$$= \left[\frac{\tau_{B_s}}{\tau_{B_d}} \frac{1-y_d^2}{1-y_s^2} \frac{1+\mathcal{A}_{\Delta\Gamma}^d y_d}{1+\mathcal{A}_{\Delta\Gamma}^s y_s} \frac{\sqrt{m_{B_s}^2 - 4m_\mu^2}}{\sqrt{m_{B_d}^2 - 4m_\mu^2}} \left(\frac{f_{B_s}}{f_{B_d}}\right)^2 \left|\frac{V_{ts}}{V_{td}}\right|^2 \frac{\bar{\mathcal{B}}(B_d \to \mu^+\mu^-)}{\bar{\mathcal{B}}(B_s \to \mu^+\mu^-)}\right]^{1/2}. \tag{8.70}$$

Therefore, presenting it in a compact way:

$$U_{\mu\mu}^{ds} \propto \left[\left|\frac{V_{ts}}{V_{td}}\right|^2 \frac{\bar{\mathcal{B}}(B_d \to \mu^+\mu^-)}{\bar{\mathcal{B}}(B_s \to \mu^+\mu^-)}\right]^{1/2}, \tag{8.71}$$

we observe that it requires knowledge of the side R_t via the term $|V_{ts}/V_{td}|$. The main advantage of using this ratio compared to the individual branching ratios of the leptonic modes is that common parameters and uncertainties drop out. Within the SM, the quantity $U_{\mu\mu}^{ds}$ is equal to 1, offering a very powerful test of the SM, as any deviation from 1 would be a hint of NP.

8.2.5 Testing Lepton Flavour Universality with Semileptonic $b \to s\ell^+\ell^-$ Modes

Before closing this Chapter, we make a small parenthesis and present a recent highlight related to the analysis of the rare semileptonic B decays, which are mediated by $b \to s\ell^+\ell^-$ transitions. An important feature of the SM is the Lepton Flavour Universality (LFU), hence the universality of electroweak couplings across different lepton flavours.

A very useful and theoretically clean observable which plays a key role in testing the LFU is the ratio $R_{K^{(*)}}$ which combines information from the $B \to K^{(*)}\mu^+\mu^-$ and $B \to K^{(*)}e^+e^-$ channels.[71] It is defined as follows:

$$\langle R_K \rangle \equiv \frac{\Gamma(B^- \to K^-\mu^+\mu^-) + \Gamma(B^+ \to K^+\mu^+\mu^-)}{\Gamma(B^- \to K^-e^+e^-) + \Gamma(B^+ \to K^+e^+e^-)}. \tag{8.72}$$

In an analogous way, we define R_{K^*}. In the SM, this ratio is equal to 1 with excellent precision. The data used to indicate values for $R_{K^{(*)}}$ in the regime of 0.8, hence suggesting a deviation from the SM at the level of 3 σ. This would be a hint of electron-muon universality violation in the SM.

However, in December 2022, new results were reported by the LHCb Collaboration which were compatible with 1 [144, 314]:

$$\langle R_K \rangle = 0.949 \pm 0.05, \quad \text{for momentum transfer } q^2 \in [1.1, 6.0] \text{ GeV}. \tag{8.73}$$

A similar pattern was found for the R_{K^*}. These results seem to agree with LFU, bringing new perspectives for testing the electron-muon universality. On the other hand, the differential rates for $B \to K\mu^+\mu^-$, which are experimentally not updated yet, are still too low with respect to the SM predictions. Deviations at the level of $3.5\,\sigma$ level have been found in comparison with the state-of-the-art calculations. This still suggests possible NP through these decays.

Hence, it is important to search how much space for electron-muon universality violation is possibly still left for this NP, which is now constrained by $\langle R_K \rangle$. Ref. [146] indicates that there is still significant room for violating the electron-muon universality, if there is CP-violating NP entering. In the future, it would be important to perform experimental studies focusing on differences in the CP asymmetries between the $b \to se^+e^-$ and $b \to s\mu^+\mu^-$ modes in order to test LFU.

[71] We note that the $R_{K^{(*)}}$ observable is one of the two cases for testing possible violation of LFU. The second case refers to the ratio $R(D^{(*)})$ which we already presented in Sec. 3.4.3.

8.3 Summary

In this Chapter, we have discussed the rare leptonic decays $B_q^0 \to \mu^+\mu^-$, which are excellent probes for searches of NP. We set up the theoretical framework, highlighting again that this is the simplest class of B decays. Particularly interesting is the sensitivity to non-SM pseudoscalar and scalar sectors, which may lift the helicity suppression. Useful observables are the branching ratios and the $\mathcal{A}_{\Delta\Gamma_s}^{\mu\mu}$.

Throughout this thesis, and especially in Chapters 3 and 5, we have explicitly pointed out how the discrepancies between the different determinations of the CKM factors have an impact on both the UT apex determination and the searches of NP in B_q^0–$\bar{B}_q^0$ mixing. Here, we studied how they affect other interesting NP searches, focusing on the branching ratio of the $B_s^0 \to \mu^+\mu^-$ modes.

As a first step, we introduced the ratio between the experimental and the SM branching fractions of the $B_s^0 \to \mu^+\mu^-$ decay. We determined its value for the inclusive, exclusive and hybrid CKM determination. We explored how our choice of the CKM input values was reflected on the $|P|$–$|S|$ plane. As a result, we obtained constraints on the allowed space for the pseudoscalar and scalar NP contributions in the leptonic decays, coming from the branching ratio. Key role in constraining this parameter space plays the $\mathcal{A}_{\Delta\Gamma_s}^{\mu\mu}$ observable. Recent pioneering measurements linked to the effective lifetime of the $B_q^0 \to \mu^+\mu^-$ channel allow the determination of the $\mathcal{A}_{\Delta\Gamma_s}^{\mu\mu}$. Unfortunately, the uncertainties are currently too large to draw any conclusion but in the future, it will be important to obtain improved measurements.

Given that the branching ratio depends on $|V_{cb}|$, our next goal was to eliminate its dependence when allowing for NP. For this purpose, we utilised the ratio of the branching ratio of the $B_s^0 \to \mu^+\mu^-$ mode with respect to the mass difference Δm_s. In the SM, the dependence on the CKM factors cancels in this ratio. However, the mixing parameter Δm_s could in principle be affected by NP. Therefore, we generalised our approach in order to include possible NP effects to B_s^0–$\bar{B}_s^0$ mixing. As a result, the NP parameters κ_s and σ_s appeared in the ratio $\mathcal{R}_{s\mu}$. Due to these NP parameters, a dependence on CKM matrix elements entered. However, the dependence on the CKM matrix elements is weaker now. Making use of our numerical results, coming from our most general analysis for the NP parameters in Chapter 5, we obtained alternative constraints on the $|P|$–$|S|$ plane for the inclusive, exclusive and hybrid case. Therefore, following this strategy, the CKM parameters and the apex of UT enter only via NP in B_s^0–$\bar{B}_s^0$ mixing.

So far, this analysis has been performed in the $B_s^0 \to \mu^+\mu^-$ channel. In principle, we can follow the same methodology in $B_d^0 \to \mu^+\mu^-$. However, here we do not have access to $\mathcal{A}_{\Delta\Gamma_s}^{\mu\mu}$ since $\Delta\Gamma_d$ is tiny. This channel has not been observed yet. It will be important in the future

to have accurate branching ratio data, so to be able to apply the above considerations here as well. Ratios of the branching fractions of $B_d^0 \to \mu^+\mu^-$ and $B_s^0 \to \mu^+\mu^-$ in the SM are also interesting players. These ratios provide an alternative determination of the UT side R_t. Current experimental uncertainties related to the branching fractions are unfortunately too large. However, more precise experimental searches in the future will allow us to further explore studies of NP in the B_q^0–$\bar{B}_q^0$ mixing. Last but not least, we introduced another interesting quantity $U_{\mu\mu}^{ds}$, which is proportional to this ratio as well as to $|V_{ts}/|V_{td}|$. Since in the SM, this quantity is equal to 1, it can be utilised as a powerful test of the SM by determining its value and comparing with the SM.

Our Decays Roadmap - Highlights

Decays with Different Dynamics

UT
Important to study inclusive & exclusive cases separately for $|V_{ub}|$ & $|V_{cb}|$

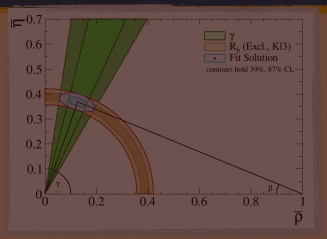

$B_d \to J/\psi K_S$, $B_s \to J/\psi\phi$

Performing combined fit with their control channels
↓
allows the determination of the mixing phases $\phi_{d,s}$
including the impact of penguins on CP asymmetries

CP Violation in different manifestations

$B_s \to D_s^{\pm} K^{\mp}$ & related modes

- Intriguing puzzles in CP violation and in branching ratio
- Utilising our model independent strategy in high precision era of B physics ⟶ may establish new sources of CP Violation

$B \to \pi K$

These modes also indicate interesting puzzles

- Highlights
- Key mode $B_d^0 \to \pi^0 K_S$: the only one exhibiting mixing-induced CP asymmetry $\xrightarrow{\text{obtain correlations}} A_{CP}^{\pi^0 K_S} - S_{CP}^{\pi^0 K_S}$
- New Belle II measurement of $A_{CP}^{\pi^0 K_S}$, $S_{CP}^{\pi^0 K_S}$ — Might resolve $B \to \pi K$ puzzle
- New Strategy for extracting ϕ, q — EW penguin parameters

Rare Decays $B_q^0 \to \mu^+\mu^-$

CP Violation: also interesting here

- Highlights
- Branching ratio

$$R_{s\mu} = \bar{\mathbf{B}}\left(B_s \to \mu^+\mu^-\right)/\Delta m_s$$

→ minimises leading dependence on $|V_{cb}|$ when allowing for New Physics in the (Pseudo)-Scalar sector

- $A_{\Delta\Gamma_s}^{\mu\mu}$: next interesting observable but we need better measurements
- Future: CP violation searches with mixing-induced CP asymmetry
- $B_d \to \mu^+\mu^-$ can also offer useful applications but is not measured yet

9 Conclusions

As demonstrated throughout this thesis, studies of CP violation and searches of physics beyond the SM through decays of B mesons are at the core of quark flavour physics. In order to have a clear picture of the theoretical framework, we have provided a detailed overview of the SM description of CP violation and discussed the dynamics of the B-meson system. Working at the high precision frontier, we have explored CP violation and have been searching for indirect signals of NP through benchmark B decays. Theoretical approaches, such as effective field theories, are powerful tools in the analysis of these decays, both within the SM and for accounting NP contributions. Utilising the B transitions and their observables, we have suggested strategies, which are very promising and have revealed exciting future prospects. In this Chapter, we summarise the key findings of our studies.

We have emphasized that CP violation manifests itself in different ways. This allows us to categorise the different decays according to their dynamics. Examining CP violation in every category from a theoretical perspective, we gained useful insights and presented highlights that may also point towards possible hints of NP. Consequently, we have discussed:

- decays which are *dominated by tree* topologies but also receive important corrections from penguins, such as the $B^0_d \to J/\psi K^0_S$ and $B^0_s \to J/\psi\phi$ modes,
- *pure tree* transitions, like the $B^0_s \to D^\mp_s K^\pm$ system and modes with similar dynamics,
- decays that are *dominated by penguin* topologies, like the $B \to \pi K$ system,
- rare processes arising from *EW penguins and box topologies*, i.e. $B^0_q \to \mu^+\mu^-$.

This outline represents our main research pillars.

The first category refers to the $B^0_d \to J/\psi K^0_S$ and $B^0_s \to J/\psi\phi$ channels, which are the "golden modes" for analysing CP violation in B decays. Involving neutral B^0_q mesons, B^0_q–$\bar{B}^0_q$ mixing provides interesting interference effects. The mixing phases ϕ_q, which are associated to this phenomenon, have played a key role in our analysis. Both $B^0_d \to J/\psi K^0_S$ and $B^0_s \to J/\psi\phi$ are colour-suppressed tree modes with penguin contributions, which are doubly-Cabibbo suppressed. The theoretical precision of the ϕ_q phases is limited by the presence of these penguin effects. However, we have reached a level of sophistication, where hadronic uncertainties from the doubly Cabibbo-suppressed penguin topologies must be

included for proper interpetation of the data. Since we cannot calculate these contributions from first principles, we use control channels, more specifically the $B_d^0 \to J/\psi\pi^0$, $B_s^0 \to J/\psi K_S^0$ and $B_d^0 \to J/\psi\rho^0$ modes, which do not suffer from this suppression. We have developed a combined strategy of the original two modes and their control channels, employing the $SU(3)$ flavour symmetry of strong interactions. This analysis utilises information from the mixing-induced CP asymmetries, which depends on the ϕ_q phases. As a result, the strategy allows us to determine the mixing phases, properly including the impact of the penguin effects on the CP asymmetries. In this way, we obtain state-of-the-art values of these phases.

These mixing phases, in particular ϕ_d, play an important role, in the analysis of the UT. In order to put them into context, we have performed a determination of the UT apex that is considered to be robust with respect to NP. We have chosen to determine it via the angle γ and the side R_b, which depends on $|V_{ub}|$ and $|V_{cb}|$. These CKM matrix elements can be determined through methods utilising inclusive and exclusive semileptonic B-meson decays. Interestingly, there are deviations between the results arising from these two methods. This long-standing issue requires special attention. Consequently, we consider separately the inclusive and exclusive values of these parameters. In addition, we consider another hybrid case, combining exclusive $|V_{ub}|$ and inclusive $|V_{cb}|$ values. We have determined the UT apex by performing a fit to γ and R_b for all these three cases and have found sizeable differences between these determinations. A proper treatment, resolving these differences, is essential in order to identify NP contributions in future.

The UT apex enters the SM prediction for the B_q^0–$\bar{B}_q^0$ mixing parameters. Comparing the SM predictions with the experimental values, we explore the remaining space for NP effects in this phenomena. On the one hand, for the B_s system, an impressive precision for ϕ_s has been obtained. On the other hand, the SM prediction of ϕ_d suffers from significant uncertainties. Introducing NP parameters κ_q and σ_q for the size of NP effects and the phase for additional CP-violating effects, respectively, we have performed fits exploring the available space for NP in B_q^0–$\bar{B}_q^0$ mixing. Making future projections, we have shown that NP searches in the B_s system are more promising than the B_d for testing the SM. However, we are interested in constraining NP as much as possible in both systems. Future prospects of improvement are also related to the angle γ of the UT.

Discussing other perspectives of decays of a B_q^0 meson into J/ψ (vector) and a P (pseudoscalar) meson, the branching ratio of these modes plays also an important role. We have proposed a method where we have combined this observable from $B_s^0 \to J/\psi K_S^0$ and $B_d^0 \to J/\psi\pi^0$ channels with information from the branching fractions of their semileptonic partner modes; $B_s^0 \to K^-\ell^+\nu_\ell$ and $B_d^0 \to \pi^-\ell^+\nu_\ell$. This method allows the extraction of the colour-suppression factor $|a_2|$ in a theoretically clean way. Comparing the resulting

values with naive factorisation, we have found that they are in the ballpark of theoretical predictions. This is a surprising finding, suggesting that factorisation in the colour-suppressed modes works better than naively expected. This also gives us confidence that non-factorisable $SU(3)$ breaking corrections for the penguin effects should be under control. When moving to higher precision, this strategy can be used to further explore the impact of these non-factorisable $SU(3)$ breaking effects, providing valueable insights into the physics of strong interactions.

The second category we discussed is given by pure tree decays, i.e., the $B_s^0 \to D_s^\mp K^\pm$ system. This analysis is of central importance in this thesis. These $B_s^0 \to D_s^\mp K^\pm$ decays allow a theoretically clean extraction of the UT angle γ, despite being non-leptonic decays. This system reveals two puzzling cases, which are connected to each other. The first puzzle is in CP violation measurements, reflected by the γ angle. Comparing the experimentally measured γ value with the one coming from the global UT analyses, deviations arise. Should this puzzle eventually be confirmed by future data, we would have a "smoking-gun" signal of CP-violating NP at the amplitude level. If there are NP effects entering at the decay amplitude, they should also manifest themselves in the branching ratios, which suggests the second puzzle. The phenomenological colour factor $|a_1|$ is the key quantity.

The $|a_1|$ factor is determined theoretically using the framework of factorisation. Factorisation is expected to work very well for the $b \to c$ transitions. Introducing the ratio between the branching fractions of the non-leptonic $\bar{B}_s^0 \to D_s^+ \ell \bar{\nu}_\ell$ decay and its semileptonic partner $\bar{B}_s^0 \to D_s^+ \ell \bar{\nu}_\ell$, we have determined the experimental values of $|a_1|$ in a clean way from the data. We follow the same strategy in other $b \to c$ decays with similar dynamics, and extract the corresponding experimental $|a_1|$. Comparing these $|a_1|$ values, we have found intriguing deviations up to 4.8σ, with the experimental results being surprisingly small with respect to the theoretical ones. Interestingly, a similar pattern appears in $b \to u$ transitions, such as $B_s^0 \to D_s^- K^+$ and similar modes, despite factorisation being on less solid ground in this case. Here the uncertainties involved are still very large though, so that we cannot yet draw any further conclusions.

In view of these puzzling patterns, we have allowed for NP and presented a model-independent strategy in order to include such NP effects with new sources of CP violation. We have generalised the expressions that provide the extraction of γ utilising the CP-violating observables. Regarding direct CP asymmetries, LHCb asumed that $C = -\bar{C}$, which holds in the SM. However, we have seen that this assumption can be affected by NP. Hence, we have generalised this relation in a way that it also holds in the presence of NP effects. Introducing NP parameters, we have applied our strategy to the current data and obtained correlations between these parameters. NP effects are found to be strongly

correlated and could have large CP-violating phases. We have shown that NP effects of moderate size could accommodate the data. It will be exciting to see how the data will evolve in the future and whether it will be possible to finally establish new sources of CP violation exploiting our strategy.

The third category refers to decays which are penguin dominated. The main focus here is on the $B \to \pi K$ system, which is another non-leptonic system of decays. They are dominated by QCD penguins but EW penguins, and especially the colour-allowed ones, play also a prominent role. Hence, we have paid special attention to the EW penguin sector. For studies of CP violation, the most interesting $B \to \pi K$ channel is $B_d^0 \to \pi^0 K_S$, which is the only mode exhibiting mixing-induced CP violation. Thus, measuring CP violation in this channel with highest precision is particularly interesting.

Isospin relations between charged and neutral $B \to \pi K$ decay amplitudes can be utilised in order to obtain correlations between the mixing-induced and the direct CP asymmetry of the $B_d^0 \to \pi^0 K_S$ channel. These correlations set a particularly clean reference in the SM. Eliminating discrete ambiguities, only one solution finally survives. This solution following from the isospin analysis turns out to show tension with the measurement. In order for this puzzle to be resolved, either the experimental data should "move" in order to become consistent with the SM, or NP effects in the EW penguin sector should be present. Interestingly, a new Belle II measurement of the CP asymmetries of this channel has recently been reported, which moved towards the SM prediction. It will be very interesting to follow the future experimental developments. Will the long-standing $B \to \pi K$ puzzle finally be resolved or will we find NP in the EW penguin sector?

Concerning NP searches in this channel, EW penguins offer an interesting way for effects of new particles to enter. Introducing parameters q and ϕ, which characterise these penguin topologies, we have proposed a new strategy to extract their values from the data. Applying this strategy to a future benchmark scenario, we have found that the experimental precision can match the theoretical predictions. This shows how powerful this method is. In the future, with data from Belle II and the LHCb Upgrade(s), this method can offer useful insights into the EW penguin sector and finally, either confirm the SM or reveal NP with new sources of CP violation.

The last category focuses on rare decays which are pure loop processes. In this thesis, we have explored the purely leptonic and very clean $B_q^0 \to \mu^+\mu^-$ system. Our main focus is on studies of NP. In this respect, we get a nice application of the constraints on NP in B_q^0–$\bar{B}_q^0$ mixing.

The first important observable is the branching ratio, which exhibits helicity suppression

in the SM. Interestingly, this suppression could be lifted by new (pseudo)-scalar contributions. Thus, NP may enhance or reduce the branching ratio, which depends on $|V_{ts}|$. Utilising unitarity relations, this CKM element is determined through $|V_{cb}|$ and the apex of the UT. Consequently, NP searches with branching ratios also depend on $|V_{cb}|$ and the UT apex (which plays a minor role entering only via higher order corrections), thereby yielding again dependence on inclusive and exclusive determinations. In other words, CKM parameters have an impact on NP studies. In order to determine NP in the (pseudo)-scalar sector, it is essential to minimise this dependence on the CKM parameters.

For this purpose, key quantity is the ratio between the $B_s^0 \to \mu^+\mu^-$ branching ratio and the mixing parameter Δm_s. In the SM, the CKM elements drop out. However, we have to allow for possible NP in B_q^0–$\bar{B}_q^0$ mixing. Hence, we have included NP effects in Δm_s, using our NP results on B_q^0–$\bar{B}_q^0$ mixing, and generalised the above mentioned ratio. This allows us to constrain the (pseudo)-scalar parameters. Similar considerations can be applied to the $B_d^0 \to \mu^+\mu^-$ mode. However, this channel has not been observed yet and only upper bounds on the decay rate are currently available. In the future, it will be exciting to measure the branching fraction of this mode, and to compare with the one from $B_s^0 \to \mu^+\mu^-$ exploring the ratio of these two branching ratios.

The second interesting observable for constraining NP is $\mathcal{A}_{\Delta\Gamma_s}^{\mu\mu}$. Recent measurements of the effective lifetime $\tau_{\mu\mu}^s$ by ATLAS, CMS and LHCb allow us to convert these values into bounds on $\mathcal{A}_{\Delta\Gamma_s}^{\mu\mu}$. However, unfortunately, the current uncertainties are too large to draw further conclusions and we need improved measurements in the future. Concerning the $B_d \to \mu^+\mu^-$ mode, we do not have access to $\mathcal{A}_{\Delta\Gamma_s}^{\mu\mu}$, since $\Delta\Gamma_d$ is negligibly small.

In the future, it will be important to focus on the topic of CP violation, which is also very interesting in these rare leptonic decays but has not received a lot of attention. As already suggested in the literature, e.g., in Ref. [313], the mixing-induced CP asymmetry will play a central role in this endeavour. Finally, regarding other rare decays, semileptonic modes offer also very useful insights, including studies of CP violation.

Concluding, where do we stand now with our exploration of the flavour sector? Throughout this thesis, we have provided theoretical work that allows us to utilise experimental input and interpret measurements. This shows that theory and experiment are closely connected. The studies presented in this thesis are very promising for the future data taking, moving towards the high-precision frontier. The study of CP violation is particularly interesting, also in the context of NP. Hence, it is desirable to obtain improved measurements of CP violation for the channels we have discussed. The arising puzzling patterns could be indirect indications of NP. Moving towards higher and higher precision, the LHCb Upgrade(s) and Belle II are the key players in this quest. Our main goal is to perform the best testing of

the SM in this sector, bringing the analysis to a higher level of precision, and check whether these studies will finally allow us to establish new sources of CP violation.

Looking at the broader picture, if deviations from the SM are finally established in the future, this would be a spectacular result. The next question would be to explore specifically the underlying NP. In this case, further deviations would be expected to emerge in other observables and processes, and correlations would allow us to narrow down the underlying NP framework. Another central point would be: Can we also find directly new particles at colliders? Would the LHC be sufficient? Are the new particles so elusive that we have not observed them yet or do we have to move to the high–energy frontier? Such findings would be very interesting in the context of future collider physics studies, going beyond the LHC. This would open up a completely new era in particle physics research. Exciting times lie ahead – we should all stay tuned.

Our Decays Roadmap - Highlights

Decays with Different Dynamics

UT
Important to study
inclusive & exclusive cases
separately for $|V_{ub}|$ & $|V_{cb}|$

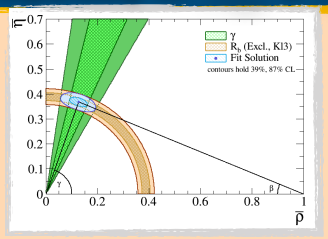

$B_d \to J/\psi K_S$, $B_s \to J/\psi\phi$

Performing combined fit with their control channels
↓
allows the determination of the mixing phases $\phi_{d,s}$
including the impact of penguins on CP asymmetries

CP Violation in different manifestations

$B_s \to D_s^{\pm} K^{\mp}$ & related modes

- Intriguing puzzles in CP violation and in branching ratio
- Utilising our model independent strategy in high precision era of B physics → may establish new sources of CP Violation

$B \to \pi K$

These modes also indicate interesting puzzles
- Highlights
- Key mode $B_d^0 \to \pi^0 K_S$: the only one exhibiting mixing-induced CP asymmetry $\xrightarrow{\text{obtain correlations}} A_{CP}^{\pi^0 K_S} - S_{CP}^{\pi^0 K_S}$
- New Belle II measurement of $A_{CP}^{\pi^0 K_S}$, $S_{CP}^{\pi^0 K_S}$ — Might resolve $B \to \pi K$ puzzle
- New Strategy for extracting ϕ, q — EW penguin parameters

Rare Decays
$B_q^0 \to \mu^+\mu^-$

CP Violation: also interesting here
- Highlights
- Branching ratio
$$R_{s\mu} = \bar{\mathbf{B}}\left(B_s \to \mu^+\mu^-\right)/\Delta m_s$$
→ minimises leading dependence on $|V_{cb}|$ when allowing for New Physics in the (Pseudo)-Scalar sector
- $A_{\Delta\Gamma_s}^{\mu\mu}$: next interesting observable but we need better measurements
- Future: CP violation searches with mixing-induced CP asymmetry
- $B_d \to \mu^+\mu^-$ can also offer useful applications but is not measured yet

Appendix

A Pauli and Gell-Mann Matrices

The Pauli matrices $\vec{\sigma} = [\sigma^1,\ \sigma^2,\ \sigma^3]$ are written as:

$$\sigma^1 = \begin{pmatrix} 0 & 1 \\ 1 & 0 \end{pmatrix}, \quad \sigma^2 = \begin{pmatrix} 0 & -i \\ i & 0 \end{pmatrix}, \quad \sigma^3 = \begin{pmatrix} 1 & 0 \\ 0 & -1 \end{pmatrix}. \tag{A.1}$$

The Gell-Mann matrices L_α are given as:

$$L_1 = \begin{pmatrix} 0 & 1 & 0 \\ 1 & 0 & 0 \\ 0 & 0 & 0 \end{pmatrix}, \quad L_2 = \begin{pmatrix} 0 & -i & 0 \\ i & 0 & 0 \\ 0 & 0 & 0 \end{pmatrix}, \quad L_3 = \begin{pmatrix} 1 & 0 & 0 \\ 0 & -1 & 0 \\ 0 & 0 & 0 \end{pmatrix}, \tag{A.2}$$

$$L_4 = \begin{pmatrix} 0 & 0 & 1 \\ 0 & 0 & 0 \\ 1 & 0 & 0 \end{pmatrix}, \quad L_5 = \begin{pmatrix} 0 & 0 & -i \\ 0 & 0 & 0 \\ i & 0 & 0 \end{pmatrix}, \quad L_6 = \begin{pmatrix} 0 & 0 & 0 \\ 0 & 0 & 1 \\ 0 & 1 & 0 \end{pmatrix}, \tag{A.3}$$

$$L_7 = \begin{pmatrix} 0 & 0 & 0 \\ 0 & 0 & -i \\ 0 & i & 0 \end{pmatrix}, \quad L_8 = \frac{1}{\sqrt{3}} \begin{pmatrix} 1 & 0 & 0 \\ 0 & 1 & 0 \\ 0 & 0 & -2 \end{pmatrix}. \tag{A.4}$$

B Q_k Operators

1) Current-Current Operators

$$Q_1^{jr} = (\bar{r}_\alpha j_\beta)_{V-A}(\bar{j}_\beta b_\alpha)_{V-A} \tag{B.1}$$

$$Q_2^{jr} = (\bar{r}_\alpha j_\alpha)_{V-A}(\bar{j}_\beta b_\beta)_{V-A} \tag{B.2}$$

2) QCD Penguin Operators

$$Q_3^r = (\bar{r}_\alpha b_\alpha)_{V-A} \sum_{q'} (\bar{q}'_\beta q'_\beta)_{V-A} \tag{B.3}$$

$$Q_4^r = (\bar{r}_\alpha b_\beta)_{V-A} \sum_{q'} (\bar{q}'_\beta q'_\alpha)_{V-A} \tag{B.4}$$

$$Q_5^r = (\bar{r}_\alpha b_\alpha)_{V-A} \sum_{q'} (\bar{q}'_\beta q'_\beta)_{V+A} \tag{B.5}$$

$$Q_6^r = (\bar{r}_\alpha b_\beta)_{V-A} \sum_{q'} (\bar{q}'_\beta q'_\alpha)_{V+A} \tag{B.6}$$

3) Ew Penguin Operators

$$Q_7^r = \frac{3}{2}(\bar{r}_\alpha b_\alpha)_{V-A} \sum_{q'} e_{\bar{q}'} (\bar{q}'_\beta q'_\beta)_{V+A} \tag{B.7}$$

$$Q_8^r = \frac{3}{2}(\bar{r}_\alpha b_\beta)_{V-A} \sum_{q'} e_{\bar{q}'} (\bar{q}'_\beta q'_\alpha)_{V+A} \tag{B.8}$$

$$Q_9^r = \frac{3}{2}(\bar{r}_\alpha b_\alpha)_{V-A} \sum_{q'} e_{\bar{q}'} (\bar{q}'_\beta q'_\beta)_{V-A} \tag{B.9}$$

$$Q_{10}^r = \frac{3}{2}(\bar{r}_\alpha b_\beta)_{V-A} \sum_{q'} e_{\bar{q}'} (\bar{q}'_\beta q'_\alpha)_{V-A} \tag{B.10}$$

We note that α and β are $SU_C(3)$ indices, $q' \in \{u, d, c, s, b\}$, $V \pm A$ refers to $\gamma_\mu(1 \pm \gamma_5)$ and the e_q denote the electrical charges.

C Puzzles in the Measurements of the $R(D)$ and $R(D^*)$ Ratios

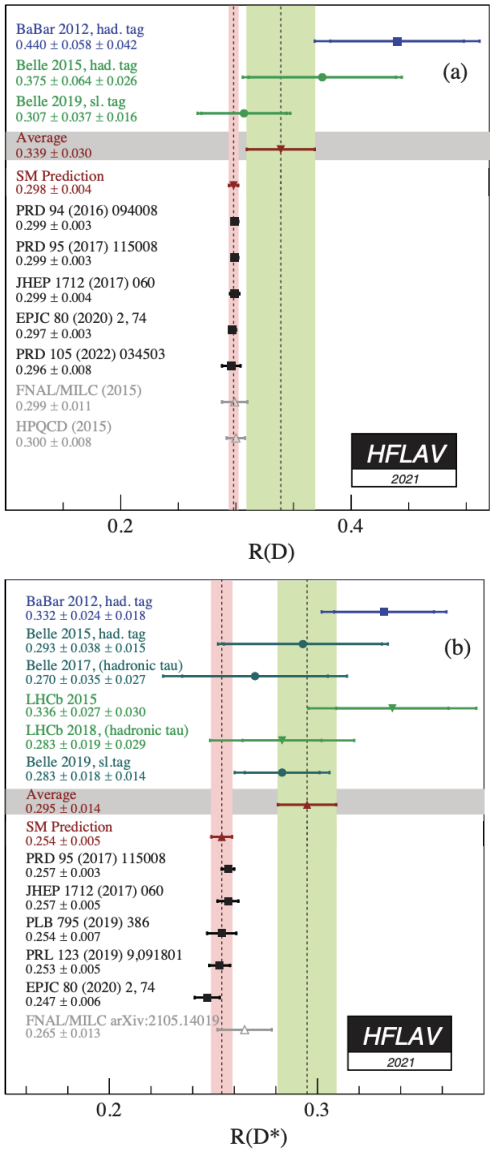

Figure 62: Measurements of the ratio $R(D)$ (left) and $R(D^*)$ (right) [11]. The green band corresponds to the current world average while the red band to the SM prediction suggesting the tension between theory and experiment.

D GammaCombo fits for the κ_q–σ_q NP parameters

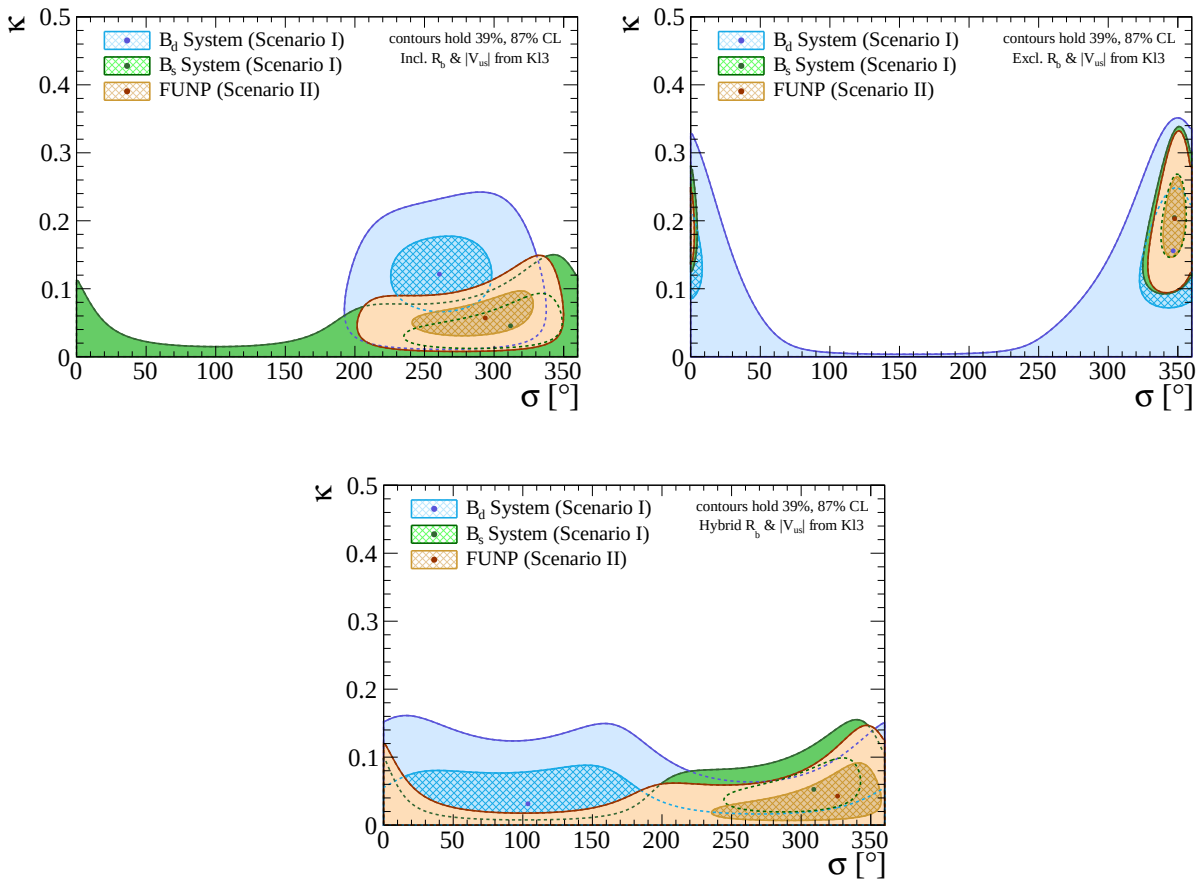

Figure 63: Comparison between the Scenario I (for the B_d and B_s system) and Scenario II fits for κ_q and σ_q, which parametrise NP contributions in B_q^0–$\bar{B}_q^0$ mixing for the inclusive (left), exclusive (right) and hybrid (bottom) case [124].

E Additional Illustrations Related to $B_s^0 \to D_s^{\mp} K^{\pm}$ System

E.1 Plot for the $|a_1|$ parameter

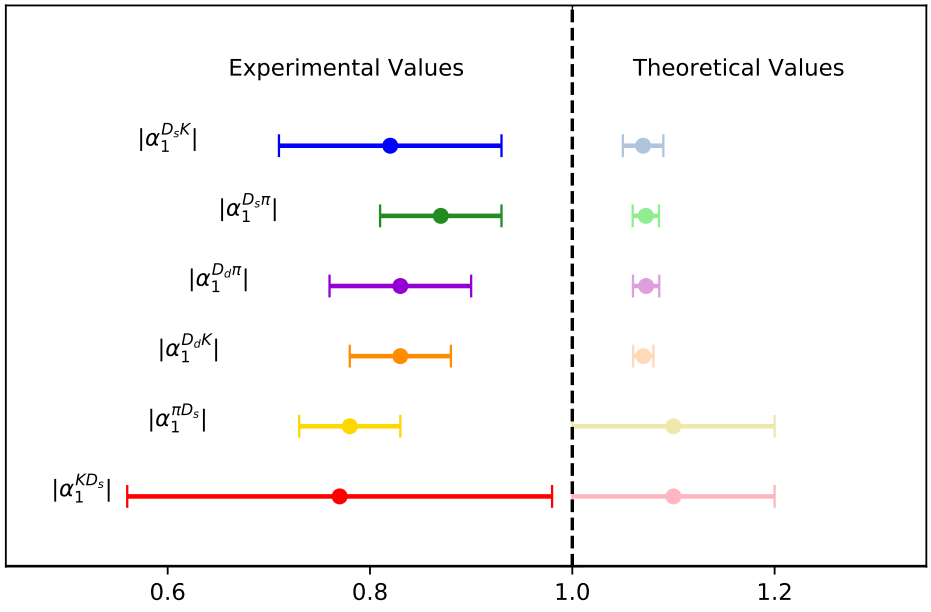

Figure 64: Comparing the $|a_1|$ experimental and theoretical SM values for various decay processes [115], as discussed in Chapter 6.

E.2 Different Scenarios for $\bar{\varphi}$, φ, $\bar{\rho}$, ρ Correlations in $B_s^0 \to D_s^{\mp} K^{\pm}$

Changing the central values of b and $\bar{b}$ observables

1. When $b = 1$ and $\bar{b} = 1$ (SM case)

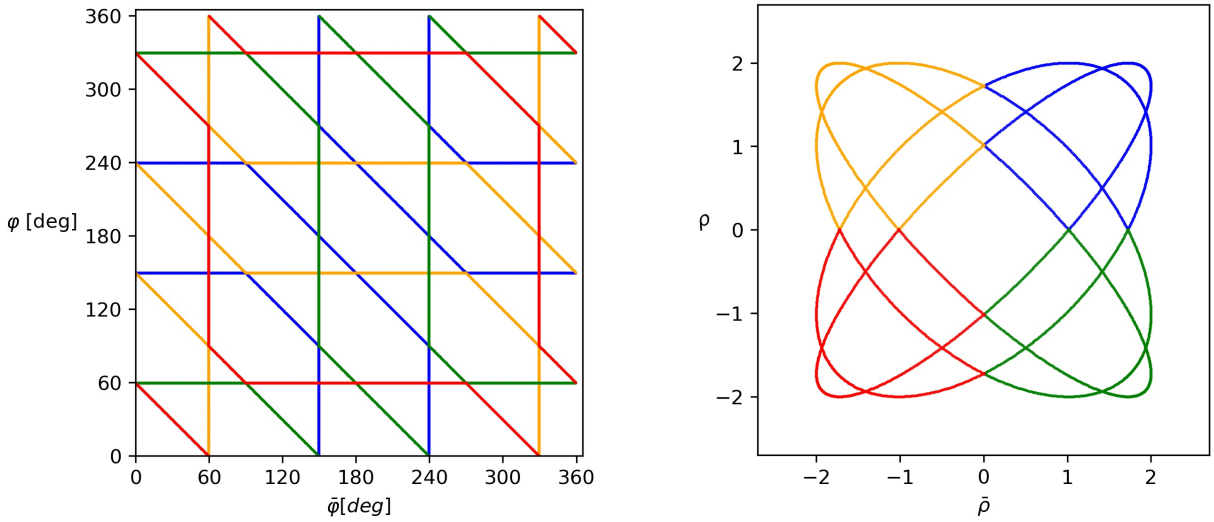

2. When $b = 1$ and $\bar{b} = 1.4$

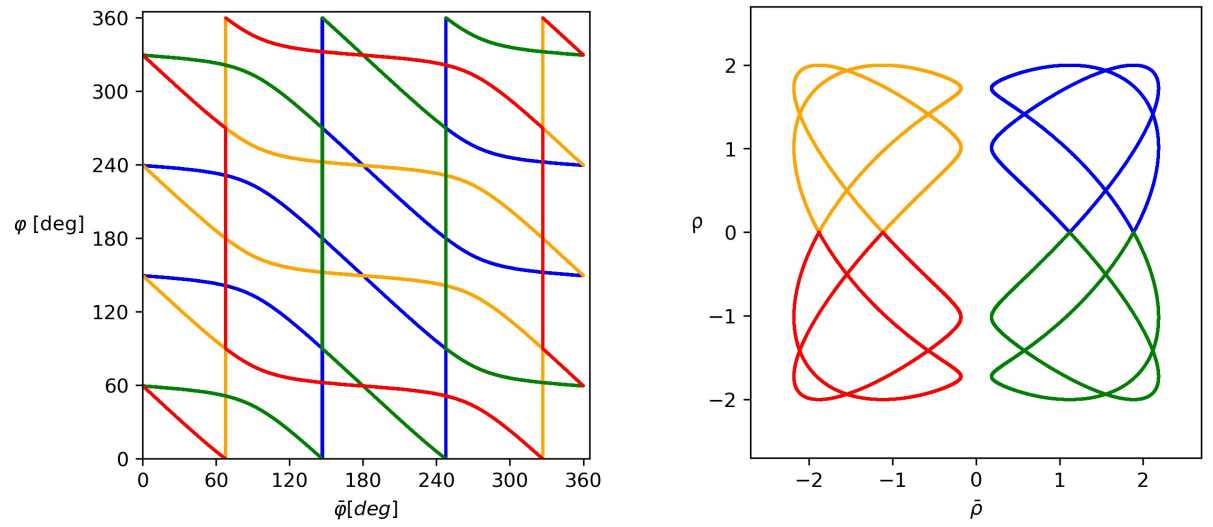

3. When $b = 1.4$ and $\bar{b} = 1$

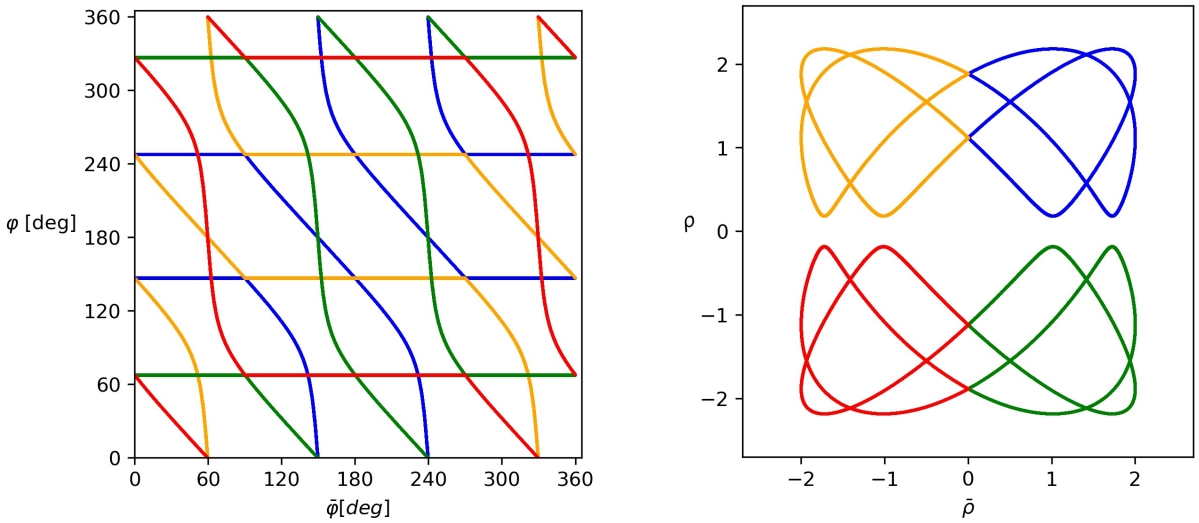

Comments

i. When both b and $\bar{b}$ are equal to 1, thus as in the SM case, we get connected lines in the $(\rho, \bar{\rho})$ plot.

ii. When b is 1 and $\bar{b}$ either greater or smaller than 1, we obtain a vertical "gap" area around $\bar{\rho} = 0$. The further we move away from 1 (either to bigger or to smaller values), the bigger the gap area becomes.

iii. On the other hand, when $\bar{b} = 1$ and b are either greater or smaller than 1, we get a horizontal "gap" area around $\rho = 0$. Similarly to the previous case, the gap gets bigger if we move away from 1.

iv. Finally, when neither b nor $\bar{b}$ is 1, there are no connected lines in the $\bar{\rho}$–ρ plane and we have "gaps" along both the ρ axis and the $\bar{\rho}$ axis (just like the plot we obtain for the current data in Fig. 41).

We also notice in all these cases that the points of 0^o and 180^o in the $\bar{\varphi}$–φ, as well as the (0,0) points on the $\bar{\rho}$–ρ plane, are not included. How can we approach the (0,0) point in the $(\rho, \bar{\rho})$ plot? In the way we have constructed the plots, we realise that even though ρ and $\bar{\rho}$ depend on b and $\bar{b}$, respectively, the values of ρ and $\bar{\rho}$ are derived from the pairs of φ and $\bar{\varphi}$, for which we obtain, following Eq. (6.201):

$$0 = \tan\Delta\varphi(1 + \rho\cos\varphi + \bar{\rho}\cos\bar{\varphi} + \rho\bar{\rho}\cos(\bar{\varphi} + \varphi)) - \rho\sin\varphi - \bar{\rho}\sin\bar{\varphi} - \rho\bar{\rho}\sin(\bar{\varphi} + \varphi).$$

Then, we check what changes in the determination of φ and $\bar{\varphi}$ and the only parameter that enters in their derivation is the $\tan(\Delta\varphi)$, thus the $\Delta\varphi$.

F Plots for the $B \to \pi K$ System

F.1 Constructing the neutral triangles

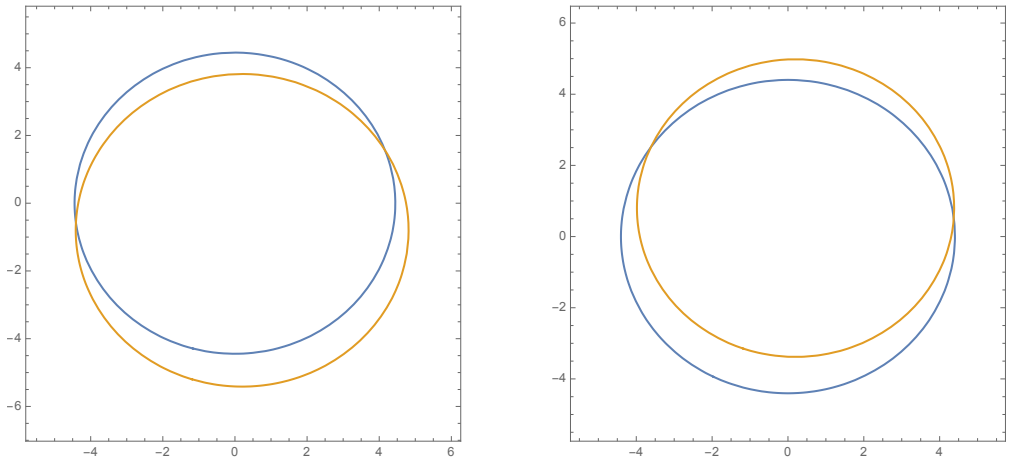

Figure 68: Circles providing the two A_{00} solutions (intersecting points) in the left panel and the $\bar{A}_{00}$ solutions for the CP-conjugate case in the right panel.

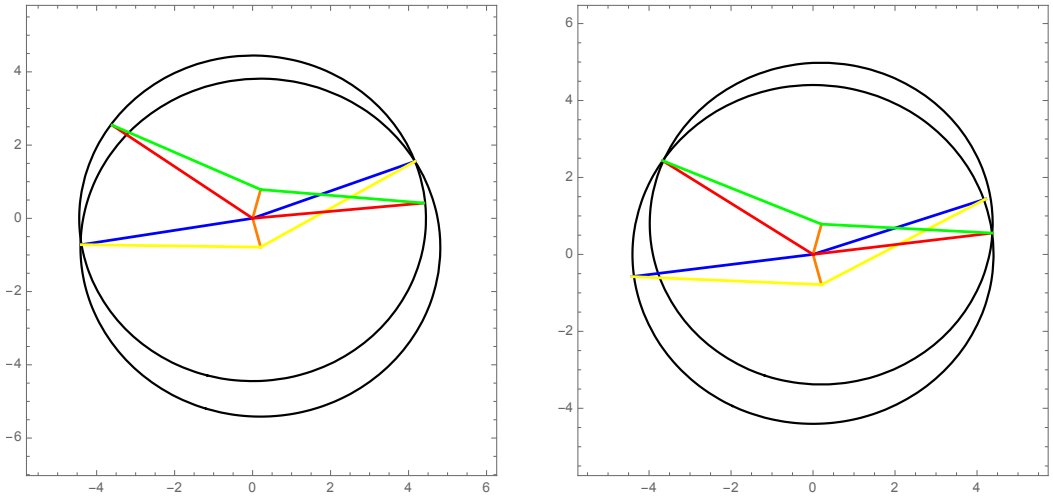

Figure 69: The drawing of the triangles with the help of the circles.

F.2 $S_{CP}^{\pi^0 K_S}$-$A_{CP}^{\pi^0 K_S}$ Correlations

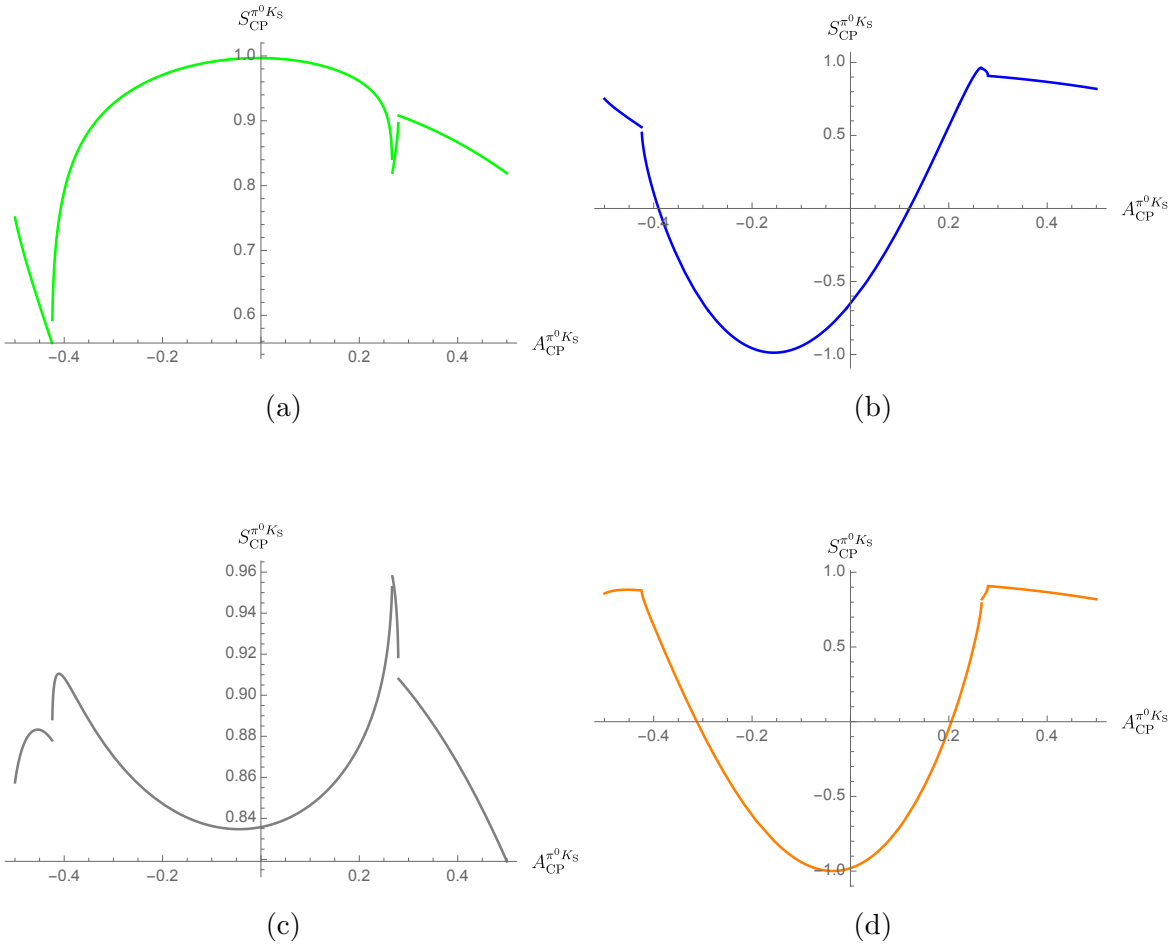

Figure 70: Correlations between $S_{CP}^{\pi^0 K_S}$ and $A_{CP}^{\pi^0 K_S}$ for the central values. The four branches correspond to the four different ϕ_{00} angles.

F.3 The angle $\phi_\pm$

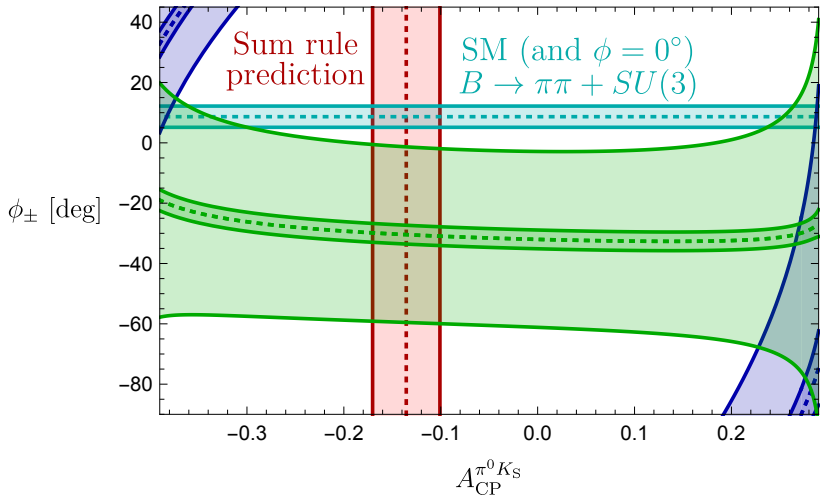

(a)

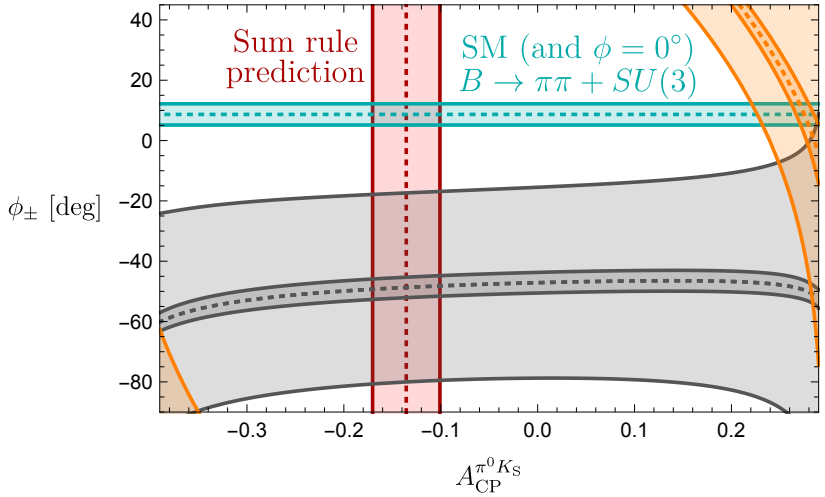

(b)

Figure 71: Angle $\phi_\pm$ in terms of the direct asymmetry for every triangle configuration [281]. The petrol horizontal band gives the constraint from the current SM prediction for the $\phi_\pm$ value in Eq. (7.130). The red vertical band shows the sum rule prediction. The colours correspond to the colours of the four ϕ_{00} angles, thus (a) includes the green and the blue band and (b) the grey and the orange. The narrow bands show a future theory scenario.

F.4 Constructing the charged triangles

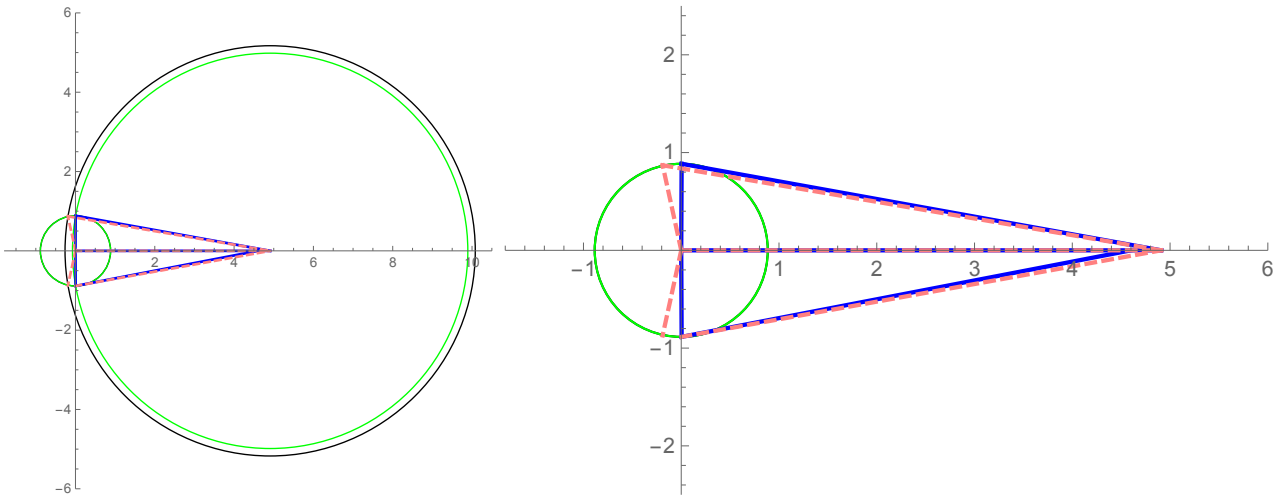

(a) (b)

Figure 72: (a) System of Eqs. (7.138)-(7.139) and the corresponding isospin triangles. (b) Zooming in to show the triangles for the central values of the charged $B \to \pi K$ decays.

F.5 Determination of the EW parameters q and ϕ

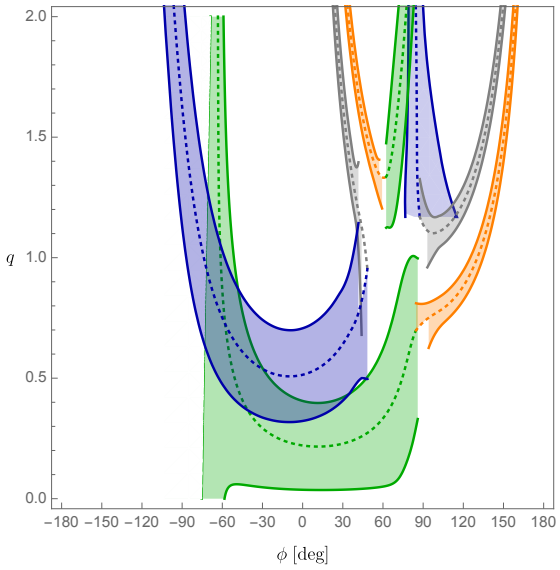

Figure 73: Contours in the ϕ-q plane following the triangle analysis for the charged $B \to \pi K$ decays, before imposing any constraints [281].

G CMS and LHCb combined results for $B_s^0 \to \mu^+\mu^-$

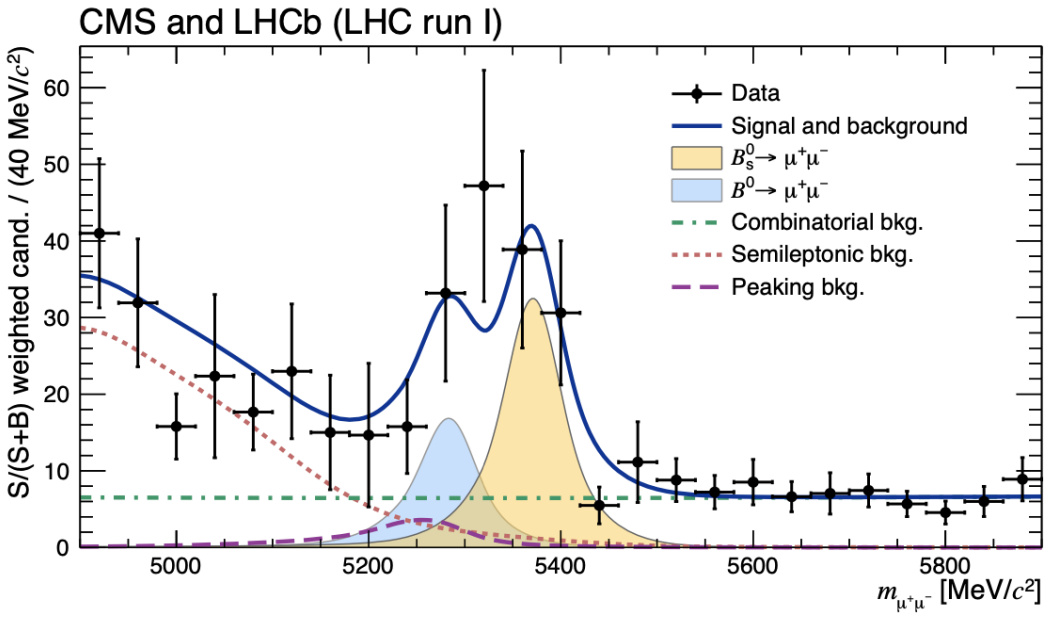

Figure 74: The signal candidates with a combined fit sharing signal and nuisance parameters as described in [331].

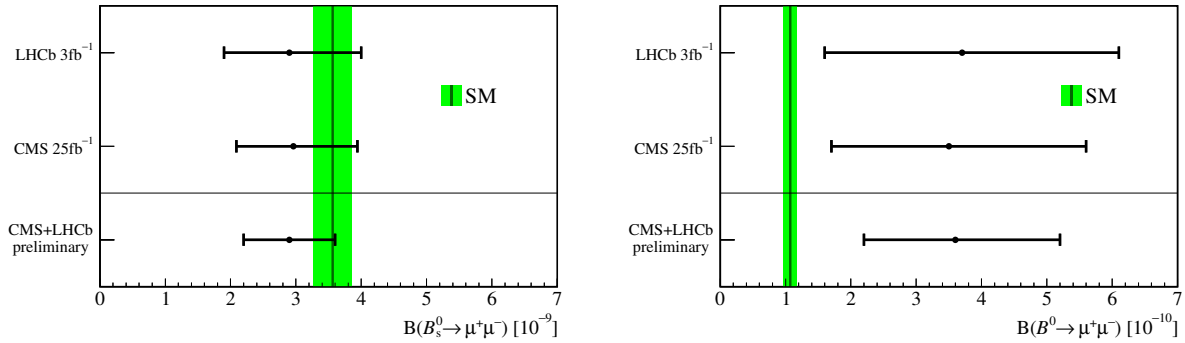

Figure 75: Measurements of the branching ratios of $B_s^0 \to \mu^+\mu^-$ and $B^0 \to \mu^+\mu^-$, from the LHCb and CMS collaborations, the combined results as well as the SM predictions [332].

References

[1] S. Weinberg, *A Model of Leptons*, *Phys. Rev. Lett.* **19** (1967) 1264–1266.

[2] A. Salam, *Weak and Electromagnetic Interactions*, *Conf. Proc. C* **680519** (1968) 367–377.

[3] S. L. Glashow, J. Iliopoulos and L. Maiani, *Weak Interactions with Lepton-Hadron Symmetry*, *Phys. Rev. D* **2** (1970) 1285–1292.

[4] ATLAS collaboration, G. Aad et al., *Observation of a new particle in the search for the Standard Model Higgs boson with the ATLAS detector at the LHC*, *Phys. Lett. B* **716** (2012) 1–29, [1207.7214].

[5] CMS collaboration, S. Chatrchyan et al., *Observation of a New Boson at a Mass of 125 GeV with the CMS Experiment at the LHC*, *Phys. Lett. B* **716** (2012) 30–61, [1207.7235].

[6] P. Langacker, *The Standard Model and Beyond (Series in High Energy Physics, Cosmology and Gravitation)*. ISBN 13: 9781498763219, 2009.

[7] Y. Nagashima, *Beyond the standard model of elementary particle physics*. Wiley-VCH, Weinheim, USA, 2014.

[8] J. H. Christenson, J. W. Cronin, V. L. Fitch and R. Turlay, *Evidence for the* 2π *Decay of the* K_2^0 *Meson*, *Phys. Rev. Lett.* **13** (1964) 138–140.

[9] F. Zwicky, *Die Rotverschiebung von extragalaktischen Nebeln*, *Helv. Phys. Acta* **6** (1933) 110–127.

[10] V. C. Rubin and W. K. Ford, Jr., *Rotation of the Andromeda Nebula from a Spectroscopic Survey of Emission Regions*, *Astrophys. J.* **159** (1970) 379–403.

[11] HFLAV collaboration, Y. S. Amhis et al., *Averages of b-hadron, c-hadron, and* τ*-lepton properties as of 2021*, *Phys. Rev. D* **107** (2023) 052008, [2206.07501].

[12] LHCb collaboration, R. Aaij et al., *Measurement of* CP*-Averaged Observables in the* $B^0 \to K^{*0}\mu^+\mu^-$ *Decay*, *Phys. Rev. Lett.* **125** (2020) 011802, [2003.04831].

[13] CMS collaboration, *Angular analysis of the* $B^0 \to K^{*0}(892)\mu^+\mu^-$ *decay at* $\sqrt{s} = 13$ *TeV*, .

[14] LHCb, ATLAS, CMS collaboration, *Combination of the ATLAS, CMS and LHCb results on the $B^0_{(s)} \to \mu^+\mu^-$ decays*, LHCb-CONF-2020-002.

[15] LHCb collaboration, R. Aaij et al., *Measurement of the $B^0_s \to \mu^+\mu^-$ decay properties and search for the $B^0 \to \mu^+\mu^-$ and $B^0_s \to \mu^+\mu^-\gamma$ decays*, *Phys. Rev. D* **105** (2022) 012010, [2108.09283].

[16] A. D. Sakharov, *Violation of CP Invariance, C asymmetry, and baryon asymmetry of the universe*, *Pisma Zh. Eksp. Teor. Fiz.* **5** (1967) 32–35.

[17] M. Trodden, *Electroweak baryogenesis*, *Rev. Mod. Phys.* **71** (1999) 1463–1500, [hep-ph/9803479].

[18] CMS, LHCb collaboration, V. Khachatryan et al., *Observation of the rare $B^0_s \to \mu^+\mu^-$ decay from the combined analysis of CMS and LHCb data*, *Nature* **522** (2015) 68–72, [1411.4413].

[19] W. N. Cottingham and D. A. Greenwood, *An Introduction to the Standard Model of Particle Physics*. Cambridge University Press, 2007.

[20] D. Goldberg, *The Standard Model in a Nutshell*. ISBN: 9780691167596, 2017.

[21] C. Burgess and G. Moore, *The Standard Model: A Primer*. Cambridge University Press,, 2007.

[22] C. Quigg, *Gauge Theories of the Strong, Weak and Electromagnetic Interactions*, vol. 56. ISBN: 978-0-8053-6020-2, 1983.

[23] F. Halzen and A. D. Martin, *Quarks and Leptons: An Itroductory Course in Modern Partticle Physics*. ISBN: 978-0-471-88741-6, 1984.

[24] D. H. Perkins, *Introduction to high energy physics*. ISBN: 978-0-521-62196-0, 1982.

[25] I. J. R. Aitchison and A. J. G. Hey, *Gauge Theories in Particle Physics: A Practical Introduction*. 1989.

[26] P. Renton, *Electroweak Interactions: An Introduction to the Physics of Quarks and Leptons*. ISBN: 978-0-521-36692-2, 1990.

[27] E. Leader and E. Predazzi, *An Introduction to gauge theories and modern particle physics. Vol. 1: Electroweak interactions, the new particles and the parton model*. ISBN: 978-0-511-88573-0, 978-0-521-46840-4, Cambridge University Press, 4, 2011.

[28] S. F. Novaes, *Standard model: An Introduction*, in *10th Jorge Andre Swieca Summer School: Particle and Fields*, pp. 5–102, 1, 1999. hep-ph/0001283.

[29] G. Altarelli, *The Standard model of particle physics*, hep-ph/0510281.

[30] D. Griffiths, *Introduction to elementary particles*. ISBN: 978-3-527-40601-2, 2008.

[31] M. Thomson, *Modern particle physics*. Cambridge University Press, New York, 2013, 10.1017/CBO9781139525367.

[32] F. Englert and R. Brout, *Broken Symmetry and the Mass of Gauge Vector Mesons*, *Phys. Rev. Lett.* **13** (1964) 321–323.

[33] P. W. Higgs, *Broken Symmetries and the Masses of Gauge Bosons*, *Phys. Rev. Lett.* **13** (1964) 508–509.

[34] G. 't Hooft, *The Glorious days of physics: Renormalization of gauge theories*, hep-th/9812203.

[35] S. L. Glashow, *The renormalizability of vector meson interactions*, *Nucl. Phys.* **10** (1959) 107–117.

[36] A. Salam and J. C. Ward, *Weak and electromagnetic interactions*, *Nuovo Cim.* **11** (1959) 568–577.

[37] D. G. Charlton, *LEP, SLC and the standard model*, *eConf* **C020805** (2002) TW05, [hep-ex/0211003].

[38] G. 't Hooft and M. J. G. Veltman, *Regularization and Renormalization of Gauge Fields*, *Nucl. Phys. B* **44** (1972) 189–213.

[39] G. 't Hooft, *When was asymptotic freedom discovered? or the rehabilitation of quantum field theory*, *Nucl. Phys. B Proc. Suppl.* **74** (1999) 413–425, [hep-th/9808154].

[40] K. G. Wilson, *The renormalization group and critical phenomena*, *Rev. Mod. Phys.* **55** (1983) 583–600.

[41] D. J. Gross and F. Wilczek, *Ultraviolet Behavior of Nonabelian Gauge Theories*, *Phys. Rev. Lett.* **30** (1973) 1343–1346.

[42] D. J. Gross and F. Wilczek, *Asymptotically Free Gauge Theories - I*, *Phys. Rev. D* **8** (1973) 3633–3652.

[43] D. J. Gross and F. Wilczek, *ASYMPTOTICALLY FREE GAUGE THEORIES. 2.*, *Phys. Rev. D* **9** (1974) 980–993.

[44] H. D. Politzer, *Reliable Perturbative Results for Strong Interactions?*, *Phys. Rev. Lett.* **30** (1973) 1346–1349.

[45] H. Georgi and S. L. Glashow, *Unity of All Elementary Particle Forces*, *Phys. Rev. Lett.* **32** (1974) 438–441.

[46] J. C. Pati and A. Salam, *Lepton Number as the Fourth Color*, *Phys. Rev. D* **10** (1974) 275–289.

[47] A. Buras, *Gauge Theory of Weak Decays*. Cambridge University Press, 6, 2020, 10.1017/9781139524100.

[48] K. Nishijima, *Charge Independence Theory of V Particles*, *Prog. Theor. Phys.* **13** (1955) 285–304.

[49] M. Gell-Mann, *The interpretation of the new particles as displaced charge multiplets*, *Nuovo Cim.* **4** (1956) 848–866.

[50] S. L. Glashow, *Partial Symmetries of Weak Interactions*, *Nucl. Phys.* **22** (1961) 579–588.

[51] A. Pich, *The Standard model of electroweak interactions*, in *2006 European School of High-Energy Physics*, pp. 1–49, 2007. 0705.4264.

[52] J. D. Bjorken and S. D. Drell, *Relativistic quantum fields*. 1965.

[53] M. E. Peskin and D. V. Schroeder, *An Introduction to quantum field theory*. ISBN: 978-0-201-50397-5, Addison-Wesley, Reading, USA, 1995.

[54] https://www.nikhef.nl/ h71/Lectures/2015/ppII-cpviolation 19032018.pdf, *Lectures on CP violation by P. Kooijman and N. Tuning*. 2015.

[55] https://www.nikhef.nl, *Particle Physics 1, Lecture notes for the first year master course on the electroweak part of the Standard Model by M. Merk, I. van Vulpen and W. Hulsbergen*. 2018.

[56] N. Cabibbo, *Unitary Symmetry and Leptonic Decays*, *Phys. Rev. Lett.* **10** (1963) 531–533.

[57] M. Kobayashi and T. Maskawa, *CP Violation in the Renormalizable Theory of Weak Interaction*, *Prog. Theor. Phys.* **49** (1973) 652–657.

[58] C. S. Wu, E. Ambler, R. W. Hayward, D. D. Hoppes and R. P. Hudson, *Experimental Test of Parity Conservation in β Decay*, *Phys. Rev.* **105** (1957) 1413–1414.

[59] G. C. Branco, L. Lavoura and J. P. Silva, *CP Violation*, vol. 103. 1999.

[60] I. I. Bigi and A. I. Sanda, *CP violation*, vol. 9. Cambridge University Press, 9, 2009, 10.1017/CBO9780511581014.

[61] T. Mannel, *Effective Field Theories in Flavor Physics*, *Springer Tracts Mod. Phys.* **203** (2004) 1–175.

[62] M. Gronau, *CP violation in beauty decays*, *Int. J. Mod. Phys. A* **22** (2007) 1953–1982, [0704.0076].

[63] V. Baluni, *CP Violating Effects in QCD*, *Phys. Rev. D* **19** (1979) 2227–2230.

[64] R. J. Crewther, P. Di Vecchia, G. Veneziano and E. Witten, *Chiral Estimate of the Electric Dipole Moment of the Neutron in Quantum Chromodynamics*, *Phys. Lett. B* **88** (1979) 123.

[65] R. D. Peccei and H. R. Quinn, *CP Conservation in the Presence of Instantons*, *Phys. Rev. Lett.* **38** (1977) 1440–1443.

[66] Particle Data Group collaboration, R. L. Workman et al., *Review of Particle Physics*, *PTEP* **2022** (2022) 083C01.

[67] Z. Maki, M. Nakagawa and S. Sakata, *Remarks on the unified model of elementary particles*, *Prog. Theor. Phys.* **28** (1962) 870–880.

[68] B. Pontecorvo, *Inverse beta processes and nonconservation of lepton charge*, *Zh. Eksp. Teor. Fiz.* **34** (1957) 247.

[69] L. Wolfenstein, *Parametrization of the Kobayashi-Maskawa Matrix*, *Phys. Rev. Lett.* **51** (1983) 1945.

[70] A. J. Buras, M. E. Lautenbacher and G. Ostermaier, *Waiting for the top quark mass, K+ —> pi+ neutrino anti-neutrino, B(s)0 - anti-B(s)0 mixing and CP asymmetries in B decays*, *Phys. Rev. D* **50** (1994) 3433–3446, [hep-ph/9403384].

[71] C. Jarlskog, *Commutator of the Quark Mass Matrices in the Standard Electroweak Model and a Measure of Maximal CP Nonconservation*, *Phys. Rev. Lett.* **55** (1985) 1039.

[72] J. Bernabeu, G. C. Branco and M. Gronau, *CP Restrictions on Quark Mass Matrices*, *Phys. Lett. B* **169** (1986) 243–247.

[73] A. J. Buras, *The ϵ'/ϵ-Story: 1976-2021*, *Acta Phys. Polon. B* **52** (2021) 7–41, [2101.00020].

[74] NA48 collaboration, V. Fanti et al., *A New measurement of direct CP violation in two pion decays of the neutral kaon*, *Phys. Lett. B* **465** (1999) 335–348, [hep-ex/9909022].

[75] KTeV collaboration, A. Alavi-Harati et al., *Observation of direct CP violation in $K_{S,L} \to \pi\pi$ decays*, *Phys. Rev. Lett.* **83** (1999) 22–27, [hep-ex/9905060].

[76] BaBar collaboration, B. Aubert et al., *Observation of CP violation in the B^0 meson system*, *Phys. Rev. Lett.* **87** (2001) 091801, [hep-ex/0107013].

[77] Belle collaboration, K. Abe et al., *Observation of large CP violation in the neutral B meson system*, *Phys. Rev. Lett.* **87** (2001) 091802, [hep-ex/0107061].

[78] LHCb collaboration, R. Aaij et al., *Observation of CP Violation in Charm Decays*, *Phys. Rev. Lett.* **122** (2019) 211803, [1903.08726].

[79] R. Aleksan, B. Kayser and D. London, *Determining the quark mixing matrix from CP violating asymmetries*, *Phys. Rev. Lett.* **73** (1994) 18–20, [hep-ph/9403341].

[80] R. Fleischer, *Theoretical overview of CP violation in B meson decay*, *Acta Phys. Polon. B* **31** (2000) 2633–2643, [hep-ph/0006132].

[81] K. De Bruyn, R. Fleischer, E. Malami and P. van Vliet, *New physics in $B_q{}^0$–mixing: present challenges, prospects, and implications for*, *J. Phys. G* **50** (2023) 045003, [2208.14910].

[82] CKMfitter Group collaboration, J. Charles, A. Hocker, H. Lacker, S. Laplace, F. R. Le Diberder, J. Malcles et al., *CP violation and the CKM matrix: Assessing the impact of the asymmetric B factories*, *Eur. Phys. J. C* **41** (2005) 1–131, [[hep-ph/0406184], updated results and plots available at: http://ckmfitter.in2p3.fr].

[83] ARGUS collaboration, H. Albrecht et al., *Reconstruction of B Mesons*, *Phys. Lett. B* **185** (1987) 218.

[84] ARGUS collaboration, H. Albrecht et al., *Observation of B0 - anti-B0 Mixing*, *Phys. Lett. B* **192** (1987) 245–252.

[85] ARGUS collaboration, H. Albrecht et al., *Measurement of the Decay B0 —> D*-Lepton+ Neutrino*, *Phys. Lett. B* **197** (1987) 452–456.

[86] CLEO collaboration, S. Behrends et al., *Observation of Exclusive Decay Modes of B Flavored Mesons*, *Phys. Rev. Lett.* **50** (1983) 881–884.

[87] CLEO collaboration, J. Green et al., *The D0 Spectrum From B Meson Decay*, *Phys. Rev. Lett.* **51** (1983) 347.

[88] CLEO collaboration, P. Avery et al., *Limits on rare exclusive decays of B mesons*, *Phys. Lett. B* **183** (1987) 429–433.

[89] BaBar collaboration, B. Aubert et al., *Measurements of branching fractions and CP-violating asymmetries in $B^0 \to \pi^+\pi^-$, $K^+\pi^-$, K^+K^- decays*, *Phys. Rev. Lett.* **89** (2002) 281802, [hep-ex/0207055].

[90] Belle collaboration, K. Abe et al., *Observation of large CP violation and evidence for direct CP violation in $B^0 \to \pi^+\pi^-$ decays*, *Phys. Rev. Lett.* **93** (2004) 021601, [hep-ex/0401029].

[91] CDF collaboration, F. Abe et al., *Measurement of $B^0\overline{B}^0$ mixing at the Fermilab Tevatron collider*, *Phys. Rev. Lett.* **67** (1991) 3351–3355.

[92] CDF collaboration, A. Abulencia et al., *Observation of $B_s^0 - \bar{B}_s^0$ Oscillations*, *Phys. Rev. Lett.* **97** (2006) 242003, [hep-ex/0609040].

[93] D0 collaboration, V. M. Abazov et al., *Measurement of B_d mixing using opposite-side flavor tagging*, *Phys. Rev. D* **74** (2006) 112002, [hep-ex/0609034].

[94] D0 collaboration, V. M. Abazov et al., *Measurement of B_s^0 mixing parameters from the flavor-tagged decay $B_s^0 \to J/\psi\phi$*, *Phys. Rev. Lett.* **101** (2008) 241801, [0802.2255].

[95] LHCb collaboration, A. A. Alves, Jr. et al., *The LHCb Detector at the LHC*, *JINST* **3** (2008) S08005.

[96] ATLAS collaboration, G. Aad et al., *The ATLAS Experiment at the CERN Large Hadron Collider*, *JINST* **3** (2008) S08003.

[97] CMS collaboration, S. Chatrchyan et al., *The CMS Experiment at the CERN LHC*, *JINST* **3** (2008) S08004.

[98] FCC collaboration, A. Abada et al., *FCC-ee: The Lepton Collider: Future Circular Collider Conceptual Design Report Volume 2*, *Eur. Phys. J. ST* **228** (2019) 261–623.

[99] R. Fleischer, *Flavour Physics and CP Violation: Expecting the LHC*, in *4th CERN-CLAF School of High-Energy Physics*, pp. 105–157, 2, 2008. 0802.2882.

[100] https://www.nikhef.nl/ h71/Lectures/2020/ppII-cpviolation 14022020.pdf, *Lectures Notes on CP violation by N. Tuning.* 2020.

[101] A. J. Buras and R. Fleischer, *Quark mixing, CP violation and rare decays after the top quark discovery*, *Adv. Ser. Direct. High Energy Phys.* **15** (1998) 65–238, [hep-ph/9704376].

[102] T. Inami and C. S. Lim, *Effects of Superheavy Quarks and Leptons in Low-Energy Weak Processes k(L) —> mu anti-mu, K+ —> pi+ Neutrino anti-neutrino and K0 <—> anti-K0*, *Prog. Theor. Phys.* **65** (1981) 297.

[103] A. J. Buras, M. Jamin and P. H. Weisz, *Leading and Next-to-leading QCD Corrections to ϵ Parameter and $B^0 - \bar{B}^0$ Mixing in the Presence of a Heavy Top Quark*, *Nucl. Phys. B* **347** (1990) 491–536.

[104] G. Buchalla, A. J. Buras and M. E. Lautenbacher, *Weak decays beyond leading logarithms*, *Rev. Mod. Phys.* **68** (1996) 1125–1144, [hep-ph/9512380].

[105] G. Banelli, R. Fleischer, R. Jaarsma and G. Tetlalmatzi-Xolocotzi, *Decoding (Pseudo)-Scalar Operators in Leptonic and Semileptonic B Decays*, *Eur. Phys. J. C* **78** (2018) 911, [1809.09051].

[106] Belle collaboration, A. Sibidanov et al., *Search for $B^- \to \mu^- \bar{\nu}_\mu$ Decays at the Belle Experiment*, *Phys. Rev. Lett.* **121** (2018) 031801, [1712.04123].

[107] Belle collaboration, N. Satoyama et al., *A Search for the rare leptonic decays B+ —> mu+ nu(mu) and B+ —> e+ nu(nu)*, *Phys. Lett. B* **647** (2007) 67–73, [hep-ex/0611045].

[108] Belle collaboration, K. Ikado et al., *Evidence of the Purely Leptonic Decay B- —> tau- anti-nu(tau)*, *Phys. Rev. Lett.* **97** (2006) 251802, [hep-ex/0604018].

[109] E. Fermi, *Tentativo di una teoria dell'emissione dei raggi beta*, *Ric. Sci.* **4** (1933) 491–495.

[110] R. Fleischer, R. Jaarsma and G. Tetlalmatzi-Xolocotzi, *Mapping out the space for new physics with leptonic and semileptonic $B_{(c)}$ decays*, *Eur. Phys. J. C* **81** (2021) 658, [2104.04023].

[111] D. Bigi and P. Gambino, *Revisiting $B \to D\ell\nu$*, *Phys. Rev. D* **94** (2016) 094008, [1606.08030].

[112] R.-H. Li, C.-D. Lu, W. Wang and X.-X. Wang, *B —> S Transition Form Factors in the PQCD approach*, *Phys. Rev. D* **79** (2009) 014013, [0811.2648].

[113] P. Colangelo, F. De Fazio, R. Ferrandes and T. N. Pham, *Exclusive B —> $K(*)$ $l+$ $l-$, B —> $K(*)$ nu anti-nu and B —> $K*$ gamma transitions in a scenario with a single Universal Extra Dimension*, *Phys. Rev. D* **73** (2006) 115006, [hep-ph/0604029].

[114] W.-F. Wang and Z.-J. Xiao, *The semileptonic decays $B/B_s \to (\pi, K)(\ell^+\ell^-, \ell\nu, \nu\bar{\nu})$ in the perturbative QCD approach beyond the leading-order*, *Phys. Rev. D* **86** (2012) 114025, [1207.0265].

[115] R. Fleischer and E. Malami, *Using $B_s^0 \to D_s^{\mp} K^{\pm}$ Decays as a Portal to New Physics*, *Phys. Rev. D* **106** (2022) 056004, [2109.04950].

[116] M. Neubert, *Heavy quark effective theory*, *Subnucl. Ser.* **34** (1997) 98–165, [hep-ph/9610266].

[117] J. Charles, A. Le Yaouanc, L. Oliver, O. Pene and J. C. Raynal, *Heavy to light form-factors in the heavy mass to large energy limit of QCD*, *Phys. Rev. D* **60** (1999) 014001, [hep-ph/9812358].

[118] https://pdg.lbl.gov/2021/reviews/rpp2021-rev-vcb vub.pdf, *76. Semileptonic b-Hadron Decays, Determination of V_{cb}, V_{ub}*. 2021.

[119] P. Gambino, P. Giordano, G. Ossola and N. Uraltsev, *Inclusive semileptonic B decays and the determination of —V(ub)—*, *JHEP* **10** (2007) 058, [0707.2493].

[120] HFLAV collaboration, Y. Amhis et al., *Averages of b-hadron, c-hadron, and τ-lepton properties as of 2021*, 2206.07501.

[121] M. Bordone, B. Capdevila and P. Gambino, *Three loop calculations and inclusive Vcb*, *Phys. Lett. B* **822** (2021) 136679, [2107.00604].

[122] J. Charles et al., *Current status of the Standard Model CKM fit and constraints on $\Delta F = 2$ New Physics*, *Phys. Rev. D* **91** (2015) 073007, [1501.05013].

[123] UTfit collaboration, M. Bona et al., *The Unitarity Triangle Fit in the Standard Model and Hadronic Parameters from Lattice QCD: A Reappraisal after the Measurements of Delta m(s) and BR(B —> tau nu(tau))*, *JHEP* **10** (2006) 081, [hep-ph/0606167].

[124] K. De Bruyn, R. Fleischer, E. Malami and P. van Vliet, *Studies of New Physics in $B_q^0 - \bar{B}_q^0$ Mixing and Implications for Leptonic Decays*, in *8th Symposium on Prospects in the Physics of Discrete Symmetries*, 1, 2023. 2301.13649.

[125] G. Ricciardi, *Theory: Semileptonic B Decays and $|V_{xb}|$ update*, *PoS* **BEAUTY2020** (2021) 031, [2103.06099].

[126] C.-Y. Seng, D. Galviz, M. Gorchtein and U.-G. Meißner, *Complete theory of radiative corrections to K_3 decays and the V_{us} update*, *JHEP* **07** (2022) 071, [2203.05217].

[127] M. Bordone, N. Gubernari, D. van Dyk and M. Jung, *Heavy-Quark expansion for $\bar{B}_s \to D_s^{(*)}$ form factors and unitarity bounds beyond the $SU(3)_F$ limit*, *Eur. Phys. J. C* **80** (2020) 347, [1912.09335].

[128] A. J. Buras and E. Venturini, *The exclusive vision of rare K and B decays and of the quark mixing in the standard model*, *Eur. Phys. J. C* **82** (2022) 615, [2203.11960].

[129] https://gammacombo.github.io.

[130] W. R. Inc., *Mathematica, Version 14.0*, https://www.wolfram.com/mathematica.

[131] A. J. Buras and M. Jamin, *epsilon-prime / epsilon at the NLO: 10 years later*, *JHEP* **01** (2004) 048, [hep-ph/0306217].

[132] S. Bertolini, M. Fabbrichesi and J. O. Eeg, *Theory of the CP Violating Parameter ϵ'/ϵ*, *Rev. Mod. Phys.* **72** (2000) 65–93, [hep-ph/9802405].

[133] A. Pich, *Epsilon-prime/epsilon in the standard model: Theoretical update*, in *32nd International Conference on High Energy Physics*, 10, 2004. hep-ph/0410215.

[134] J. Brod, M. Gorbahn and E. Stamou, *Standard-Model Prediction of ϵ_K with Manifest Quark-Mixing Unitarity*, *Phys. Rev. Lett.* **125** (2020) 171803, [1911.06822].

[135] Flavour Lattice Averaging Group (FLAG) collaboration, Y. Aoki et al., *FLAG Review 2021*, *Eur. Phys. J. C* **82** (2022) 869, [2111.09849].

[136] A. J. Buras, D. Guadagnoli and G. Isidori, *On ϵ_K Beyond Lowest Order in the Operator Product Expansion*, *Phys. Lett. B* **688** (2010) 309–313, [1002.3612].

[137] K. G. Chetyrkin, J. H. Kuhn and M. Steinhauser, *RunDec: A Mathematica package for running and decoupling of the strong coupling and quark masses*, *Comput. Phys. Commun.* **133** (2000) 43–65, [hep-ph/0004189].

[138] B. Schmidt and M. Steinhauser, *CRunDec: a C++ package for running and decoupling of the strong coupling and quark masses*, *Comput. Phys. Commun.* **183** (2012) 1845–1848, [1201.6149].

[139] J. Brod, S. Kvedaraitė and Z. Polonsky, *Two-loop electroweak corrections to the Top-Quark Contribution to ϵ_K*, *JHEP* **12** (2021) 198, [2108.00017].

[140] LHCb collaboration, *Measurement of the ratios of branching fractions $\mathcal{R}(D^*)$ and $\mathcal{R}(D^0)$*, *Phys. Rev. Lett.* **131** (2023) 111802, [2302.02886].

[141] BaBar collaboration, J. P. Lees et al., *Measurement of Branching Fractions and Rate Asymmetries in the Rare Decays $B \to K^{(*)} l^+ l^-$*, *Phys. Rev. D* **86** (2012) 032012, [1204.3933].

[142] BELLE collaboration, S. Choudhury et al., *Test of lepton flavor universality and search for lepton flavor violation in $B \to K\ell\ell$ decays*, *JHEP* **03** (2021) 105, [1908.01848].

[143] LHCb collaboration, R. Aaij et al., *Test of lepton universality in beauty-quark decays*, *Nature Phys.* **18** (2022) 277–282, [2103.11769].

[144] LHCb collaboration, R. Aaij et al., *Measurement of lepton universality parameters in $B^+ \to K^+ \ell^+ \ell^-$ and $B^0 \to K^{*0} \ell^+ \ell^-$ decays*, *Phys. Rev. D* **108** (2023) 032002, [2212.09153].

[145] R. Fleischer, E. Malami, A. Rehult and K. K. Vos, *Fingerprinting CP-violating New Physics with $B \to K\mu^+\mu$*, *JHEP* **03** (2023) 113, [2212.09575].

[146] R. Fleischer, E. Malami, A. Rehult and K. K. Vos, *New perspectives for testing electron-muon universality*, *JHEP* **06** (2023) 033, [2303.08764].

[147] K. G. Wilson, *Nonlagrangian models of current algebra*, *Phys. Rev.* **179** (1969) 1499–1512.

[148] K. G. Wilson and W. Zimmermann, *Operator product expansions and composite field operators in the general framework of quantum field theory*, *Commun. Math. Phys.* **24** (1972) 87–106.

[149] E. Witten, *Short Distance Analysis of Weak Interactions*, *Nucl. Phys. B* **122** (1977) 109–143.

[150] F. J. Gilman and M. B. Wise, *Effective Hamiltonian for Delta s = 1 Weak Nonleptonic Decays in the Six Quark Model*, *Phys. Rev. D* **20** (1979) 2392.

[151] G. Altarelli, G. Curci, G. Martinelli and S. Petrarca, *Weak Nonleptonic Decays Beyond Leading Logarithms in QCD*, *Phys. Lett. B* **99** (1981) 141–146.

[152] A. J. Buras and P. H. Weisz, *QCD Nonleading Corrections to Weak Decays in Dimensional Regularization and 't Hooft-Veltman Schemes*, *Nucl. Phys. B* **333** (1990) 66–99.

[153] M. Neubert and B. Stech, *Nonleptonic weak decays of B mesons*, *Adv. Ser. Direct. High Energy Phys.* **15** (1998) 294–344, [hep-ph/9705292].

[154] A. J. Buras, *QCD factors a1 and a2 beyond leading logarithms versus factorization in nonleptonic heavy meson decays*, *Nucl. Phys. B* **434** (1995) 606–618, [hep-ph/9409309].

[155] A. J. Buras and L. Silvestrini, *Generalized factorization in nonleptonic two-body B decays: A Critical look*, *Nucl. Phys. B* **548** (1999) 293–308, [hep-ph/9806278].

[156] M. Bauer, B. Stech and M. Wirbel, *Exclusive Nonleptonic Decays of D, D(s), and B Mesons*, *Z. Phys. C* **34** (1987) 103.

[157] S. Nussinov and W. Wetzel, *Comparison of Exclusive Decay Rates for b —> u and b —> c Transitions*, *Phys. Rev. D* **36** (1987) 130.

[158] A. Szczepaniak, E. M. Henley and S. J. Brodsky, *Perturbative QCD Effects in Heavy Meson Decays*, *Phys. Lett. B* **243** (1990) 287–292.

[159] M. J. Dugan and B. Grinstein, *QCD basis for factorization in decays of heavy mesons*, *Phys. Lett. B* **255** (1991) 583–588.

[160] H. D. Politzer and M. B. Wise, *Perturbative corrections to factorization in anti-B decay*, *Phys. Lett. B* **257** (1991) 399–402.

[161] O. Haan and B. Stech, *Violation of the Delta-I=1/2 rule in non-leptonic decays*, *Nucl. Phys. B* **22** (1970) 448–460.

[162] A. J. Buras and J. M. Gerard, *1/n Expansion for Kaons*, *Nucl. Phys. B* **264** (1986) 371–392.

[163] A. J. Buras, J. M. Gerard and R. Ruckl, *1/n Expansion for Exclusive and Inclusive Charm Decays*, *Nucl. Phys. B* **268** (1986) 16–48.

[164] M. Beneke, G. Buchalla, M. Neubert and C. T. Sachrajda, *QCD factorization for exclusive, nonleptonic B meson decays: General arguments and the case of heavy light final states*, *Nucl. Phys. B* **591** (2000) 313–418, [hep-ph/0006124].

[165] M. Neubert, *Aspects of QCD factorization*, *AIP Conf. Proc.* **602** (2001) 168–179, [hep-ph/0110093].

[166] C. W. Bauer, D. Pirjol and I. W. Stewart, *A Proof of factorization for B —> D pi*, *Phys. Rev. Lett.* **87** (2001) 201806, [hep-ph/0107002].

[167] C. W. Bauer, B. Grinstein, D. Pirjol and I. W. Stewart, *Testing factorization in B —> D(*)X decays*, *Phys. Rev. D* **67** (2003) 014010, [hep-ph/0208034].

[168] H.-n. Li and H.-L. Yu, *Perturbative QCD analysis of B meson decays*, *Phys. Rev. D* **53** (1996) 2480–2490, [hep-ph/9411308].

[169] Y.-Y. Keum, H.-n. Li and A. I. Sanda, *Fat penguins and imaginary penguins in perturbative QCD*, *Phys. Lett. B* **504** (2001) 6–14, [hep-ph/0004004].

[170] J. D. Bjorken, *Topics in B Physics*, *Nucl. Phys. B Proc. Suppl.* **11** (1989) 325–341.

[171] https://atlas.web.cern.ch/Atlas/GROUPS/PHYSICS/CombinedSummaryPlots/EXOTICS/.

[172] R. Fleischer, G. Isidori and J. Matias, *Shedding light on the ' dark side ' of $B_d^0 - \bar{B}_d^0$ mixing through $B_d \to \pi^+\pi^-$, $K \to \pi\nu\bar{\nu}$ and B(d, s) $\to \mu^+\mu^-$*, *JHEP* **05** (2003) 053, [hep-ph/0302229].

[173] M. Neubert, *B decays and CP violation*, *Int. J. Mod. Phys. A* **11** (1996) 4173–4240, [hep-ph/9604412].

[174] Y. Nir, *CP violation: A New era*, in *55th Scottish Universities Summer School in Physics: Heavy Flavor Physics (SUSSP 2001)*, pp. 147–200, 9, 2001. hep-ph/0109090.

[175] H. Quinn, *B physics and CP violation*, *ICTP Lect. Notes Ser.* **10** (2002) 1–54, [hep-ph/0111177].

[176] A. J. Buras, *Flavor physics and CP violation*, in *2004 European School of High-Energy Physics*, pp. 95–168, 5, 2005. hep-ph/0505175.

[177] LHCb collaboration, R. Aaij et al., *Measurement of the CP asymmetry in $B_s^0 - \overline{B}_s^0$ mixing*, *Phys. Rev. Lett.* **117** (2016) 061803, [1605.09768].

[178] R. Fleischer and K. K. Vos, *B_s^0-$\bar{B}_s^0$ Oscillations as a New Tool to Explore CP Violation in $D_s^\pm$ Decays*, *Phys. Lett. B* **770** (2017) 319–324, [1606.06042].

[179] R. Fleischer, *CP violation and the role of electroweak penguins in nonleptonic B decays*, *Int. J. Mod. Phys. A* **12** (1997) 2459–2522, [hep-ph/9612446].

[180] R. Fleischer, *Constraining penguin contributions and the CKM angle γ through $B_d \to \pi^+\pi^-$*, *Eur. Phys. J. C* **16** (2000) 87–95, [hep-ph/0001253].

[181] M. Gronau and J. L. Rosner, *Convention independent study of CP violating asymmetries in B —> pi pi*, *Phys. Rev. D* **66** (2002) 053003, [hep-ph/0205323].

[182] M. Gronau, E. Lunghi and D. Wyler, *Reducing the error on alpha in B —> pi pi, rho rho, rho pi*, *Phys. Lett. B* **606** (2005) 95–102, [hep-ph/0410170].

[183] R. Fleischer and T. Mannel, *Penguin zoology in B —> pi pi and the extraction of the CKM angle alpha*, *Phys. Lett. B* **397** (1997) 269–274, [hep-ph/9610357].

[184] M. Gronau, *Large penguin effects in the CP asymmetry of B(d)0 —> pi+ pi-*, *Phys. Lett. B* **300** (1993) 163–168, [hep-ph/9209279].

[185] M. Gronau and D. London, *Isospin analysis of CP asymmetries in B decays*, *Phys. Rev. Lett.* **65** (1990) 3381–3384.

[186] A. J. Buras, R. Fleischer, S. Recksiegel and F. Schwab, *Anatomy of prominent B and K decays and signatures of CP violating new physics in the electroweak penguin sector*, *Nucl. Phys. B* **697** (2004) 133–206, [hep-ph/0402112].

[187] HFLAV collaboration, Y. S. Amhis et al., *Averages of b-hadron, c-hadron, and τ-lepton properties as of 2018*, *Eur. Phys. J. C* **81** (2021) 226, [1909.12524].

[188] LHCb collaboration, *Measurement of CP asymmetry in $B_s^0 \to D_s^{\mp} K^{\pm}$ decays*, .

[189] LHCb collaboration, R. Aaij et al., *Measurement of CP asymmetry in $B_s^0 \to D_s^{\mp} K^{\pm}$ decays*, *JHEP* **03** (2018) 059, [1712.07428].

[190] R. Fleischer and E. Malami, *Revealing new physics in $B_s^0 \to D_s^{\mp} K^{\pm}$ decays*, *Eur. Phys. J. C* **83** (2023) 420, [2110.04240].

[191] M. Z. Barel, K. De Bruyn, R. Fleischer and E. Malami, *In Pursuit of New Physics with $B_d^0 \to J/\psi K^0$ and $B_s^0 \to J/\psi\phi$ Decays at the High-Precision Frontier*, *J. Phys. G* **48** (2021) 065002, [2010.14423].

[192] S. Iguro and T. Kitahara, *Implications for new physics from a novel puzzle in $\bar{B}_{(s)}^0 \to D_{(s)}^{(*)+}\{\pi^-, K^-\}$ decays*, *Phys. Rev. D* **102** (2020) 071701, [2008.01086].

[193] F.-M. Cai, W.-J. Deng, X.-Q. Li and Y.-D. Yang, *Probing new physics in class-I B-meson decays into heavy-light final states*, *JHEP* **10** (2021) 235, [2103.04138].

[194] M. Bordone, A. Greljo and D. Marzocca, *Exploiting dijet resonance searches for flavor physics*, *JHEP* **08** (2021) 036, [2103.10332].

[195] M. Gronau and D. Wyler, *On determining a weak phase from CP asymmetries in charged B decays*, *Phys. Lett. B* **265** (1991) 172–176.

[196] R. Fleischer and D. Wyler, *Exploring CP violation with B(c) decays*, *Phys. Rev. D* **62** (2000) 057503, [hep-ph/0004010].

[197] LHCb collaboration, R. Aaij et al., *Simultaneous determination of CKM angle γ and charm mixing parameters*, *JHEP* **12** (2021) 141, [2110.02350].

[198] LHCb collaboration, R. Aaij et al., *Measurement of the CKM angle γ in $B^{\pm} \to DK^{\pm}$ and $B^{\pm} \to D\pi^{\pm}$ decays with $D \to K_S^0 h^+ h^-$*, *JHEP* **02** (2021) 169, [2010.08483].

[199] J. Charles, O. Deschamps, S. Descotes-Genon and V. Niess, *Isospin analysis of charmless B-meson decays*, *Eur. Phys. J. C* **77** (2017) 574, [1705.02981].

[200] A. J. Buras and R. Fleischer, *A General analysis of gamma determinations from B —> pi K decays*, *Eur. Phys. J. C* **11** (1999) 93–109, [hep-ph/9810260].

[201] M. Z. Barel, K. De Bruyn, R. Fleischer and E. Malami, *Penguin Effects in $B_d^0 \to J/\psi K_S^0$ and $B_s^0 \to J/\psi\phi$*, in *11th International Workshop on the CKM Unitarity Triangle*, 3, 2022. 2203.14652.

[202] R. Fleischer, R. Jaarsma and K. K. Vos, *Zooming into CP violation in $B_{(s)} \to hh$ decays*, *JHEP* **02** (2023) 081, [2211.08346].

[203] R. Fleischer, *New strategies to extract Beta and gamma from B(d) —> pi+ pi- and B(S) —> K+ K-*, *Phys. Lett. B* **459** (1999) 306–320, [hep-ph/9903456].

[204] Y. Nir, *CP violation in meson decays*, in *Les Houches Summer School on Theoretical Physics: Session 84: Particle Physics Beyond the Standard Model*, pp. 79–145, 2006. hep-ph/0510413.

[205] R. Fleischer, *CP Violation in B Decays: Recent Developments and Future Perspectives*, 2, 2024. 2402.00710.

[206] V. Chobanova et al., *Summary of Working Group 4: Mixing and mixing-related CP violation in the B system: Δm, $\Delta\Gamma$, ϕ_s, ϕ_1/β, ϕ_2/α, ϕ_3/γ*, in *1st Pan-African Astro-Particle and Collider Physics Workshop*, 5, 2022. 2205.15662.

[207] E. Malami, *CP Violation and Mixing in Beauty Sector: A Theoretical Overview*, in *10th Large Hadron Collider Physics Conference*, 10, 2022. 2210.16904.

[208] R. Fleischer, *Extracting γ from $B(s/d) \to J/\psi K_S$ and $B(d/s) \to D^+(d/s)D^-(d/s)$*, *Eur. Phys. J. C* **10** (1999) 299–306, [hep-ph/9903455].

[209] Flavour Lattice Averaging Group collaboration, S. Aoki et al., *FLAG Review 2019: Flavour Lattice Averaging Group (FLAG)*, *Eur. Phys. J. C* **80** (2020) 113, [1902.08191].

[210] R. Fleischer, *Extracting CKM phases from angular distributions of B(d,s) decays into admixtures of CP eigenstates*, *Phys. Rev. D* **60** (1999) 073008, [hep-ph/9903540].

[211] K. De Bruyn and R. Fleischer, *A Roadmap to Control Penguin Effects in $B_d^0 \to J/\psi K_S^0$ and $B_s^0 \to J/\psi\phi$*, *JHEP* **03** (2015) 145, [1412.6834].

[212] S. Faller, R. Fleischer and T. Mannel, *Precision Physics with $B_s^0 \to J/\psi\phi$ at the LHC: The Quest for New Physics*, *Phys. Rev. D* **79** (2009) 014005, [0810.4248].

[213] R. Fleischer, *Recent theoretical developments in CP violation in the B system*, *Nucl. Instrum. Meth. A* **446** (2000) 1–17, [hep-ph/9908340].

[214] M. Ciuchini, M. Pierini and L. Silvestrini, *The Effect of penguins in the B(d) —> J / psi K0 CP asymmetry*, *Phys. Rev. Lett.* **95** (2005) 221804, [hep-ph/0507290].

[215] S. Faller, M. Jung, R. Fleischer and T. Mannel, *The Golden Modes B0 —> J/psi K(S,L) in the Era of Precision Flavour Physics*, *Phys. Rev. D* **79** (2009) 014030, [0809.0842].

[216] M. Ciuchini, M. Pierini and L. Silvestrini, *Theoretical uncertainty in sin 2β: An Update*, in *6th International Workshop on the CKM Unitarity Triangle*, 2, 2011. 1102.0392.

[217] M. Jung, *Determining weak phases from $B \to J/\psi P$ decays*, *Phys. Rev. D* **86** (2012) 053008, [1206.2050].

[218] X. Liu, W. Wang and Y. Xie, *Penguin pollution in $B \to J/\psi V$ decays and impact on the extraction of the $B_s - \bar{B}_s$ mixing phase*, *Phys. Rev. D* **89** (2014) 094010, [1309.0313].

[219] P. Frings, U. Nierste and M. Wiebusch, *Penguin contributions to CP phases in $B_{d,s}$ decays to charmonium*, *Phys. Rev. Lett.* **115** (2015) 061802, [1503.00859].

[220] I. Dunietz, R. Fleischer and U. Nierste, *In pursuit of new physics with B_s decays*, *Phys. Rev. D* **63** (2001) 114015, [hep-ph/0012219].

[221] K. De Bruyn, R. Fleischer, R. Knegjens, P. Koppenburg, M. Merk and N. Tuning, *Branching Ratio Measurements of B_s Decays*, *Phys. Rev. D* **86** (2012) 014027, [1204.1735].

[222] K. De Bruyn, R. Fleischer and P. Koppenburg, *Extracting γ and Penguin Topologies through CP Violation in $B_s^0 \to J/\psi K_S$*, *Eur. Phys. J. C* **70** (2010) 1025–1035, [1010.0089].

[223] LHCb collaboration, R. Aaij et al., *Measurement of the time-dependent CP asymmetries in $B_s^0 \to J/\psi K_{\rm S}^0$*, *JHEP* **06** (2015) 131, [1503.07055].

[224] LHCb collaboration, R. Aaij et al., *Updated measurement of time-dependent CP-violating observables in $B_s^0 \to J/\psi K^+K^-$ decays*, *Eur. Phys. J. C* **79** (2019) 706, [1906.08356].

[225] LHCb collaboration, R. Aaij et al., *Measurement of the CP-violating phase β in $B^0 \to J/\psi\pi^+\pi^-$ decays and limits on penguin effects*, *Phys. Lett. B* **742** (2015) 38–49, [1411.1634].

[226] A. Cerri et al., *Report from Working Group 4: Opportunities in Flavour Physics at the HL-LHC and HE-LHC*, *CERN Yellow Rep. Monogr.* **7** (2019) 867–1158, [1812.07638].

[227] Belle-II collaboration, W. Altmannshofer et al., *The Belle II Physics Book*, *PTEP* **2019** (2019) 123C01, [1808.10567].

[228] LHCb collaboration, R. Aaij et al., *Physics case for an LHCb Upgrade II - Opportunities in flavour physics, and beyond, in the HL-LHC era*, 1808.08865.

[229] A. J. Buras and L. Silvestrini, *Nonleptonic two-body B decays beyond factorization*, *Nucl. Phys. B* **569** (2000) 3–52, [hep-ph/9812392].

[230] HPQCD collaboration, D. Hatton, C. T. H. Davies, B. Galloway, J. Koponen, G. P. Lepage and A. T. Lytle, *Charmonium properties from lattice QCD+QED : Hyperfine splitting, J/ψ leptonic width, charm quark mass, and a_μ^c*, *Phys. Rev. D* **102** (2020) 054511, [2005.01845].

[231] C. Bourrely, I. Caprini and L. Lellouch, *Model-independent description of B —> pi l nu decays and a determination of —V(ub)—*, *Phys. Rev. D* **79** (2009) 013008, [0807.2722].

[232] A. Sirlin, *Large m(W), m(Z) Behavior of the O(alpha) Corrections to Semileptonic Processes Mediated by W*, *Nucl. Phys. B* **196** (1982) 83–92.

[233] Particle Data Group collaboration, P. A. Zyla et al., *Review of Particle Physics*, *PTEP* **2020** (2020) 083C01.

[234] LHCb collaboration, R. Aaij et al., *First observation of the decay $B_s^0 \to K^-\mu^+\nu_\mu$ and Measurement of $|V_{ub}|/|V_{cb}|$*, *Phys. Rev. Lett.* **126** (2021) 081804, [2012.05143].

[235] LHCb collaboration, R. Aaij et al., *Precise determination of the B_s^0–$\overline{B}_s^0$ oscillation frequency*, *Nature Phys.* **18** (2022) 1–5, [2104.04421].

[236] L. Di Luzio, M. Kirk, A. Lenz and T. Rauh, *ΔM_s theory precision confronts flavour anomalies*, *JHEP* **12** (2019) 009, [1909.11087].

[237] P. Ball and R. Fleischer, *Probing new physics through B mixing: Status, benchmarks and prospects*, *Eur. Phys. J. C* **48** (2006) 413–426, [hep-ph/0604249].

[238] R. Barbieri, D. Buttazzo, F. Sala and D. M. Straub, *Flavour physics from an approximate $U(2)^3$ symmetry*, *JHEP* **07** (2012) 181, [1203.4218].

[239] J. Charles, S. Descotes-Genon, Z. Ligeti, S. Monteil, M. Papucci and K. Trabelsi, *Future sensitivity to new physics in B_d, B_s, and K mixings*, *Phys. Rev. D* **89** (2014) 033016, [1309.2293].

[240] R. J. Dowdall, C. T. H. Davies, R. R. Horgan, G. P. Lepage, C. J. Monahan, J. Shigemitsu et al., *Neutral B-meson mixing from full lattice QCD at the physical point*, *Phys. Rev. D* **100** (2019) 094508, [1907.01025].

[241] R. Aleksan, I. Dunietz and B. Kayser, *Determining the CP violating phase gamma*, *Z. Phys. C* **54** (1992) 653–660.

[242] R. Fleischer, *New strategies to obtain insights into CP violation through B(s) —> D(s)+- K-+, D(s)*+- K-+, ... and B(d) —> D+- pi-+, D*+- pi-+, ... decays*, *Nucl. Phys. B* **671** (2003) 459–482, [hep-ph/0304027].

[243] K. De Bruyn, R. Fleischer, R. Knegjens, M. Merk, M. Schiller and N. Tuning, *Exploring $B_s \to D_s^{(*)\pm} K^\mp$ Decays in the Presence of a Sizable Width Difference $\Delta\Gamma_s$*, *Nucl. Phys. B* **868** (2013) 351–367, [1208.6463].

[244] A. S. Dighe, I. Dunietz and R. Fleischer, *Extracting CKM phases and $B_s - \bar{B}_s$ mixing parameters from angular distributions of nonleptonic B decays*, *Eur. Phys. J. C* **6** (1999) 647–662, [hep-ph/9804253].

[245] UTfit collaboration, http://www.utfit.org/UTfit/.

[246] E. Malami and R. Fleischer, *Puzzles in the $B_s^0 \to D_s^\pm K^\mp$ System*, *PoS* **CKM2021** (2023) 077, [2203.13758].

[247] E. Malami and R. Fleischer, *Searching for New Physics with $B_s^0 \to D_s^\pm K^\mp$ Decays*, *PoS* **PANIC2021** (2022) 159, [2112.00569].

[248] E. Malami, *$B_s^0 \to D_s^\pm K^\mp$ decays: Can they reveal New Physics?*, *PoS* **CORFU2019** (2020) 026.

[249] R. Fleischer, N. Serra and N. Tuning, *Tests of Factorization and SU(3) Relations in B Decays into Heavy-Light Final States*, *Phys. Rev. D* **83** (2011) 014017, [1012.2784].

[250] C. J. Monahan, H. Na, C. M. Bouchard, G. P. Lepage and J. Shigemitsu, *$B_s \to D_s \ell\nu$ Form Factors and the Fragmentation Fraction Ratio f_s/f_d*, *Phys. Rev. D* **95** (2017) 114506, [1703.09728].

[251] E. McLean, C. T. H. Davies, J. Koponen and A. T. Lytle, *$B_s \to D_s \ell\nu$ Form Factors for the full q^2 range from Lattice QCD with non-perturbatively normalized currents*, *Phys. Rev. D* **101** (2020) 074513, [1906.00701].

[252] T. Huber, S. Kränkl and X.-Q. Li, *Two-body non-leptonic heavy-to-heavy decays at NNLO in QCD factorization*, *JHEP* **09** (2016) 112, [1606.02888].

[253] M. Bordone, N. Gubernari, T. Huber, M. Jung and D. van Dyk, *A puzzle in $\bar{B}^0_{(s)} \to D^+_{(s)}\{\pi^-, K^-\}$ decays and extraction of the f_s/f_d fragmentation fraction*, *Eur. Phys. J. C* **80** (2020) 951, [2007.10338].

[254] M. Beneke, P. Böer, G. Finauri and K. K. Vos, *QED factorization of two-body non-leptonic and semi-leptonic B to charm decays*, *JHEP* **10** (2021) 223, [2107.03819].

[255] A. Khodjamirian and A. V. Rusov, *$B_s \to K\ell\nu_\ell$ and $B_{(s)} \to \pi(K)\ell^+\ell^-$ decays at large recoil and CKM matrix elements*, *JHEP* **08** (2017) 112, [1703.04765].

[256] LHCb collaboration, R. Aaij et al., *Measurement of $|V_{cb}|$ with $B^0_s \to D_s^{(*)-}\mu^+\nu_\mu$ decays*, *Phys. Rev. D* **101** (2020) 072004, [2001.03225].

[257] I. Caprini, L. Lellouch and M. Neubert, *Dispersive bounds on the shape of anti-B —> D(*) lepton anti-neutrino form-factors*, *Nucl. Phys. B* **530** (1998) 153–181, [hep-ph/9712417].

[258] J. L. Rosner, S. Stone and R. S. Van de Water, *Leptonic Decays of Charged Pseudoscalar Mesons - 2015*, 1509.02220.

[259] J. M. Flynn, T. Izubuchi, T. Kawanai, C. Lehner, A. Soni, R. S. Van de Water et al., *$B \to \pi\ell\nu$ and $B_s \to K\ell\nu$ form factors and $|V_{ub}|$ from 2+1-flavor lattice QCD with domain-wall light quarks and relativistic heavy quarks*, *Phys. Rev. D* **91** (2015) 074510, [1501.05373].

[260] Fermilab Lattice, MILC collaboration, A. Bazavov et al., *$B_s \to K\ell\nu$ decay from lattice QCD*, *Phys. Rev. D* **100** (2019) 034501, [1901.02561].

[261] I. Sentitemsu Imsong, A. Khodjamirian, T. Mannel and D. van Dyk, *Extrapolation and unitarity bounds for the $B \to \pi$ form factor*, *JHEP* **02** (2015) 126, [1409.7816].

[262] J. Flynn, R. Hill, A. Jüttner, A. Soni, J. T. Tsang and O. Witzel, *Semileptonic $B \to \pi\ell\nu$, $B \to D\ell\nu$, $B_s \to K\ell\nu$, and $B_s \to D_s\ell\nu$ decays*, *PoS* **LATTICE2019** (2019) 184, [1912.09946].

[263] R. Fleischer, R. Jaarsma and K. K. Vos, *New strategy to explore CP violation with $B_s^0 \to K^- K^+$*, *Phys. Rev. D* **94** (2016) 113014, [1608.00901].

[264] G. Hiller, *Lepton nonuniversality anomalies \& implications*, in *53rd Rencontres de Moriond on QCD and High Energy Interactions*, pp. 43–48, 2018. 1804.02011.

[265] S. Fajfer, *Theory Status - Puzzles in B Meson Decays and LFU?*, *SciPost Phys. Proc.* **1** (2019) 010.

[266] F. U. Bernlochner, M. F. Sevilla, D. J. Robinson and G. Wormser, *Semitauonic b-hadron decays: A lepton flavor universality laboratory*, *Rev. Mod. Phys.* **94** (2022) 015003, [2101.08326].

[267] J. Albrecht, D. van Dyk and C. Langenbruch, *Flavour anomalies in heavy quark decays*, *Prog. Part. Nucl. Phys.* **120** (2021) 103885, [2107.04822].

[268] M. Jung and D. M. Straub, *Constraining new physics in $b \to c\ell\nu$ transitions*, *JHEP* **01** (2019) 009, [1801.01112].

[269] S. Iguro and R. Watanabe, *Bayesian fit analysis to full distribution data of $\overline{\mathrm{B}} \to \mathrm{D}^{(*)}\ell\overline{\nu}$: $|\mathrm{V_{cb}}|$ determination and new physics constraints*, *JHEP* **08** (2020) 006, [2004.10208].

[270] J. Brod, A. Lenz, G. Tetlalmatzi-Xolocotzi and M. Wiebusch, *New physics effects in tree-level decays and the precision in the determination of the quark mixing angle γ*, *Phys. Rev. D* **92** (2015) 033002, [1412.1446].

[271] A. Lenz and G. Tetlalmatzi-Xolocotzi, *Model-independent bounds on new physics effects in non-leptonic tree-level decays of B-mesons*, *JHEP* **07** (2020) 177, [1912.07621].

[272] Y. Nir and H. R. Quinn, *Measuring CKM parameters with CP asymmetry and isospin analysis in B —> pi K*, *Phys. Rev. Lett.* **67** (1991) 541–544.

[273] M. Gronau, O. F. Hernandez, D. London and J. L. Rosner, *Electroweak penguins and two-body B decays*, *Phys. Rev. D* **52** (1995) 6374–6382, [hep-ph/9504327].

[274] M. Beneke and M. Neubert, *QCD factorization for B —> PP and B —> PV decays*, *Nucl. Phys. B* **675** (2003) 333–415, [hep-ph/0308039].

[275] A. J. Buras, R. Fleischer, S. Recksiegel and F. Schwab, *B —> pi pi, new physics in B —> pi K and implications for rare K and B decays*, *Phys. Rev. Lett.* **92** (2004) 101804, [hep-ph/0312259].

[276] Belle-II collaboration, T. Abe et al., *Belle II Technical Design Report*, 1011.0352.

[277] N. B. Beaudry, A. Datta, D. London, A. Rashed and J.-S. Roux, *The $B \to \pi K$ puzzle revisited*, *JHEP* **01** (2018) 074, [1709.07142].

[278] V. Barger, L. L. Everett, J. Jiang, P. Langacker, T. Liu and C. E. M. Wagner, *b —> s Transitions in Family-dependent U(1)-prime Models*, *JHEP* **12** (2009) 048, [0906.3745].

[279] V. Barger, L. Everett, J. Jiang, P. Langacker, T. Liu and C. Wagner, *Family Non-universal U(1)-prime Gauge Symmetries and b —> s Transitions*, *Phys. Rev. D* **80** (2009) 055008, [0902.4507].

[280] R. Fleischer, *Theoretical prospects for B physics*, *PoS* **FPCP2015** (2015) 002, [1509.00601].

[281] R. Fleischer, R. Jaarsma, E. Malami and K. K. Vos, *Exploring $B \to \pi\pi, \pi K$ decays at the high-precision frontier*, *Eur. Phys. J. C* **78** (2018) 943, [1806.08783].

[282] E. Malami, *Exploring New Physics in $B \to \pi K$ Decays*, *PoS* **CORFU2019** (2020) 025, [2008.08468].

[283] R. Fleischer, R. Jaarsma, E. Malami and K. K. Vos, *Utilising $B \to \pi K$ Decays at the High-Precision Frontier*, in *53rd Rencontres de Moriond on QCD and High Energy Interactions*, pp. 85–88, 2018. 1805.06705.

[284] R. Fleischer, R. Jaarsma, E. Malami and K. K. Vos, *Probing New Physics in $B \to \pi K$ Decays*, *PoS* **LHCP2018** (2018) 176, [1812.02672].

[285] M. Gronau, *Elimination of penguin contributions to CP asymmetries in B decays through isospin analysis*, *Phys. Lett. B* **265** (1991) 389–394.

[286] M. Neubert, *Rescattering effects, isospin relations and electroweak penguins in B —> pi K decays*, *Phys. Lett. B* **424** (1998) 152–160, [hep-ph/9712224].

[287] M. Gronau, D. Pirjol and T.-M. Yan, *Model independent electroweak penguins in B decays to two pseudoscalars*, *Phys. Rev. D* **60** (1999) 034021, [hep-ph/9810482].

[288] Particle Data Group collaboration, C. Patrignani et al., *Review of Particle Physics*, *Chin. Phys. C* **40** (2016) 100001.

[289] R. Fleischer, R. Jaarsma and K. K. Vos, *Towards New Frontiers in the Exploration of Charmless Non-Leptonic B Decays*, *JHEP* **03** (2017) 055, [1612.07342].

[290] R. Fleischer, *CP violation in the B system and relations to K —> pi nu anti-nu decays*, *Phys. Rept.* **370** (2002) 537–680, [hep-ph/0207108].

[291] R. Fleischer, *Strategies for fixing the CKM angle gamma and obtaining experimental insights into the world of electroweak penguins*, *Phys. Lett. B* **365** (1996) 399–406, [hep-ph/9509204].

[292] M. Neubert and J. L. Rosner, *New bound on gamma from B+- —> pi K decays*, *Phys. Lett. B* **441** (1998) 403–409, [hep-ph/9808493].

[293] R. Fleischer, S. Jager, D. Pirjol and J. Zupan, *Benchmarks for the New-Physics Search through CP Violation in B0 —> pi0 K(S)*, *Phys. Rev. D* **78** (2008) 111501, [0806.2900].

[294] R. Fleischer, *Rescattering and electroweak penguin effects in strategies to constrain and determine the CKM angle gamma from B —> pi K decays*, *Eur. Phys. J. C* **6** (1999) 451–470, [hep-ph/9802433].

[295] R. Fleischer and T. Mannel, *Constraining the CKM angle gamma and penguin contributions through combined B —> pi K branching ratios*, *Phys. Rev. D* **57** (1998) 2752–2759, [hep-ph/9704423].

[296] M. Gronau, J. L. Rosner and D. London, *Weak coupling phase from decays of charged B mesons to pi K and pi pi*, *Phys. Rev. Lett.* **73** (1994) 21–24, [hep-ph/9404282].

[297] M. Gronau, *A Precise sum rule among four B —> K pi CP asymmetries*, *Phys. Lett. B* **627** (2005) 82–88, [hep-ph/0508047].

[298] M. Gronau and J. L. Rosner, *Rate and CP-asymmetry sum rules in B —> K pi*, *Phys. Rev. D* **74** (2006) 057503, [hep-ph/0608040].

[299] BELLE II collaboration, M. Veronesi, *Time-dependent CP violation results at Belle II*, in *57th Rencontres de Moriond on Electroweak Interactions and Unified Theories*, 5, 2023. 2305.09153.

[300] E. Malami, *Manifestations of CP Violation in the B Meson System: Theoretical Perspective*, in *21st International Conference on B-Physics at Frontier Machines*, 2, 2024. 2402.10023.

[301] E. Malami, *Theoretical Highlights of CP Violation in B Decays*, in *16th International Conference on Heavy Quarks and Leptons*, 2, 2024. 2402.16976.

[302] R. Fleischer, R. Jaarsma and K. K. Vos, *Towards new frontiers with $B \to \pi K$ decays*, *Phys. Lett. B* **785** (2018) 525–529, [1712.02323].

[303] R. Fleischer, R. Jaarsma and G. Tetlalmatzi-Xolocotzi, *In Pursuit of New Physics with $B^0_{s,d} \to \ell^+\ell^-$*, *JHEP* **05** (2017) 156, [1703.10160].

[304] C. Bobeth, M. Gorbahn, T. Hermann, M. Misiak, E. Stamou and M. Steinhauser, *$B_{s,d} \to l^+l^-$ in the Standard Model with Reduced Theoretical Uncertainty*, *Phys. Rev. Lett.* **112** (2014) 101801, [1311.0903].

[305] G. Borissov, R. Fleischer and M.-H. Schune, *Rare Decays and CP Violation in the B_s System*, *Ann. Rev. Nucl. Part. Sci.* **63** (2013) 205–235, [1303.5575].

[306] K. De Bruyn, R. Fleischer, R. Knegjens, P. Koppenburg, M. Merk, A. Pellegrino et al., *Probing New Physics via the $B^0_s \to \mu^+\mu^-$ Effective Lifetime*, *Phys. Rev. Lett.* **109** (2012) 041801, [1204.1737].

[307] LHCb collaboration, R. Aaij et al., *Measurement of the $B^0_s \to \mu^+\mu^-$ branching fraction and effective lifetime and search for $B^0 \to \mu^+\mu^-$ decays*, *Phys. Rev. Lett.* **118** (2017) 191801, [1703.05747].

[308] P. Langacker and M. Plumacher, *Flavor changing effects in theories with a heavy Z' boson with family nonuniversal couplings*, *Phys. Rev. D* **62** (2000) 013006, [hep-ph/0001204].

[309] S. Davidson and S. Descotes-Genon, *Minimal Flavour Violation for Leptoquarks*, *JHEP* **11** (2010) 073, [1009.1998].

[310] W. Altmannshofer, S. Gori, M. Pospelov and I. Yavin, *Quark flavor transitions in $L_\mu - L_\tau$ models*, *Phys. Rev. D* **89** (2014) 095033, [1403.1269].

[311] A. J. Buras, R. Fleischer, J. Girrbach and R. Knegjens, *Probing New Physics with the $B_s \to \mu + \mu-$ Time-Dependent Rate*, *JHEP* **07** (2013) 077, [1303.3820].

[312] W. Altmannshofer, C. Niehoff and D. M. Straub, *$B_s \to \mu^+\mu^-$ as current and future probe of new physics*, *JHEP* **05** (2017) 076, [1702.05498].

[313] R. Fleischer, D. G. Espinosa, R. Jaarsma and G. Tetlalmatzi-Xolocotzi, *CP Violation in Leptonic Rare B_s^0 Decays as a Probe of New Physics*, *Eur. Phys. J. C* **78** (2018) 1, [1709.04735].

[314] LHCb collaboration, R. Aaij et al., *Test of lepton universality in $b \to s\ell^+\ell^-$ decays*, *Phys. Rev. Lett.* **131** (2023) 051803, [2212.09152].

[315] R. Fleischer, E. Malami, A. Rehult and K. K. Vos, *Targeting (Pseudo)-Scalar CP Violation with $B_s \to \mu^+\mu^-$*, 2405.10366.

[316] A. J. Buras, *Relations between Δ M(s, d) and B(s, d) $\to \mu\bar{\mu}$ in models with minimal flavor violation*, *Phys. Lett. B* **566** (2003) 115–119, [hep-ph/0303060].

[317] C. Bobeth and A. J. Buras, *Searching for New Physics with $\bar{\mathcal{B}}(B_{s,d} \to \mu\bar{\mu})/\Delta M_{s,d}$*, *Acta Phys. Polon. B* **52** (2021) 1189, [2104.09521].

[318] A. J. Buras and E. Venturini, *Searching for New Physics in Rare K and B Decays without $|V_{cb}|$ and $|V_{ub}|$ Uncertainties*, *Acta Phys. Polon. B* **53** (9, 2021) 6–A1, [2109.11032].

[319] A. J. Buras, J. Girrbach, D. Guadagnoli and G. Isidori, *On the Standard Model prediction for BR(Bs,d to mu+ mu-)*, *Eur. Phys. J. C* **72** (2012) 2172, [1208.0934].

[320] P. A. M. Dirac, *The Principles of Quantum Mechanics*. Clarendon Press, 1930.

[321] ATLAS collaboration, G. Aad et al., *Measurement of the $B_s^0 \to \mu\mu$ effective lifetime with the ATLAS detector*, *JHEP* **09** (2023) 199, [2308.01171].

[322] CMS collaboration, A. Tumasyan et al., *Measurement of the $B_{\rm S}^0 \to \mu^+\mu^-$ decay properties and search for the $B^0 \to \mu^+\mu^-$ decay in proton-proton collisions at $\sqrt{s} = 13$ TeV*, *Phys. Lett. B* **842** (2023) 137955, [2212.10311].

[323] CMS collaboration, A. M. Sirunyan et al., *Measurement of properties of $B_s^0 \to \mu^+\mu^-$ decays and search for $B^0 \to \mu^+\mu^-$ with the CMS experiment*, *JHEP* **04** (2020) 188, [1910.12127].

[324] CMS collaboration, *Measurement of $\mathrm{B}_\mathrm{s}^0 \to \mu^+\mu^-$ decay properties and search for the $\mathrm{B}^0 \to \mu\mu$ decay in proton-proton collisions at $\sqrt{s} = 13$ TeV*, CMS-PAS-BPH-21-006.

[325] LHCb collaboration, R. Aaij et al., *Analysis of Neutral B-Meson Decays into Two Muons*, *Phys. Rev. Lett.* **128** (2022) 041801, [2108.09284].

[326] ATLAS collaboration, M. Aaboud et al., *Study of the rare decays of B_s^0 and B^0 mesons into muon pairs using data collected during 2015 and 2016 with the ATLAS detector*, *JHEP* **04** (2019) 098, [1812.03017].

[327] L.-S. Geng, B. Grinstein, S. Jäger, S.-Y. Li, J. Martin Camalich and R.-X. Shi, *Implications of new evidence for lepton-universality violation in $b \to s\ell+\ell$- decays*, *Phys. Rev. D* **104** (2021) 035029, [2103.12738].

[328] W. Altmannshofer and P. Stangl, *New physics in rare B decays after Moriond 2021*, *Eur. Phys. J. C* **81** (2021) 952, [2103.13370].

[329] T. Hurth, F. Mahmoudi, D. M. Santos and S. Neshatpour, *More Indications for Lepton Nonuniversality in $b \to s\ell^+\ell^-$*, *Phys. Lett. B* **824** (2022) 136838, [2104.10058].

[330] M. Beneke, C. Bobeth and R. Szafron, *Power-enhanced leading-logarithmic QED corrections to $B_q \to \mu^+\mu^-$*, *JHEP* **10** (2019) 232, [1908.07011].

[331] LHCb collaboration, C. Langenbruch, *Rare decays at LHCb*, in *51st Rencontres de Moriond on QCD and High Energy Interactions*, pp. 175–178, ARISF, 5, 2016. 1605.07075.

[332] CMS, LHCb collaboration, *Combination of results on the rare decays $B^0_{(s)} \to \mu^+\mu^-$ from the CMS and LHCb experiments*, CERN-LHCb-CONF-2013-012.

[333] https://home.cern/science/physics/standard model.

A Tale of Beauty and Puzzles

Since ancient times, people try to obtain a deeper understanding of the Universe and unravel its secrets. Questions like "what is nature made of?" or "what are the fundamental interactions?" are at the heart of this quest. The theory that describes the subatomic world, giving answers to such questions, is the Standard Model (SM) of particle physics.

The SM classifies the elementary constituents of the matter and explains their interactions. The building blocks of matter are leptons and quarks. There are six types of leptons, the "electron" and "electron neutrino", the "muon" and "muon neutrino" as well as the "tau" and "tau neutrino". Leptons exist independently. There are also six different types of quarks, called flavours, the "up" and "down", "charm" and "strange", "top" and "bottom". Each one of these also has an anti-particle associated with it. Contrary to leptons, quarks bind together and form either triplets, called baryons, or doublets, called mesons, which are combinations of a quark and an anti-quark.

In addition, the SM describes the forces that govern the interactions. The fundamental forces which act in the universe are four: the strong, the weak, the electromagnetic and the gravitational. The SM describes three of them, as gravity is not part of the SM. These forces are mediated by particles called bosons: the photon γ for electromagnetism, the W and Z bosons for the weak force, the gluon for the strong force. In 2012, the breakthrough discovery of another particle, the Higgs boson, completed the SM picture. The Higgs boson is responsible for giving mass to particles. A full description of the SM of particle physics is given in Fig. 1.

The SM is a successful theory, but it is incomplete, as there are still unresolved issues and phenomena it cannot explain. Looking at the bigger picture, among these challenges, one of the key questions is: Why does matter dominate over antimatter in our universe? When trying to understand this baryon asymmetry within the SM framework, the predictions fall short by many orders of magnitude. What could be missing? CP violation! Let us explore this term. CP symmetry suggests that the laws of physics should remain unchanged if particles are swapped with their antiparticles and spatial coordinates are inverted. Violation of this symmetry indicates that the behaviour of particles and antiparticles differs, pointing to possible effects of physics beyond the SM.

In general, there are two approaches for searching for New Physics (NP):

- the *direct* way, where we try to find new particles at colliders at very high energies,
- the *indirect* way, where we perform calculations of very high precision.

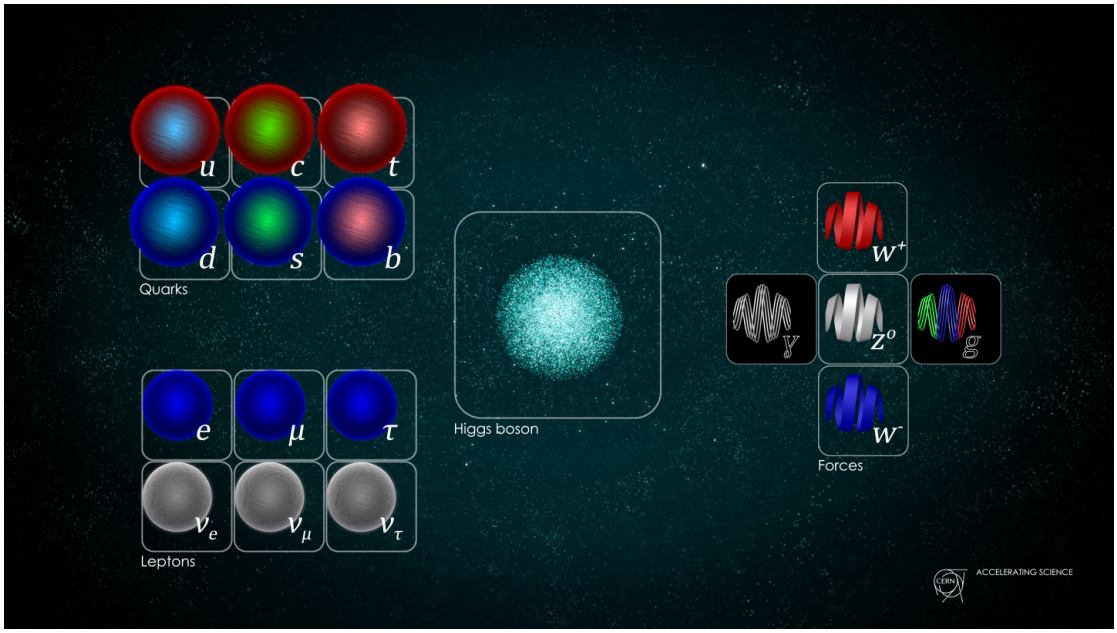

Figure 1: The Standard Model of particle physics (Image: Daniel Dominguez/CERN) [333].

CP violation is an excellent probe for searching for physics beyond the SM in an indirect way. This approach allows us to detect signs of new interactions or particles that may be too heavy to be directly observed at colliders. The most powerful collider is currently the Large Hadron Collider (LHC), which plays a key role in experimental particle physics. In order to explore CP violation in the laboratory, B mesons are fantastic tools. More specifically, B mesons are bound states of an anti-bottom quark and a light quark (up, down, strange or even charm). So, their decays are important for both testing the SM and searching for NP.

In this dissertation, I have presented a beautiful tale of beauty and puzzles. What is beauty? It is just another name for the bottom quark. And what do we mean by the term "puzzles"? It refers to the deviations that might arise between SM predictions and experimental data. So, we focus on decays with puzzling patterns where CP violation plays the key role. One of the main theoretical tools we utilize to explore these phenomena is quantum field theory (QFT). Simply speaking, QFT provides a theoretical framework for describing the behaviour and the interactions between subatomic particles, combining the principles of quantum mechanics and relativity.

B mesons can decay into other particles, referred to as the final state. There are three types of final states: those consisting only of leptons, those that include both leptons and mesons, and those made up exclusively of mesons with no leptons. In our analysis, we focus on the following decays:

Meson	Quark Content	Meson	Quark Content
K^+	$u\bar{s}$	D_s^+	$c\bar{s}$
K^-	$\bar{u}s$	D_s^-	$\bar{c}s$
K^0	$d\bar{s}$	π^+	$u\bar{d}$
$\bar{K}^0$	$\bar{d}s$	π^-	$\bar{u}d$
J/ψ	$c\bar{c}$	π^0	$\frac{u\bar{u}-d\bar{d}}{\sqrt{2}}$
ϕ	$s\bar{s}$		

Table 1: Quark content of various mesons.

- $B_d^0 \to J/\psi K_S^0$ and $B_s^0 \to J/\psi\phi$,
- $B_s^0 \to D_s^{\mp} K^{\pm}$,
- $B \to \pi K$,
- $B_{(s)}^0 \to \mu^+\mu^-$,

where J/ψ, K, ϕ, D and π are mesons while μ denotes the "muon" lepton. For completeness, the quark content of these mesons is shown in Table 1. These processes have very different and, in some cases, very complicated dynamics, providing us with a broader and thus more complete picture of our field. They serve as benchmark cases for studying CP violation and exploring NP, as they are very sensitive to new particles and interactions.

Fortunately, we live in a time where there is a plethora of experimental data. These data sets of the measured observables can be compared to the corresponding theory predictions. What do we observe in these cases? Within the studies presented in this thesis, we have found intriguing discrepancies between the theory and the measurements. It is very exciting that we have reached a level of precision, where it is possible to reveal such discrepancies. These puzzling cases suggest that there is room for NP! These first hints are very promising, especially in view of the future era of B physics, where even higher precision will be achieved.

Our strategy in the study of each one of these decays involves the following steps:

i) We perform theoretical analyses.

ii) We utilise the experimental data.

iii) We compare theory with experiment, resulting in puzzling patterns in these processes.

iv) We aim at answering the question: are these puzzles really signals of New Physics?

Each decay studied in this thesis shows very interesting patterns and offers very useful insights in the exploration of CP violation. It is important to keep improving the measurements of CP violation in these benchmark processes, which highlights the close connection between theory and experiment. We have proposed methods which can be fully exploited in the future as we move towards more accurate measurements. These methods allow us to better understand and interpret the results, which are very promising in the context of potential NP searches. The upcoming upgrades to the LHCb detector as well as the Belle II experiment, leading to more precise measurements, will play a key role in these endeavours.

Our main goal is to test the SM as thoroughly as possible and, by utilizing our analysis, hopefully identify New Physics and reveal new sources of CP violation. In the bigger picture, if significant deviations from the SM are finally established in the future, it would mark a breakthrough result, opening up a completely new era in particle physics studies. Exciting developments are just around the corner – stay tuned for what's next!

OUR STUDIES IN A NUTSHELL

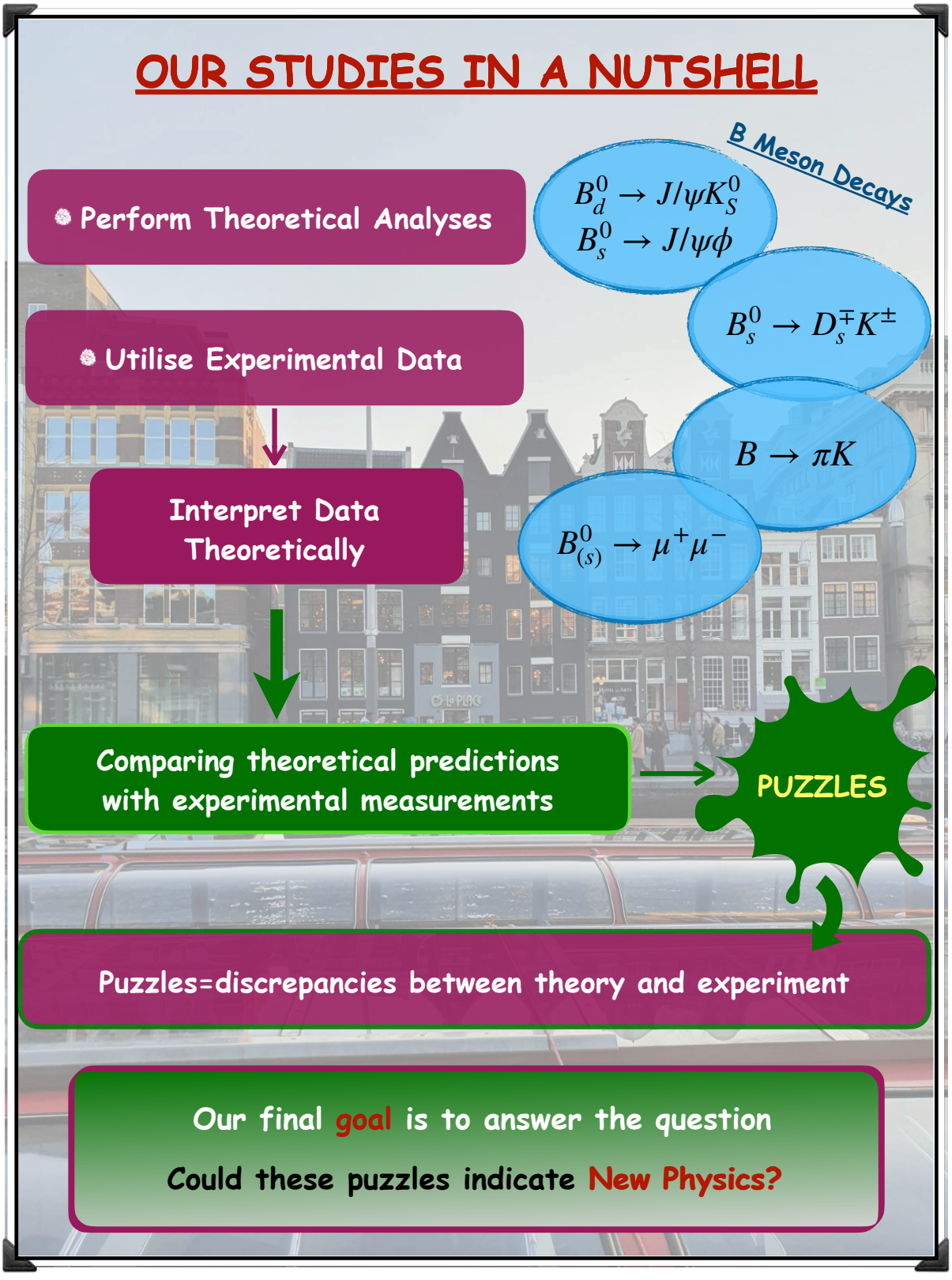

Een Verhaal van Beauty en de Puzzels

Sinds de oudheid proberen mensen een dieper begrip van het Universum te verkrijgen en de geheimen ervan te ontrafelen. Vragen zoals “waar is de natuur uit opgebouwd?” of “wat zijn de fundamentele interacties?” staan centraal in deze zoektocht. De theorie die de subatomaire wereld beschrijft en antwoorden geeft op dergelijke vragen, is het Standaardmodel (SM) van de deeltjesfysica.

Het SM classificeert de elementaire bestanddelen van materie en legt uit hoe ze interacteren. De bouwstenen van materie zijn leptonen en quarks. Er zijn zes soorten leptonen: “elektron” en “elektron neutrino”, “muon” en “muon neutrino”, evenals “tau” en “tau neutrino”. Leptonen bestaan onafhankelijk van elkaar. Er zijn ook zes verschillende soorten quarks, genaamd smaken: “up” en “down”, “charm” en “strange”, “top” en “bottom”. Elk van deze heeft ook een bijbehorend antideeltje. In tegenstelling tot leptonen binden quarks zich samen en vormen ze ofwel triplets, genaamd baryonen, of doublets, genaamd mesonen, die combinaties zijn van een quark en een antiquark.

Daarnaast beschrijft het SM de krachten die de interacties tussen de deeltjes bepalen. De fundamentele krachten die in het universum werkzaam zijn, zijn er vier: de sterke kernkracht, de zwakke kernkracht, de elektromagnetische kracht en de gravitatiekracht. Het SM beschrijft er drie van, aangezien zwaartekracht geen onderdeel is van het SM. Deze krachten worden overgebracht door deeltjes die bosonen worden genoemd: de foton γ voor de elektromagnetisme, de W- en Z-bosonen voor de zwakke kernkracht, en het gluon voor de sterke kernkracht. In 2012 voltooide de belangrijke ontdekking van een ander deeltje, het Higgs-boson, het beeld van het SM. Het Higgs-deeltje is verantwoordelijk voor het geven van massa aan de deeltjes. Een volledige beschrijving van het SM van de deeltjesfysica is te zien in Fig. 2.

Het SM is een succesvolle theorie, maar het is incompleet, aangezien er nog steeds onopgeloste problemen en fenomenen zijn die het niet kan verklaren. Als we naar het grotere geheel kijken, is een van de belangrijke vragen: Waarom domineert materie over antimaterie in ons universum? Bij pogingen om deze baryonische asymmetrie binnen het kader van het SM te begrijpen, schieten de voorspellingen tekort met vele ordes van grootte. Wat zou er kunnen ontbreken? CP-violatie! Laten we deze term verkennen. CP-symmetrie duid aan dat de natuurwetten onveranderd zouden moeten blijven als deeltjes worden verwisseld met hun antideeltjes en de ruimtelijke coördinaten worden omgekeerd. Schending van deze symmetrie duidt erop dat het gedrag van deeltjes en antideeltjes verschilt, wat wijst op mogelijke effecten van fysica die verder gaan dan het SM.

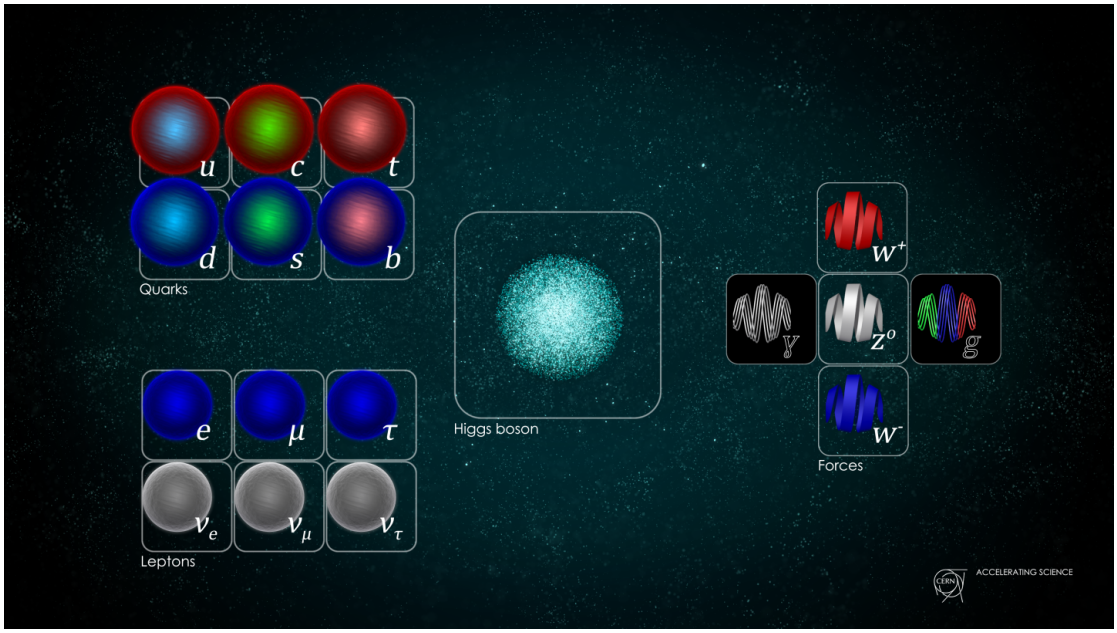

Figure 2: Het Standaardmodel van de deeltjesfysica (Afbeelding: Daniel Dominguez, CERN) [333].

In het algemeen zijn er twee benaderingen om naar Nieuwe Fysica (NP) te zoeken:

- de *directe* manier, waarbij we proberen nieuwe deeltjes te vinden bij deeltjesversnellers bij zeer hoge energieën,
- de *indirecte* manier, waarbij we berekeningen met een zeer hoge precisie uitvoeren.

CP-violatie is een uitstekende manier om te zoeken naar fysica die verder gaat dan het SM op een indirecte manier. Deze benadering stelt ons in staat om tekenen van nieuwe interacties of deeltjes te detecteren die mogelijk te zwaar zijn om direct waargenomen te worden bij deeltjesversnellers. De krachtigste deeltjesversneller is momenteel de Large Hadron Collider (LHC), die een sleutelrol speelt in de experimentele deeltjesfysica. Om CP-violatie in het laboratorium te onderzoeken, zijn B-mesonen fantastische hulpmiddelen. In het specifiek zijn B-mesonen gebonden toestanden van een anti-bottom quark en een licht quark (up, down, strange of zelfs charm). Hun verval is dus belangrijk zowel voor het testen van het SM als voor het zoeken naar NP.

In deze dissertatie heb ik een prachtig verhaal gepresenteerd over beauty en de puzzels. Wat is beauty? Het is gewoon een andere naam voor de bottomquark. En wat bedoelen we met de term "puzzels"? Het verwijst naar de afwijkingen die kunnen optreden tussen de voorspellingen van het SM en experimentele gegevens. Daarom richten we ons op vervalprocessen met puzzelende patronen waarbij CP-violatie een sleutelrol speelt. Een van de

Meson	Quarkinhoud	Meson	Quarkinhoud
K^+	$u\bar{s}$	D_s^+	$c\bar{s}$
K^-	$\bar{u}s$	D_s^-	$\bar{c}s$
K^0	$d\bar{s}$	π^+	$u\bar{d}$
$\bar{K}^0$	$\bar{d}s$	π^-	$\bar{u}d$
J/ψ	$c\bar{c}$	π^0	$\frac{u\bar{u}-d\bar{d}}{\sqrt{2}}$
ϕ	$s\bar{s}$		

Table 2: Quarkinhoud van mesonen.

belangrijkste theoretische hulpmiddelen die we gebruiken om deze fenomenen te verkennen, is de kwantumveldentheorie (QFT). Eenvoudig gezegd biedt QFT een theoretisch kader voor het beschrijven van het gedrag en de interacties tussen subatomaire deeltjes, door de principes van de kwantummechanica en relativiteit te combineren.

B-mesonen kunnen vervallen in andere deeltjes, die de eindtoestand worden genoemd. Er zijn drie typen eindtoestanden: degene die uitsluitend uit leptonen bestaan, degene die zowel leptonen als mesonen bevatten, en degene die uitsluitend uit mesonen bestaan zonder leptonen. In onze analyse richten we ons op de volgende vervalprocessen:

- $B_d^0 \to J/\psi K_S^0$ en $B_s^0 \to J/\psi\phi$,
- $B_s^0 \to D_s^{\mp} K^{\pm}$,
- $B \to \pi K$,
- $B_{(s)}^0 \to \mu^+\mu^-$,

waarbij J/ψ, K, ϕ, D en π mesonen zijn, terwijl μ het "muon" lepton aanduidt. Voor de volledigheid wordt de quarkinhoud van deze mesonen weergegeven in Table 2. Deze processen hebben zeer verschillende en, in sommige gevallen, zeer ingewikkelde dynamica, wat ons een breder en dus vollediger beeld van ons vakgebied geeft. Ze dienen als benchmarks voor het bestuderen van CP-violatie en het verkennen van NP, omdat ze zeer gevoelig zijn voor nieuwe deeltjes en interacties.

Gelukkig leven we in een tijd waarin er een overvloed aan experimentele gegevens beschikbaar is. Deze gegevenssets van de gemeten observabelen kunnen worden vergeleken met de bijbehorende theoretische voorspellingen. Wat observeren we in deze gevallen? Binnen de studies die in dit proefschrift worden gepresenteerd, hebben we intrigerende

discrepanties tussen de theorie en de metingen gevonden. Het is zeer opwindend dat we een precisieniveau hebben bereikt waarop het mogelijk is om dergelijke discrepanties te onthullen. Deze puzzelende gevallen suggereren dat er ruimte is voor NP! Deze eerste aanwijzingen zijn veelbelovend, vooral met het oog op het toekomstige tijdperk van B-fysica, waar nog hogere precisie zal worden bereikt.

Onze strategie bij het bestuderen van elk van deze vervallen omvat de volgende stappen:

i) We voeren theoretische analyses uit.

ii) We maken gebruik van de experimentele gegevens.

iii) We vergelijken theorie met experiment, wat leidt tot puzzelende gevallen in deze processen.

iv) We streven ernaar de vraag te beantwoorden: zijn deze puzzels echt signalen van Nieuwe Fysica?

Elke verval dat is geanaliseerd in dit proefschrift laat zeer interessante patronen zien en biedt waardevolle inzichten in de verkenning van CP-violatie. Het is belangrijk om de metingen van CP-violatie in deze benchmarks voortdurend te verbeteren, wat de nauwe verbinding tussen theorie en experiment onderstreept. We hebben methoden voorgesteld die in de toekomst volledig benut kunnen worden zodra nauwkeuriger metingen beschikaar zijn. Deze methoden stellen ons in staat de resultaten beter te begrijpen en te interpreteren, wat veelbelovend is in de context van mogelijke zoektochten naar NP. De aankomende upgrades van de LHCb-detector en het Belle II-experiment, die zullen leiden tot meer precieze metingen, zullen een sleutelrol spelen in deze inspanningen.

Ons belangrijkste doel is om het SM zo grondig mogelijk te testen en, door gebruik te maken van onze analyse, hopelijk Nieuwe Fysica te identificeren en nieuwe bronnen van CP-violatie te onthullen. Op de lange termijn, als er in de toekomst significante afwijkingen van het SM worden vastgesteld, zou dit een baanbrekend resultaat markeren en een volledig nieuw tijdperk in de deeltjesfysica openen. Spannende ontwikkelingen liggen in het verschiet – blijf op de hoogte van wat komen gaat!

ONZE STUDIES IN EEN NOTENDOP

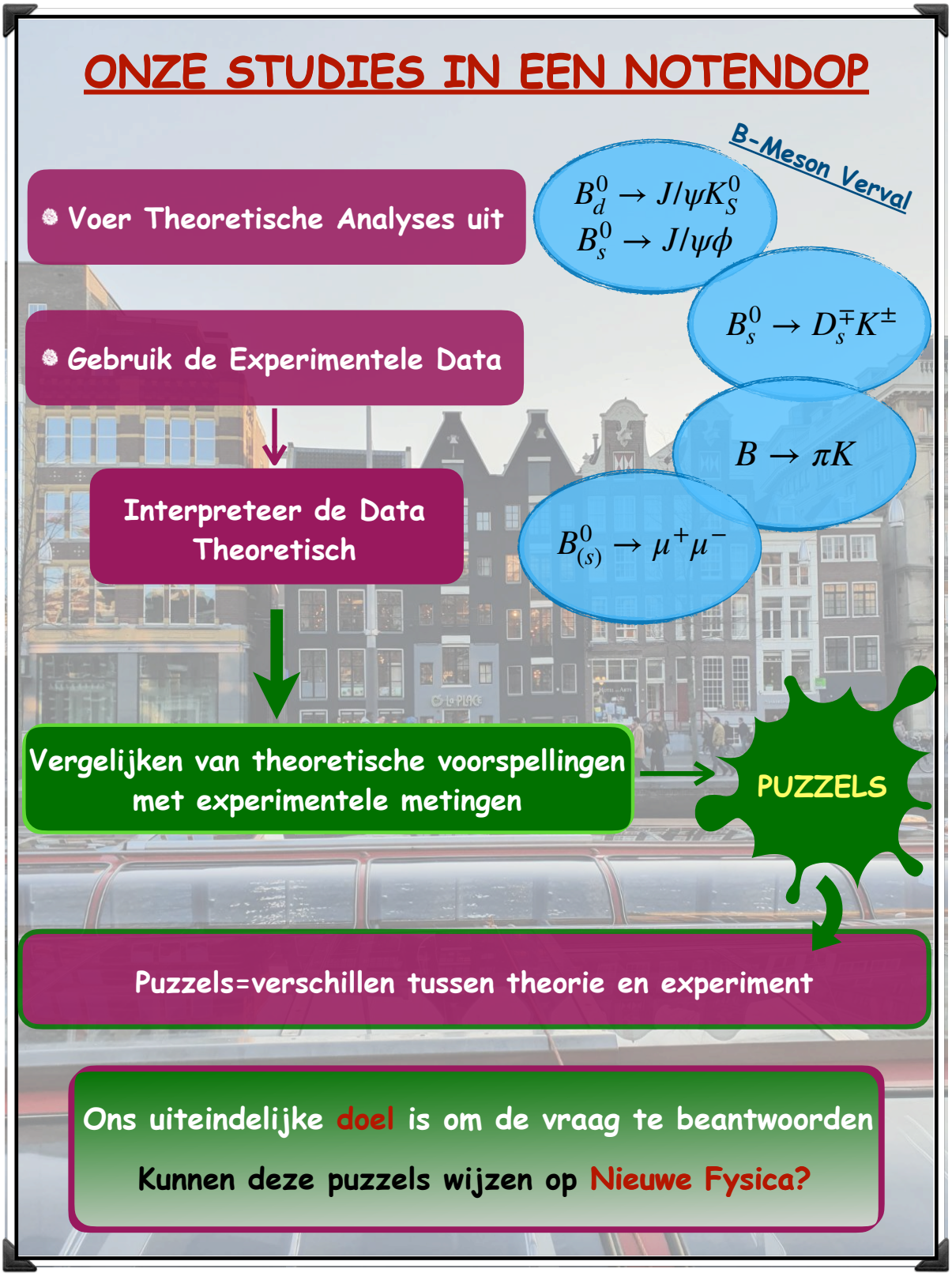

Acknowledgements

This thesis is dedicated to my parents, who fully supported my choices and my decision to study in Amsterdam, to my entire family, relatives, and my cherished long-time friends, who have always stood by my side throughout my journey.

Throughout my time in Amsterdam, I had the chance to meet many new people in both academic and personal settings. They provided me with valuable experiences and insights, greatly enriching my life and contributing to my growth. In these final pages, I would like to acknowledge and thank the new additions to my life, who have brought so much knowledge, as well as many joyful moments, and have enriched my circle of friends.

First, I would like to express my deepest gratitude to my supervisor, Robert Fleischer. He has been a mentor and a scientific father to me. It has been a great experience working with him − learning from the best, brainstorming ideas, and making the entire research journey truly remarkable. I deeply appreciate that he has always been there to support me, whether I had questions about physics, needed help with bureaucratic or organizational matters, or sought advice on things outside the pure world of academia. I am sincerely thankful for his insightful feedback, encouragement, and availability. He has inspired me and helped me develop both as a researcher and as an individual. I am happy that our collaboration continues and look forward to exploring many more exciting topics together in the future!

I would like to extend my thanks to my co-promotor, Marcel Merk, for all his help. It has been a great opportunity to benefit from his expertise on the experimental side. His insights have been invaluable for gaining a deeper understanding of the field. It is unfortunate that the challenging COVID situation limited interactions between theorists and experimentalists during my PhD years.

Next, I would like to express my sincere gratitude to all the members of my Reading Committee: Juan Rojo, Eric Laenen, Auke-Pieter Colijn, Danny van Dyk, Ann-Kathrin Perrevoort, and Jordy de Vries. Their expert review has been essential in ensuring the quality of my work. I appreciate their time and effort not only in evaluating my thesis promptly and efficiently but also for their availability and help in finalising the practical steps leading to my PhD ceremony.

Special thanks to Piet Mulders, who accepted to serve as the Chair of the Exam Committee for my PhD ceremony. He has been extremely helpful and supportive since I began

working at Nikhef, even before my PhD contract, starting from my time as a Master's student. His guidance and advice have consistently provided a significant boost for me!

When it comes to organizational matters, I cannot omit to thank the Secretary Group at Vrije Universiteit (VU), and especially Marja Herronen, who has consistently responded to all of my questions and assisted with the bureaucratic processes. Similarly, the entire team at Bureau Pedel has been very helpful throughout.

Discussing things related to the final PhD ceremony, it is time to give a big thanks to my two amazing paranymphs: Alice and Fabian! Alice, from the corridors of Nikhef to drinking cocktails and traveling through Germany, how many unforgettable moments have we shared? Fabian, from sharing an office as Master's students at Nikhef to endlessly bothering you with programming questions, look at where life has brought us. Thank you both for being there for me through all the ups and downs! Cheers to what's coming next!

Over the course of my PhD, I have had the opportunity to collaborate on projects and produce papers with outstanding individuals in our field, including both senior researchers and younger scholars, in addition to my supervisor. Working as a teaching assistant and engaging in one-on-one supervision with younger scientists has significantly contributed to my professional development, enhancing my skills in mentoring, communication, and research methodology.

In light of this, I would like to thank the following colleagues: Kristof, thank you especially for the invaluable expertise you have shared with us, including tools like GammaCombo. I have always enjoyed our collaborations. Keri, I deeply appreciate all your help and enthusiasm every time we work together, starting from our very first paper at the beginning of my PhD. Ruben, it has been wonderful working together and sharing an office as young PhD students. I always look back on those times with fantastic memories. Philine, collaborating with you on papers and coordinating classes as TAs has always been a pleasure. Anders and Marten, our collaborations have been very enjoyable. Jeannine, Yoran, and Pablo, our discussions have always been interesting, useful, and highly productive. Ilija, from our time at Nikhef to the coincidence of both moving to Siegen, our interactions have always been great.

I feel very lucky to have been working at Nikhef during my PhD years. It is an incredibly inspiring institution, with a stimulating environment where everyone is very friendly, approachable, and helpful. It has been a great opportunity to have discussions and exchange ideas with so many talented and smart people, gaining so much knowledge and experience. I will always have the sweetest memories from my time at Nikhef. I would like to heartily thank all the members of the Theory group, both senior and junior, for creating such a welcoming environment. I should not neglect to mention our experimental counterparts, with whom we had pleasant interactions from time to time, as well as the ad-

ministrative staff at Nikhef, who were always extremely helpful and polite. So many thanks first of all to my amazing officemates over the years: Jorinde, Jort, Pedro, Solange, Darren, and almost officemates Andreas, Elena and Anastasiia as well as to everyone with whom I shared enjoyable lunch and coffee break discussions and events, including both past and current members (senior and younger colleagues): Jos, Jan-Willem, Bert, Bernard, Wouter, Marieke, Franz, Valerio, Rudy, Lorenzo, Emanuele, Jacob, Nathan, Michi, Avanish, Sonia, Rabah, Rhorry, Evangelos, Giulio, Marco, Melissa, Max, Jaco, Giacomo, Andrea, Tommaso, Pieter, Marieke, Jelle, Heleen, Jacco, Robin, Sofia, Jordy, Patrick, Martijn, Ed, Eveline, Karin − hoping I don't miss names.

Being a part of the Dutch Research School of Theoretical Physics (DRSTP) was a great opportunity to meet fellow physicists across the Netherlands, in addition to gaining more knowledge through classes in other fields of theoretical physics. I also really enjoyed my role as a member of the PhD council for the DRSTP. Gabriele and Beatrix, I still strongly believe that the school in Brazil was the highlight of our time studying in Amsterdam. Thanks for all the fantastic memories, guys (both within and outside the European continent)! Also, thanks to the rest of the great colleagues and other members of the Council who made every DRSTP event a fun activity, including Guada, Perseas, Marrit, Aleksandar, Savvas, Dora, Jorgos, Ruud, Yuan, Carlos, Greg, Antonio, Eric, Joren, Peters, Alba.

On top of interacting with amazing people within academia, I also had the chance to meet fantastic individuals outside of research. First of all, special mention to our, let's call it, Greek-Amsterdam group − starting together in Amsterdam years ago and with the main core of people still holding strong: Maria, Nikos, Eftychia, Olympia, Georgia, Michalis, and Petros. Cheers to all our moments over the years!

I also had the opportunity to meet and connect with numerous great people from all over the world. The pandemic slowed everything down for a while, but despite the situation, continuing with activities like playing piano and singing, participating in theater groups, dancing, forming book clubs, or simply hanging out with neighbors brought wonderful people into my life and made the pandemic feel far less gloomy. So, a special shout out to all these people − yes, some of them are again physicists − including: Bram, Jim, Shanna, Nadine, Clara, and especially Sofia and Facundo (we still need to plan a trip with the three of us, guys!), Daphne (how many corona walks!), Stratos, Nikos, Melina, George, Dimitra, Peter, Rien, Michelle, Jasper, Aaltje, Jacob, Daan, Marco, Kimberley, Thijs, Stephan, Misha, Tina, Grazyna, Rox, Antonio, George, Angy, Angelos, Maria, Davide, Elodie, Arman, Francesca, Sofia, Celine, Lieke, Rachel, Lizzie, Richie, Anna, Harris, Lefteris, Maria, Lina, Evi, Dionysia, Peggy, Ricardo, Caroline, Pilar.

Last but not least, I could not neglect to mention how thankful I am to the people from the University of Siegen (and the whole CRC community) for welcoming me to their

group and being extremely helpful with everything I needed. First of all, I would like to extend my sincere gratitude to Thomas Mannel, Tobias Huber (as my immediate PI), and Thorsten Feldmann, who offered me a position for my next step in academia and for all their assistance. Many thanks also to Alex Lenz for his help and for including me in our fantastic "Physik im Apollo" shows! And of course, I would like to thank the entire group – PIs, senior and junior members – who have all been so friendly and created such a wonderful environment in Siegen: Guido, Alexander, Wolfgang, Björn, Rusa, Alexei, Oliver, Claus, Vlad, Maria Laura, Gilberto, Aleksey, Tom, Pia, Kevin, Nico, Jack, Anshika, Méril, Martin, Anastasia, Zac, Jacob, Dennis, Philip, Marta, Tobias, Matthew, Nils, Sebastian, Ali, Arzu.

Of course, at this point I should also add special thanks to my professors from the University of Athens, Theodore Mertzimekis and Eirene Mavrommatis. They have generously provided me with recommendation letters, which are crucial for continuing my academic career. These two have been the first to introduce me to the world of research and have supported me since the beginning of my studies.

Looking back, I feel very happy and lucky that I have managed to follow my dream and pursue the research path in physics. Participating in a lot of conferences, being invited numerous times to give talks to promote my research, and having the chance to write an article for the CERN Courier have all gone beyond what I had hoped for. It is cool to see how things have developed, from the time I was a school student discussing the idea of becoming a physicist with Giota, Vasiliki, Demetra, Maria, and Nia, to describing it to Peggy above the piano clavier, to starting my bachelor's degree and studying with Maria (before she also joined us in Amsterdam, rejoining forces for even more amazing experiences! – cheers to dream trip team), Fey, Sophia, and Maria, and finally moving to Amsterdam for my postgraduate studies. I still miss the typical Greek Sunday meals though (Vaso, Panos, Costas, Maria – yes, all the Marias mentioned are different – and our furry friend Tommy). However, as I promised at the start of these acknowledgments, I will focus on mentioning the new people that Amsterdam has brought into my path. So, I'll stick to that promise before this section turns into a whole volume.

My last comment is that I also dedicate this thesis to my grandparents, who have all passed away, but I am sure they would be really proud.

I heartily thank everyone who has been part of my life while conducting my research!